

Georgia State University

ScholarWorks @ Georgia State University

Physics and Astronomy Dissertations

Department of Physics and Astronomy

8-8-2023

Orbital Architectures of M Dwarf Companions

Eliot H. Vrijmoet

Georgia State University

Follow this and additional works at: https://scholarworks.gsu.edu/phy_astr_diss

Recommended Citation

Vrijmoet, Eliot H., "Orbital Architectures of M Dwarf Companions." Dissertation, Georgia State University, 2023.

doi: <https://doi.org/10.57709/35866812>

This Dissertation is brought to you for free and open access by the Department of Physics and Astronomy at ScholarWorks @ Georgia State University. It has been accepted for inclusion in Physics and Astronomy Dissertations by an authorized administrator of ScholarWorks @ Georgia State University. For more information, please contact scholarworks@gsu.edu.

Orbital Architectures of M Dwarf Companions

by

Eliot Halley Vrijmoet

Under the Direction of Todd J. Henry, Ph.D.

A Dissertation Submitted in Partial Fulfillment of the Requirements for the Degree of

Doctor of Philosophy

in the College of Arts and Sciences

Georgia State University

2023

ABSTRACT

The M dwarfs are the most numerous stars in our neighborhood, and considering that 27% of them are in systems of two or more stars, this dissertation surveys how these multiples behave dynamically to establish the orbital parameter distributions for companions with orbital periods up to 30 years. This work encompasses the regimes of several observing techniques: (1) astrometry from the 23-year RECONS program at CTIO, (2) speckle interferometry from SOAR HRCam+SAM, and (3) imaging and spectroscopic orbits from the literature. Through this effort we have increased the number of nearby M dwarf orbits by roughly a third, and updated or improved several dozen as well. This combined data set of nearly 200 orbits reveals three new fundamental results. The first is that the tidal circularization period is within 4–7 days for M dwarfs, shorter than for solar-type binaries. The second is that the eccentricity distribution at periods >5 years depends on the primary star mass and potentially the mass ratio, as nearly-circular orbits occur only for systems in which at least one component is $<0.1 M_{\odot}$. The third result is that mass ratios of M dwarf multiples are strongly weighted toward unity, with most having $q = M_2/M_1 \geq 0.9$. This suggests these low-mass systems’ dynamical evolution is dominated by migration through circumstellar disks. Our picture of companions spans the entire low-mass main sequence as well as brown dwarfs, showing that formation and dynamical evolution processes mold a continuum of mass all the way beyond the smallest stars.

INDEX WORDS: astronomy, astrometry, binary stars, brown dwarfs, orbits, dynamics, speckle interferometry

Copyright by
Eliot Halley Vrijmoet
2023

Orbital Architectures of M Dwarf Companions

by

Eliot Halley Vrijmoet

Committee Chair:

Todd J. Henry

Committee:

Jessie Christiansen

Sébastien Lépine

Russel White

Electronic Version Approved:

Office of Graduate Studies

College of Arts and Sciences

Georgia State University

August 2023

TABLE OF CONTENTS

LIST OF TABLES	vii
LIST OF FIGURES	xxxii
1 Introduction: Motivating Orbital Architectures of the Ubiquitous Red Dwarfs	1
1.1 Terms and Conditions	3
1.2 How To Form a System of Multiple Stars	7
1.2.1 <i>Turbulent Fragmentation of Cores and Filaments</i>	8
1.2.2 <i>Disks Broken via Gravitational Instability</i>	11
1.2.3 <i>Capture of Neighboring Stars</i>	13
1.3 Orbital Evolution After a Multiple is Formed	15
1.3.1 <i>Orbital Evolution Due to Gas and Dust</i>	15
1.3.2 <i>Orbital Evolution Due to Kozai-Lidov Cycles</i>	16
1.3.3 <i>Orbital Evolution Due to Tides</i>	17
1.4 Trends Observed for Stellar Multiples and their Properties	19
1.4.1 <i>Properties of High-mass Multiples</i>	20
1.4.2 <i>Properties of Solar-mass Multiples</i>	22
1.4.3 <i>Properties of Low-mass Multiples</i>	24
2 Defining the Sample of Nearby M Dwarfs	29
2.1 Setting Distance Limits	30
2.2 Deriving Absolute Magnitude Limits for M Dwarfs	33
2.2.1 <i>One MLR to Rule Them All</i>	35
2.2.2 <i>Extending the MLR to New Bandpasses</i>	39
2.3 Verifying the Photometric M Dwarf Definitions	45
3 The RECONS Astrometry Contribution	50

3.1	Targets Observed by the RECONS Astrometry Program	50
3.2	Observing at the CTIO/SMARTS 0.9m for RECONS astrometry .	52
3.3	Data Reduction for RECONS Astrometry	55
3.4	Fitting Orbits to RECONS Astrometry	59
3.4.1	<i>Principles of Photocentric Orbits</i>	59
3.4.2	<i>The MCMC Orbit Fitting Algorithm for RECONS Astrometry</i>	62
3.4.3	<i>Fitting Orbits Longer than the Astrometric Time Baseline</i>	66
4	The SOAR Speckle Contribution	70
4.1	Choosing Targets for SOAR Speckle	71
4.1.1	<i>189 SOAR Targets from the Literature</i>	73
4.1.2	<i>123 SOAR Targets from RECONS Astrometry</i>	74
4.1.3	<i>252 SOAR targets from Gaia DR2</i>	77
4.2	SOAR Speckle Observing and Data Reduction	82
4.3	SOAR Speckle Data Results	85
4.4	Fitting Orbits to SOAR Speckle	86
5	Results from Three Sources of Orbits	89
5.1	The RECONS Astrometry Results	89
5.1.1	<i>Orbits from RECONS Astrometry</i>	90
5.1.2	<i>Sensitivity of the RECONS Astrometry Data</i>	92
5.2	The SOAR Speckle Data	106
5.2.1	<i>Orbits from SOAR Speckle Interferometry</i>	106
5.2.2	<i>Sensitivity of the SOAR Speckle Data</i>	107
5.3	Adding Orbits from the Literature	115
5.3.1	<i>Selecting Literature Orbits of Nearby M Dwarfs</i>	115
5.3.2	<i>Sensitivity of the Literature Results</i>	116
5.3.3	<i>Distinguishing Binaries from Higher-Order Multiples</i>	118

6	The P_{orb} vs. e Distribution for M Dwarfs and its Implications	120
6.1	193 M Dwarf Orbits on One Plot	120
6.2	Zoom-in on P_{orb} vs. e Regimes	121
6.2.1	<i>Empirical P_{circ} for M Dwarf Systems</i>	121
6.2.2	<i>The Observed Upper Envelope of e</i>	127
6.2.3	<i>Eccentricities at Long P_{orb}</i>	128
6.3	Estimating Masses for Every M Dwarf	129
6.4	P_{orb} vs. e by Mass and Mass Ratio	137
6.4.1	<i>Masses Among the Shortest-P_{orb} Orbits</i>	139
6.4.2	<i>Masses Among the Longest-P_{orb} Orbits</i>	140
6.4.3	<i>Mass Ratios</i>	141
6.4.4	<i>Comparing M Dwarfs to Solar-like Systems</i>	144
6.4.5	<i>Comparing M Dwarfs to Very Low-Mass Systems</i>	146
6.5	The Picture of M Dwarf Formation	147
7	Summary, Conclusions, and the Future	164
7.1	The Author's Specific Contributions to this Dissertation	164
7.2	Conclusion to This Study	166
	Appendices	170
	REFERENCES	347

LIST OF TABLES

Table 2.1	Absolute magnitude ranges and key values used to determine the specific absolute magnitudes corresponding to $0.62 M_{\odot}$ and $0.075 M_{\odot}$, the highest and lowest masses adopted for M dwarfs. The final adopted magnitudes for those mass limits are highlighted in yellow.	41
Table 5.1	Techniques used to observe and characterize the literature orbits used in this work. Relative astrometry refers to observations of a companion orbiting a primary star, while absolute astrometry refers to observing the pair's unresolved photocenter orbiting its center of mass.	117
Table 6.1	Systems with P_{orb} between 3 and 10 days, with binaries highlighted in yellow. The precision shown is as given in the original publications for these systems, given in the last column. The full references for the reference codes shown here are given in Table 1.	125
Table 6.2	Masses and mass estimates used for the analysis described in §6.4 and thereafter. Column 4 indicates the technique used to produce the values in the preceding columns; masses that are not dynamical are estimates based on either magnitude differences, photocentric orbits, or combined magnitudes assuming $\Delta K = 0.8$ mag (described in §6.3).	131
Table 6.2	Masses and mass estimates used for the analysis described in §6.4 and thereafter. Column 4 indicates the technique used to produce the values in the preceding columns; masses that are not dynamical are estimates based on either magnitude differences, photocentric orbits, or combined magnitudes assuming $\Delta K = 0.8$ mag (described in §6.3).	132
Table 6.2	Masses and mass estimates used for the analysis described in §6.4 and thereafter. Column 4 indicates the technique used to produce the values in the preceding columns; masses that are not dynamical are estimates based on either magnitude differences, photocentric orbits, or combined magnitudes assuming $\Delta K = 0.8$ mag (described in §6.3).	133
Table 6.2	Masses and mass estimates used for the analysis described in §6.4 and thereafter. Column 4 indicates the technique used to produce the values in the preceding columns; masses that are not dynamical are estimates based on either magnitude differences, photocentric orbits, or combined magnitudes assuming $\Delta K = 0.8$ mag (described in §6.3).	134

Table 6.2	Masses and mass estimates used for the analysis described in §6.4 and thereafter. Column 4 indicates the technique used to produce the values in the preceding columns; masses that are not dynamical are estimates based on either magnitude differences, photocentric orbits, or combined magnitudes assuming $\Delta K = 0.8$ mag (described in §6.3).	135
Table 6.2	Masses and mass estimates used for the analysis described in §6.4 and thereafter. Column 4 indicates the technique used to produce the values in the preceding columns; masses that are not dynamical are estimates based on either magnitude differences, photocentric orbits, or combined magnitudes assuming $\Delta K = 0.8$ mag (described in §6.3).	136
Table 6.2	Masses and mass estimates used for the analysis described in §6.4 and thereafter. Column 4 indicates the technique used to produce the values in the preceding columns; masses that are not dynamical are estimates based on either magnitude differences, photocentric orbits, or combined magnitudes assuming $\Delta K = 0.8$ mag (described in §6.3).	137
Table 1	Five-letter reference codes and their corresponding formal references, as used in tables throughout this dissertation.	170
Table 2	List of M dwarf systems within 25 pc drawn from <i>Gaia</i> DR2, as described in §2.3. These systems have not been vetted to distinguish single stars from multiples, but in cases where a system was resolved in <i>Gaia</i> but not 2MASS, a “J” flag is listed in column 12.	171
Table 2	List of M dwarf systems within 25 pc drawn from <i>Gaia</i> DR2, as described in §2.3. These systems have not been vetted to distinguish single stars from multiples, but in cases where a system was resolved in <i>Gaia</i> but not 2MASS, a “J” flag is listed in column 12.	172
Table 2	List of M dwarf systems within 25 pc drawn from <i>Gaia</i> DR2, as described in §2.3. These systems have not been vetted to distinguish single stars from multiples, but in cases where a system was resolved in <i>Gaia</i> but not 2MASS, a “J” flag is listed in column 12.	173
Table 2	List of M dwarf systems within 25 pc drawn from <i>Gaia</i> DR2, as described in §2.3. These systems have not been vetted to distinguish single stars from multiples, but in cases where a system was resolved in <i>Gaia</i> but not 2MASS, a “J” flag is listed in column 12.	174

Table 2	List of M dwarf systems within 25 pc drawn from <i>Gaia</i> DR2, as described in §2.3. These systems have not been vetted to distinguish single stars from multiples, but in cases where a system was resolved in <i>Gaia</i> but not 2MASS, a “J” flag is listed in column 12.	175
Table 2	List of M dwarf systems within 25 pc drawn from <i>Gaia</i> DR2, as described in §2.3. These systems have not been vetted to distinguish single stars from multiples, but in cases where a system was resolved in <i>Gaia</i> but not 2MASS, a “J” flag is listed in column 12.	176
Table 2	List of M dwarf systems within 25 pc drawn from <i>Gaia</i> DR2, as described in §2.3. These systems have not been vetted to distinguish single stars from multiples, but in cases where a system was resolved in <i>Gaia</i> but not 2MASS, a “J” flag is listed in column 12.	177
Table 2	List of M dwarf systems within 25 pc drawn from <i>Gaia</i> DR2, as described in §2.3. These systems have not been vetted to distinguish single stars from multiples, but in cases where a system was resolved in <i>Gaia</i> but not 2MASS, a “J” flag is listed in column 12.	178
Table 2	List of M dwarf systems within 25 pc drawn from <i>Gaia</i> DR2, as described in §2.3. These systems have not been vetted to distinguish single stars from multiples, but in cases where a system was resolved in <i>Gaia</i> but not 2MASS, a “J” flag is listed in column 12.	179
Table 2	List of M dwarf systems within 25 pc drawn from <i>Gaia</i> DR2, as described in §2.3. These systems have not been vetted to distinguish single stars from multiples, but in cases where a system was resolved in <i>Gaia</i> but not 2MASS, a “J” flag is listed in column 12.	180
Table 2	List of M dwarf systems within 25 pc drawn from <i>Gaia</i> DR2, as described in §2.3. These systems have not been vetted to distinguish single stars from multiples, but in cases where a system was resolved in <i>Gaia</i> but not 2MASS, a “J” flag is listed in column 12.	181
Table 2	List of M dwarf systems within 25 pc drawn from <i>Gaia</i> DR2, as described in §2.3. These systems have not been vetted to distinguish single stars from multiples, but in cases where a system was resolved in <i>Gaia</i> but not 2MASS, a “J” flag is listed in column 12.	182
Table 2	List of M dwarf systems within 25 pc drawn from <i>Gaia</i> DR2, as described in §2.3. These systems have not been vetted to distinguish single stars from multiples, but in cases where a system was resolved in <i>Gaia</i> but not 2MASS, a “J” flag is listed in column 12.	183

Table 2	List of M dwarf systems within 25 pc drawn from <i>Gaia</i> DR2, as described in §2.3. These systems have not been vetted to distinguish single stars from multiples, but in cases where a system was resolved in <i>Gaia</i> but not 2MASS, a “J” flag is listed in column 12.	184
Table 2	List of M dwarf systems within 25 pc drawn from <i>Gaia</i> DR2, as described in §2.3. These systems have not been vetted to distinguish single stars from multiples, but in cases where a system was resolved in <i>Gaia</i> but not 2MASS, a “J” flag is listed in column 12.	185
Table 2	List of M dwarf systems within 25 pc drawn from <i>Gaia</i> DR2, as described in §2.3. These systems have not been vetted to distinguish single stars from multiples, but in cases where a system was resolved in <i>Gaia</i> but not 2MASS, a “J” flag is listed in column 12.	186
Table 2	List of M dwarf systems within 25 pc drawn from <i>Gaia</i> DR2, as described in §2.3. These systems have not been vetted to distinguish single stars from multiples, but in cases where a system was resolved in <i>Gaia</i> but not 2MASS, a “J” flag is listed in column 12.	187
Table 2	List of M dwarf systems within 25 pc drawn from <i>Gaia</i> DR2, as described in §2.3. These systems have not been vetted to distinguish single stars from multiples, but in cases where a system was resolved in <i>Gaia</i> but not 2MASS, a “J” flag is listed in column 12.	188
Table 2	List of M dwarf systems within 25 pc drawn from <i>Gaia</i> DR2, as described in §2.3. These systems have not been vetted to distinguish single stars from multiples, but in cases where a system was resolved in <i>Gaia</i> but not 2MASS, a “J” flag is listed in column 12.	189
Table 2	List of M dwarf systems within 25 pc drawn from <i>Gaia</i> DR2, as described in §2.3. These systems have not been vetted to distinguish single stars from multiples, but in cases where a system was resolved in <i>Gaia</i> but not 2MASS, a “J” flag is listed in column 12.	190
Table 2	List of M dwarf systems within 25 pc drawn from <i>Gaia</i> DR2, as described in §2.3. These systems have not been vetted to distinguish single stars from multiples, but in cases where a system was resolved in <i>Gaia</i> but not 2MASS, a “J” flag is listed in column 12.	191
Table 2	List of M dwarf systems within 25 pc drawn from <i>Gaia</i> DR2, as described in §2.3. These systems have not been vetted to distinguish single stars from multiples, but in cases where a system was resolved in <i>Gaia</i> but not 2MASS, a “J” flag is listed in column 12.	192

Table 2	List of M dwarf systems within 25 pc drawn from <i>Gaia</i> DR2, as described in §2.3. These systems have not been vetted to distinguish single stars from multiples, but in cases where a system was resolved in <i>Gaia</i> but not 2MASS, a “J” flag is listed in column 12.	193
Table 2	List of M dwarf systems within 25 pc drawn from <i>Gaia</i> DR2, as described in §2.3. These systems have not been vetted to distinguish single stars from multiples, but in cases where a system was resolved in <i>Gaia</i> but not 2MASS, a “J” flag is listed in column 12.	194
Table 2	List of M dwarf systems within 25 pc drawn from <i>Gaia</i> DR2, as described in §2.3. These systems have not been vetted to distinguish single stars from multiples, but in cases where a system was resolved in <i>Gaia</i> but not 2MASS, a “J” flag is listed in column 12.	195
Table 2	List of M dwarf systems within 25 pc drawn from <i>Gaia</i> DR2, as described in §2.3. These systems have not been vetted to distinguish single stars from multiples, but in cases where a system was resolved in <i>Gaia</i> but not 2MASS, a “J” flag is listed in column 12.	196
Table 2	List of M dwarf systems within 25 pc drawn from <i>Gaia</i> DR2, as described in §2.3. These systems have not been vetted to distinguish single stars from multiples, but in cases where a system was resolved in <i>Gaia</i> but not 2MASS, a “J” flag is listed in column 12.	197
Table 2	List of M dwarf systems within 25 pc drawn from <i>Gaia</i> DR2, as described in §2.3. These systems have not been vetted to distinguish single stars from multiples, but in cases where a system was resolved in <i>Gaia</i> but not 2MASS, a “J” flag is listed in column 12.	198
Table 2	List of M dwarf systems within 25 pc drawn from <i>Gaia</i> DR2, as described in §2.3. These systems have not been vetted to distinguish single stars from multiples, but in cases where a system was resolved in <i>Gaia</i> but not 2MASS, a “J” flag is listed in column 12.	199
Table 2	List of M dwarf systems within 25 pc drawn from <i>Gaia</i> DR2, as described in §2.3. These systems have not been vetted to distinguish single stars from multiples, but in cases where a system was resolved in <i>Gaia</i> but not 2MASS, a “J” flag is listed in column 12.	200
Table 2	List of M dwarf systems within 25 pc drawn from <i>Gaia</i> DR2, as described in §2.3. These systems have not been vetted to distinguish single stars from multiples, but in cases where a system was resolved in <i>Gaia</i> but not 2MASS, a “J” flag is listed in column 12.	201

Table 2	List of M dwarf systems within 25 pc drawn from <i>Gaia</i> DR2, as described in §2.3. These systems have not been vetted to distinguish single stars from multiples, but in cases where a system was resolved in <i>Gaia</i> but not 2MASS, a “J” flag is listed in column 12.	202
Table 2	List of M dwarf systems within 25 pc drawn from <i>Gaia</i> DR2, as described in §2.3. These systems have not been vetted to distinguish single stars from multiples, but in cases where a system was resolved in <i>Gaia</i> but not 2MASS, a “J” flag is listed in column 12.	203
Table 2	List of M dwarf systems within 25 pc drawn from <i>Gaia</i> DR2, as described in §2.3. These systems have not been vetted to distinguish single stars from multiples, but in cases where a system was resolved in <i>Gaia</i> but not 2MASS, a “J” flag is listed in column 12.	204
Table 2	List of M dwarf systems within 25 pc drawn from <i>Gaia</i> DR2, as described in §2.3. These systems have not been vetted to distinguish single stars from multiples, but in cases where a system was resolved in <i>Gaia</i> but not 2MASS, a “J” flag is listed in column 12.	205
Table 2	List of M dwarf systems within 25 pc drawn from <i>Gaia</i> DR2, as described in §2.3. These systems have not been vetted to distinguish single stars from multiples, but in cases where a system was resolved in <i>Gaia</i> but not 2MASS, a “J” flag is listed in column 12.	206
Table 2	List of M dwarf systems within 25 pc drawn from <i>Gaia</i> DR2, as described in §2.3. These systems have not been vetted to distinguish single stars from multiples, but in cases where a system was resolved in <i>Gaia</i> but not 2MASS, a “J” flag is listed in column 12.	207
Table 2	List of M dwarf systems within 25 pc drawn from <i>Gaia</i> DR2, as described in §2.3. These systems have not been vetted to distinguish single stars from multiples, but in cases where a system was resolved in <i>Gaia</i> but not 2MASS, a “J” flag is listed in column 12.	208
Table 2	List of M dwarf systems within 25 pc drawn from <i>Gaia</i> DR2, as described in §2.3. These systems have not been vetted to distinguish single stars from multiples, but in cases where a system was resolved in <i>Gaia</i> but not 2MASS, a “J” flag is listed in column 12.	209
Table 2	List of M dwarf systems within 25 pc drawn from <i>Gaia</i> DR2, as described in §2.3. These systems have not been vetted to distinguish single stars from multiples, but in cases where a system was resolved in <i>Gaia</i> but not 2MASS, a “J” flag is listed in column 12.	210

Table 2	List of M dwarf systems within 25 pc drawn from <i>Gaia</i> DR2, as described in §2.3. These systems have not been vetted to distinguish single stars from multiples, but in cases where a system was resolved in <i>Gaia</i> but not 2MASS, a “J” flag is listed in column 12.	211
Table 2	List of M dwarf systems within 25 pc drawn from <i>Gaia</i> DR2, as described in §2.3. These systems have not been vetted to distinguish single stars from multiples, but in cases where a system was resolved in <i>Gaia</i> but not 2MASS, a “J” flag is listed in column 12.	212
Table 2	List of M dwarf systems within 25 pc drawn from <i>Gaia</i> DR2, as described in §2.3. These systems have not been vetted to distinguish single stars from multiples, but in cases where a system was resolved in <i>Gaia</i> but not 2MASS, a “J” flag is listed in column 12.	213
Table 2	List of M dwarf systems within 25 pc drawn from <i>Gaia</i> DR2, as described in §2.3. These systems have not been vetted to distinguish single stars from multiples, but in cases where a system was resolved in <i>Gaia</i> but not 2MASS, a “J” flag is listed in column 12.	214
Table 2	List of M dwarf systems within 25 pc drawn from <i>Gaia</i> DR2, as described in §2.3. These systems have not been vetted to distinguish single stars from multiples, but in cases where a system was resolved in <i>Gaia</i> but not 2MASS, a “J” flag is listed in column 12.	215
Table 2	List of M dwarf systems within 25 pc drawn from <i>Gaia</i> DR2, as described in §2.3. These systems have not been vetted to distinguish single stars from multiples, but in cases where a system was resolved in <i>Gaia</i> but not 2MASS, a “J” flag is listed in column 12.	216
Table 2	List of M dwarf systems within 25 pc drawn from <i>Gaia</i> DR2, as described in §2.3. These systems have not been vetted to distinguish single stars from multiples, but in cases where a system was resolved in <i>Gaia</i> but not 2MASS, a “J” flag is listed in column 12.	217
Table 2	List of M dwarf systems within 25 pc drawn from <i>Gaia</i> DR2, as described in §2.3. These systems have not been vetted to distinguish single stars from multiples, but in cases where a system was resolved in <i>Gaia</i> but not 2MASS, a “J” flag is listed in column 12.	218
Table 2	List of M dwarf systems within 25 pc drawn from <i>Gaia</i> DR2, as described in §2.3. These systems have not been vetted to distinguish single stars from multiples, but in cases where a system was resolved in <i>Gaia</i> but not 2MASS, a “J” flag is listed in column 12.	219

Table 2	List of M dwarf systems within 25 pc drawn from <i>Gaia</i> DR2, as described in §2.3. These systems have not been vetted to distinguish single stars from multiples, but in cases where a system was resolved in <i>Gaia</i> but not 2MASS, a “J” flag is listed in column 12.	220
Table 2	List of M dwarf systems within 25 pc drawn from <i>Gaia</i> DR2, as described in §2.3. These systems have not been vetted to distinguish single stars from multiples, but in cases where a system was resolved in <i>Gaia</i> but not 2MASS, a “J” flag is listed in column 12.	221
Table 2	List of M dwarf systems within 25 pc drawn from <i>Gaia</i> DR2, as described in §2.3. These systems have not been vetted to distinguish single stars from multiples, but in cases where a system was resolved in <i>Gaia</i> but not 2MASS, a “J” flag is listed in column 12.	222
Table 2	List of M dwarf systems within 25 pc drawn from <i>Gaia</i> DR2, as described in §2.3. These systems have not been vetted to distinguish single stars from multiples, but in cases where a system was resolved in <i>Gaia</i> but not 2MASS, a “J” flag is listed in column 12.	223
Table 2	List of M dwarf systems within 25 pc drawn from <i>Gaia</i> DR2, as described in §2.3. These systems have not been vetted to distinguish single stars from multiples, but in cases where a system was resolved in <i>Gaia</i> but not 2MASS, a “J” flag is listed in column 12.	224
Table 2	List of M dwarf systems within 25 pc drawn from <i>Gaia</i> DR2, as described in §2.3. These systems have not been vetted to distinguish single stars from multiples, but in cases where a system was resolved in <i>Gaia</i> but not 2MASS, a “J” flag is listed in column 12.	225
Table 2	List of M dwarf systems within 25 pc drawn from <i>Gaia</i> DR2, as described in §2.3. These systems have not been vetted to distinguish single stars from multiples, but in cases where a system was resolved in <i>Gaia</i> but not 2MASS, a “J” flag is listed in column 12.	226
Table 2	List of M dwarf systems within 25 pc drawn from <i>Gaia</i> DR2, as described in §2.3. These systems have not been vetted to distinguish single stars from multiples, but in cases where a system was resolved in <i>Gaia</i> but not 2MASS, a “J” flag is listed in column 12.	227
Table 2	List of M dwarf systems within 25 pc drawn from <i>Gaia</i> DR2, as described in §2.3. These systems have not been vetted to distinguish single stars from multiples, but in cases where a system was resolved in <i>Gaia</i> but not 2MASS, a “J” flag is listed in column 12.	228

Table 2	List of M dwarf systems within 25 pc drawn from <i>Gaia</i> DR2, as described in §2.3. These systems have not been vetted to distinguish single stars from multiples, but in cases where a system was resolved in <i>Gaia</i> but not 2MASS, a “J” flag is listed in column 12.	229
Table 2	List of M dwarf systems within 25 pc drawn from <i>Gaia</i> DR2, as described in §2.3. These systems have not been vetted to distinguish single stars from multiples, but in cases where a system was resolved in <i>Gaia</i> but not 2MASS, a “J” flag is listed in column 12.	230
Table 2	List of M dwarf systems within 25 pc drawn from <i>Gaia</i> DR2, as described in §2.3. These systems have not been vetted to distinguish single stars from multiples, but in cases where a system was resolved in <i>Gaia</i> but not 2MASS, a “J” flag is listed in column 12.	231
Table 2	List of M dwarf systems within 25 pc drawn from <i>Gaia</i> DR2, as described in §2.3. These systems have not been vetted to distinguish single stars from multiples, but in cases where a system was resolved in <i>Gaia</i> but not 2MASS, a “J” flag is listed in column 12.	232
Table 2	List of M dwarf systems within 25 pc drawn from <i>Gaia</i> DR2, as described in §2.3. These systems have not been vetted to distinguish single stars from multiples, but in cases where a system was resolved in <i>Gaia</i> but not 2MASS, a “J” flag is listed in column 12.	233
Table 2	List of M dwarf systems within 25 pc drawn from <i>Gaia</i> DR2, as described in §2.3. These systems have not been vetted to distinguish single stars from multiples, but in cases where a system was resolved in <i>Gaia</i> but not 2MASS, a “J” flag is listed in column 12.	234
Table 2	List of M dwarf systems within 25 pc drawn from <i>Gaia</i> DR2, as described in §2.3. These systems have not been vetted to distinguish single stars from multiples, but in cases where a system was resolved in <i>Gaia</i> but not 2MASS, a “J” flag is listed in column 12.	235
Table 2	List of M dwarf systems within 25 pc drawn from <i>Gaia</i> DR2, as described in §2.3. These systems have not been vetted to distinguish single stars from multiples, but in cases where a system was resolved in <i>Gaia</i> but not 2MASS, a “J” flag is listed in column 12.	236
Table 2	List of M dwarf systems within 25 pc drawn from <i>Gaia</i> DR2, as described in §2.3. These systems have not been vetted to distinguish single stars from multiples, but in cases where a system was resolved in <i>Gaia</i> but not 2MASS, a “J” flag is listed in column 12.	237

Table 2	List of M dwarf systems within 25 pc drawn from <i>Gaia</i> DR2, as described in §2.3. These systems have not been vetted to distinguish single stars from multiples, but in cases where a system was resolved in <i>Gaia</i> but not 2MASS, a “J” flag is listed in column 12.	238
Table 2	List of M dwarf systems within 25 pc drawn from <i>Gaia</i> DR2, as described in §2.3. These systems have not been vetted to distinguish single stars from multiples, but in cases where a system was resolved in <i>Gaia</i> but not 2MASS, a “J” flag is listed in column 12.	239
Table 2	List of M dwarf systems within 25 pc drawn from <i>Gaia</i> DR2, as described in §2.3. These systems have not been vetted to distinguish single stars from multiples, but in cases where a system was resolved in <i>Gaia</i> but not 2MASS, a “J” flag is listed in column 12.	240
Table 2	List of M dwarf systems within 25 pc drawn from <i>Gaia</i> DR2, as described in §2.3. These systems have not been vetted to distinguish single stars from multiples, but in cases where a system was resolved in <i>Gaia</i> but not 2MASS, a “J” flag is listed in column 12.	241
Table 2	List of M dwarf systems within 25 pc drawn from <i>Gaia</i> DR2, as described in §2.3. These systems have not been vetted to distinguish single stars from multiples, but in cases where a system was resolved in <i>Gaia</i> but not 2MASS, a “J” flag is listed in column 12.	242
Table 2	List of M dwarf systems within 25 pc drawn from <i>Gaia</i> DR2, as described in §2.3. These systems have not been vetted to distinguish single stars from multiples, but in cases where a system was resolved in <i>Gaia</i> but not 2MASS, a “J” flag is listed in column 12.	243
Table 2	List of M dwarf systems within 25 pc drawn from <i>Gaia</i> DR2, as described in §2.3. These systems have not been vetted to distinguish single stars from multiples, but in cases where a system was resolved in <i>Gaia</i> but not 2MASS, a “J” flag is listed in column 12.	244
Table 2	List of M dwarf systems within 25 pc drawn from <i>Gaia</i> DR2, as described in §2.3. These systems have not been vetted to distinguish single stars from multiples, but in cases where a system was resolved in <i>Gaia</i> but not 2MASS, a “J” flag is listed in column 12.	245
Table 2	List of M dwarf systems within 25 pc drawn from <i>Gaia</i> DR2, as described in §2.3. These systems have not been vetted to distinguish single stars from multiples, but in cases where a system was resolved in <i>Gaia</i> but not 2MASS, a “J” flag is listed in column 12.	246

Table 2	List of M dwarf systems within 25 pc drawn from <i>Gaia</i> DR2, as described in §2.3. These systems have not been vetted to distinguish single stars from multiples, but in cases where a system was resolved in <i>Gaia</i> but not 2MASS, a “J” flag is listed in column 12.	247
Table 2	List of M dwarf systems within 25 pc drawn from <i>Gaia</i> DR2, as described in §2.3. These systems have not been vetted to distinguish single stars from multiples, but in cases where a system was resolved in <i>Gaia</i> but not 2MASS, a “J” flag is listed in column 12.	248
Table 2	List of M dwarf systems within 25 pc drawn from <i>Gaia</i> DR2, as described in §2.3. These systems have not been vetted to distinguish single stars from multiples, but in cases where a system was resolved in <i>Gaia</i> but not 2MASS, a “J” flag is listed in column 12.	249
Table 2	List of M dwarf systems within 25 pc drawn from <i>Gaia</i> DR2, as described in §2.3. These systems have not been vetted to distinguish single stars from multiples, but in cases where a system was resolved in <i>Gaia</i> but not 2MASS, a “J” flag is listed in column 12.	250
Table 3	Systems targeted for the M dwarf speckle interferometry program at SOAR. The WDS code (column 3) is the name each system would have in the Washington Double Star Catalog (Mason et al. 2001) if it were included there. The subsets justifying each target’s inclusion are marked in columns 8–10, and are discussed in §4.1.1, §4.1.2, and §4.1.3.	251
Table 3	Systems targeted for the M dwarf speckle interferometry program at SOAR. The WDS code (column 3) is the name each system would have in the Washington Double Star Catalog (Mason et al. 2001) if it were included there. The subsets justifying each target’s inclusion are marked in columns 8–10, and are discussed in §4.1.1, §4.1.2, and §4.1.3.	252
Table 3	Systems targeted for the M dwarf speckle interferometry program at SOAR. The WDS code (column 3) is the name each system would have in the Washington Double Star Catalog (Mason et al. 2001) if it were included there. The subsets justifying each target’s inclusion are marked in columns 8–10, and are discussed in §4.1.1, §4.1.2, and §4.1.3.	253
Table 3	Systems targeted for the M dwarf speckle interferometry program at SOAR. The WDS code (column 3) is the name each system would have in the Washington Double Star Catalog (Mason et al. 2001) if it were included there. The subsets justifying each target’s inclusion are marked in columns 8–10, and are discussed in §4.1.1, §4.1.2, and §4.1.3.	254

Table 3	Systems targeted for the M dwarf speckle interferometry program at SOAR. The WDS code (column 3) is the name each system would have in the Washington Double Star Catalog (Mason et al. 2001) if it were included there. The subsets justifying each target's inclusion are marked in columns 8–10, and are discussed in §4.1.1, §4.1.2, and §4.1.3.	255
Table 3	Systems targeted for the M dwarf speckle interferometry program at SOAR. The WDS code (column 3) is the name each system would have in the Washington Double Star Catalog (Mason et al. 2001) if it were included there. The subsets justifying each target's inclusion are marked in columns 8–10, and are discussed in §4.1.1, §4.1.2, and §4.1.3.	256
Table 3	Systems targeted for the M dwarf speckle interferometry program at SOAR. The WDS code (column 3) is the name each system would have in the Washington Double Star Catalog (Mason et al. 2001) if it were included there. The subsets justifying each target's inclusion are marked in columns 8–10, and are discussed in §4.1.1, §4.1.2, and §4.1.3.	257
Table 3	Systems targeted for the M dwarf speckle interferometry program at SOAR. The WDS code (column 3) is the name each system would have in the Washington Double Star Catalog (Mason et al. 2001) if it were included there. The subsets justifying each target's inclusion are marked in columns 8–10, and are discussed in §4.1.1, §4.1.2, and §4.1.3.	258
Table 3	Systems targeted for the M dwarf speckle interferometry program at SOAR. The WDS code (column 3) is the name each system would have in the Washington Double Star Catalog (Mason et al. 2001) if it were included there. The subsets justifying each target's inclusion are marked in columns 8–10, and are discussed in §4.1.1, §4.1.2, and §4.1.3.	259
Table 3	Systems targeted for the M dwarf speckle interferometry program at SOAR. The WDS code (column 3) is the name each system would have in the Washington Double Star Catalog (Mason et al. 2001) if it were included there. The subsets justifying each target's inclusion are marked in columns 8–10, and are discussed in §4.1.1, §4.1.2, and §4.1.3.	260
Table 3	Systems targeted for the M dwarf speckle interferometry program at SOAR. The WDS code (column 3) is the name each system would have in the Washington Double Star Catalog (Mason et al. 2001) if it were included there. The subsets justifying each target's inclusion are marked in columns 8–10, and are discussed in §4.1.1, §4.1.2, and §4.1.3.	261

Table 3	Systems targeted for the M dwarf speckle interferometry program at SOAR. The WDS code (column 3) is the name each system would have in the Washington Double Star Catalog (Mason et al. 2001) if it were included there. The subsets justifying each target's inclusion are marked in columns 8–10, and are discussed in §4.1.1, §4.1.2, and §4.1.3.	262
Table 3	Systems targeted for the M dwarf speckle interferometry program at SOAR. The WDS code (column 3) is the name each system would have in the Washington Double Star Catalog (Mason et al. 2001) if it were included there. The subsets justifying each target's inclusion are marked in columns 8–10, and are discussed in §4.1.1, §4.1.2, and §4.1.3.	263
Table 3	Systems targeted for the M dwarf speckle interferometry program at SOAR. The WDS code (column 3) is the name each system would have in the Washington Double Star Catalog (Mason et al. 2001) if it were included there. The subsets justifying each target's inclusion are marked in columns 8–10, and are discussed in §4.1.1, §4.1.2, and §4.1.3.	264
Table 3	Systems targeted for the M dwarf speckle interferometry program at SOAR. The WDS code (column 3) is the name each system would have in the Washington Double Star Catalog (Mason et al. 2001) if it were included there. The subsets justifying each target's inclusion are marked in columns 8–10, and are discussed in §4.1.1, §4.1.2, and §4.1.3.	265
Table 3	Systems targeted for the M dwarf speckle interferometry program at SOAR. The WDS code (column 3) is the name each system would have in the Washington Double Star Catalog (Mason et al. 2001) if it were included there. The subsets justifying each target's inclusion are marked in columns 8–10, and are discussed in §4.1.1, §4.1.2, and §4.1.3.	266
Table 3	Systems targeted for the M dwarf speckle interferometry program at SOAR. The WDS code (column 3) is the name each system would have in the Washington Double Star Catalog (Mason et al. 2001) if it were included there. The subsets justifying each target's inclusion are marked in columns 8–10, and are discussed in §4.1.1, §4.1.2, and §4.1.3.	267
Table 3	Systems targeted for the M dwarf speckle interferometry program at SOAR. The WDS code (column 3) is the name each system would have in the Washington Double Star Catalog (Mason et al. 2001) if it were included there. The subsets justifying each target's inclusion are marked in columns 8–10, and are discussed in §4.1.1, §4.1.2, and §4.1.3.	268

Table 3	Systems targeted for the M dwarf speckle interferometry program at SOAR. The WDS code (column 3) is the name each system would have in the Washington Double Star Catalog (Mason et al. 2001) if it were included there. The subsets justifying each target's inclusion are marked in columns 8–10, and are discussed in §4.1.1, §4.1.2, and §4.1.3.	269
Table 3	Systems targeted for the M dwarf speckle interferometry program at SOAR. The WDS code (column 3) is the name each system would have in the Washington Double Star Catalog (Mason et al. 2001) if it were included there. The subsets justifying each target's inclusion are marked in columns 8–10, and are discussed in §4.1.1, §4.1.2, and §4.1.3.	270
Table 3	Systems targeted for the M dwarf speckle interferometry program at SOAR. The WDS code (column 3) is the name each system would have in the Washington Double Star Catalog (Mason et al. 2001) if it were included there. The subsets justifying each target's inclusion are marked in columns 8–10, and are discussed in §4.1.1, §4.1.2, and §4.1.3.	271
Table 3	Systems targeted for the M dwarf speckle interferometry program at SOAR. The WDS code (column 3) is the name each system would have in the Washington Double Star Catalog (Mason et al. 2001) if it were included there. The subsets justifying each target's inclusion are marked in columns 8–10, and are discussed in §4.1.1, §4.1.2, and §4.1.3.	272
Table 3	Systems targeted for the M dwarf speckle interferometry program at SOAR. The WDS code (column 3) is the name each system would have in the Washington Double Star Catalog (Mason et al. 2001) if it were included there. The subsets justifying each target's inclusion are marked in columns 8–10, and are discussed in §4.1.1, §4.1.2, and §4.1.3.	273
Table 3	Systems targeted for the M dwarf speckle interferometry program at SOAR. The WDS code (column 3) is the name each system would have in the Washington Double Star Catalog (Mason et al. 2001) if it were included there. The subsets justifying each target's inclusion are marked in columns 8–10, and are discussed in §4.1.1, §4.1.2, and §4.1.3.	274
Table 3	Systems targeted for the M dwarf speckle interferometry program at SOAR. The WDS code (column 3) is the name each system would have in the Washington Double Star Catalog (Mason et al. 2001) if it were included there. The subsets justifying each target's inclusion are marked in columns 8–10, and are discussed in §4.1.1, §4.1.2, and §4.1.3.	275

Table 3	Systems targeted for the M dwarf speckle interferometry program at SOAR. The WDS code (column 3) is the name each system would have in the Washington Double Star Catalog (Mason et al. 2001) if it were included there. The subsets justifying each target’s inclusion are marked in columns 8–10, and are discussed in §4.1.1, §4.1.2, and §4.1.3.	276
Table 4	Results of the SOAR speckle interferometry campaign for nearby M dwarfs. The meanings of columns 8–10 differ depending on whether or not the companion was resolved in that observation, hence the two lines in those columns’ headers. The “:” flag in the last column indicates highly uncertain results; the rest of the flags are described in §4.2.	277
Table 4	Results of the SOAR speckle interferometry campaign for nearby M dwarfs. The meanings of columns 8–10 differ depending on whether or not the companion was resolved in that observation, hence the two lines in those columns’ headers. The “:” flag in the last column indicates highly uncertain results; the rest of the flags are described in §4.2.	278
Table 4	Results of the SOAR speckle interferometry campaign for nearby M dwarfs. The meanings of columns 8–10 differ depending on whether or not the companion was resolved in that observation, hence the two lines in those columns’ headers. The “:” flag in the last column indicates highly uncertain results; the rest of the flags are described in §4.2.	279
Table 4	Results of the SOAR speckle interferometry campaign for nearby M dwarfs. The meanings of columns 8–10 differ depending on whether or not the companion was resolved in that observation, hence the two lines in those columns’ headers. The “:” flag in the last column indicates highly uncertain results; the rest of the flags are described in §4.2.	280
Table 4	Results of the SOAR speckle interferometry campaign for nearby M dwarfs. The meanings of columns 8–10 differ depending on whether or not the companion was resolved in that observation, hence the two lines in those columns’ headers. The “:” flag in the last column indicates highly uncertain results; the rest of the flags are described in §4.2.	281
Table 4	Results of the SOAR speckle interferometry campaign for nearby M dwarfs. The meanings of columns 8–10 differ depending on whether or not the companion was resolved in that observation, hence the two lines in those columns’ headers. The “:” flag in the last column indicates highly uncertain results; the rest of the flags are described in §4.2.	282

Table 4	Results of the SOAR speckle interferometry campaign for nearby M dwarfs. The meanings of columns 8–10 differ depending on whether or not the companion was resolved in that observation, hence the two lines in those columns’ headers. The “:” flag in the last column indicates highly uncertain results; the rest of the flags are described in §4.2.	283
Table 4	Results of the SOAR speckle interferometry campaign for nearby M dwarfs. The meanings of columns 8–10 differ depending on whether or not the companion was resolved in that observation, hence the two lines in those columns’ headers. The “:” flag in the last column indicates highly uncertain results; the rest of the flags are described in §4.2.	284
Table 4	Results of the SOAR speckle interferometry campaign for nearby M dwarfs. The meanings of columns 8–10 differ depending on whether or not the companion was resolved in that observation, hence the two lines in those columns’ headers. The “:” flag in the last column indicates highly uncertain results; the rest of the flags are described in §4.2.	285
Table 4	Results of the SOAR speckle interferometry campaign for nearby M dwarfs. The meanings of columns 8–10 differ depending on whether or not the companion was resolved in that observation, hence the two lines in those columns’ headers. The “:” flag in the last column indicates highly uncertain results; the rest of the flags are described in §4.2.	286
Table 4	Results of the SOAR speckle interferometry campaign for nearby M dwarfs. The meanings of columns 8–10 differ depending on whether or not the companion was resolved in that observation, hence the two lines in those columns’ headers. The “:” flag in the last column indicates highly uncertain results; the rest of the flags are described in §4.2.	287
Table 4	Results of the SOAR speckle interferometry campaign for nearby M dwarfs. The meanings of columns 8–10 differ depending on whether or not the companion was resolved in that observation, hence the two lines in those columns’ headers. The “:” flag in the last column indicates highly uncertain results; the rest of the flags are described in §4.2.	288
Table 4	Results of the SOAR speckle interferometry campaign for nearby M dwarfs. The meanings of columns 8–10 differ depending on whether or not the companion was resolved in that observation, hence the two lines in those columns’ headers. The “:” flag in the last column indicates highly uncertain results; the rest of the flags are described in §4.2.	289

Table 4 Results of the SOAR speckle interferometry campaign for nearby M
 dwarfs. The meanings of columns 8–10 differ depending on whether or not
 the companion was resolved in that observation, hence the two lines in those
 columns’ headers. The “:” flag in the last column indicates highly uncertain
 results; the rest of the flags are described in §4.2. 290

Table 4 Results of the SOAR speckle interferometry campaign for nearby M
 dwarfs. The meanings of columns 8–10 differ depending on whether or not
 the companion was resolved in that observation, hence the two lines in those
 columns’ headers. The “:” flag in the last column indicates highly uncertain
 results; the rest of the flags are described in §4.2. 291

Table 4 Results of the SOAR speckle interferometry campaign for nearby M
 dwarfs. The meanings of columns 8–10 differ depending on whether or not
 the companion was resolved in that observation, hence the two lines in those
 columns’ headers. The “:” flag in the last column indicates highly uncertain
 results; the rest of the flags are described in §4.2. 292

Table 4 Results of the SOAR speckle interferometry campaign for nearby M
 dwarfs. The meanings of columns 8–10 differ depending on whether or not
 the companion was resolved in that observation, hence the two lines in those
 columns’ headers. The “:” flag in the last column indicates highly uncertain
 results; the rest of the flags are described in §4.2. 293

Table 4 Results of the SOAR speckle interferometry campaign for nearby M
 dwarfs. The meanings of columns 8–10 differ depending on whether or not
 the companion was resolved in that observation, hence the two lines in those
 columns’ headers. The “:” flag in the last column indicates highly uncertain
 results; the rest of the flags are described in §4.2. 294

Table 4 Results of the SOAR speckle interferometry campaign for nearby M
 dwarfs. The meanings of columns 8–10 differ depending on whether or not
 the companion was resolved in that observation, hence the two lines in those
 columns’ headers. The “:” flag in the last column indicates highly uncertain
 results; the rest of the flags are described in §4.2. 295

Table 4 Results of the SOAR speckle interferometry campaign for nearby M
 dwarfs. The meanings of columns 8–10 differ depending on whether or not
 the companion was resolved in that observation, hence the two lines in those
 columns’ headers. The “:” flag in the last column indicates highly uncertain
 results; the rest of the flags are described in §4.2. 296

Table 4	Results of the SOAR speckle interferometry campaign for nearby M dwarfs. The meanings of columns 8–10 differ depending on whether or not the companion was resolved in that observation, hence the two lines in those columns’ headers. The “:” flag in the last column indicates highly uncertain results; the rest of the flags are described in §4.2.	297
Table 4	Results of the SOAR speckle interferometry campaign for nearby M dwarfs. The meanings of columns 8–10 differ depending on whether or not the companion was resolved in that observation, hence the two lines in those columns’ headers. The “:” flag in the last column indicates highly uncertain results; the rest of the flags are described in §4.2.	298
Table 4	Results of the SOAR speckle interferometry campaign for nearby M dwarfs. The meanings of columns 8–10 differ depending on whether or not the companion was resolved in that observation, hence the two lines in those columns’ headers. The “:” flag in the last column indicates highly uncertain results; the rest of the flags are described in §4.2.	299
Table 4	Results of the SOAR speckle interferometry campaign for nearby M dwarfs. The meanings of columns 8–10 differ depending on whether or not the companion was resolved in that observation, hence the two lines in those columns’ headers. The “:” flag in the last column indicates highly uncertain results; the rest of the flags are described in §4.2.	300
Table 4	Results of the SOAR speckle interferometry campaign for nearby M dwarfs. The meanings of columns 8–10 differ depending on whether or not the companion was resolved in that observation, hence the two lines in those columns’ headers. The “:” flag in the last column indicates highly uncertain results; the rest of the flags are described in §4.2.	301
Table 4	Results of the SOAR speckle interferometry campaign for nearby M dwarfs. The meanings of columns 8–10 differ depending on whether or not the companion was resolved in that observation, hence the two lines in those columns’ headers. The “:” flag in the last column indicates highly uncertain results; the rest of the flags are described in §4.2.	302
Table 4	Results of the SOAR speckle interferometry campaign for nearby M dwarfs. The meanings of columns 8–10 differ depending on whether or not the companion was resolved in that observation, hence the two lines in those columns’ headers. The “:” flag in the last column indicates highly uncertain results; the rest of the flags are described in §4.2.	303

Table 4	Results of the SOAR speckle interferometry campaign for nearby M dwarfs. The meanings of columns 8–10 differ depending on whether or not the companion was resolved in that observation, hence the two lines in those columns’ headers. The “:” flag in the last column indicates highly uncertain results; the rest of the flags are described in §4.2.	304
Table 4	Results of the SOAR speckle interferometry campaign for nearby M dwarfs. The meanings of columns 8–10 differ depending on whether or not the companion was resolved in that observation, hence the two lines in those columns’ headers. The “:” flag in the last column indicates highly uncertain results; the rest of the flags are described in §4.2.	305
Table 4	Results of the SOAR speckle interferometry campaign for nearby M dwarfs. The meanings of columns 8–10 differ depending on whether or not the companion was resolved in that observation, hence the two lines in those columns’ headers. The “:” flag in the last column indicates highly uncertain results; the rest of the flags are described in §4.2.	306
Table 4	Results of the SOAR speckle interferometry campaign for nearby M dwarfs. The meanings of columns 8–10 differ depending on whether or not the companion was resolved in that observation, hence the two lines in those columns’ headers. The “:” flag in the last column indicates highly uncertain results; the rest of the flags are described in §4.2.	307
Table 4	Results of the SOAR speckle interferometry campaign for nearby M dwarfs. The meanings of columns 8–10 differ depending on whether or not the companion was resolved in that observation, hence the two lines in those columns’ headers. The “:” flag in the last column indicates highly uncertain results; the rest of the flags are described in §4.2.	308
Table 4	Results of the SOAR speckle interferometry campaign for nearby M dwarfs. The meanings of columns 8–10 differ depending on whether or not the companion was resolved in that observation, hence the two lines in those columns’ headers. The “:” flag in the last column indicates highly uncertain results; the rest of the flags are described in §4.2.	309
Table 4	Results of the SOAR speckle interferometry campaign for nearby M dwarfs. The meanings of columns 8–10 differ depending on whether or not the companion was resolved in that observation, hence the two lines in those columns’ headers. The “:” flag in the last column indicates highly uncertain results; the rest of the flags are described in §4.2.	310

Table 4	Results of the SOAR speckle interferometry campaign for nearby M dwarfs. The meanings of columns 8–10 differ depending on whether or not the companion was resolved in that observation, hence the two lines in those columns’ headers. The “:” flag in the last column indicates highly uncertain results; the rest of the flags are described in §4.2.	311
Table 4	Results of the SOAR speckle interferometry campaign for nearby M dwarfs. The meanings of columns 8–10 differ depending on whether or not the companion was resolved in that observation, hence the two lines in those columns’ headers. The “:” flag in the last column indicates highly uncertain results; the rest of the flags are described in §4.2.	312
Table 4	Results of the SOAR speckle interferometry campaign for nearby M dwarfs. The meanings of columns 8–10 differ depending on whether or not the companion was resolved in that observation, hence the two lines in those columns’ headers. The “:” flag in the last column indicates highly uncertain results; the rest of the flags are described in §4.2.	313
Table 4	Results of the SOAR speckle interferometry campaign for nearby M dwarfs. The meanings of columns 8–10 differ depending on whether or not the companion was resolved in that observation, hence the two lines in those columns’ headers. The “:” flag in the last column indicates highly uncertain results; the rest of the flags are described in §4.2.	314
Table 4	Results of the SOAR speckle interferometry campaign for nearby M dwarfs. The meanings of columns 8–10 differ depending on whether or not the companion was resolved in that observation, hence the two lines in those columns’ headers. The “:” flag in the last column indicates highly uncertain results; the rest of the flags are described in §4.2.	315
Table 4	Results of the SOAR speckle interferometry campaign for nearby M dwarfs. The meanings of columns 8–10 differ depending on whether or not the companion was resolved in that observation, hence the two lines in those columns’ headers. The “:” flag in the last column indicates highly uncertain results; the rest of the flags are described in §4.2.	316
Table 4	Results of the SOAR speckle interferometry campaign for nearby M dwarfs. The meanings of columns 8–10 differ depending on whether or not the companion was resolved in that observation, hence the two lines in those columns’ headers. The “:” flag in the last column indicates highly uncertain results; the rest of the flags are described in §4.2.	317

Table 4	Results of the SOAR speckle interferometry campaign for nearby M dwarfs. The meanings of columns 8–10 differ depending on whether or not the companion was resolved in that observation, hence the two lines in those columns’ headers. The “:” flag in the last column indicates highly uncertain results; the rest of the flags are described in §4.2.	318
Table 4	Results of the SOAR speckle interferometry campaign for nearby M dwarfs. The meanings of columns 8–10 differ depending on whether or not the companion was resolved in that observation, hence the two lines in those columns’ headers. The “:” flag in the last column indicates highly uncertain results; the rest of the flags are described in §4.2.	319
Table 4	Results of the SOAR speckle interferometry campaign for nearby M dwarfs. The meanings of columns 8–10 differ depending on whether or not the companion was resolved in that observation, hence the two lines in those columns’ headers. The “:” flag in the last column indicates highly uncertain results; the rest of the flags are described in §4.2.	320
Table 4	Results of the SOAR speckle interferometry campaign for nearby M dwarfs. The meanings of columns 8–10 differ depending on whether or not the companion was resolved in that observation, hence the two lines in those columns’ headers. The “:” flag in the last column indicates highly uncertain results; the rest of the flags are described in §4.2.	321
Table 4	Results of the SOAR speckle interferometry campaign for nearby M dwarfs. The meanings of columns 8–10 differ depending on whether or not the companion was resolved in that observation, hence the two lines in those columns’ headers. The “:” flag in the last column indicates highly uncertain results; the rest of the flags are described in §4.2.	322
Table 4	Results of the SOAR speckle interferometry campaign for nearby M dwarfs. The meanings of columns 8–10 differ depending on whether or not the companion was resolved in that observation, hence the two lines in those columns’ headers. The “:” flag in the last column indicates highly uncertain results; the rest of the flags are described in §4.2.	323
Table 4	Results of the SOAR speckle interferometry campaign for nearby M dwarfs. The meanings of columns 8–10 differ depending on whether or not the companion was resolved in that observation, hence the two lines in those columns’ headers. The “:” flag in the last column indicates highly uncertain results; the rest of the flags are described in §4.2.	324

Table 4	Results of the SOAR speckle interferometry campaign for nearby M dwarfs. The meanings of columns 8–10 differ depending on whether or not the companion was resolved in that observation, hence the two lines in those columns’ headers. The “:” flag in the last column indicates highly uncertain results; the rest of the flags are described in §4.2.	325
Table 4	Results of the SOAR speckle interferometry campaign for nearby M dwarfs. The meanings of columns 8–10 differ depending on whether or not the companion was resolved in that observation, hence the two lines in those columns’ headers. The “:” flag in the last column indicates highly uncertain results; the rest of the flags are described in §4.2.	326
Table 4	Results of the SOAR speckle interferometry campaign for nearby M dwarfs. The meanings of columns 8–10 differ depending on whether or not the companion was resolved in that observation, hence the two lines in those columns’ headers. The “:” flag in the last column indicates highly uncertain results; the rest of the flags are described in §4.2.	327
Table 4	Results of the SOAR speckle interferometry campaign for nearby M dwarfs. The meanings of columns 8–10 differ depending on whether or not the companion was resolved in that observation, hence the two lines in those columns’ headers. The “:” flag in the last column indicates highly uncertain results; the rest of the flags are described in §4.2.	328
Table 4	Results of the SOAR speckle interferometry campaign for nearby M dwarfs. The meanings of columns 8–10 differ depending on whether or not the companion was resolved in that observation, hence the two lines in those columns’ headers. The “:” flag in the last column indicates highly uncertain results; the rest of the flags are described in §4.2.	329
Table 4	Results of the SOAR speckle interferometry campaign for nearby M dwarfs. The meanings of columns 8–10 differ depending on whether or not the companion was resolved in that observation, hence the two lines in those columns’ headers. The “:” flag in the last column indicates highly uncertain results; the rest of the flags are described in §4.2.	330
Table 4	Results of the SOAR speckle interferometry campaign for nearby M dwarfs. The meanings of columns 8–10 differ depending on whether or not the companion was resolved in that observation, hence the two lines in those columns’ headers. The “:” flag in the last column indicates highly uncertain results; the rest of the flags are described in §4.2.	331

Table 4 Results of the SOAR speckle interferometry campaign for nearby M
 dwarfs. The meanings of columns 8–10 differ depending on whether or not
 the companion was resolved in that observation, hence the two lines in those
 columns’ headers. The “:” flag in the last column indicates highly uncertain
 results; the rest of the flags are described in §4.2. 332

Table 4 Results of the SOAR speckle interferometry campaign for nearby M
 dwarfs. The meanings of columns 8–10 differ depending on whether or not
 the companion was resolved in that observation, hence the two lines in those
 columns’ headers. The “:” flag in the last column indicates highly uncertain
 results; the rest of the flags are described in §4.2. 333

Table 5 Parameters for every orbit in this work, with the source of the orbit
 listed in column (1): RECONS refers to RECONS astrometry (Chapter 3),
 SOAR is speckle interferometry from SOAR (Chapter 4), and the 5-letter
 reference codes are defined in Table 1. Note that for all the RECONS orbits
 and many of the literature orbits, the semi-major axis given is photocentric
 rather than relative. 334

Table 5 Parameters for every orbit in this work, with the source of the orbit
 listed in column (1): RECONS refers to RECONS astrometry (Chapter 3),
 SOAR is speckle interferometry from SOAR (Chapter 4), and the 5-letter
 reference codes are defined in Table 1. Note that for all the RECONS orbits
 and many of the literature orbits, the semi-major axis given is photocentric
 rather than relative. 335

Table 5 Parameters for every orbit in this work, with the source of the orbit
 listed in column (1): RECONS refers to RECONS astrometry (Chapter 3),
 SOAR is speckle interferometry from SOAR (Chapter 4), and the 5-letter
 reference codes are defined in Table 1. Note that for all the RECONS orbits
 and many of the literature orbits, the semi-major axis given is photocentric
 rather than relative. 336

Table 5 Parameters for every orbit in this work, with the source of the orbit
 listed in column (1): RECONS refers to RECONS astrometry (Chapter 3),
 SOAR is speckle interferometry from SOAR (Chapter 4), and the 5-letter
 reference codes are defined in Table 1. Note that for all the RECONS orbits
 and many of the literature orbits, the semi-major axis given is photocentric
 rather than relative. 337

Table 5	Parameters for every orbit in this work, with the source of the orbit listed in column (1): RECONS refers to RECONS astrometry (Chapter 3), SOAR is speckle interferometry from SOAR (Chapter 4), and the 5-letter reference codes are defined in Table 1. Note that for all the RECONS orbits and many of the literature orbits, the semi-major axis given is photocentric rather than relative.	338
Table 5	Parameters for every orbit in this work, with the source of the orbit listed in column (1): RECONS refers to RECONS astrometry (Chapter 3), SOAR is speckle interferometry from SOAR (Chapter 4), and the 5-letter reference codes are defined in Table 1. Note that for all the RECONS orbits and many of the literature orbits, the semi-major axis given is photocentric rather than relative.	339
Table 5	Parameters for every orbit in this work, with the source of the orbit listed in column (1): RECONS refers to RECONS astrometry (Chapter 3), SOAR is speckle interferometry from SOAR (Chapter 4), and the 5-letter reference codes are defined in Table 1. Note that for all the RECONS orbits and many of the literature orbits, the semi-major axis given is photocentric rather than relative.	340
Table 5	Parameters for every orbit in this work, with the source of the orbit listed in column (1): RECONS refers to RECONS astrometry (Chapter 3), SOAR is speckle interferometry from SOAR (Chapter 4), and the 5-letter reference codes are defined in Table 1. Note that for all the RECONS orbits and many of the literature orbits, the semi-major axis given is photocentric rather than relative.	341
Table 5	Parameters for every orbit in this work, with the source of the orbit listed in column (1): RECONS refers to RECONS astrometry (Chapter 3), SOAR is speckle interferometry from SOAR (Chapter 4), and the 5-letter reference codes are defined in Table 1. Note that for all the RECONS orbits and many of the literature orbits, the semi-major axis given is photocentric rather than relative.	342
Table 5	Parameters for every orbit in this work, with the source of the orbit listed in column (1): RECONS refers to RECONS astrometry (Chapter 3), SOAR is speckle interferometry from SOAR (Chapter 4), and the 5-letter reference codes are defined in Table 1. Note that for all the RECONS orbits and many of the literature orbits, the semi-major axis given is photocentric rather than relative.	343

Table 5	Parameters for every orbit in this work, with the source of the orbit listed in column (1): RECONS refers to RECONS astrometry (Chapter 3), SOAR is speckle interferometry from SOAR (Chapter 4), and the 5-letter reference codes are defined in Table 1. Note that for all the RECONS orbits and many of the literature orbits, the semi-major axis given is photocentric rather than relative.	344
Table 5	Parameters for every orbit in this work, with the source of the orbit listed in column (1): RECONS refers to RECONS astrometry (Chapter 3), SOAR is speckle interferometry from SOAR (Chapter 4), and the 5-letter reference codes are defined in Table 1. Note that for all the RECONS orbits and many of the literature orbits, the semi-major axis given is photocentric rather than relative.	345
Table 5	Parameters for every orbit in this work, with the source of the orbit listed in column (1): RECONS refers to RECONS astrometry (Chapter 3), SOAR is speckle interferometry from SOAR (Chapter 4), and the 5-letter reference codes are defined in Table 1. Note that for all the RECONS orbits and many of the literature orbits, the semi-major axis given is photocentric rather than relative.	346

LIST OF FIGURES

- Figure 1.1 Illustration of a secondary star (M_2) orbiting a primary star (M_1) that is fixed in the reference frame, with the angular parameters of the orbit labeled. The primary reference point for the orbit is the vector direction of the vernal equinox, represented by the Aries symbol (Υ), in the plane of the sky, represented by the black outlined rectangle. The longitude of the ascending node is described by the angle Ω , which is measured from the reference vector to a point on the line of nodes at which M_2 is moving from below to above the plane of the sky (i.e., away from the observer). The angle ω orients the orbit with an angle that swings from the location of the line of nodes to the periapsis, which is the location of closest approach of M_2 to M_1 . The true anomaly ν describes the current location of M_2 with respect to M_1 and the line of nodes. Finally, the inclination i of the orbit is defined to be 90° when the orbit is oriented edge-on to the observer; in this schematic, the inclination is $\sim 30^\circ$ 6
- Figure 1.2 Summary of formation scenarios, reproduced here from Offner et al. (2022) Figure 5. *Top row*: schematic of the main formation scenarios discussed here, including typical time- and length scales. *Middle row*: Observational results that are potential examples for each scenario (from Pineda et al. 2015; Kirk et al. 2017; Reynolds et al. 2021; Rodriguez et al. 2018). *Bottom row*: Results from numerical simulations showing examples of each scenario (from Guszejnov et al. 2021; Offner et al. 2016; Bate 2018; Muñoz et al. 2015). . . 9
- Figure 1.3 Multiplicity (or “multiplicity fraction”) of stars as a function of spectral type, reproduced here from Figure 1 of Offner et al. (2022) using a wide accumulation of stellar surveys. The thick lines represent multiplicity of all types, while the thin lines reflect only the fractions of triples/higher-order multiples (“THF;” not discussed here). The letters along the top indicate the approximate spectral type of each stellar mass. 20

- Figure 2.1 Hertzsprung-Russell Diagrams in $V - K$ vs. M_V (*left*) and M_K (*right*), showing stars within 25 pc that have no evidence of multiplicity. All stars have spectral types confirmed using a consistent technique (see text), distances from *Gaia* DR2, *Gaia* DR3 RUWE < 1.4, and no evidence of a perturbation in RECONS astrometry (if RECONS data are available). Light red symbols are M dwarfs from the RECONS astrometry program, those in dark red are L dwarfs from the RECONS astrometry program, and those in black are sources from the RECONS 25 pc Database that are not on the RECONS astrometry program. Dashed horizontal lines indicate the end of the main sequence as defined for this work (§2.2.2). 35
- Figure 2.2 *Top*: Masses of 289 *bona fide* single M dwarfs within 25 pc, as determined from their M_V vs. as determined from M_K . The orange line indicates the 1:1 relation. *Middle left*: HRD of the same targets, with a 3rd-order polynomial fit marked in black. The colors indicate the stars' deviation from that fit. *Middle right*: The same mass vs. mass plot as at top, but with colors marked as at middle left. The black line is a 3rd-order polynomial fit, and the orange line again is 1:1. *Bottom*: The K -band Benedict et al. (2016) MLR (light blue) and our corrected $V+K$ -band MLR (dark blue). 37
- Figure 2.3 Estimated masses from the corrected $V+K$ -band MLR (§2.2.1) for 289 single M dwarfs plotted against their absolute magnitudes in (*left to right panels*) G , B_G , R_G , and I bands. 40
- Figure 2.4 Hertzsprung-Russell Diagrams of the same set of nearby single M dwarf stars, shown in different filters with respect to K . From *top left* to *bottom right* are M_G vs. $G - K$, M_{BG} vs. $B_G - K$, M_{RG} vs. $R_G - K$, and M_I vs. $I - K$. The colors and symbols are the same as in Figure 2.1. 43
- Figure 2.5 Differences between apparent B_G and V magnitudes as a function of B_G . The colors and symbols are the same as in Figure 2.1. 44
- Figure 2.6 Absolute magnitudes in G and B_G against those in V and K for the *bona fide* single M dwarfs. The colors and symbols are the same as in Figure 2.1. Dashed black lines mark the adopted M_V and M_K values for the stellar/substellar lines. Orange curves are fits for each relation derived using the 33% faintest stars in the samples. The analogous plots for R_G and I are shown in Figure 2.7. 46

Figure 2.7 Absolute magnitudes in R_G and I against those in V and K for the *bona fide* single M dwarfs. The colors and symbols are the same as in Figure 2.1. Dashed black lines mark the adopted M_V and M_K values for the stellar/substellar lines. Orange curves are fits for each relation derived using the 33% faintest stars in the samples. The analogous plots for G B_G are shown in Figure 2.6. 47

Figure 2.8 *Left panel:* Number of systems within a given distance in the 25 pc sample. Curves of constant density in black, dark red, and light red illustrate the number of systems expected given the average density within 25 pc, 15 pc, and 10 pc, respectively. *Right panel:* HRD of the 25 pc sample. Each point color roughly indicates the quality of that system’s *Gaia* data (and thus the reliability of its HRD position): light points have parallax error ≥ 0.40 mas or are missing B_G or R_G , dark points have no such issues with their data, and open points (of either color) have more than one star included in their 2MASS K_s measurement (joint photometry). 49

Figure 3.1 *Left panel:* Distribution of targets added to the RECONS astrometry program each year since it began in 1999, considering only the M dwarfs within 25 pc. Targets are added to (or subtracted from) the program to keep the core survey volume-complete as new nearby M dwarfs are detected, with additional modifications as the RECONS research priorities shifted over time. Nearly all systems added earlier than 2021 (539 total) have enough data to be monitored for orbits for this thesis. On the vertical axis, to “set up” a target means to begin monitoring it on the continuous observing program. *Right panel:* HRD of the same sample of 25 pc M dwarfs, with points colored according to their observing baselines on the RECONS program. Brown dwarfs followed by RECONS are also shown here to emphasize our coverage, but we do not consider them for this thesis analysis; these systems are below the horizontal dashed “stars-brown dwarfs” line. 53

Figure 3.2 Examples of target star fields from the CTIO/SMARTS 0.9m for three targets: WT 2180 (*left*), LP 754-8 (*middle*), and LP 717-36 AB (*right*). Colors have been inverted such that darker pixels indicate more counts (i.e., brighter). In each panel, the target star is marked with a cyan double circle and the reference stars are marked with yellow single circles. The field in the left panel is excellent, with stars clustered around the target and near to it. The middle field is not as good because the reference stars are more dispersed, but the distribution is still reasonable — this field is typical of most targets. The right panel’s field is poor, as the references are spread far across the image and are generally all to one side of the target star. 56

Figure 3.3 Examples of residuals to the proper motion and parallax fit for four target stars: (*upper left to lower right*): LP 655-48, G 99-49, GJ 1111, and GJ 273. Each system’s residuals are represented by two panels: the upper showing residuals with respect to R.A. over time, and the lower showing residuals with respect to Decl. over time. The nightly (per-epoch) uncertainties of LP 655-48 (the first system) are unusually low (~ 2 mas), and those of GJ 273 (the last system) are unusually high (10–15 mas), while G 99-49 and GJ 1111 are typical. 60

Figure 3.4 Two examples of RECONS astrometry perturbations (PBs) characteristic of orbital motion; the systems shown here are the binaries LP 848-50 AB (*left*) and LHS 2071 AB (*right*). These PBs are with respect to the “single-star” astrometric model, i.e., they are the residuals left after fitting for the target star’s proper motion and parallax. In each column, the top panel shows residuals with respect to R.A. over time, and the bottom panel shows residuals with respect to Decl. 61

Figure 3.5 Examples of well-converged probability distribution functions for an astrometric binary (WT 460 AB) fit by the Dieterich et al. (2018) MCMC code. For space reasons, only a subset of the ten fit parameters are shown. *Top left to bottom right*: parallax (in mas), R.A. proper motion (mas yr^{-1}), Decl. proper motion (mas yr^{-1}), semi-major axis of the photocentric orbit (mas), orbital period (days), and eccentricity. The top of each plot lists the distribution’s mean, median, and standard deviation. 67

Figure 4.1 Venn diagram illustrating the three subsets of systems with M dwarfs targeted in the SOAR speckle survey, comprising 337 systems total. Each circle is labeled according to the subset’s source: “0.9 m PB” for targets showing perturbations (PBs) in the RECONS astrometry program at the CTIO/SMARTS 0.9m (§3), “Lit. mult.” for known multiples from the literature, and “DR2 sus.” for systems suspected to be multiples based on their *Gaia* DR2 results. The number of targets is given under each subset name, and the numbers in the overlapping sections indicate the number of targets common to multiple subsets. The area of each circle is proportional to the number of targets in that subset, although the overlapping regions are not to scale. 72

Figure 4.2 Two examples of astrometric perturbations (PBs) in RECONS data that are ambiguous, or not clearly astrophysical: GJ 693 (*left column*) and G 169-29 (*right column*). To contrast, compare these to the PBs showing clear orbital motion in Figure 3.4. For each system, each panel shows residuals in R.A. or Decl. with respect to time, computed after fitting proper motion and parallax to the system’s astrometry. 77

- Figure 4.3 Four astrometric fit parameters in DR2 that are useful for selecting potential unresolved multiples. Unresolved multiples are red symbols and hatched bars, resolved components are light blue dots/bars, and presumed singles are dark blue dots/bars. *Left column:* parameters for these systems in *Gaia* DR2, plotted against their *G* mags. *Middle column:* distributions of these parameters for systems from the left, separated again by multiplicity. *Right column:* each bar shows the fraction of systems above each cutoff value that are single or unresolved multiple. The values above which 75% of our systems are unresolved multiples are indicated with a black line. 80
- Figure 4.4 Four astrometric fit parameters in *Gaia* DR2 that are less useful for choosing potential unresolved multiples. The color schemes and columns are the same as for Figure 4.3, and any systems with values exceeding these ranges are noted with an arrow and text in each panel. For these quantities, the distributions of single and unresolved systems do not differ as significantly as those in Figure 4.3, making them less useful for identifying potential unresolved systems. The parameter `astrometric_excess_noise` does show a distinction between singles and multiples, but it is less useful than the very similar `astrometric_excess_noise_sig` because it strongly depends on *G* magnitude (faint singles have values similar to brighter unresolved multiples). 81
- Figure 5.1 Hertzsprung-Russell diagram of every system with an orbit presented in this work. One point is plotted per system, representing combined magnitudes for unresolved pairs. Circular points are binaries and triangular points are subsystems of higher-order multiples, and boxes indicate systems that are likely young. Colors refer to the source of the orbit: RECONS astrometry (red; Chapter 3), SOAR speckle interferometry (blue; Chapter 4), or the literature (black; §5.3). 91
- Figure 5.2 Orbits fit from RECONS astrometry (shown in R.A. order). For each system, the upper panel shows residuals with respect to R.A. over time, the bottom panel shows residuals with respect to Decl. over time, and the blue curve shows the orbit model fit (§3.4). 93
- Figure 5.3 Orbits fit from RECONS astrometry (shown in R.A. order). For each system, the upper panel shows residuals with respect to R.A. over time, the bottom panel shows residuals with respect to Decl. over time, and the blue curve shows the orbit model fit (§3.4). 94
- Figure 5.4 Orbits fit from RECONS astrometry (shown in R.A. order). For each system, the upper panel shows residuals with respect to R.A. over time, the bottom panel shows residuals with respect to Decl. over time, and the blue curve shows the orbit model fit (§3.4). 95

Figure 5.5 Orbits fit from RECONS astrometry (shown in R.A. order). For each system, the upper panel shows residuals with respect to R.A. over time, the bottom panel shows residuals with respect to Decl. over time, and the blue curve shows the orbit model fit (§3.4). 96

Figure 5.6 Example of a circular orbit used in the simulations that underpin the RECONS sensitivity plots. *Top panel:* simulated positions of a companion in a randomly oriented orbit on the sky, with each point representing its position at the time of RECONS observation. For the purpose of this demonstration, the random inclination angle were restricted to $\pm 30^\circ$ of face-on. *Middle panels:* simulated R.A. and Decl. displacements vs. time for the orbit snippet shown in the top panel. The red dashed line is the linear fit to the astrometry, representing the RECONS single-star model fit to the photocenter’s proper motion. Note that parallactic motion is not simulated nor fit here because those residuals are usually much smaller than the orbital motion (see step 4e). *Bottom panels:* simulated R.A. and Decl. residuals to the single-star fit, with the red line the same as in the middle panels. Error bars representing typical uncertainties are also illustrated now (and omitted from the top and middle panels for clarity). This residual is then multiplied by the $B - \beta$ factor for this (M_1, M_2) combination to produce the final simulated astrometric PB (not shown). 101

Figure 5.7 Example of an $e = 0.9$ orbit used in the simulations that underpin the RECONS sensitivity plots. Each panel is the same as in Figure 5.6, with the only differences being this orbit’s higher eccentricity and different randomly selected orientation angles. 102

Figure 5.8 Examples of average sensitivity plots for two single stars: (*left panel*) G034-023, a star with limited coverage over only ~ 3.5 years, and (*right panel*) G141-021, a star with modest coverage over ~ 9 years. The color indicates the percentage of simulated orbits that were detectable given that system’s typical nightly astrometric uncertainty. The teal vertical line in each plot indicates the length of RECONS observations for that system to date; orbits longer than those baselines may be detectable, but cannot usually be fit reliably. . . . 103

Figure 5.9 Average detection sensitivity in P_{orb} vs. e space for the subset of the RECONS 16.67 pc volume-complete sample which had enough data to be considered (258 red dwarfs). The colors represent the percentage of orbits that were detectable, calculated via the injection-recovery process described in §5.1.2 averaged over all systems in the sample. It is evident that at least 70% of orbits would have been detected for orbital periods of ≤ 30 years at effectively all eccentricities. 103

Figure 5.10 *Left panel:* average percentage of orbits that can be fit, as a function of P_{orb} vs. e , for 127 multiples and suspected multiples followed by the RECONS astrometry program. For clarity, the exact values for the patches in the topmost row are printed in white. This fit capability map was created by averaging the fit capability maps of the individual multiples (following §5.1.2). The variation is quite low in e because coverage is generally excellent for these systems and their detectability plot was nearly uniform, as noted in the text. Overplotted are P_{orb} vs. e values for the orbits fit from RECONS astrometry, with circles for binaries and triangles for subsystems of triples and quadruples. *Right panel:* Hertzsprung-Russell diagram of the multiples analyzed in this sensitivity analysis, with each point's color indicating the time baseline over which it has been observed. 105

Figure 5.11 Orbits fit to SOAR speckle interferometry (filled points) combined with available high-imaging data from the literature (open points). The systems are shown here in order of R.A., and each blue curve is the best-fit orbit model. 108

Figure 5.12 Orbits fit to SOAR speckle interferometry (filled points) combined with available high-imaging data from the literature (open points). The systems are shown here in order of R.A., and each blue curve is the best-fit orbit model. 109

Figure 5.13 Orbits fit to SOAR speckle interferometry (filled points) combined with available high-imaging data from the literature (open points). The systems are shown here in order of R.A., and each blue curve is the best-fit orbit model. 110

Figure 5.14 Orbits fit to SOAR speckle interferometry (filled points) combined with available high-imaging data from the literature (open points). The systems are shown here in order of R.A., and each blue curve is the best-fit orbit model. 111

Figure 5.15 Orbits fit to SOAR speckle interferometry (filled points) combined with available high-imaging data from the literature (open points). The systems are shown here in order of R.A., and each blue curve is the best-fit orbit model. 112

Figure 5.16 *Left panel:* average percentage of orbits that can be fit, as a function of P_{orb} vs. e , for multiples followed by the SOAR speckle program. This plot is analogous to that of Figure 5.10, but with fit capability defined as a companion moving through 40% of 360° over the observations (described in detail in §5.2.2). Overplotted is P_{orb} vs. e for the orbits fit from the SOAR speckle program, with circles for binaries and triangles for subsystems of triples and quadruples. *Right panel:* Hertzsprung-Russell diagram of the multiples analyzed in this sensitivity analysis, with each point's color indicating the time baseline over which it has been observed, including literature data. The lack of low-mass systems (compared to, e.g., the RECONS program in the right panel of Figure 5.10) is mainly due to the $I \leq 14$ mag limit of the SOAR speckle program. 114

Figure 6.1 The distribution of P_{orb} vs. e for 193 systems with red dwarf stellar primaries shown in terms of $\log P_{\text{orb}}$. An equivalent plot with P_{orb} scaled linearly is given in Figure 6.2. Each point's color indicates its source: fit from RECONS astrometry (red, 19 points), fit from SOAR speckle interferometry (blue, 42 points), and published in the literature (black, 132 points). Each point's shape indicates multiplicity, with binaries as circles and triples and quadruples as triangles. Points known to be young systems are marked with open squares. The vertical dashed line indicates the $P_{\text{orb}} = 7$ days limit discussed in the text (§6.2.1). The dotted curve marks the limit at which two mid-M dwarfs would collide at periastron (§6.2.2). 122

Figure 6.2 The distribution of P_{orb} vs. e for 193 systems with red dwarf stellar primaries shown in terms of linear P_{orb} . This plot is identical to Figure 6.1 with only the P_{orb} scaling changed, thus the symbols and curves are the same as in that figure: each point's color indicates the source of its orbit fit (RECONS astrometry, SOAR speckle interferometry, or literature publications), each point's shape indicates the multiplicity of that system (binary or triple/quadruple), and the dotted curve marks the limit at which two mid-M dwarfs would collide at periastron (§6.2.2). 123

Figure 6.3 Distributions of orbital period (*left panels*) and eccentricity (*right panels*) for the orbits presented in this work (e.g., as shown in Figures 6.1 and 6.2). In every panel here, the non-hatched bars indicate binaries and hatched bars represent subsystems of higher-order multiples. For P_{orb} in the left column, both panels are the full set of orbits, with the bottom panel as a zoom-in to better show the distribution for systems with $P_{\text{orb}} > 1$ year. For e in the right column, the top panel is the full set of orbits and the bottom panel is the set with $P_{\text{orb}} < 7$ days excluded, as those shortest-period orbits all fall in the lowest e bin. 124

- Figure 6.4 Distribution of eccentricity in three regimes of P_{orb} : $P_{\text{orb}} < 7$ days (*top panel*), $7 \text{ days} \leq P_{\text{orb}} < 7 \text{ years}$ (*middle panel*), and $P_{\text{orb}} \geq 7 \text{ years}$ (*bottom panel*). In every panel, the non-hatched bars indicate binaries and the hatched bars indicate subsystems of higher-order multiples. This figure is discussed in §6.2.3. 150
- Figure 6.5 The P_{orb} vs. e plot showing the same systems as in Figures 6.1 and 6.2, but with points colored by primary mass (*top*), secondary mass (*middle*), or mass ratio (*bottom*). Open symbols indicate masses estimated assuming $\Delta K = 0.8 \text{ mag}$, as those estimates are the least reliable. This figure is introduced in §6.4. 151
- Figure 6.6 These P_{orb} vs. e plots are identical to those in Figure 6.5, but here the plots are in terms of linear P_{orb} instead of $\log P_{\text{orb}}$. Again, the points are colored by primary mass (*top*), secondary mass (*middle*), or mass ratio (*bottom*). Open symbols indicate masses estimated by assuming $\Delta K = 0.8 \text{ mag}$, as those estimates are the least reliable. This figure is introduced in §6.4. 152
- Figure 6.7 Distributions of eccentricity for multiples with different M dwarf primaries, shown for all systems (*left column*) and those with $P_{\text{orb}} > 7 \text{ years}$ (*right column*). Systems with $P_{\text{orb}} < 7 \text{ days}$ were excluded. Binaries are shown with non-hatched bars and higher-order multiples are indicated with hatched bars. Masses were either dynamical or estimated as described in §6.3. The analogous plot organized by M dwarf secondary mass is given in Figure 6.8. This figure is introduced in §6.4. 153
- Figure 6.8 Distributions of eccentricity for multiples with different M dwarf secondaries, shown for all systems (*left column*) and those with $P_{\text{orb}} > 7 \text{ years}$ (*right column*). Systems with $P_{\text{orb}} < 7 \text{ days}$ were excluded. Binaries are shown with non-hatched bars and higher-order multiples are indicated with hatched bars. Masses were either dynamical or estimated as described in §6.3. The analogous plot organized by M dwarf primary mass is given in Figure 6.7. This figure is introduced in §6.4. 154
- Figure 6.9 Distribution of mass ratios for M dwarf systems presented in this work. For systems without dynamical mass, masses were estimated following §6.3. Systems were excluded if their mass estimates required assuming $\Delta K = 0.8 \text{ mag}$, as those masses are the least reliable. Binaries are represented here with non-hatched bars and higher-order multiples are indicated with hatched bars. The bars are colored to match the color scheme for q used in other plots in this chapter. This figure is introduced in §6.4.3. 155

- Figure 6.10 Distributions of mass ratios for multiples with different primary masses (*left column*) and secondary masses (*right column*). In every panel, the non-hatched bars represent binaries and the hatched bars indicate subsystems of higher-order multiples. This figure is introduced in §6.4.3. 156
- Figure 6.11 Distributions of mass ratios for multiples of different P_{orb} . In every panel, the non-hatched bars represent binaries and the hatched bars indicate subsystems of higher-order multiples. This figure is introduced in §6.4.3. . . 157
- Figure 6.12 Distributions of eccentricity for systems of different mass ratios, given for all systems (*left column*) and those with $P_{\text{orb}} > 7$ years (*right column*). All masses (and thus mass ratios) that were not dynamical masses were estimated using the procedure in §6.3. This figure is introduced in §6.4.3. 158
- Figure 6.13 Distribution of eccentricity with respect to mass ratio as q vs. e , excluding systems for which masses were estimated by assuming $\Delta K = 0.8$ mag. All masses (and thus mass ratios) that were not dynamical masses were estimated using the procedure in §6.3. The symbol shapes indicate the types of system: circles are binaries and triangles are subsystems of higher-order multiples. This figure is introduced in §6.4.3. 159
- Figure 6.14 Distribution of orbital period with respect to mass ratio as P_{orb} vs. q . The open symbols indicate the systems for which masses were estimated by assuming $\Delta K = 0.8$ mag, while the filled symbols are systems for which masses were either dynamical or estimated using the procedure in §6.3. The symbol shapes indicate the types of system: circles are binaries and triangles are subsystems of higher-order multiples. This plot is discussed in §6.4.3. . . 160
- Figure 6.15 P_{orb} vs. e for multiples of solar-type stars (yellow points; Raghavan et al. 2010) and M dwarfs (black points; this work). The same distribution is shown in terms of $\log P_{\text{orb}}$ (*left panel*) and linear P_{orb} (*right panel*). The 12-day tidal circularization period for solar-type stars is shown with the yellow dashed line, and the black dashed line indicates the 7-day period that is the upper limit of P_{circ} for M dwarfs. This figure is discussed in §6.4.4. 161

Figure 6.16 Comparison of the eccentricity distributions for three populations of multiples. *Top panel:* multiples of F, G, and K dwarfs (“solar-type”) from Raghavan et al. (2010); *middle panel:* multiples of M dwarfs from this work (repeated from Figure 6.3); *bottom panel:* multiples of very low-mass (VLM) stars and brown dwarfs from Dupuy & Liu (2017). Note that the scale for the VLM distribution is much smaller, as they have fewer orbits than the other sets. In every panel, the bars represent the sum of all multiples (binary, triple, etc.), and systems with $P_{\text{orb}} < P_{\text{circ}}$ for that population are excluded (except for the VLM set, which contains no tidally circularized systems). This figure is introduced in §6.4.4. 162

Figure 6.17 P_{orb} vs. e for multiples of very low-mass (VLM) stars and brown dwarfs (blue points; Dupuy & Liu 2017) and M dwarfs (black points; this work). The distribution is given in terms of $\log P_{\text{orb}}$ (*left panel*) as well as for linear P_{orb} (*right panel*). The black dashed line indicates the 7-day limit below which all M dwarf systems are nearly circular; P_{circ} is not indicated for the VLM sample because there are not enough of those systems with short P_{orb} observed to constrain it. This figure is introduced in §6.4.5. 163

CHAPTER 1

Introduction: Motivating Orbital Architectures of the Ubiquitous Red Dwarfs

As we carry out our urge to explore, discover, and learn, we measure every new place or experience against our own home and its environments — either to rediscover the familiar, or to identify the most strange.

In the context of modern astronomy, this tendency is most visible in our search for extrasolar planets (“exoplanets”), but our search for the familiar can also be seen in studies of stars and galaxies, as we compare each observed phenomenon to the Sun or the Milky Way. Despite phenomenal success in finding distant worlds, astronomical exploration has yet to discover another multi-planet system exactly like our own. Rather than discouraging us, this difficulty has motivated us toward the longer journey of unraveling how planetary systems form, evolve, and are influenced by their stellar environments and histories. Those environments are, in turn, affected by how those stars form and evolve, and those processes are affected by how the diversity of other stars in their neighborhood form and evolve — and each of these things depends on factors spanning molecular to galactic scales.

It is with this motivation that we embark on this dissertation that examines low-mass stars in systems with multiple stellar components. In this work, each star considered has less than 60% the mass of our Sun and is gravitationally bound to other low-mass stars (or, in a few cases, to brown dwarfs), which admittedly makes them more strange than familiar. On the other hand, these non-solar systems are an inevitable part of the discussion on star and planet formation, as the chain of processes that forms stars has produced both

our Sun as well as these small stars; it produces the low-mass stars in such abundance that they comprise three out of every four stars in our neighborhood (Henry et al. 2006, 2018). Predicting the frequency and multiplicity of these stars is thus an essential test of our models of star formation. Predicting the subsequent properties of these multiples — the most common stellar pairs, how widely they are separated, and the orbits they settle into — then tests our understanding of how stars interact with the gas, dust, and other stars in their post-formation environments.

This dissertation addresses that final line of inquiry. We begin by formally asking,

What are the orbital architectures of companions to red dwarf stars?

Our goals are to establish empirically the sizes and shapes of primarily stellar companions’ orbits around low-mass stars, and in doing so, to provide constraints for models of star formation and dynamical evolution. The key relationship that will be explored is the comparison of orbital periods (representing the sizes of orbits) to eccentricities (orbital shapes), or the plot of P_{orb} vs. e . The P_{orb} vs. e plot reveals a remarkable amount of information about which formation scenarios apply to various types of stars. These models and empirical results will, in turn, have implications for all phenomena that depend on stellar properties and histories, including planet formation and evolution.

In this first chapter we begin with nomenclature on multiple stars (§1.1), then discuss the current family of paradigms of star formation (§1.2) and how stellar orbits change and evolve (§1.3). We then review what observations have revealed on these topics for a variety of types of main sequence stars (§1.4), including our low-mass “red dwarf” stars of interest.

The remaining chapters of this dissertation describe our investigation of the orbital architectures of low-mass multiples: Chapter 2 defines our stellar regime of focus, Chapter 3 and Chapter 4 explain our observations of several hundred low-mass star systems, Chapter 5 presents the results of each of those observing campaigns, and Chapter 6 synthesizes those results and explores the implications for these star systems’ formation and dynamical evolution. Finally, Chapter 7 outlines the conclusions that can be drawn from this work and posits the next steps for future studies.

1.1 Terms and Conditions

Throughout this dissertation, we will frequently refer to vocabulary specific to systems of multiple stars and their orbits. Here we pause to define some of these terms, for clarity.

First, the subjects of this dissertation are the stars on the main sequence with masses of $0.075\text{--}0.60 M_{\odot}$ that have spectral types of M0.0V to L2.5V. We will refer to these objects as “M dwarfs” or “red dwarfs” throughout.

In this work, a *system* is considered to be one or more stars; thus, a single star is considered to be a system. A system consisting of two or more stars that are gravitationally bound is known as a multi-star system or *multiple system*. A multiple of exactly two stars is a binary, three stars is a triple, and four is a quadruple. The stars in these systems are sometimes referred to as its *components*, and individually these components are named the primary star (denoted “A”), the secondary star (“B”), the tertiary star (“C”), etc. The latter stars are generally called companions of the primary. These components are named in

order of most massive to least massive, using each star’s maximum mass (over its lifetime) as the distinguishing factor. Note that this means in a binary with a white dwarf and M dwarf, the white dwarf is the primary, because earlier in the system’s history the white dwarf was the most massive component. In systems with no white dwarfs, the brightest component is assumed to be the most massive — the primary star (component A) is identified to be the one that is brightest at visible wavelengths, first considered in the *Gaia* G photometric band, or in the Johnson system V photometric band if G is not available. Component B is the next brightest, component C the third brightest, etc.

Due to their mutual gravitation, the stars in a multiple orbit their common center of mass. Often we will consider the alternate reference frame centered on the primary star, in which case the companions are said to orbit the primary. Most of the parameters describing an orbit do not change with this change of reference frame (with the exception of the semi-major axis).

The parameters describing the orbit are illustrated in Figure 1.1 and described as follows:

- Orbital period (P_{orb}): the time required for each star to complete its orbital path and return to a given point. In a binary system, the period of the primary and secondary around their center of mass are identical. The orbital period of the secondary in the frame where it orbits the primary is the same as in that center of mass frame.
- Eccentricity (e): the shape of the orbit, given as a dimensionless value where a perfectly circular orbit has $e = 0$. For these bound systems, eccentricity is limited as $e < 1$.

- Semi-major axis (a): the size of the orbit, defined as its length along its longest axis.
The semi-major axis of the relative orbit is the sum of the semi-major axes of the primary and secondary's orbits around the center of mass: $a = a_1 + a_2$. In this work, this property is typically measured in arcseconds, milliarcseconds (mas), and astronomical units (AU).
- Argument of periastron (ω): angular location along the orbit at which the primary and secondary are closest, measured with respect to the ascending node (see below) and the primary star or center of mass.
- Longitude of the ascending node (Ω): angular location at which the orbit crosses the plane of the sky and the orbiting body is receding from the observer (the other intersection point, at which the star is approaching the observer, is the descending node). This angle is typically measured with respect to the vernal equinox.
- Inclination (i): angle between the plane of the orbit and the plane of the sky, with $i = 90^\circ$ corresponding to an “edge-on” orbit from the observer's perspective.
- Time of periastron passage (T_0): the date at which the stars in a binary cross their orbit's periastron, in the center of mass frame, or the date when the secondary crosses its periastron with respect to the primary. Some authors give alternative reference times in lieu of periastron passage time — for example, eclipsing binary publications refer to the epoch of the first observed primary eclipse.

More detailed descriptions of these parameters are given in Chapter 2 of Hilditch (2001).

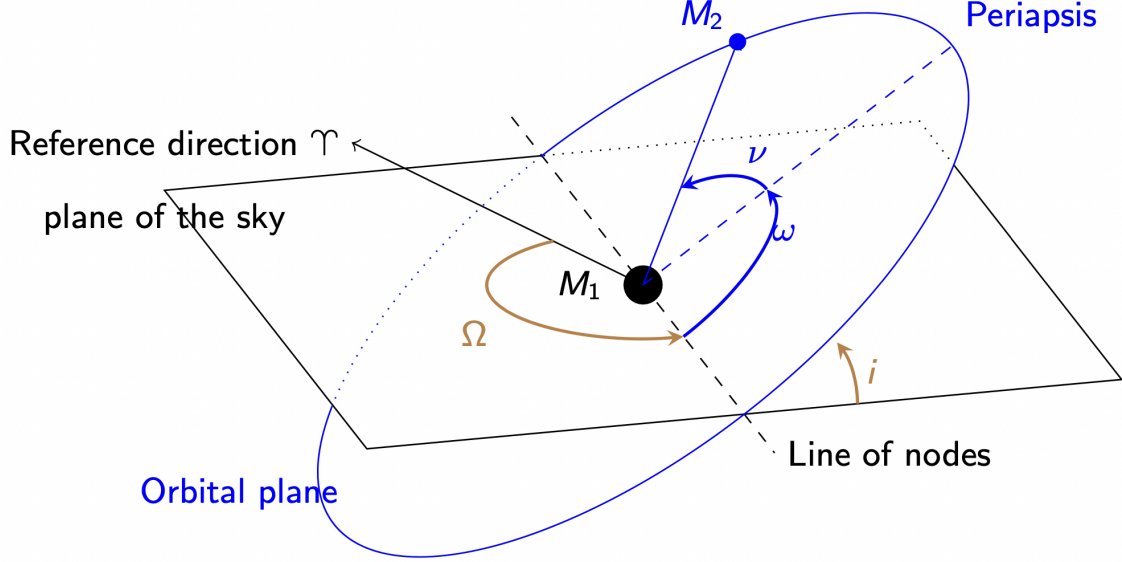


Figure 1.1 Illustration of a secondary star (M_2) orbiting a primary star (M_1) that is fixed in the reference frame, with the angular parameters of the orbit labeled. The primary reference point for the orbit is the vector direction of the vernal equinox, represented by the Aries symbol (Υ), in the plane of the sky, represented by the black outlined rectangle. The longitude of the ascending node is described by the angle Ω , which is measured from the reference vector to a point on the line of nodes at which M_2 is moving from below to above the plane of the sky (i.e., away from the observer). The angle ω orients the orbit with an angle that swings from the location of the line of nodes to the periastris, which is the location of closest approach of M_2 to M_1 . The true anomaly ν describes the current location of M_2 with respect to M_1 and the line of nodes. Finally, the inclination i of the orbit is defined to be 90° when the orbit is oriented edge-on to the observer; in this schematic, the inclination is $\sim 30^\circ$.

For any pair of stars in a binary or triple, we will also discuss their *mass ratio* (q), which will always be the ratio of the mass of the secondary or tertiary star to that of the primary star, e.g., $q = M_2/M_1$ or M_3/M_1 . In some instances, we will refer to the *mass fraction* (f), which quantifies the amount of mass in one component relative to the total mass in the system, e.g., $f = M_1/(M_1 + M_2)$ or $M_2/(M_1 + M_2)$ or $M_1/(M_1 + M_2 + M_3)$, etc.

1.2 How To Form a System of Multiple Stars

In each multiple system of two (or more) objects, the components are moving along paths that are the cumulative result of how those objects formed and how they have subsequently evolved dynamically. Observing the formation processes from start to finish is not an option because they take longer than the modern astronomical record, but we have gleaned some understanding by matching physics-heavy models to observational snapshots of large sets of systems. In this section we review our current understanding of the different formation paths for systems of low-mass stars and brown dwarfs, as well as the subsequent dynamical evolution that could proceed in each of those scenarios.

In general, stars form from the collapse of localized regions (typically about a parsec in size) within molecular clouds that are relatively more dense than surrounding regions in the clouds. These overdense regions range from spherical to filamentary in shape, and are the natural result of the cloud's balance of turbulence, gas molecule kinetics, gravitational pressure, and magnetic fields. These overdensities are unstable, and prone to collapse when they experience a perturbative event, such as the collision of two molecular clouds, when a cloud passes through galaxy's spiral arm, or when a shock event occurs, such as a supernova. As gas within a localized region falls toward a central point, it quickly forms a disk with a dense, spherical center as angular momentum is conserved. If the central sphere grows enough, the pressure at the center triggers hydrogen to begin fusing into helium in the core, and a star is born. The star's contraction slows to a stop as hydrostatic equilibrium is established, and its leftover material spins around it in the form of a disk that slowly thins

in the breeze of the stellar winds.

Two or more stars may end up gravitationally bound at several points during the above formation process, or even shortly afterward. As detailed in the following subsections, current models group the formation of multiples into three methods: first, one molecular cloud breaking into multiple stellar cores through turbulence (§1.2.1); second, the disk around a stellar core fragmenting into additional cores (§1.2.2); third, fully-formed stars capturing neighboring stars (§1.2.3). Additional dynamical evolution may follow these events due to local gas mechanics (§1.3). Many of these models were constrained by observations of multi-star systems and trends of multiplicity with stellar mass, which are discussed in §1.4.

Figure 5 in Offner et al. (2022) summarizes these scenarios, including their typical length scales and timescales, and is reproduced here as Figure 1.2.

1.2.1 Turbulent Fragmentation of Cores and Filaments

The earliest point at which a star might gain a companion is just as it begins to form, during the collapse of local gas in its molecular cloud. The balance of turbulence vs. rotation keeps the cloud stable, and this turbulence naturally leads to the overdense regions discussed above to be shaped as filamentary structures as well as spherical cores. Each of these structures (and the spectrum of morphologies in between) could form multiples if the conditions are right during their gravitational collapse. In both cases the fragmentation of the structure into collapsing sub-structures is triggered by existing density anomalies within the core or filament exceeding a critical threshold that depends on the region’s size, temperature, mass, and — for filaments in particular — magnetic field pressure.

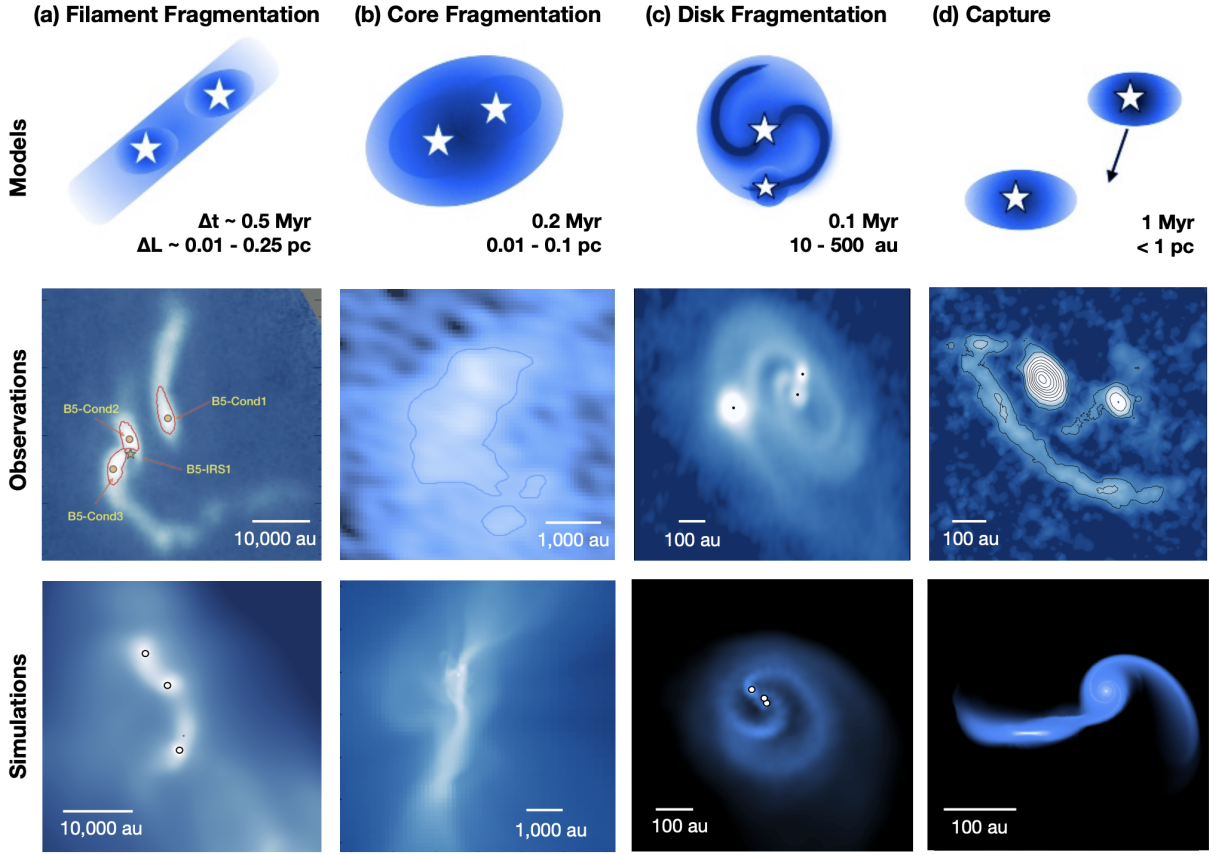


Figure 1.2 Summary of formation scenarios, reproduced here from Offner et al. (2022) Figure 5. *Top row*: schematic of the main formation scenarios discussed here, including typical time- and length scales. *Middle row*: Observational results that are potential examples for each scenario (from Pineda et al. 2015; Kirk et al. 2017; Reynolds et al. 2021; Rodriguez et al. 2018). *Bottom row*: Results from numerical simulations showing examples of each scenario (from Guszejnov et al. 2021; Offner et al. 2016; Bate 2018; Muñoz et al. 2015).

When filaments collapse and fragment they do so along their lengths, creating multiple cores. Such cores would thus be aligned like “beads on a string,” and if they are within ~ 0.1 pc of each other they may be gravitationally bound. Multiples that form from fragmentation of more spherical overdensities (molecular cloud cores) would be similarly separated but have no particular alignment with one another. Each overdensity collapse suppresses the

propagation and growth of additional perturbations in its vicinity as material is depleted, so each multiple formed is typically restricted to 2–3 members (Offner et al. 2016; Guszejnov et al. 2017).

Measurable attributes of multiple systems formed via turbulent fragmentation include:

Mass ratios — Very low-mass companions ($\lesssim 0.08 M_{\odot}$) are expected to be uncommon because the collapsing and fragmenting overdensities are relatively massive and these processes occur while the local gas is plentiful (Fisher 2004), although this is subject to debate. Furthermore, when each protostar forms, its radiation suppresses further smaller-scale fragmentation within a few hundred AU (Offner et al. 2009; Bate 2012). Small mass ratios are thus unlikely.

Initial separations — The initial separations of stars formed in multiples via this method is $\gtrsim 100$ AU, regardless of the specific physics that sets the minimum fragmentation scale (e.g., Guszejnov et al. 2017; Lee & Hennebelle 2018). If the stars are connected by gas “bridges” (as suggested by Kuffmeier et al. 2019) and actively accreting, they would migrate inward to $\lesssim 100$ AU within a Myr through gas-dynamical friction (Bate & Bonnell 1997; Zhao & Li 2013; Lee et al. 2019).

Additional observational signatures — Due to their initially wide separations and isolated development, the spin axes and early circumstellar disks of the stars in each system should be distributed randomly (Offner et al. 2016; Bate 2018).

A complicating facet of the formation of multiples via turbulent fragmentation is that some properties of the systems may also reflect the initial turbulence of their molecular cloud,

thereby skewing trends of mass ratios vs. orbital periods for binaries (Fisher 2004). These dependencies are not straightforward to untangle, however, for more complicated physics involving magnetic fields.

1.2.2 Disks Broken via Gravitational Instability

As a single protostar is collapsing, it may also gain companions that coalesce from leftover material of its circumstellar disk. At its outer edge, the disk is receiving infalling gas from the collapsing molecular cloud, and at its inner edge its material is falling onto the newly forming star. This growing star heats the disk, providing thermal stabilization, thus the overall stability of the disk is dictated by the balance of accretion onto the star vs. accretion onto the outer disk. The disk will fragment if the cold outer region grows too quickly while its temperature remains constant, or if the central star's luminosity drops (e.g., if accretion slows) and the disk loses temperature. Regardless of the cause, disk fragmentation occurs at roughly the boundary between the protostar-heated region and accretion-fed region, or ~ 100 AU.

The result is that the fragmented part of the disk quickly collapses to a single mass orbiting the original protostar. Initially the companion may be larger than its own Hill radius (the companion's radius of gravitational influence), which places it in danger of being sheared apart by the competing gravitational influence of the protostar and surrounding material. The companion does not survive unless it becomes small enough to be contained within the safety of its own Hill sphere, thus it must cool efficiently enough and become dense enough to collapse quickly. The companion may migrate inward during this process,

but doing so shrinks its Hill sphere even smaller, as the Hill radius is directly proportional to the semi-major axis of the companion’s orbit. Thus, to avoid tidal disruption, the companion must migrate inward slowly enough that its shrinking Hill radius stays larger than its still-collapsing physical radius (Gammie 2001; Kratter & Murray-Clay 2011).

Measurable attributes of multiple systems formed via broken disks include:

Mass ratios — The companion formed from this scenario tends to be similar in mass to the initial protostar due to the conditions that led to the disk fragmentation in the first place — the bountiful infall of gas onto the outer disk. The new companion will also tend to outpace the first star’s accretion rate from the disk, making an equal mass ratio even more likely.

Initial separations — The heat from the central star gives thermal support to the disk within tens to hundreds of AU (depending on the star). Thus, fragmentation occurs only in the outer region, and the resulting stars are separated by $\gtrsim 100$ AU.

Additional observational signatures — Given that the new companion is born into the remnants of the leftover disk, the properties of the resulting binaries depend substantially on how that leftover disk affects the companion’s dynamical evolution. How the companion’s migration is affected by disk properties will determine the distributions of companion separations and mass ratios expected from this formation scenario. Gas-driven migration is discussed in detail in §1.3.

1.2.3 Capture of Neighboring Stars

Even if a star remains single through its entire formation, it could gain a bound companion if another star passes near enough to enter its gravitational well and loses so much energy that it cannot escape. There are two main categories of capture scenarios: gasless and gaseous, depending on whether gas is available to assist with the capture.

In a gasless scenario, enough energy can be lost to capture the new companion if the stars pass closely enough to generate tidal forces (Fabian et al. 1975), or if the addition is initially a third companion and the subsequent dynamical evolution ejects one of the stars (usually the least massive member; Valtonen & Mikkola 1991). Neither of these scenarios are likely enough to account for a significant fraction of field binaries (Bate 2015).

For gaseous capture, however, the odds of gaining a companion are improved, as long as there is enough gas in circumstellar disks that two closely passing stars lose energy to that material as they move through it (a process termed “gas-mediated capture”). This mechanism requires close stellar passes and stellar velocities that are relatively slow to avoid simply truncating the disks, making it more likely in smaller, dense clusters (Clarke & Pringle 1991a,b). Because this scenario requires substantial disk material, it is only an option during a star’s initial formation phase.

Measurable attributes of multiple systems formed via capture include:

Mass ratios — Dynamical gasless capture leaves systems with mass ratios closer to unity, as the ejected companion tends to be the least massive of the three. Capture via gaseous disks, however, produces a distribution of systems with mass ratios that dramatically rise

toward lower values (McDonald & Clarke 1995), primarily because lower mass stars are more easily captured than massive stars.

Initial separations — Gasless capture usually leaves the resulting binary with a similar separation as the original pair, as ejecting the least massive companion does not dramatically change the total angular momentum and energy (Kratter 2011). Gaseous capture, on the other hand, results in separations necessarily closer than the initial size of the circumstellar disk, which observations suggest are tens of AU in radius for low-mass stars (Pascucci et al. 2016; Burn et al. 2021). Migration to wider orbits (as discussed in §1.3) is not expected in this case because the disk is likely to be truncated (Cuello et al. 2023) or destroyed by the capture, with the latter scenario significantly more likely for higher-mass companions (Olczak et al. 2006).

Additional observational signatures — The capture of another star would not leave an orbit with any particular eccentricity or orientation, although the stars’ random initial trajectories make circular orbits less likely unless there is subsequent gas-driven evolution (§1.3). In general, then, there are no observational signatures that allow us to distinguish between multiples formed via gaseous capture and fragmentation of a disk (§1.2.2), or between gasless capture and turbulent core/filament fragmentation (§1.2.1) — unless the ages of the components can be shown as very different, which is only possible in a capture scenario. The only other smoking gun would be circumstellar disks in the system that are on clearly colliding paths, especially if their morphologies indicate they collided with each other previously. However, the lifetimes of those disks are relatively short compared to the average

age of field stars, so this line of evidence has presumably been erased in samples of multiples found anywhere other than young clusters.

1.3 Orbital Evolution After a Multiple is Formed

As discussed above (§1.2), models indicate that most multiples form with relatively wide separations (tens to thousands of AU) and no particular orbital eccentricity. The large numbers of closely-separated multiples we observe today at separations $\lesssim 10$ AU are thus the result of subsequent orbital evolution. Models currently suggest that that evolution is mainly the result of (1) interactions between the stars and the gas and dust in their environment — the circumstellar disks as well as any surrounding molecular cloud — and in some cases also (2) tidal forces.

1.3.1 *Orbital Evolution Due to Gas and Dust*

If there is substantial gas left in the surrounding molecular cloud, interactions between the stars and that gas creates torque, which in turn reduces the stars’ separations via a process known as “gas-dynamical friction.” These interactions include accretion and the effects of the gas distribution that forms a wake trailing behind each star. Angular momentum may also be lost by magnetic braking as the stars move through the gas (Zhao & Li 2013). In less than a Myr, these combined processes can drive stars from thousands of AU apart to tens of AU (Offner et al. 2022). Thus, it appears that substantial gas — either in the leftover molecular cloud or in circumstellar disks — *is required* to create the distributions of companion separations for various types of main sequence stars.

If there are disks around both stars in a binary and both are still accreting from the surrounding cloud, the balance of the torques from these processes may drive the stars closer together or further apart. Early simulations showed that a single circumbinary disk will consistently induce *only* inward migration (Lubow & Artymowicz 1996). The options changed when star formation models included circumstellar disks and accretion torque, although the specific results depend substantially on the initial parameters of a binary pair, such as its mass ratio, disk morphologies and densities, and orbital eccentricity. For typical disks, pairs with initially low mass ratios will generally migrate inward, whereupon the companion will accrete mass from the disk and drive the mass ratio closer to unity. As the mass ratio increases, the migration slows and potentially reverses direction (Tokovinin & Moe 2020), resulting in a distribution of separations wherein not all companions are at very small distances from their primaries.

1.3.2 Orbital Evolution Due to Kozai-Lidov Cycles

It has been suggested that pairs at separations $\lesssim 10$ AU could also be the result of Kozai-Lidov cycles (Kozai 1962; Lidov 1962) in combination with tidal friction (Fabrycky & Tremaine 2007). This mechanism can shrink an orbit if there is a third, wide companion in the system, as angular momentum exchanged between the outer and inner orbits induces oscillations in eccentricity and relative inclination. During the period when the inner pair is eccentric, tidal forces during periastron passage circularize its orbit and generally reduce its semi-major axis.

This process, however, is generally not rapid enough to explain all current $\lesssim 10$ AU orbits. Kozai-Lidov oscillations occur on timescales of a Gyr, whereas most binaries evolved to their

current $\lesssim 10$ AU semi-major axes on Myr timescales, as described by Moe & Kratter (2018). Gas-driven migration is more efficient and thus more likely.

1.3.3 Orbital Evolution Due to Tides

Under the right circumstances, one of the most efficient mechanisms of orbital evolution is loss of angular momentum to the tidal force arising between two or more bodies. The tidal force is induced when one object passes near to a second object and the gravitational force on its near side is greater than the force on its far side. This differential force deforms the object along that force axis, creating a tidal bulge that lags ahead or behind the force axis (depending on the rotation direction) as the object continues to rotate, inducing a torque. This torque adjusts the rotation of the object until the tidal bulge is aligned with the force axis, synchronizing rotation with orbital motion, and in the process the orbit is circularized.

The torque due to the tidal force is inversely proportional to a^8 (Zahn 1977), where a is the separation between the objects, and the subsequent rate of change of a is proportional to $1/a^5$. Consequently, the torque is ineffective unless the objects are close enough together to mitigate the a^8 or a^5 factor, at which point its proportionalities to the objects' masses, radii, and interior structure constants become significant. The tidal torque then works efficiently such that the orbit is synchronized and circularized on Myr timescales (typically within the pre-main sequence phase), set by the two objects' initial separation, eccentricity, and mass ratio (Zahn & Bouchet 1989).

The tidal dependence on stellar properties implies that for a population of identical binaries of a specific age, every orbit with a semi-major axis smaller than some specific

threshold will be completely circularized. That threshold would then move outward as that population ages and tides less efficiently move the wider binaries closer together; Mathieu & Mazeh (1988) even proposed using this mechanism to age-date binaries. In observational studies, that semi-major axis threshold is discussed in terms of the equivalent orbital period, denoted P_{circ} , below which all orbits are circularized. The P_{circ} threshold has been observed to range from ~ 2 days for high-mass binaries to ~ 12 days for solar-type binaries (§1.4.1 vs. §1.4.2). The larger radii of high-mass stars improves the efficiency of tides, increasing the P_{circ} at which they are effective, but the stellar lifetimes of the high-mass stars are so short that circularization can only occur for the closest pairs before evolution removes one or both components from the tidal process. In the same vein, Meibom & Mathieu (2005) showed that P_{trans} (analogous to P_{circ} , as discussed below) for G-type stars in clusters increases with increasing population age, from ~ 7 days (Pleiades) to 10 days (Solar neighborhood) to 16 days (halo).

One complication in the discussion of P_{circ} is that the timescale for circularization of a particular binary depends strongly on its mass ratio; for example, Mazeh (2008) pointed out that the mass ratio can change the circularization timescale by a factor of 8, corresponding to a factor of 1.5 in P_{circ} . Mass ratio can vary significantly even among relatively uniform samples like “solar-type stars,” thus if we have a rich data set we are unlikely to find a P_{circ} for which zero orbits above it are circular (and zero orbits below it are eccentric). Most likely this ambiguity is why techniques to determine P_{circ} for an observed population vary substantially, adding difficulty to comparing results across studies. To address this issue,

Meibom & Mathieu (2005) proposed a “transition period” P_{trans} replace the concept of P_{circ} : below P_{trans} , the *average* eccentricity of the set is zero, and above it the *average* eccentricity rises exponentially. This approach may be important if the results of this thesis show signs of a transition period rather than P_{circ} cutoff.

1.4 Trends Observed for Stellar Multiples and their Properties

Among main-sequence field stars, observations have established that multiplicity increases with stellar mass. At the lowest masses, $\sim 30\%$ of M dwarfs are multiples, as found initially in a sample of 27 M dwarfs within 5 pc in (Henry & McCarthy 1990), to the much larger sample of more than 1000 M dwarfs over the entire sky in (Winters et al. 2019). In contrast, at the highest masses of the O and B stars, $>90\%$ are multiples, as shown by Mason et al. (1998, 2009) and later (Moe & Di Stefano 2017). Solar-type stars have multiplicity rates of $\sim 50\%$ (e.g., Raghavan et al. 2010), falling between the rates for the highest and lowest mass stars. This overall trend of multiplicity with mass is summarized in Figure 1 in Offner et al. (2022), reproduced here in Figure 1.3.

Whereas the multiplicity fraction is well-determined for stars along the main sequence, trends among the *properties* of these multiples are not yet evenly established for all stellar masses or spectral types. As discussed in §1.2, the distributions of mass ratios, semi-major axes, orbital periods, and eccentricities are our strongest observational clues to the how these systems formed and evolved dynamically. In this section we review what observations have shown to date about how stellar multiples’ properties compare between systems of different

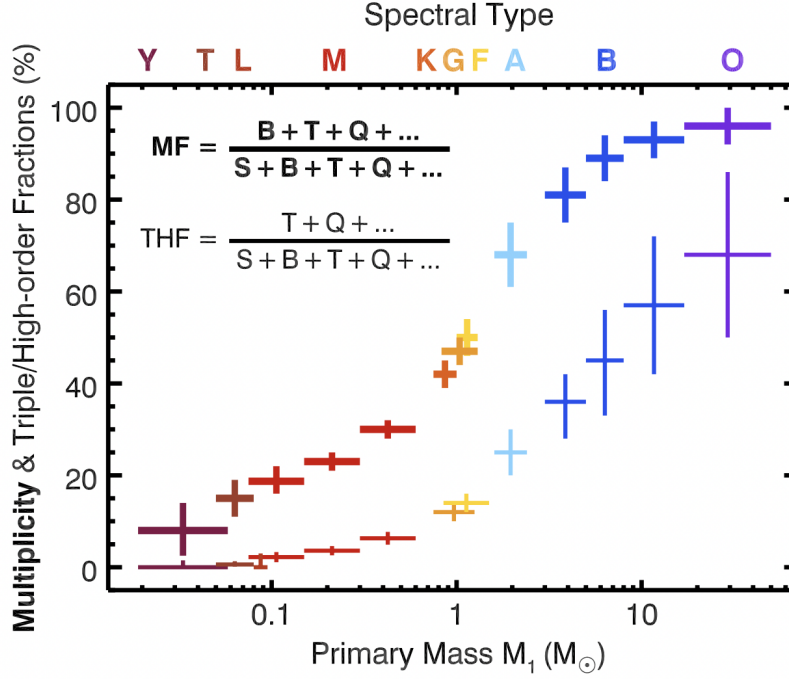


Figure 1.3 Multiplicity (or “multiplicity fraction”) of stars as a function of spectral type, reproduced here from Figure 1 of Offner et al. (2022) using a wide accumulation of stellar surveys. The thick lines represent multiplicity of all types, while the thin lines reflect only the fractions of triples/higher-order multiples (“THF;” not discussed here). The letters along the top indicate the approximate spectral type of each stellar mass.

masses.

1.4.1 Properties of High-mass Multiples

Multiples among the O, B, and A stars (main sequence stars with masses of at least $1.5 M_\odot$) have been studied extensively through spectroscopy, long-baseline interferometry, adaptive optics, and eclipsing binaries. These techniques are generally sensitive to companions $\gtrsim 10\%$ the mass of their primary star ($q \gtrsim 0.1$). For the highest-mass stars in this group, the O stars, binary and dynamical evolution quickly and strongly alters the multiples’ properties (Hoogerwerf et al. 2001), so multiplicity studies often avoid targets that have undergone

evolution by considering only O stars that are members of young star clusters.

Earlier notable surveying of the highest-mass stars was done by Mason et al. (1998), then updated in Mason et al. (2009), who established these systems’ remarkable multiplicity and used those results to infer their significant degree of dynamical evolution. Nearly a decade later, Moe & Di Stefano (2017) presented an even more comprehensive survey of these stars by combining data from several earlier studies (e.g., Abt et al. 1990; Shatsky & Tokovinin 2002; Rizzuto et al. 2013). They showed that separations between companions and primary stars are distributed uniformly in $\log a$, known as “Öpik’s law” (Öpik 1924). All three spectral types in this group also follow a similar trend for companion mass ratios, keeping in mind the *caveat* that these surveys miss the lowest mass companions: at close separations ($\lesssim 0.5\text{--}1$ AU) the mass ratio distribution is uniform, at moderate separations (1–100 AU) it peaks at $q \approx 0.3$, and at wide separations ($\gtrsim 100$ AU) mass ratios are skewed toward small mass ratios (Offner et al. 2022, and references therein). On top of these trends, however, these systems have an excess of “twin” companions ($q \gtrsim 0.95$) that is strong at the closest separations and small but still significant at moderate separations.

The eccentricities of high-mass multiples in Moe & Di Stefano (2017) generally increased as P_{orb} increased, with this rise somewhat steeper for more massive primary stars ($\gtrsim 5 M_{\odot}$). We will show this distribution and discuss it in detail in Chapter 6. For systems with $P_{\text{orb}} \lesssim 15$ days this P_{orb} vs. e trend is partly related to their ages: the systems with B and A primaries are significantly older than O stars, and thus have had more time to accumulate the effects of the tidal forces that are felt at those separations. Beyond $P_{\text{orb}} \gtrsim 15$ days,

higher-eccentricity orbits for higher-mass systems can only be explained by these systems being systematically more eccentric at formation. Moe & Di Stefano (2017) proposed two potential explanations:

- The more massive stars have a higher frequency of triples and higher-order multiples, which more efficiently drive their eccentricities upward during the first ~ 1 Myr of the pre-main sequence phase.
- All O, B, and A systems are born with high eccentricities, but the less massive stars spend more time contracting during pre-main sequence and thus more time under the influence of tides. This lets them accumulate more eccentricity damping than their O-star cousins. Similarly, circumstellar disks are longer-lived around less massive stars, adding another potential source of eccentricity damping.

The idea that evolution within disks is a factor is also well supported by the observation that twins are more common at tighter separations, as the accretion that comes with interactions between companion and disk drives a system’s mass ratio toward unity (§1.3).

1.4.2 Properties of Solar-mass Multiples

The F, G, and K dwarf stars (main sequence stars with masses of $0.6\text{--}1.5 M_{\odot}$, frequently grouped together as “solar-type”) are established to have a multiplicity rate of $\sim 50\%$ (Duquennoy & Mayor 1991; Raghavan et al. 2010).

The distribution of their separations is normal in logarithmic space (“log-normal”), peaking at ~ 40 AU (Raghavan et al. 2010; Tokovinin 2014), although certainly increasing to

smaller separations in linear space, with more companions found per AU within 10 AU than at any other distance. The mass ratio distribution over all separations is roughly uniform, but at the closest separations the occurrence of “twin” companions ($q \gtrsim 0.95$) is $\sim 30\%$ higher than the uniform distribution. This excess decreases but persists at intermediate separations, and even at wide separations there remains a notable twins excess (El-Badry et al. 2019). This trend of twin companions is consistent with these companions forming from disk fragmentation (§1.2.2) and migrating inward or outward (§1.3).

The most complete eccentricity distribution for solar-type multiples is presented by Raghavan et al. (2010), who completed a comprehensive multiplicity study of F, G, and K dwarfs within 25 pc, with companions revealed using multiple observational methods. We will show and discuss this distribution in detail in Chapter 6. To summarize, they showed that the eccentricities of solar-type multiples generally increase as orbital period increases, with long orbits ($P_{\text{orb}} \gtrsim 100$ days) being rarely circular, and very short orbits ($P_{\text{orb}} \lesssim 12$ days) exclusively circular for systems with no signs of youth. The latter structure is due to tidal forces, which are so efficient those smaller semi-major axes that they have circularized every close orbit in that field-age population (§1.3).

The upper envelope to the Raghavan et al. (2010) P_{orb} vs. e distribution is well below the limit at which two stars would collide at periastron, and is most likely set by early dynamical interactions with neighboring systems. They also noted that the highest-eccentricity systems at each P_{orb} are triples, thus these extreme eccentricities are the result of the triple-specific Kozai-Lidov cycles (§1.3).

1.4.3 *Properties of Low-mass Multiples*

The low-mass multiples that are the subject of this work include systems with primary star masses of 0.075–0.60 M_{\odot} — these are main sequence dwarfs with M and L spectral types. Their companions have the same spectral types, with the exception of the few percent that are the rare substellar brown dwarfs. Pre-2000 efforts targeting these stars struggled with their intrinsic faintness, limiting the current availability of historical and long-term data coverage. As newer instruments made lower-mass stars accessible, efforts focused on them for exoplanet searches, intentionally avoiding targets with stellar companions in the process. The result is that stellar multiples among M and L dwarfs are somewhat less well-studied than their solar-mass neighbors, particularly for the orbits of those multiples.¹

Low-mass multiples are a particularly critical population to study, however, because they are ubiquitous (Henry et al. 2006, 2018) and encompass a wide range of stellar physics that presents persistent challenges to interior models (e.g., Dieterich et al. 2021; Brandner et al. 2023). Their interiors may be partially or fully convective, depending on their mass (Chabrier & Baraffe 1997; Jao et al. 2018), and these stellar structures are partly to blame for the breakdown of the standard stellar rotation vs. age relations at M dwarf masses (Newton et al. 2016; Douglas et al. 2017; Pass et al. 2022). At the same time, these stars have grown in popularity as targets of searches for habitable exoplanets (e.g., Irwin et al. 2009; Law et al. 2011; Muirhead et al. 2018; Ribas et al. 2023). This combination of persistent challenges

¹Most surveys targeting low-mass stars are sensitive to brown dwarf companions as well, and it is challenging to exclude them entirely from the results. Because the brightness of the lowest-mass stars drops steeply with mass below $\sim 0.1 M_{\odot}$ (e.g., Benedict et al. 2016), and because brown dwarfs lose brightness over time as they cool, it is generally not possible to determine whether or not a very low-mass companion is above or below $0.075 M_{\odot}$ without precisely measuring its dynamical mass.

and the demand for exoplanet host star characterization escalates our need to understand how these stars form and how they affect their immediate environments on Gyr timescales.

Winters et al. (2019) completed the most comprehensive survey of nearby M dwarf multiplicity to date by combining several previous studies with their own imaging observations. They found that 27% of M dwarfs are in systems of multiples, with this fraction smaller for less massive vs. more massive M dwarf primaries. Their separations are log-normally distributed around 20 AU, somewhat closer than the 40 AU peak of solar-type binaries (Raghavan et al. 2010). Limiting the sample to primary stars $\lesssim 0.15 M_{\odot}$ produced an even closer peak at ~ 4 AU. As with the solar-type multiples, in linear separation space there are more companions orbiting M dwarfs per AU at the smallest separations than at wider realms. Because comprehensive surveys for the closest companions are still underway (e.g., with radial velocity searches), the peak of the separation distribution will most likely be revised as further inward in future work.

The mass ratios of Winters et al. (2019) were uniformly distributed for M dwarfs $\gtrsim 0.3 M_{\odot}$ and skewed toward higher q for lower-mass M dwarfs. This trend is not due to formation or evolution, but rather the result of the survey’s cutoff in mass at the end of the main sequence, as that exclusion leaves the lowest-mass M dwarfs without the possibility of companions of $q \lesssim 0.5$. Although the survey was sensitive to substellar companions to some stars, those that were detected were excluded from the multiplicity results and not corrected for observational biases. After taking this effect into account, no excess of twins is evident in the M dwarf mass ratios, although the distributions are not broken down by separation. This contrasts

with the twins excesses seen in different separation regimes around solar-type and massive multiples (§1.4.2 and §1.4.1), potentially indicating a very different formation or dynamical history for these lower-mass systems.

The Winters et al. (2019) multiples did not have orbits, and thus no eccentricities determined, but a preliminary eccentricity distribution was presented by Udry et al. (2000) using 48 binaries characterized via radial velocities. Their P_{orb} vs. e plot was similar to the solar-type distribution, with $P_{\text{orb}} \gtrsim 11$ days orbits exclusively eccentric and orbits with $P_{\text{orb}} \lesssim 10$ days tidally circularized. For the lack of circular orbits they suggest a range of explanations, e.g., circular orbits may be unlikely to form, or star-disk interactions may have increased the systems’ eccentricities (modeled by Lubow & Artymowicz 2000). These scenarios are difficult to corroborate further without information about the systems’ mass ratios.

This picture of low-mass multiples was supplemented at the very end of the main sequence by Dupuy & Liu (2017), who presented 27 orbits for systems with total masses $0.2 M_{\odot}$ and less, including brown dwarfs. They showed an eccentricity distribution that peaks strongly at $e \approx 0.1$, significantly lower than the uniform distribution for solar-type stars from Raghavan et al. (2010) and the preliminary M dwarf distribution of Udry et al. (2000). Underscoring that result, their P_{orb} vs. e plot shows $\sim 20\%$ of their very low-mass systems with $P_{\text{orb}} \gtrsim 5$ years have $e \lesssim 0.1$ — whereas these orbits were entirely absent among the solar-type systems with $P_{\text{orb}} \leq 30$ years, and at greater P_{orb} only subsets of higher-order multiples had $e \lesssim 0.1$.

Although the Dupuy & Liu (2017) survey design did not allow them to draw conclusions on the distribution of mass ratios or prevalence of twin binaries, their eccentricity results

indicate a clear difference in the formation and dynamical evolution of the lowest-mass stars and brown dwarfs vs. the solar-type stars. The potential explanations mirror those of the analogous situation with the high-mass stars (§1.4.1): either the two classes of objects have different distributions of orbit shapes from birth, or the distributions are initially similar but evolve differently due to different eccentricity-damping environments. Considering that observational evidence shows circumstellar disks persist for much longer around M dwarfs vs. higher-mass stars such as G dwarfs (e.g., Mamajek 2009; Ribas et al. 2015, and references therein), the latter explanation is perhaps more likely.

Extrapolating the Dupuy & Liu (2017) results to the slightly more massive M dwarfs is hazardous due to the prevalence of brown dwarfs in their sample, which may form from the similar processes as low-mass stars but with significant deviations that affect their final statistics (Whitworth et al. 2007; Ma & Ge 2014). Differences in post-formation evolution of stars vs. brown dwarfs are also inevitable because a star’s luminosity is higher and sustained, whereas a brown dwarf starts fainter and diminishes in output forever. This will have significant impacts on the temperatures, viscosities, and ultimately the lifetimes of the disks in those young systems, as photoevaporation is the mechanism that ultimately dissipates the disks (Clarke et al. 2001).

Given our relatively poor understanding of M dwarf orbital architectures, we have undertaken this study of the companions to low-mass stars. Our goals are to establish the distribution of P_{orb} vs. e for these systems and identify any trends (or absence of trends in this distribution with respect to primary stars, secondary stars, and mass ratios. By

accumulating many of these orbits and carefully distinguishing the stellar companions from the brown dwarfs, we can explore the extent to which those populations are similar to or different from the outcomes from formation and evolution for more massive stars.

CHAPTER 2

Defining the Sample of Nearby M Dwarfs

To understand how well our results represent the true population of M dwarf multiples, we must carefully define the sample of objects that we will consider in this group. This task requires defining the observational attributes of M dwarf stars, then identifying the list of stars to be targeted and monitored for detecting orbits.

In fact, our samples for orbit monitoring extend slightly beyond the end of the M spectral sequence and into the early L types because we adopt an astrophysical cutoff — the line between stars and brown dwarfs — rather than lettering in a spectral sequence. RECONS member Serge Dieterich determined this cutoff using the minimum in the radius sequence at spectral type L2.0V (Dieterich et al. 2014), and this is the line we will adopt as the end of the stellar main sequence. Thus, our sample is really the “red dwarfs” rather than limited to “M dwarfs,” although hereafter we refer to the sample as M dwarfs.

Also note that in this work, we are studying systems in which the primary is a main sequence M dwarf, although we include a few cool subdwarfs and young stars that are of spectral type M.

Ideally, we would define the M dwarf by mass, as the M dwarfs include all stars 62% the mass of the Sun or less (Benedict et al. 2016). But mass is not a directly observable quantity or able to be determined model-independently for most systems, hence we need to use other properties that strongly depend on mass. In this thesis we use absolute magnitude as a proxy for luminosity and thus mass, and if necessary we also consider colors from several

combinations of photometric bandpasses.

In this chapter we first discuss in §2.1 the stellar distances from which each star’s absolute magnitude will be derived. The absolute magnitude limits defining an M dwarf are determined in §2.2, which involves a reconciliation of mass-luminosity relations (§2.2.1) and then an extension of those relations to additional bandpasses (§2.2.2). Finally, in §2.3 we review the sample resulting from these definitions. This broad sample will be the set from which we will draw smaller samples for each observing program.

2.1 Setting Distance Limits

In order to derive the absolute magnitudes corresponding to M dwarf masses, we must establish reliable distances to an ensemble of *bona fide* M dwarfs. Although there are several methods to determine distances to astronomical objects, for the most nearby stars the most accurate method is trigonometric parallax.

Trigonometric parallax is a purely geometric technique, requiring no assumptions about the properties of the star of interest. The observer measures the angle between the Earth, nearby star of interest, and the Sun — known as the *parallax angle* — and the distance to the star is proportional to the inverse of that angle following the small-angle approximation. If the angle is expressed in arcseconds and the Earth-Sun distance is 1 AU, then the constant of proportionality is 1.0, giving the formula the convenient form $d = 1/\pi$ (where d is the distance in parsecs (pc) and π is the trigonometric parallax angle in arcseconds).

The strength of this method is its simplicity, but the catch is that the largest parallax

angles in our neighborhood (for the most nearby stars) are tenths to hundredths of an arc-second in size, which itself is only $1/3600$ of a degree on the sky. These tiny angles made parallaxes impossible to measure until the 1830s, when they were measured independently by Friedrich Bessel, Wilhelm Struve, and then Thomas Henderson, after several centuries of astronomers’ dedicated efforts toward that goal (Perryman 2012, and references therein). Measuring parallaxes for stars beyond a few tens of parsecs required late-20th century techniques and instrumentation (in particular, charge-coupled devices or CCDs), and achieving precision better than $\sim 5\%$ for stars beyond 100 parsecs was not possible until the space-based astrometric mission *Hipparcos* and, more recently, the space-based *Gaia* mission (Gaia Collaboration et al. 2016). Now that we have moved beyond the instrumental difficulties of the 1800s and have entered an era of highly accurate and precise astrometry, the straightforward geometry underpinning parallax makes it the ideal technique for measuring stellar distances, especially for stars in our immediate neighborhood.

In every sample in this work for which we have set a distance limit, each target is required to have a trigonometric parallax placing its distance within that stated limit. All samples considered here are larger than $0''.040$, or 40 milliarcseconds (mas), corresponding to a distance of 25 pc.¹ The two primary sources of parallaxes used here are the RECONS program and the *Gaia* mission due to these efforts’ reliability and precision.

The RECONS astrometry program began in 1999 on the 0.9m CTIO/SMARTS² telescope, and throughout its tenure it has focused almost exclusively on red dwarfs within 25

¹A few systems considered here are slightly beyond 25 pc, but these are not used for statistical treatments.

²The Small and Moderate Aperture Research Telescope System (SMARTS) at Cerro Tololo Inter-American Observatory (CTIO) near La Serena, Chile.

pc. RECONS parallaxes are measured relative to reference grids of background stars, then corrected to absolute parallaxes using the distances to the reference stars. The program continues regular observations on a volume-complete sample of Southern Hemisphere red dwarfs with parallaxes of at least 60 mas (within 16.7 pc), a distance which provides ~ 500 M dwarfs that can each be observed a few times per year. At the thesis sample definition stage in August 2018, RECONS had determined parallaxes for 482 M dwarfs, and a further 155 M dwarfs were expected to have enough data to measure their parallaxes by the thesis conclusion in 2023.

Gaia is a space telescope launched in 2013 for the purposes of measuring parallaxes and other astrometry for stars across the entire sky. Their Data Release 2 (DR2) in April 2018 gave parallaxes for 1.7 billion objects, including for ~ 3000 red dwarfs within 25 pc, with a median precision of 0.08 mas. *Gaia* parallaxes are absolute, as they are linked to a reference grid of distant quasars having zero parallax. Comparison between RECONS and *Gaia* results in Vrijmoet et al. (2020) showed that the *Gaia* and RECONS parallaxes were reliably consistent for single stars to within ~ 2.5 mas.

To be included in any sample discussed here, at least one of those two programs must have measured the target star’s parallax to be within the stated distance limit. Other sources of parallax measurements (e.g., *Hipparcos*) are only considered if there is no RECONS or *Gaia* measurement for that object. A weighted average of the RECONS and *Gaia* parallaxes is not used because, at the time that the observational samples were established for this thesis, the available *Gaia* results showed that parallaxes for unresolved multiples tended to deviate

from the RECONS values by $\gtrsim 2.5$ mas, often $\gtrsim 5$ mas (Vrijmoet et al. 2020).

2.2 Deriving Absolute Magnitude Limits for M Dwarfs

In this section we establish the absolute magnitudes corresponding to the most and least massive M dwarf stars. These photometric limits are then used to select a large sample of M dwarfs to monitor for orbital motion during the observing campaigns detailed in Chapters 3 and 4. In short, the procedure is to use an empirical mass-luminosity relation to estimate masses of a sample of M dwarfs, then use the photometry of those systems in other bandpasses to derive those bandpasses' absolute magnitude limits corresponding to specific masses.

First, we gathered an ensemble of 327 *bona fide* M and L dwarf stars within 25 pc that have no known close or unresolved companions. Objects with spectral types of L2.5 or cooler were considered substellar and thus excluded, with this cutoff based on the results of Dieterich et al. (2014). Requiring that these sources be single, without companions, ensured that the photometric limits were representative of individual objects rather than unique combinations of two or more luminous bodies. Although most of these sources were stars, brown dwarfs were not excluded at this stage because one goal of this exercise was to determine the line dividing stars from brown dwarfs.

Of the 327 objects, 163 were selected from systems on the RECONS astrometry program (discussed in detail in Chapter 3). Selecting from the astrometry program allowed us to exclude targets that showed evidence of an unresolved companion orbiting on multi-year to multi-decade scales. The median baseline of these 163 RECONS systems was 18.55 years,

and the shortest-observed system had a baseline of 6.58 years. This list was supplemented by 164 single stars from the RECONS 25 pc Database, which also includes systems well-vetted for companions, bringing the total sample to 327. To ensure that this final *bona fide* single-star sample would be suitable for deriving absolute magnitude cutoffs and would be free from any remaining unseen companions, we imposed the following requirements on all stars:³:

- *Gaia* DR2 RUWE ≤ 1.4 . Reduced unit weight error, or RUWE, is a measure of the deviation between a star's *Gaia* DR2 astrometry and the single-star model fit to that data (Lindgren et al. 2018). For stars with no orbital motion over *Gaia* DR2's 2.4 years of observations, RUWE ≈ 1 .
- no flags indicative of youth in the RECONS 25 pc Database or astrometry program
- measured *V* magnitude available from RECONS or another similar source (Reid et al. 2003; Weis 1991, 1996)
- measured *K* magnitude available from 2MASS (Skrutskie et al. 2006; Cutri et al. 2003)
- confirmed spectroscopically to be an M or L dwarf in systematic spectroscopic surveys of low mass dwarfs, including RECONS efforts, Reid et al. (1995), Hawley et al. (1996), and Gray et al. (2003, 2006)

The full sample of 327 *bona fide* single M and L dwarfs is shown in the Hertzsprung-Russell diagrams (HRDs) of Figure 2.1. Red and dark red symbols indicate sources chosen

³*Gaia* DR2 results were not used in creating this initial sample because stars were not as well-vetted for companions as for the RECONS astrometry program and RECONS 25 pc Database.

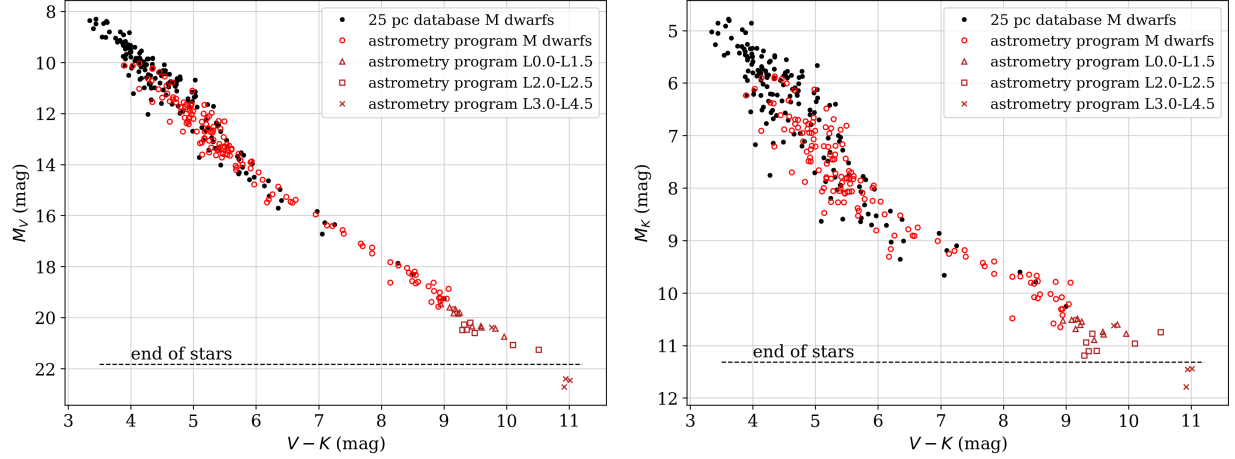


Figure 2.1 Hertzsprung-Russell Diagrams in $V - K$ vs. M_V (left) and M_K (right), showing stars within 25 pc that have no evidence of multiplicity. All stars have spectral types confirmed using a consistent technique (see text), distances from *Gaia* DR2, *Gaia* DR3 RUWE < 1.4 , and no evidence of a perturbation in RECONS astrometry (if RECONS data are available). Light red symbols are M dwarfs from the RECONS astrometry program, those in dark red are L dwarfs from the RECONS astrometry program, and those in black are sources from the RECONS 25 pc Database that are not on the RECONS astrometry program. Dashed horizontal lines indicate the end of the main sequence as defined for this work (§2.2.2).

from the RECONS astrometry program, and black symbols are from the RECONS 25 pc database. Additional lines shown in that Figure are discussed later in §2.2.1.

2.2.1 One MLR to Rule Them All

To pinpoint the absolute magnitudes corresponding to the highest and lowest mass M dwarfs, we use the mass-luminosity relations (MLRs) of Benedict et al. (2016), which provides conversions between mass and V and K absolute magnitudes specifically for M dwarf stars. These empirical MLRs are based on dynamical masses of 46 M dwarfs, making them the most comprehensive relations in a multi-decade series of incrementally improving M dwarf MLRs (Popper 1980; Henry & McCarthy 1993; Henry et al. 1999; Delfosse et al. 2000). The

similarly precise MLR of Mann et al. (2019) was not used for this sample because it offers a relation only in K band, and because it is based on mass sums rather than individual dynamical masses.

Because Benedict et al. (2016) provides two MLRs (V and K band), estimating the mass of any one target requires choosing between one of these two relations. This choice is not necessarily straightforward: in K band the M dwarfs show less photometric scatter from stellar activity, resulting in a tighter relation between dynamical mass and M_K than for M_V . At V , however, the M dwarfs span twice as many absolute magnitudes, allowing any M_V measurement to provide relatively more leverage in placing an object at a given mass compared to an M_K measurement.

The sample selection discussed below in §2.3 required a single relation to be applied to all targets. To determine the best choice, we estimated the mass of each target in the *bona fide* single M and L dwarf sample using their M_V magnitudes, then we estimated their masses again using their M_K magnitudes. The comparison of those values is shown in the top panel of Figure 2.2. Targets with magnitudes outside the stated limits of the Benedict et al. (2016) MLR (i.e., with $M_V > 19$ or $M_K > 10$) were excluded from this part of the analysis, which eliminated all L dwarfs and reduced the sample to 289 stars. The comparison (Figure 2.2, top panel) showed significant scatter around the 1:1 line with masses from M_K often larger than masses from M_V . These trends did not depend on whether the target was drawn from the RECONS 25 pc Database or the astrometry program with its extra years of monitoring, hence undetected multiplicity was unlikely to play a role.

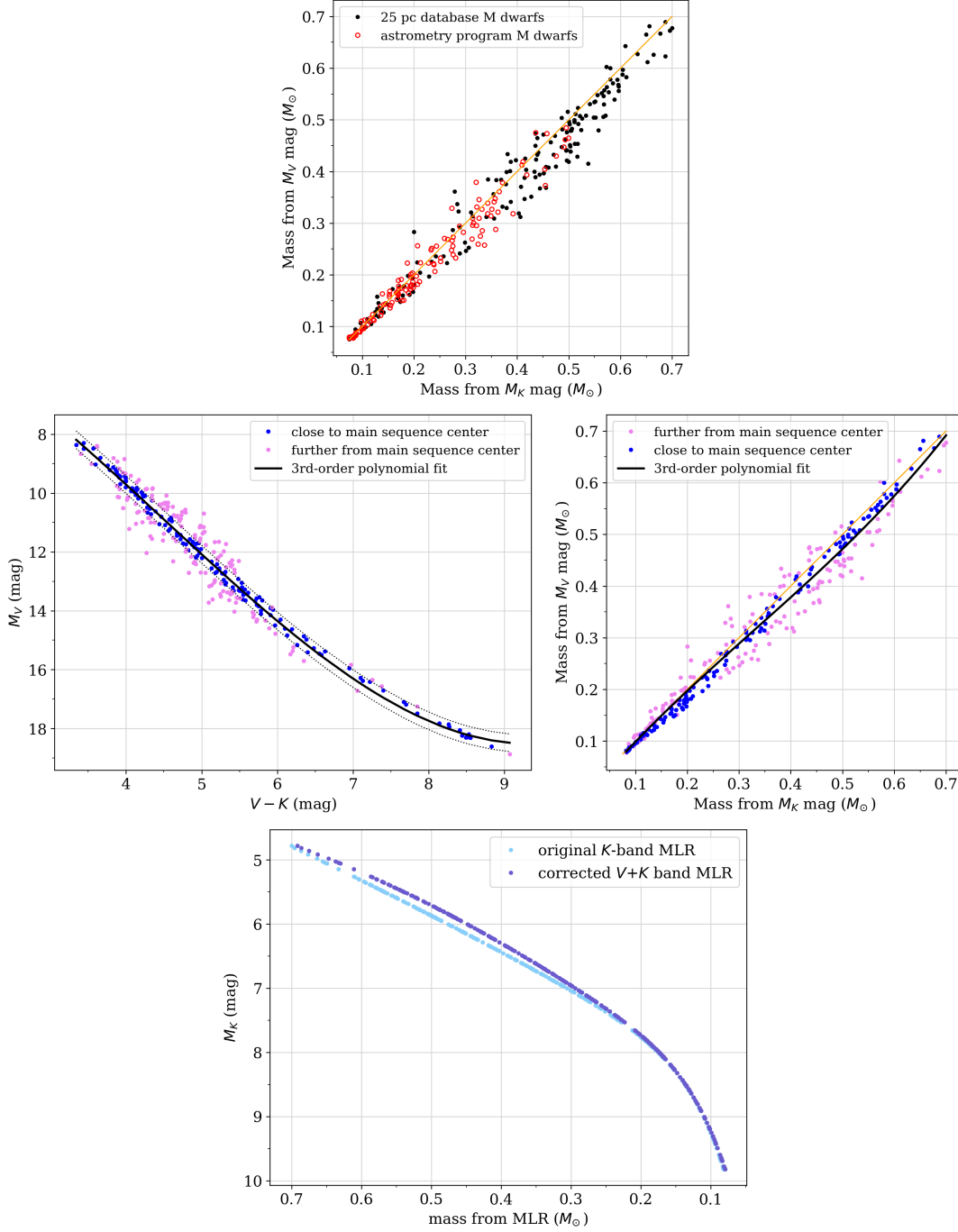


Figure 2.2 *Top:* Masses of 289 *bona fide* single M dwarfs within 25 pc, as determined from their M_V vs. as determined from M_K . The orange line indicates the 1:1 relation. *Middle left:* HRD of the same targets, with a 3rd-order polynomial fit marked in black. The colors indicate the stars' deviation from that fit. *Middle right:* The same mass vs. mass plot as at top, but with colors marked as at middle left. The black line is a 3rd-order polynomial fit, and the orange line again is 1:1. *Bottom:* The K -band Benedict et al. (2016) MLR (light blue) and our corrected $V+K$ -band MLR (dark blue).

Next, we constructed the HRD of these points in terms of $V - K$ and M_V , and fit a 3rd-order polynomial to the main sequence using a standard least-squares algorithm (Python’s `numpy.polyfit` package, default settings). This HRD is shown in Figure 2.2, middle left panel, with the polynomial fit in black, and the points colored based on their proximity to the main sequence fit — those within 0.3 magnitudes are in blue, and those outside 0.3 magnitudes are pink. The point color thus indicates whether each star is near the center of the main sequence or more scattered.

Finally, in the middle right panel of Figure 2.2 we again plotted mass from M_V vs. mass from M_K with the points colored according to the HRD position/scatter from the Figure 2.2 middle left panel. This second mass vs. mass plot shows that the scatter in mass estimate roughly tracks with scatter on the HRD. Below $\sim 0.25 M_\odot$, the HRD-scattered stars show consistently higher mass from M_V than the HRD-tight stars; this may reflect the effects of metallicity, especially because for $M_V \gtrsim 13.5$ on the HRD the scattered points are always bluer than the main sequence fit.

The magnitude of the scatter in Figure 2.2 indicates that it would be hazardous to use either the V -band or K -band MLR alone; the mass estimate for any single system could vary by up to $0.1 M_\odot$ depending on the bandpass used, and the direction of this variation is not predictable. To compromise between these relations, we fit a 3rd-order polynomial to the full set of M_K mass vs. M_V mass values, including the scattered points as well as the tighter main sequence points. This fit is shown in Figure 2.2, middle right panel, as the thick black curve. The polynomial order was set at 3rd to capture the broad trends without inducing

any additional features. In testing, 4th-order (and greater) polynomials added curves that were not visible by eye in these data; thus, higher orders did not provide significantly better fits. Going forward, then, a system’s mass can be estimated by first determining its mass from M_K using the MLR in Benedict et al. (2016), then choosing the corrected value of mass at that M_K from the polynomial fit of M_K mass vs. M_V mass.

2.2.2 Extending the MLR to New Bandpasses

Although the Benedict et al. (2016) MLRs provide mass estimates for M dwarfs using their M_V and M_K values, later in the sample construction we need to draw a deeper pool of targets from larger catalogs with measurements in other, different bandpasses. In this section we determine absolute magnitudes at the $0.62 M_\odot$ highest mass and $0.075 M_\odot$ lowest mass points for M dwarfs in the *Gaia* G , B_G , and R_G bands, as well as in the Johnson-Kron-Cousins I band. As discussed later in this section, a different process will be needed for the $0.62 M_\odot$ limit vs. the $0.075 M_\odot$; we thus begin with the $0.62 M_\odot$ limit.

For stars in the *bona fide* single M dwarf sample bright enough to apply the Benedict et al. (2016) MLRs ($M_V < 19$ mag and $M_K < 10$ mag), we estimated their masses using the $V+K$ corrected MLR discussed in §2.2.1. We then collected their *Gaia* and I band photometry measurements, and Figure 2.3 shows these stars’ absolute magnitudes in G , B_G , R_G , and I with respect to those mass estimates. For each of these bandpasses, we identified the nine stars with mass estimates within 10% of $0.62 M_\odot$, and took the median of their absolute magnitudes. We then adopted the $0.62 M_\odot$ absolute magnitude limits as the median magnitudes of “similar” stars in each bandpass. Table 2.1 lists the ranges of those

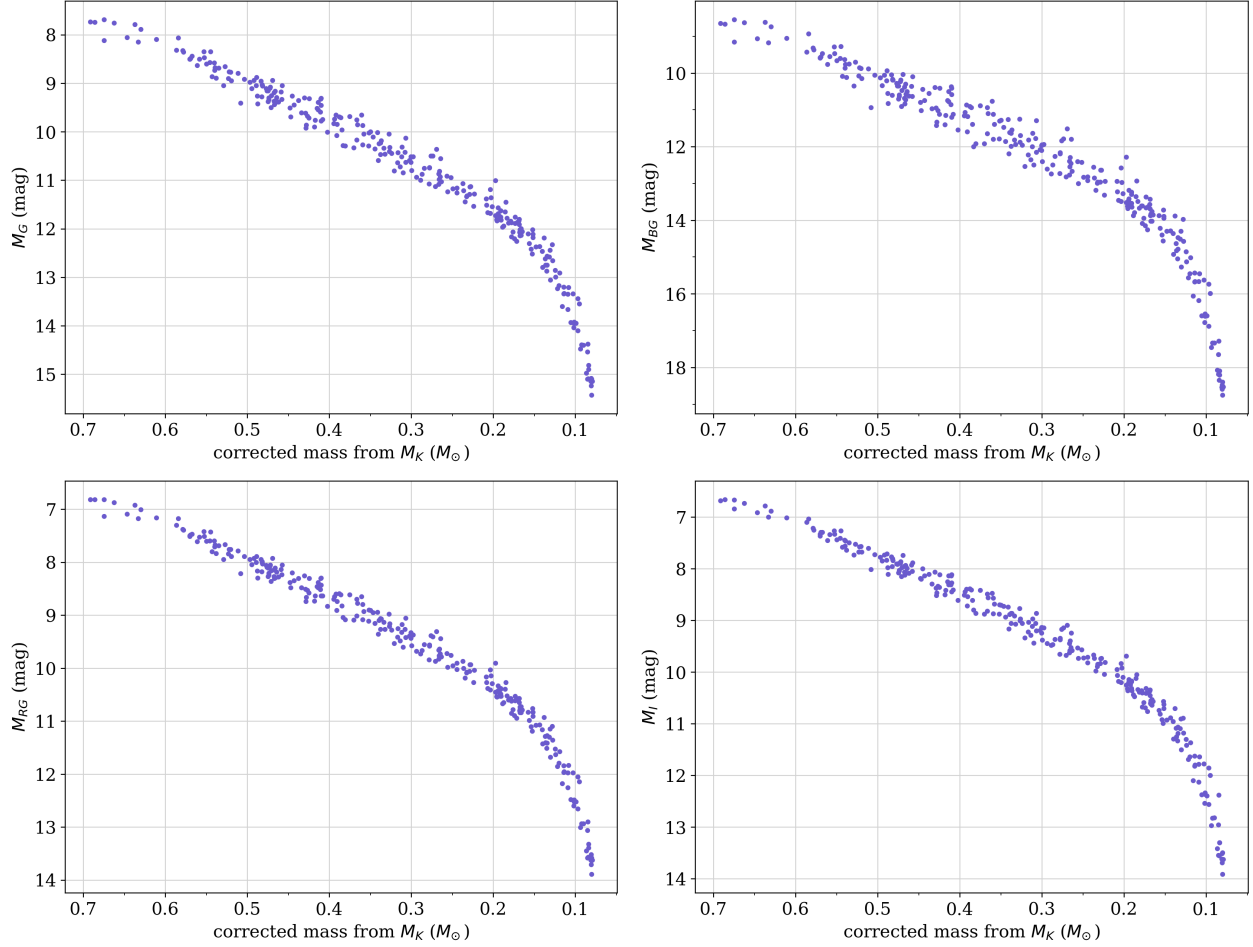


Figure 2.3 Estimated masses from the corrected $V+K$ -band MLR (§2.2.1) for 289 single M dwarfs plotted against their absolute magnitudes in (*left to right panels*) G , B_G , R_G , and I bands.

similar stars' magnitudes in each band and the subsequent adopted absolute magnitudes for $0.62 M_\odot$.

We applied the same procedure to the V and K bands as well, rather than taking the values offered by the Benedict et al. (2016) MLRs or the single $V+K$ corrected MLR derived in §2.2.1. This approach ensured we were applying a consistent technique to derive each mass limit. The Benedict et al. (2016) MLR offers V - and K -band absolute magnitude limits

Bandpass	Abs. mags within 10% of $0.62 M_{\odot}$	Adopted abs. mag at $0.62 M_{\odot}$	Abs. mag fit at $M_V = 21.825$	Abs. mag fit at $M_K = 11.318$	Adopted abs. mag at $0.075 M_{\odot}$
G	7.686–8.632	8.23	17.841	17.733	17.79
V	8.299–9.551	8.99	—	21.575	21.82
B_G	8.547–9.758	9.24	20.627	20.580	20.60
R_G	6.818–7.611	7.24	16.256	16.153	16.20
I	6.669–7.451	7.07	16.411	16.296	16.35
K	4.858–5.398	5.26	11.334	—	11.32

Table 2.1 Absolute magnitude ranges and key values used to determine the specific absolute magnitudes corresponding to $0.62 M_{\odot}$ and $0.075 M_{\odot}$, the highest and lowest masses adopted for M dwarfs. The final adopted magnitudes for those mass limits are highlighted in yellow.

marking the most and least massive M dwarfs — here we find that the resulting V -band absolute magnitude for $0.62 M_{\odot}$ is nearly identical to the Benedict et al. (2016) MLR (8.99 mag instead of 9.03 mag) and the K -band absolute magnitude is 0.06 mag brighter (5.26 mag instead of 5.32 mag). The difference between the original and corrected relations rises to ~ 0.25 mag between between $0.35 M_{\odot}$ and $0.60 M_{\odot}$ (Figure 2.2, bottom panel).

For the absolute magnitudes marking the end of the main sequence, we used the above process as a starting point, although not as the final result. Dieterich et al. (2014) established that the hydrogen-burning limit occurs around spectral type L2.5V. Comparing the M_V and M_K magnitudes of spectroscopically confirmed L dwarfs with the predictions for $0.075 M_{\odot}$ by the Benedict et al. (2016) MLRs shows that the MLRs’ predicted magnitudes of $M_V \sim 19$ and $M_K \sim 10$ are too bright for L2.5V. This is evident in the HRD of Figure 2.1, as the L2.0V–L2.5V dwarfs span $M_V = 20.0$ – 21.5 , and the sources around $M_V = 19$ all have M spectral types. The discrepancy between the MLR value and the spectroscopy value adopted here is unsurprising given that there are few stars with dynamical masses near the end of

the main sequence used in the MLR, coupled with the significant drop in flux for stars as masses decrease toward the end of the main sequence.

The L2.0V–L2.5V dwarfs significantly overlap with the L0.0V–L1.5V dwarfs, making it difficult to pinpoint precise absolute magnitudes corresponding to any one of those spectral types. In M_V as well as M_K there is, however, a significant gap between those sources and three of the four plotted L3.0–L4.5 dwarfs.⁴ This main-sequence gap is the expected observational result for the hydrogen-burning limit because the brown dwarfs below that point should cool and lose luminosity quickly over time, moving down and to the right on the HRD. Further establishing the stellar/substellar line is beyond the scope of this dissertation, thus we set the dividing line as the midpoint between the last object above the gap and the first object below the gap: at $M_V = 21.82$ mag and $M_K = 11.32$ mag.

We also need to establish this stellar/substellar line in the G , B_G , R_G , and I bandpasses. Figure 2.4 shows that most of the HRDs in these bands show similar gaps as seen in M_V and M_K , but the width and clarity of the gaps vary. In particular, the B_G HRD shows a turn-back in color near the end of the main sequence instead of a gap, wherein progressively less massive objects become more blue starting around \sim L2.0V. This turn-back occurs primarily because there are features in the spectra of the lowest mass red dwarfs that cause $B_G - K$ colors to reach a maximum value, before lower mass objects appear bluer in that bandpass combination. In addition, *Gaia* B_G measurements become less reliable for sources fainter than $B_G \sim 19$ mag, as illustrated in Figure 2.5. The variation in *Gaia* reliability with brightness means we need a more careful approach than the simple gap-midpoint applied

⁴Beyond type L2.5V, the V denoting main sequence stellar dwarf is not used.

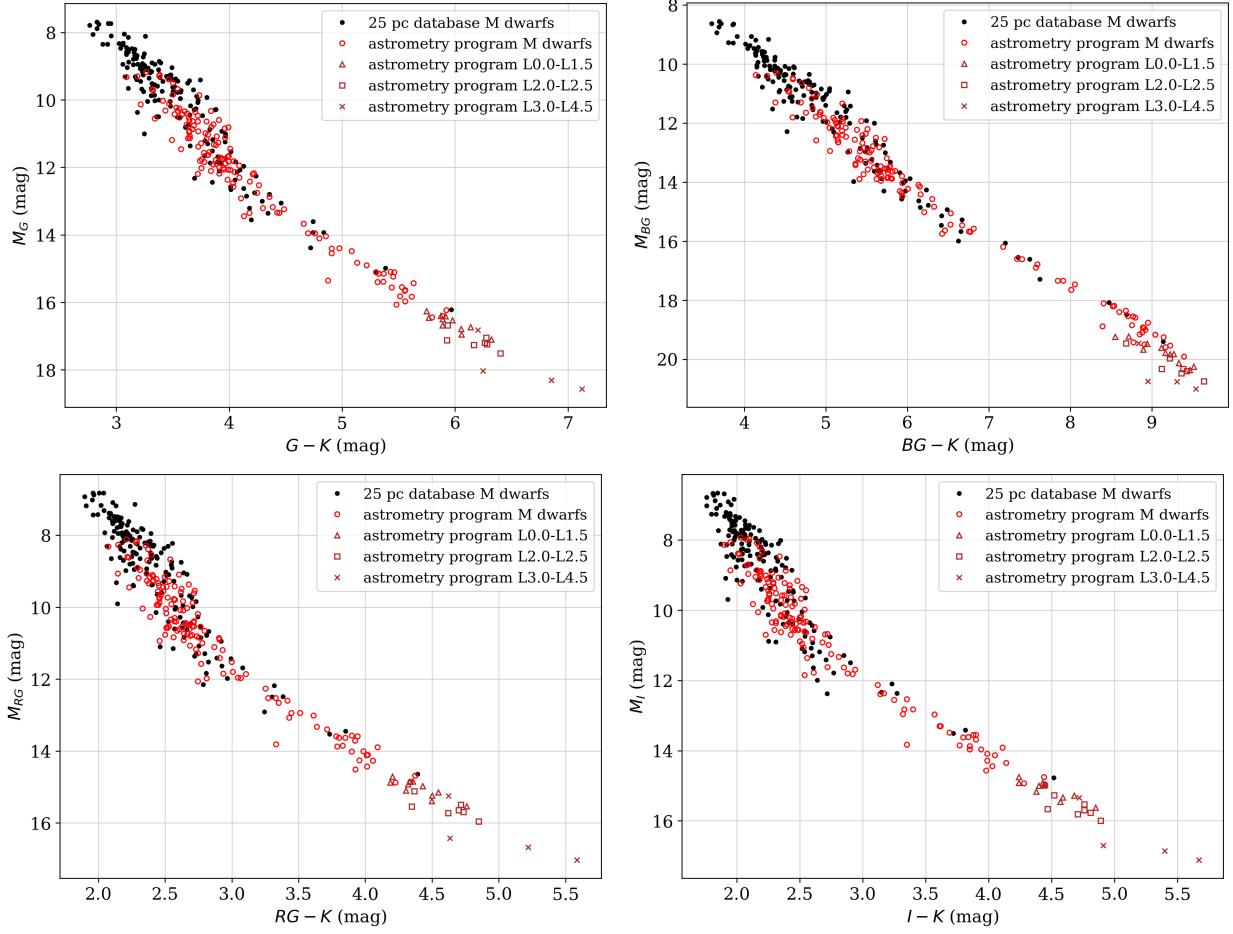


Figure 2.4 Hertzsprung-Russell Diagrams of the same set of nearby single M dwarf stars, shown in different filters with respect to K . From *top left* to *bottom right* are M_G vs. $G - K$, M_{BG} vs. $B_G - K$, M_{RG} vs. $R_G - K$, and M_I vs. $I - K$. The colors and symbols are the same as in Figure 2.1.

above for V and K .

The stellar/substellar lines in the bandpasses must be consistent with each other — e.g., an object identified as stellar according to M_V should not be marked as substellar according to M_{BG} . With this in mind, we used the stellar/substellar lines already set for M_V and M_K to determine the lines for M_G , M_{BG} , M_{RG} , and M_I . Figures 2.6 and 2.7 shows each of these absolute magnitudes plotted against M_V (left column) and M_K (right column) for

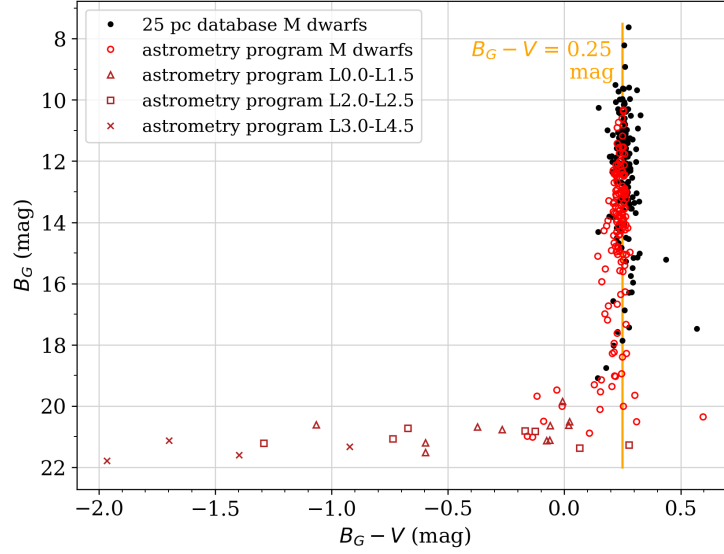


Figure 2.5 Differences between apparent B_G and V magnitudes as a function of B_G . The colors and symbols are the same as in Figure 2.1.

the *bona fide* single M and L dwarf sample, creating absolute magnitude-absolute magnitude relations for each bandpass. Dotted lines in the panels of Figures 2.6 and 2.7 indicate the stellar/substellar lines already established in M_V and M_K ; the goal here is to establish the alternate absolute magnitude corresponding to that M_V or M_K limit.

In each bandpass X , the stars' M_X values become more scattered around the M_V and M_K values at the end of the main sequence, making it hazardous to choose the M_X limit using a simple median or mean. Instead, we selected the intrinsically faintest 33% of the *bona fide* sample and fit a 2nd-order polynomial to those points' magnitude-magnitude relation (M_X - M_V or M_X - M_K). The fits are shown in each panel of Figures 2.6 and 2.7 as orange lines. We did not fit the full sample because the goal was to replicate the behavior for only these faint stars, regardless of how the brighter 66% were related. The relations in those areas are thus given by the orange polynomial fits, and the intersections with the established M_V or M_K

lines mark the M_X corresponding to those M_V or M_K . We adopted the stellar/substellar line for each bandpass X as the average of the two M_X - M_V and M_X - M_K intersections. The final values are listed in Table 2.1.

2.3 Verifying the Photometric M Dwarf Definitions

Applying the photometric limits in Table 2.1 to the *Gaia* DR2 catalog (requiring that each star meet the criteria in at least one bandpass) yields 5866 sources across the entire sky with parallaxes indicating they are within 25 pc. Because the goal of defining these limits was to establish samples for observing from facilities in the Southern Hemisphere, we drew only the 4565 sources in these limits below Decl. $+25^\circ$. Finally, we omitted white dwarfs from the sample by excluding sources with $B_G - R_G < 1.80$, leaving 3415 potential M dwarfs. Systems that included white dwarfs were excluded because each white dwarf was once a more massive star, making it ineligible for this work that focuses on systems with M dwarf primaries (discussed in §1.1).

Not every source in this extraction of the *Gaia* catalog corresponds to a true star, however, as *Gaia* DR2 contains many spurious entries due to source confusion and sources near the detection limits of the instruments. Although there are several methods to “clean” the *Gaia* catalog in an automated way by removing entries with poor-quality data flags, such as the “ABC” cuts (Lindgren et al. 2018, Appendix C), those methods are dangerous to apply to our particular target sample. This is because we are gathering very nearby stars for which photocentric motions from orbiting companions could be large enough to look like

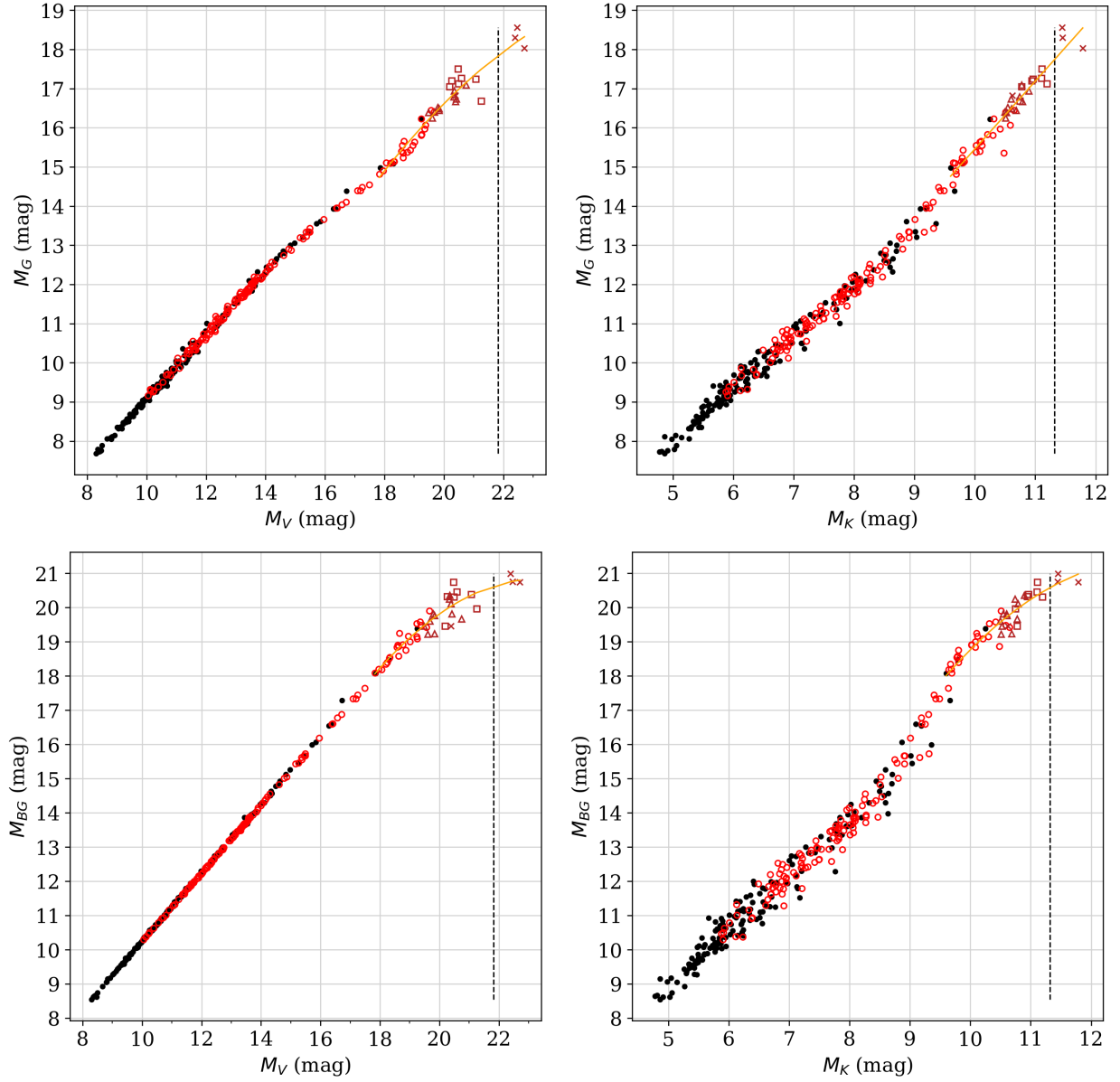


Figure 2.6 Absolute magnitudes in G and B_G against those in V and K for the *bona fide* single M dwarfs. The colors and symbols are the same as in Figure 2.1. Dashed black lines mark the adopted M_V and M_K values for the stellar/substellar lines. Orange curves are fits for each relation derived using the 33% faintest stars in the samples. The analogous plots for R_G and I are shown in Figure 2.7.

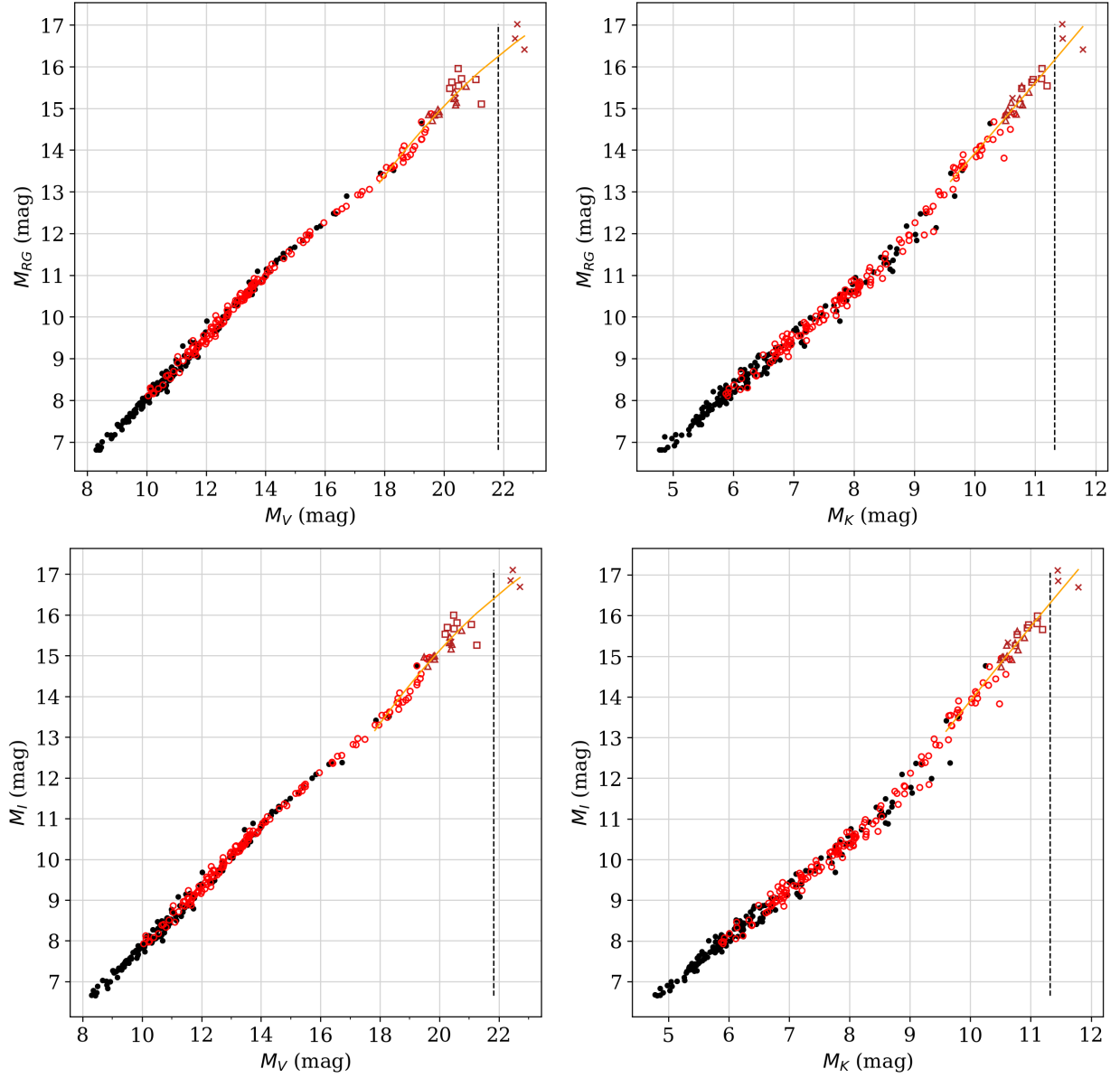


Figure 2.7 Absolute magnitudes in R_G and I against those in V and K for the *bona fide* single M dwarfs. The colors and symbols are the same as in Figure 2.1. Dashed black lines mark the adopted M_V and M_K values for the stellar/substellar lines. Orange curves are fits for each relation derived using the 33% faintest stars in the samples. The analogous plots for G B_G are shown in Figure 2.6.

poor quality astrometric fits to the data. In fact, many of the targets we desire for orbit mapping are binaries that would be culled using the ABC cuts. Additionally, some of our lowest-mass M dwarfs are too faint to have reliable *Gaia* magnitudes, which are generally limited to $G \lesssim 20$ and $B_G \lesssim 19$.

To clean the sample, we identified the sources in the 2MASS catalog (Skrutskie et al. 2006) that correspond to each *Gaia* source, as most M dwarfs are bright in the 2MASS K_s bandpass. This process required using each source’s proper motion (as measured by *Gaia*) to convert its *Gaia* DR2 2015.5 coordinates to epoch 2000.0, then matching it to the nearest 2MASS source on the sky. For most of the *Gaia* sources, a corresponding 2MASS source was located less than $0''.05$ away. To verify the matches that were not so close, we checked each visually in Aladin using the *Gaia* catalog overlaid on the 2MASS images and catalog positions, supplemented by the CDS-composited Digitized Sky Survey II images (Lasker et al. 1996) for bluer or very high proper motion sources. This process yielded 2592 M dwarfs in 2461 systems within 25 pc.

Finally, we added 45 systems from the RECONS astrometry program that were not already represented in the above *Gaia* sample. Most of these systems were astrometric multiples or had $\pi < 40$ mas in *Gaia* DR2 but $\pi \geq 40$ mas from RECONS data. The final set of 2637 sources in 2506 systems comprises an effectively volume-complete sample of M dwarf stars within 25 pc south of Decl. $+25^\circ$, as demonstrated in Figure 2.8. The only systems that may be missing would be nearby red dwarfs with no entry in *Gaia* that remain unknown to the RECONS team, even after more than two decades targeting exactly

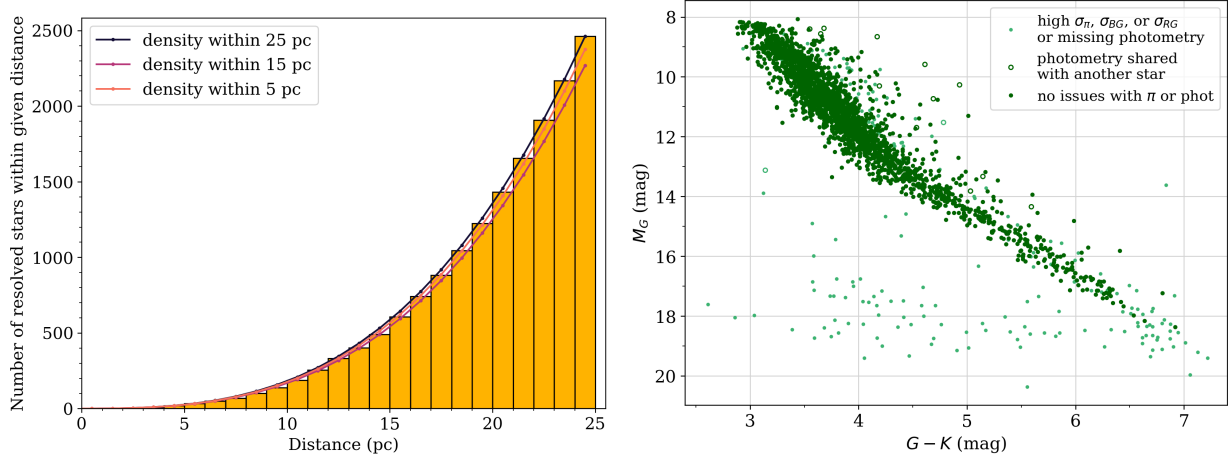


Figure 2.8 *Left panel:* Number of systems within a given distance in the 25 pc sample. Curves of constant density in black, dark red, and light red illustrate the number of systems expected given the average density within 25 pc, 15 pc, and 10 pc, respectively. *Right panel:* HRD of the 25 pc sample. Each point color roughly indicates the quality of that system’s *Gaia* data (and thus the reliability of its HRD position): light points have parallax error ≥ 0.40 mas or are missing B_G or R_G , dark points have no such issues with their data, and open points (of either color) have more than one star included in their 2MASS K_s measurement (joint photometry).

these systems in the southern sky. From this sample of 2506 systems, we drew the target lists to add to the RECONS astrometry program (§3) and to begin the new SOAR speckle interferometry program (§4). The full list is given in Table 2 (Appendix 7.2).

CHAPTER 3

The RECONS Astrometry Contribution

In order to form a big-picture view of orbit sizes and shapes for the smallest stars, we need orbits on multi-decade scales to complement the days- and years-long orbits available in the literature. Accurate long-period orbits are difficult to accumulate, however, because to map a significant portion of these orbits requires more years than typically allocated to observing programs. To alleviate this problem we have turned to the astrometry program of the REsearch Consortium On Nearby Stars (RECONS), which has been taking data on the nearest M dwarfs at the CTIO/SMARTS 0.9m telescope since 1999. Having more than 20 years of data from a single observing program with consistent protocols gives us access to multi-decade orbits while simplifying the later task of analyzing observational biases affecting the results. For this thesis, we are focused on M dwarf primaries with companions orbiting in periods of 0–30 years.

3.1 Targets Observed by the RECONS Astrometry Program

The RECONS astrometry program is a broad survey that primarily targets a volume-complete sample of M dwarfs with parallaxes ≥ 60 mas (i.e., within ~ 16.67 pc) and Decl. $\leq 0^\circ$ (the southern sky). The program continues to observe ~ 300 low-mass targets outside these limits, including targets as far north as $+30^\circ$ Decl., M dwarfs of interest out to 25 pc, a few young M dwarfs at larger distances, and a few dozen white dwarfs and brown dwarfs. The “interesting” M dwarf additions are generally systems with orbital motion or with evidence of stellar activity and cycles, hence the multiplicity or photometric variability statistics

must be interpreted with care for RECONS systems beyond 16.67 pc. But, out to that horizon, 97% of the final sample systems described in Chapter 2 are currently targeted at the CTIO/SMARTS 0.9m. Only 32 stars are not being observed for the volume-complete survey — these are too bright (generally having $V < 10$ mag), have very poor reference star fields, and/or are corrupted by nearby sources.

Prior to 2019, the volume-complete RECONS survey was limited to M dwarfs with $5.0 < V - K < 12.0$, corresponding to stars with masses $\lesssim 0.3 M_{\odot}$. As this thesis began in August 2018, the volume-complete survey was redefined to include more massive M dwarfs up to $0.62 M_{\odot}$, set by M_V and M_K values that correspond roughly to $3.9 \leq V - K \leq 10.5$, to enable stronger comparisons between partially convective and fully convective stars. This broadening of the survey required defining an M dwarf in terms of absolute magnitudes, which is discussed in detail in Chapter 2.

Expanding the RECONS astrometry survey required adding ~ 126 targets to the program’s observing list for ongoing monitoring, bringing the total survey to 461 systems as of May 2023. The final member of this sample was set up for monitoring on August 31, 2021, as the CTIO/SMARTS 0.9m was closed for most of 2020 during the global pandemic. Considerations of the astrometric technique does prevent this sample from being truly 100% volume-complete. As mentioned above, systems brighter than ~ 10 mag in V , R , and I usually cannot be monitored because the short exposure times for those targets leave the potential reference stars in those fields too faint to be used. Further details of this requirement are discussed in §3.2. This issue disproportionately affects the more massive M dwarfs

due to their intrinsic brightness.

The addition of 126 systems to the observing program for this thesis effort was not the only time the RECONS observing list was modified. Over the 20+ years of this program, targets have been added to or removed from the observing list as new nearby M dwarfs were discovered (or refuted) and as the active goals of the RECONS group evolved and shifted. The end result is that targets on the astrometry program have been observed over a range of timescales, as illustrated in Figure 3.1, which represents the 782 M dwarf systems that the program has ever monitored. Of these systems, 539 have enough data to be considered for this thesis, as an astrometric fit requires at least 2 years of data and 60 frames total.

For the purposes of this dissertation, our goal in observing these 539 M dwarfs is to characterize the orbits of the multiples within that sample. The varied distribution of time coverage (Figure 3.1) does affect the type of orbits we are sensitive to for each system. Despite this complication, our observations allow us to fit orbits to most systems with P_{orb} up to 20 years, and in some cases even longer (discussed further in §5.1.2).

3.2 Observing at the CTIO/SMARTS 0.9m for RECONS astrometry

Observations for the RECONS astrometry program are carried out at Cerro Tololo Inter-American Observatory (CTIO) in Chile at the CTIO/SMARTS 0.9m telescope. The program is discussed in detail in Jao et al. (2005) and Henry et al. (2018); here we give a brief summary of the observing procedures.

Observing runs are carried out 4–6 times per year, with runs lasting 10–20 nights each.

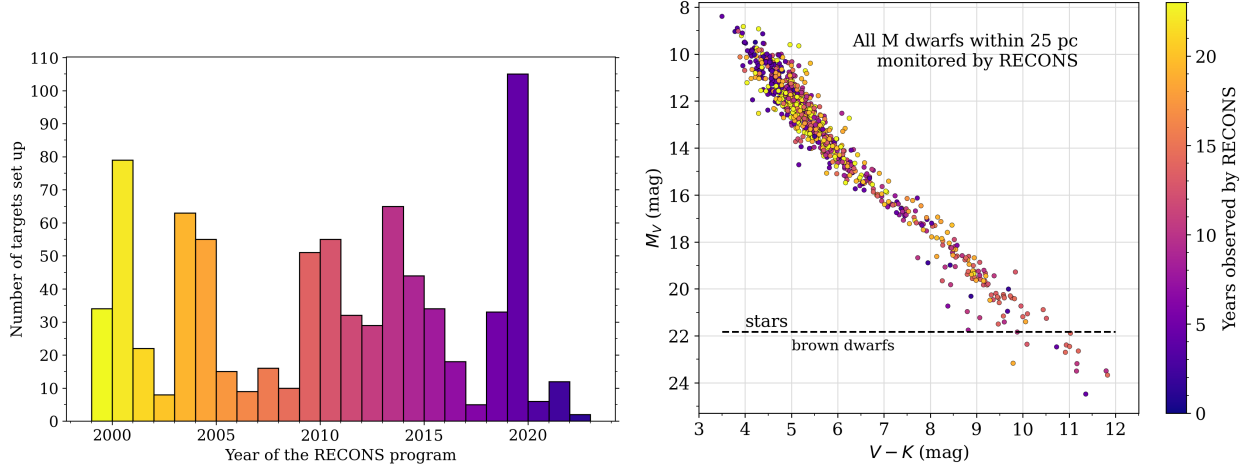


Figure 3.1 *Left panel:* Distribution of targets added to the RECONS astrometry program each year since it began in 1999, considering only the M dwarfs within 25 pc. Targets are added to (or subtracted from) the program to keep the core survey volume-complete as new nearby M dwarfs are detected, with additional modifications as the RECONS research priorities shifted over time. Nearly all systems added earlier than 2021 (539 total) have enough data to be monitored for orbits for this thesis. On the vertical axis, to “set up” a target means to begin monitoring it on the continuous observing program. *Right panel:* HRD of the same sample of 25 pc M dwarfs, with points colored according to their observing baselines on the RECONS program. Brown dwarfs followed by RECONS are also shown here to emphasize our coverage, but we do not consider them for this thesis analysis; these systems are below the horizontal dashed “stars-brown dwarfs” line.

During a night, typically ~ 20 targets are observed at airmasses less than 2.0. Throughout a run, 200–300 targets are typically observed at least once, with a visit consisting of 3–5 images spanning roughly 30 minutes. These images are routinely combined into nightly mean astrometric points because the astrometric positions of stars do not change markedly during a night. The end result is that most nearby M dwarfs receive 2–4 total observations per year.

The raw data are images taken on the Tek2k CCD, which has a full extent of 2048×2046 pixels and $0''.401$ per pixel plate scale. Only the central quarter of the chip is used for this

program, so images are 1024×1024 pixels and the field size is $6.8' \times 6.8'$. The filters used are V , R , or I on the Johnson-Kron-Cousins system, depending on the brightness of the target and its surrounding field stars. A single filter is used for all astrometric frames on a given target, and is selected to provide an exposure time giving $\sim 50,000$ peak counts to the brightest star used in the field (nearly always the target star) in typical seeing of $1''.2$. A set of 5–29 stars surrounding the target star is used as reference stars during data reduction (§3.3), and ideally, at least a few have $\gtrsim 10,000$ peak counts. Exposures are generally 30–300 seconds long, with some very faint targets requiring 600 or 900 seconds per image. Exposure times are adjusted on-the-fly during observations to ensure maximum counts during changing sky conditions, e.g., seeing fluctuations and clouds.

For each target, the filter used remains consistent through the entire span of its observations — for example, if we began observing a star in 1999 in V filter, every astrometric observation on that target since then has been carried out in V . This consistency is essential to obtaining reliable astrometry from the data, as it ensures the specific shifts in the field induced by the different colors of the stars as seen through a specific filter remain consistent from frame to frame and epoch to epoch.

Calibration images are taken either nightly or every two nights during the run, and consist of 17 bias frames and 11 dome flats in each of the three filters, for a total of 50 frames. After each observing run, the data are bias-subtracted and flat-fielded using a set of IRAF scripts, then organized into target-specific subfolders so a given target can have all its entire time series of data reduced as a single continuous data set¹.

¹My own role in these processes is that between 2018 and 2023 I completed $\sim 20\%$ of the observing

3.3 Data Reduction for RECONS Astrometry

Every time a target’s data are reduced, all suitable images — going back to the first image taken of that target for this program — are reduced together as one continuous data set, rather than processing the new data separately and adding it to the previous solution. This is essential to ensure that (1) the parallactic ellipse is as well-sampled by the data as possible, which improves the parallax fit; and (2) the time baseline of the data is as long as possible, which ensures the most accurate proper motion fit.

In general, the data reduction procedure consists of:

1. measuring the positions of the target and several (5–29) reference stars in each image,
2. using those positions to calibrate the target’s position in R.A./Decl. space in those images, then
3. fitting those positions in time series to an astrometric model that includes proper motion and parallactic motion.
4. If any orbital motion is evident in the residuals of that first astrometric fit, we re-fit the data with a more comprehensive model that includes orbital motion in addition to proper motion and parallax (§3.4).

What follows in this section is a more detailed description of each of the above steps.

The first time a target’s data are reduced, reference stars are chosen for that field. These stars are distant (beyond 300 pc) and collectively have small proper motions so they move

(excluding 2020–2021 during the pandemic), all of the IRAF data processing and organizing, and nearly all of the astrometry data reductions. My role is discussed in more detail in Chapter 7.

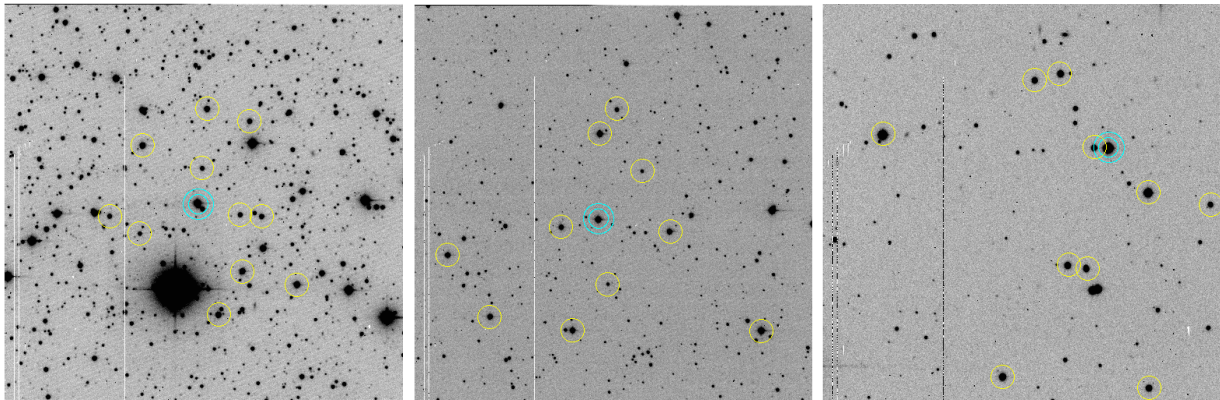


Figure 3.2 Examples of target star fields from the CTIO/SMARTS 0.9m for three targets: WT 2180 (*left*), LP 754-8 (*middle*), and LP 717-36 AB (*right*). Colors have been inverted such that darker pixels indicate more counts (i.e., brighter). In each panel, the target star is marked with a cyan double circle and the reference stars are marked with yellow single circles. The field in the left panel is excellent, with stars clustered around the target and near to it. The middle field is not as good because the reference stars are more dispersed, but the distribution is still reasonable — this field is typical of most targets. The right panel's field is poor, as the references are spread far across the image and are generally all to one side of the target star.

minimally over time, which allows them to be used to calibrate the grid of R.A./Decl. in the image. The ideal reference stars are therefore located near to the target on the image (minimizing the area of the CCD to be calibrated) and distributed evenly in R.A. and Decl. (ensuring the CCD is well-sampled). Figure 3.2 gives examples of excellent, good, and poor reference star distributions.

The same set of reference stars is used for every image, with minor adjustments made for individual images if a telescope pointing error placed a reference star off the field or on a bad pixel on the CCD. If the reference set is revised, that new set is then used for all of the target's images, following the requirement that the all the old and new data for a given field be processed uniformly together.

First, each image is checked for poor seeing (worse than $2''.4$ FWM) or errors in telescope tracking, both of which affect all stars of interest. In addition, checks are made for cosmic rays, bad pixels, or other anomalies that alter the PSFs of either the target star or any of the designated reference stars. If such an issue affects a reference star in a given image, then that star can later be excluded from that image’s data, but if the issue affects the target star then the whole frame must be discarded. Every frame must be checked using this procedure, although if this target’s data have been reduced before, then previous frames were already verified and only the new/additional frames need to be checked.

Next, the rough positions of the target star and reference stars are noted (“tagged”) in each image. This is generally done via a script that asks the user to mark the stars in one representative image, then propagates these positions to the rest of the images, taking into account the proper motion of the target star supplied by the user. These tagged positions can be manually adjusted later by the user if necessary.

The stars’ tagged positions are then used to determine the precise positions of these stars. SExtractor (Bertin & Arnouts 1996) fits a 2D Gaussian window function to each tagged star; this is an efficient technique that approximates fitting a 3D Gaussian to each star’s PSF. This procedure outputs the precise positions of those stars’ centroids in each image, as well as their instrumental magnitudes. At this stage, reference stars that had issues in some frames (often noted in the first step during the frame-checking) can be excluded from those frames to ensure their spurious data are not used.

Those stellar positions are used next to calibrate the field to the R.A./Decl. grid. The

user selects a high-quality frame taken at minimal hour angle, in good seeing, and with maximized signal-to-noise, to use as the “trail plate.” The trail plate’s stellar positions are then matched to the 2MASS catalog (Cutri et al. 2003; Skrutskie et al. 2006) to determine the rotation and scaling of that frame with respect to R.A./Decl. space. That solution is applied to the rest of the frames in the data set, so the measured positions now reflect those stars’ motions due to proper motion and parallax only.

Next, the target and reference star positions in each frame are corrected for the effects of differential color refraction (DCR). This effect is a result of each star’s light being refracted — by different amounts, based on the star’s color — as it passes through Earth’s atmosphere. The DCR correction was empirically determined for the RECONS program in each of the V , R , and I filters as described in Jao et al. (2005), and ultimately amounts to a small (\sim few mas) shift in the measured positions of the target and reference stars in each frame. Observations are typically made within one hour of the target’s transit in order to minimize DCR effects. At this stage, we also use the precise observation times of each image to generate the parallax factors in R.A. and Decl., which indicate the Earth’s position in its orbit during the observation. These factors must be taken into account when fitting the astrometric model to the data.

Finally, the GaussFit program (Jefferys et al. 1988) uses a least-squares algorithm to determine the plate constants that describe the scale, rotation, and stretch for each frame, as well as the relative proper motions of the reference stars and science target star. This solution assumes that the reference stars’ proper motions and parallaxes sum to zero². The

²Alternatively, the positions could be matched to the *Gaia* catalog, and *Gaia* parallaxes and proper mo-

relative parallax determined here for the target star is corrected to absolute parallax using the photometric distances of the reference stars, which are derived using *VRI* photometry of the fields also acquired at the CTIO/SMARTS 0.9m.

We evaluate the results by computing the residuals between the parallax + proper motion model and the target star’s position data over the duration of the data set. Some representative examples are shown in Figure 3.3. If any data point has an unusually high residual relative to the rest, we check that frame for common issues (cosmic rays or bad pixels on stars, bad background, misshapen PSFs). If any are found, we exclude those frames and re-compute the fit.

3.4 Fitting Orbits to RECONS Astrometry

When a target star has a bound stellar or brown dwarf companion, its orbital motion is often visible in the residuals to the astrometric fit described above (§3.3). Figure 3.4 shows two examples of such signals. These perturbations with respect to the astrometric model, or “PBs,” are usually tracing orbital motion, but occasionally a false or ambiguous PB is induced by instrumental effects or when the target star passes very near a background star on the CCD over time. §4.1.2 revisits this topic of false/ambiguous PBs.

3.4.1 *Principles of Photocentric Orbits*

The motion evident in these residuals is not that of the primary star nor secondary star; rather, it is motion of the photocenter (center of light) of the two stars. The photocenter

tions could be used to account for the stars’ motions during the observations. This substantial improvement is planned for a future upgrade to the RECONS data pipeline.

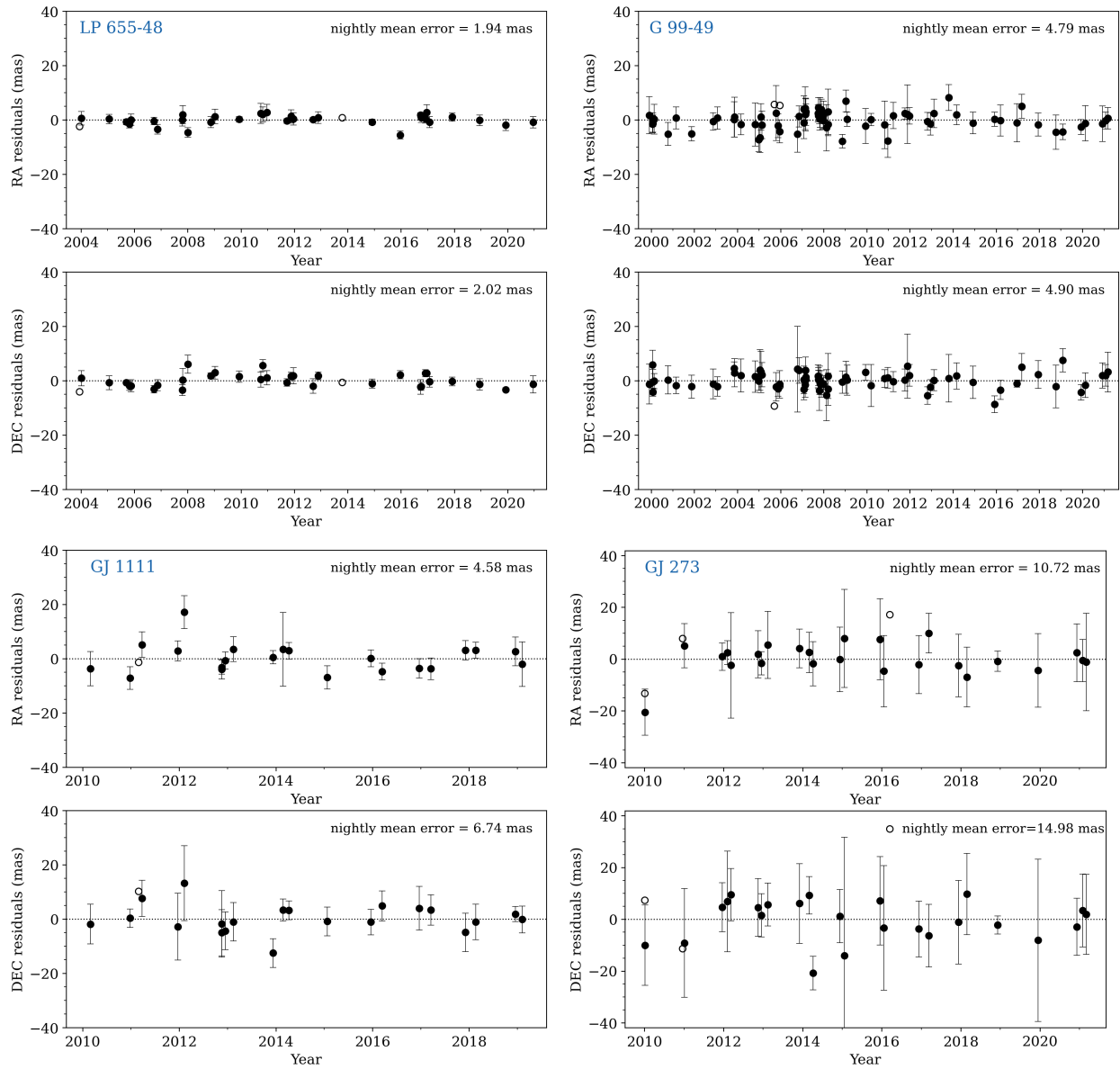


Figure 3.3 Examples of residuals to the proper motion and parallax fit for four target stars: (*upper left to lower right*): LP 655-48, G 99-49, GJ 1111, and GJ 273. Each system's residuals are represented by two panels: the upper showing residuals with respect to R.A. over time, and the lower showing residuals with respect to Decl. over time. The nightly (per-epoch) uncertainties of LP 655-48 (the first system) are unusually low (~ 2 mas), and those of GJ 273 (the last system) are unusually high (10–15 mas), while G 99-49 and GJ 1111 are typical.

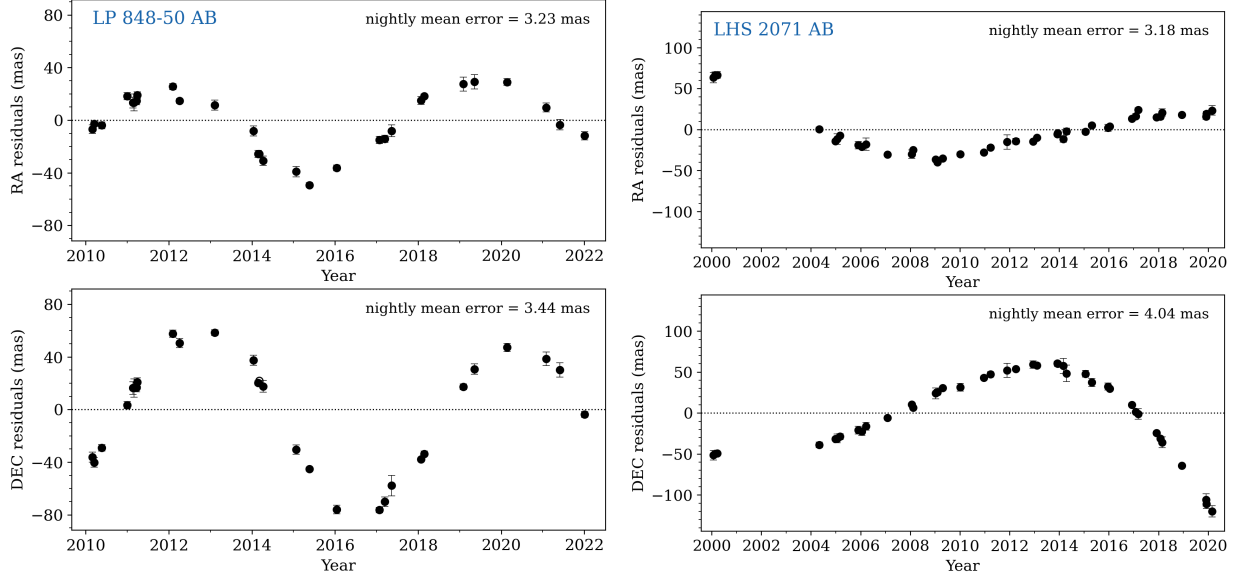


Figure 3.4 Two examples of RECONS astrometry perturbations (PBs) characteristic of orbital motion; the systems shown here are the binaries LP 848-50 AB (*left*) and LHS 2071 AB (*right*). These PBs are with respect to the “single-star” astrometric model, i.e., they are the residuals left after fitting for the target star’s proper motion and parallax. In each column, the top panel shows residuals with respect to R.A. over time, and the bottom panel shows residuals with respect to Decl.

position with respect to the system’s center of mass, p , is the same as that of the secondary companion (ρ) but scaled down by the difference between the companion’s fractional mass (B) and fractional luminosity (β) with respect to the primary star (Van De Kamp 1967):

$$p = \rho \cdot \left(\frac{M_B}{M_A + M_B} - \frac{F_B}{F_A + F_B} \right) = \rho \cdot (B - \beta) \quad (3.1)$$

Following this principle, the semi-major axis of the photocentric orbit (α) is proportional to the semi-major axis of the relative orbit (a) by the same factor:

$$\alpha = a \cdot (B - \beta). \quad (3.2)$$

The shape of the photocentric orbit is thus identical to that of the relative orbit, with

only the size reduced by the $(B - \beta)$ scale factor, whereas the orientation is similar but flipped by 180° . This proportionality makes some binary orbits more difficult to detect than others — for example, two equal-mass stars with equal fluxes would exhibit no apparent photocentric orbit ($\alpha = 0$). The consequences of this selection function on the sensitivity of the RECONS program are discussed in §5.1.2.

Although orbital motion is visible in the residuals to the proper motion and parallax fit, an accurate orbital fit requires fitting the orbit to the data simultaneously with fitting the proper and parallactic motions, rather than fitting the sets of residuals. Fitting all three motions simultaneously rather than in sequence allows the algorithm to balance them equally, rather than optimizing the first model fit (parallax+proper motion) at the expense of the second (orbital motion). In testing these two approaches, we found that fitting proper motion and parallax first, separately from orbital motion, resulted in orbits with systematically lower eccentricities than fits of the same systems using relative astrometry data (which reflects only orbital motion, no proper motion and parallax).

3.4.2 The MCMC Orbit Fitting Algorithm for RECONS Astrometry

To fit the proper, parallactic, and orbital motions simultaneously, we used the Markov chain Monte Carlo (MCMC) IDL code of Dieterich et al. (2018) designed specifically for RECONS astrometry data taken at the CTIO/SMARTS 0.9m. This code is open-source and available on GitHub (Dieterich 2018). The inputs for the Dieterich et al. (2018) orbit fitter are the target star’s R.A. and Decl. displacements from its initial position after DCR and the trail plate calibration have been applied (§3.3). The user specifies hard limits on each of the 10

parameters to fit — proper motions in R.A. and Decl., parallax, and the 7 orbital parameters — as well as ranges from which each parameter will be drawn. The MCMC code draws values uniformly from within these ranges, thus they constitute uniform priors.

Formally, the astrometric model computed by the code gives the displacement at time t of the photocenter in R.A. and Decl. ($\Delta\alpha$ and $\Delta\delta$) from the center of mass as:

$$\Delta\alpha = \mu_\alpha (t - t_0) + \pi p_\alpha + (B X + G Y), \quad (3.3)$$

$$\Delta\delta = \mu_\delta (t - t_0) + \pi p_\delta + (A X + F Y), \quad (3.4)$$

where t_0 is the time of the first observation, μ_α and μ_δ are the proper motions in R.A. and Decl., π is the parallax, and p_α and p_δ are the parallax factors in each direction. Several of the orbital parameters are encoded in the Thiele-Innes constants A , B , F , and G above via:

$$A = a (\cos \Omega \cos \omega - \sin \Omega \sin \omega \cos i)$$

$$B = a (\sin \Omega \cos \omega + \cos \Omega \sin \omega \cos i)$$

$$F = a (-\cos \Omega \sin \omega - \sin \Omega \cos \omega \cos i)$$

$$G = a (-\sin \Omega \sin \omega + \cos \Omega \cos \omega \cos i)$$

where a is the semi-major axis, Ω is the longitude of the ascending node, ω is the argument of periastron, and i is the inclination of the orbit such that $i = 90^\circ$ is along the line of sight. Figure 1.1 illustrates these parameters of the orbit. Finally, the rectilinear coordinates X

and Y above are

$$\begin{aligned} X &= \cos E - e, \\ Y &= \sqrt{1 - e^2} \sin E, \end{aligned}$$

with e indicating the orbital eccentricity and E the eccentric anomaly, as given by Kepler's equation:

$$E - e \sin E = \frac{2\pi}{P}(t - T). \quad (3.5)$$

The orbital period is P and the time of periastron passage is T .

The goal of the algorithm is thus to find the combination of orbital parameters a , e , i , Ω , ω , T , P , and astrometric parameters μ_α , μ_δ , π , that best matches the model given the values $\Delta\alpha$, $\Delta\delta$, p_α , p_δ , and t for each data point. The MCMC algorithm effectively accomplishes this goal by exploring the parameter spaces and building distributions of where it explored, i.e., the “posterior” distributions, that indicate the most likely values for the best-fit model. For this process to work, the algorithm needs to draw models from the entire possible range of each parameter, but also draw more values around models that are relatively better fits to the data than the others.

The user specifies two ranges of values for each parameter: an “initial values” range, from which the MCMC algorithm uniformly draws random starting values for each parameter, and a “hard limit” range, from which the parameters are not allowed to escape. After drawing parameter values on each iteration, the MCMC algorithm chooses a small step for each

parameter and evaluates whether or not that new model is an improved fit to the data over the previous model. To make this decision, the algorithm uses the χ^2 to compute the probability that each model matches the data, then takes the ratio of these probabilities to determine if the new model is a sufficient improvement. A modified Metropolis-Hastings procedure is used to determine this threshold (see Dieterich et al. 2018, Appendix A, for further details). Improved models are accepted, while worse models are rejected and a new random step is chosen. These incremental steps form a “chain” of models, and after a specified number of them — for this thesis, 200 steps — the chain is declared finished and a new chain is begun with new random parameter values drawn again from the “initial values” ranges. The MCMC process terminates when 51 chains have completed.

The algorithm varies the step size for each parameter based on the partial derivatives at those points, which avoids the potential of one parameter dominating the effect of each step. This issue is particularly a danger for the orientation angles Ω , ω , and i , as certain values of these angles would cause small changes in motion to be particularly large or small on the sky through their projection effects.

To avoid over-exploring one small part of the parameter space, every 200 steps the Dieterich et al. (2018) algorithm also takes a “spider step” for one of the parameters (selected at random) wherein it chooses a completely new random value within the hard-limits range. After varying the chain normally for 100 more steps, the algorithm evaluates whether the spider step was an improvement; if not, it reverts that parameter to its pre-spider value and continues the chain. At any point, if a step generates a value that it outside the “hard

limit” range set by the user, then the algorithm rejects that step and computes a new one at random. The spider step mechanism allows the user to set very broad ranges for the parameters, as it ensures the algorithm will not get sidetracked by a local minimum. This avoids the potential of the posteriors reflecting the user’s parameter starting ranges (i.e., the user’s initial guesses).

The code terminates when it reaches a specified number of chains — for this thesis, 51 chains were usually enough to reach convergence. Then a separate code is used to extract the last 100,000 models and plot the distributions of parameter values of these models, i.e., the posteriors (also referred to as the probability density functions or PDFs). If they show Gaussian peaks around specific parameter values, the chains have converged and the best-fit model can be inferred from the median of those PDFs. Examples of these PDFs are shown in Figure 3.5.

All the 19 orbits fit from the RECONS astrometry program that are contributing to this work are shown and discussed in §5.1.1.

3.4.3 Fitting Orbits Longer than the Astrometric Time Baseline

Our orbit fitting procedure works reliably as long as the entire orbit is visible in the astrometric observations — i.e., for systems with P_{orb} shorter than the observed time baseline. Orbits that are not completely observed in these data are difficult or even impossible to constrain because the orbital motion cannot be distinguished from proper motion. For example, a short curved arc of motion could be fit by a decade-long orbit or a century-long orbit, depending on the proper motion (both angle and total amount) assumed to be contributing

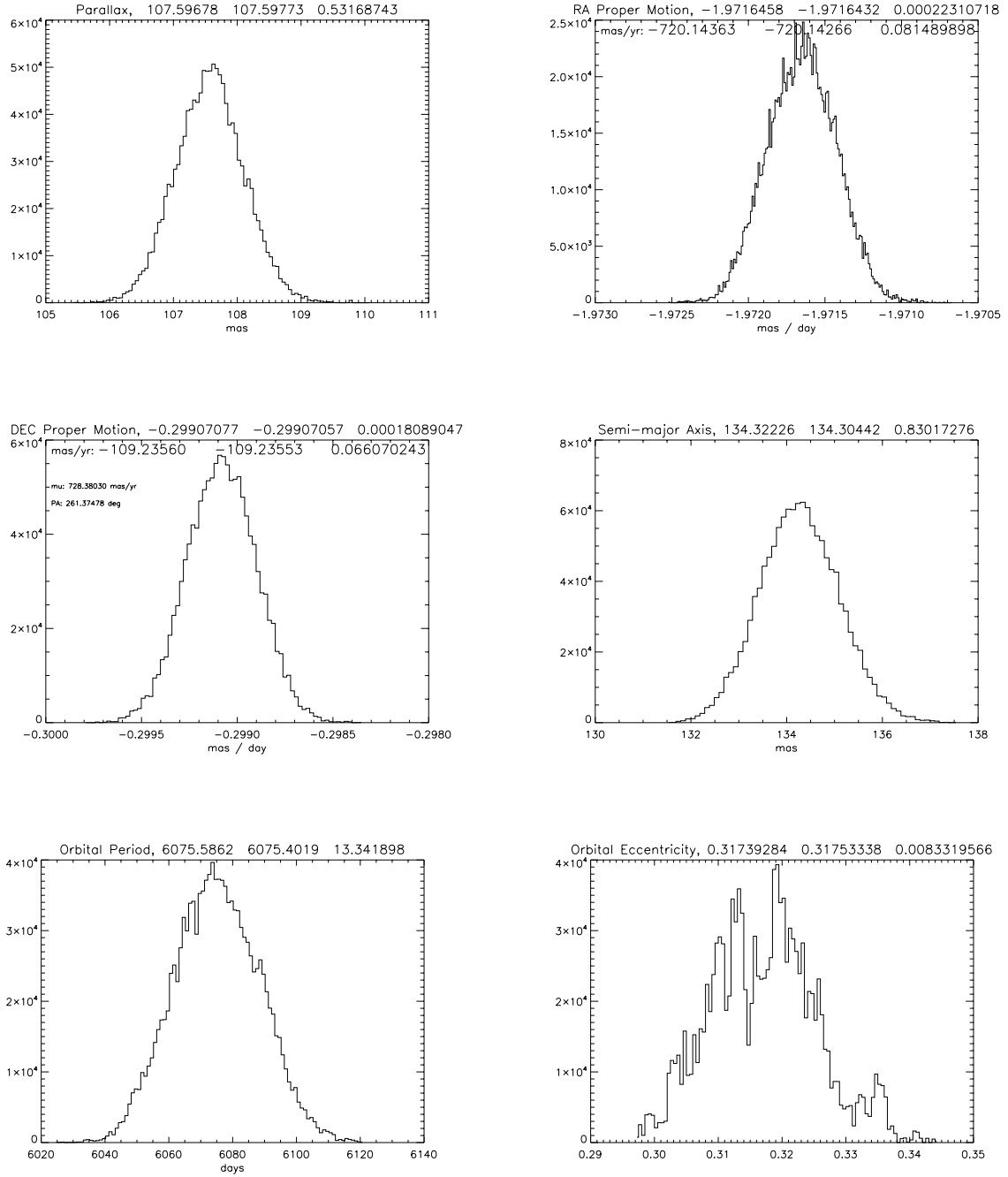


Figure 3.5 Examples of well-converged probability distribution functions for an astrometric binary (WT 460 AB) fit by the Dieterich et al. (2018) MCMC code. For space reasons, only a subset of the ten fit parameters are shown. *Top left to bottom right*: parallax (in mas), R.A. proper motion (mas yr^{-1}), Decl. proper motion (mas yr^{-1}), semi-major axis of the photocentric orbit (mas), orbital period (days), and eccentricity. The top of each plot lists the distribution's mean, median, and standard deviation.

to that arc³. This degeneracy is thus unique to absolute astrometry such as the RECONS data, and is not a factor when fitting relative astrometry (such as from the SOAR program; Chapter 4).

In practice we have found that this proper vs. orbital motion degeneracy means we can only fit orbits that are less than $\sim 110\%$ the length of a given system’s observational baseline. If sufficient motion is visible (at least two “turns” in R.A. and one in Decl., or vice versa), we can fit longer orbits by holding the proper motion fixed while fitting the rest of the orbital parameters and parallax. For this dissertation, this method was only applied when an initial 10-parameter fit showed:

1. orbit size parameters (period and semi-major axis) were constrained even if not converged,
2. PDFs of μ_α and μ_δ were well-constrained to within a few tenths of mas per day (the medians of these distributions were chosen as the fixed values),
3. eccentricity well converged despite the orbit size parameters (period and semi-major axis) being poorly constrained.

Given these caveats, this technique of holding proper motion fixed was only applied when $\gtrsim 80\%$ of the orbit was observed over the given time baseline. Shorter orbital arcs did not allow these parameters to be well enough constrained. This technique also induces some bias toward less-eccentric orbits, as those show more orbital motion over shorter time period;

³The eccentricities will necessarily be different between the best-fitting decade-long orbit vs. century-long orbit, thus this degeneracy between proper motion and orbital motion makes these partially-observed orbits difficult to include responsibly in both the P_{orb} and e distributions.

partially observed eccentric orbits look more linear unless the observations happen to catch them at periastron. Biases related to orbit shape for RECONS astrometry are discussed in more detail in §5.1.2.

CHAPTER 4

The SOAR Speckle Contribution

The speckle program was initiated in 2019 at the Southern Astrophysical Research (SOAR) 4.1m telescope to map orbits that complement the RECONS astrometry results. Because the SOAR effort has been underway for nearly four years, it is particularly good for determining orbits with periods less than a few years, while the RECONS astrometry effort is best in providing systems with periods of 3 years and longer. Although the cadence of the SOAR observations is similar to that of the RECONS program, these data map relative orbits directly — proper motion and parallactic motion thus need not be considered because the motion seen is only the orbital motion of the secondary star about the primary. This feature also makes it straightforward to combine SOAR speckle data with other high-resolution imaging data in the literature to form a longer or more complete observing time baseline for a given system.

In this chapter we begin with the target selection for the SOAR program, which includes multiples and suspected multiples from the literature (§4.1.1), from the RECONS astrometry program (§4.1.2), and from *Gaia* DR2 (§4.1.3). We then explain the procedures for observing and reduction of these data (§4.2), and finally describe how orbits are fit to those results (§4.4).

Many of the details shown here regarding the SOAR speckle target list and observations were first presented in Vrijmoet et al. (2022), which described results from the first 1.5 years of our SOAR speckle observing program.

4.1 Choosing Targets for SOAR Speckle

To increase the likelihood of companion detections and to maximize efficiency during the allocated observing time, the SOAR program targeted only known or very likely multiples. These included systems identified in the literature (§4.1.1), from the RECONS astrometry program (§4.1.2), and from *Gaia* DR2 (§4.1.3). These three subsets had substantial overlap; for example, many systems with perturbations in RECONS data were also known multiples in the literature (sometimes from previous RECONS work). The overlap between these subsamples is illustrated in Figure 4.1. In total there were 337 systems targeted with M dwarf primaries, with the majority — but not all — being confirmed multiples at the beginning of the program. Many of those confirmed multiples had not been resolved prior to this program, as they were detected with techniques such as spectroscopy. Table 3 (Appendix 7.2) gives the full target list, with the subsets from Figure 4.1 (and discussed below) marked in columns 8–10.

Regardless of their subset, the instrument configuration on SOAR required that all targets be brighter than $I = 14.0$ mag in the Johnson-Cousins I band, which was the filter used for these observations. For targets with no previous I measurements, brightnesses were estimated by assuming the *Gaia* R_G magnitude was roughly equivalent. Collaborator and SOAR/HRCam+SAM Instrument Scientist, Andrei Tokovinin, carried out the observations and found that none of these targets were too faint to observe, thus the $R_G \approx I$ estimate was sufficiently valid.

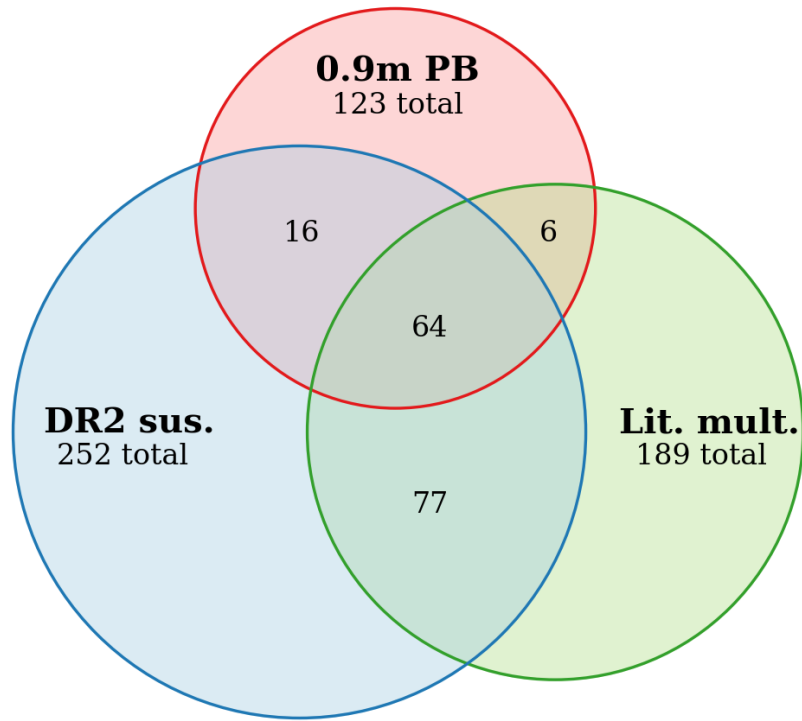


Figure 4.1 Venn diagram illustrating the three subsets of systems with M dwarfs targeted in the SOAR speckle survey, comprising 337 systems total. Each circle is labeled according to the subset’s source: “0.9 m PB” for targets showing perturbations (PBs) in the RECONS astrometry program at the CTIO/SMARTS 0.9m (§3), “Lit. mult.” for known multiples from the literature, and “DR2 sus.” for systems suspected to be multiples based on their *Gaia* DR2 results. The number of targets is given under each subset name, and the numbers in the overlapping sections indicate the number of targets common to multiple subsets. The area of each circle is proportional to the number of targets in that subset, although the overlapping regions are not to scale.

4.1.1 189 SOAR Targets from the Literature

Roughly 50% of the SOAR speckle targets were already identified as known multiples in the literature, some via high-resolution imaging and others through spectroscopy or (unresolved) astrometry, e.g., the RECONS astrometry program. In observing these known multiples with HRCam+SAM, our goals were:

1. Obtain separations and position angles for companions that were previously unresolved from their primary stars.
2. Map each companion’s motion through relative astrometry to enable fitting its relative orbit, incorporating any previous data available to extend its time baseline.
3. Improve upon any existing orbit fits, in particular by improving the accuracy of the orbital elements.

To select known multiples that would have pre-existing data, we matched the sample of 25 pc M dwarfs (Chapter 2) against the Sixth Catalog of Orbits of Visual Binary Stars (ORB6; Hartkopf et al. 2001) and the Washington Double Star Catalog (WDS; Mason et al. 2001). Some additional targets were identified through private communication with collaborators.

Cross-matching with known orbits in ORB6 allowed us to exclude systems with preliminary orbits much longer than the 0–30 year regime targeted by this thesis. For the systems without previous orbits (e.g., from WDS), we excluded potentially long orbits by requiring each pair to be separated by $\lesssim 2''$ at its widest separation recorded to date. Matching against ORB6 also ensured that many of these M dwarf multiples already had characterized

orbits, supporting our goal of improving on previous characterizations, and allowing us to supplant those with new measurements of magnitude differences to better characterize each component. Roughly one-third of the systems in this literature sample also had never been resolved in high-resolution imaging before, as their orbits were spectroscopic or astrometric. Resolving these systems gives valuable information about the components' physical separation and flux ratio (in this case, in the I band), both of which can be used to help constrain their masses.

Through this process, the SOAR target list included 189 known systems with M dwarf primaries, 81 of which already had orbits in the literature.

4.1.2 123 SOAR Targets from RECONS Astrometry

About one-third of the targets on the SOAR observing list were drawn from the RECONS astrometry program (Chapter 3), which reveals multiples based on perturbations detected in the positions of target stars' photocenters. These SOAR targets all had evidence of potential multiplicity based on those data, but many did not yet have a companion confirmed — and a substantial number had ambiguous signals that could not be clearly classified as orbital, as discussed below. Adding speckle data for these targets accomplishes several aims to aid this thesis:

1. Every result — both resolutions and non-resolutions — constrains orbital parameters for orbits that are incompletely mapped in the RECONS astrometry.
2. When no companion is resolved around a given star, this non-resolution places con-

straints on the potential companion’s luminosity (and thus its mass) and its separation from the primary star.

3. For systems with ambiguous signals in RECONS astrometry (discussed below), the speckle data either alleviates that ambiguity with a detection or mitigates it by revealing the absence of a companion within specific luminosity (thus mass) and separation limits.
4. When an orbit is completely mapped by RECONS astrometry and the companion is also resolved in speckle data, the combination of those data allows the determination of the components’ individual dynamical masses.

A unresolved multiple is identified in the RECONS data when the changing orbital position of the two components causes a perturbation (or “PB”) of the source’s position after solving for proper motion and parallax. The position shifts observed are that of the photocenter (center of light) of the unresolved pair of stars; as discussed in §3.4, this photocentric orbit is identical to the relative orbit of the secondary star about the primary, but is rotated 180° (in argument of periastron) and is smaller in size (semi-major axis), typically by a factor of 2–3.

Observing photocentric motion creates some limitations on the types of companions that can be detected in the RECONS data. On the plus side, a multiple can generally be *identified* with this technique when as little as 10% of its orbit is observed, as long as those observations have captured some of the orbit’s curved shape. An orbit thus need not be fully mapped in RECONS data to be a good candidate for our SOAR speckle follow-up program. On

the other hand, no perturbation is detected in cases of planetary-mass companions and for systems where the components have nearly-identical fluxes (in which case the center of light is halfway between the two sources at all times and hence, does not shift; §3.4.1). Orbital motion is also more difficult to detect when the astrometric precision is poor, such as for bright stars ($\lesssim 10$ mag for RECONS data), or when the orbit is poorly sampled, e.g., when the orbital period is short so that many orbits are completed between observations.

Although many systems show a PB with clear orbital motion that can be fit by an astrometric model (§3.4), a similar number have a PB that is clearly evident but more ambiguous in nature. Two examples are shown in Figure 4.2. These ambiguous PBs could represent true orbits that are poorly sampled or unfortunately oriented on the sky, or they could be non-astrophysical artefacts, such as star positions that have been mis-measured because the target has moved in front of a background star or if its PSF overlaps bad CCD pixels. Another notable class of non-astrophysical PBs were created by changing the V filter to a supposedly identical copy. The “new V ” filter was photometrically identical, but its bandpass curve — and thus the way stars shifted in the astrometric field due to their different colors — was slightly different than the previous one, so the positions of the stars as measured in the “old V ” were several milliarcseconds different than those measured in the “new V .”

Ultimately, of the 123 systems contributed to the SOAR target list by RECONS astrometry, 62 were resolved with SOAR (§5.2).

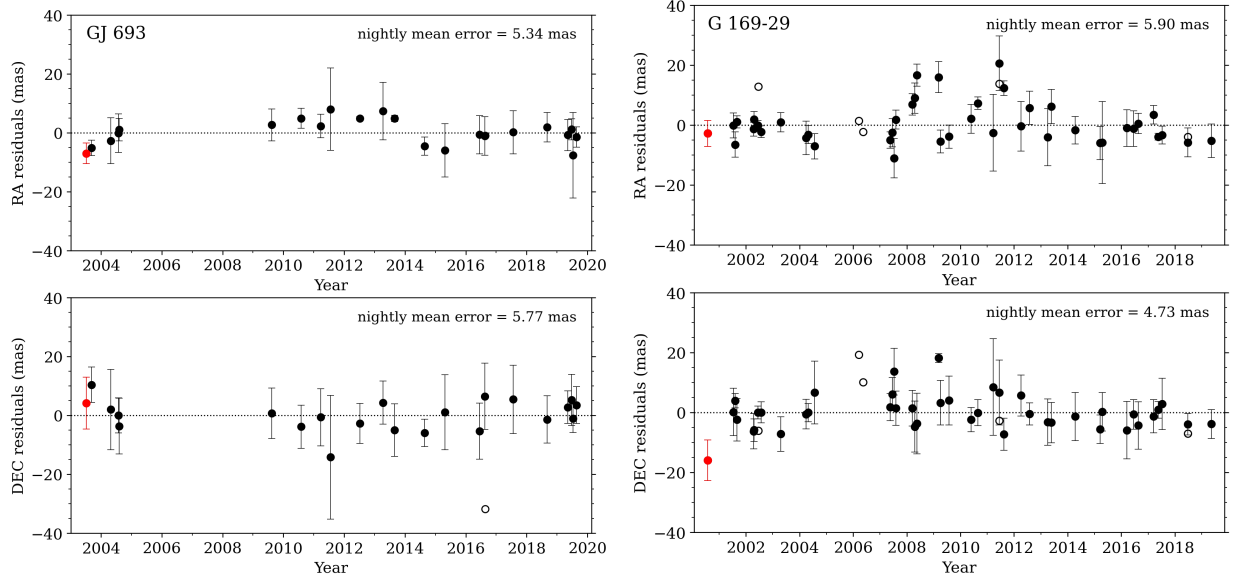


Figure 4.2 Two examples of astrometric perturbations (PBs) in RECONS data that are ambiguous, or not clearly astrophysical: GJ 693 (*left column*) and G 169-29 (*right column*). To contrast, compare these to the PBs showing clear orbital motion in Figure 3.4. For each system, each panel shows residuals in R.A. or Decl. with respect to time, computed after fitting proper motion and parallax to the system’s astrometry.

4.1.3 252 SOAR targets from Gaia DR2

To supplement the SOAR target list beyond known M dwarf multiples, we added 95 systems that showed evidence of *potential* multiplicity based only on the quality of their astrometry in *Gaia* DR2. These are the targets among the 252 total systems from DR2 represented in the blue region of Figure 4.1 that are not in either the literature and RECONS lists. Applying the criteria outlined below to the entire SOAR target list showed that 75% had this evidence of multiplicity in *Gaia*, indicating these criteria were reliable for selecting potential multiples. The targets added from *Gaia* that were not yet known multiples were included in the SOAR campaign to:

1. Identify and confirm new multiples and begin building their long-term data sets for

the astronomical community.

2. Measure magnitude differences at I to characterize components of any new multiples.
3. Map orbits of multiples with $P_{\text{orb}} \lesssim 6$ years, to which these *Gaia* DR2 data should be particularly sensitive because DR2 only observed for 22 months.

The specific criteria used to construct this list of “Gaia suspects” (potential multiples) are outlined in the analysis presented in Vrijmoet et al. (2020). In that work, we compared RECONS astrometry results to *Gaia* DR2 to identify the most useful parameters for potential multiplicity in the *Gaia* catalog. The steps of that analysis are summarized as follows:

1. We matched all the systems — singles or multiples — ever published by RECONS to their counterparts in *Gaia* DR2. This allowed us to consider the *Gaia* results for ~ 500 systems for which we already had access to their time-series astrometry data.
2. *Gaia* provides a substantial suite of parameters describing different aspects of the data and the quality of their fit to the astrometric and photometric models. From this list, we considered eight parameters that might be affected by the presence of a companion.
3. We distinguished the known multiples from the systems with perturbations in RECONS astrometry (as described in §3.4 and §4.1.2) and plotted the values of those eight parameters. These plots are shown in Figures 4.3 and 4.4.
4. The four parameters shown in Figure 4.3 revealed clear differences in the distributions for multiples vs. single stars and could be used to identify unresolved multiples in *Gaia* DR2 data. The remaining four parameters, shown in Figure 4.4, were not so helpful.

5. Based on the distributions of “helpful” parameters in Figure 4.3, we identified the value of each parameter for which 75% of the stars above that value were unresolved multiples. Stars below that value were not necessarily single, but stars above that value were overwhelmingly likely to be multiple. These “cutoff” values form the criteria for selecting likely unresolved multiples in *Gaia* DR2.

The above analysis indicates that three out of four stars that fulfilled the following criteria in *Gaia* DR2 were unresolved multiples:

1. missing *Gaia* DR2 parallax or missing DR2 catalog entry,
2. `parallax_err` ≥ 0.32 mas for $G \lesssim 18$ mag (≥ 0.40 mas otherwise),
3. `astrometric_gof_al` ≥ 56.0 ,
4. `astrometric_excess_noise_sig` ≥ 108.0 , and
5. `ruwe` ≥ 2.0 .

Note that the above statement does not *guarantee* that a system meeting these criteria has a companion — 25% of stars in that group had no evidence of multiplicity in RECONS data or the literature. Other factors such as high proper motion or very crowded fields could have affected the quality of those systems’ *Gaia* DR2 astrometric fits instead. These could include systems with very small astrometric signals (§3.4), with very slow orbital motions (long P_{orb}), or with orbital motions that mimicked a single star’s linear motion during the *Gaia* observations (such as a minimally curved portion of an eccentric orbit).

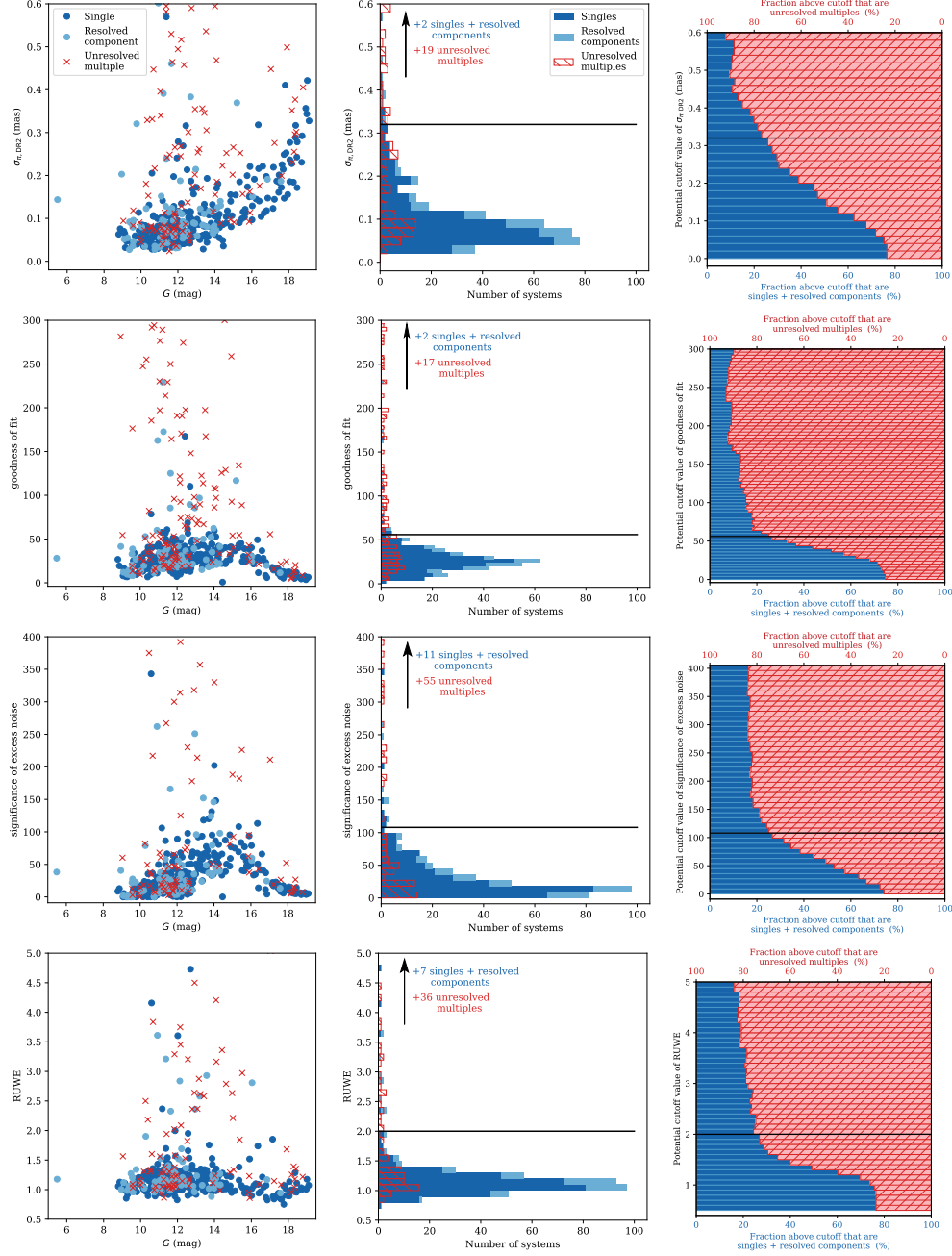


Figure 4.3 Four astrometric fit parameters in DR2 that are useful for selecting potential unresolved multiples. Unresolved multiples are red symbols and hatched bars, resolved components are light blue dots/bars, and presumed singles are dark blue dots/bars. *Left column:* parameters for these systems in *Gaia* DR2, plotted against their G mags. *Middle column:* distributions of these parameters for systems from the left, separated again by multiplicity. *Right column:* each bar shows the fraction of systems above each cutoff value that are single or unresolved multiple. The values above which 75% of our systems are unresolved multiples are indicated with a black line.

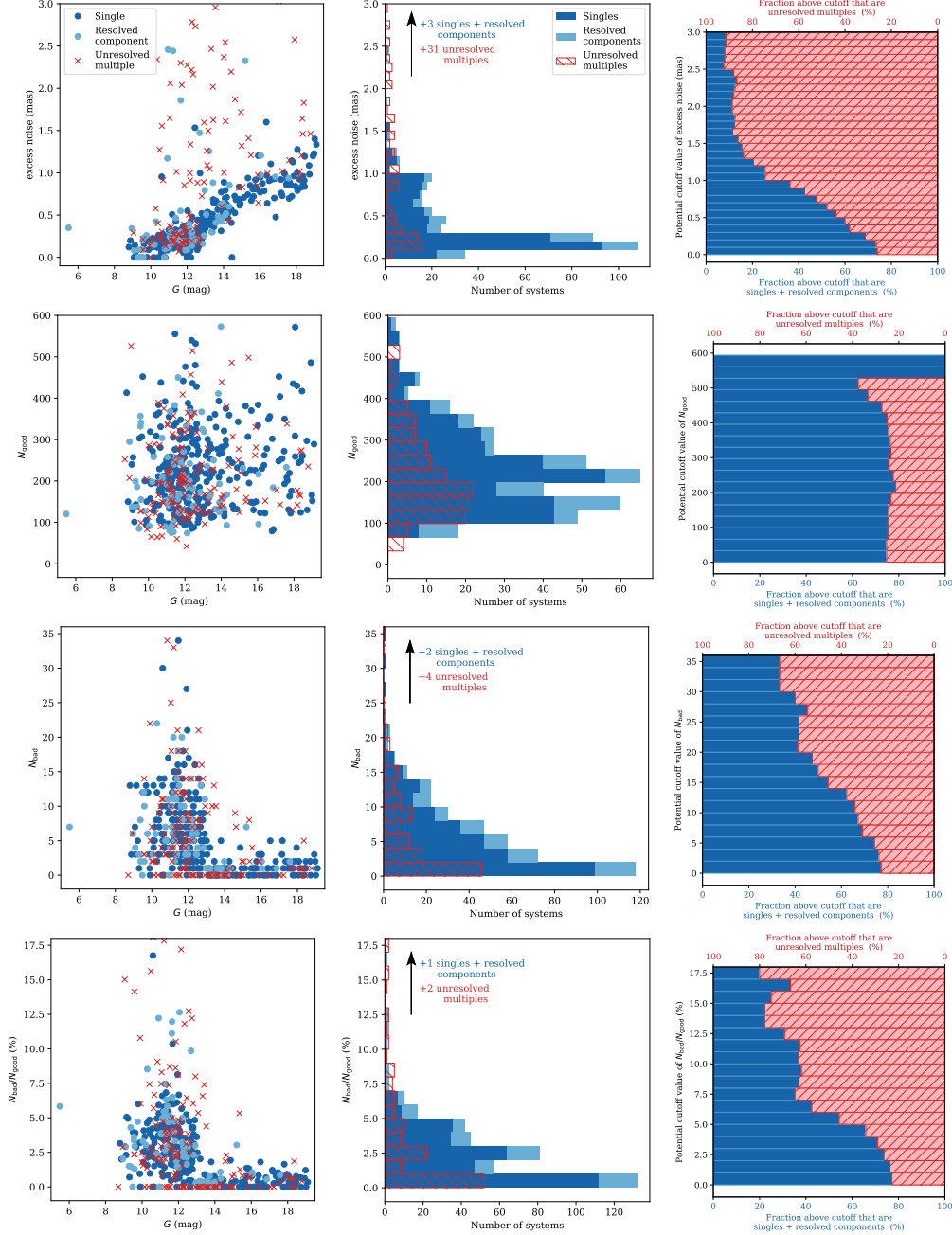


Figure 4.4 Four astrometric fit parameters in *Gaia* DR2 that are less useful for choosing potential unresolved multiples. The color schemes and columns are the same as for Figure 4.3, and any systems with values exceeding these ranges are noted with an arrow and text in each panel. For these quantities, the distributions of single and unresolved systems do not differ as significantly as those in Figure 4.3, making them less useful for identifying potential unresolved systems. The parameter `astrometric_excess_noise` does show a distinction between singles and multiples, but it is less useful than the very similar `astrometric_excess_noise_sig` because it strongly depends on G magnitude (faint singles have values similar to brighter unresolved multiples).

While selecting targets for the “*Gaia* suspects” subset, we also chose several dozen targets that had parameters slightly lower than the formal criteria from Vrijmoet et al. (2020). This supplementary list of 32 systems was included to leave the door open for possibly revising the criteria later once the SOAR speckle campaign revealed or confirmed new multiples.

4.2 SOAR Speckle Observing and Data Reduction

Data for this program were collected at the 4.1m Southern Astrophysical Research (SOAR) telescope by the high-resolution camera (HRCam) mounted on the SOAR adaptive optics module (SAM; Tokovinin et al. 2016). Since 2007 this instrument+telescope configuration has been imaging stellar multiples using the speckle interferometry technique (Tokovinin 2018), with regular results published in a yearly paper series (e.g., Tokovinin et al. 2020, 2021, 2022). Although M dwarfs have been occasionally included in those results, no dedicated M dwarf speckle observing program existed on SOAR before this thesis effort.

The observations for this thesis program were conducted from July 2019 to March 2023, with all data taken and reduced by HRCam Instrument Scientist Andrei Tokovinin. The telescope time for the program was allocated by NSF’s NOIRLab through several standard and long-term proposals. The allocated time was always combined with that of other observing programs on HRCam+SAM to increase the opportunities for timely observations of fast-orbiting systems. Typically, targets received 2–5 observations per year. In preparation for each observing run, we considered previous SOAR observations and RECONS astrometry to prioritize systems that exhibited rapid orbital motion. This procedure improved the

likelihood that defining features of the orbit shapes, e.g., epochs of periastron, would not be missed.

These HRCam+SAM observations were conducted in the instrument’s seeing-limited mode, meaning that no laser guide star was used during image acquisition. Frames were taken almost exclusively in the Kron–Cousins *I* filter, usually in 2–3 sets (data cubes) of 400 frames per target, with integrations typically 24 ms per frame. These sets were each processed independently to verify results. Most observations used the HRCam narrow 3'' field of 200×200 pixels, whereas pairs known to have separations of 1''.4 or more were observed with the 6'' field of 400×400 pixels. The formal resolution limit in *I* on the SOAR 4.1m is 45 mas, but the ultimate separation limit reached depends on target brightness and sky conditions. In some cases, good conditions and the data reduction procedure (discussed below) allow a system to be “super-resolved” down to 35 mas, beyond the formal definition of resolution (as shown in Figure 1 of Tokovinin et al. 2020). Targets that are unresolved in the first two attempts are usually observed a third time, then retired from the program if still unresolved.

The data are processed and reduced for this program using the standard procedures described in Tokovinin et al. (2010) and Tokovinin (2018), and representative images of the reduced data products are shown in Tokovinin (2018). In brief, for each target the power spectrum and autocorrelation function are calculated, and companions are noted via power spectrum fringes or secondary peaks in the autocorrelation function. Fitting an empirical model to the power spectrum yields the parameters of each detected pair: the separation

between components (ρ), the position angle (θ) of the secondary with respect to primary star (north = 0° through east = 90°), and the difference in magnitude between components (Δm). In addition to the those three measurements from the data reduction, important details about these results are:

1. The position angle determined through this procedure is only ascertainable modulo 180° , leaving some ambiguity in the secondary’s true position on the sky. This ambiguity has been eliminated whenever possible by applying a shift-and-add procedure to each target’s data (Tokovinin 2018); this process reveals the true quadrant for companions that are not too faint but still have some magnitude difference with their primary star ($\Delta m \gtrsim 0$ mag).

These results are noted with the “q” flag in Table 4 (Appendix 7.2), indicating that the quadrant has been determined.

2. For some observations of wider pairs, a separate procedure is used to determine the magnitude difference using the average image for a target (described in detail in Tokovinin et al. 2010). This method produces more reliable photometry for cases where the stars’ separations are greater than the size of the isoplanatic patch, which is the angular size of coherent turbulent cells in the atmosphere.

Observations with Δm determined with this method are marked by a “p” in Table 4 (Appendix 7.2), indicating that this photometric method has been used.

3. For observations in which no companion was detected, a contrast curve is computed to

report the detection (magnitude) limits as a function of the distance from the primary star on the sky (for example, see Figure 5 of Tokovinin 2018). The parameters of this curve are reported in the results (§4.3 and Table 4 in Appendix 7.2) as the minimum separation resolvable for pairs with $\Delta m < 1$ mag, as determined from the maximum spatial frequency of the power spectrum, and the maximum detectable magnitude difference at separations of $0''.15$ and $1''.0$ (the dynamic range).

4.3 SOAR Speckle Data Results

Here we briefly present the data obtained from the SOAR speckle campaign, as the results of interest for the remaining dissertation chapters will be the orbits fit to these data rather than the data points themselves.

Overall, of the 337 M dwarf systems in the SOAR program, 1289 total speckle observations were made on all 337 systems. Of these, 216 (64%) were resolved. Notably, this includes new companions for 76% of the subset selected from Gaia DR2. Among the supplemental sample of 32 stars, 13 (41%) were resolved, indicating that stretching the criteria slightly does reveal additional multiples. In all, we report the first direct detections of 97 new stellar companions to the observed M dwarfs. Each of these companions was consistent with being physically associated with its primary star; a background star was resolved for one system (GJ 1068) and confirmed through the source’s motion in subsequent observations, thus that system is not included in the 97 here. The system-by-system results are given in Table 4 (Appendix 7.2).

To augment the SOAR speckle results, we also searched the literature for additional high-resolution imaging data on these targets to add to their data sets. These literature results were essential for (1) extending the time baseline of the observations to enable fitting longer orbits, and (2) informing or confirming the correct quadrant for the SOAR speckle data’s ambiguous position angles. The full list of references contributing data to each orbit fit is given alongside those orbits in Chapter 5.

4.4 Fitting Orbits to SOAR Speckle

An orbit is ready for its first fit when its shape becomes apparent in its imaging data. This state typically occurs when $\sim 40\%$ of the orbit is mapped by the data. Before the orbit’s true period and orientation are known, this coverage is estimated by computing the position angle change between the first and most recent observations and comparing the coverage to the 360° of a full orbit. Some consideration is also made for the companion’s speed — if the companion has considerably slowed or sped up over the course of the observations, the available observations (regardless of position angle percentage) may constrain the orbital eccentricity and thus period. A revised orbital fit is attempted when we acquire more data for a system, as the richer data set invariably improves the certainty of the result.

Each orbit is fit with the `ORBIT` code of Tokovinin (2016). This IDL routine uses a Levenberg-Marquardt least-squares algorithm to find the orbit model that minimizes the differences between the model and data in R.A. and Decl. Each data point is weighted by the inverse square of its uncertainty, with the uncertainty set to nominal values depending

on the instrument used for that observation. If an orbit is well-constrained by the data, varying these uncertainties by ± 1 mas does not significantly change the resulting best-fit orbit model.

The initial positions of the orbit parameters for **ORBIT** are set by the user. For this thesis, we began with either a previous fit from the literature, a photocentric orbit from RECONS astrometry, or a rough estimate of the orbital period and parameters set to nominal values ($e = 0.5$, $i = 45^\circ$, etc.). The fit was checked for robustness by adjusting these parameters (to $e = 0.3$, $i = 80^\circ$, etc.) and computing a new fit. Well-constrained orbits would quickly converge to the same result regardless of these adjustments.

If there are any points for which the position angle is still ambiguous modulo 180° — i.e., that flipping the position angle 180° produces an equally plausible path of motion — then we make that adjustment, re-compute the orbit fit, and compare that result with the prior fit. One of these two models must clearly fit the data better in order to be considered robust; if both are equally plausible, then the data are not constraining the models well enough for any model to be considered reliable.

For every model computed (including the data-flipping variations discussed above), we check the result by computing the total mass of the system and comparing that to the masses expected from the absolute magnitudes of those individual stars. Spectral types are also considered if they are available — in particular, the combination of I magnitudes and/or spectral types for a pair of stars can be used to determine whether or not either component is a white dwarf. This procedure provides a very rough check on the feasibility and robustness

of the result. Occasionally, the procedure at this stage reveals that the code is converging to a P_{orb} that is significantly too large or too small, and several speckle data points need to be flipped 180° to find the orbit that makes physical sense. If a published orbit was already available for this system, those results were compared to our new fit to determine if we were consistent within the uncertainties.

All the orbits we have fit from the SOAR speckle program are illustrated and discussed in §5.2.1.

CHAPTER 5

Results from Three Sources of Orbits

With our sample defined (§2) and observations completed and characterized from the RECONS astrometry program at the CTIO/SMARTS 0.9m (Chapter 3) and the speckle imaging program at the SOAR 4.1m (Chapter 4), we are now in a position to synthesize the results. In this chapter we describe the RECONS astrometry orbits (§5.1) and SOAR speckle orbits (§5.2), including our procedure for assessing the sensitivity of both surveys in P_{orb} vs. e space. Then we augment the sample with results selected from the literature (§5.3).

5.1 The RECONS Astrometry Results

Of the 696 systems on the RECONS astrometry program on 1 April 2023, 132 showed some sort of perturbation (PB) in their single-star fit residuals (§3.4) potentially due to a companion, and 78 of those 132 PBs clearly traced out orbital motion. Here we discuss 19 of those systems to which we fit orbits. Of the remaining 59 systems with orbital motion but no RECONS orbit presented here, many already had orbits published in the literature; if a literature orbit for a system was more precise, we used that in this dissertation in lieu of our RECONS characterization. Many clearly orbiting systems also have no fit here because the orbit was not yet fully mapped by the data, a situation which causes considerable difficulty with obtaining a reliable fit (§3.4.3). §5.1.1 presents the 19 unique RECONS orbits and their general statistics, and §5.1.2 analyzes how well those orbits represent the P_{orb} vs. e parameter space for this thesis, driven primarily by our desire to map orbits on timescales of 0–30 years.

5.1.1 Orbits from RECONS Astrometry

The RECONS astrometry program yielded 19 systems for which we determined a reliable orbit fit. These orbits span 5–29 years in orbital period and 0.06–0.87 in e , as shown in Table 5 (Appendix 7.2). Roughly half of the systems have primary stars with masses $\lesssim 0.35 M_{\odot}$, as suggested by the HRD in Figure 5.1, in which $M_V = 11.37$ mag corresponds to $0.35 M_{\odot}$. The astrometric technique of measuring the target’s position with respect to reference stars generally favors the lower mass M dwarfs (12–16 mag, for the 0.9m program) because fainter stars allow longer exposures, which in turn result in smoother point spread functions (PSFs) and better centroids (§3.2). Hence, somewhat counterintuitively, the sensitivity to companions for faint stars is better than for bright stars.

Orbits that could be reliably determined include every orbit with:

- $P_{\text{orb}} \gtrsim 3$ years and signal-to-noise (S/N) $\geq 3\sigma$ in R.A. and/or Decl., where σ represents the average uncertainty of the per-epoch position measurement — resulting in clearly traced orbital motion considering our cadence of 2–4 data points per year per target, and
- Orbital period shorter than the time baseline of observations — allowing proper motion to be clearly disentangled from orbital motion (§3.4).

A few systems that violated the time baseline rule were added by holding the proper motion fixed to the most likely value determined from a preliminary fit of proper motion, parallax, and orbital motion.

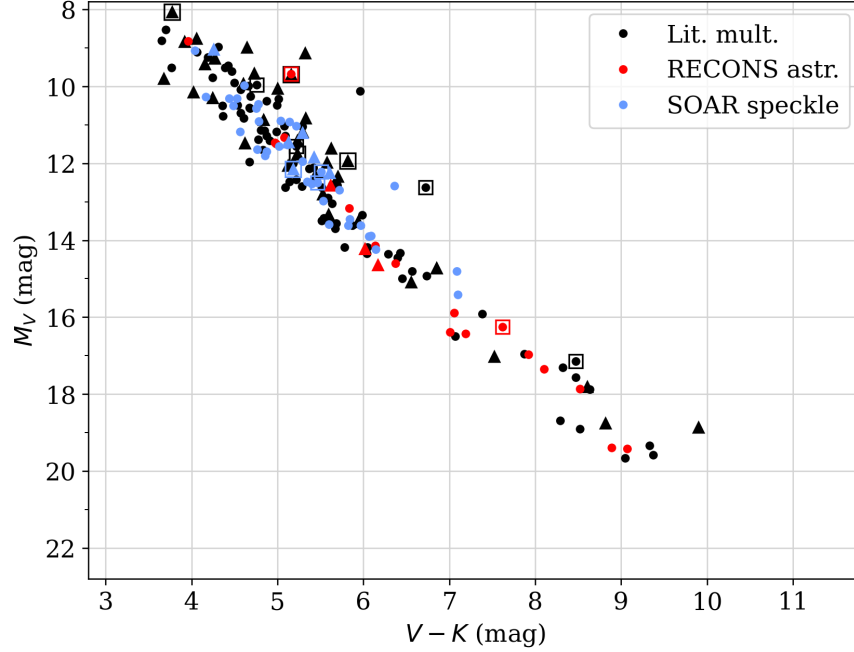


Figure 5.1 Hertzsprung-Russell diagram of every system with an orbit presented in this work. One point is plotted per system, representing combined magnitudes for unresolved pairs. Circular points are binaries and triangular points are subsystems of higher-order multiples, and boxes indicate systems that are likely young. Colors refer to the source of the orbit: RECONS astrometry (red; Chapter 3), SOAR speckle interferometry (blue; Chapter 4), or the literature (black; §5.3).

Systems with projected separations exceeding $\sim 0''.8$ at maximum were usually excluded, as this is the limit where the two stars' PSFs look like two peaks rather than one unresolved source, depending on the seeing. This consideration is important because the overlap in the PSFs shifts the peaks' positions toward each other, and as the seeing changes the PSFs' shapes, so too does it change those peak positions. The typical seeing at the CTIO/SMARTS varies over $0''.8$ – $2''.0$ from night to night, thus point sources with separation in that range will be unresolved in bad seeing and resolved (but with PSFs superimposed) in good seeing. This issue may be alleviated by the labor-intensive process of fitting the PSFs of both stars

simultaneously in every image, but this is only done in particularly compelling cases, such as the nearby young binary AT Mic AB (Holden et al. 2023). The potential bias introduced by excluding systems with $\gtrsim 0''.8$ separation are explored at the end of §5.1.2.

Figures 5.2–5.5 show all 19 orbits determined from RECONS astrometry, and their orbit parameters are given in Table 5 in Appendix 7.2. We fit each orbit with the Dieterich et al. (2018) MCMC code, as discussed in §3.4. Three of these orbits also have fits published in the literature from other groups using other techniques. Results are consistent between previous orbits and the new results shown here, and for the cases shown here our RECONS orbits are improvements over those previously published results, usually because we have significantly longer data timelines. The remaining 16 orbits are new, with no orbit characterization published before this work. Every RECONS orbit presented here has P_{orb} determined to 5% or better, with three-quarters of the orbits having P_{orb} determined to better than 3%.

5.1.2 Sensitivity of the RECONS Astrometry Data

To understand how well the RECONS contribution of orbits represents the full distribution of orbits in the solar neighborhood, we have undertaken an analysis of the sensitivity of the RECONS astrometry as a function of P_{orb} and e . This sensitivity analysis required simulating 2500 orbits for each system observed and counting how many of those orbits would create astrometric signals we could detect — effectively an injection-recovery procedure.

The simulations for the sensitivity analysis were generated as follows:

1. for every target in the RECONS volume-complete sample ($\pi < 60$ mas and Decl. $< 0^\circ$), we calculated its absolute K magnitude. We then identified every combination of

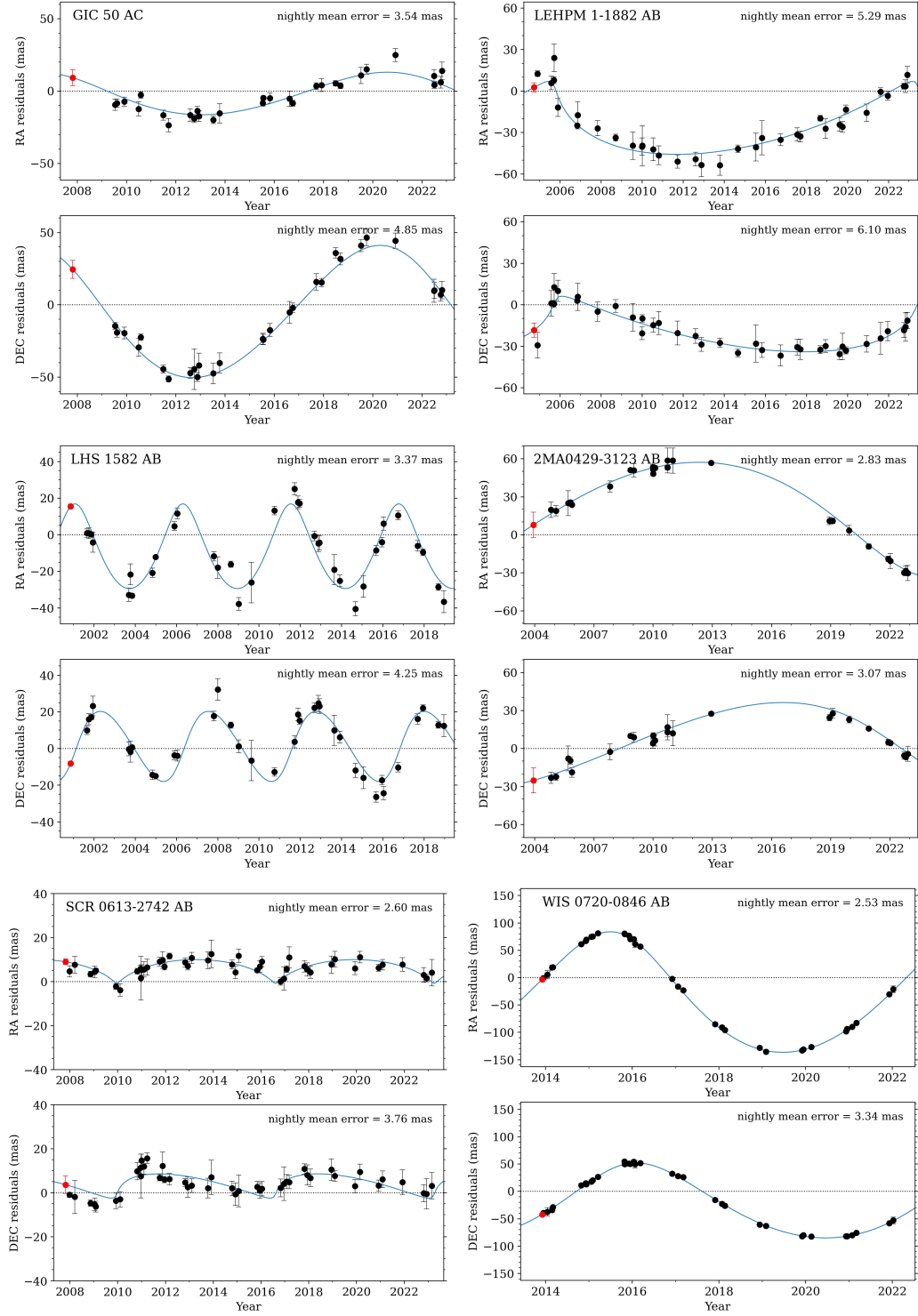


Figure 5.2 Orbits fit from RECONS astrometry (shown in R.A. order). For each system, the upper panel shows residuals with respect to R.A. over time, the bottom panel shows residuals with respect to Decl. over time, and the blue curve shows the orbit model fit (§3.4).

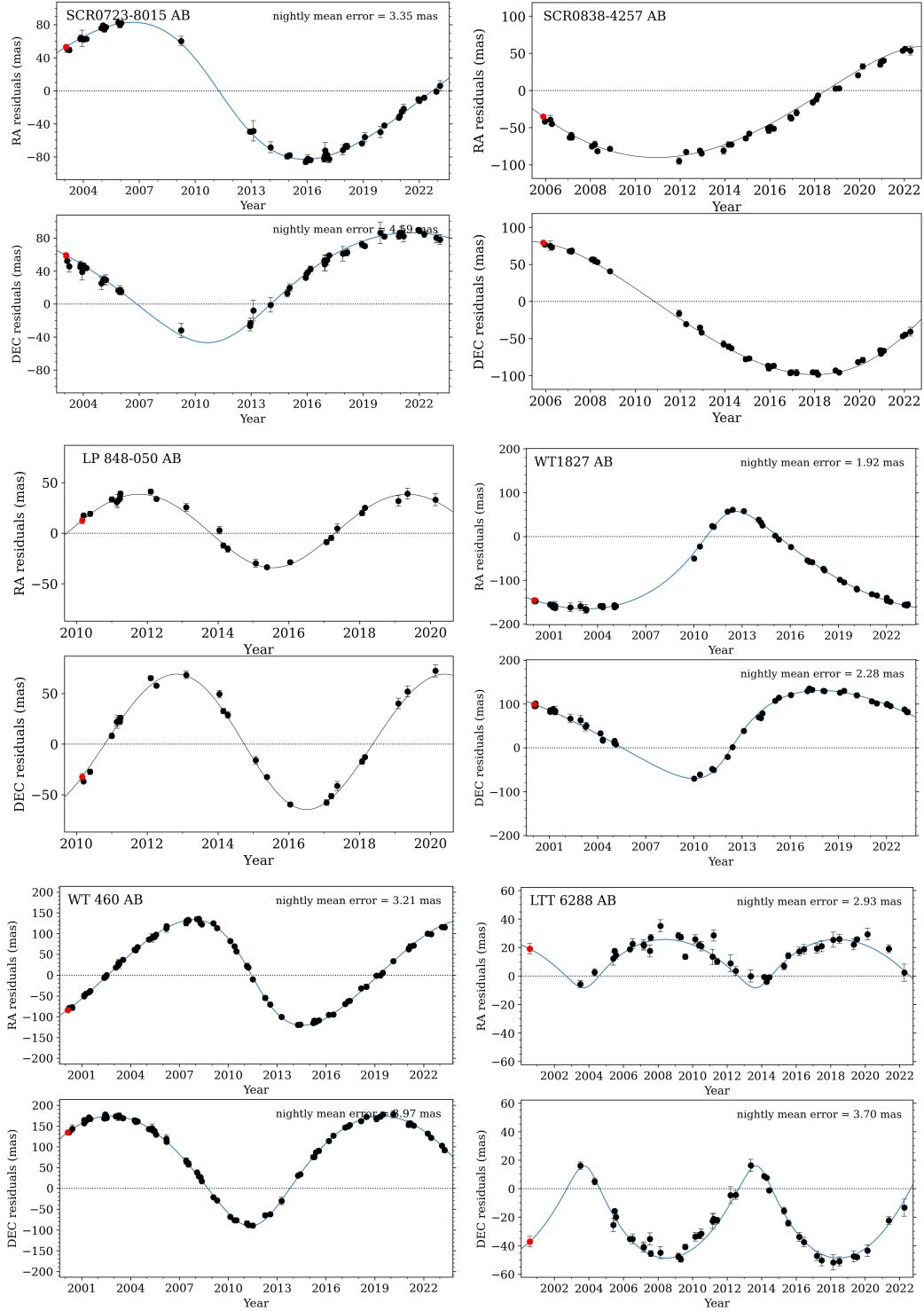


Figure 5.3 Orbits fit from RECONS astrometry (shown in R.A. order). For each system, the upper panel shows residuals with respect to R.A. over time, the bottom panel shows residuals with respect to Decl. over time, and the blue curve shows the orbit model fit (§3.4).

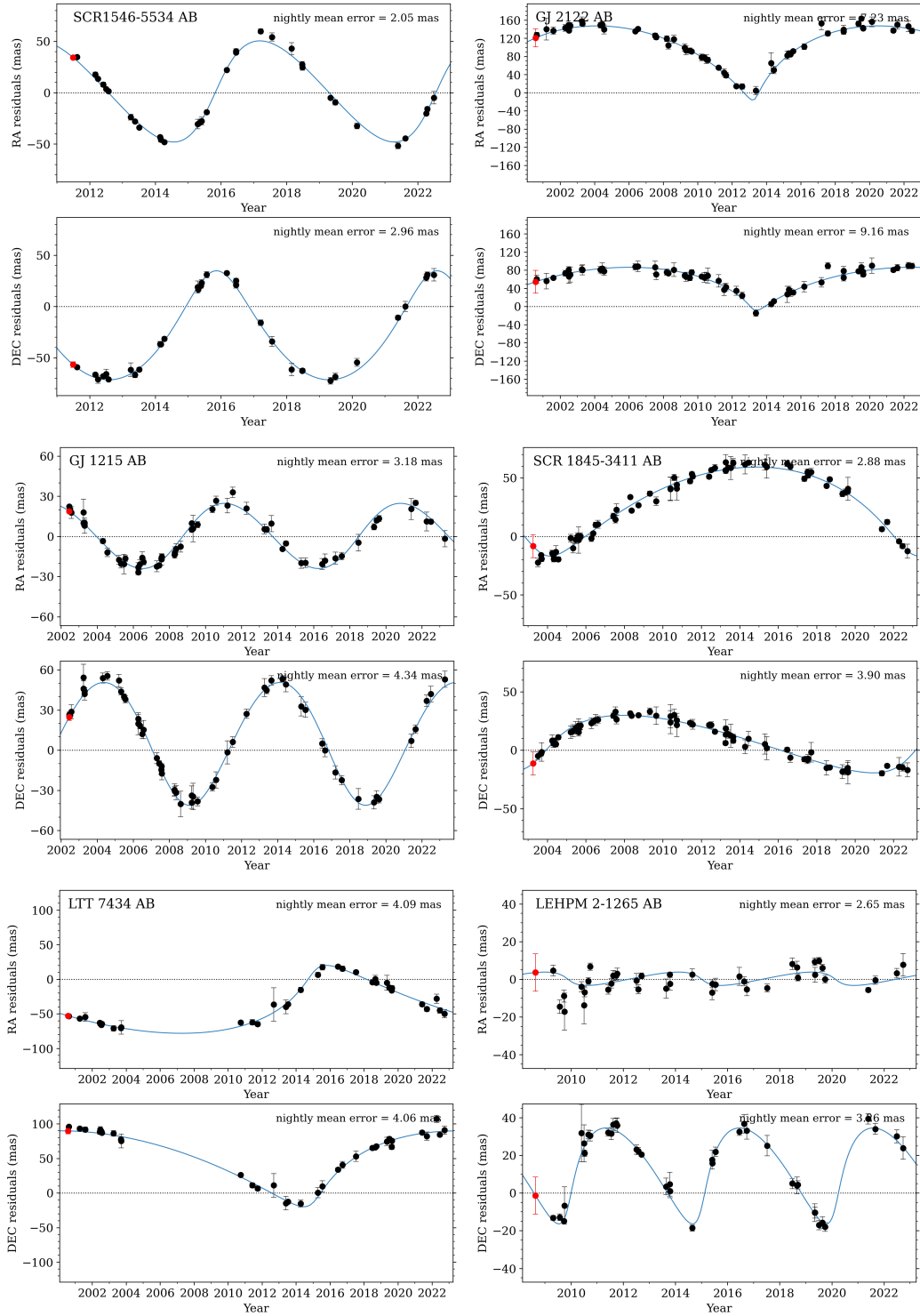


Figure 5.4 Orbits fit from RECONS astrometry (shown in R.A. order). For each system, the upper panel shows residuals with respect to R.A. over time, the bottom panel shows residuals with respect to Decl. over time, and the blue curve shows the orbit model fit (§3.4).

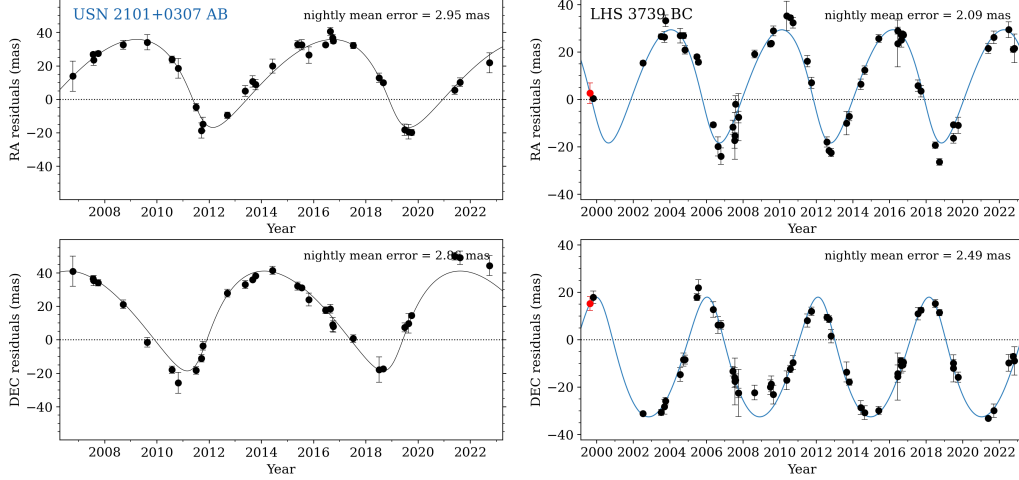


Figure 5.5 Orbits fit from RECONS astrometry (shown in R.A. order). For each system, the upper panel shows residuals with respect to R.A. over time, the bottom panel shows residuals with respect to Decl. over time, and the blue curve shows the orbit model fit (§3.4).

primary and secondary mass (M_1 and M_2) that could have a combined M_K matching that measured value according to our corrected K -band MLR (§2.2.1).

To ensure reasonable computation time, before beginning this analysis we generated a grid of combined M_K values corresponding to each possible M_1 and M_2 combination. M_1 was varied between $0.60 M_\odot$ and $0.08 M_\odot$, and M_2 between $0.60 M_\odot$ and $0.06 M_\odot$, both in steps of $0.01 M_\odot$. No mass combinations were duplicated in this grid — i.e., for the row corresponding to a given M_1 , only the columns for which $M_2 < M_1$ were populated (the grid was thus triangular in shape).

An extended grid was also calculated to use when a system could not find a match on the standard grid. This extended grid included masses every $0.001 M_\odot$ below $0.1 M_\odot$, to ameliorate the fact that absolute magnitude changes so rapidly with respect to mass below $0.1 M_\odot$.

2. For every compatible M_1 and M_2 combination, we calculated the threshold at which a PB would be detectable as three times the target's mean epoch uncertainty (i.e., 3σ). This threshold was chosen based on experience evaluating these signals by-eye throughout the program.
3. Each compatible M_1 and M_2 combination also corresponding to a specific mass and flux ratio, given as B and β in Eq. 3.1 (§3.4). These values were later required to calculate the photocentric PB of each simulated unresolved pair.
4. For every compatible (M_1, M_2) pair, we then stepped through each potential (P_{orb}, e) combination in our P_{orb} vs. e parameter space of interest (0–30 years in P_{orb} and 0.0–1.0 in e). To reduce computation time, the step sizes were 2 years for P_{orb} and 0.1 for e . For each of those potential orbits we calculated the expected PB of 2500 random snippets of randomly-oriented orbits using the following procedure:
 - (a) The semi-major axis of the simulated orbit was computed from Kepler's law given the M_1 , M_2 , and P_{orb} being considered. The distance to the system was then used to scale this semi-major axis from AU to arcseconds.
 - (b) An orbit orientation was chosen by selecting a random value of i and Ω between 0° and 180° and a random ω between 0° and 360° . To reduce computation time, these angles were restricted to multiples of 10° . These random angles were then converted to the corresponding Thiele-Innes constants (§3.4.2).
 - (c) A random point within the orbit was chosen as the starting point of simulated

observations. Because a companion moves quickly through periastron and thus is more likely to be observed at apastron, the potential starting point angles were evenly spaced but were each weighted by the time the companion takes to reach the following angle. The random starting point was thus drawn from this weighted distribution of angles. The procedure thus takes into account the role of e in the orbit's observability.

- (d) With all orbit parameters now determined, the companion's positions on the sky were computed from the chosen starting point to the end of the simulated observations, with that end point determined by the number of RECONS observations actually obtained for that target to date. An example for one simulated circular system is shown in the top panel of Figure 5.6 and for one simulated eccentric system in the top panel of Figure 5.7.
- (e) To mirror the process we use with real observations to detect PBs, we computed residuals of a single-star astrometric fit to this simulated orbit. We omitted parallax motion from these simulations because experience has shown that its contribution to the single-star residuals is minimal even when there is dramatic orbital motion¹ The proper motion fit was then assigned by a fitting a line to the simulated motion in R.A. vs. time and another line to Decl. vs. time. These fits are illustrated in the middle panels of Figures 5.6 and 5.7 with red dashed lines.

¹This is primarily because the parallax residuals are much smaller than the semi-major axis of the photocentric orbit (~ 1.5 mas vs. $\gtrsim 20$ mas). These residuals are small because the parallax ellipse wraps exactly once per year and we typically have many years of observations, so the ellipse is exceedingly well-determined.

- (f) We then multiplied the residuals to those fits, shown in the bottom panels of Figures 5.6 and 5.7, by the factor $B - \beta$ determined earlier for this (M_1, M_2) combination. That scaling shrunk the residuals to represent the photocentric orbit and create the final simulated PB.
- (g) Finally, we computed the amplitude of the simulated PB residuals and compared it to the threshold of detectability that was determined earlier for this system based on its mean nightly uncertainties (step 2). This random snippet of randomly-oriented orbit was thus counted as either a detection or non-detection for this (P_{orb}, e) combination.
- (h) After the above process was completed for one random starting point, steps 4c–4g were repeated until 50 random starting points (and associated orbit snippets) had been simulated. Then a new random orientation was selected, restarting the process at step 4b, until 50 random orientations had been explored. The end result was a count of the total orbits detected, out of 2500 simulated data sets, for that single (P_{orb}, e) combination.
5. The result of step 4 was a full accounting of what percentage of orbits would be detected for every (P_{orb}, e) for that (M_1, M_2) . The process was repeated for the next (M_1, M_2) combination compatible with the measured combined M_K . There were 5–15 of these compatible mass combinations for most systems.
6. After all compatible mass combinations had been simulated, we took the average of

their P_{orb} vs. e sensitivity results, generating a single P_{orb} vs. e sensitivity plot for each target. Two examples are given in Figure 5.8.

This process produced an assessment of sensitivity in P_{orb} vs. e space for each individual target. To assess the observing program as a whole, we then combined these single-target results by averaging over all the plots from the RECONS volume-complete sample that had enough data to be considered, which numbered 258 M dwarfs within 16.67 pc. The result, shown in Figure 5.9, indicates that for the volume-complete sample the RECONS program detects $\gtrsim 70\%$ of companions as long as they have $P_{\text{orb}} < 30$ years. The overall coverage is quite good, with only a few “softer spots” at $P_{\text{orb}} < 3$ years and at the longest-period + highest-eccentricity orbits. This validates that the volume-complete sample can be used to determine multiplicity statistics.

Not every detectable orbit in Figure 5.9 can be characterized, however, as the length of the observing baseline places a hard limit on our ability to distinguish proper motion from orbital motion (discussed further in §3.4). Additionally, the RECONS orbits presented in this dissertation are drawn not only from the volume-complete 16.67 pc sample, but also from targets we monitor out to 25 pc. The targets between 16.67 pc and 25 pc cannot be used to infer multiplicity statistics because they are only included if they are “interesting” (e.g., if they are multiple or exhibit significant photometric variability); thus, the more distant sample is affected by numerous selection biases. We can sidestep that potential overrepresentation of multiples, however, if we redefine our question as: *Given that a system is multiple, in which regions of P_{orb} vs. e space are we able to fit orbits?*

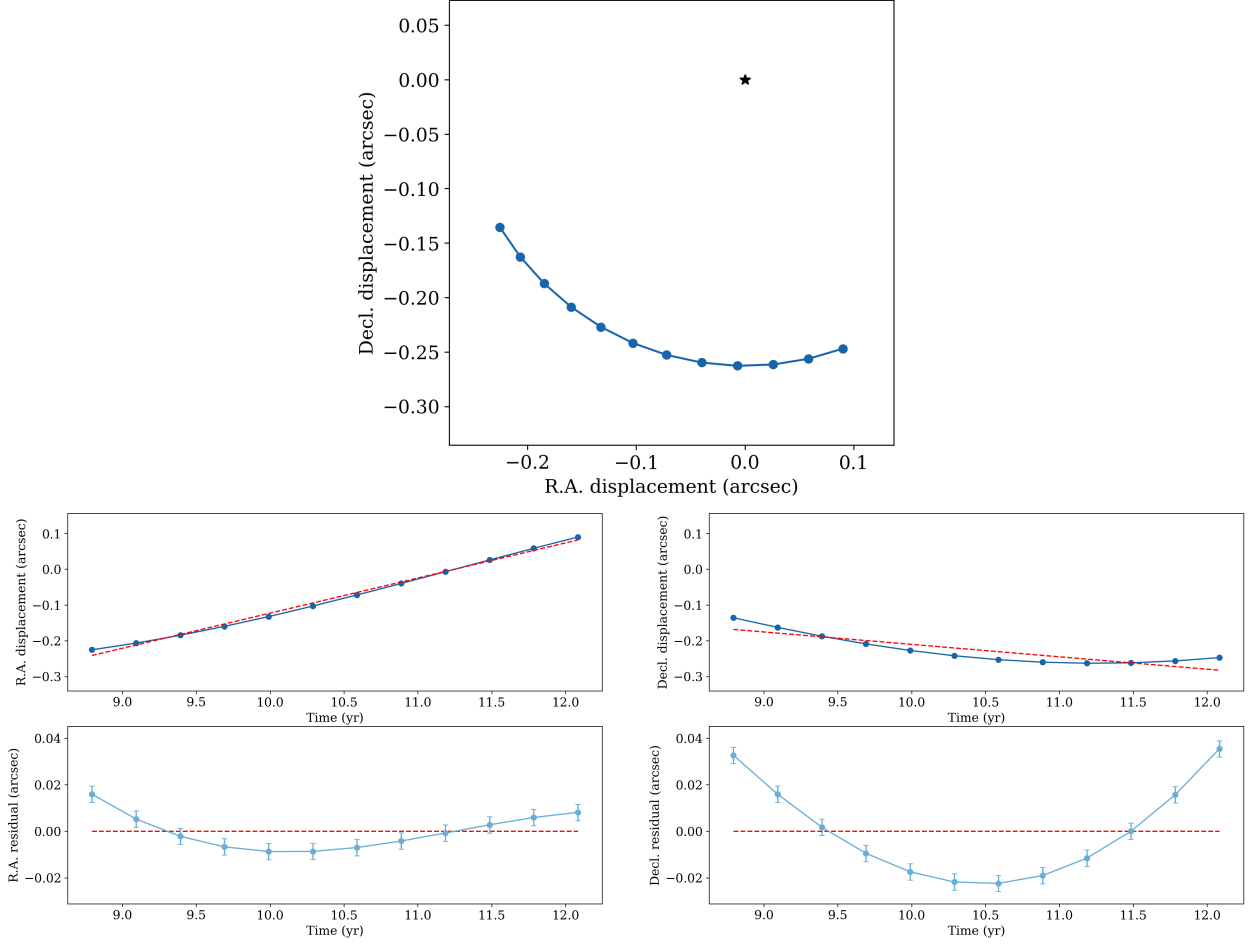


Figure 5.6 Example of a circular orbit used in the simulations that underpin the RECONS sensitivity plots. *Top panel:* simulated positions of a companion in a randomly oriented orbit on the sky, with each point representing its position at the time of RECONS observation. For the purpose of this demonstration, the random inclination angle were restricted to $\pm 30^\circ$ of face-on. *Middle panels:* simulated R.A. and Decl. displacements vs. time for the orbit snippet shown in the top panel. The red dashed line is the linear fit to the astrometry, representing the RECONS single-star model fit to the photocenter’s proper motion. Note that parallactic motion is not simulated nor fit here because those residuals are usually much smaller than the orbital motion (see step 4e). *Bottom panels:* simulated R.A. and Decl. residuals to the single-star fit, with the red line the same as in the middle panels. Error bars representing typical uncertainties are also illustrated now (and omitted from the top and middle panels for clarity). This residual is then multiplied by the $B - \beta$ factor for this (M_1, M_2) combination to produce the final simulated astrometric PB (not shown).

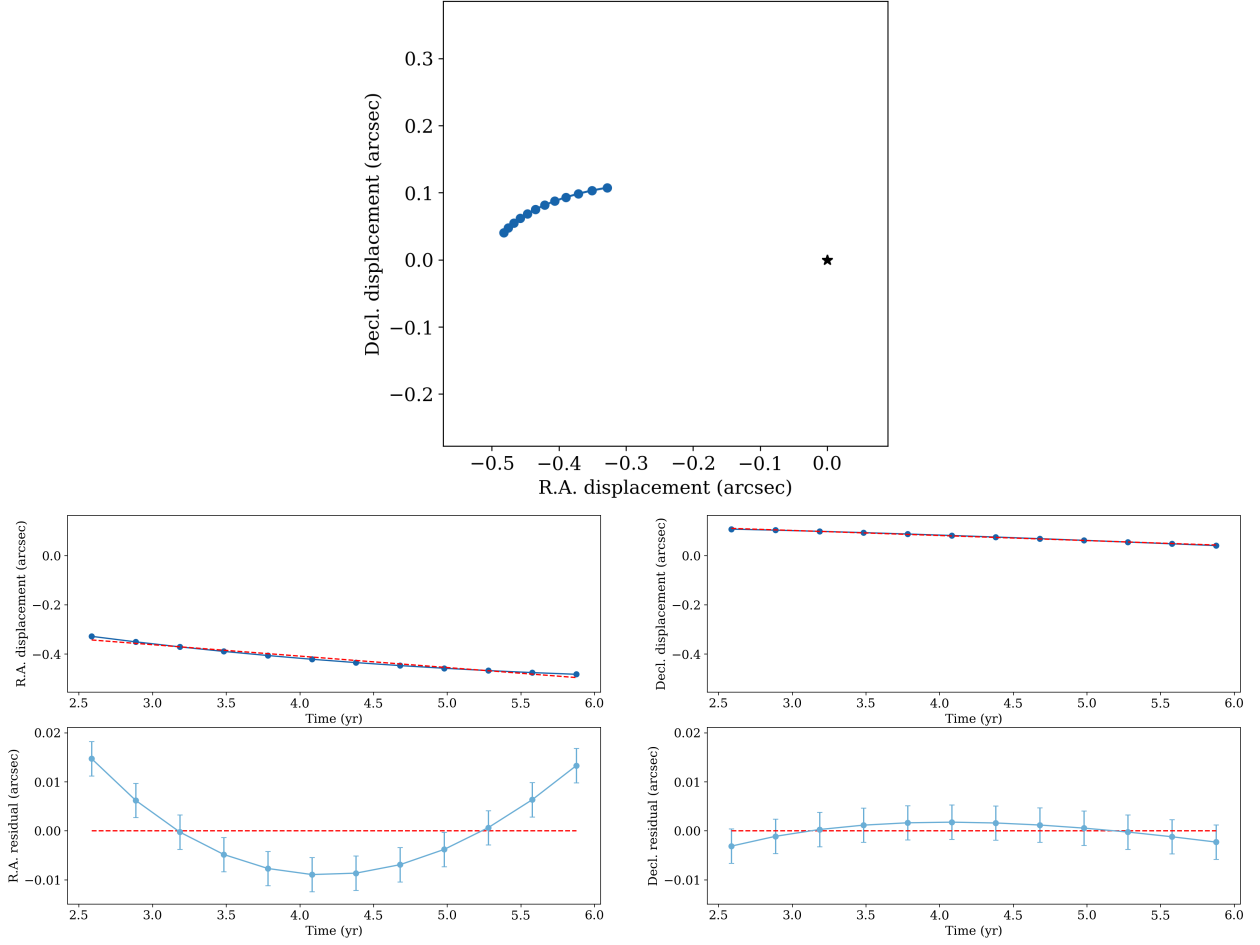


Figure 5.7 Example of an $e = 0.9$ orbit used in the simulations that underpin the RECONS sensitivity plots. Each panel is the same as in Figure 5.6, with the only differences being this orbit’s higher eccentricity and different randomly selected orientation angles.

To address this revised question of fitting capability, we completed the above sensitivity analysis using only confirmed and suspected multiples monitored by RECONS. This analysis included 127 multiples, after excluding 5 systems separated by $\gtrsim 0''.8$ because our current procedure for these systems does not produce astrometry suitable for orbit characterization (see §5.1.1)². We then zeroed out each multiple’s sensitivity plot for P_{orb} greater than

²This expanded sample of 127 systems is used in lieu of the 78 with clearly traced orbital motion because many of these systems are retained on the program only because of their astrometric PBs, regardless of

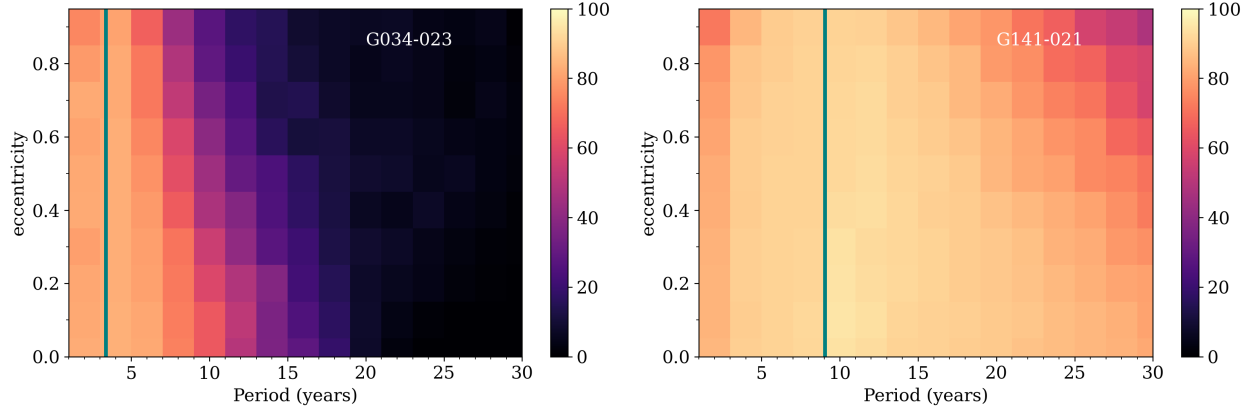


Figure 5.8 Examples of average sensitivity plots for two single stars: (*left panel*) G034-023, a star with limited coverage over only ~ 3.5 years, and (*right panel*) G141-021, a star with modest coverage over ~ 9 years. The color indicates the percentage of simulated orbits that were detectable given that system’s typical nightly astrometric uncertainty. The teal vertical line in each plot indicates the length of RECONS observations for that system to date; orbits longer than those baselines may be detectable, but cannot usually be fit reliably.

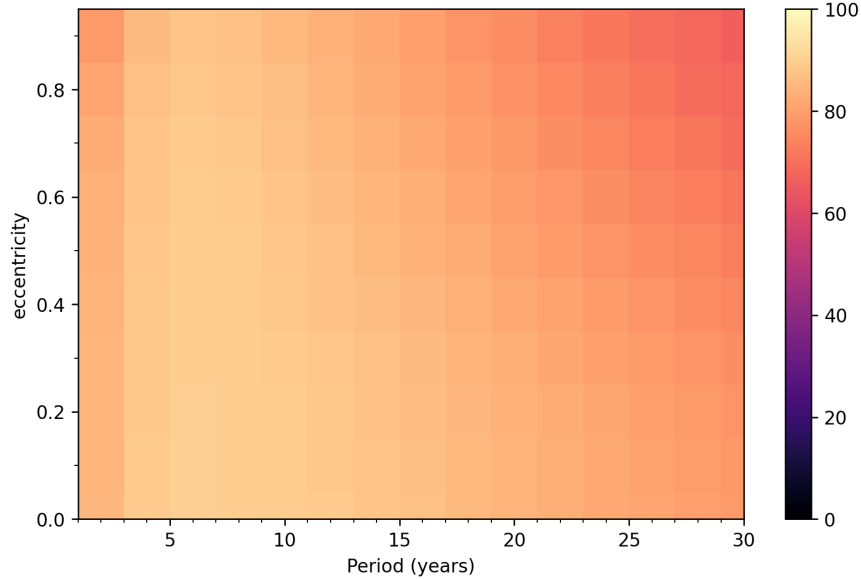


Figure 5.9 Average detection sensitivity in P_{orb} vs. e space for the subset of the RECONS 16.67 pc volume-complete sample which had enough data to be considered (258 red dwarfs). The colors represent the percentage of orbits that were detectable, calculated via the injection-recovery process described in §5.1.2 averaged over all systems in the sample. It is evident that at least 70% of orbits would have been detected for orbital periods of ≤ 30 years at effectively all eccentricities.

110% of that target’s observed baseline. This effectively transformed the plot from *detection sensitivity* to *capability of an orbit fit*. We then re-computed the average over all the multiples monitored.

The left panel of Figure 5.10 shows the fraction of orbits we are able to fit, given that a system is multiple (or potentially multiple), across P_{orb} vs. e space. The plot varies very little in e because the detection sensitivity for this sample of multiples is nearly identical to Figure 5.9 due to our generally excellent time coverage of these systems (right panel of Figure 5.10); cutting off systems at 110% their time baseline to translate that plot to fit capability then creates the striped pattern of the final plot. This result shows that as expected, we are best at fitting binaries with orbital periods of $\sim 5\text{--}10$ years, and worst at fitting very short and very long P_{orb} . This efficacy distribution is driven by the decades-long RECONS data sets for most of these systems; overall, the median observing baseline for these multiples is 18.26 years. The right panel of Figure 5.10 shows the multiples considered in this analysis on the HRD, to give a sense of how well they represent the M dwarf main sequence.

Overplotted on Figure 5.10 are the P_{orb} vs. e values for the 19 orbits characterized for this dissertation. Although the distribution is sparse, the number of stars in each 5 year bin of P_{orb} does increase somewhat from $30 \rightarrow 5$ years, following the prediction of the fit capability map. Orbits with $P_{\text{orb}} \lesssim 3$ years are missing because the MCMC fitting algorithm currently does not usually converge on e in those cases. This issue is related to the low

whether those PBs are clearly orbital (78 systems) or questionable in nature but not consistent with single-star motion (49 systems). Internally within RECONS these sets are known as “PB!” and “PB?”, respectively.

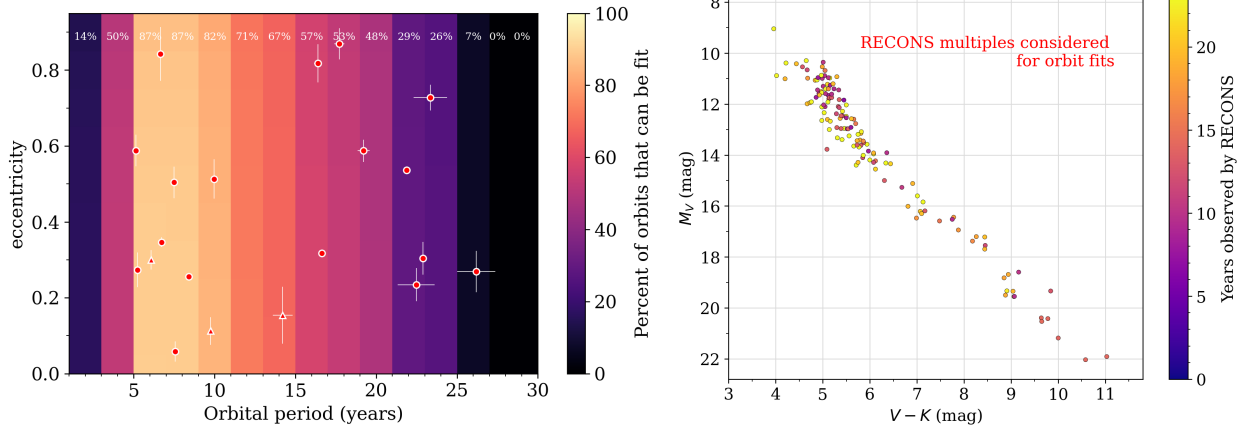


Figure 5.10 *Left panel:* average percentage of orbits that can be fit, as a function of P_{orb} vs. e , for 127 multiples and suspected multiples followed by the RECONS astrometry program. For clarity, the exact values for the patches in the topmost row are printed in white. This fit capability map was created by averaging the fit capability maps of the individual multiples (following §5.1.2). The variation is quite low in e because coverage is generally excellent for these systems and their detectability plot was nearly uniform, as noted in the text. Overplotted are P_{orb} vs. e values for the orbits fit from RECONS astrometry, with circles for binaries and triangles for subsystems of triples and quadruples. *Right panel:* Hertzsprung-Russell diagram of the multiples analyzed in this sensitivity analysis, with each point’s color indicating the time baseline over which it has been observed.

S/N of those systems (their orbits have relatively small photocentric semi-major axes) and our sparse observing cadence of only 2–4 epochs per year. Because we could not model this unsolved issue in our sensitivity analysis, here we have assumed that only 20% of orbits with $P_{\text{orb}} \leq 3$ years can be fit, as experience has shown that that is the fraction that are unaffected by this non-convergence issue.

Finally, in §5.1 we discussed that our RECONS sample excluded systems with separations $\gtrsim 0''.8$ because their PSFs were seeing-dependent. This sampling biases the results somewhat against high-eccentricity orbits and against the most massive M dwarfs. This is because two M dwarfs with total mass $\gtrsim 0.55 M_{\odot}$ and separation of $0''.8$ could have an orbital period in

the 20–30 years range if they are very nearby, such as at 10 pc. The potentially excluded mass range is even wider if their orbits are eccentric and $0''.8$ represents those systems’ apastrons. As discussed in §3.4.1, our astrometric technique can rarely observe stars with $\gtrsim 0.5 M_\odot$ or with very similar-mass components, and both these biases are incorporated into the sensitivity analysis presented here. The $0''.8$ sample bias thus excludes systems for which the primary is $0.325\text{--}0.475 M_\odot$ and secondary is $0.075\text{--}0.275 M_\odot$ (such that the primary and secondary sum to $\geq 0.55 M_\odot$). These requirements are fulfilled by 5% of the mass combinations (for systems nearer than 15 pc) considered in the sensitivity analysis above, thus the sensitivity in the 20–30 year P_{orb} range may be inflated by $\sim 5\%$.

5.2 The SOAR Speckle Data

As outlined in Chapter 4, the SOAR speckle program imaged 337 potential multiples between July 2019 and March 2023, and continued observing 225 of these systems to map their companions’ motions. Of those resolved pairs, 42 yielded enough data (in combination with other imaging in the literature) to enable reliable orbit fits. In §5.2.1 we present these SOAR speckle orbits and their basic demographics, and in §5.2.2 we analyze how well those orbits represent the population we were sensitive to in P_{orb} vs. e space.

5.2.1 Orbits from SOAR Speckle Interferometry

The SOAR orbits span 0.7–28 years in P_{orb} and 0.02–0.90 in e , providing an excellent complement to the RECONS orbits by extending toward shorter orbital periods. Many of the systems have orbits mapped using SOAR data previous to our ~ 4 year program, supple-

mented by data from the literature. Figure 5.1 shows that these systems are concentrated in the $\sim 0.15\text{--}0.60 M_{\odot}$ area of the main sequence, balancing the RECONS sample in the mass regime as well. Many of the lowest-mass targets on the SOAR program were supplied by the RECONS astrometry program (Chapter 3), which can reach much fainter stars. The SOAR sample was limited mainly by the $I = 14$ mag faintness limit of HRCam+SAM (§4.2).

For this sample from SOAR, we fit every orbit with more than four observations and $\gtrsim 144^{\circ}$ of motion in position angle, corresponding to at least 40% of a complete orbit. We omitted orbit fits for a handful of systems that were well-observed but had short periods ($\lesssim 1$ year) and already had high-quality orbits available in the literature, as the 180° ambiguity in position angle that affects these speckle data proved to be considerably challenging in those cases. The SOAR program also yielded several orbits with P_{orb} too long to be included in this study (>30 years) that will be incorporated into future efforts.

The SOAR orbits are shown in R.A. vs. Decl. space in Figures 5.11–5.15. As discussed in §4.4, each system was fit with the IDL code `ORBIT` (Tokovinin 2016). This code fits relative astrometry and (optionally) RV data simultaneously using a Levenberg-Marquardt algorithm to find the best-fit orbit model.

5.2.2 Sensitivity of the SOAR Speckle Data

To assess the representation of the SOAR P_{orb} vs. e results, we completed a sensitivity analysis that closely mirrored the procedure used for the RECONS astrometry program sensitivity (§5.1.2). For this analysis we omitted the program’s detectability assessment (i.e., Figure 5.9), as every system on the SOAR target list was either a suspected multiple or

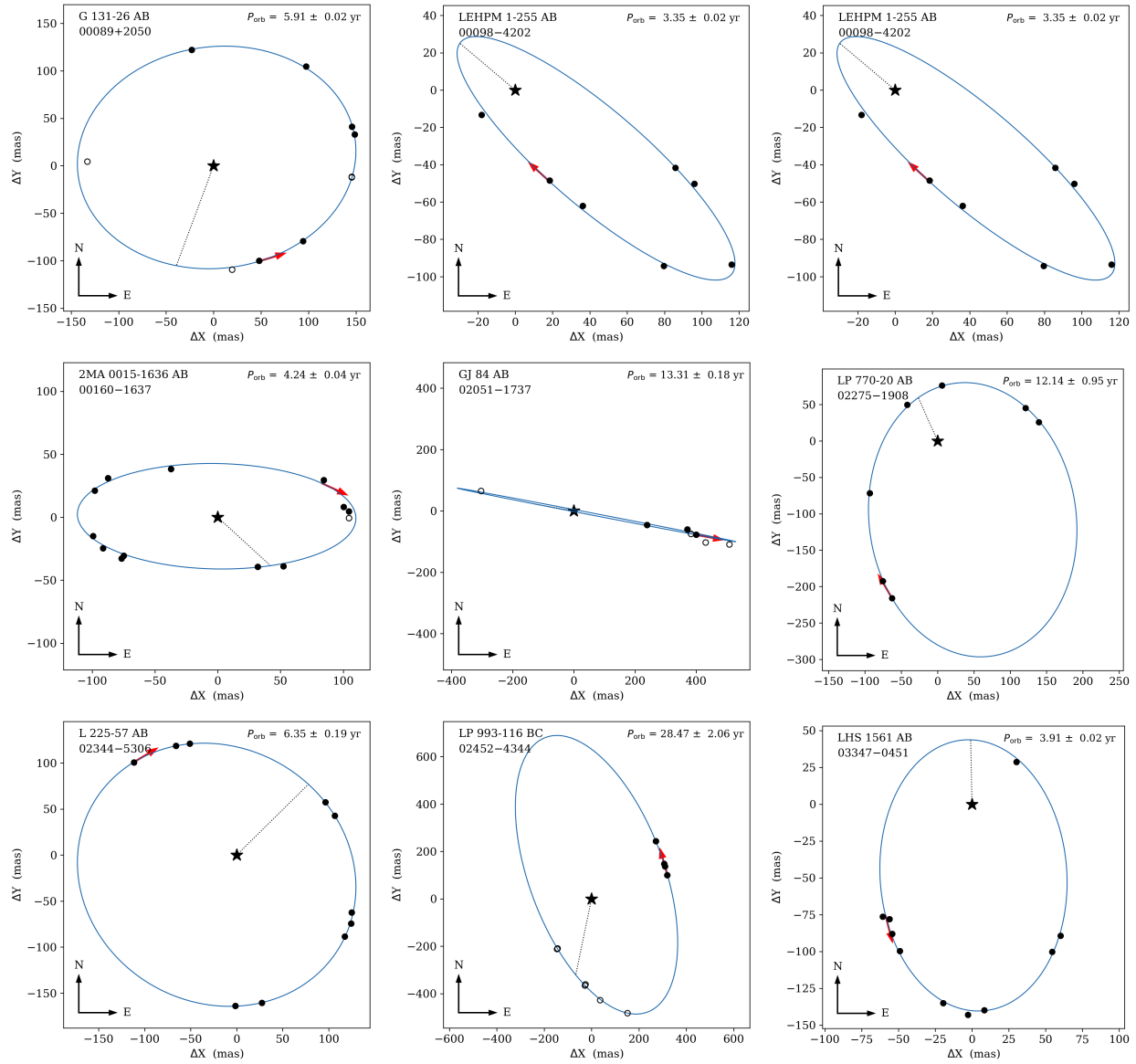


Figure 5.11 Orbits fit to SOAR speckle interferometry (filled points) combined with available high-imaging data from the literature (open points). The systems are shown here in order of R.A., and each blue curve is the best-fit orbit model.

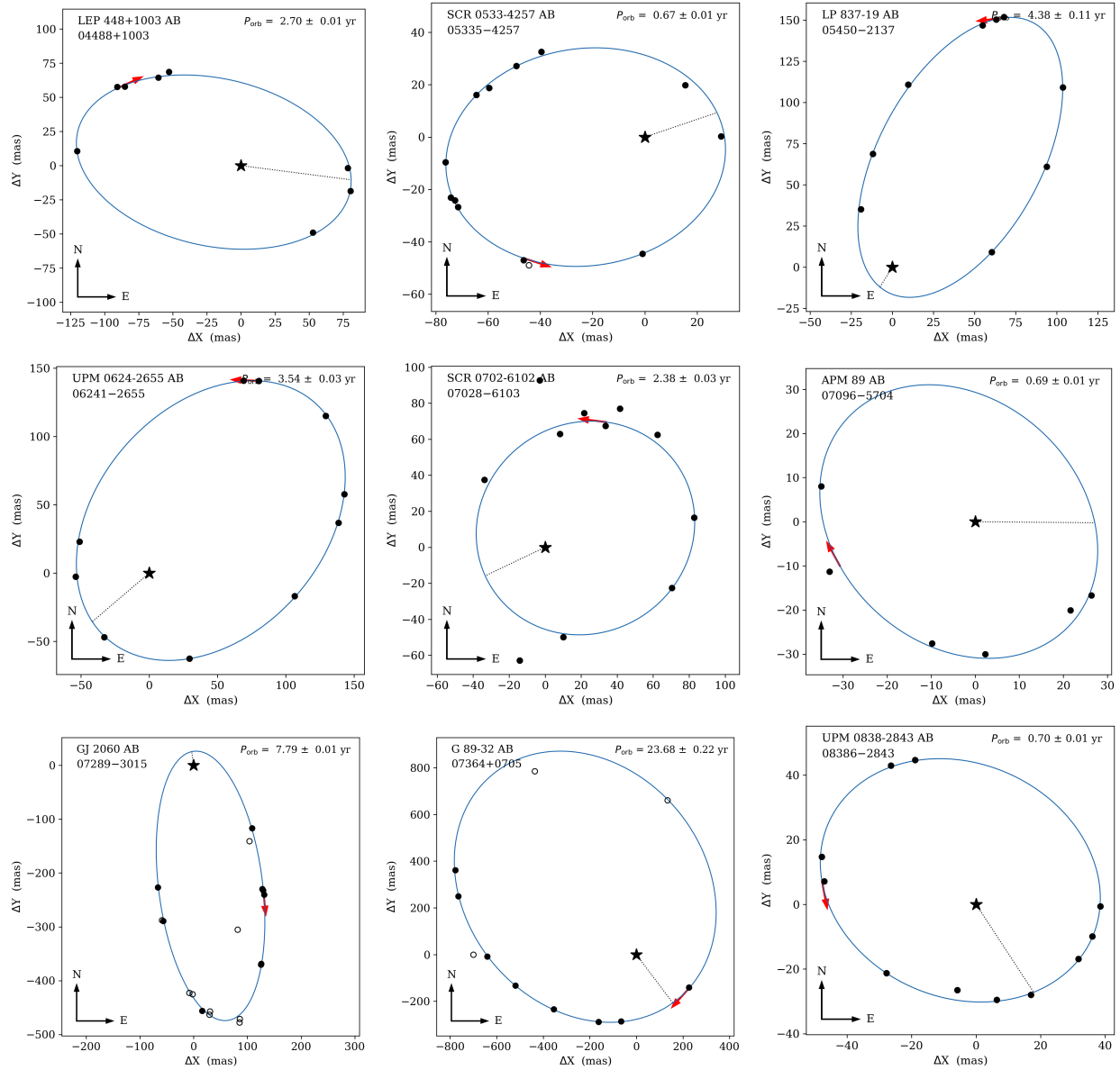


Figure 5.12 Orbits fit to SOAR speckle interferometry (filled points) combined with available high-imaging data from the literature (open points). The systems are shown here in order of R.A., and each blue curve is the best-fit orbit model.

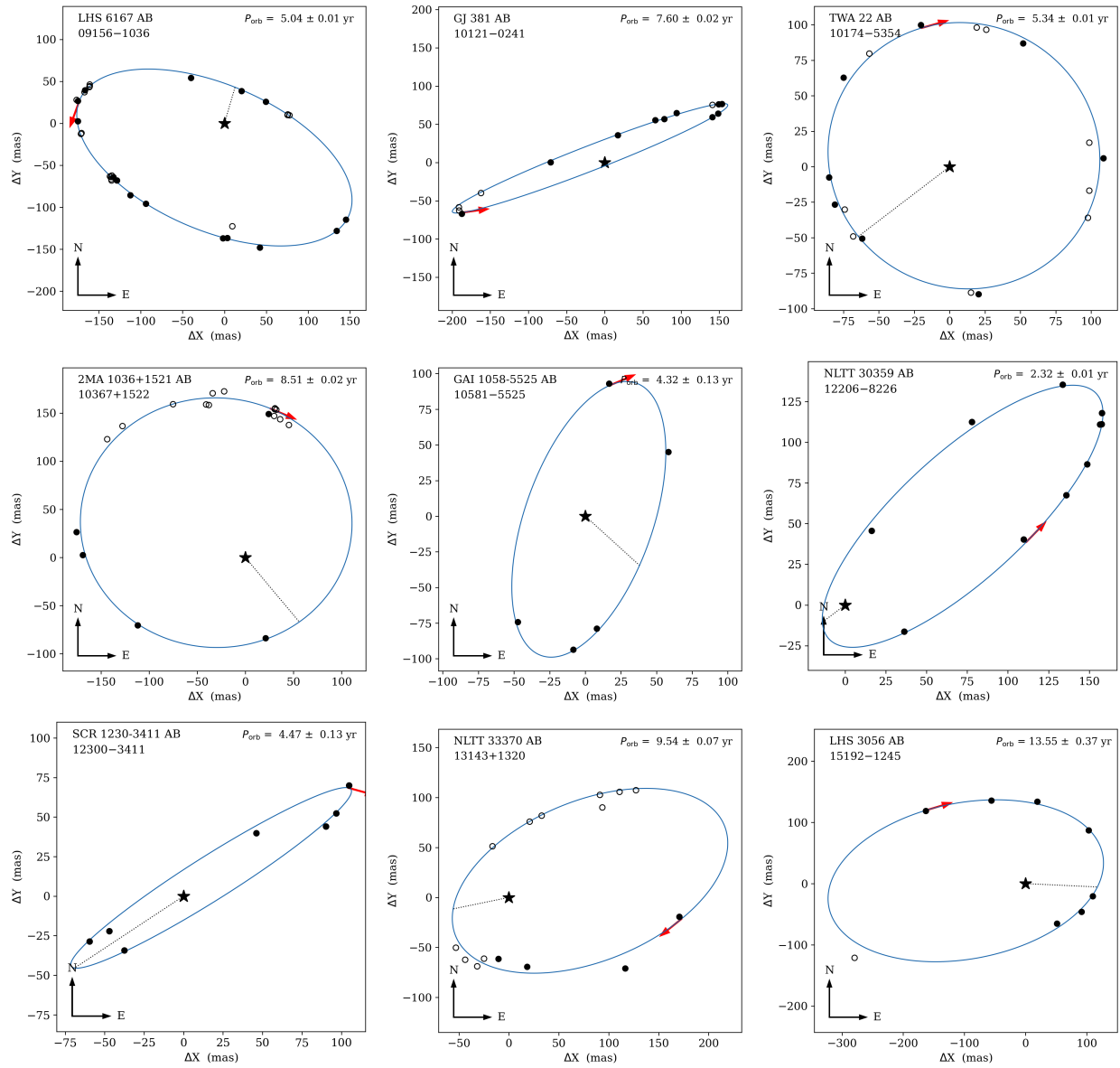


Figure 5.13 Orbits fit to SOAR speckle interferometry (filled points) combined with available high-imaging data from the literature (open points). The systems are shown here in order of R.A., and each blue curve is the best-fit orbit model.

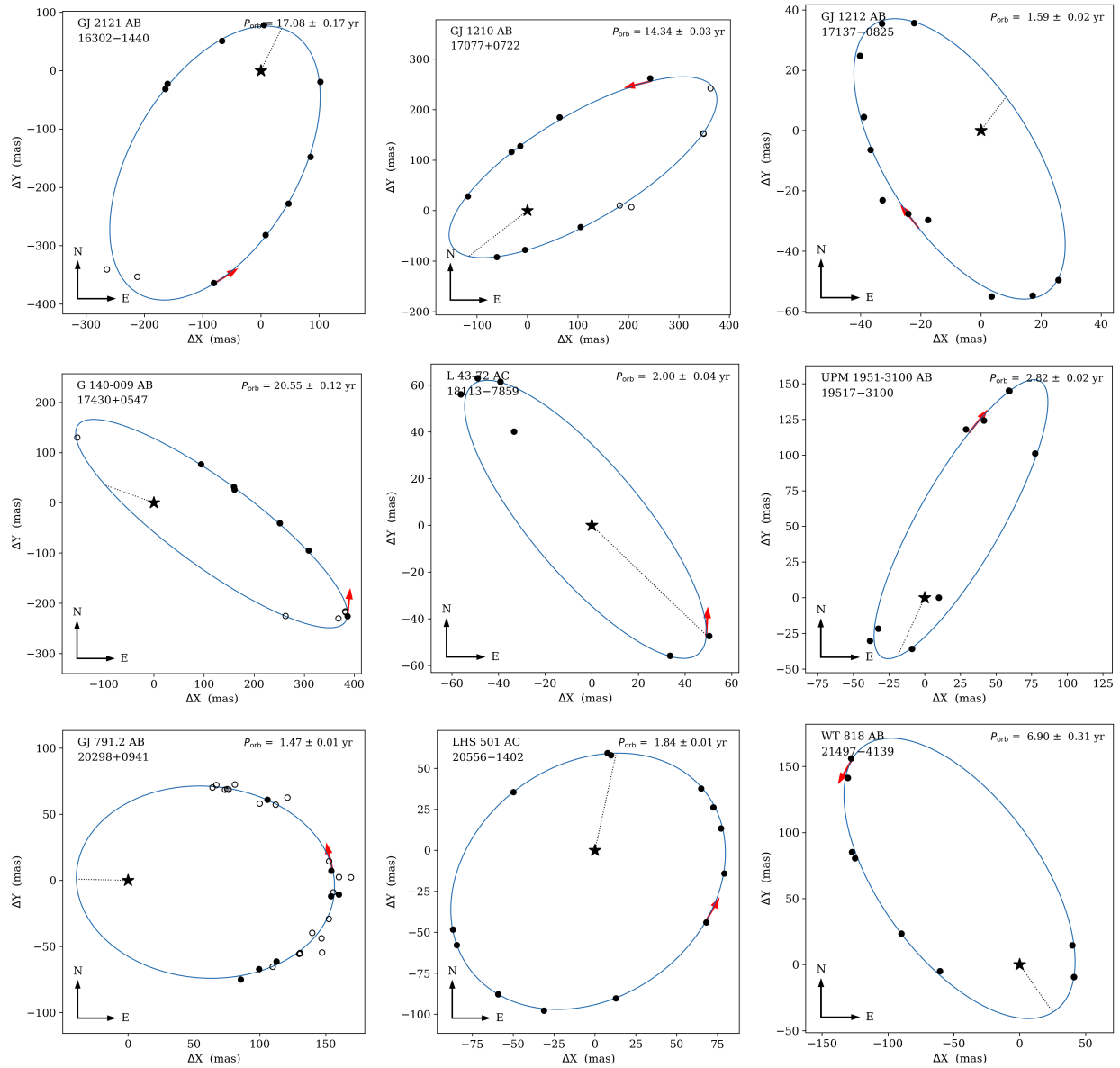


Figure 5.14 Orbits fit to SOAR speckle interferometry (filled points) combined with available high-imaging data from the literature (open points). The systems are shown here in order of R.A., and each blue curve is the best-fit orbit model.

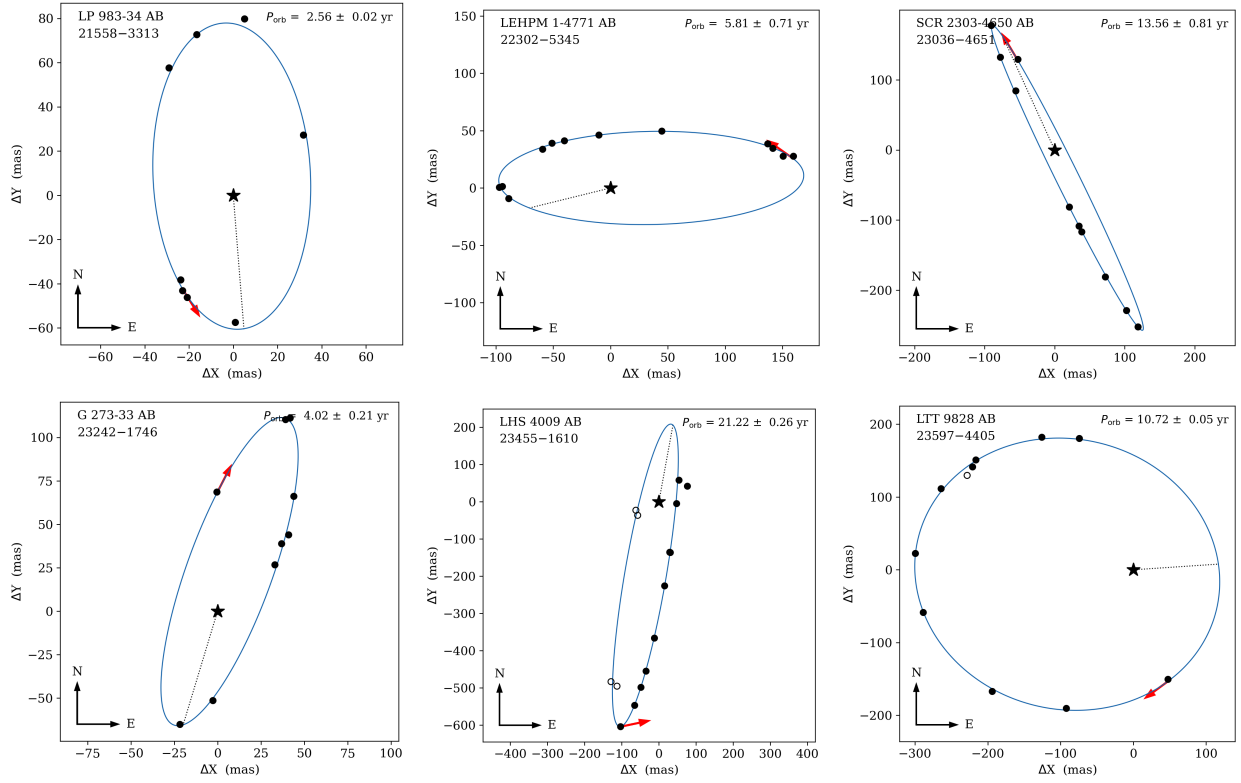


Figure 5.15 Orbits fit to SOAR speckle interferometry (filled points) combined with available high-imaging data from the literature (open points). The systems are shown here in order of R.A., and each blue curve is the best-fit orbit model.

known multiple established from a diverse array of previous data. We thus proceeded to the fitting step, computing the average fit capability plot for SOAR using only the targets with successfully detected companions. The goal of this analysis was to address the question: *For the given set of multiples monitored by the SOAR program, in which areas of P_{orb} vs. e space are we able to fit orbits?*

The simulations were conducted exactly as described in §5.1.2, with a few key differences for this relative astrometry data:

- Because the SOAR data provided ΔI magnitudes for every resolved system, for each

pair we calculated the M_I mag of each component and estimated their masses using the I -band pseudo-MLR derived in §2.2.2 (Figure 2.3). This step replaced the grid of combined M_K values and related steps used for the RECONS astrometry simulations (i.e., step 1 and the repetition for different compatible mass combinations).

Because we did not fit a mathematical function to those pseudo-MLRs, for each star in the pair we identified every point in the pseudo-MLR with M_I within 0.02 mag of that star, then averaged those points' mass estimates to arrive at a single mass for the star of interest.

- A system's simulated relative astrometry was deemed able to be fit if the simulated companion moved at least 144° in position angle (i.e., 40% of 360°) over its entire data set. These data included the 3.67 years of SOAR as well as imaging results from the literature if those were available. The fit capability criterion of 40% position angle coverage was chosen based on prior experience fitting orbits to these data (§4.4).

This simulated position angle calculation entirely replaced the simulated PB calculation (i.e., the linear fit and amplitude of residuals) in steps 4e–4g of §5.1.2.

As for the RECONS sensitivity analysis, at each (P_{orb}, e) point 50 randomly oriented orbits were simulated for each of the binaries, then each orbit was repeated for 50 simulated observing start times. This meant for each (P_{orb}, e) a total of 2500 orbit snippets were simulated and evaluated for fit capability.

Figure 5.16 presents the results of that sensitivity analysis for the SOAR data. It shows that our program should fit nearly all orbits with $P_{\text{orb}} \lesssim 8$ years, with 50% of orbits able to

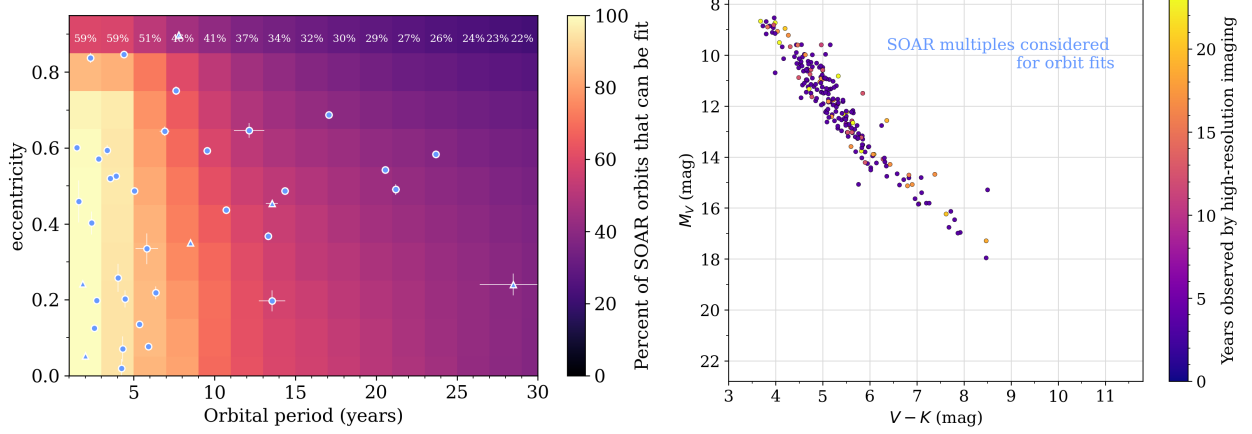


Figure 5.16 *Left panel:* average percentage of orbits that can be fit, as a function of P_{orb} vs. e , for multiples followed by the SOAR speckle program. This plot is analogous to that of Figure 5.10, but with fit capability defined as a companion moving through 40% of 360° over the observations (described in detail in §5.2.2). Overplotted is P_{orb} vs. e for the orbits fit from the SOAR speckle program, with circles for binaries and triangles for subsystems of triples and quadruples. *Right panel:* Hertzsprung-Russell diagram of the multiples analyzed in this sensitivity analysis, with each point’s color indicating the time baseline over which it has been observed, including literature data. The lack of low-mass systems (compared to, e.g., the RECONS program in the right panel of Figure 5.10) is mainly due to the $I \leq 14$ mag limit of the SOAR speckle program.

be fit out to 15 years. A dropoff in sensitivity is evident for $e \gtrsim 0.75$ regardless of P_{orb} , which matches the bias first described by Harrington & Miranian (1977) based on the difficulty of fitting very eccentric orbits. Tokovinin & Kiyayeva (2016) also confirmed this trend in the context of binaries of solar-type stars.

Overplotted on Figure 5.16 is P_{orb} vs. e for the 42 orbits we have fit from the SOAR program. That distribution mainly follows the expectation from our fit capability plot, although for $P_{\text{orb}} \gtrsim 10$ years we lack orbits with $e \lesssim 0.3$ despite no strong decrease in sensitivity in that area. This suggests a lack of low- e orbits in the underlying population, the implications of which are discussed further in Chapter 6.

5.3 Adding Orbits from the Literature

Although our two observing campaigns have provided an avalanche of data, the rich history of binary star astronomy means the literature holds many well-characterized orbits as well. Because these orbits are from campaigns with different techniques or faster cadences than the observing programs carried out for this dissertation, these literature orbits fill critical gaps in the orbital period, eccentricity, and mass ratio parameter spaces.

5.3.1 *Selecting Literature Orbits of Nearby M Dwarfs*

To select literature orbits, we relied on the database of the Sixth Catalog of Orbits of Visual Binaries (“ORB6”; Hartkopf et al. 2001). We extracted systems with primary stars having masses $\leq 0.6 M_{\odot}$ from ORB6 by matching the coordinates of the 25 pc sample (from Chapter 2) to the ORB6 catalog coordinates. This selection was thus made based on each system’s photometry (all components combined) in *Gaia* DR2, so individual component masses were not strictly required. Each match was allowed a wide radius (1′5) to account for potential coordinate errors in individual publications, then any coordinates that were different by $\gtrsim 0′5$ between the catalogs were displayed over 2MASS images in Aladin to check (by eye) if they could belong to two separate sources instead of one.

Two sources of published orbits not included in ORB6 were also added to the selection. We identified M dwarfs in Mann et al. (2019) by computing their absolute K magnitudes and verifying they matched the M_K criteria in Table 2.1 (§2.2.2). Next, we identified astrometric M and L dwarf binaries from the *Gaia* DR3 Non-Single Star catalog (NSS; Gaia

Collaboration et al. 2022) via a cross-matching process identical to that described above for ORB6. Spectroscopic orbits given by *Gaia* NSS were also checked, but none had absolute magnitudes consistent with red dwarf primaries.

After this selection process, we located the publication cited for each literature orbit and verified the quality of their model fits. This process allowed us also to note the techniques used for their observations, any flags for system youth, and any masses or mass estimates for the system’s components. Orbits were omitted at this stage if their authors noted them as preliminary or if the orbital eccentricity or period had to be fixed (rather than treated as a free parameter) to reach a solution. Orbits were also omitted if their uncertainty in eccentricity was greater than 0.08; this restriction meant that the included orbits’s other parameters were determined to better than 3% uncertainty for all but a few systems.

Through this process we selected 132 orbits from published works. In the HRD of Figure 5.1, these literature systems (black points) span the entire main sequence, including near the hydrogen-burning limit of $M_V = 21.82$ mag (although they are elevated above that line in Figure 5.1 because that plot uses combined magnitudes).

5.3.2 Sensitivity of the Literature Results

The orbits published in the literature were obtained with a diverse array of techniques using a variety of instruments, adding considerable complexity to the task of assessing their observational biases. Some were the results of systematic surveys that reported all they detected, while many others were more sporadic efforts to characterize specific systems. We therefore did not conduct an extensive sensitivity analysis of this subset.

Table 5.1 Techniques used to observe and characterize the literature orbits used in this work. Relative astrometry refers to observations of a companion orbiting a primary star, while absolute astrometry refers to observing the pair’s unresolved photocenter orbiting its center of mass.

Technique	Number of orbits
absolute astrometry	24
relative astrometry	16
relative astrometry + absolute astrometry	15
radial velocities	42
radial velocities + eclipsing light curves	15
radial velocities + rel. or abs. astrometry	18

Instead, we can gain a sense of the parameter space explored by the literature by considering the methods used to map those orbits. The 132 orbits reported by the literature were obtained using the following techniques:

- relative astrometry from high-resolution imaging (e.g., speckle interferometry, adaptive optics, *HST* Fine Guidance Sensors)
- radial velocities (RVs) obtained via spectroscopy (both single-lined/SB1 and double-lined/SB2 systems)
- absolute astrometry of photocentric (unresolved) orbits (mainly the *Gaia* DR3 Non-Single Stars catalog and the CFHT/WIRCam survey of Dupuy & Liu (2017))
- light curves of eclipsing binaries (often in conjunction with RV data)

A significant fraction of the characterizations used a combination of these methods. The complete breakdown is given in Table 5.1.

These efforts ranged from three to 10 years in length, and 80% of the orbits they produced had $P_{\text{orb}} \leq 6$ years. These orbits also had to be at least 40% mapped by observations to

pass our informal quality check (§5.3.1). Together, these factors suggest that these literature sources were unable to fit orbits longer than 7.5–25 years (for campaigns 3–10 years long) — and indeed it is the case that 78% of the literature orbits used here have P_{orb} within that minimum 7.5 year limit (and 98% have P_{orb} within 25 years).

The most significant *caveat* of the literature sample is that the short P_{orb} regimes are dominated by orbits determined from RVs. Obtaining RV data requires a bright primary star — and, in SB2 cases, a similarly bright secondary star — which means a P_{orb} regime dominated by RV orbits may overrepresent massive M dwarfs and equal-mass pairs. In this dissertation, literature authors used RVs to characterize all of the orbits with $P_{\text{orb}} \leq 10$ days, and 55% of the orbits with $10 \text{ days} \leq P_{\text{orb}} \leq 1 \text{ year}$. Neither the SOAR nor RECONS observing program are very sensitive for $P_{\text{orb}} \leq 1 \text{ year}$, as those orbits are too tight for our speckle imaging and too fast for our sparse RECONS astrometry cadence. We must therefore apply caution in our later discussion (§6.4) about the mass ratio distributions and parameters that depend on mass ratios.

5.3.3 Distinguishing Binaries from Higher-Order Multiples

Finally, in this work we only briefly consider the dynamical evolution of systems with three or more components (triples, quadruples, etc.), which may proceed differently than that of binaries. With this potential issue in mind, we used *Gaia* DR3 to search each orbit reported here for common proper motion companions separated by 1–5 arcmin from the primary star. *Gaia* reports resolved companions with separations as low as $0''.7$, and reliably detects $\sim 100\%$ of companions separated by at least $1''.0$ within *Gaia*’s magnitude limit and

for applicable brightness ratios. A potential companion meeting these criteria was deemed to be a gravitationally bound companion if its parallax was within 8.0 mas of the primary star and its proper motion was within 50 mas/year of the primary's proper motion in both R.A. and Decl. directions. These specific limits were set by the values found in *Gaia* for widely-separated companions already evaluated during the RECONS program for binaries within 50 pc. This search for wide companions identified several dozen systems as triples or higher-order multiples, all of which were previously noted in the literature.

Overall, these thesis results include 138 binaries and 51 triples or higher-order multiples. These results are not indicative of the true fraction of higher-order multiples vs. simple binaries, as systems with more than two components are often noted but not characterized in orbit fitting work. Throughout this dissertation, the triples and higher-order multiples are always distinguished with triangular symbols or, for histograms, hatched bars.

CHAPTER 6

The P_{orb} vs. e Distribution for M Dwarfs and its Implications

In this chapter we finally present the full results of our accumulation of 193 M dwarf multiples' orbits. We discuss the overall assessments of orbital periods and eccentricities in §6.1, and in §6.2 we examine the short- and long-period regimes in detail. Next, in §6.3, we estimate masses of the systems, and in §6.4 we discuss the P_{orb} vs. e results in light of those mass estimates. In §6.4.4 we compare these M dwarf multiple results to those of solar-like and very low-mass multiples. Finally, in §6.5 we summarize the implications for M dwarf formation and dynamical evolution.

6.1 193 M Dwarf Orbits on One Plot

With orbits from the RECONS astrometry program, the SOAR speckle program, and the literature, Figures 6.1 and 6.2 show the full P_{orb} vs. e for 193 M dwarf systems. This includes 19 orbits from RECONS, 42 from the SOAR program, and 132 from the literature. These figures show the plot in terms of $\log P_{\text{orb}}$ (Figure 6.1) and linear P_{orb} (Figure 6.2) separately to highlight the behaviors in the short- and long-period regimes, respectively. At very short P_{orb} nearly all the orbits are circular, and at longer periods their eccentricities vary widely between an upper envelope and loose lower envelope of e .

As shown in the left panels of Figure 6.3, there are many systems with $P_{\text{orb}} \leq 1$ year. There is then a gentle dropoff in numbers from 1–8 years and a smattering of orbits out to 30 years. This pattern most likely reflects the longevity of observing programs focused on orbit determinations, because short-period orbits are easier to map completely and char-

acterize well than long period orbits. Nonetheless, it is encouraging that nearly 60 orbits are now available for M dwarf pairs with $P_{\text{orb}} = 10\text{--}30$ years, allowing us to evaluate their distribution for comparisons to formation scenarios.

In concert, the eccentricity histograms shown in the right panels of Figure 6.3 reveal a relatively flat overall distribution for $e = 0.1\text{--}0.6$, with a rather precipitous dropoff beyond $e = 0.6$. It appears that high eccentricity orbits are present, but not common, in populations of M dwarf multiple systems. These overall characteristics for $e > 0.1$ should be robust, given the detection capability evaluations described in Chapter 5 showing that we are sensitive to orbits of all eccentricities.

6.2 Zoom-in on P_{orb} vs. e Regimes

Specific regions of P_{orb} vs. e space can reveal important information about how these systems evolved, and we will later note differences in these regions with stellar mass. Here we introduce the “zoom-in” regions of most significance.

6.2.1 *Empirical P_{circ} for M Dwarf Systems*

Given sufficient time, every two-body system in an eccentric orbit will eventually migrate toward a circular configuration with tidally-locked components because every periastron passage raises tides that sap orbital energy. Thus, for the sample of M dwarfs with orbits presented here, there should be an orbital period below which all aged M dwarf systems are found in circular orbits. The log P_{orb} view of P_{orb} vs. e (Figure 6.1) shows that orbits with $P_{\text{orb}} \lesssim 7$ days are almost exclusively circular. The one exception to that rule is the

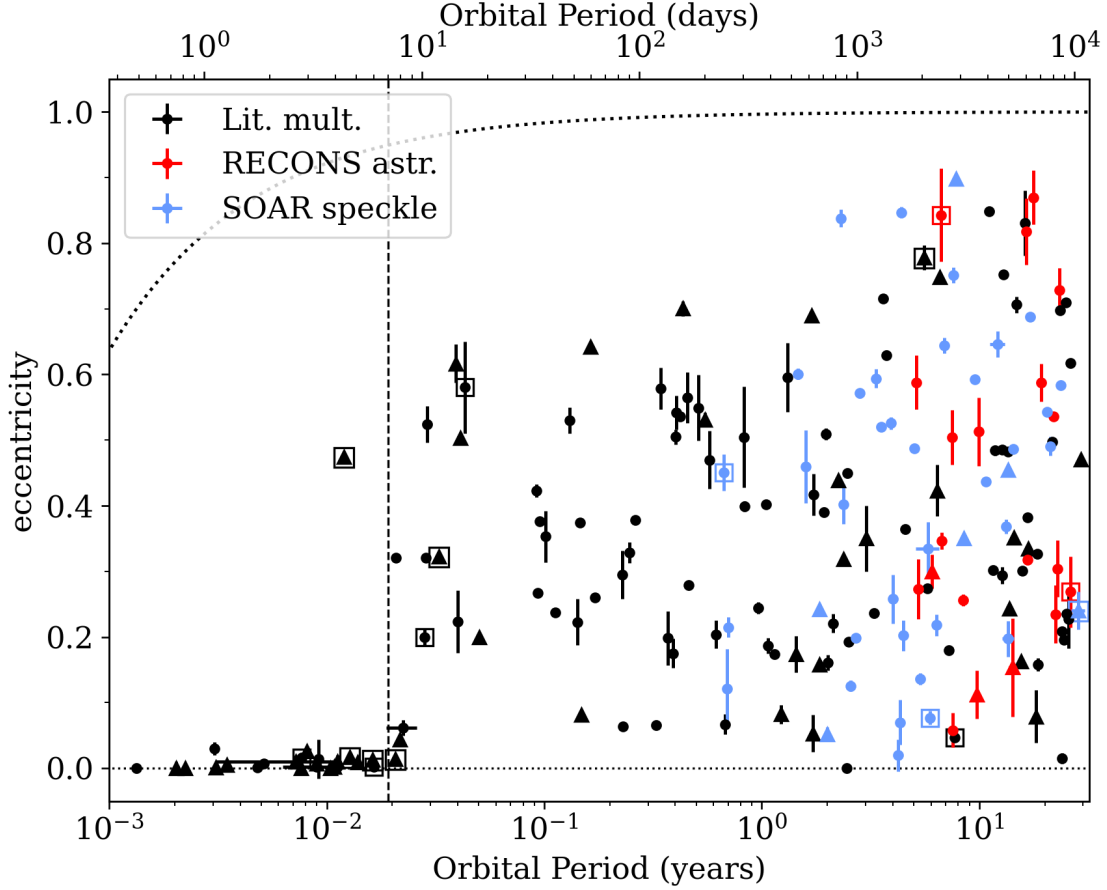


Figure 6.1 The distribution of P_{orb} vs. e for 193 systems with red dwarf stellar primaries shown in terms of $\log P_{\text{orb}}$. An equivalent plot with P_{orb} scaled linearly is given in Figure 6.2. Each point’s color indicates its source: fit from RECONS astrometry (red, 19 points), fit from SOAR speckle interferometry (blue, 42 points), and published in the literature (black, 132 points). Each point’s shape indicates multiplicity, with binaries as circles and triples and quadruples as triangles. Points known to be young systems are marked with open squares. The vertical dashed line indicates the $P_{\text{orb}} = 7$ days limit discussed in the text (§6.2.1). The dotted curve marks the limit at which two mid-M dwarfs would collide at periastron (§6.2.2).

young system HIP 47133 AB, which is a β Pictoris moving group member (Alonso-Floriano et al. 2015) and thus only ~ 24 Myr old (Bell et al. 2015), and is noted by Sperauskas et al. (2019) as synchronized but not circularized. That result is consistent with the prediction that tidal torques synchronize a binary pair’s rotation more quickly than it circularizes their

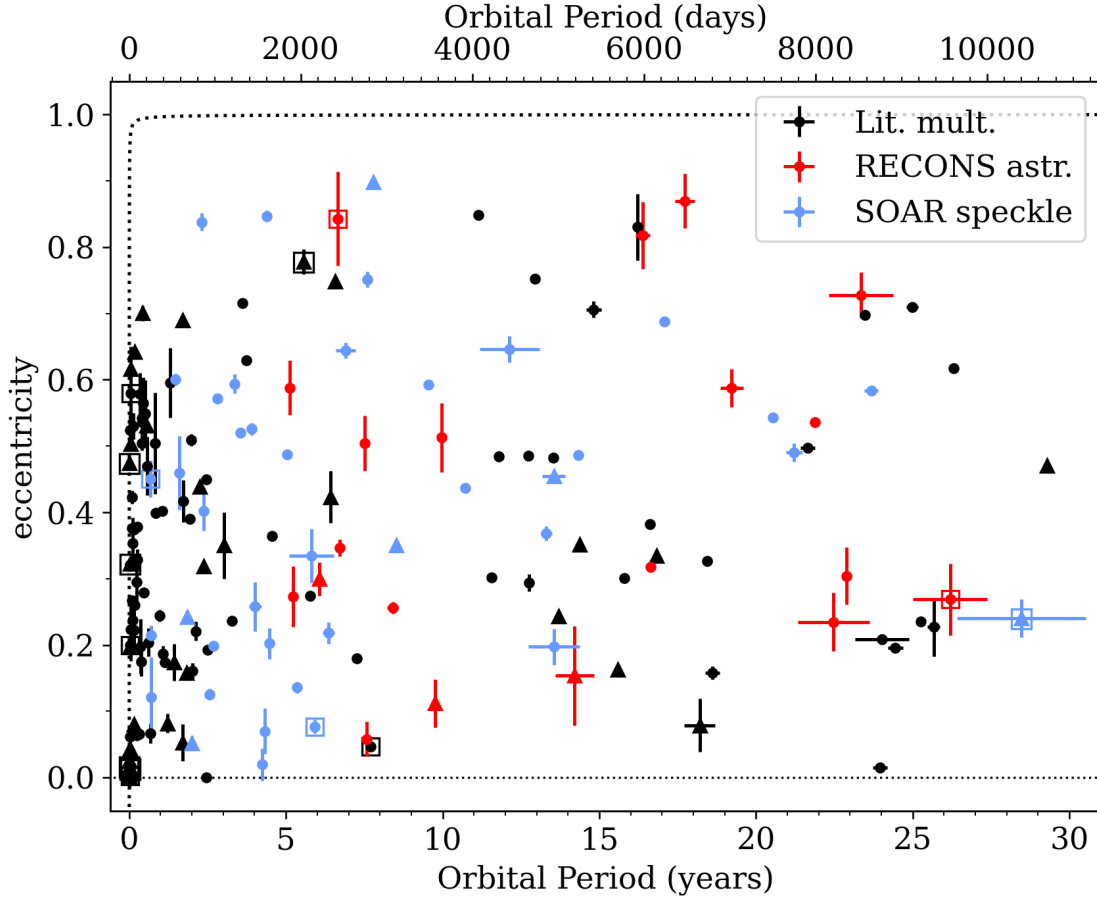


Figure 6.2 The distribution of P_{orb} vs. e for 193 systems with red dwarf stellar primaries shown in terms of linear P_{orb} . This plot is identical to Figure 6.1 with only the P_{orb} scaling changed, thus the symbols and curves are the same as in that figure: each point's color indicates the source of its orbit fit (RECONS astrometry, SOAR speckle interferometry, or literature publications), each point's shape indicates the multiplicity of that system (binary or triple/quadruple), and the dotted curve marks the limit at which two mid-M dwarfs would collide at periastron (§6.2.2).

orbit (§1.3.3 and Zahn & Bouchet (1989)).

Although a line at $P_{\text{orb}} \approx 7$ days cleanly separates eccentric systems from those with nearly circular orbits, considering their characterizations more precisely reveals more nuance.

Table 6.1 shows 21 systems with $3 \text{ days} \lesssim P_{\text{orb}} \lesssim 15 \text{ days}$, with binaries highlighted in yellow to easily distinguish them from higher-order multiples. Column 5 of that table gives each

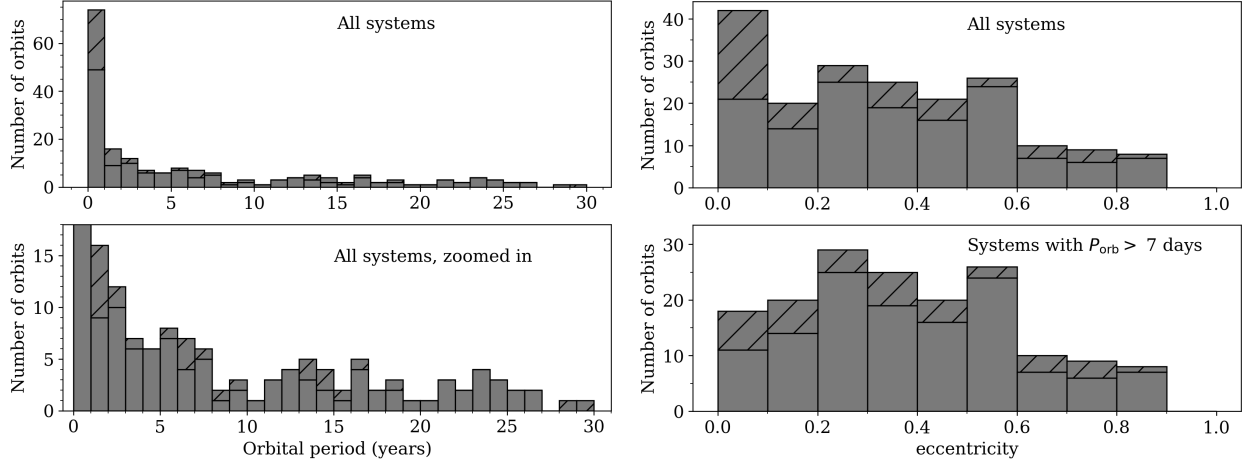


Figure 6.3 Distributions of orbital period (*left panels*) and eccentricity (*right panels*) for the orbits presented in this work (e.g., as shown in Figures 6.1 and 6.2). In every panel here, the non-hatched bars indicate binaries and hatched bars represent subsystems of higher-order multiples. For P_{orb} in the left column, both panels are the full set of orbits, with the bottom panel as a zoom-in to better show the distribution for systems with $P_{\text{orb}} > 1$ year. For e in the right column, the top panel is the full set of orbits and the bottom panel is the set with $P_{\text{orb}} < 7$ days excluded, as those shortest-period orbits all fall in the lowest e bin.

system’s lower bound of e given its published uncertainty, allowing us to determine which systems have e consistent with zero. Note that subtracting more than 1σ (i.e., if the published uncertainties are underestimated) does not change the following discussion in any meaningful way.

Including only binaries in the sample, the longest period for a circular orbit is 4.08 days. If we exclude the five young systems because they may not have had time to circularize, the shortest-period eccentric system is NGT 2143-3801 AB at $P_{\text{orb}} = 7.62$ days. Thus, P_{circ} for these binaries is in the 4–8 days range. Despite this wide range of uncertainty, the M dwarfs’ P_{circ} is firmly below the 12-day P_{circ} that Raghavan et al. (2010) demonstrated for binaries of solar-type stars.

Table 6.1: Systems with P_{orb} between 3 and 10 days, with binaries highlighted in yellow.

The precision shown is as given in the original publications for these systems, given in the last column. The full references for the reference codes shown here are given in Table 1.

Name	N_{comp}	P_{orb} (days)	e	$e - \sigma_e$	Flag (ref.)	Orbit ref.
(1)	(2)	(3)	(4)	(5)	(6)	(7)
GJ0815 AC	3	3.276188 ± 0.00005	0.007 ± 0.007	0.000		Duq88
G203-060 AB	2	3.29 ± 0.99	0.002 ± 0.002	0.000		Ski18
HAT-TR-318-007 AB	2	3.3439539 ± 0.0000002	0.014 ± 0.03	-0.016		Har18
GJ0866 AC	3	3.786516 ± 0.000005	0.0 ± 0.0	0.0		Seg00
GJ1006 AC	3	3.956523 ± 0.000092	0.00220 ± 0.00096	0.00124		Bar18
LP827-020 AB	2	4.077017 ± 0.000001	0.002 ± 0.002	0.000		Zho15
GJ0867 AC	4	4.08322 ± 0.00004	0.010 ± 0.010	0.000		Her65
HIP47133 AB	3	4.38804 ± 0.00001	0.474 ± 0.005	0.469	young (Alo15)	Spe19
PARANAGO-1802 AB	3	4.67390 ± 0.00006	0.017 ± 0.003	0.014	young? (Gom12)	Gom12
GJ1230 AC	3	5.06880 ± 0.00005	0.009 ± 0.001	0.008		Del99
LP790-002 AC	3	5.922845 ± 0.000061	0.01350 ± 0.0012	0.0123	young? (Bar18)	Bar18
PTF0850+1948 AB	2	6.015742 ± 0.000002	0.0017 ± 0.0006	0.0011	young? (Kra17)	Kra17
G041-014 AC	3	7.5555 ± 0.0002	0.014 ± 0.002	0.012	young (Rie14)	Del99
NGT2143-3801 AB	2	7.61793 ± 0.00000544	0.32034 ± 0.00120	0.31914		Act20
G229-018 AD	4	7.9461 ± 0.0002	0.044 ± 0.007	0.037		Spe19
G212-034 AB	2	8.17 ± 1.31	0.062 ± 0.012	0.050		Ski18
GJ0735 AB	2	10.3191 ± 0.0008	0.200 ± 0.012	0.188	young (Dal11)	Duq88
GJ0268 AB	2	10.42672 ± 0.00006	0.3203 ± 0.0009	0.3194		Bar12
LHS1610 AB	2	10.588495 ± 0.001312	0.5239050 ± 0.027422	0.49683		Gaia3
LP476-207 AC	3	11.9623 ± 0.0005	0.323 ± 0.006	0.317	young (Rie14)	Del99
LHS1955 AC	3	14.325696 ± 0.001731	0.6166959 ± 0.029570	0.587126		Gaia3
G093-033 AB	2	14.646202 ± 0.003492	0.2232439 ± 0.047969	0.175275		Gaia3

Including higher-order multiples allows GJ1230 AC to set the upper P_{circ} limit to 5.07 days, although that system's third component is close enough to have possibly influenced the inner pair — both Delfosse et al. (1999) and *Gaia* DR3 place that third companion at $5''$ (~ 50 AU), giving it a potential P_{orb} of only several centuries. We also note that all higher-order multiples below $P_{\text{orb}} = 4.08$ days are circular with the exception of GJ1006 AC, which has an orbit that is only barely eccentric at $e = 0.00220$. Triples with their third component

at \sim a few hundred AU will evolve under the additional effects of Kozai-Lidov cycles with tidal friction (Fabrycky & Tremaine 2007), which ultimately drives the inner pair toward circular. This makes them not comparable to simple binaries in our evaluation of P_{circ} . If the third component is further out (e.g., beyond 1000 AU) then the inner pair may effectively function as a simple binary, but not many M dwarf systems with those configurations are known and have accurate orbits for their inner pairs.

Another unusual feature is that in the $P_{\text{orb}} = 4\text{--}8$ days range an unusually high number of systems are noted as young (marked with boxes in Figures 6.1 and 6.2). This feature should be interpreted with caution, as the entire sample has not been uniformly searched for signs of youth. The results in this short- P_{orb} regime are dominated by orbits determined from radial velocities, thus these systems all have spectroscopic data available to assess their potential ages — which is not the case for every system on the P_{orb} vs. e plot.

On the other hand, if there is a formation path that sets some systems quickly migrating inward toward circular orbits with tidally-locked components, we would expect the region of P_{circ} orbits to be dominated by those young, quickly-migrating systems. Models of disk fragmentation show migration inward can happen on astronomically short timescales of a few Myr, but this process also results in accretion of mass onto the companion. In the bottom panel of Figure 6.5 (discussed in §6.4) we see that high mass ratios are not overrepresented in this P_{orb} regime, so this is not a compelling formation path for the shortest period systems.

6.2.2 The Observed Upper Envelope of e

A clear envelope of maximum eccentricity extends from the P_{circ} line to our survey limit of 30 years. As P_{orb} increases from ~ 10 days to 30 years, this upper envelope extends from $e \approx 0.65$ to $e \approx 0.95$.

This envelope is well below the limit at which two M mid-M dwarfs would pass close enough to collide, represented in Figures 6.1 and 6.2 with the dotted black curve. This limit was drawn assuming two stars of $0.30 M_{\odot}$ and $0.33 R_{\odot}$ (Mann et al. 2015) each collide when their periastron distance is $\leq 0.66 R_{\odot}$. We tested additional combinations of masses and radii from the M dwarf sequence and found no significant difference in the result — i.e., in all cases, the observed points fall well below the collision curve in P_{orb} vs. e space.

The line of stars along the upper edge of the e envelope are almost exclusively subsystems of triples or higher-order multiples. These systems also populate lower eccentricities, thus they do not necessarily have higher eccentricities than binaries; rather, they have a somewhat higher- e upper envelope. This is presumably a sign of an eccentricity-pumping mechanism only accessible to higher-order multiples, such as the Kozai-Lidov mechanism (§1.3.2).

Interpreting the specific shape of the upper e envelope — such as its gradual slope upward with increasing P_{orb} — is treacherous for this data set, as most of the shape is set by our diverse set of literature orbits. Roughly 50% of the orbits between 10 days and 1 year were obtained with radial velocities (RVs), while the rest were from absolute astrometry and eclipsing binaries. Without a careful analysis of those surveys’ sensitivities, we cannot be confident that they can characterize high- e orbits just as easily as low- e orbits, so the true

slope of the M dwarf multiples' upper envelope remains uncertain. Its somewhat abrupt rise in the SOAR-sensitive region ($P_{\text{orb}} \gtrsim 1$ year) validates these suspicions.

6.2.3 *Eccentricities at Long P_{orb}*

Beyond $P_{\text{orb}} \approx 10$ years, the density of orbits in P_{orb} vs. e space decreases, although the bottom left panel of Figure 6.3 shows that the distribution is only slightly decreasing beyond that threshold. This lack of long-period orbits is due to the declining sensitivity of the RECONS and SOAR observational programs in this regime (see Figure 5.10 and Figure 5.16), as well as the decline of the literature efforts' sensitivities (§5.3.2) because most observing programs are short in duration.

That said, orbits with $P_{\text{orb}} \geq 7$ years are generally contained between $e \approx 0.1$ and $e \approx 0.9$, with only a few exceptions to that lower bound. This distribution is demonstrated in the bottom panel of Figure 6.4. To interpret this feature, we must consider the sensitivity of our observing programs. The SOAR speckle program shows a notable decrease in fitting capability with increasing e ; for example, at $P_{\text{orb}} = 24$ years, the percentage of orbits that can be fit decreases from 45% to 26% from $e = 0$ to $e = 0.9$. The RECONS astrometry program does not have such a strong dependence on e because its sensitivity is mostly flat for multiples (nearly identical to Figure 5.9) and its fit capability depends only on P_{orb} , not e , resulting in the vertical striped pattern in Figure 5.10. Considering those analyses together suggests that the lack of circular orbits at long P_{orb} is reflective of the underlying population, while the lack of very eccentric orbits may or may not be real.

6.3 Estimating Masses for Every M Dwarf

Because in Chapter 1 we noted so much variation in P_{orb} vs. e between high-mass, solar-type, and very low-mass systems (§1.4), our M dwarf results will be richer if we interpret their distributions in light of their masses as well. For 52 of our 193 systems we have dynamical masses of the individual stars, but for the remaining systems we need to estimate their masses using alternative means.

When dynamical masses are not available, our most reliable technique to estimate component masses in a system is to use the absolute magnitudes of its individual components. Of our 193 pairs, 69 have magnitude difference (Δm) measurements of their components, either from our SOAR speckle program or from various efforts published in the literature. For these systems, we estimated component masses using either the corrected M_K MLR described in §2.2.1 or the I -band pseudo-MLR presented in §2.2.2. A few systems had only Δm measurements from alternative bandpasses at optical or near-infrared wavelengths, often from narrow-band filters used in speckle surveys, and in these cases we considered the shapes of those filters' throughput functions and chose either K or I , depending on which was most similar.

For six systems there were no Δm measurements or dynamical masses, but we did have a photocentric orbit determined by RECONS. In those cases we used that photocentric orbit to constrain the individual masses through the following procedure:

1. We began by finding every potential mass combination that could have produced the measured M_K for the combined pair. This process was identical to that used for step 1

of §5.1.2: we created a grid of mass combinations between $0.08 M_{\odot}$ and $0.6 M_{\odot}$ in steps of $0.01 M_{\odot}$, computed the M_K expected from each component mass on that grid using the corrected MLR (§2.2.1), then computed the M_K expected for each combination of those absolute magnitudes. These simulated combined magnitudes needed to be within 0.02 mag of the measured M_K to be considered a match. The grid contained no duplicated mass combinations.

As we did in §5.1.2, if the measured M_K did not match any grid values, we matched it against an extended grid that included masses every $0.001 M_{\odot}$ below $0.1 M_{\odot}$. This was necessary because the change in absolute magnitude with respect to mass becomes quite steep in that region.

2. Next, we computed B and β (the fractional mass and luminosity; §3.4.1) of each potential mass combination from the previous step.
3. We also computed the semi-major axis a of each mass combination given their combined masses and the orbit's measured P_{orb} .
4. Finally, we used the B , β , and a computed above for each mass combination to determine $\alpha = a(B - \beta)$ (Eq. 3.1), where α is the semi-major axis of the photocentric orbit. The mass combination for which α was closest to the orbit's measured value was considered most likely, and its component masses were adopted for the system.

After checking each of the above possibilities for estimating masses, there were 62 systems that did not have appropriate data to use any of the above mass estimating procedures. For

these systems, we assumed $\Delta K \approx 0.8$ mag and followed the procedure described above for when magnitude differences were available. This specific value was the average for the entire sample with measured Δm in any bandpass, after converting Δm in other bandpasses to Δm at K .

The result is that dynamical masses make up slightly less than 1/3 of the sample, masses estimated for systems with Δm measurements make up slightly more than 1/3, and systems with combined magnitudes assumed to have $\Delta K = 0.8$ mag make up slightly more than 1/3. Mass estimates from photocentric orbits only account for a few percent. These masses and mass estimates are given in Table 6.2.

Table 6.2: Masses and mass estimates used for the analysis described in §6.4 and thereafter. Column 4 indicates the technique used to produce the values in the preceding columns; masses that are not dynamical are estimates based on either magnitude differences, photocentric orbits, or combined magnitudes assuming $\Delta K = 0.8$ mag (described in §6.3).

Name	M_1 (M_\odot)	M_2 (M_\odot)	mass type
(1)	(2)	(3)	(4)
G131-026AB	0.23	0.22	ΔI
LEHPM1-0255AB	0.23	0.15	ΔI
GJ1005AB	0.179	0.112	dynamical
2MA0015-1636AB	0.24	0.24	ΔI
GJ1006AC	0.430	0.151	dynamical
GJ2005BC	0.0844	0.0804	dynamical
LP349-025AB	0.1585	0.0093	dynamical
GJ0022AC	0.405	0.157	dynamical
GIC0050AC	0.25	0.10	ΔI
GJ0046AB	0.31	0.20	combined phot
GJ1029AB	0.142	0.101	dynamical
GJ0054AB	0.432	0.301	dynamical
LP707-017AB	0.15	0.11	combined phot

Table 6.2: Masses and mass estimates used for the analysis described in §6.4 and thereafter. Column 4 indicates the technique used to produce the values in the preceding columns; masses that are not dynamical are estimates based on either magnitude differences, photo-centric orbits, or combined magnitudes assuming $\Delta K = 0.8$ mag (described in §6.3).

GJ0065AB	0.120	0.117	dynamical
LEHPM1-1882AB	0.29	0.23	ΔI
GJ0084AB	0.47	0.10	ΔI
GJ0084.2AB	0.52	0.39	combined phot
2MA0213+3648AB	0.17	0.09	$\Delta \text{mag K}$
GJ1046AB	0.36	0.24	combined phot
LP770-020AB	0.28	0.14	ΔI
GJ0098AB	0.69	0.69	ΔI
GJ0099AB	0.69	0.67	$\Delta \text{mag K}$
L225-057AB	0.33	0.32	ΔI
LP993-116BC	0.24	0.16	combined phot
GJ0125AB	0.69	0.08	$\Delta \text{mag K}$
BD+60-0637AC	0.69	0.65	combined phot
SIP0320-0446AB	0.080	0.054	dynamical
LTT01628AB	0.42	0.30	combined phot
LHS1561AB	0.38	0.27	ΔI
LHS1582AB	0.21	0.09	ΔI
LHS1610AB	0.13	0.10	combined phot
GJ0164AB	0.20	0.13	combined phot
KELT0416-6200AB	0.48	0.35	combined phot
LEHPM1-3719AB	0.13	0.09	combined phot
LP415-020AB	0.149	0.087	dynamical
2MA0429-3123AB	0.10	0.08	ΔI
LP655-043AB	0.38	0.27	combined phot
DQTAUAB	0.69	0.69	combined phot
LEP0448+1003AB	0.34	0.29	ΔI
LSPM0448+3648AB	0.14	0.10	combined phot
LP476-207AC	0.59	0.42	ΔI
LTT11586AC	0.26	0.17	combined phot
GJ0190AB	0.39	0.38	ΔI
NGT0522-2507AB	0.1742	0.1739	dynamical
GJ1081AB	0.325	0.205	dynamical
SCR0533-4257AB	0.20	0.20	ΔI
PARANAGO-1802AB	0.69	0.69	combined phot

Table 6.2: Masses and mass estimates used for the analysis described in §6.4 and thereafter. Column 4 indicates the technique used to produce the values in the preceding columns; masses that are not dynamical are estimates based on either magnitude differences, photocentric orbits, or combined magnitudes assuming $\Delta K = 0.8$ mag (described in §6.3).

APM0206AB	0.21	0.14	combined phot
LP837-019AB	0.36	0.34	ΔI
LP827-020AB	0.25	0.17	combined phot
GJ0220AB	0.602	0.200	dynamical
G098-052AB	0.32	0.21	combined phot
LHS1817AB	0.22	0.15	combined phot
SCR0613-2742AB	0.60	0.58	photocentric orbit
UPM0624-2655AB	0.43	0.41	ΔI
GJ0234AB	0.223	0.109	dynamical
LHS0221AB	0.350	0.187	dynamical
SCR0702-6102AB	0.11	0.11	ΔI
LHS0224AB	0.126	0.124	dynamical
GJ0263AB	0.39	0.37	ΔI
APM0089AB	0.19	0.19	ΔI
GJ0268AB	0.22599	0.19248	dynamical
LHS1901AB	0.1079	0.0945	dynamical
GJ0268.3AB	0.39	0.28	combined phot
WIS0720-0846AB	0.083	0.059	dynamical
SCR0723-8015AB	0.10	0.07	photocentric orbit
GJ2060AB	0.59	0.38	ΔI
GJ0278CD	0.599	0.599	dynamical
G089-032AB	0.15	0.13	ΔI
2MA0746+2000AB	0.079	0.075	dynamical
LHS1955AC	0.25	0.17	combined phot
LHS2010AB	0.35	0.24	combined phot
GJ2069AC	0.433	0.398	dynamical
GJ0310AB	0.65	0.28	$\Delta \text{mag K}$
SCR0838-5855AB	0.09	0.08	ΔI
UPM0838-2843AB	0.27	0.26	ΔI
SCR0840-4044AB	0.12	0.09	combined phot
HAT-TR-318-007AB	0.42	0.30	combined phot
PTF0850+1948AB	0.33	0.22	combined phot
G041-014AC	0.27	0.23	ΔI
G041-014AB	0.30	0.20	combined phot

Table 6.2: Masses and mass estimates used for the analysis described in §6.4 and thereafter. Column 4 indicates the technique used to produce the values in the preceding columns; masses that are not dynamical are estimates based on either magnitude differences, photocentric orbits, or combined magnitudes assuming $\Delta K = 0.8$ mag (described in §6.3).

LHS6167AB	0.13	0.13	ΔI
2MA0920+3517AB	0.1107	0.0678	dynamical
2MA0930+0227AB	0.26	0.17	combined phot
GJ0352AB	0.43	0.36	ΔI
HIP47133AB	0.69	0.54	combined phot
GJ0372AB	0.53	0.39	combined phot
GJ0375AB	0.49	0.36	combined phot
GJ0381AB	0.37	0.36	ΔI
2MA1017+1308AB	0.077	0.072	dynamical
TWA022AB	0.24	0.23	ΔI
LP790-002AC	0.401	0.232	dynamical
LHS0283AB	0.323	0.164	dynamical
2MA1036+1521BC	0.26	0.24	ΔI
LP848-050AB	0.08	0.08	photocentric orbit
WT1827AB	0.12	0.10	ΔI
LP168-021AB	0.12	0.09	combined phot
2MA1047+4026BC	0.093	0.076	dynamical
WIS1055-7356AB	0.09	0.09	ΔI
GAI1058-5525AB	0.12	0.12	ΔI
LSPM1112+7626AB	0.39	0.27	combined phot
LHS2397AAB	0.0888	0.0630	dynamical
HIP56229AB	0.69	0.69	combined phot
LP734-034AB	0.28	0.18	combined phot
NLTT30359AB	0.35	0.13	ΔI
GJ0469AB	0.332	0.188	dynamical
SCR1230-3411AB	0.24	0.13	ΔI
GJ0473AB	0.124	0.113	dynamical
G123-045AB	0.15	0.11	combined phot
LHS5221AB	0.14	0.10	combined phot
GJ0487AB	0.38	0.26	combined phot
GJ0494AB	0.58	0.09	$\Delta \text{mag K}$
KELU-1AB	0.08	0.08	$\Delta \text{mag K}$
NLTT33370AB	0.12	0.11	ΔI
GJ0507AB	0.48	0.40	dynamical

Table 6.2: Masses and mass estimates used for the analysis described in §6.4 and thereafter. Column 4 indicates the technique used to produce the values in the preceding columns; masses that are not dynamical are estimates based on either magnitude differences, photocentric orbits, or combined magnitudes assuming $\Delta K = 0.8$ mag (described in §6.3).

GJ0508AC	0.61	0.46	combined phot
WT0460AB	0.10	0.09	ΔI
GJ1182AB	0.157	0.104	dynamical
GJ0569BC	0.45	0.30	$\Delta \text{mag K}$
LHS3056AC	0.32	0.31	ΔI
LHS3056AB	0.39	0.28	combined phot
GUBOAB	0.616	0.600	dynamical
GJ0595AB	0.20	0.13	combined phot
LTT06288AB	0.33	0.13	ΔI
SCR1546-5534AB	0.08	0.08	ΔI
USCOCTIO-5AB	0.3336	0.3200	dynamical
LSR1610-0040AB	0.095	0.070	dynamical
EPIC203710387AB	0.1183	0.1076	dynamical
GJ0623AB	0.379	0.114	dynamical
GJ2121AB	0.36	0.34	ΔI
GJ0630.1AC	0.2310	0.2141	dynamical
GJ2122AB	0.59	0.46	ΔI
GJ0644AB	0.6609	0.4155	dynamical
GJ0644BD	0.3466	0.3143	dynamical
GJ1210AB	0.14	0.13	ΔI
GJ0661AB	0.35	0.32	$\Delta \text{mag K}$
GJ0660.1AC	0.36	0.24	combined phot
GJ1212AB	0.37	0.36	ΔI
GJ1215AB	0.14	0.06	photocentric orbit
G203-060AB	0.26	0.17	combined phot
LP388-055AB	0.0954	0.0840	dynamical
G140-009AB	0.52	0.49	ΔI
G249-020AC	0.36	0.24	combined phot
LTT07077AB	0.27	0.17	combined phot
LP044-162AB	0.09	0.08	combined phot
L043-072AC	0.25	0.19	ΔI
GJ1230AC	0.29	0.19	combined phot
SCR1845-6357AB	0.08	0.07	photocentric orbit
LTT07434AB	0.31	0.26	ΔI

Table 6.2: Masses and mass estimates used for the analysis described in §6.4 and thereafter. Column 4 indicates the technique used to produce the values in the preceding columns; masses that are not dynamical are estimates based on either magnitude differences, photocentric orbits, or combined magnitudes assuming $\Delta K = 0.8$ mag (described in §6.3).

GJ0735AB	0.51	0.38	combined phot
G229-018AD	0.69	0.63	combined phot
GJ0747AB	0.214	0.200	dynamical
GJ0748AB	0.369	0.190	dynamical
2MA1912-5016AB	0.16	0.11	combined phot
L274-089AB	0.20	0.14	combined phot
G260-022AB	0.10	0.13	combined phot
G125-018AB	0.36	0.24	combined phot
UPM1951-3100AB	0.29	0.14	ΔI
GJ1245AC	0.111	0.076	dynamical
LP395-008AC	0.621	0.348	dynamical
GJ0791.2AB	0.237	0.114	dynamical
LEHPM2-1265AB	0.15	0.09	photocentric orbit
GJ0802AC	0.280	0.063	dynamical
GJ0802AB	0.14	0.14	dynamical
LHS0501AC	0.24	0.23	ΔI
GJ0815AB	0.55	0.41	combined phot
GJ0815AC	0.55	0.41	combined phot
USN2101+0307AB	0.08	0.08	photocentric orbit
L117-123AB	0.54	0.41	combined phot
G212-034AB	0.54	0.40	combined phot
GJ0829AB	0.29	0.29	ΔI
GJ0831AB	0.27	0.145	dynamical
LTT16329AB	0.46	0.33	combined phot
2MA2140+1625AB	0.1088	0.0659	dynamical
NGT2143-3801AB	0.4545	0.4256	dynamical
G093-033AB	0.39	0.28	combined phot
WT0818AB	0.31	0.18	ΔI
LP983-034AB	0.38	0.25	ΔI
LHS3739BC	0.14	0.09	ΔI
GJ0844AB	0.49	0.44	ΔI
2MA2206-2047AB	0.0974	0.0821	dynamical
LEHPM1-4771AB	0.14	0.14	ΔI
GJ0866AB	0.12	0.11	ΔI

Table 6.2: Masses and mass estimates used for the analysis described in §6.4 and thereafter. Column 4 indicates the technique used to produce the values in the preceding columns; masses that are not dynamical are estimates based on either magnitude differences, photo-centric orbits, or combined magnitudes assuming $\Delta K = 0.8$ mag (described in §6.3).

GJ0866AC	0.15	0.11	combined phot
GJ0867AC	0.54	0.40	combined phot
LEP2249+0459AB	0.20	0.13	combined phot
SCR2303-4650AB	0.17	0.16	ΔI
G273-033AB	0.35	0.34	ΔI
LHS4009AB	0.14	0.13	ΔI
LTT09828AB	0.25	0.23	ΔI

6.4 P_{orb} vs. e by Mass and Mass Ratio

With masses (or mass estimates) available for every system, we now have the values needed to look for trends with respect to this fundamental parameter. Figures 6.5 and 6.6 show the P_{orb} vs. e plot of Figures 6.1 and 6.2, but with the points colored by either the primary’s mass (top plot in each Figure), secondary’s mass (middle plot), or mass ratio (bottom plot). In the mass ratio plots, systems with masses estimated by assuming $\Delta K = 0.8$ mag are shown as open symbols, as those masses are the least reliable.

Distributions of eccentricity with respect to primary mass are shown in Figure 6.7, with $P_{\text{orb}} < 7$ days excluded to avoid tidally circularized systems. These distributions show that the highest-mass M dwarf multiples have a roughly flat distribution of eccentricity, but this distribution skews toward lower e for the lower-mass M_1 cohorts. The distribution shapes are qualitatively different between the 0.15–0.30 M_{\odot} vs. 0.075–0.15 M_{\odot} groups, but we caution

against interpreting this feature because the peak numbers of those histograms are somewhat low. Of the 1/3 of systems with masses estimated from combined photometry (§6.3), ~40% fall into these two lower bins, but in general those estimated masses' eccentricity distributions match that of the full set (see the bottom panels of Figures 6.5 and 6.6). The right panels of Figure 6.7 also show statistically too few systems to interpret, but they do hint that the systems with $P_{\text{orb}} > 7$ years match the trend of the full set in the left panels.

Figure 6.8 shows the eccentricity distributions with respect to secondary mass, again with $P_{\text{orb}} < 7$ days excluded. The trends are consistent with the primary mass plots of Figure 6.7, with the $0.075\text{--}0.15 M_{\odot}$ cohort now strongly peaked around $e \approx 0.35$ and the more massive $0.15\text{--}0.30 M_{\odot}$ group peaked at $e \approx 0.2$. Estimated masses are evenly distributed between the top three mass groups, so they should have less of an effect here. The shift in peak from lower to higher e runs counter to the overall trend of e decreasing with stellar mass (discussed in §1.4 and later in §6.4.4 and §6.4.5). It is likely, however, that the decrease in low-mass orbits at $P_{\text{orb}} \lesssim 3$ years is playing a role in this trend, as e generally decreases in that region as well (Figure 6.5), and the trend is not significant when the orbits are restricted to $P_{\text{orb}} \gtrsim 7$ years (right panel of Figure 6.8). We have not conducted an extensive analysis of the biases with respect to mass and mass ratio for the literature orbits that dominate this region, thus we cannot draw conclusions about whether the decrease in low-mass systems below $P_{\text{orb}} \lesssim 3$ years represents the underlying population — and, similarly, whether the eccentricity trend that follows from it is representative.

Adding the dimension of masses to the P_{orb} vs. e plots reveals a few important features

to specific regions of P_{orb} vs. e space, discussed next.

6.4.1 Masses Among the Shortest- P_{orb} Orbits

Figure 6.5 shows that among the circular or nearly-circular orbits with $P_{\text{orb}} \lesssim 7$ days, many systems have primaries with masses of $0.3 M_{\odot}$ or higher. This feature is likely a selection effect, as every one of those systems were characterized using RVs from spectroscopy, which requires brighter targets than the other techniques contributing to this plot.

On the other hand, it is important to note that the migration that would bring a companion closer to its primary star — before, or while tidal forces circularize the orbit — would cause that companion to accrete material and drive its mass closer to that of the primary (§1.3.1). If this scenario is the only one by which companions could migrate inward, then we would expect this short- P_{orb} regime to be exclusively populated by systems with high mass ratios. The bottom panel of Figure 6.5 shows that this is indeed the case because all but one of the 25 systems with $P_{\text{orb}} \lesssim 7$ days have q values of at least 0.5, and the middle panel of that Figure confirms that almost none of those $q \gtrsim 0.5$ systems are higher-mass M dwarfs with very low-mass companions. With this result we must also tread carefully, however, as more massive companions are more detectable via RV than less massive companions.

We therefore conclude that for short- P_{orb} orbits of M dwarfs, the evidence is consistent with migration+tides being responsible for populating that regime, but the evidence is also not sufficient to disprove that scenario. To form stronger conclusions requires a uniform survey of companions that targets these short- P_{orb} orbits, can easily characterize orbits of the lowest-mass companions, and has its fitting capability space well mapped (analogous to

§5.1.2 and §5.2.2).

6.4.2 Masses Among the Longest- P_{orb} Orbits

In the $P_{\text{orb}} \gtrsim 7$ years region, the primary masses represented span the entire M dwarf sequence, as shown in the top panel of Figure 6.6 and the right column of Figure 6.7. The lowest-mass cohort is slightly more prevalent, which is unsurprising given that many of these orbits are from RECONS astrometry, which is generally better suited to fainter stars (§3.2) and has shorter time baselines for M dwarfs with masses $\gtrsim 0.3 M_{\odot}$ because they were added to the observing program relatively recently (Figure 5.10, right panel).

The most notable feature among these long orbits ($\gtrsim 7$ years) is that seven of the 11 systems with $e < 0.2$ have primaries with masses of $0.075\text{--}0.15 M_{\odot}$. In the same plot showing secondary masses (Figure 6.6, middle panel), nine of the 11 systems have secondaries $\leq 0.15 M_{\odot}$. Only two systems in this long- P_{orb} , low- e region have both stars $\geq 0.15 M_{\odot}$. In summary, for P_{orb} longer than a few years, nearly all systems with $e \lesssim 0.2$ are those with at least one very low-mass star or brown dwarf.

This result is consistent with the findings of Dupuy & Liu (2017), who showed that the very low-mass systems have lower eccentricities than solar-type systems. Our comparison with their results is discussed in more depth in §6.4.5. Those authors suggested that this difference could be due to the lower-mass stars and brown dwarfs having longer-lived disks that impart additional eccentricity damping. The bottom panel of Figure 6.6, however, shows that four of the eleven systems with $P_{\text{orb}} \geq 7$ years and $e < 0.2$ have $q < 0.5$. It would be surprising for so many companions to move through disks enough to dampen their

eccentricities without accreting significant material.

On the other hand, three of those four high- P_{orb} , low- e , low- q systems have brown dwarf rather than stellar companions. Furthermore, in the bottom panels of Figure 6.8 we also note that brown dwarf companions exclusively have $e < 0.5$. Brown dwarfs' lower luminosities and potentially different formation processes are most likely playing a role here.

6.4.3 Mass Ratios

The mass ratios of the M dwarf multiples are potentially their most telling property. Figure 6.9 presents the mass ratio distribution for all systems in our sample excluding those that required assuming $\Delta K = 0.8$ mag to estimate mass. This distribution reveals that twin multiples ($q \geq 0.9$) vastly outnumber all other pairs in our sample. Figure 6.10 demonstrates that this twin prevalence does not depend on mass of the primary or secondary — this mass ratio is common in the sample regardless of the type of system. The only panel in Figure 6.10 that does not show these excess twins is that for brown dwarf secondaries, which will never have many similar-mass primaries in this sample because we excluded systems with primaries of mass $\leq 0.075 M_{\odot}$.

This twins excess could have strong implications for M dwarf multiples' dynamical evolution, but there is also high potential for observational bias to contribute to this result. The bottom panel of Figure 6.5 shows that the $q > 0.9$ systems become prevalent for $P_{\text{orb}} \gtrsim 1$ year, which is precisely the region where high-resolution imaging methods become sensitive (e.g., see Figures 5.16 and 6.1 for SOAR speckle). These imaging techniques excel when companions are similar in brightness. Additionally, as we consider longer-period orbits that rely on

data from older instruments, we might expect brighter companions to be better represented due to those instruments' reduced sensitivities. Figure 6.11 shows the distributions of q for different regimes of P_{orb} , and indeed the twin pairs become less overrepresented as P_{orb} decreases. To determine the full extent of the role observational bias is playing here requires a more complete sensitivity analysis of each observing program — including literature efforts — with respect to mass ratio.

If our sample were a truly volume-complete representation of all multiples' orbits in the Solar Neighborhood, the additional systems included would most likely include the less massive companions that have gone undetected or uncharacterized in this work. Spectroscopic and visual binaries are both biased toward brighter (more massive) companions, and these techniques contribute the most to the entirety of the P_{orb} parameter space investigated here. Unresolved astrometry from RECONS, on the other hand, is sensitive to companions that are massive but of lesser brightness than their primary star, but RECONS orbits make up only 11% of the orbits in this work because they must be fully mapped to be accurately characterized. If these biases were not baked into the results shown in, e.g., Figure 6.11, we would expect the numbers of low- q systems to increase in most P_{orb} bins, softening the steepness of the rise at $q \geq 0.9$. Any change in formation at the star/BD line (such as a lack of brown dwarf companions) would then be evident in the shape of the distribution toward the $q < 0.25$ end. And if significant accretion during migration is required to bring companions to decades-long orbits or shorter, we would see the distribution's rise from low q to high q become steeper as P_{orb} decreases (i.e., as we consider tighter orbits). Future, more

volume-complete samples of multiples' orbits would thus reveal many more features of these systems' formation and evolution.

Figure 6.12 shows the eccentricity distribution for systems in different cohorts of mass ratio. Considering either the full sample (left column) or the long-period orbits alone (right column), the eccentricity distribution is roughly flat regardless of mass ratio. In most panels there are not enough orbits to discern details of the distributions' shapes. Figure 6.13 confirms this lack of structure and shows that there is no correlation between eccentricity and our estimated mass ratios.

To further assess observational bias, we consider the distribution of mass ratio with respect to P_{orb} , which is shown in Figure 6.14. The open symbols in that plot indicate systems for which the mass was estimated by assuming $\Delta K = 0.8$ mag; predictably, they pile up around $q = 0.7$, and excluding those systems would produce a roughly flat mass ratio distribution between $q = 0.3$ and 0.8. Considering only the more reliable mass ratios (filled symbols), only the near-twin pairs ($q \geq 0.9$) are well represented at all P_{orb} . The moderately high mass ratios between 0.5 and 0.9 skew toward $P_{\text{orb}} \gtrsim 1$ year, and the $q < 0.5$ systems are entirely confined to that higher P_{orb} region with only one exception. The edges of this distribution adhere well to the boundaries of the regimes of different observational techniques:

- all orbits within 0–10 days originate from radial velocities;
- 50% of orbits between 10 days and 1 year are still from RVs; and
- the orbits above 1 year are evenly distributed between relative astrometry from SOAR,

absolute astrometry from RECONS, and a variety of astrometric and spectroscopic techniques from the literature.

It is striking that in the regime with the most variety of observations the mass ratios are most varied and also distributed in an unstructured way (beyond the number of systems generally increasing as q increases). The sudden cutoff of $q < 0.5$ systems at the $P_{\text{orb}} \approx 1$ year boundary of SOAR and RECONS sensitivity hints that those features could be related, and the prevalence of low- q systems might continue if the orbit mapping techniques below 1 year were sensitive to them. Any results that hinge on q and systems with $P_{\text{orb}} \lesssim 1$ year should be considered with careful regard to this potential bias of observational technique.

6.4.4 Comparing M Dwarfs to Solar-like Systems

The P_{orb} vs. e distribution for systems of solar-type stars was presented by Raghavan et al. (2010), who collected multiples from a sample of 454 F, G, and K stars to determine the multiplicity of that population, as discussed in §1.4.2. In doing so, they also showed that the solar-type multiples circularize at $P_{\text{orb}} \approx 12$ days and rarely have circular orbits for $P_{\text{orb}} \gtrsim 100$ days. Figure 6.15 shows their distribution (yellow points) over our M dwarf distribution (black points), with P_{circ} for the solar-type stars marked at 12 days with the dashed yellow line.

There are no fewer than eight eccentric M dwarf systems to the left of that 12-day line, along with a handful of nearly (but not quite) circular systems. This firmly demonstrates that P_{circ} for M dwarfs is shorter than P_{circ} for solar-type stars, validating our analysis in §6.2.1.

On an intuitive level it seems reasonable that the M dwarf multiples would have a shorter P_{circ} than solar-type multiples, as their lower mass means the stars must be closer together to feel the same amount of gravitational force and thus comparable tides. In order for a $0.6+0.3 M_{\odot}$ pair to feel the same gravity as a $1.0+0.5 M_{\odot}$ pair with $P_{\text{orb}} = 12$ days and semi-major axis 0.117 AU, the M dwarfs need to orbit at 0.071 AU, corresponding to $P_{\text{orb}} = 7.2$ days. For less massive M dwarfs, a $0.3+0.15 M_{\odot}$ pair would need to orbit at 3.6 days. The observed P_{circ} of 4–8 days is thus what we would expect over the wide range of M dwarf masses, although important factors such as their stellar radii and internal structures should also be considered.

Just beyond the P_{circ} lines, the solar-type multiples exhibit a somewhat tighter correlation of e with respect to P_{orb} than the M dwarf multiples. For $P_{\text{orb}} \gtrsim 100$ days, the solar-type e distribution is roughly the same width as the M dwarf distribution, but is shifted toward higher e ; this is also evident in the top panel of Figure 6.16 as compared to the bottom right panel of Figure 6.3. Low- e orbits are entirely lacking among the solar-type multiples, while the M dwarfs only see that behavior past P_{orb} of ~ 7 years (§6.2.1), and systems that include very low-mass components can violate this rule. These differing features suggest differences in the migration paths that led to these orbits and/or differences in stable orbits available after the migration process. We elaborate upon these scenarios in §6.5.

Finally, the upper envelope of the solar-type multiples' eccentricity distribution is somewhat higher than the M dwarfs (see Figure 14 of Raghavan et al. 2010). Considering that for the solar-type systems this envelope is dominated by higher-order multiples just as it is for

our M dwarfs, it is again likely due to the Kozai-Lidov mechanism, or a similar evolutionary process in systems with more than two components.

6.4.5 Comparing M Dwarfs to Very Low-Mass Systems

For very low-mass (VLM) systems with $M_1 \lesssim 0.1 M_\odot$, Dupuy & Liu (2017) showed that the eccentricity distribution firmly skews toward lower e at high P_{orb} . This distribution is reproduced in the bottom panel of Figure 6.16. Their sample is somewhat small (25 multiples) because VLM systems are intrinsically faint and thus difficult to observe. We compare those 25 multiples to our M dwarfs in Figure 6.17, in which blue points indicate the VLM systems and black points are once again our M dwarf multiples. The VLM sample overlaps the M dwarfs (and hence some points are aligned), but the VLMs also include the systems with brown dwarf primaries that we excluded from our sample.

The logarithmic view of P_{orb} (Figure 6.17, left panel) is not particularly revealing, as the VLM systems lack observations of short-period orbits. The two short-period orbits both have $P_{\text{orb}} < 12$ days and are still moderately eccentric ($e > 0.3$), consistent with our conclusion that lower-mass systems have a shorter P_{circ} than solar-type systems. Although one of these VLM systems has an eccentric orbit shorter than our 7-day upper limit for the M dwarf P_{circ} , that orbit is a young system (Pleiades member; Basri & Martín 1999), thus may not have had time to circularize yet. We thus cannot draw more conclusions about P_{circ} for VLM systems.

The linear P_{orb} view (Figure 6.17, right panel) demonstrates that these systems have representatives out to similar P_{orb} as our M dwarf multiples, and yet their upper envelope

of eccentricity remains firmly below that of the M dwarfs. Only 13% of the VLM orbits (two systems) have $e > 0.5$, whereas 32% of our M dwarfs (53 systems) exceed that limit. Although this upper envelope is composed of higher-order multiples among the M dwarfs, the highest- e VLM systems are binaries, not triples or quadruples (shown in Figure 18 of Dupuy & Liu 2017). The maximum eccentricity being higher for the higher-mass population matches what we observed in our comparison of solar-type vs. M dwarf multiples. On the other hand, it is surprising that the upper e envelope of VLM systems is *not* dominated by higher-order multiples. This suggests that eccentricity-pumping mechanisms for subsystems of higher-order multiples are less efficient for these VLM systems. The orbital evolution of Kozai-Lidov cycles, for example, has several dependencies on the components' masses (Fabrycky & Tremaine 2007). The necessary *caveat* to this conjecture is, of course, that there not many VLM systems with well-determined orbits.

The most notable feature of the VLM P_{orb} vs. e distribution is that 88% of the orbits have $e < 0.5$. In contrast, 70% of the M dwarf orbits and 58% of the solar-type orbits are below the $e = 0.50$ line. There is thus a clear trend for orbits to be less eccentric as the stellar masses decrease. We explore the implications of this result in §6.5.

6.5 The Picture of M Dwarf Formation

With evidence in hand for the M dwarfs as well as the two mass regimes that bookend them, we are well positioned to draw comparative conclusions regarding how these systems form and dynamically evolve.

As outlined in Chapter 1, current models suggest systems of multiple stars form with components separated by tens to tens of thousands of AU. Considering that all of the M dwarf systems presented here have $P_{\text{orb}} \leq 30$ years and thus $a \lesssim 10$ AU, every companion in our sample has undergone significant migration to arrive at its orbit that we observe today.

At $P_{\text{orb}} \gtrsim 7$ years, orbits are generally eccentric among solar-type multiples, somewhat less eccentric among M dwarf multiples, and appear to be even less eccentric for very low-mass (VLM) multiples. This trend creates the characteristic lack of nearly-circular orbits at long P_{orb} for solar-type and higher-mass M dwarf systems. Previous work (Dupuy & Liu 2017) suggested that this trend is a consequence of disk lifetimes increasing as stellar mass decreases; lower-mass companions and their primary stars spend more time swimming through circumstellar material, losing more angular momentum to those disks than higher mass stars do before the disks dissipate.

An essential piece of that orbital evolution process is accretion of disk material onto the secondary star. If the overabundance of twins observed for M dwarfs (§6.4, esp. Figures 6.10 and 6.11) is not entirely due to observational bias, we can be assured that most companions experience a significant amount of accretion to arrive at their current positions. On the other hand, the lack of correlation between eccentricity and mass ratio (Figure 6.13) throws a wrench into this interpretation — why would some very low-mass systems evolve to low eccentricity without significant accretion?

We obtain more clues as we look toward shorter P_{orb} . The eccentricity distribution of solar-type multiples narrows as P_{orb} decreases (Figure 6.15), whereas the M dwarfs' distri-

bution narrows by an insignificant amount. This is another counterintuitive set of features: if M dwarfs spend *more* time exchanging angular momentum with disk material than solar-type stars, we might expect their final orbits to be *more* strictly regulated. The simplest explanation may be that M dwarf companions arrive at those orbits with less disk interaction than solar-type companions. This may mean the disk fragmentation radius is smaller or the disks themselves are smaller or less dense. This scenario could also explain why we find a few low-mass stars with low eccentricities and low mass ratios, assuming the odds of a multiple forming with $e = 0.1$ are not very different than one forming with $e = 0.8$.

The final clue to the M dwarf binary formation process comes from their tidal circularization period (P_{circ}). In §6.2.1 we noted that the observed range of potential P_{circ} is remarkably close to what we would expect given the solar-type multiples' P_{circ} and the difference in gravitational force between those two populations. The timescale of tidal orbital evolution depends on other important factors, however, such as the stars' radii, internal structures, and initial eccentricity at the moment the tidal force becomes significant. The agreement of reality with our back-of-the-envelope calculation thus suggests that the post-migration distributions of M dwarf systems and solar-type systems are different by roughly the amount needed to cancel out their differences in the other important tidal factors. The finer details of the tidal evolution timescales could thus be constrained by a very complete, well-characterized set of observed multiples and their orbits. The dissertation work presented here may qualify if we update our orbits with more reliable mass ratios for systems with $P_{\text{orb}} \lesssim 1$ year.

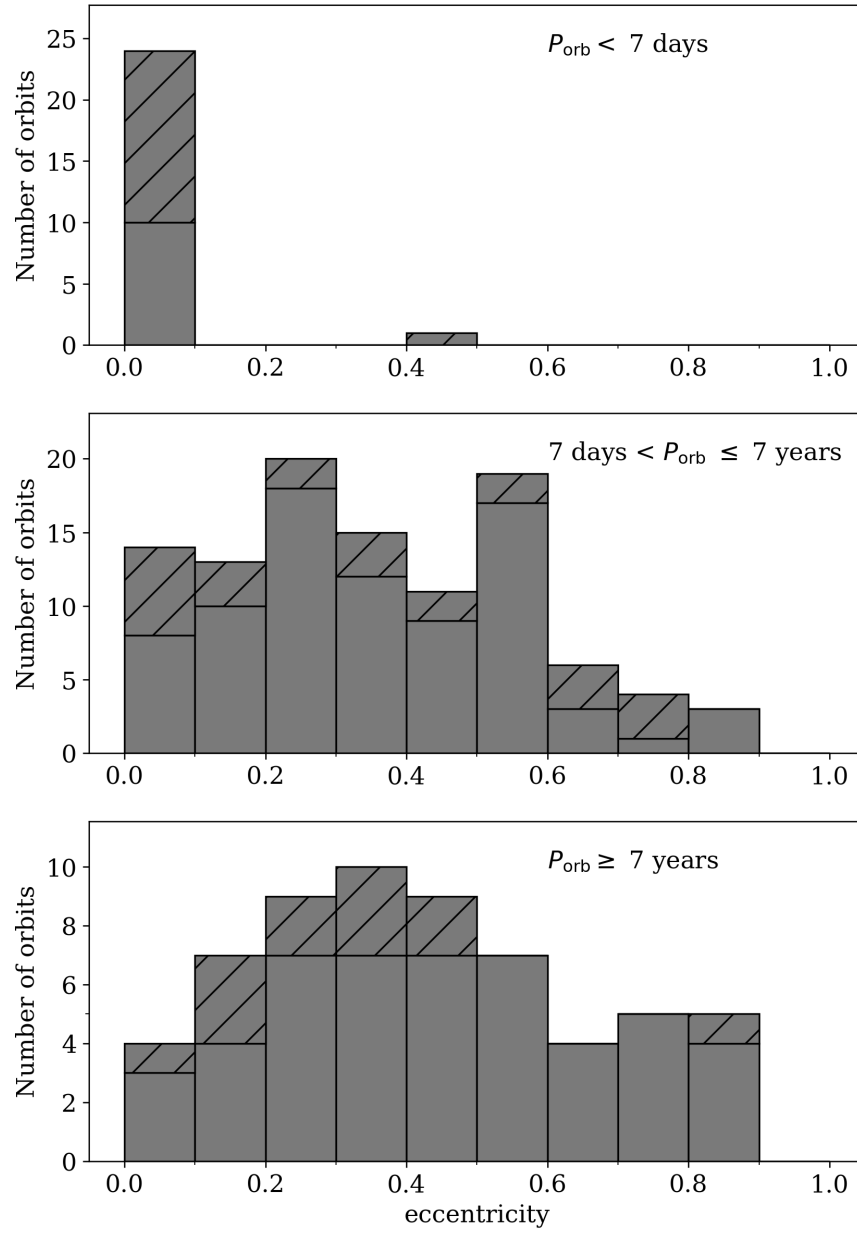


Figure 6.4 Distribution of eccentricity in three regimes of P_{orb} : $P_{\text{orb}} < 7 \text{ days}$ (*top panel*), $7 \text{ days} \leq P_{\text{orb}} < 7 \text{ years}$ (*middle panel*), and $P_{\text{orb}} \geq 7 \text{ years}$ (*bottom panel*). In every panel, the non-hatched bars indicate binaries and the hatched bars indicate subsystems of higher-order multiples. This figure is discussed in §6.2.3.

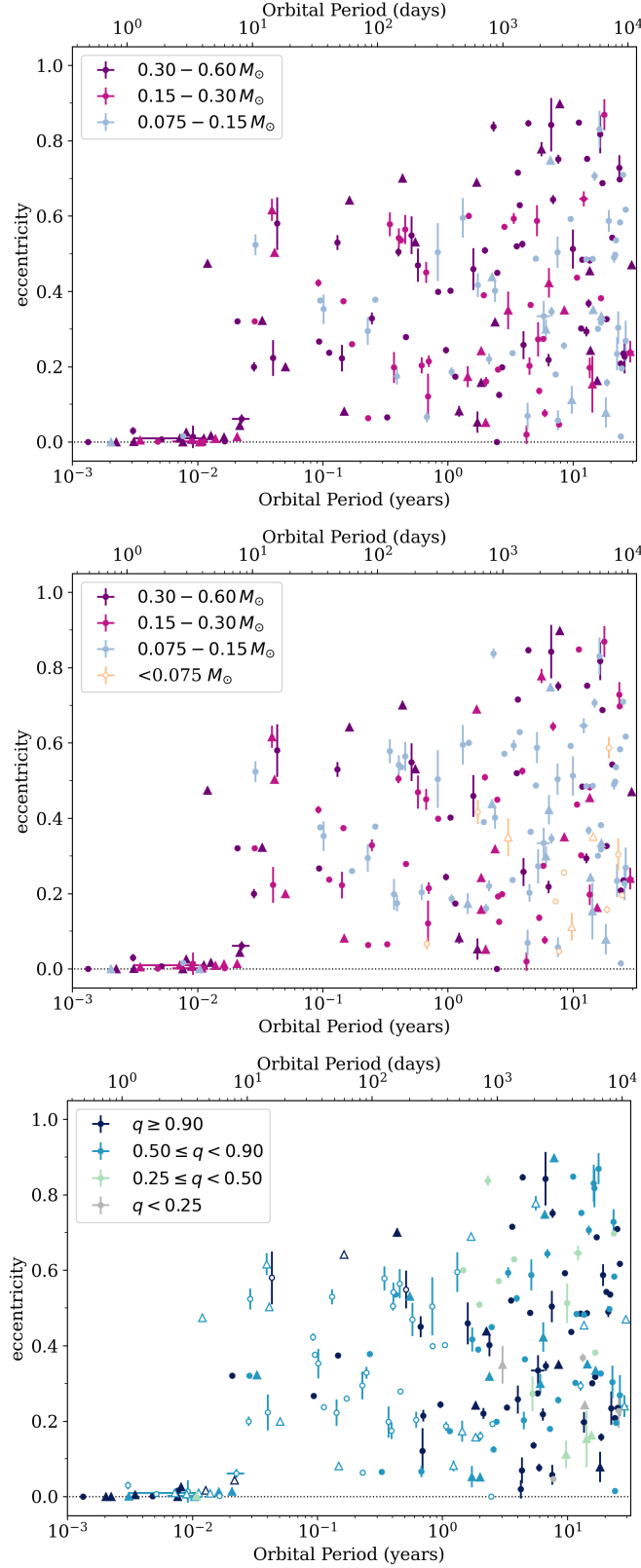


Figure 6.5 The P_{orb} vs. e plot showing the same systems as in Figures 6.1 and 6.2, but with points colored by primary mass (*top*), secondary mass (*middle*), or mass ratio (*bottom*). Open symbols indicate masses estimated assuming $\Delta K = 0.8$ mag, as those estimates are the least reliable. This figure is introduced in §6.4.

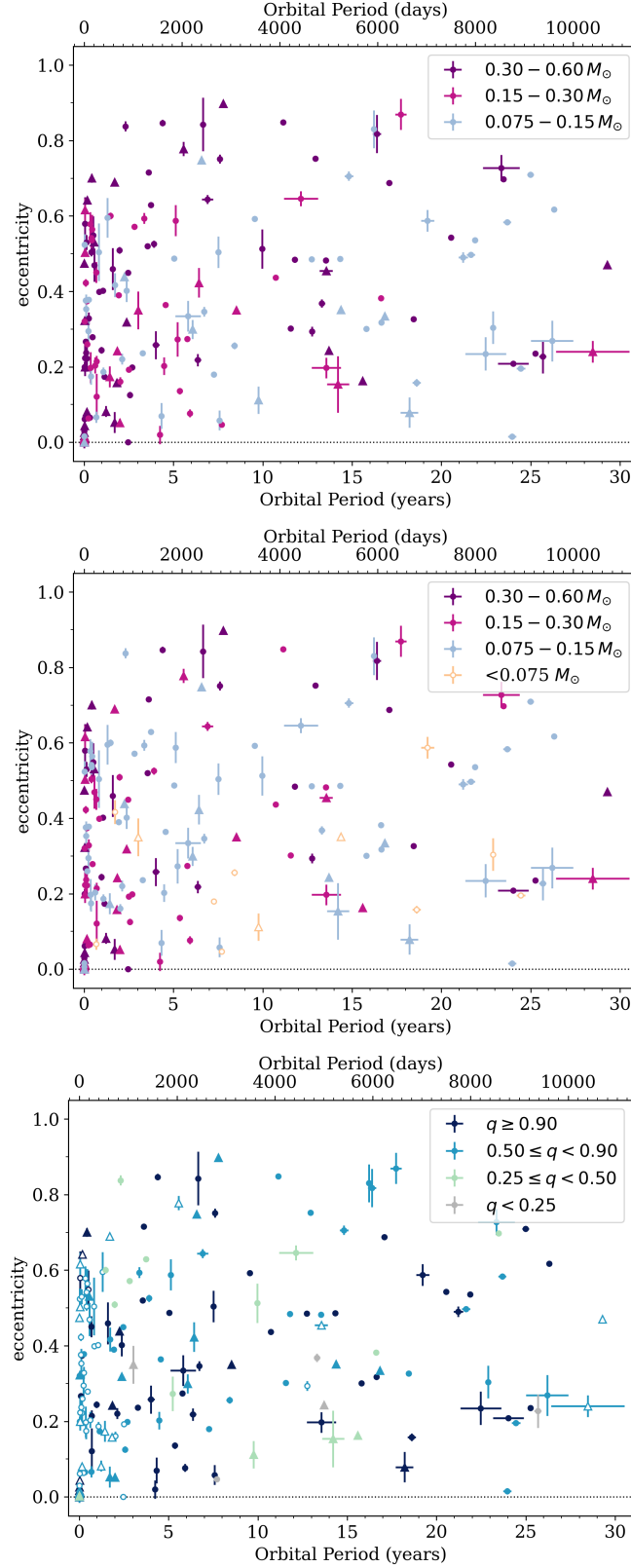


Figure 6.6 These P_{orb} vs. e plots are identical to those in Figure 6.5, but here the plots are in terms of linear P_{orb} instead of $\log P_{\text{orb}}$. Again, the points are colored by primary mass (*top*), secondary mass (*middle*), or mass ratio (*bottom*). Open symbols indicate masses estimated by assuming $\Delta K = 0.8$ mag, as those estimates are the least reliable.

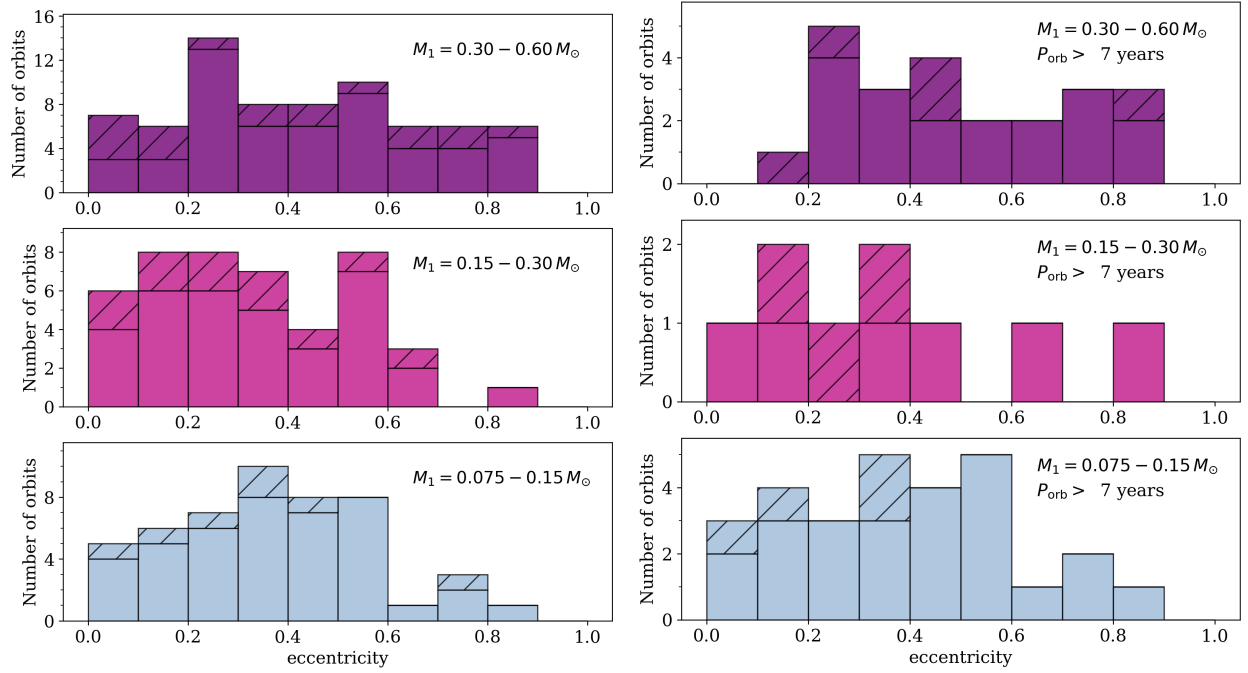


Figure 6.7 Distributions of eccentricity for multiples with different M dwarf primaries, shown for all systems (*left column*) and those with $P_{\text{orb}} > 7$ years (*right column*). Systems with $P_{\text{orb}} < 7$ days were excluded. Binaries are shown with non-hatched bars and higher-order multiples are indicated with hatched bars. Masses were either dynamical or estimated as described in §6.3. The analogous plot organized by M dwarf secondary mass is given in Figure 6.8. This figure is introduced in §6.4.

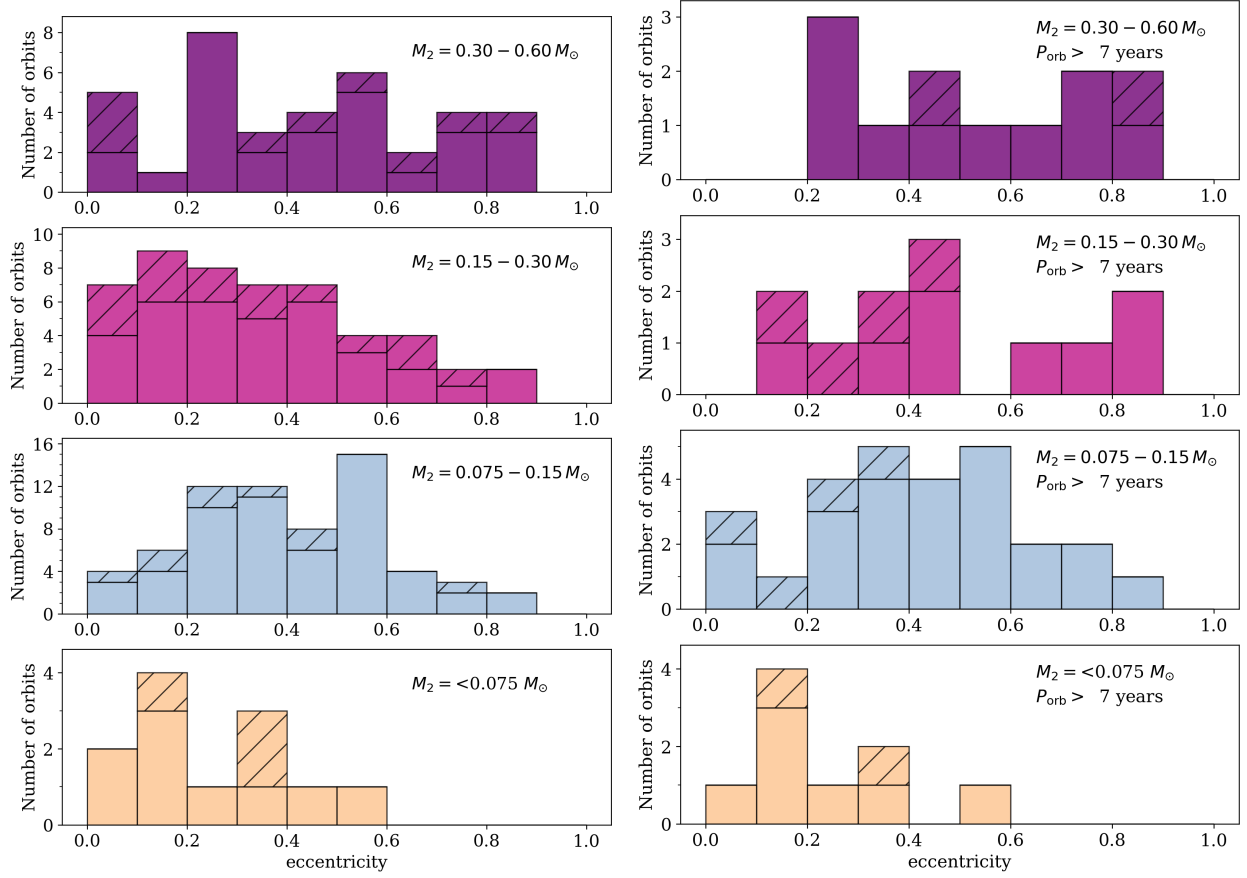


Figure 6.8 Distributions of eccentricity for multiples with different M dwarf secondaries, shown for all systems (*left column*) and those with $P_{\text{orb}} > 7$ years (*right column*). Systems with $P_{\text{orb}} < 7$ days were excluded. Binaries are shown with non-hatched bars and higher-order multiples are indicated with hatched bars. Masses were either dynamical or estimated as described in §6.3. The analogous plot organized by M dwarf primary mass is given in Figure 6.7. This figure is introduced in §6.4.

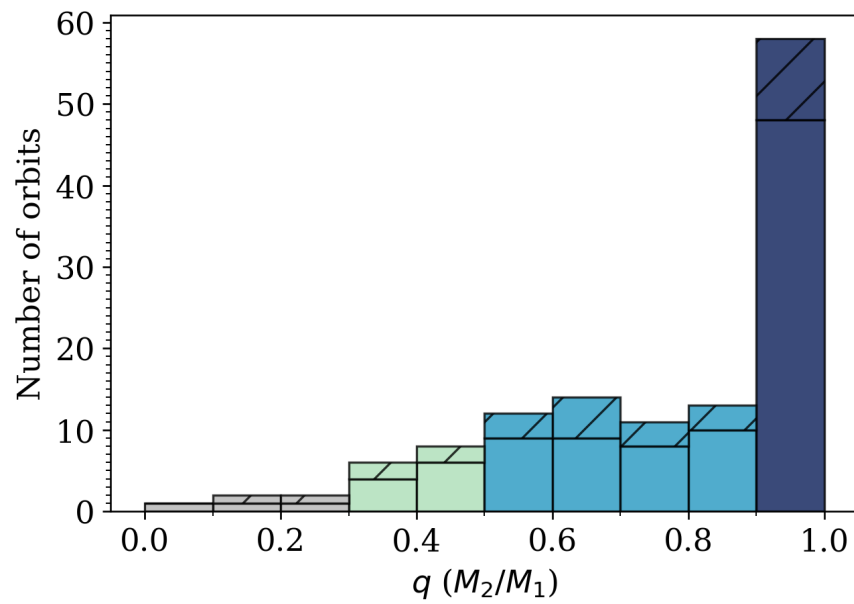


Figure 6.9 Distribution of mass ratios for M dwarf systems presented in this work. For systems without dynamical mass, masses were estimated following §6.3. Systems were excluded if their mass estimates required assuming $\Delta K = 0.8$ mag, as those masses are the least reliable. Binaries are represented here with non-hatched bars and higher-order multiples are indicated with hatched bars. The bars are colored to match the color scheme for q used in other plots in this chapter. This figure is introduced in §6.4.3.

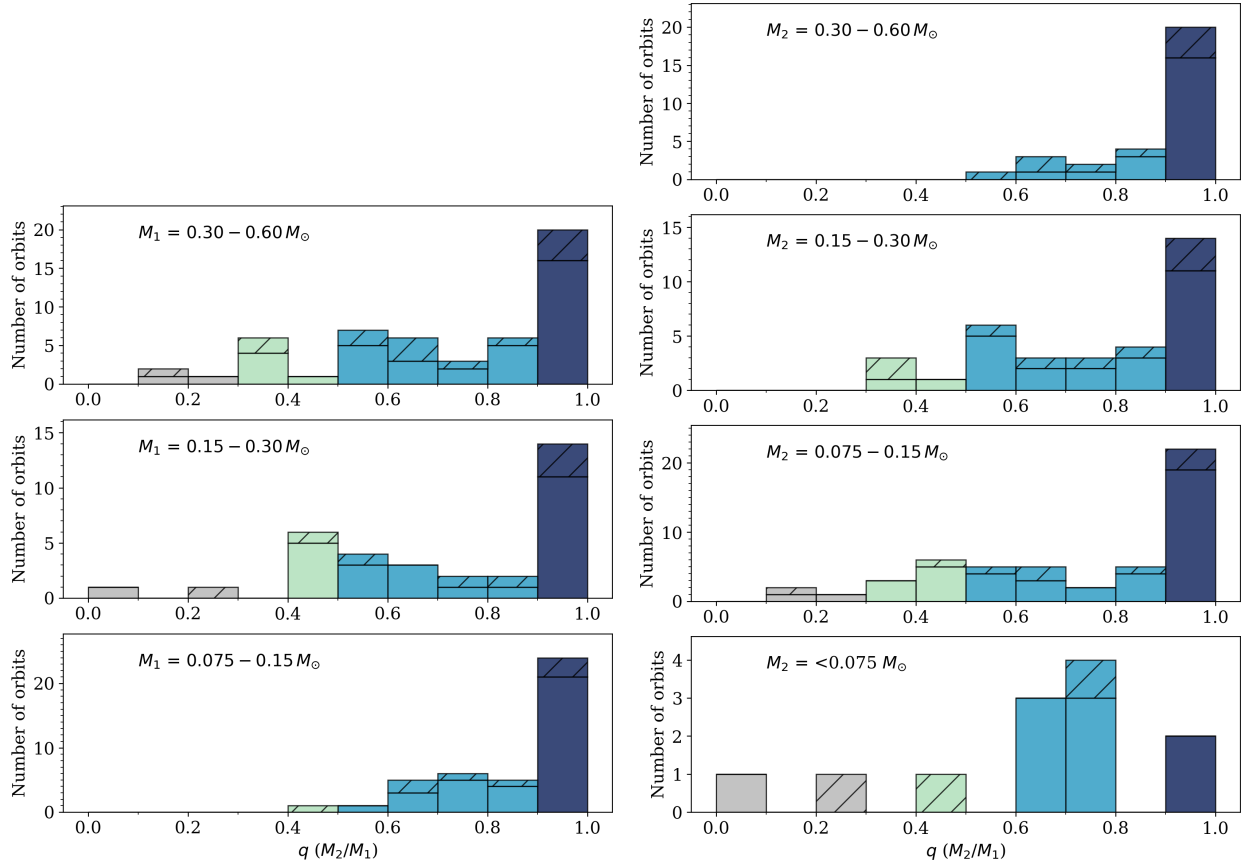


Figure 6.10 Distributions of mass ratios for multiples with different primary masses (*left column*) and secondary masses (*right column*). In every panel, the non-hatched bars represent binaries and the hatched bars indicate subsystems of higher-order multiples. This figure is introduced in §6.4.3.

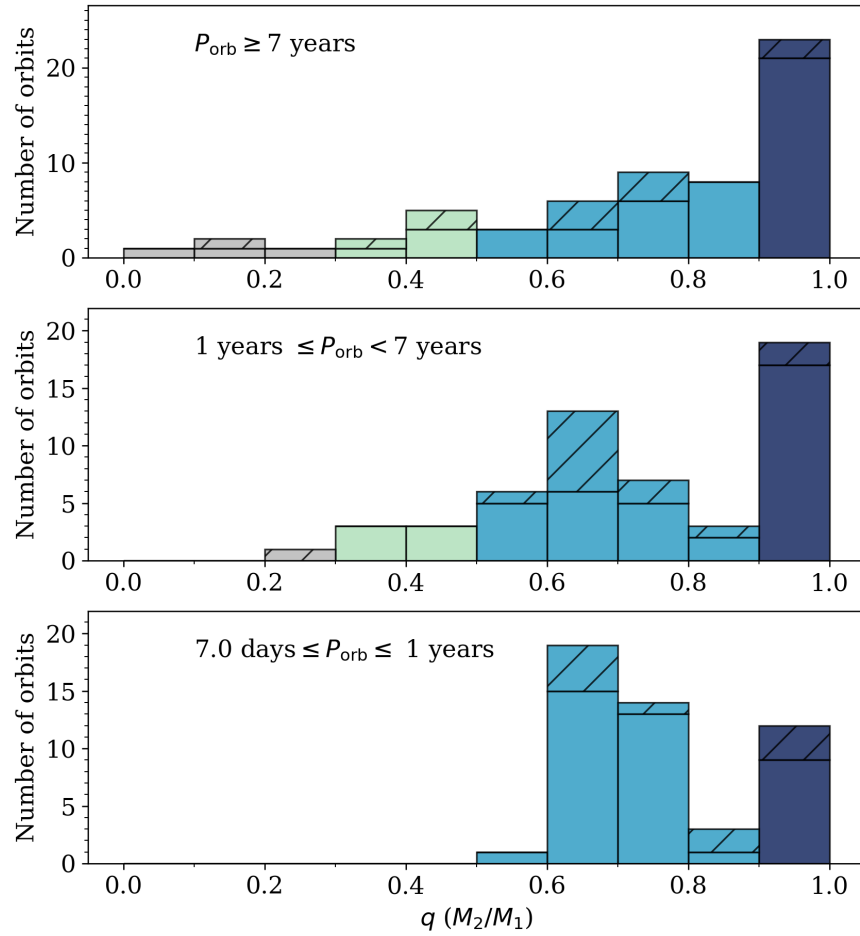


Figure 6.11 Distributions of mass ratios for multiples of different P_{orb} . In every panel, the non-hatched bars represent binaries and the hatched bars indicate subsystems of higher-order multiples. This figure is introduced in §6.4.3.

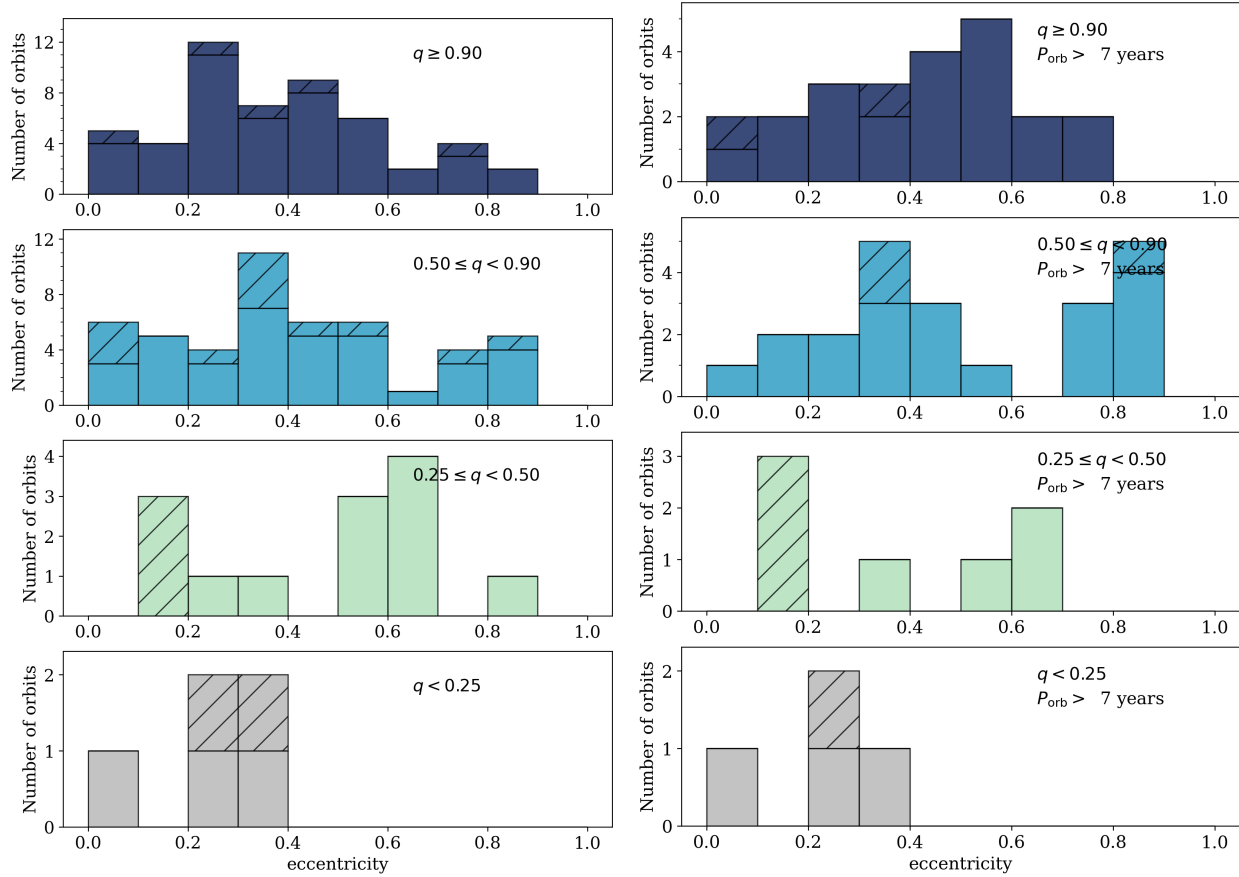


Figure 6.12 Distributions of eccentricity for systems of different mass ratios, given for all systems (*left column*) and those with $P_{\text{orb}} > 7$ years (*right column*). All masses (and thus mass ratios) that were not dynamical masses were estimated using the procedure in §6.3. This figure is introduced in §6.4.3.

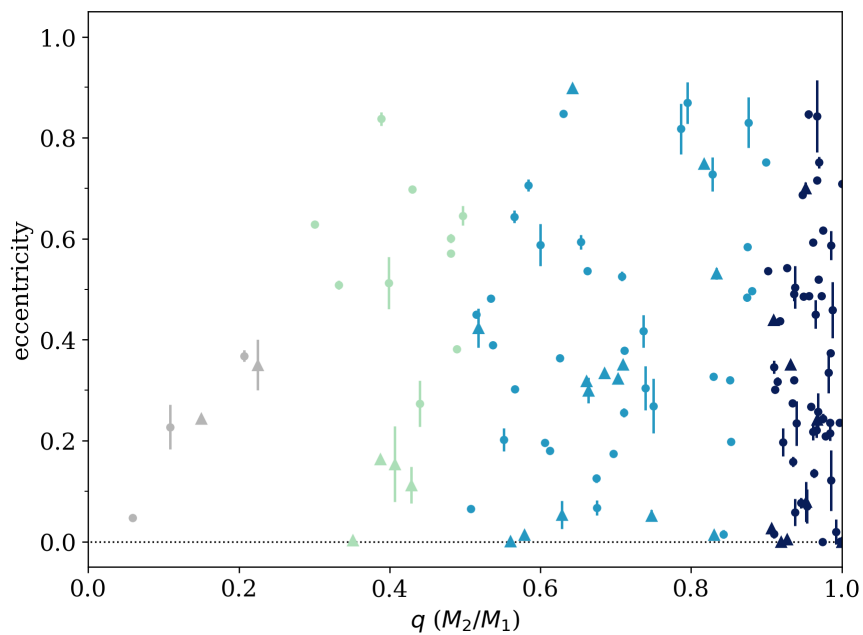


Figure 6.13 Distribution of eccentricity with respect to mass ratio as q vs. e , excluding systems for which masses were estimated by assuming $\Delta K = 0.8$ mag. All masses (and thus mass ratios) that were not dynamical masses were estimated using the procedure in §6.3. The symbol shapes indicate the types of system: circles are binaries and triangles are subsystems of higher-order multiples. This figure is introduced in §6.4.3.

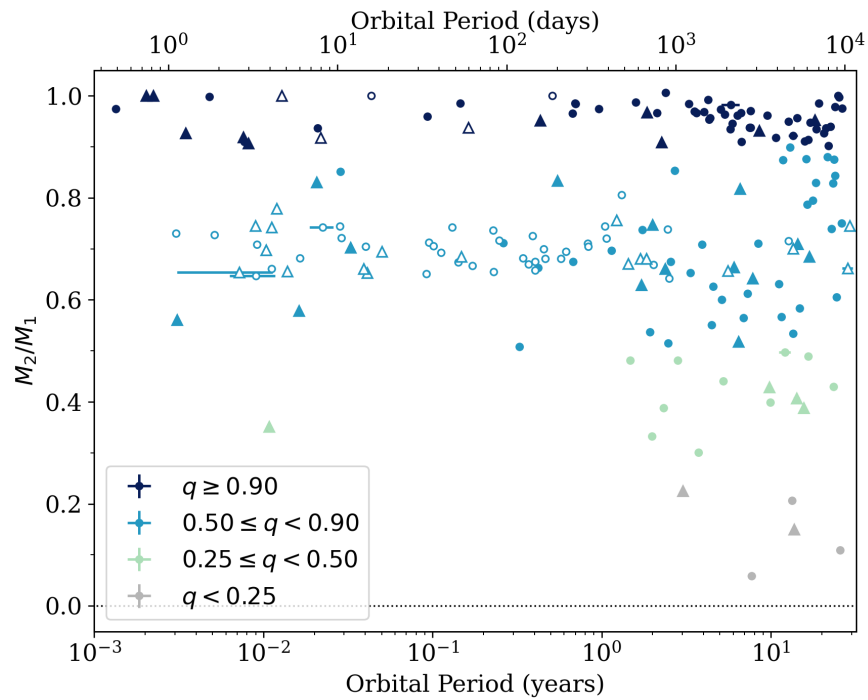


Figure 6.14 Distribution of orbital period with respect to mass ratio as P_{orb} vs. q . The open symbols indicate the systems for which masses were estimated by assuming $\Delta K = 0.8$ mag, while the filled symbols are systems for which masses were either dynamical or estimated using the procedure in §6.3. The symbol shapes indicate the types of system: circles are binaries and triangles are subsystems of higher-order multiples. This plot is discussed in §6.4.3.

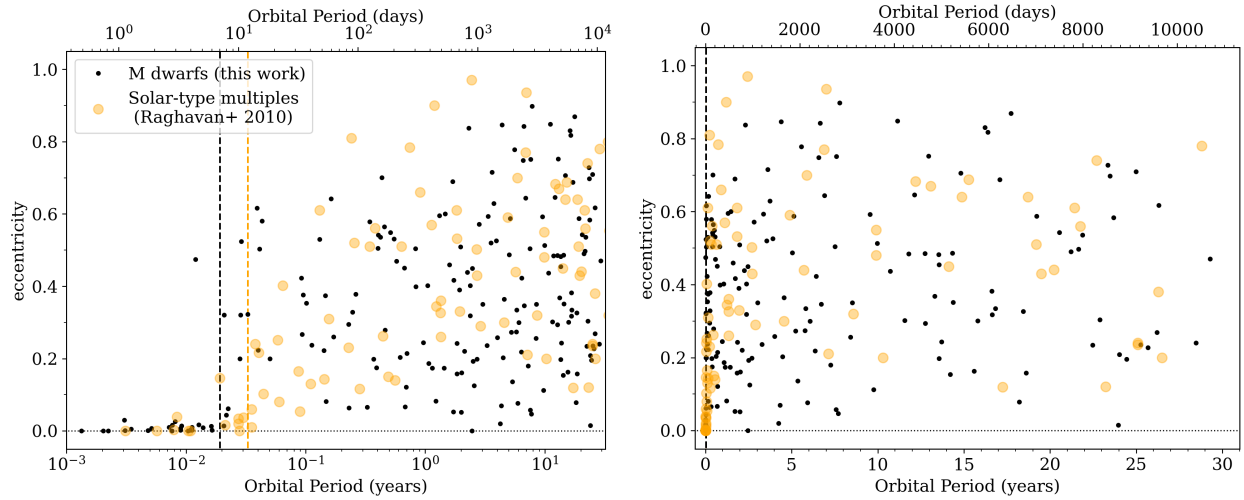


Figure 6.15 P_{orb} vs. e for multiples of solar-type stars (yellow points; Raghavan et al. 2010) and M dwarfs (black points; this work). The same distribution is shown in terms of $\log P_{\text{orb}}$ (*left panel*) and linear P_{orb} (*right panel*). The 12-day tidal circularization period for solar-type stars is shown with the yellow dashed line, and the black dashed line indicates the 7-day period that is the upper limit of P_{circ} for M dwarfs. This figure is discussed in §6.4.4.

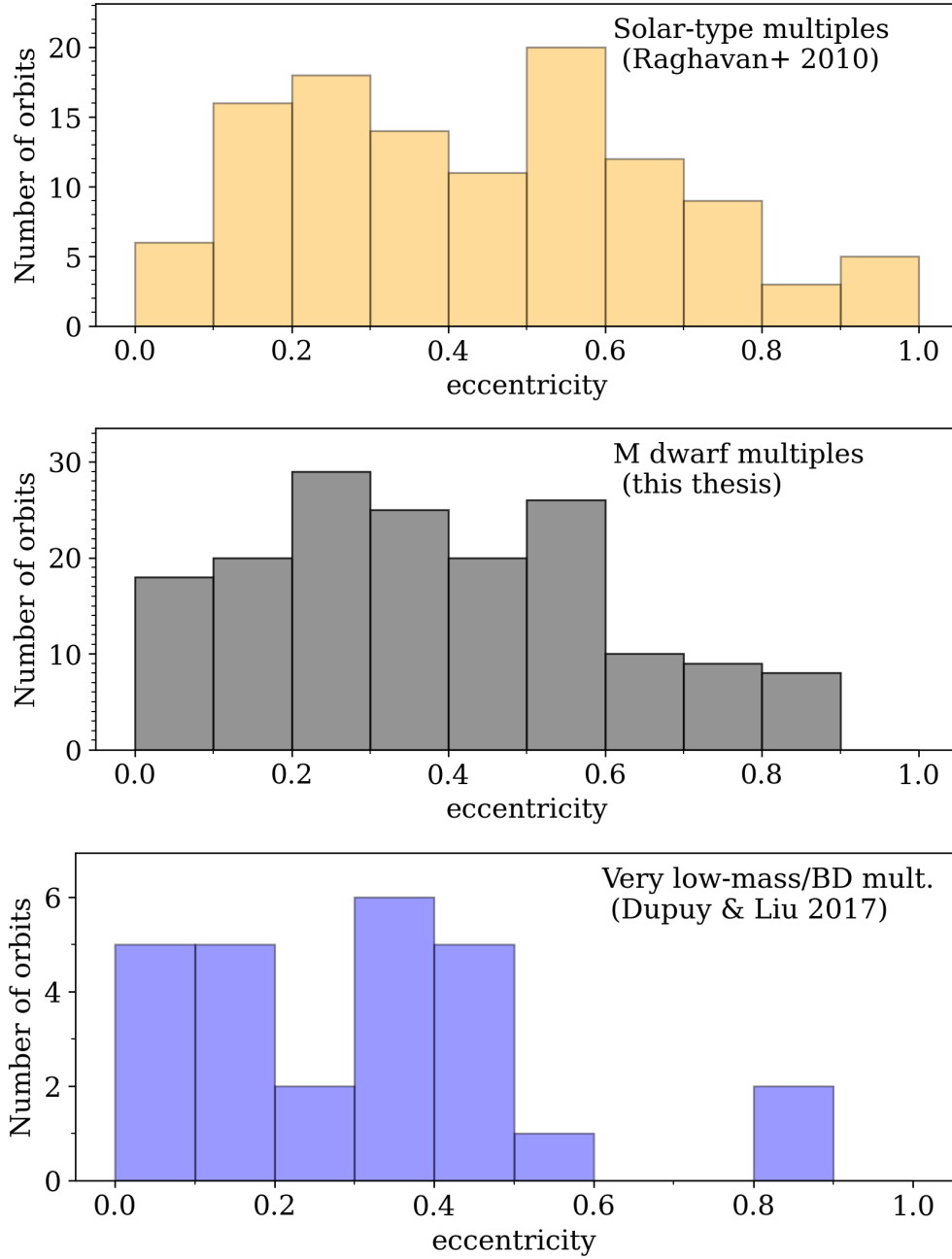


Figure 6.16 Comparison of the eccentricity distributions for three populations of multiples. *Top panel:* multiples of F, G, and K dwarfs (“solar-type”) from Raghavan et al. (2010); *middle panel:* multiples of M dwarfs from this work (repeated from Figure 6.3); *bottom panel:* multiples of very low-mass (VLM) stars and brown dwarfs from Dupuy & Liu (2017). Note that the scale for the VLM distribution is much smaller, as they have fewer orbits than the other sets. In every panel, the bars represent the sum of all multiples (binary, triple, etc.), and systems with $P_{\text{orb}} < P_{\text{circ}}$ for that population are excluded (except for the VLM set, which contains no tidally circularized systems). This figure is introduced in §6.4.4.

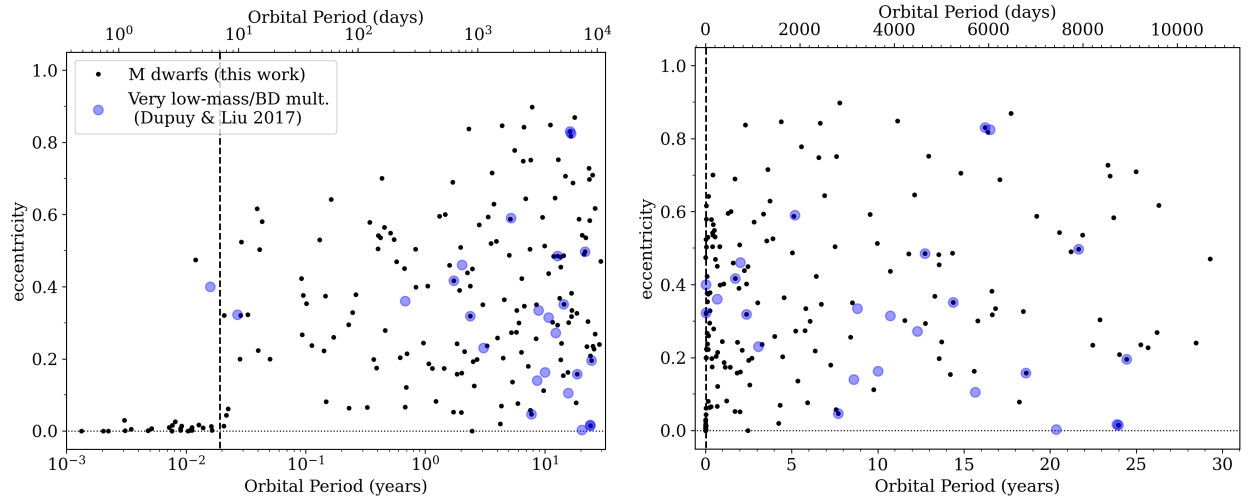


Figure 6.17 P_{orb} vs. e for multiples of very low-mass (VLM) stars and brown dwarfs (blue points; Dupuy & Liu 2017) and M dwarfs (black points; this work). The distribution is given in terms of $\log P_{\text{orb}}$ (*left panel*) as well as for linear P_{orb} (*right panel*). The black dashed line indicates the 7-day limit below which all M dwarf systems are nearly circular; P_{circ} is not indicated for the VLM sample because there are not enough of those systems with short P_{orb} observed to constrain it. This figure is introduced in §6.4.5.

CHAPTER 7

Summary, Conclusions, and the Future

7.1 The Author’s Specific Contributions to this Dissertation

The work in this document has been presented in the voice of a group effort — i.e., as “our” work rather than “my work” (that of the first author alone). This narrative choice adds clarity to the scientific and procedural descriptions, and also reflects the collaborative nature of the project.

It is impossible to completely separate my own work from that of the larger RECONS group (both past and present), considering that every individual in the group regularly conducts observations for each other and consults on analyses. To celebrate the conclusion of the project and the PhD, however, here I distinguish the main highlights.

- Although most of the RECONS astrometry data used in this work were secured many years before my involvement in this group, I personally completed five observing runs (spanning 64 nights) at the CTIO 0.9m during my years with RECONS. These account for $\sim 20\%$ of the observing runs taken for this program during that time, and a full third of the runs undertaken by U.S.-based RECONS members. All data were taken classically by visiting the 0.9m telescope itself.
- During the period 2018–2022 I was also responsible for calibrating and organizing all the data taken at the CTIO 0.9m for the RECONS program, regardless of whether or not I was the observer for each run.

- I reduced the astrometry and photometric variability data for more than 700 data sets representing ~ 400 systems, with many systems reduced more than once as new data were added. Each system's data reduction takes roughly half an hour (but can take up to 1.5 hours in some cases), and requires human assessments and decision-making at several points despite many steps of the pipeline being automated.
- I personally completed the orbits fits for every orbit presented here from both the RECONS astrometry (using the Dieterich 2018, code) and SOAR speckle interferometry (using the Tokovinin 2016, code), as well as ~ 40 orbits that were not included here because they were poor quality or simply not as precise as other characterizations in the literature.
- To improve the computation time of the Dieterich et al. (2018) orbit fitting code, I completed some minor upgrades to how it solves Kepler's equation and how it stores some variables. I also altered its output to allow it to run remotely without interruption during the global pandemic of 2020.
- To improve the efficiency of the RECONS data pipeline, I created for it a new front-end user interface using a combination of Python and IRAF. Although the underlying procedures were unchanged by this upgrade, the new interface made the data reduction process faster to complete and less susceptible to user errors.
- Most of the SOAR speckle data shown in this dissertation was secured through standard and long-term proposals to NSF's NOIRLab. I led these proposals for the semesters

2019A, 2020A, 2020B–2022A, and 2022B–2023A, and as the proposal lead I drafted all text and figures as well as solicited and incorporated feedback from several collaborators.

- The sample construction presented in Chapter 2 of this dissertation was designed and completed by myself alone, with advisor guidance only for the initial concept of an M dwarf sample and some revision regarding its presentation.

7.2 Conclusion to This Study

We have presented here a comprehensive study of the orbits of M dwarf multiples, focusing primarily on the population within 25 pc (augmented by a few systems beyond that radius). By combining data from two observing programs as well as the literature, we have mapped the distribution of P_{orb} vs. e between 0.3 days and 30 years. These results show that the low-mass systems demonstrate tidal circularization at very short orbits and exhibit a diverse range of shapes for longer orbits, with the most eccentric systems being higher-order multiples. The M dwarf multiples' orbital eccentricity distributions lie intermediate between those of the solar-type multiples and brown dwarf multiples, forming a continuum across stellar mass.

The multiples considered for this study most likely formed at wide separations (at least tens of AU) and migrated to their current configurations ($\lesssim 10$ AU). The only efficient method for this process is if the stars travel through each others' circumstellar disks and lose angular momentum to that material before it disperses. This process shrinks the stars' orbits as they accrete material from the disks, which is also expected to drive the orbits toward circular architectures. Among our M dwarfs we observed a high incidence of very high mass ratios

($q \gtrsim 0.9$), a result that is consistent with the majority of the systems migrating through accretion, although we caution that observational biases are undoubtedly present because low mass/low flux companions are more difficult to detect than higher mass/higher flux companions. These selection effects drive up the number of roughly equal mass systems in our sample.

Future improvements to this study should address those observational biases first and foremost. The continuation of the RECONS volume-complete astrometric survey over the next 10 years should ameliorate some of the biases described here, as many of the higher-mass M dwarfs in that survey currently have extremely short timelines of observation that limit their data’s usefulness. More impactful, however, would be if the sensitivity space of the diverse set of literature orbits were better characterized by re-fitting each publication’s data in a uniform matter, although some variations will be required for the different combinations of types of data employed. Each data set could also be characterized in terms of its sensitivity to different mass ratios, which would allow us to calibrate the observed mass ratio distributions to determine the underlying populations. Our current interpretations are somewhat conservative because of the poorly constrained selection effects for mass ratio.

Another significant dimension to this work could be added if the entire sample were uniformly assessed for indicators of system youth or age. Although most orbital evolution occurs quickly, we do occasionally find a system that is in the midst of these rapid processes (such as HIP47133 AB, discussed in §6.2.1). Separating the systems that are decidedly post-evolution from those that are potentially still mid-evolution could add an unusually

empirical view of how these processes change the distributions of orbits. Although it is notoriously difficult to determine an age for an M dwarf system, a first step in estimating ages for the overall M dwarf sample would be to derive UVW space motions for all of the systems considered here.

Of course, as is the case with nearly every astrophysical study, more data points on virtually every plot presented here would further clarify the trends we have already outlined. Nonetheless, this study presents 193 M dwarf orbits that have been well-characterized and used to reach the conclusions given. This is four times more than any previous study for these stars and extends out to three decades of orbital coverage, matching the orbit of Saturn around our Sun.

Significant improvements could also be made to the RECONS data if we incorporated the new results from the *Gaia* mission into our data reduction process. If we matched our reference stars to the *Gaia* catalog instead 2MASS, we could use the *Gaia* parallaxes and proper motions to determine their true positions at each observation, and from those determine a more accurate and precise measurement of the non-astrophysical shape of the field (i.e., the shape imparted by the optics between the CCD and sky). This upgrade would improve the RECONS program's sensitivity to equal-mass and very low-mass companions down to Jovian planet masses, and reduce the number of signals of ambiguous origin (such as those shown in Figure 4.2 in §4.1.2). Characterizing the non-astrophysical field shape so precisely would also allow RECONS data to be combined with the *Gaia* time-series data when that is released in the coming years (Data Release 4, planned for late 2025). This

upgrade is already planned for the coming years at RECONS by members of the group.

Finally, the most telling extension to this study would be to include even lower-mass systems using various techniques, including both brown dwarfs and gas giant planets. Both of these populations are expected to be rare companions to M dwarfs, and a comprehensive survey of their occurrence rates would add another dimension to the results of their dynamics. This study is already planned for the coming years. Observing programs are also underway to search for giant planets on short orbits around M dwarfs (Cañas et al. 2022, 2023; Kanodia et al. 2023), and the RECONS data will complement these by opening the door to long-period orbits once it is improved with the *Gaia* results described above. Having the P_{orb} vs. e parameter space mapped for planetary companions as well would allow us to compare the stellar and brown dwarf results directly with a population that is well known to form and evolve in circumstellar disks. We would then have one big picture of formation and dynamical evolution across the entire mass spectrum of the main sequence — and beyond.

Appendix of Long Tables Used in this Work

Ref. code	Reference
Act20	Acton et al. (2020)
Bal10	Balega et al. (2010)
Bar12	Barry et al. (2012)
Bar18	Baroch et al. (2018)
Ben16	Benedict et al. (2016)
Bla10	Blake et al. (2010)
Cas18	Casewell et al. (2018)
Dal11	Dal & Evren (2011)
Dav16	David et al. (2016)
Del99	Delfosse et al. (1999)
Dia07	Díaz et al. (2007)
Die18	Dieterich et al. (2018)
Dup17	Dupuy & Liu (2017)
Duq88	Duquennoy & Mayor (1988)
Gaia3	Gaia Collaboration et al. (2022)
Gom12	Gómez Maqueo Chew et al. (2012)
Har18	Hartman et al. (2018)
Har96	Harlow (1996)
Her65	Herbig & Moorhead (1965)
Ire08	Ireland et al. (2008)
Irw11	Irwin et al. (2011)
Kor16	Koren et al. (2016)
Kra17	Kraus et al. (2017)
Kur08	Kürster et al. (2008)
Laz18	Lazorenko & Sahlmann (2018)
Lop05	López-Morales & Ribas (2005)
Lub17	Lubin et al. (2017)
Man19	Mann et al. (2019)
Mar09	Martinache et al. (2009)
Mat97	Mathieu et al. (1997)
Maz01	Mazeh et al. (2001)
Mor09	Morales et al. (2009)
Nid02	Nidever et al. (2002)
Rie14	Riedel et al. (2014)
Sah15	Sahlmann et al. (2015)
Seg00	Ségransan et al. (2000)
Ski18	Skinner et al. (2018)
Spe19	Sperauskas et al. (2019)
Tok15	Tokovinin et al. (2015)
Tok97	Tokovinin (1997)
Win20	Winters et al. (2020)
Xia19	Xia et al. (2019)
Zho15	Zhou et al. (2015)

Table 1 Five-letter reference codes and their corresponding formal references, as used in tables throughout this dissertation.

Table 2: List of M dwarf systems within 25 pc drawn from *Gaia* DR2, as described in §2.3.

These systems have not been vetted to distinguish single stars from multiples, but in cases

where a system was resolved in *Gaia* but not 2MASS, a “J” flag is listed in column 12.

R.A. J2000.0 (1)	Decl. J2000.0 (2)	<i>Gaia</i> DR2 ID (3)	2MASS ID (4)	π (mas) (5)	μ_α (mas yr ⁻¹) (6)	μ_δ (mas yr ⁻¹) (7)	G (mag) (8)	B_G (mag) (9)	R_G (mag) (10)	K_s (mag) (11)	Joint phot? (12)
00 01 15.82	+06 59 35.50	2745860763717896448	00011579+0659355	42.75 ± 0.08	−436.74	−83.49	14.693	16.801	13.339	10.418	–
00 02 06.22	+01 15 36.14	2738415592529108096	00020623+0115360	48.05 ± 0.14	463.38	61.41	16.337	19.449	14.804	11.129	–
00 03 16.71	−55 16 29.10	4923590430409730048	00031670−5516292	42.07 ± 0.05	448.53	−235.67	13.702	15.403	12.450	9.849	–
00 04 36.44	−40 44 02.89	4996141155411983744	00043643−4044020	81.23 ± 0.11	677.73	−1505.12	11.499	13.103	10.307	7.737	–
00 04 41.47	−20 58 29.88	2340736324254735488	00044144−2058298	66.33 ± 0.16	758.23	85.20	16.869	20.484	15.249	11.396	–
00 04 57.55	−17 09 36.96	2414623952318068224	00045753−1709369	58.68 ± 0.12	145.14	−8.50	14.605	16.971	13.201	10.084	–
00 05 24.99	−50 02 52.98	4976609705736840960	00052498−5002529	41.35 ± 0.04	−155.91	−11.36	11.008	12.230	9.958	7.627	–
00 05 34.87	−06 07 06.87	2442074771933927424	00053484−0607070	40.21 ± 0.06	177.31	−55.30	11.979	13.395	10.822	8.411	–
00 06 19.19	−65 50 25.92	4899957905439144320	00061920−6550262	57.34 ± 0.07	197.07	−549.22	11.103	12.442	9.988	7.631	–
00 06 39.24	−07 05 35.93	2441755840548967424	00063925−0705354	50.87 ± 0.62	−100.95	118.25	13.102	14.971	11.768	8.958	–
00 06 43.20	−07 32 17.02	2441630500517079808	00064325−0732147	206.21 ± 0.13	−811.48	−1892.90	11.780	14.096	10.405	7.439	–
00 07 05.45	−56 05 04.62	4922569671300905088	00070543−5605045	40.08 ± 0.04	339.79	−7.32	12.315	13.754	11.150	8.710	–
00 08 17.38	−57 05 52.91	4919497979411495296	00081737−5705528	78.12 ± 0.06	−355.45	−44.45	10.935	12.390	9.793	7.395	–
00 08 27.28	+17 25 27.46	2772804845911842944	00082730+1725274	46.00 ± 0.05	−92.73	−65.91	10.026	11.032	9.070	6.980	–
00 08 53.92	+20 50 25.59	2798766647610195456	00085391+2050252	55.26 ± 0.76	−48.64	−260.19	11.990	13.773	10.716	8.010	–
00 09 04.36	−27 07 19.68	2333676738049780352	00090428−2707196	42.12 ± 0.05	692.25	90.14	10.919	11.933	9.947	7.856	–
00 09 18.71	−55 05 57.43	4922947628424508544	00091870−5505573	41.99 ± 0.06	185.10	−125.76	12.921	14.622	11.670	9.011	–
00 09 19.95	−21 14 41.41	2364492097606462336	00091993−2114411	43.01 ± 0.11	146.24	−103.21	11.203	12.404	10.167	7.937	–
00 09 43.29	−41 17 35.58	4996252755842227072	00094327−4117355	43.65 ± 0.07	193.59	105.96	14.090	15.940	12.799	10.077	–
00 09 45.04	−42 01 39.30	4995796699034222464	00094508−4201396	57.20 ± 0.24	268.49	−16.08	12.147	13.899	10.886	8.223	–
00 11 04.61	−05 47 02.31	2443632711190063872	00110458−0547023	41.21 ± 0.07	255.87	8.37	10.106	11.085	9.167	7.119	–
00 11 53.03	+22 59 04.59	2848646203058386560	00115302+2259047	48.86 ± 0.08	120.81	−211.90	11.757	13.276	10.571	7.987	–
00 12 02.68	+02 06 23.69	2546762984866318080	00120264+0206236	41.93 ± 0.08	301.46	65.44	13.709	15.466	12.439	9.721	–
00 13 46.60	−04 57 37.18	2444078253918146944	00134659−0457371	41.90 ± 0.34	600.59	−162.58	15.464	18.288	13.980	10.479	–
00 14 55.77	−48 44 16.90	4977142934516994176	00145575−4844171	50.11 ± 0.39	870.73	281.47	19.068	21.418	17.362	12.723	–
00 15 49.24	+13 33 22.32	2768048564768256512	00154919+1333218	81.87 ± 0.09	618.00	329.32	11.396	12.849	10.244	7.807	–
00 15 51.53	−67 59 51.82	4706483441369292288	00155156−6759519	53.27 ± 0.02	556.40	−130.02	10.106	11.184	9.114	6.949	–
00 15 58.07	−16 36 57.62	2368212771939556992	00155808−1636578	55.94 ± 0.20	−115.82	6.00	11.748	13.428	10.514	7.909	–

Table 2: List of M dwarf systems within 25 pc drawn from *Gaia* DR2, as described in §2.3.

These systems have not been vetted to distinguish single stars from multiples, but in cases

where a system was resolved in *Gaia* but not 2MASS, a “J” flag is listed in column 12.

00 16 01.97	-48 15 39.13	4977352700719796864	00160199-4815392	40.19 ± 0.49	-43.12	-244.69	10.531	11.807	9.442	7.112	-
00 16 14.63	+19 51 37.53	2797745549200763520	00161455+1951385	65.72 ± 0.10	714.51	-761.42	10.897	12.534	9.686	7.087	-
00 16 18.66	-17 08 52.93	2367899071824176384	00161866-1708535	40.34 ± 0.08	51.62	435.43	14.050	15.640	12.831	10.327	-
00 16 36.58	-50 16 08.47	4973763482448692096	00163656-5016086	42.20 ± 0.04	332.54	269.53	11.413	12.628	10.359	8.168	-
00 16 37.72	-52 41 36.10	4924503128140880512	00163769-5241361	43.87 ± 0.06	101.79	12.74	14.374	16.381	13.041	10.205	-
00 16 56.30	+05 07 26.40	2741452134407577216	00165629+0507261	56.07 ± 0.09	-89.89	-623.75	12.398	14.070	11.148	8.587	-
00 18 16.59	+10 12 10.04	2752746111688997248	00181659+1012100	59.60 ± 0.09	2.39	-29.32	10.001	11.148	8.964	6.741	-
00 18 44.78	-34 50 15.09	2309132133824849152	00184479-3450151	41.88 ± 0.04	-26.87	-273.41	11.800	13.225	10.646	8.157	-
00 19 04.78	+04 20 53.14	2741149940509219072	00190475+0420530	41.99 ± 0.08	-393.25	-219.13	12.976	14.519	11.772	9.274	-
00 19 27.49	+04 50 29.92	2741250786341356288	00192745+0450297	40.47 ± 0.12	-485.54	-300.21	15.342	17.554	13.964	11.085	-
00 20 00.58	-38 52 08.43	4998040286871047680	00200058-3852084	40.89 ± 0.07	-203.40	-62.24	14.803	16.832	13.468	10.622	-
00 20 08.38	-17 03 41.00	2367938722962185088	00200837-1703409	43.78 ± 0.05	141.89	-13.17	10.843	11.923	9.842	7.695	-
00 21 16.55	+18 43 55.67	2794420351160369920	00211645+1843558	43.93 ± 0.14	637.03	-69.44	14.843	17.102	13.459	10.420	-
00 21 19.62	-45 44 47.11	4978671015158662528	00211961-4544465	56.86 ± 0.03	69.91	-815.29	9.629	10.642	8.659	6.544	-
00 21 37.26	-46 05 33.38	4978625041828782848	00213729-4605331	52.22 ± 0.10	-305.84	-360.68	11.072	12.498	9.943	7.447	-
00 21 56.04	-31 24 21.81	2316867885320845696	00215604-3124215	55.39 ± 0.04	63.30	-193.89	10.177	11.397	9.119	6.785	-
00 23 18.53	-50 53 37.94	4972971284318252160	00231851-5053380	49.63 ± 0.05	549.11	0.10	10.857	12.152	9.763	7.375	-
00 23 27.99	+24 18 24.61	2801216123294143360	00232802+2418244	60.03 ± 0.10	-224.83	118.04	12.838	14.540	11.572	8.867	-
00 24 24.63	-01 58 19.97	2541756977144595712	00242463-0158201	79.97 ± 0.22	-77.16	141.11	16.596	19.853	14.993	10.539	-
00 25 04.31	-36 46 17.86	4998699749034263808	00250428-3646176	50.00 ± 0.28	242.78	50.27	11.342	12.750	10.223	7.828	-
00 25 20.60	+22 53 11.11	2800823799506215168	00252063+2253121	61.87 ± 0.09	-233.86	-463.66	12.792	14.521	11.531	8.868	-
00 26 31.64	+14 59 22.75	2780347152080719872	00263162+1459223	44.44 ± 0.07	-66.46	-389.03	13.168	14.797	11.929	9.388	-
00 26 56.33	-54 28 52.80	4923179694098110848	00265632-5428530	43.59 ± 0.14	349.51	-192.61	16.840	19.855	15.275	11.344	-
00 27 23.45	-54 01 46.05	4923251780829182080	00272343-5401461	41.11 ± 0.09	401.51	37.92	16.472	19.357	14.951	11.338	-
00 28 39.46	-06 39 49.18	2430731144829585280	00283948-0639481	74.77 ± 0.10	-327.52	-800.49	10.895	12.432	9.716	7.189	-
00 31 04.25	-72 01 05.90	4689958778035794048	00310412-7201061	50.68 ± 0.04	417.07	141.11	12.317	13.929	11.092	8.445	-
00 31 19.27	-38 40 36.08	4997505546262260096	00311925-3840356	41.31 ± 0.69	558.09	-31.92	19.070	21.182	17.397	12.924	-
00 31 35.41	-05 52 13.08	2526862202360516224	00313539-0552115	70.97 ± 0.05	351.21	-1055.18	11.558	13.039	10.384	7.945	-
00 31 36.96	-36 06 50.41	5004776376139340672	00313696-3606504	45.65 ± 0.06	-53.45	-14.01	10.849	12.101	9.774	7.442	-
00 32 05.08	+02 19 01.84	2547532539925750784	00320509+0219017	41.05 ± 0.45	406.69	-326.81	19.182	21.321	17.553	12.802	-
00 32 29.22	-79 21 17.18	4634641351610758400	00322917-7921172	43.35 ± 0.06	86.08	-239.49	15.121	17.439	13.721	10.682	-

Table 2: List of M dwarf systems within 25 pc drawn from *Gaia* DR2, as described in §2.3.

These systems have not been vetted to distinguish single stars from multiples, but in cases

where a system was resolved in *Gaia* but not 2MASS, a “J” flag is listed in column 12.

00 32 53.12	−04 34 07.31	2528227035593363840	00325313−0434068	52.45 ± 0.14	84.43	−129.09	12.534	14.263	11.213	8.350	−
00 33 13.51	−47 33 16.52	4975847194422433280	00331349−4733165	68.47 ± 0.06	277.06	142.24	13.876	16.047	12.513	9.538	−
00 33 21.77	−24 25 19.82	2348070616567676288	00332179−2425187	42.18 ± 0.06	−180.06	−716.76	14.417	16.257	13.133	10.512	−
00 33 23.87	−15 21 30.87	2373841073178592512	00332386−1521309	43.63 ± 0.93	302.15	23.07	20.355	21.046	18.667	13.410	−
00 35 44.12	−05 41 10.57	2526788363283721984	00354412−0541102	55.85 ± 0.09	−9.26	−266.69	14.152	16.323	12.784	9.711	−
00 35 55.52	+10 28 35.51	2751296646125543040	00355557+1028352	69.47 ± 0.07	1085.01	−384.93	13.584	15.648	12.239	9.367	−
00 36 24.63	−34 07 03.02	5005435876957437696	00362466−3407025	44.50 ± 0.04	−429.30	−311.19	13.121	14.535	11.960	9.603	−
00 36 30.17	−00 54 40.73	2542537011925737600	00363014−0054403	40.31 ± 0.09	400.93	−199.28	14.084	15.869	12.805	10.136	−
00 37 24.96	−13 43 05.65	2374484527999034112	00372495−1343057	40.13 ± 0.09	52.66	−153.04	12.897	14.250	11.737	9.220	−
00 37 36.30	−15 11 52.91	2374036786248265856	00373627−1511526	40.32 ± 0.06	−193.28	46.94	11.534	12.724	10.475	8.234	−
00 38 03.86	+16 56 02.82	2782423820307949952	00380386+1656028	47.65 ± 0.04	−104.69	−96.24	12.087	13.490	10.933	8.523	−
00 39 58.82	−44 15 11.58	4980466929964496128	00395880−4415117	42.33 ± 0.05	482.47	−220.76	10.579	11.672	9.570	7.394	−
00 40 26.42	−00 08 40.90	2543062097446318080	00402642−0008408	40.10 ± 0.08	−171.87	−54.93	11.527	12.873	10.428	8.019	−
00 41 30.47	−33 37 32.03	5006921282807193856	00413051−3337317	50.95 ± 0.05	−347.52	−251.05	9.835	10.783	8.906	6.884	−
00 42 16.94	−36 43 05.41	5001098681543159040	00421695−3643053	45.36 ± 0.07	−155.19	45.44	11.553	12.956	10.410	7.970	−
00 43 26.00	−41 17 34.03	4999067471248893952	00432603−4117337	97.73 ± 0.08	−488.56	−582.33	11.561	13.272	10.323	7.710	−
00 44 19.33	+12 37 02.69	2775987485397299072	00441933+1237027	50.58 ± 0.10	283.98	−183.80	11.612	13.075	10.461	8.083	−
00 44 38.17	−78 45 09.19	4634695708716644864	00443799−7845092	48.14 ± 0.10	404.78	205.51	15.397	17.873	13.791	10.367	J
00 44 59.33	−15 16 17.54	2371032916186181760	00445930−1516166	66.70 ± 0.07	317.58	−596.62	12.671	14.435	11.399	8.821	−
00 45 21.42	+16 34 44.74	2781513733917711616	00452143+1634446	65.02 ± 0.23	358.92	−48.07	18.168	20.992	16.540	11.366	−
00 45 55.86	−36 04 56.61	5001224335106301824	00455585−3604565	41.06 ± 0.12	−61.51	−93.12	15.365	17.635	13.990	11.057	−
00 46 53.29	+16 03 02.68	2781242085825625088	00465328+1603028	49.80 ± 0.06	−117.66	−52.45	10.892	12.128	9.823	7.576	−
00 47 07.96	−23 30 28.16	2348794198298597376	00470794−2330279	51.01 ± 0.15	167.95	−152.48	12.907	14.615	11.648	9.071	−
00 48 13.33	−05 08 07.70	2525688198820543360	00481333−0508074	40.20 ± 0.06	182.16	−120.16	11.142	12.300	10.134	7.932	−
00 49 29.06	−61 02 32.76	4902689745157488128	00492903−6102326	51.26 ± 0.04	1122.68	−78.13	11.163	12.409	10.085	7.837	−
00 50 33.25	+24 49 00.18	2805045756653326080	00503319+2449009	66.81 ± 0.12	203.42	−31.92	11.217	12.446	9.676	7.119	−
00 50 51.99	−46 04 22.82	4982134992183239424	00505198−4604228	47.13 ± 0.05	521.19	48.91	13.474	15.176	12.227	9.595	−
00 51 22.30	+18 44 11.37	2788907296779605376	00512228+1844120	44.80 ± 0.14	51.50	−276.30	15.331	17.686	13.904	10.787	−
00 52 15.33	−62 01 54.37	4902366110781708288	00521529−6201545	42.37 ± 0.09	1084.91	131.54	15.874	18.694	14.413	11.370	−
00 52 54.70	−27 05 59.56	2342686956666281728	00525468−2705597	40.18 ± 0.23	50.52	73.09	18.194	21.374	16.573	12.540	−
00 53 12.96	+19 03 26.92	2789002576334151808	00531297+1903270	44.76 ± 0.09	−110.31	−118.21	11.368	12.674	10.265	7.912	−

Table 2: List of M dwarf systems within 25 pc drawn from *Gaia* DR2, as described in §2.3.

These systems have not been vetted to distinguish single stars from multiples, but in cases

where a system was resolved in *Gaia* but not 2MASS, a “J” flag is listed in column 12.

00 53 18.98	−36 31 10.19	5001668709601989248	00531899−3631102	41.46 ± 0.92	67.15	−108.27	19.653	21.855	17.854	12.937	—
00 56 01.51	−48 26 47.38	4932698441137787264	00560151−4826474	40.03 ± 0.04	232.86	−50.94	12.840	14.417	11.627	9.063	—
00 56 38.37	+17 27 34.95	2787758616366123136	00563841+1727347	54.71 ± 0.08	683.29	−291.82	12.348	14.011	11.111	8.374	—
00 57 12.48	−64 15 23.94	4708990018643008896	00571247−6415240	56.96 ± 0.04	350.87	180.35	11.195	12.657	10.033	7.596	—
00 57 44.55	+05 51 20.62	2553195883802687104	00574455+0551205	56.19 ± 0.07	−55.75	1.25	9.559	10.499	8.633	6.640	—
00 58 27.94	−27 51 25.37	5032683355641241472	00582789−2751251	83.52 ± 0.46	1295.43	−301.20	10.565	12.053	9.399	6.892	—
01 00 56.37	−04 26 56.56	2525276565243086080	01005643−0426561	80.92 ± 0.08	1248.82	438.94	11.976	13.578	10.757	8.224	—
01 02 51.05	−37 37 43.77	4989399774745144448	01025100−3737438	87.87 ± 0.12	1470.13	251.19	15.368	18.759	13.801	10.069	—
01 03 14.15	+20 05 52.28	2788769028896753664	01031408+2005523	62.63 ± 0.04	672.25	50.85	10.657	11.906	9.570	6.832	—
01 03 21.23	−13 47 58.49	2372192767810059008	01032122−1347585	63.05 ± 0.10	73.00	33.43	10.621	11.978	9.501	7.076	—
01 04 06.96	−65 22 27.19	4705628051386514304	01040695−6522272	80.19 ± 0.04	−310.22	−173.52	12.465	14.237	11.201	8.532	—
01 04 28.90	−38 27 48.73	4989114210959175808	01042892−3827485	44.00 ± 0.05	−6.99	−193.16	11.747	13.177	10.594	8.135	—
01 04 53.80	−18 07 28.63	2358022227591374336	01045368−1807292	102.32 ± 0.08	1292.25	488.25	12.713	14.799	11.370	8.453	—
01 06 36.97	+19 13 33.16	2785466581298775680	01063697+1913336	40.39 ± 0.08	−41.46	−222.70	12.117	13.547	10.951	8.497	—
01 06 41.51	+15 16 22.09	2783324526489429504	01064151+1516229	44.96 ± 0.05	−108.21	−251.27	10.504	11.700	9.451	7.159	—
01 07 38.53	+22 57 20.72	2791782794564103680	01073851+2257218	48.85 ± 0.11	97.31	−495.20	12.626	14.307	11.372	8.673	—
01 08 12.30	+00 27 56.54	2537831170877143552	01081230+0027563	51.85 ± 0.10	−250.88	−353.40	13.303	15.143	12.012	9.166	—
01 08 18.29	−28 48 20.57	5032989500911228928	01081826−2848207	77.90 ± 0.06	732.28	−122.28	12.023	13.665	10.794	8.228	—
01 08 46.43	−37 10 21.44	4989657094825384064	01084644−3710212	43.94 ± 0.06	−558.87	−432.31	14.347	16.301	13.031	10.248	—
01 09 01.52	−51 00 49.40	4928644747924606848	01090150−5100494	62.85 ± 0.11	219.19	77.70	16.672	19.889	15.078	11.092	—
01 09 12.50	−24 41 20.92	5041018993810217984	01091250−2441209	49.07 ± 0.08	300.21	24.63	11.117	12.515	10.011	7.608	—
01 09 17.22	−72 12 42.24	4687511776265158400	01091706−7212429	51.90 ± 0.03	583.08	439.49	11.874	13.159	10.749	8.476	—
01 09 18.73	−24 30 23.68	5041034524411980288	01091872−2430236	55.92 ± 0.07	278.62	−183.80	13.029	14.809	11.759	9.066	—
01 09 51.20	−03 43 26.39	2531195858721613056	01095117−0343264	94.40 ± 0.32	371.96	8.73	16.351	19.559	14.770	10.428	—
01 10 17.51	−11 51 17.41	2468929239634877824	01101752−1151175	54.43 ± 0.11	217.49	−120.26	11.390	12.912	10.232	7.656	—
01 10 22.88	−67 26 41.95	4704272495284592512	01102281−6726425	121.45 ± 1.19	393.81	584.03	8.700	10.076	7.562	5.132	—
01 11 13.49	+03 06 40.89	2538865845678493312	01111347+0306408	42.36 ± 0.10	−44.23	28.28	13.848	15.685	12.555	9.799	—
01 11 36.67	+12 05 07.03	2583721522045243008	01113666+1205074	48.68 ± 0.05	−0.78	−292.96	11.364	12.555	10.308	8.087	—
01 11 47.52	−49 08 08.86	4929042942932181888	01114752−4908087	53.73 ± 0.09	−290.02	−451.69	15.335	17.975	13.883	10.607	—
01 11 55.59	+04 55 05.18	2564020472698316416	01115562+0455048	63.59 ± 0.15	398.95	−534.97	11.719	13.148	10.508	7.951	—
01 12 30.64	−16 59 56.36	2358524597030794112	01123052−1659570	269.36 ± 0.08	1205.18	637.76	10.429	12.356	9.150	6.420	—

Table 2: List of M dwarf systems within 25 pc drawn from *Gaia* DR2, as described in §2.3.

These systems have not been vetted to distinguish single stars from multiples, but in cases

where a system was resolved in *Gaia* but not 2MASS, a “J” flag is listed in column 12.

01 12 47.49	+01 54 39.47	2538451703458011264	01124752+0154395	48.09 ± 0.08	447.76	49.34	12.665	14.347	11.421	8.769	—
01 13 05.36	−70 50 37.67	4690736923033593728	01130536−7050378	57.29 ± 0.07	−74.33	7.64	13.834	15.823	12.506	9.665	—
01 13 16.43	−54 29 13.82	4914733005253271040	01131639−5429138	56.43 ± 0.05	382.36	123.66	12.653	14.416	11.383	8.684	—
01 13 24.03	−22 54 07.75	2351469138289894528	01132401−2254077	44.26 ± 0.06	151.17	27.12	12.899	14.561	11.658	9.038	—
01 14 08.60	−36 56 43.25	5012890771951532672	01140858−3656432	51.92 ± 0.04	676.60	360.33	12.500	14.042	11.295	8.808	—
01 14 34.20	−53 56 31.61	4915139584039259392	01143421−5356316	60.14 ± 0.03	103.37	310.99	10.201	11.335	9.179	6.966	—
01 16 29.20	+24 19 26.78	294014808041906688	01162893+2419282	46.59 ± 0.09	1678.84	−680.14	13.650	15.319	12.403	9.909	—
01 17 15.41	−35 42 57.21	5013816835621197440	01171538−3542569	57.48 ± 0.04	91.81	−172.81	10.310	11.537	9.247	6.938	—
01 17 21.88	−57 05 20.09	4910314961376339584	01172190−5705199	43.22 ± 0.09	−17.50	−34.39	15.224	17.566	13.809	10.662	—
01 17 53.25	+05 28 26.15	2564324345929277184	01175325+0528256	55.21 ± 0.05	87.77	−634.34	10.193	11.277	9.194	7.020	—
01 18 16.01	−12 53 59.38	2456594643316646784	01181599−1253581	42.10 ± 0.06	174.00	−675.71	10.828	12.045	9.767	7.550	—
01 21 34.59	−41 39 23.05	4984184825454337408	01213447−4139226	59.87 ± 0.03	1239.52	−455.78	9.462	10.385	8.540	6.581	—
01 21 45.39	−46 42 51.77	4933912198893332224	01214538−4642518	44.46 ± 0.05	−111.21	−79.83	10.552	11.692	9.526	7.294	—
01 22 44.04	−25 47 07.69	5039735554502890752	01224403−2547078	51.10 ± 0.05	54.09	9.36	11.882	13.315	10.723	8.282	—
01 22 44.97	+00 32 04.11	2534338503471881728	01224500+0032042	65.51 ± 0.31	−184.99	−527.98	12.555	14.090	11.027	8.299	—
01 23 18.03	−12 56 22.86	2457862762476854656	01231802−1256233	63.65 ± 0.05	−12.21	331.31	11.858	13.253	10.712	8.350	—
01 23 24.78	−30 45 34.04	5028912580514933248	01232479−3045339	43.60 ± 0.04	−107.25	−173.46	10.845	11.873	9.871	7.817	—
01 23 31.73	−23 45 41.63	5040636634346210432	01233175−2345413	42.24 ± 0.08	−201.12	−223.51	14.399	16.342	13.082	10.312	—
01 28 26.64	−55 45 34.24	4910850865919078016	01282664−5545343	54.02 ± 0.23	−234.95	108.24	18.596	—	—	12.336	—
01 28 37.04	−47 54 12.83	4930524225613187456	01283702−4754127	40.01 ± 0.05	115.83	−187.52	12.907	14.315	11.756	9.384	—
01 28 39.51	−14 58 04.70	2452167910719793664	01283952−1458042	78.25 ± 0.27	−1.98	−29.95	12.162	13.859	10.883	8.198	—
01 30 29.01	−35 12 00.45	5014775163084430976	01302899−3512002	44.26 ± 0.07	247.24	−293.02	14.387	16.248	13.094	10.433	—
01 30 29.88	−16 24 17.50	2451701339832959232	01302989−1624174	50.04 ± 0.05	−138.61	−131.96	12.677	14.131	11.505	9.047	—
01 32 26.20	−21 54 18.44	5042734468172061440	01322625−2154172	53.73 ± 0.04	−588.12	−888.15	10.290	11.406	9.276	7.100	—
01 33 58.00	−17 38 23.81	2450599697900838912	01335800−1738235	67.96 ± 0.08	43.16	−186.04	11.742	13.308	10.539	7.972	—
01 35 53.67	−61 27 11.08	4715859664213969024	01355366−6127111	40.86 ± 0.06	−262.31	−53.07	13.005	14.570	11.791	9.244	—
01 36 08.75	−26 52 16.25	5036026145867484672	01360872−2652161	40.59 ± 0.04	231.59	−37.03	12.032	13.495	10.859	8.411	—
01 36 55.18	−06 47 38.00	2478001486169801216	01365516−0647379	41.72 ± 0.11	173.47	−100.14	12.730	14.382	11.490	8.862	—
01 37 23.49	−41 48 56.27	4959814287663518080	01372347−4148563	43.17 ± 0.06	183.00	131.90	13.779	15.569	12.502	9.780	—
01 37 34.34	+06 56 49.90	2565529071371410048	01373434+0656497	40.13 ± 0.05	243.71	−8.80	11.913	13.221	10.803	8.496	—
01 37 41.31	−64 27 00.55	4711216151731060608	01374129−6427004	44.63 ± 0.04	−19.65	218.85	12.715	14.270	11.476	8.854	—

Table 2: List of M dwarf systems within 25 pc drawn from *Gaia* DR2, as described in §2.3.

These systems have not been vetted to distinguish single stars from multiples, but in cases

where a system was resolved in *Gaia* but not 2MASS, a “J” flag is listed in column 12.

01 38 01.13	−60 29 56.02	4716158215980519552	01380110−6029559	42.34 ± 0.05	571.92	54.03	14.705	16.816	13.337	10.292	−
01 38 29.94	+00 39 05.72	2510475768254568832	01382998+0039059	48.22 ± 0.10	517.99	165.48	10.643	11.846	9.589	7.324	−
01 38 43.49	−45 14 31.52	4955395178633330304	01384349−4514314	59.69 ± 0.03	−150.95	−70.21	9.651	10.621	8.707	6.659	−
01 39 01.38	−17 57 02.40	5140693571158739840	01390120−1757026	369.93 ± 0.27	3385.83	532.04	10.487	12.848	9.103	5.343	J
01 39 21.73	−39 36 08.97	4960651016012601856	01392170−3936088	114.40 ± 0.07	143.42	−228.72	12.590	14.716	11.238	8.274	−
01 41 03.25	+18 04 50.18	94712996769289856	01410321+1804502	42.30 ± 0.29	409.55	−55.16	18.725	21.280	17.083	12.492	−
01 43 20.18	+04 19 17.96	2560771312759450496	01432015+0419172	88.34 ± 0.05	−422.19	−765.21	9.898	11.176	8.811	6.516	−
01 43 45.14	−06 02 40.20	2479453696216295296	01434512−0602400	46.85 ± 0.07	52.26	−27.07	11.668	13.234	10.470	7.912	−
01 43 53.36	+00 14 32.69	2509463083685544320	01435333+0014323	46.84 ± 0.53	14.90	−161.22	14.969	17.602	13.521	10.258	−
01 43 58.64	−06 54 49.48	2467242352575094784	01435863−0654497	66.22 ± 0.07	65.92	47.98	11.457	12.836	10.324	7.966	−
01 44 58.45	+16 20 39.24	91289568531757184	01445851+1620396	61.55 ± 0.06	−738.62	−420.93	12.654	14.366	11.401	8.709	−
01 45 16.81	+16 36 58.89	91490916598591616	01451680+1636588	49.32 ± 0.10	−69.11	30.63	14.518	16.617	13.166	10.239	−
01 46 29.35	−53 39 32.58	4912898156569562624	01462935−5339325	57.29 ± 0.09	162.21	−104.41	12.574	14.401	11.289	8.609	−
01 47 07.68	−14 24 44.09	2453195851012123904	01470769−1424442	57.43 ± 0.07	−85.37	145.97	11.995	13.461	10.820	8.386	−
01 47 42.51	−48 36 05.33	4941699593078093952	01474254−4836055	59.26 ± 0.59	236.91	−311.09	11.372	12.695	9.957	7.449	−
01 48 03.97	+21 12 24.26	97993497084921984	01480397+2112243	53.75 ± 0.07	346.64	−218.45	11.104	12.417	10.008	7.644	−
01 48 25.96	−70 58 28.89	4687870530577399296	01482604−7058289	47.05 ± 0.03	434.76	80.36	11.377	12.636	10.287	7.971	−
01 48 26.18	−56 58 41.46	4719084256940884608	01482616−5658414	47.77 ± 0.03	261.14	−22.12	10.730	11.979	9.649	7.319	−
01 48 38.62	−30 24 39.57	5022239300847947136	01483864−3024396	41.10 ± 0.43	−72.17	44.89	16.603	19.936	15.042	11.227	−
01 49 47.90	−13 36 32.83	2459254503678694144	01494790−1336325	43.53 ± 0.09	61.90	−105.82	14.217	16.170	12.899	10.029	−
01 50 13.25	−37 41 52.03	4962688582857278208	01501324−3741519	44.00 ± 0.05	193.48	−89.29	13.092	14.732	11.861	9.237	−
01 51 04.10	−06 07 04.99	2467732906559754496	01510405−0607047	94.49 ± 0.10	545.70	−266.85	12.717	14.735	11.392	8.552	−
01 51 05.14	−30 57 56.69	5019191935652145792	01510512−3057572	50.00 ± 0.07	100.39	300.95	14.059	15.921	12.765	10.141	−
01 51 24.17	+21 23 39.46	97334889619799168	01512417+2123399	59.09 ± 0.05	−3.40	−347.59	12.512	14.183	11.274	8.644	−
01 51 48.69	−10 48 12.49	2460983348274381696	01514865−1048120	58.16 ± 0.05	568.70	−539.60	10.857	12.064	9.793	7.631	−
01 52 51.59	−48 05 41.22	4941774600386872960	01525159−4805413	74.52 ± 0.06	−515.69	−218.28	12.294	14.080	11.020	8.243	−
01 53 30.75	+01 47 55.85	2511235633868627712	01533076+0147559	47.20 ± 0.08	420.28	45.06	14.206	16.290	12.854	9.879	−
01 53 37.02	−66 53 33.75	4697746374082330496	01533707−6653341	58.18 ± 0.21	403.32	157.10	10.596	11.966	9.470	6.990	−
01 53 50.56	−10 32 13.76	2460900300786503296	01535050−1032135	57.38 ± 0.13	617.53	−271.96	13.789	15.818	12.459	9.649	−
01 54 07.96	−15 36 22.29	5142787797211936640	01540795−1536218	65.59 ± 0.09	88.47	−296.97	12.892	14.676	11.624	8.899	−
01 55 03.55	+09 50 00.42	2570824594248255104	01550354+0950003	44.71 ± 0.67	327.44	−89.45	20.014	21.045	18.354	13.139	−

Table 2: List of M dwarf systems within 25 pc drawn from *Gaia* DR2, as described in §2.3.

These systems have not been vetted to distinguish single stars from multiples, but in cases

where a system was resolved in *Gaia* but not 2MASS, a “J” flag is listed in column 12.

01 55 11.06	−32 05 24.98	5018745774450205952	01551106−3205250	41.18 ± 0.04	−65.18	42.39	10.780	11.851	9.784	7.631	—
01 55 13.20	−53 06 30.91	4912282881031353216	01551318−5306309	45.45 ± 0.05	286.14	273.53	13.567	15.284	12.314	9.729	—
01 58 15.72	+18 07 12.90	91196316201965184	01581572+1807128	50.84 ± 0.18	−88.20	86.78	15.660	18.338	14.212	11.069	—
01 59 12.38	+03 31 09.26	2517883830925784704	01591239+0331092	41.77 ± 0.07	263.11	24.09	10.455	11.490	9.473	7.070	—
02 00 12.96	+13 03 07.02	76868614540049408	02001278+1303112	223.63 ± 0.11	1096.56	−1772.86	10.671	12.583	9.409	6.648	—
02 00 38.29	−55 58 04.62	4719430083410927232	02003830−5558047	121.74 ± 0.06	113.24	−69.69	10.545	12.141	9.351	6.773	—
02 01 43.87	−10 17 29.05	2461728194387221504	02014384−1017295	53.30 ± 0.08	274.56	243.81	13.055	14.746	11.806	9.189	—
02 02 16.24	+10 20 13.95	2571094283835172736	02021620+1020136	108.53 ± 0.12	−673.11	−281.62	13.458	15.940	12.049	8.928	—
02 02 28.29	+10 34 53.64	2571309959912985472	02022823+1034533	68.79 ± 1.20	−101.45	−58.95	12.330	13.102	10.108	7.548	J
02 02 52.08	+04 47 02.42	2518828169682982656	02025208+0447023	48.07 ± 0.05	−77.97	−129.39	11.826	13.360	10.631	8.078	—
02 03 20.74	−21 13 43.37	5136466567425127168	02032076−2113427	46.76 ± 0.06	−196.76	−429.10	10.156	11.436	9.071	6.771	—
02 03 25.89	+06 48 01.00	2519736851615952256	02032589+0648008	42.45 ± 0.07	94.06	−120.65	12.753	14.243	11.568	9.083	—
02 03 28.69	+21 34 16.74	94546596851142400	02032864+2134168	40.41 ± 0.13	353.10	−14.83	15.270	17.596	13.873	10.714	—
02 03 32.22	+06 48 59.02	2519736920335457280	02033222+0648588	42.25 ± 0.05	92.16	−122.04	13.294	14.895	12.068	9.517	—
02 04 27.50	−01 52 56.87	2506306454521815040	02042754−0152560	54.39 ± 0.07	−592.91	−569.93	12.500	14.074	11.285	8.804	—
02 05 04.88	−17 36 52.78	5138510181584617856	02050492−1736528	105.95 ± 0.11	1269.79	−166.93	9.160	10.454	8.053	5.662	—
02 05 48.55	−30 10 35.90	5020179503252128768	02054859−3010361	106.71 ± 0.06	−524.93	103.67	11.045	12.457	9.908	7.558	—
02 07 14.05	−37 21 50.31	4967628688601251200	02071403−3721502	44.04 ± 0.12	416.55	122.10	16.629	19.684	15.074	11.382	—
02 07 23.25	−66 34 11.50	4698037645878876800	02072345−6634113	81.24 ± 0.03	1739.00	368.00	10.572	11.761	9.522	7.364	—
02 09 36.13	−14 21 32.64	5148602083419126016	02093608−1421321	50.48 ± 0.05	516.20	−349.13	10.742	12.040	9.646	7.259	—
02 10 03.67	−08 52 59.55	2462263484751574144	02100364−0852598	43.28 ± 0.06	−325.37	−248.15	11.838	13.358	10.644	8.083	—
02 11 18.05	−63 13 40.93	4701057557644479232	02111797−6313413	67.45 ± 0.04	−669.70	−345.88	11.162	12.507	10.050	7.726	—
02 11 40.97	+18 33 37.97	80910659801926528	02114094+1833375	48.92 ± 0.08	196.07	271.55	11.387	12.784	10.242	7.866	—
02 12 17.20	−10 36 30.37	5151948893734911744	02121719−1036304	41.42 ± 0.15	−35.66	28.23	16.901	20.203	15.363	11.827	—
02 12 20.99	+03 34 32.23	2515037264041041536	02122090+0334310	95.16 ± 0.04	−1762.47	−1852.76	9.205	10.307	8.183	6.077	—
02 12 39.77	−33 52 06.24	4970123274326574080	02123974−3352062	42.16 ± 0.06	829.02	235.09	14.265	16.092	12.977	10.319	—
02 12 46.35	+10 32 54.82	72354810070468224	02124635+1032546	52.79 ± 0.16	−70.12	−131.90	15.186	17.813	13.734	10.523	—
02 12 51.01	−17 41 12.20	5143621433184275200	02125096−1741123	42.51 ± 0.04	493.61	203.00	10.368	11.355	9.416	7.342	—
02 12 54.62	+00 00 16.86	2507016253701863040	02125458+0000167	65.45 ± 0.07	555.65	29.00	12.113	13.822	10.862	8.168	—
02 13 08.11	−19 01 52.59	5143185923500965504	02130805−1901526	45.30 ± 0.07	800.99	−65.90	13.986	15.896	12.674	9.940	—
02 13 53.63	−32 02 28.47	4971496564348094336	02135359−3202282	78.19 ± 0.04	757.84	−531.98	9.398	10.574	8.345	6.093	—

Table 2: List of M dwarf systems within 25 pc drawn from *Gaia* DR2, as described in §2.3.

These systems have not been vetted to distinguish single stars from multiples, but in cases

where a system was resolved in *Gaia* but not 2MASS, a “J” flag is listed in column 12.

02 14 12.56	−03 57 43.58	2492866780297999232	02141251−0357434	80.05 ± 0.18	509.30	−156.27	14.171	16.678	12.745	9.485	—
02 14 18.60	−30 33 47.09	4971920872757192192	02141859−3033472	41.50 ± 0.07	239.74	95.42	11.553	12.949	10.414	7.958	—
02 14 59.81	+17 25 08.38	80530400577483904	02145978+1725089	45.42 ± 0.08	346.03	−471.02	13.047	14.745	11.798	9.100	—
02 15 08.04	−30 40 01.40	4971892010576979840	02150802−3040011	71.11 ± 0.15	768.60	−360.33	15.865	19.190	14.308	10.542	—
02 15 56.09	+10 15 17.47	72117556076986368	02155612+1015174	54.94 ± 0.13	617.39	24.49	13.953	15.994	12.619	9.660	—
02 16 21.43	−22 00 48.69	5123785831102567680	02162144−2200490	51.89 ± 0.10	−114.26	242.01	14.843	17.198	13.443	10.401	—
02 16 29.85	+13 35 12.80	74203982469858816	02162977+1335136	109.80 ± 0.19	503.86	−433.95	13.579	16.113	12.159	8.981	—
02 16 35.11	−30 58 07.49	4971869092631523200	02163510−3058073	74.42 ± 0.08	683.72	246.39	11.749	13.431	10.517	7.887	—
02 16 41.20	−30 59 18.23	4971681351020953088	02164119−3059181	74.55 ± 0.06	684.13	248.77	10.777	12.280	9.603	7.131	—
02 17 04.99	−30 06 21.68	5068036605844590976	02170499−3006219	42.69 ± 0.18	46.95	−32.50	13.782	15.633	12.483	9.717	—
02 17 28.44	−59 22 43.69	4714117865996976768	02172845−5922435	68.08 ± 0.06	−243.65	−462.54	13.832	15.964	12.468	9.542	—
02 18 17.93	−55 07 32.54	4742946236243914880	02181792−5507326	47.16 ± 0.04	445.06	176.43	12.333	13.856	11.141	8.638	—
02 18 29.10	−31 33 23.17	4971581089304028288	02182913−3133230	43.11 ± 0.57	−138.51	−124.80	19.773	21.053	18.142	13.154	—
02 18 35.96	+20 47 49.44	99279543440878208	02183595+2047501	49.91 ± 0.06	−25.55	−291.77	11.391	12.655	10.297	8.022	—
02 19 02.33	+23 52 54.97	102535064223209216	02190228+2352550	44.17 ± 0.06	296.72	−78.78	12.728	14.342	11.505	8.956	—
02 19 10.08	−36 46 41.18	4966414930843373184	02191003−3646413	65.80 ± 0.12	1391.97	546.09	10.529	11.863	9.416	7.031	—
02 20 22.37	−08 08 25.01	2486558126175258880	02202235−0808253	40.68 ± 0.09	−204.05	−210.50	14.074	15.930	12.775	10.033	—
02 20 46.25	+02 58 37.58	2514052131687080192	02204625+0258375	53.39 ± 0.10	152.15	−294.06	13.226	15.053	11.939	9.202	—
02 22 25.61	−34 33 18.25	4967212763968339712	02222560−3433184	51.44 ± 0.03	112.53	269.73	10.631	11.677	9.644	7.555	—
02 22 47.67	−27 32 35.11	5116817882319879936	02224767−2732349	58.80 ± 0.12	−194.18	−133.32	16.328	19.780	14.764	11.100	—
02 23 24.01	−23 18 24.68	5120416854460344192	02232402−2318242	46.05 ± 0.08	−226.98	−259.67	12.848	14.497	11.613	9.005	—
02 24 26.55	−47 10 23.87	4939950270078388224	02242654−4710240	45.96 ± 0.04	−28.64	249.87	11.747	13.213	10.579	8.179	—
02 24 30.70	−17 16 42.37	5143825976706932480	02243065−1716419	43.91 ± 0.11	434.97	−219.53	15.040	17.296	13.655	10.617	—
02 27 10.33	−16 24 47.65	5145416111038393216	02271036−1624479	48.79 ± 0.34	439.42	−304.24	18.402	20.860	16.809	12.143	—
02 27 27.56	+03 10 54.98	2515329665414503808	02272756+0310548	41.88 ± 0.14	−120.57	−16.99	12.948	14.574	11.714	9.143	—
02 27 30.36	−30 54 35.55	5067008970494311936	02273036−3054355	48.13 ± 0.07	448.98	−70.91	10.070	11.148	9.071	6.932	—
02 27 30.53	−19 07 40.76	5131300889999108608	02273055−1907404	64.87 ± 0.96	−356.64	−176.67	12.034	13.555	10.834	8.365	—
02 27 31.28	+19 35 25.70	86511572033828480	02273126+1935260	43.19 ± 0.11	181.55	−150.48	14.536	16.582	13.198	10.307	—
02 28 07.76	−36 28 20.40	4965689356248347648	02280771−3628204	53.14 ± 0.05	451.27	−16.29	12.721	14.386	11.482	8.866	—
02 28 09.88	+03 10 58.32	2515419825368053120	02280987+0310575	44.37 ± 0.15	38.38	−806.93	15.342	17.874	13.917	10.788	—
02 28 13.92	−62 48 04.50	4700568859085688576	02281391−6248045	40.17 ± 0.04	188.34	120.00	13.411	15.067	12.167	9.570	—

Table 2: List of M dwarf systems within 25 pc drawn from *Gaia* DR2, as described in §2.3.

These systems have not been vetted to distinguish single stars from multiples, but in cases

where a system was resolved in *Gaia* but not 2MASS, a “J” flag is listed in column 12.

02 28 17.11	+01 26 31.07	2501452449987251840	02281712+0126310	44.76 ± 0.05	281.27	−131.44	11.949	13.341	10.801	8.397	—
02 28 31.94	−20 02 26.16	5130073422706364544	02283188−2002265	50.86 ± 0.05	606.52	230.95	11.787	13.127	10.658	8.347	—
02 28 42.44	+16 39 32.99	82493612948013824	02284243+1639329	46.05 ± 0.41	400.32	−430.72	17.812	20.678	16.226	11.818	—
02 30 24.90	+16 48 25.21	82512476444934528	02302486+1648262	50.40 ± 0.14	210.19	−421.32	15.415	17.893	14.002	10.978	—
02 31 43.27	−54 32 24.84	4741518516098734592	02314328−5432248	43.39 ± 0.04	−15.59	−174.73	12.727	14.236	11.538	9.108	—
02 32 52.62	−08 33 17.86	5177244498761708416	02325262−0833179	40.20 ± 0.08	−62.52	230.47	13.957	15.655	12.706	10.094	—
02 33 27.66	+12 39 53.81	26367903742260736	02332761+1239538	40.61 ± 0.07	316.89	−20.82	12.235	13.623	11.090	8.694	—
02 33 30.52	+22 09 14.14	89186168428165632	02333051+2209144	44.23 ± 0.18	154.34	−275.31	16.739	19.942	15.194	11.739	—
02 33 37.18	+24 55 37.69	102162639019033600	02333717+2455392	100.28 ± 0.11	48.82	−676.17	11.540	13.270	10.293	7.627	—
02 33 47.48	+15 00 17.40	75339743621732608	02334741+1500173	45.27 ± 0.07	437.20	26.87	12.543	14.046	11.358	8.858	—
02 34 21.19	−53 05 36.75	4744710746248039040	02342120−5305366	50.09 ± 0.76	249.80	−326.14	11.205	12.817	9.986	7.311	—
02 35 53.31	+20 13 11.58	87921523897823872	02355328+2013119	71.16 ± 0.07	249.93	−140.40	9.706	10.921	8.639	6.328	—
02 36 15.27	+06 52 17.92	18565464288396416	02361535+0652191	138.46 ± 0.09	1801.84	1449.91	10.318	11.973	9.108	6.574	—
02 36 32.46	−59 28 05.55	4725889546721486976	02363244−5928057	99.33 ± 0.05	575.04	457.79	12.628	14.713	11.284	8.341	—
02 36 44.13	+22 40 26.20	89593331327905536	02364412+2240265	68.52 ± 0.07	−37.77	−374.56	13.469	15.531	12.125	9.194	—
02 37 29.68	+00 21 27.43	2501776500974951168	02372971+0021273	43.51 ± 0.07	502.47	−169.67	13.625	15.386	12.357	9.689	—
02 37 52.79	−58 45 11.06	4726357491998516480	02375278−5845110	71.71 ± 0.04	79.99	208.32	11.164	12.681	10.002	7.513	—
02 39 17.33	+07 28 17.14	18986817760556416	02391735+0728169	49.93 ± 0.11	480.82	−137.42	12.879	14.532	11.643	9.033	—
02 39 50.71	−34 07 57.56	5062273240775788416	02395066−3407557	92.00 ± 0.04	535.70	−1665.12	10.679	12.017	9.564	7.305	—
02 41 15.14	−04 32 17.82	5185165891628969984	02411510−0432177	80.95 ± 0.09	352.90	−58.07	12.268	14.070	10.993	8.246	—
02 42 06.13	−41 24 35.29	4948775190921234816	02420612−4124352	40.31 ± 0.06	410.34	−52.73	14.839	16.932	13.487	10.550	—
02 43 53.22	−08 49 45.74	5173999736868992512	02435317−0849448	46.88 ± 0.06	615.58	−754.06	11.051	12.178	10.024	7.922	—
02 45 10.73	−43 44 32.03	4947513157730843136	02451070−4344319	90.16 ± 0.06	31.86	−387.96	11.038	12.629	9.847	7.270	—
02 45 18.52	−13 56 23.84	5158214559529933824	02451852−1356241	40.61 ± 0.06	12.16	−237.28	12.133	13.545	10.982	8.589	—
02 46 02.26	−70 24 06.26	4646616923022587136	02460224−7024062	78.48 ± 0.05	214.81	−88.70	13.146	15.156	11.816	9.019	—
02 46 14.92	−04 59 20.56	5184938400096586112	02461477−0459182	59.68 ± 0.09	1691.12	−1881.06	14.329	16.570	12.959	10.152	—
02 46 34.71	+16 25 10.21	33732162042339072	02463486+1625115	71.46 ± 0.12	−831.31	−569.45	14.579	17.229	13.142	10.185	—
02 48 35.48	+19 16 29.13	83872744127196416	02483544+1916294	40.08 ± 0.14	248.43	−124.70	16.126	18.791	14.655	11.258	—
02 48 41.00	−16 51 22.11	5156623295621846016	02484100−1651216	44.55 ± 0.15	−33.30	−289.53	16.866	19.757	15.302	11.422	—
02 50 02.45	−08 08 41.49	5174318457801944448	02500239−0808417	41.79 ± 0.12	567.26	100.48	15.644	18.197	14.204	10.856	—
02 50 09.73	−53 08 20.29	4741883764414703232	02500975−5308204	75.72 ± 0.02	−114.61	503.08	9.794	10.978	8.743	6.495	—

Table 2: List of M dwarf systems within 25 pc drawn from *Gaia* DR2, as described in §2.3.

These systems have not been vetted to distinguish single stars from multiples, but in cases

where a system was resolved in *Gaia* but not 2MASS, a “J” flag is listed in column 12.

02 51 50.65	+06 13 41.53	6452209110182016	02515065+0613414	40.59 ± 0.05	469.13	−122.94	12.103	13.482	10.953	8.539	—
02 52 00.32	−18 09 15.97	5129236831795673088	02520030−1809160	40.90 ± 0.04	0.93	−235.07	12.507	13.843	11.380	9.078	—
02 52 04.49	−67 41 15.57	4647534190597951232	02520450−6741155	40.31 ± 0.05	−55.70	149.27	13.588	15.279	12.334	9.722	—
02 52 22.17	−63 40 47.32	4721111481504251264	02522213−6340475	85.14 ± 0.03	979.92	634.48	10.318	11.666	9.207	6.829	—
02 52 26.30	+00 56 22.61	2499091523644792832	02522628+0056223	42.75 ± 0.36	−164.36	−111.66	17.594	20.858	15.998	11.963	—
02 53 00.89	+16 52 52.64	35227046884571776	02530084+1652532	261.01 ± 0.27	3429.53	−3806.16	12.275	15.348	10.784	7.585	—
02 53 07.13	−10 19 00.36	5173021308959257344	02530709−1018597	41.14 ± 0.15	354.08	−526.77	14.489	16.363	13.190	10.601	—
02 53 26.13	+17 24 32.39	35398295820372864	02532611+1724324	52.08 ± 0.70	9.83	−250.62	11.511	12.962	10.345	7.872	—
02 53 27.22	−23 36 57.88	5076670520902556544	02532721−2336579	41.61 ± 0.14	219.72	213.31	16.216	18.914	14.729	11.314	—
02 53 44.47	−79 59 13.26	4620448786799883136	02534448−7959133	57.10 ± 0.07	77.48	83.84	15.077	17.628	13.637	10.379	—
02 54 05.82	−19 34 52.22	5128049359237940224	02540582−1934523	42.85 ± 0.35	24.92	55.98	17.648	21.027	16.022	11.906	—
02 54 39.51	−22 15 58.52	5079067147013772288	02543950−2215584	69.95 ± 0.06	383.68	−73.71	11.754	13.225	10.586	8.167	—
02 56 03.90	−00 36 33.08	2497858563088120448	02560388−0036332	61.85 ± 0.09	256.93	69.90	13.795	15.861	12.456	9.567	—
02 57 31.05	+10 47 24.57	27360698317776640	02573103+1047245	60.99 ± 0.09	1754.37	−419.07	11.897	13.314	10.742	8.428	—
02 58 10.23	−12 53 06.00	5159273530961537280	02581021−1253066	86.82 ± 0.12	274.05	539.37	11.591	12.941	10.463	8.199	—
02 58 20.09	−00 59 33.44	5187933160532891136	02582009−0059330	41.85 ± 0.09	4.92	−251.59	10.222	11.226	9.261	7.171	—
03 00 20.81	−40 29 58.98	5044165727370002304	03002075−4029595	45.02 ± 0.08	−144.43	−67.14	16.069	18.508	14.245	10.479	J
03 01 51.39	−16 35 36.02	5153091836072107136	03015142−1635356	145.55 ± 0.08	−369.20	−268.51	10.047	11.501	8.910	6.496	—
03 02 06.36	−39 50 51.91	5044297634405581696	03020638−3950516	70.10 ± 0.06	−546.50	−644.23	14.016	16.146	12.665	9.885	—
03 02 38.05	−18 09 58.77	5152365363828101632	03023801−1809587	52.44 ± 0.08	404.00	164.97	10.757	12.038	9.666	7.337	—
03 03 00.70	−55 24 52.65	4728487967576289024	03030069−5524526	45.39 ± 0.06	158.47	168.23	13.582	15.360	12.308	9.603	—
03 03 40.74	−12 50 31.87	5159136122072204416	03034071−1250317	42.60 ± 0.08	229.82	−112.35	12.265	13.780	11.077	8.548	—
03 03 47.85	−12 51 19.20	5159135847194297600	03034782−1251190	42.65 ± 0.06	234.17	−112.84	12.128	13.639	10.940	8.373	—
03 04 04.49	−20 22 42.88	5103774994355594368	03040452−2022433	58.51 ± 0.08	487.55	−485.94	11.534	13.099	10.351	7.751	—
03 05 11.21	−34 05 24.02	5051354712350091904	03051118−3405239	40.52 ± 0.05	331.04	−51.02	12.585	14.217	11.351	8.774	—
03 05 58.91	−14 04 43.24	5155946477494819712	03055888−1404432	43.43 ± 1.48	5.41	17.45	19.850	20.064	18.216	15.435	—
03 06 11.60	−36 47 52.85	5047423236725995136	03061159−3647528	75.44 ± 0.10	−172.48	−669.32	16.015	19.503	14.451	10.631	—
03 07 28.18	−27 31 53.46	5071782435802712960	03072817−2731534	46.31 ± 0.05	90.82	−115.73	13.549	15.299	12.279	9.577	—
03 07 32.11	−06 36 47.46	5180173288500392320	03073209−0636471	41.65 ± 0.08	201.38	−392.25	13.701	15.600	12.392	9.552	—
03 07 53.39	−28 14 09.92	5059643002799575424	03075341−2814098	51.03 ± 0.04	−330.14	−110.61	11.982	13.329	10.852	8.515	—
03 08 25.41	−38 12 43.06	5044867731184769280	03082540−3812432	47.93 ± 0.06	497.31	100.99	14.616	16.760	13.254	10.327	—

Table 2: List of M dwarf systems within 25 pc drawn from *Gaia* DR2, as described in §2.3.

These systems have not been vetted to distinguish single stars from multiples, but in cases

where a system was resolved in *Gaia* but not 2MASS, a “J” flag is listed in column 12.

03 09 00.17	+10 01 25.65	14912165107085184	03090015+1001257	79.51 ± 0.08	286.50	−586.47	13.209	15.224	11.886	9.066	−
03 09 51.19	−19 06 47.71	5104338008732482176	03095115−1906476	49.47 ± 0.11	367.07	−59.05	13.028	14.694	11.786	9.205	−
03 10 00.50	+07 26 50.50	13533892921879936	03100053+0726506	42.10 ± 0.17	563.37	245.20	17.311	20.560	15.729	11.775	−
03 10 03.38	+02 34 27.11	769456276704128	03100340+0234269	53.12 ± 0.10	180.23	−321.02	14.626	16.774	13.271	10.526	−
03 10 15.47	+05 54 31.47	4267552520347776	03101547+0554311	55.23 ± 0.06	−121.88	−563.22	10.882	12.140	9.799	7.532	−
03 11 15.48	+01 06 30.88	3266937637860051840	03111547+0106307	59.20 ± 0.11	113.57	−16.80	14.199	16.523	12.811	9.755	−
03 11 35.22	−38 47 23.44	4852624170381960320	03113519−3847233	44.33 ± 0.03	831.98	−263.57	12.571	14.032	11.392	9.016	−
03 11 36.69	−04 16 36.94	5183110874332308480	03113668−0416364	65.49 ± 0.08	164.59	−382.67	12.132	13.675	10.935	8.459	−
03 11 42.70	−15 37 33.02	5154606546483045888	03114269−1537327	42.56 ± 0.04	103.10	−182.07	11.748	13.089	10.625	8.253	−
03 12 29.77	−38 05 20.17	5046323965615244160	03122972−3805204	69.48 ± 0.07	1263.15	732.27	10.509	11.740	9.438	7.185	−
03 13 22.92	+04 46 29.34	3179036008830848	03132299+0446293	116.15 ± 0.09	1741.86	86.02	12.123	14.153	10.795	7.833	−
03 14 03.44	+16 03 05.48	31235033696866688	03140344+1603056	73.43 ± 0.28	−242.45	−55.11	17.232	20.461	15.633	11.238	−
03 14 18.16	−23 09 29.75	5075243629687574656	03141813−2309297	62.82 ± 0.07	331.09	170.74	11.312	12.827	10.141	7.625	−
03 14 36.75	−09 40 02.59	5166527284047995008	03143676−0940024	45.12 ± 0.05	−245.19	−199.23	10.793	11.863	9.793	7.681	−
03 16 47.81	−21 25 26.07	5099657838705246464	03164779−2125260	57.19 ± 0.05	257.07	137.33	10.071	11.294	9.014	6.691	−
03 17 18.05	−19 40 17.80	5103275609917675904	03171800−1940175	41.38 ± 0.07	515.86	−219.69	14.075	15.920	12.782	10.169	−
03 18 03.98	−30 24 11.77	5058175086056319616	03180400−3024113	45.36 ± 0.02	−175.41	−325.14	10.220	11.266	9.239	7.115	−
03 18 42.53	−50 53 06.89	4737059519708024960	03184254−5053070	49.51 ± 0.05	−35.70	179.20	13.497	15.267	12.228	9.545	−
03 18 45.48	−40 51 34.17	4851425908866023808	03184548−4051343	58.65 ± 0.03	171.94	300.20	10.957	12.332	9.831	7.392	−
03 18 58.22	−36 23 34.89	5046897017332803584	03185824−3623346	45.87 ± 0.17	−139.76	−110.13	10.836	12.154	9.732	7.395	−
03 20 17.68	−55 36 19.75	4733538780397070848	03201767−5536197	44.24 ± 0.05	178.49	115.20	13.834	15.613	12.564	9.887	−
03 20 31.45	−07 41 05.97	5168398373665537536	03203147−0741060	44.71 ± 0.05	−146.74	99.92	11.958	13.252	10.847	8.552	−
03 20 51.78	−63 51 52.42	4672462936698379520	03205178−6351524	53.80 ± 0.04	−7.97	−292.31	12.100	13.717	10.876	8.195	−
03 20 58.87	−55 20 15.72	4733921479163010688	03205885−5520157	42.14 ± 0.08	298.22	264.41	15.911	18.585	14.462	11.084	−
03 20 59.71	+18 54 22.77	56252256123908096	03205965+1854233	68.28 ± 0.15	352.96	−257.16	16.127	19.206	14.570	10.639	−
03 21 46.92	−06 40 24.22	5169649072437050496	03214689−0640242	58.04 ± 0.05	323.56	−47.46	10.352	11.585	9.287	6.983	−
03 22 04.10	+02 56 34.74	3269132022551595264	03220410+0256346	61.14 ± 0.08	340.17	−750.29	13.336	15.089	12.069	9.508	−
03 23 22.42	+11 41 13.36	16302463200535040	03232241+1141134	58.45 ± 0.09	−251.04	−147.95	11.099	12.491	9.968	7.562	−
03 24 06.48	+23 47 06.13	62948174562104448	03240643+2347073	48.30 ± 0.05	215.05	−120.24	9.948	11.001	8.935	6.267	J
03 24 12.86	+23 46 19.06	62947354224986240	03241281+2346193	48.45 ± 0.07	205.52	−110.35	10.861	12.132	9.776	7.455	−
03 25 39.69	−42 59 12.05	4847829165813317504	03253966−4259118	45.02 ± 0.09	320.85	−130.70	10.501	11.509	9.534	7.483	−

Table 2: List of M dwarf systems within 25 pc drawn from *Gaia* DR2, as described in §2.3.

These systems have not been vetted to distinguish single stars from multiples, but in cases

where a system was resolved in *Gaia* but not 2MASS, a “J” flag is listed in column 12.

03 26	44.96	+19 14	40.26	57739208163471744	03264495+1914402	55.20 ± 0.10	10.25	−160.37	13.331	15.187	12.031	9.252	—
03 28	08.35	−70 01	40.68	4643131608600380800	03280833−7001409	46.04 ± 0.02	87.34	286.91	12.006	13.309	10.894	8.585	—
03 28	34.64	+11 29	51.69	16386404041502592	03283463+1129515	55.91 ± 0.16	541.80	256.27	16.862	20.378	15.287	11.330	—
03 28	39.14	−15 37	33.29	5111963126166680192	03283911−1537333	41.86 ± 0.09	199.85	40.73	13.055	14.638	11.845	9.271	—
03 29	21.53	−38 44	02.78	4853410870951405440	03292151−3844029	43.06 ± 0.18	−32.14	75.07	11.389	12.813	10.234	7.806	—
03 31	30.26	−30 42	38.82	5055805741577757824	03313025−3042383	79.92 ± 0.11	51.76	−403.27	15.653	18.978	14.085	10.264	—
03 31	47.14	+14 19	17.74	41840029505514496	03314712+1419194	49.45 ± 0.10	39.20	−674.38	11.282	12.553	10.195	7.907	—
03 32	17.12	−54 09	39.86	4732538568412966784	03321707−5409395	40.82 ± 0.08	−134.00	−175.19	14.897	17.037	13.538	10.568	—
03 32	55.86	−44 42	07.00	4846689899968623744	03325585−4442070	91.19 ± 0.03	−311.44	133.85	10.386	11.745	9.267	6.907	—
03 34	10.66	−21 30	34.39	5100356956302641536	03341065−2130343	46.10 ± 0.12	138.05	6.73	15.797	18.476	14.322	10.870	—
03 34	12.22	−49 53	32.01	4736655036868019072	03341218−4953322	112.64 ± 0.09	2360.51	482.16	15.859	19.317	14.258	10.392	—
03 34	39.63	−04 50	33.40	3248028717923282048	03343959−0450329	42.67 ± 0.51	410.52	−319.42	11.729	13.308	10.518	7.928	—
03 34	42.92	−48 24	04.82	4833654949103051008	03344289−4824047	48.45 ± 0.05	92.86	−331.53	12.213	13.798	11.000	8.402	—
03 35	38.61	−08 29	22.79	5165286828773802880	03353849−0829223	76.56 ± 0.13	1520.91	−321.64	13.870	16.154	12.487	9.456	—
03 35	53.23	+10 17	09.09	13000080026782464	03355322+1017090	48.68 ± 0.08	175.91	−84.22	13.613	15.347	12.352	9.750	—
03 35	56.94	−10 30	56.99	5163644433279729408	03355693−1030568	43.28 ± 0.08	115.77	−145.56	14.055	15.823	12.783	10.136	—
03 35	59.70	−44 30	45.73	4848140361962951552	03355969−4430453	272.24 ± 0.07	745.29	−373.67	10.989	13.303	9.622	6.610	—
03 38	10.03	−68 56	46.15	4667304715334508672	03380997−6856460	46.00 ± 0.04	292.06	479.21	11.525	12.710	10.094	7.372	—
03 38	15.70	−11 29	13.50	5115463180914712448	03381558−1129102	61.87 ± 0.05	1458.09	−2696.80	12.078	13.276	11.010	8.831	—
03 38	55.91	−52 34	10.61	4733113441195646592	03385590−5234107	81.40 ± 0.06	144.97	224.48	12.796	14.640	11.517	8.799	—
03 39	10.67	+08 00	04.31	3278030198356627584	03391067+0800039	46.90 ± 0.05	204.49	−449.86	12.104	13.489	10.956	8.582	—
03 39	29.71	+24 58	02.52	68553931516671488	03392972+2458028	62.54 ± 0.08	116.21	197.03	11.601	13.057	10.438	7.970	—
03 39	35.25	−35 25	43.63	4860376345833699840	03393521−3525440	155.76 ± 0.10	308.87	268.19	15.465	18.920	13.873	9.548	—
03 42	57.40	−64 07	56.45	4672963867324468608	03425738−6407563	40.02 ± 0.05	642.44	−843.29	14.430	16.288	13.138	10.579	—
03 43	22.06	−09 33	50.68	5164137461165628032	03432204−0933512	49.65 ± 0.25	433.40	285.59	13.080	14.930	11.780	8.854	—
03 43	45.25	+16 40	02.17	43335537119008896	03434521+1640027	58.01 ± 0.05	156.21	−310.29	9.917	11.038	8.900	6.688	—
03 44	20.82	+07 41	54.93	3278137572540701056	03442081+0741549	64.38 ± 0.10	−164.37	20.32	13.344	15.187	12.056	9.380	—
03 44	33.53	−62 37	19.00	4673565536406558976	03443351−6237190	40.41 ± 0.04	−102.68	29.60	13.150	14.661	11.958	9.468	—
03 46	45.41	−11 17	42.44	5115590415026701184	03464538−1117422	41.82 ± 0.13	577.95	123.00	11.622	12.932	10.509	8.188	—
03 47	20.89	+08 41	47.11	3278325004913943808	03472091+0841464	80.63 ± 0.10	469.33	−653.54	12.978	14.822	11.692	9.022	—
03 47	23.34	−01 58	19.95	3250328209054347264	03472333−0158195	59.52 ± 0.06	180.67	−274.18	10.496	11.862	9.375	6.933	—

Table 2: List of M dwarf systems within 25 pc drawn from *Gaia* DR2, as described in §2.3.

These systems have not been vetted to distinguish single stars from multiples, but in cases

where a system was resolved in *Gaia* but not 2MASS, a “J” flag is listed in column 12.

03 47 58.10	+02 47 16.15	3270590765246119168	03475809+0247161	56.96 ± 0.05	−394.68	−425.03	10.227	11.304	9.232	7.110	—
03 47 58.85	+23 29 04.28	64989250397297280	03475885+2329046	41.31 ± 0.10	−62.24	−131.30	14.685	16.701	13.351	10.492	—
03 50 44.29	−06 05 41.63	3243715604392800512	03504432−0605400	100.56 ± 0.11	−445.44	−1371.12	11.456	13.086	10.267	7.751	—
03 51 00.03	−00 52 44.92	3257243312560240000	03510004−0052452	68.03 ± 0.19	11.08	−470.18	15.342	18.312	13.827	10.232	—
03 52 10.86	+02 10 48.00	3270388416449237760	03521086+0210479	51.20 ± 0.25	306.39	341.27	17.749	20.800	16.119	11.955	—
03 52 41.75	+17 01 04.17	43574131143039104	03524169+1701056	103.38 ± 0.13	433.20	−645.62	12.189	14.095	10.888	8.053	—
03 53 21.21	−34 41 39.37	4859110361272954752	03532122−3441395	41.99 ± 0.07	−182.90	113.44	15.369	17.697	13.970	10.954	—
03 54 20.09	−14 37 38.57	5110641513191522304	03542008−1437388	52.46 ± 0.65	−64.95	85.77	15.398	18.242	13.839	10.334	—
03 54 25.62	−09 09 30.94	3194816237789820544	03542561−0909316	47.39 ± 0.04	−95.44	110.84	10.535	11.685	9.502	6.950	J
03 54 25.72	−09 09 33.60	3194816237788234496	03542561−0909316	47.40 ± 0.06	−96.46	98.93	11.880	13.321	10.687	6.950	J
03 54 46.22	+24 16 24.63	65829792677145344	03544620+2416246	75.42 ± 0.19	−293.77	−221.83	14.394	16.950	12.955	9.574	—
03 59 14.42	−78 37 28.86	4626056158662812032	03591439−7837288	45.39 ± 0.04	409.70	274.73	14.050	15.928	12.748	10.004	—
03 59 55.72	−16 35 08.31	5097351956664593152	03595571−1635083	49.93 ± 0.05	277.71	322.76	13.607	15.324	12.353	9.741	—
04 00 15.59	−20 01 24.19	5094232294281977216	04001557−2001242	40.14 ± 0.05	106.81	88.52	12.718	14.224	11.527	9.012	—
04 00 28.61	−25 52 52.25	5082514940600694272	04002858−2552526	53.59 ± 0.04	368.60	274.56	12.183	13.664	11.004	8.605	—
04 02 33.29	−02 42 16.11	3252841310381645696	04023328−0242161	44.96 ± 0.06	38.66	−40.31	11.810	13.261	10.648	8.191	—
04 06 06.87	−05 34 44.62	3197487123332369536	04060688−0534444	70.76 ± 0.06	23.38	−145.27	12.003	13.568	10.801	8.304	—
04 07 20.48	−24 29 13.64	5089072526731699072	04072048−2429129	54.11 ± 0.12	186.01	−642.62	11.633	12.861	10.120	7.441	J
04 08 29.06	−14 50 33.60	5098050661942146816	04082905−1450334	45.44 ± 0.33	205.76	−111.31	19.105	21.358	17.494	12.817	—
04 08 55.60	−31 28 53.87	4883809068925124224	04085558−3128537	55.37 ± 0.06	−1.81	−250.95	13.043	14.836	11.726	8.823	—
04 09 15.67	−53 22 25.29	4780294722094459904	04091567−5322254	66.07 ± 0.03	1046.14	584.13	10.677	12.097	9.535	7.135	—
04 09 32.34	−44 35 39.41	4838250838987898880	04093234−4435395	68.07 ± 0.04	−16.86	115.59	12.664	14.538	11.365	8.561	—
04 10 28.12	−53 36 08.14	4780100658292046592	04102815−5336078	140.56 ± 0.04	−825.18	−2415.61	11.914	13.827	10.620	7.900	—
04 10 48.04	−12 51 42.06	3188811632989991168	04104810−1251421	44.87 ± 0.08	−146.29	−395.93	14.907	17.109	13.485	9.920	—
04 12 46.43	−07 34 10.16	3195979005694112768	04124640−0734097	59.69 ± 0.34	407.80	−429.58	18.528	21.275	16.892	12.278	—
04 13 39.83	−27 04 29.30	4889645826401308416	04133980−2704291	42.29 ± 0.08	260.77	−41.94	16.079	18.812	14.603	11.195	—
04 14 17.31	−09 06 54.61	3192389821785729408	04141730−0906544	40.30 ± 0.08	99.82	−145.46	12.574	14.164	11.354	8.755	—
04 15 49.05	−46 02 23.64	4837138408098045312	04154908−4602238	51.08 ± 0.69	−94.34	−103.09	11.220	12.128	9.659	7.293	—
04 16 41.68	−12 33 22.98	3177244255271333376	04164173−1233233	46.89 ± 0.26	−80.75	232.04	10.397	11.525	9.367	6.731	—
04 16 42.76	+13 10 58.29	3310480909661217664	04164276+1310587	48.11 ± 0.14	−40.37	−197.92	15.641	18.315	14.174	10.839	—
04 17 18.53	+08 49 22.01	3299381442858615936	04171852+0849220	68.55 ± 0.08	133.97	−377.25	12.249	14.094	10.962	8.182	—

Table 2: List of M dwarf systems within 25 pc drawn from *Gaia* DR2, as described in §2.3.

These systems have not been vetted to distinguish single stars from multiples, but in cases

where a system was resolved in *Gaia* but not 2MASS, a “J” flag is listed in column 12.

04 17 34.58	−48 34 39.14	4782807621559619584	04173459−4834391	60.62 ± 0.25	240.85	596.63	13.798	16.100	12.414	9.341	—
04 17 37.49	−08 00 00.60	3192982561632526208	04173745−0800007	55.29 ± 0.16	454.64	48.96	16.413	19.690	14.858	11.090	—
04 18 04.71	−49 01 30.05	4782762094906353408	04180471−4901300	40.86 ± 0.03	31.61	489.53	12.023	13.452	10.861	8.473	—
04 18 40.15	−25 07 08.44	4895945684431356672	04184013−2507085	40.29 ± 0.05	157.88	130.19	13.531	15.384	12.236	9.476	—
04 19 08.11	+09 44 48.12	3300578673582192384	04190809+0944481	40.19 ± 0.06	44.03	131.14	12.765	14.226	11.592	9.156	—
04 20 12.55	−70 05 58.62	4654435618927743872	04201249−7005594	60.29 ± 0.10	243.59	625.92	14.839	17.335	13.401	10.251	—
04 21 05.56	−48 39 07.06	4788741548375134336	04210556−4839070	47.16 ± 0.02	30.02	−533.78	13.658	14.496	12.637	9.852	—
04 21 50.08	+21 19 42.83	145333721838128896	04215005+2119433	48.55 ± 0.07	123.42	−226.00	11.835	13.303	10.673	8.205	—
04 22 12.50	−57 26 01.00	4775316442680940800	04221249−5726011	60.39 ± 0.03	−250.30	−494.03	10.712	12.052	9.598	7.210	—
04 22 31.99	+10 31 18.80	3300729031796977024	04223199+1031188	48.03 ± 0.08	245.26	32.58	11.281	12.757	10.138	7.560	—
04 23 26.88	−07 23 46.91	3198812859478372480	04232688−0723468	51.06 ± 0.06	−144.41	−177.55	13.201	14.912	11.946	9.293	—
04 23 48.58	−04 14 03.23	3203124697405667712	04234858−0414035	67.86 ± 1.51	−347.19	70.18	20.055	21.294	18.036	12.929	—
04 24 09.40	+15 05 15.38	3311213115686175616	04240936+1505155	43.35 ± 0.09	179.07	−64.67	13.528	15.365	12.236	9.472	—
04 24 11.57	−23 56 36.26	4896480390678599168	04241156−2356365	64.97 ± 0.06	−30.90	56.66	10.977	12.369	9.869	7.465	—
04 24 56.20	−40 02 47.59	4865016349710062208	04245619−4002469	69.81 ± 0.05	−96.93	−635.25	12.568	14.282	11.315	8.665	—
04 25 30.47	−09 55 51.69	3191480078993217408	04253045−0955521	44.87 ± 0.09	87.58	360.50	14.940	17.168	13.563	10.572	—
04 25 30.70	−63 55 48.04	4675599087458814464	04253069−6355483	43.89 ± 0.07	−18.08	214.52	15.037	17.318	13.641	10.563	—
04 26 00.17	−46 21 11.35	4789443208593313280	04260016−4621113	43.74 ± 0.02	−164.05	−148.79	11.868	13.215	10.738	8.398	—
04 26 19.94	+03 36 36.17	3280675417175220224	04261992+0336359	62.34 ± 0.17	−121.90	−1011.98	15.572	18.617	14.065	10.693	—
04 26 32.64	−30 48 01.86	4884761177275202176	04263264−3048013	74.60 ± 0.05	−67.27	−468.66	12.468	14.316	11.177	8.411	—
04 27 07.25	+08 59 02.69	3299496547982121216	04270723+0859027	46.05 ± 0.25	−130.11	4.51	17.405	20.562	15.786	11.727	—
04 27 25.07	+20 22 44.55	144410205086676480	04272507+2022443	40.69 ± 0.07	−84.44	−3.64	11.177	12.320	10.162	7.982	—
04 28 05.70	−62 09 25.13	4677345043203760896	04280568−6209254	54.82 ± 0.04	179.63	348.09	11.769	13.297	10.572	8.006	—
04 28 16.66	+06 00 12.86	3285714066648802816	04281667+0600130	42.61 ± 0.11	179.93	−286.80	12.925	14.468	11.722	9.157	—
04 28 35.72	−25 10 09.30	4893118771316702720	04283571−2510088	49.50 ± 0.05	−81.43	−485.47	10.979	12.309	9.874	7.486	—
04 29 18.47	−31 23 56.76	4872659466967320576	04291842−3123568	59.38 ± 0.20	66.98	100.49	14.958	17.574	13.399	9.770	—
04 29 18.48	+14 13 59.44	3307883450880112256	04291847+1413594	41.50 ± 0.06	254.31	159.24	12.289	13.880	11.071	8.472	—
04 31 09.04	−13 30 52.63	3177407910705445888	04310905−1330523	53.44 ± 0.04	−164.72	−212.95	10.520	11.806	9.427	7.048	—
04 31 43.99	−21 50 44.06	4898609629306412160	04314395−2150433	54.35 ± 0.06	450.65	−682.11	14.264	16.280	12.935	10.280	—
04 32 29.88	−48 19 16.59	4788244328600836480	04322986−4819166	47.98 ± 0.05	256.75	264.51	12.855	14.373	11.663	9.200	—
04 32 42.63	−39 47 12.15	4864160624337973248	04324261−3947112	50.28 ± 0.02	239.41	−967.77	11.540	12.747	10.469	8.264	—

Table 2: List of M dwarf systems within 25 pc drawn from *Gaia* DR2, as described in §2.3.

These systems have not been vetted to distinguish single stars from multiples, but in cases

where a system was resolved in *Gaia* but not 2MASS, a “J” flag is listed in column 12.

04 32 57.77	−57 41 46.00	4775153440082275200	04325777−5741459	47.70 ± 0.11	72.47	28.57	13.009	14.792	11.732	9.072	—
04 33 33.96	+20 44 45.84	144312344255035392	04333393+2044461	73.54 ± 0.10	454.50	−321.95	12.913	14.730	11.629	8.960	—
04 33 39.72	−51 57 22.44	4781196115469953024	04333970−5157222	44.46 ± 0.03	82.94	−269.76	11.631	12.870	10.543	8.251	—
04 34 37.83	+19 06 05.03	3410478399832994688	04343785+1906051	58.92 ± 0.07	−194.55	−64.14	14.018	16.139	12.659	9.710	—
04 34 45.33	−00 26 46.50	3230306548988683392	04344532−0026463	52.04 ± 0.13	−82.41	−231.15	12.285	13.933	11.053	8.434	—
04 35 16.15	−16 06 57.25	3171631420210205056	04351612−1606574	94.49 ± 0.25	161.28	317.77	14.629	17.920	13.084	9.352	—
04 35 36.19	−25 27 34.59	4894315447987680640	04353618−2527347	59.61 ± 0.05	67.29	−195.92	11.130	12.662	9.951	7.406	—
04 36 40.85	−27 21 18.24	4891703042724926080	04364086−2721180	41.79 ± 0.04	−287.57	−196.65	11.190	12.516	10.094	7.727	—
04 36 56.23	−29 03 27.73	4879015915487168384	04365618−2903279	57.88 ± 0.04	514.56	175.92	12.454	13.972	11.262	8.802	—
04 37 41.87	−11 02 19.97	3184351876391975808	04374188−1102198	89.17 ± 0.03	−226.99	−196.11	9.402	10.598	8.345	6.091	—
04 38 37.16	−11 30 14.78	3178132420149741824	04383718−1130145	48.90 ± 0.07	−268.26	−241.44	11.458	12.928	10.317	7.824	—
04 39 31.62	+16 15 42.96	3310083401849536384	04393163+1615447	83.90 ± 0.07	−77.93	−795.38	13.572	15.798	12.197	9.194	—
04 39 34.06	−32 35 51.57	4871414343064541824	04393407−3235516	49.59 ± 0.08	−101.53	9.71	15.353	17.862	13.911	10.633	—
04 40 23.28	−05 30 08.13	3200303384927512960	04402325−0530082	102.46 ± 0.11	333.11	128.15	14.927	18.021	13.396	9.545	—
04 40 33.23	−07 31 18.02	3186280900821901824	04403324−0731177	43.04 ± 0.06	−149.09	−271.38	13.637	15.444	12.354	9.579	—
04 40 41.65	−12 43 32.37	3174976821778062720	04404160−1243321	41.71 ± 0.06	648.98	−251.52	13.601	15.298	12.350	9.766	—
04 40 42.49	+02 13 51.82	3231329541479389440	04404249+0213522	41.83 ± 0.18	166.38	57.94	10.331	11.474	9.299	7.032	—
04 41 35.01	−65 05 36.39	4663226523630904064	04413498−6505363	43.44 ± 0.04	96.03	29.48	11.930	13.302	10.791	8.384	—
04 42 07.57	+04 44 29.59	3281805779551809024	04420757+0444296	41.72 ± 0.05	−126.90	−304.26	12.555	13.903	11.418	9.032	—
04 42 22.45	−54 59 38.46	4777244844341374208	04422244−5459385	44.98 ± 0.04	124.84	14.65	11.209	12.533	10.097	7.743	—
04 42 55.78	+18 57 29.40	3409711211681795584	04425581+1857285	105.56 ± 0.07	656.38	−1116.50	9.000	10.233	7.923	5.607	—
04 42 55.86	+21 28 22.96	3411398347466374144	04425586+2128230	71.94 ± 0.07	36.93	117.67	10.717	12.169	9.567	7.101	—
04 43 05.82	−32 02 08.70	4877448669035035520	04430581−3202090	48.31 ± 0.74	−7.12	194.41	20.493	20.594	18.553	13.877	—
04 43 23.47	+21 06 31.84	3411184458094211072	04432345+2106321	45.97 ± 2.74	13.48	14.12	20.628	20.968	18.834	15.957	—
04 43 37.61	+00 02 05.11	3230008650057256960	04433761+0002051	47.41 ± 0.19	55.11	−107.48	17.333	20.738	15.677	11.216	—
04 44 10.97	−70 19 24.36	4654969496256092032	04441107−7019247	47.51 ± 0.03	−120.47	−65.85	10.252	11.367	9.225	6.593	—
04 44 38.25	−36 55 45.12	4866394831963983744	04443824−3655452	44.78 ± 0.24	42.98	141.68	18.440	20.612	16.781	12.460	—
04 44 50.19	−37 49 40.98	4818243369494800256	04445017−3749410	46.66 ± 0.05	224.31	−65.98	13.096	14.805	11.839	9.184	—
04 45 53.90	−30 48 20.64	4878035808244168832	04455387−3048204	61.97 ± 0.18	161.48	−419.68	18.256	21.323	16.645	11.975	—
04 46 49.68	−60 34 10.88	4677731349742482176	04464970−6034109	40.72 ± 0.03	53.50	113.18	11.079	12.286	10.015	7.724	—
04 46 51.78	−11 16 47.66	3181197137010596608	04465175−1116476	52.69 ± 0.07	−142.39	−57.56	11.390	12.725	10.070	7.294	—

Table 2: List of M dwarf systems within 25 pc drawn from *Gaia* DR2, as described in §2.3.

These systems have not been vetted to distinguish single stars from multiples, but in cases

where a system was resolved in *Gaia* but not 2MASS, a “J” flag is listed in column 12.

04 47 12.25	+20 38 10.80	3410346286637015040	04471225+2038109	42.99 ± 0.08	88.68	−98.34	12.637	14.540	11.322	8.507	—
04 47 22.68	−27 50 29.31	4880837088995421952	04472266−2750295	63.82 ± 0.02	46.32	152.15	9.251	10.254	8.293	6.190	—
04 48 00.98	−26 03 01.46	4881697181966448896	04480096−2603015	46.37 ± 0.05	169.71	82.06	14.066	16.019	12.746	9.936	—
04 48 30.07	−15 44 52.03	2981185389121883520	04483006−1544519	42.13 ± 0.05	167.50	−187.47	12.032	13.431	10.882	8.562	—
04 48 40.14	−35 39 22.09	4866928335623297152	04484013−3539219	49.84 ± 0.05	−58.37	−126.31	13.814	15.733	12.500	9.652	—
04 48 47.39	+10 03 02.66	3293154736711966976	04484738+1003025	57.64 ± 0.22	−69.45	−77.55	10.912	12.371	9.756	7.306	—
04 50 50.93	+22 07 21.53	3412806512623627008	04505083+2207224	78.97 ± 0.08	628.78	−425.48	13.356	15.475	12.001	8.977	—
04 51 00.95	−34 02 14.92	4873243032763432064	04510093−3402150	45.80 ± 0.17	96.85	138.23	18.454	21.216	16.807	12.294	—
04 51 37.34	−58 18 52.04	4774420478143249536	04513734−5818519	57.15 ± 0.09	−171.89	−692.57	15.725	18.688	14.222	10.705	—
04 52 04.02	−10 58 22.02	3181367767472670080	04520400−1058218	61.43 ± 0.34	−395.04	−204.00	14.150	16.507	12.743	9.606	—
04 52 04.11	+14 40 56.70	3404727747858610432	04520415+1440581	47.20 ± 0.22	48.07	−177.10	17.443	19.339	15.786	9.756	—
04 52 05.73	+06 28 35.59	3288082758293022848	04520573+0628356	80.90 ± 0.06	153.43	−306.11	10.706	12.250	9.523	6.942	—
04 52 24.41	−16 49 21.93	2980822034888930176	04522441−1649219	63.16 ± 0.05	122.14	−210.57	10.433	11.834	9.300	6.891	—
04 52 29.31	+09 30 29.02	3289877848463999104	04522930+0930291	41.47 ± 0.09	173.20	−354.94	14.463	16.342	13.168	10.449	—
04 53 31.20	−55 51 37.10	4776266794388393472	04533119−5551372	90.12 ± 0.03	126.12	76.86	9.903	11.311	8.769	6.338	—
04 53 49.98	−17 46 24.31	2979590513145784192	04534995−1746235	83.72 ± 0.03	408.57	−644.46	9.934	11.157	8.868	6.598	—
04 54 10.42	−30 36 36.96	4875068123283035904	04541043−3036370	45.76 ± 0.05	−19.36	118.10	13.770	15.587	12.485	9.732	—
04 55 19.01	−32 12 23.37	4873878176823736192	04551900−3212234	45.68 ± 0.06	14.91	84.22	14.068	16.110	12.728	9.814	—
04 55 30.29	+02 44 23.37	3232309683080514560	04553028+0244232	40.09 ± 0.09	645.28	−417.84	15.417	17.735	14.032	11.254	—
04 55 57.75	−61 09 46.51	4761524752938019200	04555759−6109459	41.67 ± 0.02	912.58	−608.34	11.288	12.297	10.313	8.312	—
04 57 29.89	−01 48 20.88	3225643760693828480	04572991−0148205	46.22 ± 0.06	−235.77	−306.73	13.788	15.537	12.523	9.883	—
04 57 58.62	−05 06 16.48	3212318332599958784	04575862−0506161	46.03 ± 0.05	−104.23	−206.48	13.194	14.901	11.939	9.286	—
04 59 24.40	−30 55 57.79	4876309231392838528	04592436−3055577	41.59 ± 0.04	364.69	50.88	13.406	15.198	12.127	9.345	—
04 59 32.27	−61 53 04.12	4665366619931917824	04593230−6153042	50.25 ± 0.03	−197.47	24.08	11.399	12.787	10.260	7.812	—
05 00 05.68	−66 39 34.75	4662098871410185984	05000568−6639345	45.57 ± 0.05	61.64	−204.28	13.098	14.713	11.876	9.274	—
05 00 08.67	−12 16 02.31	3180270454868010368	05000865−1216025	44.96 ± 0.06	322.12	−325.79	13.156	14.799	11.918	9.313	—
05 00 48.09	+04 42 14.39	3239389064789380992	05004808+0442143	44.12 ± 0.34	127.56	−14.77	18.716	21.490	17.088	12.513	—
05 01 15.52	+24 52 24.55	3419611630606267392	05011551+2452245	44.20 ± 0.05	229.72	−394.21	10.582	11.790	9.523	7.205	—
05 01 18.02	+22 37 00.92	3418324583527645440	05011802+2237015	69.85 ± 0.10	−62.48	−351.19	13.597	15.748	12.238	9.232	—
05 01 24.09	−00 10 45.58	3228124598226930816	05012406−0010452	47.08 ± 0.89	189.25	−145.31	20.430	21.300	18.828	12.963	—
05 01 50.57	+03 45 55.24	3238437574916370048	05015057+0345551	53.03 ± 0.04	129.98	−133.95	10.420	11.533	9.401	7.233	—

Table 2: List of M dwarf systems within 25 pc drawn from *Gaia* DR2, as described in §2.3.

These systems have not been vetted to distinguish single stars from multiples, but in cases

where a system was resolved in *Gaia* but not 2MASS, a “J” flag is listed in column 12.

05 01 57.43	-06 56 46.37	3187115498866675456	05015746-0656459	186.02 ± 0.06	-551.72	-533.94	10.647	12.439	9.397	6.736	-
05 01 58.80	+09 58 59.04	3291643148740384128	05015881+0958587	41.92 ± 0.08	31.02	-121.40	10.540	11.990	9.158	6.370	J
05 03 16.09	+21 23 56.22	3409167094776800384	05031607+2123563	48.46 ± 0.06	102.35	-135.53	9.957	11.195	8.881	6.569	-
05 03 20.08	-17 22 24.72	2976850598890038784	05032009-1722245	108.33 ± 0.05	-228.06	-444.62	10.552	12.003	9.400	6.936	-
05 03 25.85	-53 53 18.71	4770840914960066176	05032583-5353188	43.44 ± 0.04	466.81	120.57	13.306	15.047	12.035	9.289	-
05 04 14.76	+11 03 23.86	3292000966760477312	05041476+1103238	98.15 ± 0.08	-63.03	194.47	12.232	14.001	10.968	8.311	-
05 04 56.63	-34 39 48.22	4825113801043230720	05045663-3439483	45.59 ± 0.02	-66.14	41.25	12.083	13.449	10.945	8.607	-
05 05 11.78	-12 00 28.62	2989642519027010560	05051180-1200285	48.13 ± 0.04	-216.25	-145.32	11.721	13.109	10.580	8.245	-
05 05 14.43	-47 56 15.53	4785886941312921344	05051443-4756154	71.39 ± 0.04	-66.09	25.08	12.894	14.723	11.610	8.900	-
05 06 04.02	+04 20 14.34	3238938265024397568	05060402+0420142	43.97 ± 0.12	398.16	109.91	10.654	11.766	9.640	7.435	-
05 06 13.81	-08 07 07.44	3183748278864953856	05061381-0807071	52.34 ± 0.05	-119.96	-179.33	12.349	13.882	11.154	8.638	-
05 06 49.92	-21 35 09.13	2962658549474035584	05064991-2135091	50.31 ± 0.04	47.14	-15.57	9.555	10.749	8.503	6.117	-
05 07 49.30	+17 58 57.66	3407150556091924736	05074924+1758584	86.10 ± 0.31	32.01	-261.58	10.688	12.074	9.558	7.178	-
05 08 35.04	-18 10 19.39	2976507997939000064	05083500-1810178	108.72 ± 0.09	503.67	-1399.81	9.044	10.572	7.857	5.314	-
05 09 21.03	-08 38 55.73	3182910554085960320	05092099-0838556	44.46 ± 0.07	390.86	-79.25	12.965	14.647	11.719	9.062	-
05 09 43.84	-43 25 17.44	4812321124989687296	05094385-4325174	48.83 ± 0.04	-133.13	194.36	12.651	14.336	11.407	8.735	-
05 10 47.96	+24 10 12.07	3418863344225339520	05104796+2410125	47.59 ± 0.07	-27.26	-212.55	13.264	14.975	12.013	9.333	-
05 10 57.43	+18 37 34.48	3407572287520660992	05105747+1837359	47.09 ± 0.07	-237.04	-648.50	12.861	14.470	11.644	9.062	-
05 12 18.32	+18 18 02.29	3395539232265931520	05121831+1818020	40.42 ± 0.08	112.50	101.59	13.941	15.716	12.672	9.984	-
05 12 42.23	+19 39 56.36	3407785622839603968	05124223+1939566	82.26 ± 0.05	279.33	240.92	9.810	11.022	8.748	6.470	-
05 13 05.96	-76 53 21.94	4624829103685457024	05130604-7653221	45.13 ± 0.03	-223.48	132.74	11.885	13.250	10.749	8.358	-
05 15 08.04	-07 20 48.51	3207120460100680448	05150804-0720486	46.40 ± 0.09	265.71	-433.63	10.693	11.785	9.683	7.518	-
05 15 46.72	-31 17 45.32	4827532078086044416	05154667-3117456	42.31 ± 0.05	494.23	249.75	11.103	12.347	10.038	7.733	-
05 16 00.35	-72 14 12.78	4651329704762754176	05160040-7214135	44.89 ± 0.03	-46.79	825.77	10.751	12.024	9.665	7.362	-
05 16 59.72	-78 17 20.30	4623882630333283328	05165967-7817203	62.84 ± 0.04	44.65	-1125.10	10.770	12.158	9.640	7.199	-
05 17 21.42	-42 52 47.23	4800721723993736576	05172143-4252473	45.03 ± 0.04	40.26	183.49	10.913	12.179	9.830	7.446	-
05 17 22.91	-35 21 54.64	4822636399484228224	05172292-3521545	86.19 ± 0.33	-218.99	-167.89	10.340	11.957	9.136	6.558	-
05 17 37.70	-33 49 03.07	4825880783419986432	05173766-3349027	59.27 ± 0.10	446.45	-332.59	16.506	19.884	14.915	10.832	-
05 18 36.63	-28 42 06.63	2954555801611979648	05183663-2842070	54.82 ± 0.05	-37.77	432.68	14.244	16.344	12.897	10.014	-
05 19 49.41	-04 36 16.59	3210380713937584768	05194942-0436165	45.24 ± 0.06	-128.51	-30.38	12.527	14.062	11.328	8.849	-
05 20 03.49	-22 57 03.17	2961704070302754304	05200348-2257032	44.28 ± 0.03	-78.85	107.48	11.736	13.029	10.632	8.371	-

Table 2: List of M dwarf systems within 25 pc drawn from *Gaia* DR2, as described in §2.3.

These systems have not been vetted to distinguish single stars from multiples, but in cases

where a system was resolved in *Gaia* but not 2MASS, a “J” flag is listed in column 12.

05 21 47.92	+17 20 34.42	3394484074763973504	05214793+1720341	60.02 ± 0.07	−16.21	130.05	13.188	14.913	11.939	9.316	—
05 23 38.22	−14 03 02.01	2985035874544160384	05233822−1403022	78.36 ± 0.19	107.25	160.90	18.057	21.473	16.441	11.638	—
05 25 15.28	+21 02 39.58	3402351217901366528	05251524+2102394	47.49 ± 0.19	244.40	50.88	17.784	20.721	16.153	12.247	—
05 26 36.02	−42 20 17.52	4805866957374888448	05263603−4220178	50.30 ± 0.02	−185.14	−2.23	10.196	11.271	9.203	6.938	—
05 26 40.79	−48 51 47.45	4796804060982392064	05264079−4851473	40.15 ± 0.03	93.71	−256.44	11.772	13.132	10.639	8.242	—
05 27 30.57	−51 29 15.81	4772342676044749952	05273058−5129158	68.58 ± 0.05	−33.22	325.33	13.731	15.877	12.372	9.460	—
05 28 00.15	+09 38 38.15	3338097377577012480	05280015+0938382	97.98 ± 0.10	−191.30	−756.77	11.181	12.713	10.001	7.542	—
05 28 14.63	+02 58 09.80	3235885299189354496	05281462+0258098	47.09 ± 0.14	−340.76	−1117.31	15.197	17.546	13.773	10.901	—
05 28 48.21	+11 20 55.11	3339136927164194176	05284820+1120551	49.56 ± 0.08	−94.45	−61.25	13.290	15.033	12.024	9.331	—
05 29 27.02	+15 34 38.24	3390818582171734656	05292704+1534383	58.20 ± 0.06	−83.43	−128.08	9.816	10.854	8.847	6.782	—
05 29 52.02	−03 26 30.07	3210711671234654848	05295204−0326295	57.76 ± 0.08	−298.56	−473.53	10.940	12.314	9.826	7.437	—
05 30 37.22	+15 14 28.48	3390044040652614656	05303723+1514286	50.75 ± 0.05	−121.95	−136.27	11.670	13.043	10.543	8.167	—
05 30 57.20	−53 30 52.26	4768702571002262912	05305719−5330521	55.19 ± 0.03	−11.24	−251.89	10.306	11.457	9.280	7.053	—
05 31 04.33	−30 11 44.71	2905516483501493120	05310430−3011442	65.30 ± 0.04	347.75	−467.26	11.849	13.347	10.666	8.190	—
05 31 27.40	−03 40 38.02	3209938366665770752	05312734−0340356	175.43 ± 0.07	761.55	−2092.32	7.099	8.207	6.081	4.039	—
05 32 14.66	+09 49 14.93	3338162729799839104	05321467+0949150	77.18 ± 0.08	−180.11	−216.94	10.243	11.766	9.070	6.560	—
05 32 26.86	−07 14 19.18	3016516095038210304	05322686−0714189	45.45 ± 0.06	−12.94	−173.03	10.160	11.181	9.198	7.094	—
05 33 10.28	−39 08 55.42	4808788016172681984	05331027−3908557	41.54 ± 0.05	135.52	440.16	13.720	15.382	12.479	9.899	—
05 33 28.04	−42 57 20.55	4805600119646735616	05332802−4257205	96.63 ± 0.34	−17.58	39.51	11.064	12.820	9.816	7.116	—
05 33 44.80	+01 56 43.46	3223516063958808064	05334480+0156434	63.60 ± 0.09	−231.22	−154.30	10.376	11.702	9.266	6.855	—
05 34 07.17	+22 39 37.08	3404065223385705600	05340714+2239363	46.81 ± 0.06	142.63	324.69	13.326	14.835	12.146	9.685	—
05 34 15.14	+10 19 14.08	3339705378973587328	05341513+1019142	45.17 ± 0.08	−85.01	−378.21	11.286	12.632	10.170	7.768	—
05 34 52.12	+13 52 46.71	3341624061123288448	05345212+1352471	83.85 ± 0.07	−118.69	−396.69	10.611	12.100	9.447	6.936	—
05 34 58.45	−15 11 43.89	2972230554107163264	05345844−1511439	50.58 ± 0.16	−117.63	69.26	17.858	20.866	16.255	11.973	—
05 35 21.30	−09 31 06.52	3013672487388307456	05352131−0931067	52.18 ± 0.13	343.89	−230.67	15.801	18.739	14.294	10.832	—
05 36 00.08	−07 38 58.43	3015684005638599168	05360007−0738580	66.30 ± 0.06	110.19	466.61	11.475	13.099	10.262	7.567	—
05 36 38.46	+11 17 48.78	3339914973377653760	05363846+1117487	87.37 ± 0.09	−3.52	−60.95	11.189	12.800	9.990	7.406	—
05 37 23.32	−08 16 06.39	3015584160150844416	05372332−0816055	42.93 ± 0.11	5.60	−421.69	16.145	18.940	14.654	11.348	—
05 37 39.77	−61 54 43.68	4757687388639045504	05373975−6154442	58.50 ± 0.06	133.22	487.10	13.260	15.055	11.980	9.227	—
05 39 52.00	−00 59 01.47	3217523558083415040	05395200−0059019	78.53 ± 0.57	162.45	321.15	19.178	20.407	17.444	12.527	—
05 40 53.90	+08 54 18.25	3336130626153639424	05405390+0854183	63.83 ± 0.07	−169.05	−7.33	13.831	15.945	12.478	9.589	—

Table 2: List of M dwarf systems within 25 pc drawn from *Gaia* DR2, as described in §2.3.

These systems have not been vetted to distinguish single stars from multiples, but in cases

where a system was resolved in *Gaia* but not 2MASS, a “J” flag is listed in column 12.

05 42 09.27	+12 29 21.61	3340477717172813568	05420897+1229252	172.71 ± 0.08	1997.71	−1569.79	10.099	11.761	8.886	6.389	—
05 42 12.70	−05 27 55.56	3023121827755777280	05421271−0527567	77.02 ± 0.06	−157.34	956.67	13.500	15.604	12.153	9.371	—
05 42 54.88	−53 14 53.26	4768909313548256640	05425488−5314533	40.51 ± 0.05	−33.34	−145.27	14.412	16.422	13.079	10.144	—
05 43 26.66	−30 41 45.33	2903754309959700224	05432664−3041452	48.73 ± 0.05	151.14	−54.86	10.469	11.814	9.352	6.880	—
05 43 46.54	−41 08 08.46	4804690376853844096	05434654−4108079	45.54 ± 0.19	150.27	−579.86	12.707	14.369	11.468	8.870	—
05 44 27.15	−04 06 01.37	3023526379315580800	05442715−0406013	42.04 ± 0.06	−49.67	−63.98	13.267	14.900	12.032	9.443	—
05 44 57.04	−21 36 55.77	2964203466393004928	05445704−2136561	41.26 ± 0.27	−91.52	338.58	11.256	12.572	10.143	7.823	—
05 45 31.99	−11 58 03.42	3009191736986345472	05453198−1158034	46.27 ± 0.06	45.90	73.39	12.673	14.405	11.408	8.716	—
05 45 50.34	−27 09 49.65	2907884728469088384	05455033−2709498	55.97 ± 0.06	−74.98	201.65	13.001	14.677	11.754	9.133	—
05 47 09.12	−05 12 11.39	3022439786949104256	05470907−0512106	56.94 ± 0.08	531.99	−554.28	13.097	14.826	11.840	9.177	—
05 47 40.58	−36 19 42.83	2887328533953284096	05474051−3619425	68.98 ± 0.03	767.68	−123.04	9.833	10.988	8.797	6.615	—
05 47 50.21	−34 19 13.80	2888823075195849728	05475019−3419138	47.11 ± 0.04	186.93	58.90	10.976	12.150	9.937	7.709	—
05 48 24.07	+07 45 38.70	3334997304542444032	05482407+0745388	44.52 ± 0.08	72.70	−272.84	12.823	14.501	11.580	8.877	—
05 48 32.21	+21 19 18.07	3400111547084348928	05483220+2119180	44.00 ± 0.07	332.72	−191.45	12.686	14.221	11.494	8.992	—
05 52 29.15	−55 06 42.49	4767716893186840320	05522915−5506424	48.40 ± 0.02	−313.09	−595.05	11.725	12.977	10.638	8.379	—
05 52 34.64	−21 00 42.68	2965774153111101696	05523464−2100428	40.75 ± 0.05	−21.84	166.72	12.749	14.230	11.568	9.075	—
05 53 26.45	−71 33 49.79	4656782698309778432	05532643−7133502	87.56 ± 0.05	12.11	397.05	14.112	16.712	12.666	9.358	—
05 53 34.60	+15 20 07.41	3347284175186268160	05533463+1520075	40.57 ± 0.78	136.55	97.13	12.716	13.710	11.084	8.552	—
05 53 40.11	−42 41 43.64	4803556711646531840	05534011−4241432	48.00 ± 0.02	−5.06	−411.75	12.117	13.487	10.979	8.596	—
05 54 05.12	−02 48 21.64	3025404791851801728	05540513−0248213	44.77 ± 0.09	13.52	−251.75	14.061	16.038	12.724	9.806	—
05 54 10.00	+01 52 28.72	3315882290597093504	05540999+0152288	40.73 ± 0.05	82.56	−94.41	11.884	13.272	10.747	8.377	—
05 54 45.73	+10 55 57.02	3342799469117920896	05544574+1055570	40.52 ± 0.05	−140.22	−69.25	11.443	12.747	10.332	7.970	—
05 55 43.21	−26 51 23.41	2910909931633597312	05554318−2651233	71.23 ± 0.03	314.77	−9.60	9.780	11.083	8.682	6.288	—
05 56 00.52	+15 46 00.86	3348805143361118464	05560053+1546011	52.53 ± 0.09	−47.52	−140.82	14.764	16.942	13.407	10.507	—
05 56 18.45	+01 46 25.94	3315824192575362176	05561845+0146261	46.45 ± 0.05	209.42	−356.82	11.552	12.719	10.499	8.372	—
05 56 40.67	−10 18 37.81	2999254213453678720	05564066−1018378	62.69 ± 0.05	−27.99	127.62	11.956	13.527	10.749	8.220	—
05 56 47.84	+15 36 24.61	3348740650136554368	05564783+1536246	40.03 ± 0.06	66.38	−88.59	13.148	14.810	11.910	9.205	—
05 56 57.23	+11 44 33.16	3342958387205080064	05565722+1144333	70.16 ± 0.12	523.17	−342.56	13.827	16.045	12.453	9.496	—
05 57 18.66	+17 08 29.67	3349805247975323392	05571864+1708299	48.86 ± 0.06	242.95	−260.97	12.801	14.316	11.614	9.248	—
05 57 48.66	+00 48 02.49	3314939979068074624	05574866+0048025	47.50 ± 0.13	−179.45	−333.16	15.736	18.516	14.251	10.901	—
05 58 17.17	−04 38 01.50	3022685905755527296	05581716−0438012	41.50 ± 0.08	78.77	−213.21	14.386	16.334	13.071	10.312	—

Table 2: List of M dwarf systems within 25 pc drawn from *Gaia* DR2, as described in §2.3.

These systems have not been vetted to distinguish single stars from multiples, but in cases

where a system was resolved in *Gaia* but not 2MASS, a “J” flag is listed in column 12.

05 58 53.29	+21 21 01.57	3423241805685345920	05585333+2121010	60.71 ± 0.77	205.41	−442.25	13.398	15.471	12.028	9.066	—
06 00 03.50	+02 42 23.60	3316364602541746048	06000351+0242236	192.07 ± 0.07	309.49	−40.64	9.897	11.579	8.674	6.042	—
06 00 38.91	−07 55 41.26	3017863275957247872	06003890−0755409	43.15 ± 0.05	160.82	−92.15	12.527	13.981	11.360	8.950	—
06 00 47.23	−37 42 19.61	2884107098026680064	06004723−3742196	44.77 ± 0.04	−97.39	87.90	12.580	14.115	11.380	8.806	—
06 01 18.94	−60 47 09.27	5482312349304478976	06011889−6047092	49.28 ± 0.05	251.51	−180.96	12.403	13.966	11.194	8.759	—
06 01 45.69	+13 05 01.51	3343573598320013440	06014571+1305015	53.22 ± 0.05	−137.18	−50.35	11.033	12.333	9.939	7.588	—
06 02 01.73	−10 01 56.64	2999321180586629120	06020172−1001565	45.64 ± 0.11	−41.01	−93.97	15.792	18.531	14.313	11.006	—
06 02 22.62	−20 19 44.14	2918040883015489408	06022261−2019447	66.52 ± 0.04	−45.35	554.95	12.025	13.542	10.836	8.374	—
06 02 54.24	−09 15 03.74	3005440443830195968	06025422−0915030	65.46 ± 0.09	116.44	−594.36	14.623	17.110	13.201	10.033	—
06 03 12.31	−37 22 42.68	2884162387142135936	06031230−3722426	47.31 ± 0.05	22.85	−107.50	13.714	15.605	12.405	9.614	—
06 04 42.08	+22 19 23.22	3423743492225744128	06044205+2219231	43.58 ± 0.66	104.97	−58.60	12.365	13.608	11.273	9.006	—
06 04 52.15	−34 33 35.77	2886233695250041216	06045215−3433360	115.40 ± 0.08	25.72	342.85	11.109	13.199	9.785	6.866	—
06 05 24.68	−16 18 06.79	2991458504218554496	06052467−1618067	46.32 ± 0.06	333.31	133.37	13.736	15.614	12.434	9.662	—
06 07 43.74	−25 44 41.50	2911981886751531648	06074375−2544414	87.67 ± 0.03	−184.90	−202.81	10.732	12.150	9.590	7.169	—
06 08 16.43	−32 16 46.05	2889899840676982912	06081642−3216462	62.37 ± 0.04	731.21	−25.78	11.960	13.575	10.736	8.200	—
06 08 22.41	−79 04 44.79	5211871624615014400	06082242−7904446	42.44 ± 0.04	172.53	−209.76	13.303	14.850	12.094	9.592	—
06 09 07.71	−49 53 17.05	5553110654636730496	06090772−4953170	52.61 ± 0.02	39.68	−54.63	10.154	11.246	9.155	6.981	—
06 09 19.21	−35 49 31.06	2885863400349980288	06091922−3549311	44.63 ± 0.03	−3.72	−56.27	10.218	11.278	9.229	7.046	—
06 10 34.62	−21 51 52.66	2940856402123426176	06103462−2151521	173.70 ± 0.05	−135.98	−719.09	7.307	8.386	6.304	4.166	—
06 10 43.01	+02 59 47.79	3316984005545134592	06104301+0259477	40.05 ± 0.06	−93.02	−17.18	13.495	15.252	12.223	9.473	—
06 10 45.04	−33 46 22.41	2886691573123995520	06104503−3346226	58.48 ± 0.08	669.10	531.45	15.091	17.645	13.663	10.656	—
06 10 52.88	−43 24 17.65	5571142580908768384	06105288−4324178	89.39 ± 0.05	130.94	733.84	10.992	12.527	9.812	7.312	—
06 11 14.65	−00 35 37.82	3121522311646906240	06111465−0035379	46.26 ± 0.30	−40.07	65.93	14.097	16.331	12.715	9.693	—
06 11 20.00	+07 11 03.32	3325157736332326784	06112000+0711033	54.08 ± 0.06	10.11	9.99	12.688	14.426	11.429	8.805	—
06 12 22.45	−08 07 16.25	3006023219353984256	06122246−0807162	43.75 ± 0.16	−113.37	7.87	14.933	17.516	13.490	10.270	—
06 12 37.91	−08 26 21.78	3005809226902815360	06123793−0826216	42.83 ± 0.06	−205.62	−152.61	14.084	15.967	12.781	9.961	—
06 12 54.65	+10 06 31.43	3329891443126668544	06125467+1006313	41.42 ± 0.12	−220.15	−1.14	12.560	13.938	11.421	9.014	—
06 13 47.18	−23 54 24.82	2913314288686472576	06134717−2354250	60.01 ± 0.04	−31.04	110.80	11.631	13.210	10.426	7.872	—
06 13 57.21	−34 37 02.34	2886405528302243712	06135730−3437024	44.65 ± 0.05	190.76	261.38	14.245	16.149	12.849	9.531	—
06 13 57.39	−34 37 02.71	2886405528302243584	06135730−3437024	44.70 ± 0.06	194.12	242.46	14.451	16.440	13.075	9.531	—
06 15 11.98	−16 26 15.43	2944727125434832768	06151198−1626152	77.55 ± 0.07	−75.94	−371.99	12.270	13.965	11.020	8.387	—

Table 2: List of M dwarf systems within 25 pc drawn from *Gaia* DR2, as described in §2.3.

These systems have not been vetted to distinguish single stars from multiples, but in cases

where a system was resolved in *Gaia* but not 2MASS, a “J” flag is listed in column 12.

06 15 49.35	−01 00 41.66	3121200807575320448	06154934−0100415	44.80 ± 0.33	199.17	−57.86	18.552	19.972	16.904	12.541	—
06 16 38.39	−31 35 22.28	2892996035358675968	06163837−3135223	42.86 ± 0.04	40.17	61.42	13.222	14.835	11.991	9.389	—
06 17 10.65	+05 07 02.36	3317901440625203968	06171064+0507024	55.54 ± 1.10	−220.20	180.29	12.093	13.563	10.822	8.267	—
06 17 47.11	−34 01 11.66	2891695137006940544	06174711−3401118	72.83 ± 0.04	−95.22	110.11	10.788	12.133	9.678	7.329	—
06 19 20.78	−06 39 22.11	3007559370624135424	06192078−0639215	59.51 ± 0.06	−36.04	−625.05	11.874	13.314	10.710	8.238	—
06 21 06.66	−49 05 37.95	5550620058937466880	06210665−4905379	85.75 ± 0.03	−26.45	255.19	12.028	13.568	10.835	8.350	—
06 21 36.58	+16 18 36.18	3369198846380425344	06213658+1618361	42.91 ± 0.05	238.75	−149.62	10.828	11.932	9.818	7.650	—
06 21 43.90	+16 19 22.28	3369198983818682624	06214389+1619223	42.96 ± 0.05	241.29	−149.09	11.589	12.847	10.500	8.223	—
06 21 50.47	+15 54 14.11	3369132536382082432	06215046+1554140	40.05 ± 0.07	49.08	−166.00	14.609	16.498	13.301	10.553	—
06 21 54.71	−47 25 31.33	5553958176239495040	06215471−4725313	40.19 ± 0.05	−24.11	−0.45	14.821	16.793	13.501	10.819	—
06 22 37.02	−62 37 34.73	5478163342178788480	missing	45.24 ± 0.04	−300.35	−185.73	12.715	14.414	11.464	—	—
06 23 38.48	−09 38 51.73	3003146828216906624	06233847−0938517	40.62 ± 0.05	−59.96	16.12	12.688	14.182	11.499	8.947	—
06 23 46.46	+05 02 41.20	3131514462863888768	06234645+0502411	40.37 ± 0.04	33.97	−71.30	10.351	11.453	9.346	7.138	—
06 24 03.94	−46 05 15.93	5554890115423215616	06240393−4605159	47.38 ± 0.02	−2.55	109.57	10.846	12.091	9.771	7.467	—
06 24 04.46	−26 58 46.11	2899039432302133632	06240446−2658462	53.07 ± 0.03	8.53	15.81	9.773	10.830	8.788	6.642	—
06 24 08.52	−26 55 23.57	2899039878978713472	06240852−2655239	49.21 ± 0.86	12.18	4.78	10.425	11.789	9.298	6.895	—
06 24 10.12	−00 16 30.50	3120174031215549824	06241011−0016301	46.24 ± 0.39	160.17	−267.61	12.699	14.387	11.456	8.843	—
06 24 41.28	+23 25 58.94	3377365057060447616	06244132+2325585	117.74 ± 0.06	550.90	−508.42	11.674	13.392	10.433	7.911	—
06 25 36.03	−48 15 59.72	5550682078265062528	06253604−4815598	42.62 ± 0.04	−92.57	−79.25	11.802	13.173	10.666	8.287	—
06 25 56.09	−60 03 27.04	5481843025342799104	06255610−6003273	74.37 ± 0.04	−25.39	110.75	11.026	12.614	9.829	7.206	—
06 26 34.08	+20 32 14.46	3375625461782073984	06263408+2032144	50.04 ± 0.13	−5.45	−39.60	13.461	15.180	12.212	9.568	—
06 27 44.74	−11 20 08.72	3000469002004888576	06274476−1120087	51.34 ± 0.78	6.16	9.00	18.206	18.883	16.658	14.190	—
06 29 23.39	−02 48 48.80	3117120863523946368	06292339−0248499	242.97 ± 0.88	750.14	−802.95	9.581	11.376	8.276	5.486	—
06 30 46.47	−76 43 09.60	5260451999700465536	06304661−7643094	112.49 ± 0.12	−37.01	523.99	13.207	15.324	11.423	7.923	—
06 32 08.92	−10 09 27.22	3002163349423052544	06320891−1009269	48.68 ± 0.82	98.03	−210.37	20.210	21.192	18.440	13.500	—
06 32 21.94	−69 57 43.85	5278882357204698624	06322189−6957445	42.41 ± 0.03	249.51	640.10	11.884	13.260	10.743	8.378	—
06 33 43.28	−75 37 47.96	5260759175761501696	06334337−7537482	113.12 ± 0.03	−297.96	280.64	9.371	10.706	8.258	5.862	—
06 33 49.97	−58 31 42.45	5482827676662168832	06334998−5831426	65.70 ± 0.03	−404.35	795.85	10.529	11.854	9.422	7.030	—
06 34 18.62	−31 52 22.92	2893677457691363584	06341862−3152227	47.96 ± 0.03	−149.63	−362.61	11.881	13.289	10.730	8.290	—
06 34 39.32	+24 13 52.76	3382740882560780928	06343934+2413528	40.37 ± 0.09	−162.22	−37.09	15.539	17.467	14.107	10.984	—
06 35 22.27	−57 37 35.17	5484571119849822464	06352229−5737349	42.77 ± 0.03	−17.49	53.22	10.286	11.288	9.318	7.153	—

Table 2: List of M dwarf systems within 25 pc drawn from *Gaia* DR2, as described in §2.3.

These systems have not been vetted to distinguish single stars from multiples, but in cases

where a system was resolved in *Gaia* but not 2MASS, a “J” flag is listed in column 12.

06 35	29.85	−04 03	18.44	3104733181410232576	06352986−0403185	79.46 ± 0.51	−100.88	78.18	12.698	14.837	11.335	8.307	−
06 36	06.39	+11 37	03.10	3352091927220152320	06360639+1137032	56.57 ± 0.11	−205.43	−851.95	12.816	14.527	11.565	8.994	−
06 36	18.28	−40 00	23.62	5570642264461522048	06361826−4000238	52.80 ± 0.29	−221.98	44.24	9.850	10.846	8.893	6.790	−
06 36	36.97	+06 19	10.31	3131963480225963392	06363696+0619102	48.63 ± 0.09	−12.91	379.22	14.873	17.210	13.466	10.321	−
06 37	10.80	+17 33	53.33	3359074685047632640	06371092+1733526	99.92 ± 0.05	−764.52	337.80	8.876	9.876	7.916	5.862	−
06 38	35.29	−14 04	58.18	2950868451932669440	06383532−1404579	40.12 ± 0.07	−247.40	−96.64	12.915	14.468	11.711	9.139	−
06 39	37.64	−55 36	34.83	5497072086021346688	06393764−5536349	75.89 ± 0.02	−392.28	11.18	9.065	10.067	8.107	6.027	−
06 39	41.07	−36 59	02.58	5580526362897086080	06394106−3659024	41.47 ± 0.03	73.75	−273.46	10.882	12.162	9.797	7.418	−
06 40	13.99	−05 52	23.37	3100542495921276160	06401397−0552226	84.72 ± 0.05	107.21	−582.86	9.303	10.505	8.251	5.962	−
06 41	18.42	−43 22	32.49	5557113083119380224	06411840−4322329	51.28 ± 0.19	211.77	632.03	18.558	21.142	16.911	12.451	−
06 41	36.31	−62 33	46.71	5478730243502292736	06413634−6233466	40.75 ± 0.06	−141.19	−72.63	14.812	16.946	13.451	10.439	−
06 41	42.88	+12 26	43.81	3352081447497931264	06414287+1226438	50.25 ± 0.08	11.05	−24.56	13.465	15.353	12.169	9.358	−
06 42	11.19	+03 34	52.63	3127503620545728128	06421118+0334527	66.35 ± 0.07	42.04	−258.75	10.893	12.313	9.750	7.334	−
06 42	27.15	−67 07	19.77	5280389615847484416	06422703−6707193	74.13 ± 0.07	697.70	−408.95	14.004	16.300	12.623	9.807	−
06 43	13.87	+16 31	42.96	3357958852543597056	06431389+1631428	49.82 ± 0.16	112.94	62.30	15.739	18.492	14.261	10.860	−
06 43	16.86	−18 43	37.37	2945455521833759744	06431685−1843375	43.07 ± 0.14	174.07	−102.57	17.569	20.744	15.963	11.803	−
06 43	29.77	−70 03	20.64	5266917261213622144	06432978−7003209	51.15 ± 0.03	5.91	192.04	11.676	13.159	10.500	7.967	−
06 43	34.77	+16 41	35.20	3358735760588625152	06433477+1641349	44.26 ± 0.54	−217.34	17.11	12.916	14.689	11.648	8.888	−
06 43	36.70	−02 23	13.15	3106548406384807680	06433670−0223130	71.92 ± 1.38	28.28	−221.22	20.680	20.946	18.750	13.624	−
06 43	40.66	−26 24	40.97	2920124904228150144	06434068−2624405	58.04 ± 0.04	−322.71	−331.03	11.696	13.164	10.526	8.129	−
06 43	42.61	−69 28	54.09	5279003887597588096	06434263−6928539	43.48 ± 0.05	−156.19	−95.85	12.674	14.310	11.444	8.803	−
06 44	53.65	−16 31	11.68	2947071425961581184	06445365−1631117	49.56 ± 0.04	175.79	28.68	10.872	12.018	9.836	7.646	−
06 46	41.08	−21 50	16.10	2926033267402660224	06464109−2150161	59.96 ± 0.07	−195.57	−50.25	14.859	17.323	13.446	10.354	−
06 46	45.74	+15 57	42.17	3357701803041885696	06464573+1557422	44.65 ± 0.05	−99.41	−25.56	10.244	11.309	9.249	7.096	−
06 48	13.54	−10 25	43.19	2954061532478049664	06481354−1025430	58.56 ± 0.04	4.11	−32.26	10.061	11.174	9.044	6.831	−
06 50	26.56	−21 35	57.63	2926101127885235712	06502653−2135576	46.29 ± 0.08	296.34	0.27	15.069	17.437	13.667	10.551	−
06 50	31.26	−09 38	44.63	3050203310249250304	06503126−0938441	40.96 ± 0.05	−142.46	−458.24	11.431	12.506	10.423	8.362	−
06 50	41.91	−50 33	29.29	5502166746165608576	06504190−5033293	43.03 ± 0.05	131.63	−122.97	14.181	16.049	12.880	10.258	−
06 50	59.49	−09 10	50.15	3050513754787437312	06505947−0910506	40.96 ± 0.04	−105.66	−574.71	12.146	13.589	10.976	8.555	−
06 51	59.02	+03 12	55.28	3126552749144643328	06515901+0312553	40.50 ± 0.04	−208.44	−34.66	11.862	13.251	10.722	8.318	−
06 52	17.08	−26 23	14.30	2919383519853573504	06521707−2623145	56.65 ± 0.03	−1.23	101.95	9.961	11.125	8.922	6.666	−

Table 2: List of M dwarf systems within 25 pc drawn from *Gaia* DR2, as described in §2.3.

These systems have not been vetted to distinguish single stars from multiples, but in cases

where a system was resolved in *Gaia* but not 2MASS, a “J” flag is listed in column 12.

06 52 19.76	−25 34 50.47	2920995300823950720	06521977−2534505	62.44 ± 0.16	−235.50	88.15	17.460	20.518	15.832	11.516	—
06 52 24.31	+18 17 04.98	3364557601640710272	06522429+1817046	44.60 ± 0.08	125.63	123.09	11.947	13.466	10.759	8.160	—
06 54 18.77	−49 56 55.29	5508256047719002240	06541877−4956552	41.21 ± 0.04	142.76	−689.05	14.371	16.227	13.074	10.387	—
06 57 11.71	−43 24 51.67	5562135411718515328	06571173−4324509	47.36 ± 0.03	72.73	−233.03	10.782	12.002	9.682	6.757	—
06 57 13.05	−72 43 31.19	5262441840867360128	06571304−7243311	41.78 ± 0.04	99.26	−13.67	12.778	14.364	11.563	8.962	—
06 57 46.50	−44 17 27.93	5559035514776717312	06574663−4417281	124.38 ± 0.05	−1173.68	−126.01	10.369	11.820	9.188	6.056	—
06 58 39.78	−20 21 53.27	2932111573841023360	06583980−2021526	46.92 ± 0.06	4.24	26.33	13.233	14.893	11.941	8.571	—
06 58 39.83	−20 21 52.08	2932111573845020672	06583980−2021526	47.02 ± 0.06	−15.57	45.03	12.898	14.374	11.510	8.571	—
06 59 09.68	−13 47 25.56	2949436372399442560	06590966−1347253	49.42 ± 0.05	290.92	−92.63	10.813	12.070	9.723	7.245	—
06 59 28.82	+19 20 55.86	3365063724883180288	06592868+1920577	129.00 ± 0.17	909.01	−894.58	12.800	15.164	11.403	8.230	—
06 59 28.85	+19 30 33.70	3365092380904700544	06592887+1930341	49.60 ± 0.10	−174.40	−205.40	11.675	13.093	10.527	8.122	—
06 59 56.17	−61 44 59.84	5287046368477870848	06595620−6145001	54.00 ± 0.05	−159.63	263.51	14.557	16.837	13.163	10.038	—
06 59 58.50	+17 17 15.80	3361210791323909504	06595849+1717162	42.08 ± 0.85	67.10	−457.51	19.725	21.710	18.054	13.021	—
07 00 09.49	−28 47 02.11	5608852393772621184	07000950−2847022	46.02 ± 0.03	−219.25	−90.31	10.066	11.021	9.133	7.120	—
07 00 34.34	−44 47 13.34	5559134436466111360	07003434−4447132	45.22 ± 0.13	−43.50	−14.42	14.481	17.064	13.027	9.787	—
07 01 36.56	−14 37 18.65	2948306177526059520	07013658−1437185	43.56 ± 0.09	−224.50	228.82	14.581	16.612	13.247	10.321	—
07 02 30.50	+21 54 29.97	3367795633320598528	07023044+2154310	42.98 ± 0.12	367.01	−539.69	14.594	16.712	13.236	10.257	—
07 02 50.33	−61 02 47.47	5479255432103480320	07025026−6102482	57.29 ± 0.19	521.51	594.67	14.109	16.933	12.632	9.522	—
07 04 17.70	−10 30 31.58	3046530292874936448	07041771−1030307	63.55 ± 0.51	−138.41	−814.62	10.098	11.564	8.940	6.427	—
07 04 34.49	+16 57 27.04	3361034083487398016	07043449+1657273	50.13 ± 0.07	−7.02	−203.54	13.783	15.710	12.468	9.639	—
07 04 45.92	−38 36 07.56	5565570359057262720	07044567−3836074	44.51 ± 0.03	1163.57	−221.55	11.886	13.000	10.674	7.868	—
07 04 47.06	+02 58 14.04	3116021729853781376	07044706+0258139	42.77 ± 0.21	−69.37	−179.78	16.671	19.599	15.116	11.473	—
07 04 49.65	+24 59 54.98	3380787325274157824	07044967+2459555	42.14 ± 0.04	−174.89	−275.52	10.709	11.862	9.669	7.417	—
07 05 11.96	−10 07 52.75	3046640175314154624	07051194−1007528	58.54 ± 0.07	127.83	71.57	13.452	15.365	12.140	9.275	—
07 05 12.31	+08 25 52.36	3154550541435395200	07051231+0825524	51.43 ± 0.06	73.34	−419.20	11.298	12.496	10.241	7.984	—
07 07 22.92	−21 27 27.31	2929062902976882304	07072291−2127271	56.98 ± 0.04	195.13	−210.38	10.136	11.363	9.074	6.799	—
07 07 53.28	−49 00 50.31	5508545421138819968	07075327−4900503	41.57 ± 0.15	−14.99	397.70	17.758	21.201	16.138	12.105	—
07 08 07.01	−22 48 47.31	2927791352138805504	07080702−2248471	59.78 ± 0.03	−411.63	−228.97	10.512	11.684	9.470	7.268	—
07 09 33.65	+08 00 56.63	3154368194301157376	07093364+0800566	43.32 ± 0.08	−109.69	−193.42	13.140	14.756	11.911	9.270	—
07 09 37.66	−57 03 42.13	5486916932205092352	07093765−5703423	57.88 ± 0.07	331.26	330.36	12.191	13.899	10.944	8.297	—
07 10 31.46	−08 42 48.25	3051343817347672576	07103147−0842485	51.60 ± 0.07	−84.57	97.62	11.928	13.468	10.732	8.164	—

Table 2: List of M dwarf systems within 25 pc drawn from *Gaia* DR2, as described in §2.3.

These systems have not been vetted to distinguish single stars from multiples, but in cases

where a system was resolved in *Gaia* but not 2MASS, a “J” flag is listed in column 12.

07 11 00.98	−38 24 46.75	5565156633450986752	07110095−3824460	62.95 ± 0.09	373.63	−782.78	14.662	17.055	13.253	10.226	—
07 11 16.92	−21 17 54.65	2928420272788743296	07111696−2117546	50.32 ± 0.04	−103.76	−64.41	13.220	14.908	11.862	9.060	—
07 11 17.10	−21 17 55.12	2928420272788743424	07111696−2117546	50.37 ± 0.04	−124.68	−67.92	13.376	15.094	12.090	9.060	—
07 12 54.06	−52 20 05.62	5503983654771355776	07125405−5220055	54.15 ± 0.02	−294.47	904.15	11.609	13.038	10.451	8.063	—
07 13 11.22	−05 11 48.62	3059182338820698624	07131123−0511482	87.03 ± 0.05	−22.71	−306.98	10.156	11.402	9.076	6.819	—
07 16 10.65	−20 11 23.39	2930012262549006336	07161063−2011232	45.57 ± 0.06	276.10	−199.25	14.576	16.556	13.260	10.485	—
07 16 29.23	−31 32 36.74	5605040794974833024	07162922−3132367	49.13 ± 0.04	22.72	−199.27	12.503	13.946	11.335	8.937	—
07 16 47.90	−06 30 36.94	3058039362114874496	07164790−0630369	41.10 ± 0.35	−12.00	145.49	18.647	21.246	17.016	12.565	—
07 17 17.09	−05 01 03.54	3059246454092369024	07171706−0501031	89.69 ± 0.08	420.91	−390.48	11.874	13.560	10.639	8.045	—
07 17 29.93	+19 34 16.65	3363266366969232128	07172997+1934170	47.57 ± 0.05	−322.56	−265.21	11.698	13.067	10.566	8.162	—
07 18 07.35	−35 02 20.98	5590736084278574464	07180734−3502209	56.68 ± 0.12	−166.29	6.86	14.536	17.194	13.072	9.795	—
07 18 12.90	+13 42 16.64	3166484739422960640	07181290+1342167	40.24 ± 0.06	−34.48	−27.58	12.170	13.657	10.987	8.448	—
07 18 41.90	+08 30 01.47	3155195714240292736	07184190+0830014	48.90 ± 0.05	−32.68	−117.58	12.614	14.068	11.448	9.020	—
07 18 44.19	−26 16 17.43	5616120681034800000	07184418−2616172	40.97 ± 0.03	37.48	−34.25	10.606	11.757	9.566	7.268	—
07 19 39.44	−26 44 41.19	5616029932658479232	07193943−2644411	40.84 ± 0.04	36.45	−31.75	12.216	13.780	11.003	8.450	—
07 20 52.04	−62 10 11.59	5292028393100840320	07205204−6210118	89.20 ± 0.03	−285.92	194.70	11.141	12.614	9.977	7.515	—
07 21 51.17	+21 14 54.32	3363902571884367232	07215116+2114544	41.33 ± 0.08	43.84	−138.96	13.656	15.433	12.378	9.640	—
07 21 54.35	−31 04 36.78	5604989633324007168	07215434−3104365	41.02 ± 0.03	52.42	−227.83	12.036	13.398	10.900	8.539	—
07 22 01.46	+02 43 54.39	3136033356873855488	07220145+0243544	47.53 ± 0.21	−146.88	−246.54	17.004	20.097	15.400	11.808	—
07 23 20.75	−60 06 13.07	5293288295987250816	07232075−6006132	51.01 ± 0.03	76.77	450.02	11.188	12.469	10.094	7.758	—
07 23 59.62	−80 15 18.04	5207997014358306816	07235966−8015179	61.19 ± 0.09	−415.66	737.91	15.041	17.731	13.583	10.440	—
07 24 17.33	+18 38 47.89	3362528491586472960	07241733+1838479	40.90 ± 0.07	−109.03	−78.30	13.718	15.492	12.440	9.739	—
07 25 35.64	−42 38 56.53	5512265038913877248	07253564−4238566	43.55 ± 0.06	−247.30	134.70	12.378	13.888	11.187	8.675	—
07 26 38.08	−30 33 08.76	5605438925569442432	07263809−3033087	52.92 ± 0.05	−316.47	59.00	13.127	14.853	11.869	9.196	—
07 27 28.61	+22 02 37.94	866016662739803008	07272865+2202383	49.31 ± 0.05	−261.05	−144.29	10.295	11.469	9.245	6.946	—
07 27 40.67	−14 04 57.99	3031748699076624768	07274064−1404577	40.56 ± 0.06	273.60	−344.71	14.428	16.168	13.156	10.525	—
07 28 45.44	−03 17 53.31	3060641356388548224	07284541−0317524	85.34 ± 0.07	439.65	−788.98	10.289	11.702	9.151	6.704	—
07 28 51.17	−30 15 52.83	5605469299570245504	07285117−3015527	65.09 ± 0.05	−134.46	−189.64	12.174	14.058	10.876	8.062	—
07 30 02.04	−28 31 03.15	5611909104822545152	07300205−2831032	55.38 ± 0.06	−152.72	90.82	13.971	16.012	12.635	9.747	—
07 30 30.39	−03 39 33.60	3060426058267356928	07303040−0339337	40.99 ± 0.12	−154.75	45.06	15.836	18.433	14.371	10.995	—
07 31 29.50	+02 49 08.46	3136232952593850496	07312949+0249084	56.55 ± 0.12	−218.37	3.82	14.844	17.259	13.429	10.237	—

Table 2: List of M dwarf systems within 25 pc drawn from *Gaia* DR2, as described in §2.3.

These systems have not been vetted to distinguish single stars from multiples, but in cases

where a system was resolved in *Gaia* but not 2MASS, a “J” flag is listed in column 12.

07 32 07.82	−36 07 22.06	5588141992752796800	07320783−3607217	65.19 ± 0.03	−245.01	−468.03	11.846	13.281	10.688	8.326	−
07 32 23.10	−23 14 48.63	5618467726035023616	07322311−2314484	79.43 ± 1.26	−2.78	−6.02	19.065	20.007	17.678	15.249	−
07 32 27.98	−25 43 04.37	5613426740110194816	07322799−2543044	40.47 ± 0.05	−140.16	60.18	14.244	16.161	12.931	10.135	−
07 34 08.90	−43 30 25.68	5535283658436274944	07340889−4330256	48.25 ± 0.84	−39.14	151.66	20.719	21.358	18.860	14.010	−
07 34 17.59	+00 59 09.27	3134682194522547968	07341758+0059092	64.09 ± 0.06	−18.97	−599.48	10.870	12.195	9.764	7.434	−
07 34 19.89	−13 14 42.14	3033364873792430208	07341985−1314421	41.68 ± 0.04	−425.73	−62.38	12.202	13.475	11.099	8.824	−
07 34 56.33	+14 45 53.83	3165346538729784192	07345632+1445544	61.80 ± 0.15	−72.46	−81.50	10.395	11.501	9.056	6.398	−
07 35 05.93	+10 00 28.27	3149589510609268352	07350593+1000283	45.04 ± 0.13	−257.84	210.56	14.454	16.436	13.136	10.326	−
07 35 51.63	−00 48 55.91	3086118793148247296	07355164−0048560	45.08 ± 0.06	−95.89	57.58	13.277	15.008	12.020	9.307	−
07 36 07.08	−03 06 38.79	3060788514846284032	07360708−0306385	71.08 ± 0.14	68.24	−289.99	9.118	10.161	8.122	5.934	−
07 36 12.02	−51 55 21.21	5492622847798742272	07361202−5155213	61.27 ± 0.03	397.97	446.87	11.296	12.716	10.142	7.755	−
07 36 56.68	−30 24 16.40	5599170330597007360	07365666−3024160	71.95 ± 0.04	223.85	−361.26	12.291	13.922	11.066	8.495	−
07 37 33.35	−22 13 36.87	5618970026754408192	07373336−2213369	42.35 ± 1.75	4.90	4.32	19.473	20.066	18.206	16.861	−
07 38 09.69	−31 12 19.11	5598366690674006912	07380970−3112192	64.78 ± 0.03	−168.24	207.83	10.789	12.124	9.679	7.298	−
07 38 29.50	+24 00 08.65	868209703104242048	07382951+2400088	51.59 ± 0.06	−152.14	−96.86	11.751	13.228	10.579	8.122	−
07 38 40.96	−21 13 28.48	5715352842388433664	07384089−2113276	95.84 ± 0.04	456.67	−475.61	10.604	12.028	9.462	7.063	−
07 38 50.82	+18 29 20.22	671436777166606976	07385081+1829205	54.42 ± 0.17	69.48	−170.30	14.372	16.652	12.985	9.808	−
07 40 11.81	−42 57 40.29	5535361753834861312	07401183−4257406	125.08 ± 0.06	−483.45	504.55	12.045	14.089	10.708	7.768	−
07 40 19.37	−17 24 45.91	5717278911884264576	07401922−1724449	109.05 ± 0.08	1152.39	−536.55	13.979	16.898	12.507	9.291	−
07 40 19.86	−22 12 22.88	5618982224466716928	07401985−2212229	45.83 ± 2.02	8.00	6.75	19.748	20.398	18.208	16.887	−
07 41 06.79	+17 38 44.85	671143035762692352	07410681+1738459	53.52 ± 0.22	−201.75	−499.07	16.086	19.184	14.553	10.942	−
07 44 40.17	+03 33 08.88	3136952686035250688	07444018+0333089	167.02 ± 0.06	−348.10	−445.88	9.681	11.440	8.436	5.698	−
07 44 50.70	+00 07 35.45	3085871437392148992	07445070+0007355	40.21 ± 0.08	−56.04	−119.51	13.022	14.611	11.802	9.227	−
07 45 50.67	−39 01 38.58	5538430941749582976	07455065−3901385	73.12 ± 2.04	−0.29	−2.11	20.017	20.130	18.169	15.551	−
07 48 16.39	+20 22 05.25	672091364541849344	07481617+2022073	68.03 ± 0.04	1449.88	−992.24	10.552	11.694	9.517	7.396	−
07 49 12.68	−76 42 06.71	5213167330349528064	07491271−7642065	91.83 ± 0.03	−102.00	−193.26	10.146	11.574	9.009	6.579	−
07 49 42.14	−03 20 33.95	3080857458209146368	07494215−0320338	58.78 ± 0.18	−161.30	−56.98	11.809	13.425	10.594	8.025	−
07 49 50.77	−03 17 19.78	3080863574242572032	07495087−0317194	58.78 ± 0.09	−139.60	−37.61	11.922	13.480	10.626	7.193	−
07 49 50.94	−03 17 19.21	3080863574244739712	07495087−0317194	58.81 ± 0.09	−174.04	−65.43	11.550	13.189	10.282	7.193	−
07 51 51.39	+05 32 57.17	3143635723866162432	07515138+0532572	67.53 ± 0.07	442.95	−409.87	13.165	15.081	11.858	9.089	−
07 51 54.67	−00 00 12.26	5 30857169903686397	44 07515465−00001	17107. ± 780	09263	38 − 756.	97 11.6	55 13.5	03 10.3	79 7.6	−

Table 2: List of M dwarf systems within 25 pc drawn from *Gaia* DR2, as described in §2.3.

These systems have not been vetted to distinguish single stars from multiples, but in cases

where a system was resolved in *Gaia* but not 2MASS, a “J” flag is listed in column 12.

07 52 23.93	+16 12 14.96	666988221840703232	07522390+1612157	52.93 ± 0.10	182.91	−350.38	14.773	17.225	13.321	9.846	—
07 53 13.48	−10 12 17.75	3037592156694079744	07531346−1012174	43.49 ± 0.09	144.43	−348.30	14.788	16.874	13.439	10.601	—
07 53 20.37	−33 26 32.10	5593952946066050304	07532037−3326322	60.02 ± 0.04	−51.42	79.27	10.452	11.781	9.345	6.916	—
07 53 37.41	−18 57 57.57	5717361100375608960	07533741−1857574	42.41 ± 0.04	−122.63	−248.28	12.537	13.984	11.367	8.989	—
07 54 35.46	−41 03 46.95	5537221685127063040	07543545−4103470	40.28 ± 0.05	−11.19	−0.74	13.760	15.517	12.485	9.817	—
07 54 54.73	−29 20 56.29	5600272625752039296	07545478−2920559	80.35 ± 0.82	358.41	−511.32	11.877	13.183	10.197	7.354	—
07 54 54.84	−38 09 37.78	5538156819768871552	07545484−3809381	80.12 ± 0.08	−75.87	367.54	13.535	15.745	12.158	9.077	—
07 55 27.46	−24 04 37.84	5698599996038907520	07552745−2404374	42.90 ± 0.10	2.07	−391.36	16.312	19.251	14.808	11.235	—
07 55 38.04	−39 28 44.87	5537831536118877184	07553808−3928449	42.62 ± 1.54	20.37	−3.36	20.096	21.265	18.605	16.191	—
07 56 13.88	−25 09 21.71	5698280927203731072	07561384−2509218	49.85 ± 2.24	−38.50	−19.42	19.783	20.629	18.231	15.740	—
07 56 53.94	−45 38 14.06	5519117229744210944	07565395−4538145	51.52 ± 0.04	−199.13	636.73	11.317	12.569	10.227	8.000	—
07 57 32.53	−71 14 53.83	5269507921064994304	07573255−7114537	44.43 ± 0.04	92.64	17.04	11.166	12.694	9.977	7.423	—
07 58 09.09	+07 17 01.46	3144499458967932672	07580909+0717015	76.13 ± 0.05	−325.54	−32.03	12.298	14.038	11.036	8.381	—
07 59 18.80	−55 28 28.66	5296104935544651520	07591880−5528286	40.62 ± 0.04	5.17	−14.89	14.060	15.999	12.740	9.885	—
08 00 54.12	−29 33 40.81	5597122765067896960	08005412−2933407	43.36 ± 0.03	−112.76	−99.80	12.147	13.609	10.973	8.531	—
08 01 43.58	+23 42 27.29	680446793919166080	08014355+2342271	52.86 ± 0.41	−124.32	−123.96	10.057	11.205	9.033	6.802	—
08 02 57.81	−83 30 07.47	5193725009832516608	08025781−8330076	43.39 ± 0.51	−109.49	124.57	14.124	16.320	12.739	9.712	—
08 03 44.69	+08 27 00.01	3146187071877364992	08034469+0827000	41.67 ± 0.11	−75.28	−203.45	15.365	17.743	13.960	11.007	—
08 05 11.02	−31 58 11.46	5595785866305529216	08051104−3158115	42.05 ± 0.14	−238.23	90.68	17.474	20.837	15.863	12.113	—
08 05 11.49	−35 22 02.86	5544880780046222464	08051148−3522029	46.72 ± 0.05	−33.92	47.26	12.959	14.601	11.729	9.142	—
08 05 36.95	−09 32 38.37	3038607830561555072	08053691−0932377	61.10 ± 0.10	486.51	−576.85	13.547	15.486	12.234	9.443	—
08 05 46.17	−59 12 50.32	5291484512805323264	08054616−5912504	59.74 ± 0.05	262.07	−565.00	13.193	14.982	11.922	9.215	—
08 05 57.14	+04 17 03.60	3094447525008511488	08055713+0417035	45.37 ± 0.13	−202.81	−1.44	15.612	18.206	14.159	10.865	—
08 06 26.42	−28 39 22.85	5597587141239788672	08062638−2839222	44.74 ± 0.22	620.08	−703.65	17.161	18.564	15.407	11.945	—
08 08 16.85	−73 01 40.16	5220893216305190528	08081689−7301399	41.03 ± 0.29	26.26	−156.06	12.914	14.631	11.651	8.992	—
08 09 30.95	+21 54 17.24	676804558572501120	08093099+2154173	47.69 ± 0.04	−319.44	−66.07	10.862	12.072	9.800	7.514	—
08 09 40.63	−37 20 02.03	5541111516746730752	08094064−3720019	46.81 ± 0.89	−149.76	−105.20	20.368	21.633	18.615	13.751	—
08 09 58.05	−52 58 05.42	5320435203722048768	08095807−5258054	61.79 ± 0.04	−514.17	668.56	10.649	12.016	9.525	7.135	—
08 10 26.46	−11 09 36.78	5727991694185495552	08102645−1109370	50.59 ± 0.05	73.33	91.05	10.796	12.027	9.726	7.441	—
08 10 34.29	−13 48 51.13	5725122965270676864	08103429−1348514	47.81 ± 0.32	−249.07	61.64	10.921	12.114	9.770	7.418	—
08 10 48.05	+01 09 11.71	3089829644889680256	08104804+0109118	51.62 ± 0.08	54.91	190.22	13.932	15.919	12.604	9.744	—

Table 2: List of M dwarf systems within 25 pc drawn from *Gaia* DR2, as described in §2.3.

These systems have not been vetted to distinguish single stars from multiples, but in cases

where a system was resolved in *Gaia* but not 2MASS, a “J” flag is listed in column 12.

08 10 53.63	+03 58 33.61	3094572113419797248	08105362+0358335	45.64 ± 0.09	114.28	−340.07	12.157	13.727	10.946	8.293	−
08 10 58.65	+14 20 38.78	653799751664331520	08105865+1420390	41.99 ± 0.17	−42.68	−128.06	17.127	20.264	15.546	11.592	−
08 11 01.44	−34 11 42.39	5546549907425468800	08110145−3411425	42.34 ± 0.04	−199.56	202.66	12.820	14.290	11.643	9.197	−
08 11 52.63	−08 55 13.00	3062730668994961024	08115263−0855131	42.07 ± 0.06	−202.39	154.53	12.218	13.693	11.038	8.602	−
08 11 56.05	−33 24 35.67	5547451060267538304	08115605−3324357	45.90 ± 0.44	−53.42	153.32	19.809	21.029	18.087	12.991	−
08 11 57.56	+08 46 22.98	3098328216938651264	08115757+0846220	145.48 ± 0.57	1078.93	−5096.18	11.376	13.156	10.159	7.660	−
08 12 31.72	−24 44 42.47	5697787766170389888	08123170−2444423	47.24 ± 0.23	135.53	−140.87	18.702	20.990	17.061	12.391	−
08 12 40.89	−21 33 06.98	5700706729031126656	08124088−2133056	123.22 ± 0.07	13.70	−694.02	10.665	12.387	9.434	6.705	−
08 12 44.25	−45 04 33.82	5520094661224351872	08124427−4504335	40.37 ± 0.08	−270.03	−332.84	15.411	17.833	13.995	10.906	−
08 12 58.37	−10 31 58.33	5728413494331031168	08125835−1031581	46.08 ± 0.05	223.54	−113.15	13.042	14.524	11.853	9.230	J
08 13 19.49	−52 32 02.99	5320834841834013568	08131950−5232031	42.81 ± 0.38	−63.32	802.12	19.822	21.698	18.064	13.287	−
08 13 42.59	−76 07 48.41	5210616497733074304	08134261−7607485	64.07 ± 0.03	−307.60	621.90	10.800	12.150	9.684	7.297	−
08 14 22.57	−25 42 19.07	5694679408146511232	08142257−2542187	42.09 ± 0.05	−64.05	−241.34	10.585	11.799	9.525	7.202	−
08 15 11.20	−23 44 15.64	5699418131466175488	08151117−2344157	101.26 ± 0.08	111.99	64.18	11.044	12.618	9.841	7.215	−
08 15 15.99	−36 00 58.91	5541659279700994944	08151599−3600595	40.02 ± 0.05	−112.57	613.53	13.850	15.605	12.583	9.881	−
08 16 07.98	+01 18 09.27	3089711447388931584	08160798+0118091	111.84 ± 0.05	−376.32	60.40	9.124	10.359	8.061	5.766	−
08 18 07.62	−68 18 46.80	5271055243163629056	08180763−6818468	94.14 ± 0.03	94.77	−340.47	10.598	11.977	9.472	7.101	−
08 18 58.01	+23 33 51.59	677439114220735616	08185804+2333522	44.39 ± 0.19	−259.68	−331.91	16.241	19.094	14.724	11.149	−
08 19 04.54	−13 45 38.23	5723469746454887936	08190454−1345384	40.82 ± 0.11	−113.58	94.94	15.874	18.463	14.421	11.008	−
08 20 13.37	+05 32 08.14	3093380483331664896	08201336+0532082	44.35 ± 0.11	−75.68	6.09	10.960	12.150	9.913	7.670	−
08 21 56.94	+17 48 56.08	656328319169788032	08215702+1748558	54.66 ± 0.10	−521.36	146.66	14.113	16.122	12.786	10.037	−
08 22 47.41	−57 26 52.95	5315595737654226304	08224744−5726530	77.49 ± 0.07	−372.24	481.33	11.871	13.597	10.546	7.802	−
08 23 03.15	−49 12 01.27	5514929155583865216	08230313−4912012	48.39 ± 0.46	−157.90	11.81	18.558	21.153	16.850	12.062	−
08 26 00.36	−08 24 21.58	5753113851249915392	08260036−0824216	41.45 ± 0.04	11.60	−98.85	10.605	11.718	9.589	7.381	−
08 26 55.72	−36 06 01.55	5542217865970083712	08265571−3606016	44.67 ± 0.05	−15.15	76.14	12.869	14.444	11.654	9.119	−
08 27 06.98	−25 26 54.20	5695264936746881536	08270699−2526544	60.51 ± 0.05	21.75	−188.38	12.570	14.181	11.351	8.784	−
08 27 11.83	−44 59 21.12	5522879208777731200	08271183−4459215	72.63 ± 0.07	−166.65	512.91	10.610	12.142	9.424	6.873	−
08 27 30.93	+08 37 13.35	599224353850405888	08273094+0837133	44.38 ± 0.08	−56.43	95.11	11.072	12.408	9.966	7.581	−
08 28 12.66	+20 08 21.57	663767443044739840	08281269+2008228	42.58 ± 0.07	−261.20	−634.29	12.035	13.349	10.913	8.681	−
08 28 34.17	−13 09 19.84	5723739672264914176	08283419−1309198	85.54 ± 0.17	−581.56	27.54	17.603	20.706	15.999	11.297	−
08 29 21.91	+03 55 09.34	3091982587439255168	08292191+0355092	54.32 ± 0.08	−93.42	−70.37	10.438	11.678	9.366	7.026	−

Table 2: List of M dwarf systems within 25 pc drawn from *Gaia* DR2, as described in §2.3.

These systems have not been vetted to distinguish single stars from multiples, but in cases

where a system was resolved in *Gaia* but not 2MASS, a “J” flag is listed in column 12.

08 30 32.57	+09 47 15.44	599891555546067072	08303256+0947153	59.90 ± 0.14	−489.58	−458.87	16.236	19.295	14.674	10.756	—
08 30 46.29	−04 13 40.44	3065768550901629056	08304629−0413405	42.56 ± 0.08	43.72	35.12	14.517	16.512	13.187	10.376	—
08 31 23.46	−10 29 53.71	5751680775281710720	08312348−1029534	58.91 ± 0.06	−593.37	−324.79	13.377	15.321	12.058	9.136	—
08 31 37.57	+19 23 39.40	662732046688476288	08313759+1923395	60.24 ± 0.08	−228.62	−119.99	10.548	12.191	9.324	6.603	—
08 32 04.52	−01 28 36.04	3073123351683582720	08320451−0128360	42.24 ± 0.42	62.53	10.49	19.005	21.236	17.390	12.712	—
08 32 24.91	+17 06 44.20	659076617202569856	08322494+1706441	46.03 ± 0.10	−114.42	41.49	13.038	14.498	11.787	9.255	—
08 32 30.48	−01 34 38.55	3073118648694573312	08323047−0134380	49.09 ± 0.12	159.58	−471.98	15.878	18.705	14.404	11.142	—
08 33 25.12	+18 31 45.24	659624826827938560	08332512+1831459	47.69 ± 0.11	−57.57	−646.27	13.306	15.013	12.047	9.513	—
08 33 43.19	−53 36 41.24	5321049521489667328	08334323−5336417	50.41 ± 0.09	−256.01	388.87	16.126	19.145	14.595	10.975	—
08 34 25.89	−01 08 39.55	3073508528645520000	08342587−0108391	74.64 ± 0.07	231.55	−419.34	11.508	12.959	10.361	8.031	—
08 35 12.90	−69 26 33.41	5223423952768191744	08351287−6926329	43.27 ± 0.14	−118.51	65.69	15.003	16.871	13.187	9.836	—
08 35 31.73	−34 00 37.22	5638902733762157184	08353172−3400369	58.89 ± 0.05	−81.70	−425.37	12.873	14.522	11.637	9.076	—
08 37 07.96	+15 07 45.53	657608666099404544	08370799+1507475	56.10 ± 0.06	−127.05	−894.34	10.734	12.037	9.631	7.321	—
08 37 30.22	+03 33 45.90	3080039799513337216	08373021+0333458	52.82 ± 0.08	61.72	−175.78	12.916	14.619	11.665	8.973	—
08 38 02.17	−58 55 58.40	5302788969813884160	08380224−5855583	90.04 ± 0.22	−61.82	−317.83	14.412	17.369	12.871	9.268	—
08 38 33.74	−28 43 26.35	5645479806157346688	08383373−2843261	73.47 ± 0.08	77.75	−145.14	10.761	12.148	9.631	7.282	—
08 40 01.73	−40 44 30.78	5528315778376852224	08400174−4044309	41.45 ± 0.11	−246.89	192.10	14.524	16.534	13.194	10.248	—
08 40 29.68	+18 24 08.73	659464504288593536	08402975+1824091	73.76 ± 0.14	−810.29	−448.99	15.019	17.766	13.519	10.046	—
08 40 40.72	−38 32 37.40	5529120822749728384	08404070−3832372	62.31 ± 0.06	107.38	−70.31	13.109	15.059	11.788	8.868	—
08 40 56.62	−31 13 32.75	5640444764457556992	08405661−3113324	46.24 ± 0.07	76.47	−227.12	13.018	14.594	11.802	9.272	—
08 40 59.21	−23 27 22.60	5701750711020088192	08405923−2327232	65.77 ± 0.06	−461.16	805.57	10.754	12.246	9.583	7.028	—
08 41 27.27	+02 37 26.22	3079124421723401856	08412726+0237262	40.93 ± 0.09	−388.76	−111.97	14.754	16.850	13.401	10.451	—
08 42 23.20	−04 53 55.16	5761555587993177216	08422320−0453547	45.59 ± 0.06	−59.38	−293.97	11.719	13.099	10.582	8.186	—
08 42 52.23	+09 33 11.18	598180646733241216	08425223+0933111	64.58 ± 0.05	223.22	−614.26	10.724	12.059	9.612	7.283	—
08 43 09.45	−29 37 30.79	5642333072596166528	08430943−2937304	41.88 ± 0.05	283.08	−423.63	13.544	15.191	12.304	9.723	—
08 43 09.76	−46 59 18.31	5329751125239019392	08430981−4659191	64.26 ± 0.07	540.27	−637.20	13.153	14.995	11.861	9.130	—
08 43 35.14	−74 03 46.33	5216850522504272384	08433510−7403461	41.07 ± 0.03	−75.55	−140.91	12.723	14.062	11.598	9.317	—
08 44 38.88	−48 05 20.98	5329084752471816192	08443891−4805218	68.66 ± 0.04	−322.11	794.30	12.450	14.219	11.183	8.562	—
08 47 19.05	−57 17 54.72	5304502936647141504	08471906−5717547	43.50 ± 0.04	−125.85	16.20	12.326	13.920	11.106	8.550	—
08 47 19.33	−46 52 44.22	5329580357345457664	08471933−4652439	60.68 ± 0.04	−122.80	−360.49	10.517	11.928	9.375	6.962	—
08 47 28.74	−15 32 37.38	5733429157137237760	08472872−1532372	56.92 ± 0.32	132.70	−199.75	18.378	20.967	16.765	12.061	—

Table 2: List of M dwarf systems within 25 pc drawn from *Gaia* DR2, as described in §2.3.

These systems have not been vetted to distinguish single stars from multiples, but in cases

where a system was resolved in *Gaia* but not 2MASS, a “J” flag is listed in column 12.

08 48 59.20	−80 35 01.60	5196680222210415104	08485911−8035017	45.27 ± 0.04	−162.31	−267.41	13.571	15.388	12.284	9.503	—
08 50 10.10	−28 22 04.90	5642693123990628480	08501009−2822050	57.56 ± 0.05	25.23	66.29	12.381	13.916	11.183	8.713	—
08 51 43.79	+18 07 29.93	659951725377466880	08514386+1807299	59.72 ± 0.06	−899.71	−53.14	10.660	11.793	9.630	7.525	—
08 52 09.55	−16 21 24.21	5730219785776085632	08520956−1621246	44.52 ± 0.05	−103.72	230.79	11.703	12.978	10.603	8.320	—
08 53 10.91	−20 17 17.44	5704445579657833856	08531090−2017172	42.20 ± 0.05	37.54	−117.45	12.050	13.446	10.900	8.482	—
08 53 28.65	−39 24 40.97	5621702867205993088	08532867−3924409	57.93 ± 0.05	−379.47	−23.68	11.209	12.579	10.091	7.717	—
08 53 36.16	−03 29 32.20	5761985432616501376	08533619−0329321	115.30 ± 0.11	−516.88	−199.41	15.909	19.083	14.333	9.942	—
08 54 05.33	−13 07 30.68	5736464668224470400	08540524−1307301	66.26 ± 0.57	333.53	−578.42	11.389	12.226	9.687	7.258	—
08 54 12.34	−08 05 00.23	5756746775106229120	08541227−0804594	51.20 ± 0.08	940.78	−803.13	15.004	17.438	13.597	10.810	—
08 54 31.99	−05 51 25.69	5760670171895209984	08543197−0551258	44.80 ± 0.21	−122.17	−52.97	12.096	13.620	10.898	8.321	—
08 55 04.74	−71 35 47.97	5222018879990530304	08550473−7135480	56.98 ± 0.05	−209.51	512.01	13.114	14.745	11.885	9.340	—
08 55 20.24	−23 52 14.65	5653063069125830016	08552032−2352151	69.21 ± 0.46	−570.43	36.24	12.328	14.126	11.038	8.201	—
08 55 51.16	−25 12 35.49	5652642883884415488	08555116−2512351	43.90 ± 0.16	−128.54	−320.31	17.777	20.782	16.177	12.202	—
08 56 06.61	−61 57 44.44	5298261284001871616	08560662−6157443	52.10 ± 0.03	−266.02	−95.78	12.187	13.596	11.035	8.669	—
08 56 19.55	+12 39 49.78	605079910398496640	08561956+1239500	85.55 ± 0.07	−47.26	−246.68	12.780	14.701	11.473	8.708	—
08 57 04.68	+11 38 48.80	604756890202697728	08570468+1138490	58.42 ± 0.91	−29.85	−308.70	9.821	10.844	8.701	6.486	—
08 58 15.07	+19 45 48.24	660597997696173440	08581519+1945470	194.72 ± 0.13	−766.03	−99.27	11.974	14.338	10.551	6.889	—
08 58 15.15	+19 45 45.86	660597997697274752	08581519+1945470	195.08 ± 0.18	−938.55	−36.24	12.491	15.040	10.969	6.889	—
08 58 29.23	−27 14 22.56	5648842486369498496	08582923−2714225	41.51 ± 0.05	−157.98	72.69	12.317	13.822	11.125	8.631	—
08 58 34.82	+07 58 55.61	585008772310106496	08583481+0758555	43.76 ± 0.11	105.40	−336.43	15.220	17.576	13.816	10.713	—
08 58 43.28	−00 41 46.62	5764544369835819776	08584330−0041466	41.52 ± 0.10	−310.86	−41.10	15.359	17.775	13.939	10.764	—
08 59 05.32	−31 13 26.61	5629282488047547648	08590526−3113259	53.19 ± 0.05	693.76	−831.71	12.414	14.057	11.180	8.586	—
08 59 31.67	−47 26 09.20	5330091595871802368	08593169−4726097	47.90 ± 0.04	−475.28	675.28	11.226	12.424	10.177	7.932	—
08 59 40.31	+11 45 32.57	604031766579902976	08594029+1145325	53.88 ± 0.16	−272.90	−85.26	17.353	20.568	15.754	11.494	—
09 00 23.55	+21 50 04.90	685103912857072640	09002359+2150054	156.76 ± 0.13	−515.66	−592.06	13.432	16.369	11.947	8.437	—
09 00 48.52	+05 14 41.46	583257314711142144	09004853+0514413	45.21 ± 0.09	−260.00	−210.11	11.232	12.591	10.133	7.816	—
09 01 10.48	+01 56 35.25	576949798755602560	09011048+0156350	42.02 ± 0.24	−377.19	−95.38	10.671	12.068	9.532	7.057	—
09 01 31.71	−65 26 40.26	5296347755815266816	09013172−6526402	55.61 ± 0.06	−67.66	206.18	13.371	15.245	12.068	9.282	—
09 01 38.96	−72 40 16.74	5217401618349014400	09013891−7240166	44.05 ± 0.03	−245.76	228.91	11.416	12.691	10.321	7.994	—
09 01 49.88	+09 05 11.17	585391024399034880	09014988+0905110	40.18 ± 0.07	−2.07	−277.68	13.532	15.286	12.261	9.530	—
09 02 06.91	+00 33 19.44	576506489410890752	09020690+0033195	46.01 ± 0.19	−465.11	−97.52	16.116	19.079	14.615	11.161	—

Table 2: List of M dwarf systems within 25 pc drawn from *Gaia* DR2, as described in §2.3.

These systems have not been vetted to distinguish single stars from multiples, but in cases

where a system was resolved in *Gaia* but not 2MASS, a “J” flag is listed in column 12.

09 02 19.88	+08 28 06.54	585132295569511168	09021988+0828064	49.02 ± 0.05	618.35	−204.45	10.713	12.005	9.618	7.310	—
09 02 23.06	+17 46 32.61	612073663345730560	09022307+1746326	47.61 ± 0.06	−133.28	−47.74	12.594	14.185	11.378	8.784	—
09 04 29.52	−25 09 12.27	5650990966446973696	09042953−2509121	40.53 ± 0.08	−341.60	−177.94	13.165	14.811	11.924	9.314	—
09 04 40.19	−12 19 12.19	5736025550767699968	09044018−1219116	54.73 ± 0.07	90.36	−681.04	13.966	15.922	12.649	9.893	—
09 04 59.69	+02 26 10.30	577355999582711040	09045968+0226102	40.03 ± 0.06	−208.02	4.42	12.152	13.423	11.052	8.746	—
09 05 04.44	+02 50 03.39	577478114092768384	09050442+0250031	42.58 ± 0.25	−312.21	29.17	10.929	11.975	9.730	7.313	—
09 05 17.93	−51 02 36.31	5324164541003506304	09051792−5102362	41.19 ± 0.03	−126.15	285.63	12.265	13.711	11.097	8.640	—
09 05 36.52	−24 53 17.64	5651024054875481856	09053652−2453176	48.33 ± 0.81	−15.51	−1.45	15.462	16.411	14.490	12.342	—
09 05 43.25	−08 41 58.39	5743757763210745216	09054323−0841581	42.17 ± 0.07	299.47	−171.58	14.152	16.103	12.826	9.961	—
09 07 02.75	−22 08 50.04	5655050092795276800	09070278−2208494	65.21 ± 0.12	−302.39	−409.07	12.632	14.481	11.346	8.645	—
09 08 48.85	+11 51 41.12	604215144503584640	09084885+1151411	45.80 ± 0.06	−458.50	192.63	13.796	15.563	12.528	9.899	—
09 09 39.15	+06 42 10.98	580925323563533056	09093916+0642109	43.31 ± 0.06	−76.27	49.91	12.095	13.555	10.920	8.440	—
09 09 57.48	−06 58 18.65	5756372799418344960	09095749−0658186	40.13 ± 0.32	−189.08	17.19	18.675	—	—	12.539	—
09 10 00.75	+09 01 38.10	590490696768123392	09100074+0901381	49.16 ± 0.07	−312.25	31.97	13.810	15.666	12.517	9.765	—
09 12 12.60	−25 55 02.61	5649998554125258368	09121259−2555025	52.77 ± 0.05	104.10	−53.22	12.580	14.148	11.369	8.827	—
09 13 07.45	−31 47 05.33	5634166037660253184	09130747−3147056	47.31 ± 0.07	−544.81	247.35	13.081	14.619	11.879	9.397	—
09 13 23.05	+03 40 42.58	578940739435580288	09132302+0340424	41.77 ± 0.08	−415.51	−76.85	13.014	14.578	11.804	9.253	—
09 14 03.18	+19 40 05.77	635964431813070848	09140320+1940060	43.66 ± 0.14	−147.03	−159.83	11.101	12.437	9.987	7.535	—
09 14 17.43	−41 34 37.85	5427791278545931264	09141746−4134383	82.38 ± 0.06	−548.46	535.19	13.274	15.275	11.943	9.120	—
09 14 41.27	+18 09 44.62	635202989946889728	09144128+1809446	40.77 ± 0.12	−151.56	−9.31	15.141	17.405	13.752	10.644	—
09 15 34.16	+04 22 04.83	579379032257250176	09153413+0422045	54.85 ± 1.10	−111.47	17.59	20.474	21.242	18.096	13.011	—
09 16 10.18	+01 53 08.83	3845035696121944576	09161018+0153088	63.91 ± 0.07	54.64	−101.54	11.699	13.265	10.493	7.960	—
09 16 20.64	−18 37 32.90	5680147991886954240	09162066−1837329	74.36 ± 0.04	−314.80	146.24	9.795	10.988	8.749	6.492	—
09 16 25.97	−62 04 15.85	5298809356198635520	09162598−6204160	51.88 ± 0.04	−683.30	645.12	11.347	12.844	10.165	7.545	—
09 16 51.04	−55 55 46.84	5309974484478157696	09165105−5555468	65.64 ± 0.03	−114.93	−458.93	12.260	13.771	11.074	8.586	—
09 17 05.32	−77 49 23.38	5203276810942065536	09170532−7749233	105.13 ± 0.04	636.47	−806.64	11.562	13.426	10.268	7.448	—
09 19 20.20	+21 54 31.87	638558836873447040	09192021+2154324	41.13 ± 0.12	−148.21	−293.43	15.906	18.469	14.469	11.349	—
09 20 57.95	+03 22 06.44	3845829101135351296	09205794+0322064	56.64 ± 0.06	314.58	−1136.49	12.116	13.599	10.938	8.520	—
09 21 14.11	−21 04 44.42	5676353096222033792	09211410−2104446	79.31 ± 0.23	245.94	−911.60	17.637	21.147	15.984	11.690	—
09 21 37.60	−60 16 55.03	5299440441521812992	09213761−6016551	95.63 ± 0.03	−840.11	182.09	8.675	9.722	7.692	5.587	—
09 21 48.13	−02 19 43.34	3838384617141390208	09214812−0219433	83.47 ± 0.06	177.19	6.58	11.037	12.358	9.932	7.611	—

Table 2: List of M dwarf systems within 25 pc drawn from *Gaia* DR2, as described in §2.3.

These systems have not been vetted to distinguish single stars from multiples, but in cases

where a system was resolved in *Gaia* but not 2MASS, a “J” flag is listed in column 12.

09 22 16.88	−08 52 10.63	5744451451968477952	09221688−0852105	48.01 ± 0.18	30.38	−89.48	15.471	18.060	14.035	10.860	−
09 22 46.32	−15 47 23.94	5683119044103789440	09224626−1547235	51.66 ± 0.07	436.43	−258.75	14.320	16.411	12.976	10.051	−
09 25 35.70	−01 55 47.55	3838046787898605184	09253570−0155476	47.92 ± 0.06	342.40	−388.23	12.309	13.571	11.211	8.919	−
09 26 05.55	−63 19 45.94	5250413836504584576	09260557−6319461	46.31 ± 0.03	−195.77	−186.94	10.877	12.113	9.804	7.478	−
09 28 53.33	−07 22 15.81	5745027080665197696	09285333−0722148	57.18 ± 0.05	−160.27	−714.31	11.034	12.361	9.932	7.630	−
09 30 44.59	+00 19 21.60	3840711729206827520	09304457+0019214	101.00 ± 0.07	−568.70	−549.79	10.494	11.994	9.332	6.871	−
09 30 50.85	+02 27 20.20	3844632759469347584	09305084+0227202	44.50 ± 0.37	−33.53	80.98	12.402	14.060	11.165	8.578	−
09 31 22.32	−17 17 42.32	5682008056323530368	09312228−1717425	72.18 ± 0.27	−367.20	−152.13	14.999	17.831	13.518	10.069	−
09 31 33.02	+20 16 56.55	634729066075133056	09313301+2016581	45.19 ± 0.11	24.65	−806.93	11.251	12.462	10.211	8.040	−
09 33 26.24	−43 53 36.48	5424690587034982144	09332625−4353366	56.91 ± 0.10	−196.75	165.15	15.363	18.057	13.886	10.432	−
09 33 56.39	−10 09 24.37	5740366044716708864	09335639−1009245	40.39 ± 0.05	77.13	240.39	11.886	13.151	10.789	8.508	−
09 34 27.93	−26 43 26.80	5661077924778519552	09342791−2643267	69.73 ± 0.05	294.30	−22.12	12.557	14.296	11.293	8.619	−
09 36 01.64	−21 39 38.88	5664814198431308288	09360161−2139371	105.88 ± 0.06	138.69	−990.31	9.880	11.190	8.792	6.475	−
09 36 04.82	−06 06 55.94	3823729157935421952	09360486−0606557	42.42 ± 0.08	−672.10	−327.21	12.722	14.265	11.518	9.006	−
09 36 19.29	−37 40 35.54	5435991775558944512	09361930−3740355	47.64 ± 0.04	−91.29	−3.73	11.956	13.324	10.820	8.483	−
09 36 50.83	−65 13 50.82	5249254676369630336	09365082−6513507	51.08 ± 0.05	272.28	122.55	14.037	16.240	12.668	9.788	−
09 36 55.65	−26 09 42.31	5661194163772723072	09365564−2609422	54.04 ± 0.12	36.47	−27.23	16.581	19.942	15.023	11.205	−
09 37 34.73	−25 47 15.56	5661231955187115136	09373473−2547156	46.38 ± 0.06	−62.89	21.21	10.916	12.214	9.825	7.465	−
09 38 53.81	−33 48 45.42	5439247193268841344	09385389−3348456	43.29 ± 0.11	−1308.21	302.50	14.959	17.179	13.587	10.776	−
09 39 29.94	+14 38 49.74	617982090939470464	09392993+1438498	51.45 ± 0.08	−161.21	−80.49	12.194	13.670	11.015	8.554	−
09 39 46.37	−41 04 03.20	5425628298649940608	09394631−4104029	104.15 ± 0.04	−527.20	356.83	9.629	11.033	8.491	6.056	−
09 41 02.05	+22 01 28.34	640862653425455360	09410199+2201291	81.26 ± 0.10	461.64	−487.48	12.716	14.543	11.438	8.813	−
09 41 10.36	+13 12 34.42	614543647497149056	09411033+1312344	86.55 ± 0.04	−660.06	−143.23	9.437	10.635	8.383	6.128	−
09 41 26.04	−05 08 24.35	3824279085547913088	09412603−0508242	40.55 ± 0.05	228.92	−89.34	11.174	12.367	10.124	7.923	−
09 42 35.67	−19 14 05.14	5677606810060597248	09423573−1914045	58.66 ± 0.06	−474.87	−217.95	10.899	12.221	9.805	7.495	−
09 42 46.34	−68 53 06.00	5243594081269535872	09424635−6853060	153.78 ± 0.06	−75.52	1128.51	11.133	13.012	9.849	7.037	−
09 42 49.60	−63 37 55.87	5249863805819472640	09424960−6337560	95.37 ± 0.04	508.55	62.77	11.771	13.575	10.498	7.771	−
09 43 29.95	−38 33 56.11	5432670704985289088	09432994−3833560	77.72 ± 0.09	−95.11	−161.64	14.735	17.540	13.271	10.029	−
09 43 39.12	−19 45 43.79	5677526343849451520	09433912−1945437	49.92 ± 0.06	287.39	88.27	12.662	14.048	11.517	9.154	−
09 43 46.16	−17 47 06.29	5684037136313018368	09434633−1747066	74.57 ± 0.04	−1420.04	225.97	12.170	13.429	11.077	8.874	−
09 44 23.74	−73 58 38.27	5217602588456509696	09442373−7358382	41.09 ± 0.31	−523.18	−97.09	13.550	15.432	12.207	9.375	−

Table 2: List of M dwarf systems within 25 pc drawn from *Gaia* DR2, as described in §2.3.

These systems have not been vetted to distinguish single stars from multiples, but in cases

where a system was resolved in *Gaia* but not 2MASS, a “J” flag is listed in column 12.

09 44 29.84	−45 46 35.42	5412250540681250560	09442986−4546351	106.21 ± 0.03	−462.55	−582.81	9.152	10.398	8.078	5.780	—
09 44 47.35	−18 12 48.96	5683871247496205312	09444731−1812489	90.82 ± 0.08	−1599.95	−171.72	11.085	12.703	9.876	7.257	—
09 44 54.19	−12 20 54.37	5690846274384548864	09445422−1220544	76.17 ± 0.09	−331.34	40.03	11.908	13.951	10.550	7.601	—
09 45 58.43	−32 53 30.00	5439029627401396096	09455843−3253299	83.23 ± 0.09	−300.41	146.02	12.419	14.308	11.117	8.279	—
09 46 09.25	−04 25 43.26	3825820772648802816	09460928−0425429	50.17 ± 0.13	−555.10	165.93	13.038	14.485	11.528	8.832	—
09 47 34.81	+12 56 39.13	614339786873867264	09473481+1256390	47.10 ± 0.07	−87.81	226.69	12.133	13.667	10.935	8.451	—
09 48 25.58	−56 44 21.98	5307525906414825216	09482557−5644220	52.90 ± 0.04	−121.04	323.53	12.522	14.158	11.290	8.665	—
09 48 50.20	+15 38 44.87	619440661833351040	09485020+1538449	58.35 ± 0.06	−19.64	228.89	12.046	13.481	10.887	8.470	—
09 49 22.23	+08 06 45.11	3853943806185777664	09492223+0806450	60.50 ± 0.20	39.54	−894.92	16.791	19.965	15.179	11.206	—
09 50 49.59	+01 18 13.63	3846639574348918528	09504959+0118135	50.80 ± 0.08	234.64	−360.55	12.633	14.176	11.432	8.951	—
09 51 09.64	−12 19 47.48	5690980582306104448	09510964−1219478	76.23 ± 0.05	1137.63	−1455.58	9.239	10.290	8.258	6.150	—
09 52 19.67	−71 32 56.92	5242285490629566592	09521968−7132568	46.80 ± 0.06	377.97	7.46	11.855	13.205	10.723	8.360	—
09 52 41.78	−15 36 13.76	5686163724944033792	09524176−1536137	56.70 ± 0.06	−118.99	−134.32	12.187	13.718	10.991	8.507	—
09 53 11.78	−03 41 24.45	3823307284773157248	09531178−0341240	62.98 ± 0.08	−103.71	−459.42	9.547	10.798	8.472	6.130	—
09 53 55.17	+20 56 46.80	628080246633611520	09535523+2056460	104.50 ± 0.12	−345.92	392.80	12.378	14.283	11.079	8.326	—
09 54 15.57	+20 25 32.92	627983081202284928	09541556+2025328	44.98 ± 0.09	36.97	−26.87	11.626	13.005	10.489	8.016	—
09 54 24.68	+06 38 45.53	3850532189108251008	09542467+0638454	40.86 ± 0.04	−270.27	61.94	11.949	13.210	10.853	8.567	—
09 56 26.96	+22 39 01.07	641821259671808896	09562699+2239015	54.49 ± 0.09	−465.09	−258.96	12.718	14.451	11.459	8.724	—
09 56 37.02	−42 34 27.79	5418335478542731136	09563699−4234273	57.94 ± 0.06	346.85	−531.63	14.221	16.261	12.889	10.210	—
09 56 45.70	+11 34 23.83	3879819059998988288	09564571+1134238	40.71 ± 0.10	−456.39	−13.86	14.299	16.144	13.006	10.241	—
09 58 34.32	−46 25 30.40	5408648849826522112	09583428−4625300	64.78 ± 0.04	479.89	−480.02	10.004	11.535	8.826	6.257	—
09 58 41.94	−53 44 47.85	5404351271207811968	09584191−5344477	46.19 ± 0.09	242.22	−198.51	15.651	18.253	14.193	10.987	—
09 59 52.16	+02 46 49.44	3836344438956110208	09595217+0246494	52.12 ± 0.12	184.31	27.96	12.825	14.354	11.633	9.133	—
10 00 30.91	−41 30 35.29	5418743844032438400	10003091−4130351	54.27 ± 0.06	−49.75	370.47	12.963	14.468	11.779	9.257	—
10 01 10.74	−30 23 24.53	5463554195989068800	10011079−3023249	62.10 ± 0.07	−1097.56	643.77	10.322	11.718	9.187	6.700	—
10 01 23.81	−38 50 24.53	5421345941377717760	10012381−3850245	47.55 ± 0.05	161.91	−207.18	10.833	12.068	9.767	7.460	—
10 02 42.45	+14 59 13.01	615779464207025152	10024246+1459127	56.49 ± 0.37	157.41	−236.42	12.748	14.455	11.494	8.803	—
10 03 19.16	−01 05 08.01	3830128624846458752	10031918−0105079	49.67 ± 0.24	−498.73	47.43	16.553	19.806	14.999	11.236	—
10 03 33.36	+05 57 48.02	3873461954734052736	10033336+0557480	42.45 ± 0.06	−564.60	−164.07	12.037	13.478	10.873	8.471	—
10 04 38.73	−33 35 09.53	5458784415381054464	10043870−3335093	53.46 ± 0.09	345.36	−345.96	12.908	14.636	11.651	9.026	—
10 04 40.30	−13 18 19.01	3765325471089276288	10044030−1318186	40.71 ± 0.66	−124.97	−196.68	19.866	21.115	18.223	13.357	—

Table 2: List of M dwarf systems within 25 pc drawn from *Gaia* DR2, as described in §2.3.

These systems have not been vetted to distinguish single stars from multiples, but in cases

where a system was resolved in *Gaia* but not 2MASS, a “J” flag is listed in column 12.

10 06 08.66	−49 49 38.26	5406897052930352512	10060866−4949380	40.39 ± 0.04	−55.98	−180.97	11.567	12.937	10.435	8.104	—
10 06 31.95	−16 53 26.31	5673602319993218560	10063197−1653266	49.83 ± 0.14	−317.43	191.48	16.176	19.159	14.659	10.992	—
10 06 57.84	+12 40 52.26	3881626244798724480	10065783+1240522	40.10 ± 0.10	−321.47	−43.85	11.149	12.293	10.117	7.916	—
10 07 09.83	−82 50 15.60	5192408069781824512	10070987−8250155	43.70 ± 0.04	−315.75	176.00	11.225	12.513	10.126	7.736	—
10 08 44.60	+02 43 56.79	3836540220745072384	10084460+0243568	41.30 ± 0.07	−82.35	−449.15	11.241	12.580	10.128	7.741	—
10 09 36.28	−17 50 27.87	5672554627146256000	10093625−1750277	46.70 ± 0.04	84.65	3.71	10.702	11.854	9.667	7.460	—
10 09 36.67	−17 48 24.85	5672555864096835840	10093664−1748248	46.73 ± 0.04	85.58	4.13	10.925	12.135	9.867	7.607	—
10 12 04.67	−02 41 05.17	3828751074215823872	10120466−0241044	86.65 ± 0.70	526.77	−600.65	9.608	10.897	8.510	6.193	—
10 12 06.49	−30 49 26.34	5461814875584141056	10120649−3049263	44.12 ± 0.12	−142.74	36.88	16.291	19.249	14.783	11.179	—
10 12 17.67	−03 44 44.39	3828238392559860992	10121768−0344441	129.79 ± 0.08	−152.93	−243.60	8.331	9.508	7.274	5.015	—
10 14 51.78	−47 09 24.19	5413438219396893568	10145184−4709244	79.25 ± 0.04	−1053.98	414.30	12.138	13.758	10.922	8.322	—
10 14 53.13	+21 23 46.02	628865130046268672	10145315+2123464	54.87 ± 0.19	−195.83	−220.69	12.882	14.719	11.596	8.881	—
10 15 53.94	+17 29 27.07	622339455521105280	10155390+1729271	71.35 ± 0.08	290.84	6.25	11.605	13.155	10.410	7.861	—
10 16 45.95	−11 57 42.40	3765772972322477696	10164599−1157412	74.23 ± 0.07	−417.59	−604.37	9.923	11.251	8.825	6.452	—
10 17 26.80	+07 19 25.89	3873864513044635648	10172680+0719260	41.14 ± 0.18	−164.97	−95.56	16.590	19.553	15.073	11.488	—
10 17 26.90	−53 54 26.46	5355751581627180288	10172689−5354265	51.00 ± 0.30	−173.10	−4.94	12.061	14.228	10.685	7.689	—
10 18 35.14	−11 43 00.24	3767281845873242112	10183516−1142599	45.46 ± 0.08	−341.41	−247.87	11.846	13.352	10.658	8.204	—
10 19 24.44	−27 07 17.08	5471876437768940416	10192447−2707171	42.85 ± 0.24	−630.24	28.43	18.196	20.934	16.578	12.471	—
10 19 51.26	−41 48 46.17	5416514034445180800	10195126−4148457	43.44 ± 0.04	−90.93	−434.53	10.748	11.896	9.716	7.489	—
10 21 32.32	−20 44 07.09	5668026421651069184	10213232−2044069	45.86 ± 0.20	−324.74	−52.28	17.700	20.695	16.097	12.068	—
10 22 24.60	−60 10 37.69	5254819339117709952	10222461−6010377	45.12 ± 0.06	346.70	−414.66	9.963	10.991	8.987	6.848	—
10 24 20.19	+11 57 20.64	3883368588478223360	10242017+1157207	51.69 ± 0.05	−24.54	176.15	11.419	12.700	10.321	8.022	—
10 25 10.84	−10 13 43.29	3767878708888402816	10251088−1013434	78.00 ± 0.10	−693.14	121.37	9.270	10.404	8.247	6.032	—
10 25 26.45	+05 12 39.01	3860610076465867520	10252645+0512391	43.54 ± 0.11	−228.15	−52.45	15.514	18.068	14.064	10.788	—
10 25 29.03	−49 54 25.73	5358900174919209984	10252904−4954258	46.88 ± 0.03	−573.94	156.64	11.670	12.880	10.603	8.412	—
10 28 07.76	−63 27 12.85	5252090488660292480	10280776−6327128	48.20 ± 0.51	58.60	443.94	20.098	21.454	18.337	13.645	—
10 28 55.55	+00 50 27.60	3855208897392952192	10285555+0050275	142.19 ± 0.05	−603.00	−732.08	8.674	9.907	7.603	5.311	—
10 30 10.50	−15 26 08.31	3749120250244516480	10301051−1526085	42.36 ± 0.09	−131.40	81.94	12.630	14.046	11.478	9.112	—
10 31 08.53	−41 27 48.91	5440359486716251904	10310854−4127490	54.43 ± 0.05	−282.63	55.07	12.187	13.636	11.021	8.610	—
10 31 12.37	−73 23 08.40	5229173470875537664	10311237−7323084	54.09 ± 0.13	39.63	−59.37	17.274	—	—	11.755	—
10 31 32.35	−53 38 01.02	5357078043648622976	10313234−5338010	45.18 ± 0.08	−420.61	207.79	15.469	17.702	14.038	10.991	—

Table 2: List of M dwarf systems within 25 pc drawn from *Gaia* DR2, as described in §2.3.

These systems have not been vetted to distinguish single stars from multiples, but in cases

where a system was resolved in *Gaia* but not 2MASS, a “J” flag is listed in column 12.

10 31 59.62	−36 49 19.74	5442306064677752832	10315965−3649198	78.97 ± 1.54	10.41	11.54	18.906	20.261	17.697	15.223	—
10 32 32.97	+06 30 07.59	3862117335108574848	10323297+0630074	51.34 ± 0.08	−232.02	−193.07	14.016	16.158	12.649	9.544	—
10 32 40.67	−52 55 05.97	5357217647259627648	10324069−5255058	41.07 ± 0.12	−489.97	214.32	15.577	17.998	14.152	11.008	—
10 35 01.12	−09 24 38.58	3762071530853756928	10350110−0924384	61.38 ± 0.08	228.33	−185.27	10.990	12.397	9.848	7.393	—
10 35 07.88	−07 32 36.04	3774703583720247552	10350789−0732357	42.10 ± 0.09	−114.45	−310.56	14.532	16.574	13.197	10.358	—
10 35 20.28	−20 58 38.31	5475243898288297088	10352029−2058382	44.15 ± 0.16	−140.93	−11.66	15.426	17.957	13.983	10.717	—
10 36 01.22	+05 07 12.80	3858896247075847680	10360120+0507128	65.38 ± 0.09	−654.07	127.13	11.365	12.943	10.160	7.598	—
10 36 08.72	+19 23 30.65	3987041475434695936	10360869+1923314	57.80 ± 0.13	228.99	−382.12	15.105	17.794	13.648	10.344	—
10 36 44.84	+15 21 39.86	3886019480945496576	10364483+1521394	50.62 ± 0.16	111.52	−79.19	12.129	13.504	10.593	7.896	—
10 37 45.31	−27 46 38.60	5468091231551021184	10374532−2746388	64.65 ± 0.08	−231.34	255.20	11.688	13.427	10.430	7.719	—
10 38 15.19	−49 33 44.52	5363990535794423680	10381517−4933446	69.10 ± 0.06	−317.61	−565.29	13.520	15.473	12.207	9.430	—
10 38 47.75	−86 32 43.93	5189170557793054848	10384782−8632441	70.36 ± 0.05	−198.17	−170.57	11.909	13.513	10.692	8.112	—
10 39 32.38	−38 20 02.52	5441169002153568512	10393240−3820020	59.09 ± 0.07	−280.47	−677.87	14.270	16.490	12.903	9.998	—
10 39 40.56	−06 55 25.50	3774789959807192064	10394061−0655255	64.19 ± 0.09	−718.37	−105.18	10.262	11.557	9.165	6.818	—
10 39 45.41	−44 30 36.97	5367095178669583360	10394540−4430368	54.35 ± 0.15	−42.94	−143.07	10.691	12.036	9.576	7.145	—
10 41 09.30	−36 53 43.67	5443030196164951168	10410932−3653436	63.98 ± 0.05	212.45	−218.65	9.259	10.211	8.162	5.993	—
10 41 44.01	−31 11 54.38	5454284595324061312	10414398−3111542	54.48 ± 0.09	350.54	−261.92	14.463	16.650	13.091	10.162	—
10 41 56.35	−82 59 23.21	5192264446075455744	10415640−8259231	48.32 ± 0.03	386.99	2.23	12.141	13.505	11.003	8.656	—
10 42 16.77	−03 23 39.94	3778200992769095808	10421676−0323396	42.69 ± 0.08	199.93	−268.02	15.170	17.339	13.818	10.991	—
10 42 37.02	−03 55 06.48	3778027269931886592	10423705−0355065	43.92 ± 0.05	−497.46	60.98	12.655	14.241	11.444	8.884	—
10 42 41.36	−24 16 04.10	5471345889049823744	10424135−2416050	96.15 ± 0.47	40.79	156.58	14.091	16.747	12.641	9.338	—
10 43 02.86	−09 12 40.92	3762231926405726720	10430293−0912410	81.40 ± 0.26	−1977.58	370.16	13.159	15.356	11.776	8.728	—
10 44 21.23	−61 12 35.26	5254061535097566848	10442131−6112384	206.82 ± 0.07	−346.43	1610.34	11.861	14.189	10.483	7.728	—
10 44 29.20	−18 38 07.18	3555173782156353536	10442927−1838063	77.27 ± 0.13	−656.31	−410.92	13.073	14.828	11.811	9.291	—
10 45 16.69	−30 48 26.96	5454500168322239872	10451668−3048268	65.27 ± 0.05	−31.40	−232.31	10.280	11.478	9.229	6.992	—
10 45 17.17	−26 07 25.12	5469802724480366848	10451718−2607249	42.40 ± 0.17	−172.35	−146.77	17.332	20.556	15.732	11.626	—
10 45 23.98	−01 49 57.77	3802665122192531712	10452400−0149576	58.66 ± 0.24	−507.70	−10.24	17.998	21.387	16.388	11.780	—
10 45 51.81	−23 09 00.50	5471516004114550784	10455184−2309001	61.22 ± 0.07	−252.73	−142.06	13.385	15.377	12.057	9.176	—
10 47 38.69	−79 27 46.03	5199087706000356096	10473868−7927458	69.79 ± 0.04	−448.19	−204.91	12.055	13.719	10.819	8.139	—
10 48 12.61	−11 20 09.61	3757613049856225792	10481258−1120082	219.12 ± 0.16	579.03	−1530.17	12.849	15.960	11.358	7.926	—
10 48 14.57	−39 56 06.84	5393446658454453632	10481463−3956062	247.22 ± 0.12	−1179.18	−988.10	14.020	17.630	12.432	8.447	—

Table 2: List of M dwarf systems within 25 pc drawn from *Gaia* DR2, as described in §2.3.

These systems have not been vetted to distinguish single stars from multiples, but in cases

where a system was resolved in *Gaia* but not 2MASS, a “J” flag is listed in column 12.

10 48 32.58	+19 09 02.04	3986412584848128000	10483255+1909022	43.26 ± 0.06	233.78	−106.78	12.290	13.732	11.123	8.677	—
10 48 42.81	+01 11 58.22	3808159454810609280	10484281+0111580	66.46 ± 0.21	−440.01	−231.47	17.703	20.915	16.090	11.623	—
10 48 56.03	+22 53 24.04	3989925872391445888	10485609+2253239	52.11 ± 0.09	−472.10	81.83	12.916	—	—	9.202	—
10 49 09.71	−01 08 12.29	3803094829375222144	10490970−0108122	44.20 ± 0.10	−9.43	−17.75	14.466	16.491	13.139	10.224	—
10 50 52.03	+06 48 29.26	3864615459886222464	10505201+0648292	143.50 ± 0.06	−856.29	−818.84	10.279	11.937	9.063	6.371	—
10 51 37.55	−48 41 52.05	5362775747244035968	10513760−4841523	45.20 ± 0.08	−913.76	442.69	15.133	17.453	13.739	10.687	—
10 52 04.24	+13 59 51.30	3873066031380105216	10520440+1359509	75.46 ± 0.06	−1124.73	199.02	11.475	12.983	10.290	7.795	—
10 52 14.25	+05 55 09.83	3864228496219589120	10521423+0555098	71.78 ± 0.09	−695.41	−60.60	13.098	15.073	11.773	8.941	—
10 54 11.06	−85 05 02.33	5190838276414527872	10541102−8505023	53.70 ± 0.12	−427.68	285.07	17.153	—	—	11.654	—
10 54 27.88	−54 31 32.41	5353308264949689728	10542786−5431322	40.81 ± 0.11	−149.65	178.44	16.456	19.341	14.940	11.289	—
10 54 41.96	−07 18 33.44	3763681215875388288	10544197−0718326	49.55 ± 0.66	−173.15	−371.88	12.230	13.532	10.647	7.970	—
10 55 05.56	+05 59 43.21	3864311616720496640	10550557+0559430	48.96 ± 0.09	−3.52	44.17	11.791	13.267	10.614	8.114	—
10 55 15.31	−73 56 09.02	5225863906515477376	10551532−7356091	72.97 ± 0.57	160.96	−221.63	14.738	17.862	13.225	9.666	—
10 55 26.62	−02 49 42.81	3801886118203373184	10552660−0249428	40.27 ± 0.07	109.52	17.32	12.528	14.050	11.333	8.845	—
10 55 34.47	−09 21 25.92	3759774208680370688	10553448−0921262	51.96 ± 0.06	−266.67	448.76	12.296	13.840	11.097	8.609	—
10 55 47.34	+08 08 42.93	3865934633321490048	10554733+0808427	53.34 ± 0.15	−329.78	−138.18	17.089	20.309	15.502	11.368	—
10 56 38.91	−15 52 53.51	3557461767066965248	10563892−1552540	56.47 ± 0.05	79.96	−453.16	10.730	12.074	9.617	7.226	—
10 58 05.31	−55 25 17.56	5353126879893514368	10580531−5525176	50.63 ± 0.26	20.53	0.32	13.851	16.011	12.485	9.577	—
10 58 27.99	−10 46 30.50	3758629475341196672	10582800−1046304	69.15 ± 0.08	−192.77	−83.86	12.768	14.672	11.467	8.640	—
10 58 34.22	−05 54 09.21	3787904732640409216	10583421−0554090	40.44 ± 0.06	52.26	−238.05	12.010	13.472	10.838	8.330	—
10 58 35.09	−31 08 38.20	5452743423618768000	10583513−3108382	49.04 ± 0.08	−566.86	−91.37	10.923	12.193	9.842	7.470	—
11 00 04.26	+22 49 58.65	3988987164339438208	11000432+2249592	148.13 ± 0.06	−426.92	−282.41	8.970	10.300	7.859	5.495	—
11 00 50.43	+12 04 10.71	3871653498240785280	11005043+1204108	46.35 ± 0.17	135.83	−126.31	14.047	16.169	12.689	9.782	—
11 02 38.34	+21 58 01.70	3988689609004982912	11023832+2158017	83.78 ± 0.06	142.85	−51.96	8.807	9.847	7.832	5.688	—
11 03 21.26	+13 37 57.02	3968118399284369280	11032125+1337571	65.59 ± 0.10	−192.36	76.62	11.673	13.273	10.454	7.914	—
11 03 25.37	−09 51 10.41	3758803507415614080	11032537−0951102	40.02 ± 0.11	128.49	−187.10	12.564	14.053	11.380	8.906	—
11 03 54.10	+24 17 47.63	3995235242243230208	11035418+2417483	44.57 ± 0.10	−532.04	−409.39	14.972	17.263	13.583	10.502	—
11 04 01.28	+19 59 21.71	3985153334796556928	11040127+1959217	55.92 ± 0.44	54.95	121.95	19.608	21.861	17.939	12.950	—
11 04 33.79	−62 32 34.47	5241011156681563136	11043379−6232344	60.28 ± 0.06	−223.55	−56.61	13.511	15.456	12.182	9.357	—
11 05 06.86	−22 12 52.31	3539057213728669184	11050685−2212520	60.06 ± 0.07	−65.46	−347.46	14.095	16.284	12.731	9.820	—
11 05 39.83	−52 47 17.27	5347825378410235264	11053986−5247173	46.47 ± 0.04	−473.34	168.61	12.542	14.104	11.338	8.809	—

Table 2: List of M dwarf systems within 25 pc drawn from *Gaia* DR2, as described in §2.3.

These systems have not been vetted to distinguish single stars from multiples, but in cases

where a system was resolved in *Gaia* but not 2MASS, a “J” flag is listed in column 12.

11 05 43.14	+10 14 09.40	3868080055385587840	11054316+1014093	55.91 ± 0.04	609.51	−703.29	11.279	12.632	10.149	7.797	—
11 06 18.97	+04 28 32.67	3815413929451499904	11061897+0428327	46.89 ± 0.16	−349.44	372.21	16.470	19.429	14.926	11.332	—
11 07 27.70	−19 17 29.36	3552000252294347392	11072772−1917293	53.40 ± 0.05	−235.02	−45.99	9.641	10.626	8.689	6.620	—
11 08 06.54	−05 13 47.14	3788190605663811840	11080654−0513468	40.06 ± 0.05	−54.87	−439.68	11.476	12.825	10.346	7.933	—
11 09 12.24	−04 36 25.10	3788517916531415552	11091225−0436249	41.22 ± 0.05	−333.88	−107.99	10.433	11.467	9.458	7.330	—
11 09 31.35	−24 35 55.12	3536123338748976256	11093138−2435548	92.78 ± 0.05	−797.37	−446.77	9.462	10.697	8.389	6.097	—
11 09 53.27	−24 14 59.52	3536327366875661056	11095327−2414594	57.05 ± 0.09	44.33	100.63	13.449	15.385	12.130	9.260	—
11 10 00.49	−74 36 15.18	5225957639881367552	11100048−7436151	44.84 ± 0.03	−587.08	398.89	12.231	13.850	11.004	8.353	—
11 11 47.04	−56 20 23.18	5340857086040057728	11114705−5620234	47.35 ± 0.03	−92.86	−295.50	10.895	12.086	9.843	7.609	—
11 11 48.24	+14 56 26.32	3968512574202866560	11114824+1456264	46.11 ± 0.07	−104.15	−94.87	13.287	15.056	12.014	9.220	—
11 12 38.97	+18 56 05.44	3972130276695660288	11123898+1856054	59.94 ± 0.05	−21.02	6.52	9.878	11.035	8.852	6.579	—
11 13 00.58	+10 25 05.77	3963458767789502336	11130059+1025059	45.16 ± 0.08	120.91	−138.83	13.058	14.745	11.811	9.199	—
11 13 01.46	+12 54 39.67	3965148618378008832	11130142+1254401	47.18 ± 0.05	508.60	−274.38	13.335	14.963	12.101	9.558	—
11 14 38.09	−27 32 28.75	3531371829316077568	11143809−2732287	45.13 ± 0.09	−63.07	−74.73	10.681	11.912	9.609	7.303	—
11 15 12.41	+19 27 11.93	3978179338700027008	11151240+1927124	53.73 ± 0.05	182.79	−478.99	11.706	13.190	10.532	8.086	—
11 15 15.51	−18 07 35.94	3558266708748472960	11151549−1807347	43.58 ± 0.06	141.65	−740.03	12.436	13.911	11.255	8.763	—
11 15 50.35	−67 31 33.14	5235273458327588224	11155037−6731332	57.53 ± 0.09	534.69	−227.09	16.407	19.698	14.839	10.964	—
11 16 00.20	−57 32 51.57	5339892367683264384	11160018−5732513	78.94 ± 0.04	−2468.48	1183.91	10.477	11.856	9.348	7.035	—
11 16 05.08	+08 00 12.40	3818557673713011712	11160506+0800123	42.63 ± 0.05	−758.47	−69.93	11.858	13.034	10.799	8.635	—
11 16 36.66	−44 07 49.59	5376651377824140288	11163668−4407495	45.42 ± 0.04	−529.24	−22.68	12.773	14.322	11.567	9.050	—
11 16 37.63	−27 57 19.24	3531294008802299392	11163766−2757186	71.10 ± 0.05	−485.93	−802.46	12.301	13.905	11.081	8.621	—
11 17 06.46	−11 22 25.31	3566338949070993536	11170644−1122251	50.02 ± 0.07	−390.13	−149.07	12.467	14.019	11.261	8.725	—
11 17 29.31	−32 02 09.83	5403804848261260288	11172930−3202095	48.57 ± 0.06	−191.37	−406.35	13.277	14.885	12.050	9.477	—
11 18 20.31	+13 47 39.04	3966634844566024960	11182030+1347392	40.16 ± 0.06	85.24	−48.16	11.897	13.319	10.730	8.258	—
11 19 48.16	−16 32 37.97	3558854607781867392	11194820−1632381	41.90 ± 0.08	−355.74	58.93	14.016	16.042	12.670	9.786	—
11 20 06.10	−10 29 46.73	3590516110254931328	11200609−1029468	52.89 ± 0.05	−197.85	19.73	10.296	11.488	9.240	6.967	—
11 20 46.54	−19 39 07.26	3545594119594716160	11204657−1939069	44.59 ± 0.09	−354.01	−164.92	11.766	13.152	10.623	8.209	—
11 21 18.14	−55 49 17.76	5346007675222666752	11211814−5549177	45.00 ± 0.04	−18.36	−21.27	12.470	13.975	11.281	8.782	—
11 21 38.50	+06 08 26.01	3814369840081992448	11213847+0608256	50.24 ± 0.07	−766.29	−1582.79	12.463	13.856	11.314	8.969	—
11 21 49.17	−13 13 08.73	3562157781229213312	11214924−1313084	69.49 ± 0.18	−472.25	−46.26	16.417	19.620	14.824	10.735	—
11 22 12.22	−11 32 16.07	3565623270081275264	11221219−1132159	41.42 ± 0.09	−323.50	−20.93	15.062	17.348	13.678	10.587	—

Table 2: List of M dwarf systems within 25 pc drawn from *Gaia* DR2, as described in §2.3.

These systems have not been vetted to distinguish single stars from multiples, but in cases

where a system was resolved in *Gaia* but not 2MASS, a “J” flag is listed in column 12.

11	22	42.55	−32	05	40.38	5403099064875400064	11224253−3205398	47.59 ± 0.10	57.09	−604.42	14.462	16.604	13.098	10.167	−
11	23	19.64	−05	09	04.79	3786550031235785344	11231964−0509045	46.75 ± 0.12	−27.36	−161.29	15.590	18.279	14.125	10.836	−
11	23	44.57	+08	33	48.55	3914019231742221568	11234456+0833483	49.63 ± 0.04	−1003.31	192.86	10.326	11.430	9.318	7.161	−
11	23	57.30	−18	21	48.75	3546332682170832128	11235737−1821485	55.62 ± 0.08	−611.06	−45.94	11.903	13.348	10.745	8.322	−
11	24	08.16	−28	40	34.11	3483307365699695232	11240816−2840340	40.72 ± 0.07	18.65	−53.45	12.087	13.477	10.937	8.561	−
11	24	23.24	−39	00	43.07	5396029063372913664	11242323−3900429	44.87 ± 0.07	22.66	−183.38	12.952	14.583	11.723	9.096	−
11	24	39.08	−42	13	11.43	5383082833650178816	11243908−4213114	49.34 ± 0.08	−144.96	−89.36	15.486	18.247	14.022	10.924	−
11	24	53.27	+13	22	52.90	3965764619767224832	11245327+1322533	52.69 ± 0.11	−26.09	−106.03	14.515	16.746	13.135	10.070	−
11	24	58.77	+02	28	24.50	3810811579936440960	11245875+0228244	42.51 ± 0.04	−232.51	146.56	10.944	12.004	9.961	7.741	−
11	25	28.55	−19	01	53.14	3546047977378251008	11252854−1901528	46.37 ± 0.10	142.49	−162.58	13.926	15.825	12.616	9.789	−
11	25	37.28	−38	34	43.04	5396067550577971072	11253730−3834428	49.29 ± 0.05	−563.42	−171.96	13.156	14.846	11.904	9.187	−
11	28	56.26	+10	10	39.25	3915363693944242304	11285624+1010395	78.09 ± 0.14	−750.05	557.73	11.338	12.878	10.151	7.671	−
11	30	41.83	−08	05	42.99	3592769731134725248	11304179−0805425	74.39 ± 0.07	−353.49	257.45	10.809	12.285	9.658	7.152	−
11	31	08.39	−14	57	21.25	3560746351897773952	11310835−1457201	87.07 ± 0.10	405.47	−1374.55	12.573	14.465	11.270	8.497	−
11	31	43.39	+22	40	01.70	3980560507224374400	11314339+2240016	63.19 ± 0.05	−584.59	32.85	9.467	10.541	8.472	6.322	−
11	31	46.51	−41	02	47.17	5382868669400908928	11314655−4102473	93.07 ± 0.08	−717.39	170.89	10.233	11.753	9.063	6.511	−
11	32	08.49	−13	19	22.25	3561220000891316736	11320850−1319223	48.45 ± 0.08	−127.48	42.11	14.173	16.128	12.853	10.040	−
11	32	19.00	−16	58	07.34	3547944531854903168	11321898−1658071	43.14 ± 0.04	167.52	−233.06	10.621	11.711	9.609	7.470	−
11	32	22.30	−46	27	56.66	5375247610713364736	11322232−4627567	46.37 ± 0.05	−387.94	95.34	11.152	12.475	10.061	7.702	−
11	32	23.01	+18	16	22.33	3974240961063678976	11322300+1816223	48.78 ± 0.07	138.13	62.51	13.257	14.978	11.993	9.338	−
11	34	02.68	+01	25	33.51	3799191837974913920	11340266+0125335	40.59 ± 0.06	−295.39	141.62	14.498	16.241	13.230	10.638	−
11	34	13.46	−74	28	45.43	5225268520968623744	11341347−7428453	44.55 ± 0.03	279.66	−33.42	11.461	12.642	10.405	8.197	−
11	34	37.96	−23	52	15.15	3540112504374165888	11343803−2352146	54.73 ± 0.05	−608.26	−295.33	10.352	11.406	9.361	7.256	−
11	34	54.93	+00	22	54.12	3797370909280252160	11345493+0022541	40.84 ± 0.20	393.17	−329.38	17.314	20.310	15.726	11.672	−
11	34	56.70	+18	17	07.83	3974251440784390016	11345670+1817081	42.59 ± 0.07	−42.08	−369.09	13.739	15.540	12.456	9.703	−
11	34	59.70	−74	36	09.14	5225219214743975552	11345970−7436090	53.51 ± 0.04	162.84	377.30	10.203	11.316	9.194	7.014	−
11	35	07.34	−05	39	23.07	3593710810008880768	11350732−0539219	54.74 ± 0.06	300.28	−948.19	13.367	15.173	12.086	9.355	−
11	35	26.95	−32	32	23.88	3478160727866058368	11352695−3232232	110.29 ± 0.04	−70.77	−850.68	8.891	10.060	7.845	5.623	−
11	36	40.97	−07	55	12.00	3592116483788799744	11364099−0755121	41.86 ± 0.10	−179.50	133.95	15.764	17.324	14.461	11.276	−
11	37	16.60	−03	17	36.66	3792473718850041216	11371665−0317359	46.71 ± 0.07	−809.85	−746.76	14.014	15.895	12.715	10.088	−
11	38	16.77	−77	21	48.58	5224460173763882496	11381671−7721484	119.25 ± 0.07	−2063.92	616.17	12.836	15.073	11.468	8.521	−

Table 2: List of M dwarf systems within 25 pc drawn from *Gaia* DR2, as described in §2.3.

These systems have not been vetted to distinguish single stars from multiples, but in cases

where a system was resolved in *Gaia* but not 2MASS, a “J” flag is listed in column 12.

11 38 24.96	−41 22 32.51	5384065896210582528	11382500−4122325	65.26 ± 0.06	−949.98	60.11	12.364	13.994	11.141	8.543	—
11 38 30.10	−34 55 35.60	3476835610197278208	11383010−3455356	48.24 ± 0.05	−55.84	129.18	12.207	13.523	11.088	8.778	—
11 39 11.07	+08 41 12.23	3911082878569883264	11391107+0841121	43.15 ± 0.19	72.24	−28.88	17.318	—	—	11.836	—
11 41 21.52	−36 24 34.56	3464485826872541440	11412152−3624346	115.20 ± 0.08	485.06	311.69	11.580	13.376	10.319	7.699	—
11 42 01.73	+14 46 36.30	3924206653650135168	11420176+1446357	40.62 ± 0.05	−272.15	226.12	11.559	12.922	10.427	7.959	—
11 42 13.05	−01 21 54.24	3793898479761174656	11421305−0121544	50.14 ± 0.07	−110.79	−18.28	11.503	12.864	10.382	7.968	—
11 42 29.94	−64 40 33.93	5332656412938844288	11422993−6440339	48.95 ± 0.07	−156.12	−134.83	13.585	15.447	12.287	9.481	—
11 43 19.82	−51 50 25.93	5369480397355535872	11431977−5150255	90.80 ± 0.04	654.54	−539.65	9.503	10.619	8.485	6.320	—
11 43 49.37	−51 35 08.77	5369584885317537408	11434939−5135087	43.82 ± 0.04	−347.62	−140.09	11.790	13.150	10.657	8.222	—
11 44 24.88	−43 02 53.45	5379241586700315904	11442489−4302535	41.00 ± 0.10	−295.89	133.40	16.020	18.784	14.550	11.197	—
11 45 34.44	−20 21 12.43	3542490095189596544	11453443−2021124	51.80 ± 0.10	162.21	66.19	10.813	12.054	9.742	7.444	—
11 45 35.40	−40 55 58.49	5381146215717550336	11453539−4055585	63.09 ± 0.07	−289.11	−130.17	12.739	14.478	11.480	8.790	—
11 46 03.48	−48 41 37.70	5371815897485266944	11460347−4841374	41.96 ± 0.05	61.20	−257.59	13.841	15.572	12.579	9.951	—
11 46 42.91	−14 00 51.78	3573119564265842432	11464282−1400504	51.59 ± 0.06	710.88	−786.44	10.607	11.953	9.486	7.069	—
11 47 22.13	−54 24 39.79	5344443383724940416	11472212−5424398	40.02 ± 0.26	−158.58	−155.89	15.960	18.582	14.497	11.018	—
11 47 37.61	+05 01 10.79	3897324590782822528	11473762+0501106	43.23 ± 0.79	64.93	43.50	11.577	12.645	9.974	7.381	—
11 47 40.75	+00 15 20.10	3795993633527490560	11474074+0015201	53.19 ± 0.07	−314.20	−100.91	11.980	13.628	10.748	8.098	—
11 47 44.40	+00 48 16.40	3796072592206250624	11474440+0048164	296.31 ± 0.07	607.68	−1223.32	9.591	11.388	8.345	5.654	—
11 47 52.48	−55 04 11.91	5344026286547761664	11475249−5504119	53.46 ± 0.04	41.02	187.88	12.480	13.972	11.294	8.811	—
11 48 25.92	−38 09 27.85	3463299110228918272	11482591−3809278	44.03 ± 0.09	9.80	49.78	14.636	16.815	13.262	10.180	—
11 48 35.48	+07 41 40.60	3911410464311357568	11483548+0741403	48.30 ± 0.07	136.54	−174.37	12.371	13.935	11.161	8.600	—
11 48 54.27	−25 44 40.53	3490715741903588992	11485427−2544404	40.17 ± 0.22	114.65	63.22	17.998	20.554	16.385	12.169	—
11 49 21.37	−67 18 42.74	5235714289453482240	11492134−6718427	45.99 ± 0.04	−216.01	−212.26	11.130	12.461	10.020	7.649	—
11 51 17.95	+18 29 22.91	3974692997781566080	11511794+1829229	40.46 ± 0.08	106.80	−79.98	12.254	13.624	11.109	8.747	—
11 51 55.30	−01 31 32.22	3794437034301022720	11515529−0131319	57.22 ± 0.10	142.27	−159.59	13.887	15.890	12.552	9.643	—
11 52 04.76	−76 31 05.76	5224385269534134912	11520475−7631056	41.40 ± 0.05	−179.21	11.24	13.933	15.619	12.683	10.121	—
11 52 57.92	+24 28 45.61	4004586348119642240	11525791+2428454	59.57 ± 0.10	−315.88	79.54	13.062	14.857	11.786	9.016	—
11 53 08.19	−01 07 14.62	3794485653330841984	11530818−0107145	44.55 ± 0.13	−6.58	−87.63	13.825	15.479	12.584	10.004	—
11 53 12.43	−31 23 56.11	3479221035031532416	11531249−3123560	65.21 ± 0.06	−1137.73	−138.37	12.285	13.920	11.049	8.555	—
11 53 16.09	−07 22 27.65	3595317540095019520	11531609−0722273	51.40 ± 0.06	−166.61	−507.89	10.843	12.115	9.756	7.445	—
11 53 52.68	+06 59 56.26	3899128064731508736	11535267+0659561	67.18 ± 0.15	314.70	−894.43	15.296	18.260	13.785	10.262	—

Table 2: List of M dwarf systems within 25 pc drawn from *Gaia* DR2, as described in §2.3.

These systems have not been vetted to distinguish single stars from multiples, but in cases

where a system was resolved in *Gaia* but not 2MASS, a “J” flag is listed in column 12.

11 54 07.89	+09 48 22.81	3912369208386557440	11540788+0948227	86.74 ± 0.08	85.04	−801.58	11.526	13.062	10.342	7.872	—
11 54 56.93	−02 06 09.19	3602189792709909504	11545693−0206091	40.67 ± 0.06	−95.26	49.79	12.239	13.637	11.085	8.685	—
11 55 39.54	−37 27 35.51	3460806448649173504	11553952−3727350	84.57 ± 0.19	43.08	−790.91	17.647	20.852	16.044	11.462	—
11 55 42.85	−22 24 58.79	3493736924979792768	11554286−2224586	91.60 ± 0.15	−374.02	−187.49	15.122	18.400	13.579	9.881	—
11 55 44.28	−18 54 31.61	3543109704351294848	11554425−1854316	41.99 ± 0.08	522.82	−312.60	12.915	14.517	11.688	9.092	—
11 55 49.16	−38 16 49.32	3460347849221303296	11554911−3816491	43.67 ± 0.05	624.09	−296.01	11.111	12.213	10.104	7.945	—
11 57 45.55	−01 49 02.70	3602406744394215936	11574552−0149023	50.14 ± 0.11	396.67	−217.82	14.248	16.280	12.910	10.024	—
11 58 59.42	−19 00 42.57	3566923923617986560	11585941−1900423	40.26 ± 0.14	43.01	−118.39	15.258	17.494	13.874	10.930	—
11 59 25.88	−36 34 49.69	3460907947316392704	11592585−3634495	50.45 ± 0.27	78.84	−140.94	17.359	20.247	15.678	11.305	—
11 59 27.36	−52 47 18.91	5368479017141170304	11592743−5247188	105.59 ± 0.13	−1068.13	−129.35	16.032	19.526	14.422	10.322	—
11 59 37.66	−42 56 39.06	5380149023092265856	11593765−4256391	50.25 ± 0.06	−403.80	−460.63	12.230	13.603	11.087	8.721	—
11 59 59.05	+21 05 02.84	3999645142864600320	11595905+2105029	49.45 ± 0.12	−119.13	−213.32	14.880	17.186	13.492	10.641	—
12 00 22.89	−49 31 11.73	6130529910504105600	12002292−4931136	48.24 ± 0.16	−373.97	96.22	12.883	14.616	11.564	7.871	—
12 00 22.91	−49 31 14.20	6130529910504105216	12002292−4931136	47.39 ± 0.06	−372.34	95.54	11.827	13.195	10.682	7.871	—
12 00 32.90	+20 48 51.38	3999432971480096640	12003292+2048513	40.62 ± 0.16	−130.13	235.46	17.103	20.368	15.537	11.861	—
12 00 44.73	+20 50 49.82	3999433452516434560	12004474+2050497	40.59 ± 0.05	−129.50	235.95	11.625	12.871	10.551	8.296	—
12 01 40.78	−12 13 53.92	3574523370032644992	12014079−1213537	40.30 ± 0.11	−55.77	−231.15	11.276	12.616	10.201	7.871	—
12 01 42.08	−27 37 46.29	3486653767994941952	12014211−2737458	41.67 ± 0.12	−273.40	−171.53	15.945	18.760	14.469	11.231	—
12 03 28.06	−29 22 59.47	3473913108288671488	12032808−2922599	43.12 ± 0.07	−237.91	216.91	13.866	15.684	12.578	9.813	—
12 03 58.13	+00 15 50.11	3698979462002285824	12035812+0015500	67.24 ± 0.56	−1217.63	−282.62	19.159	20.445	17.456	12.476	—
12 03 58.27	−33 01 26.54	3466404092409078272	12035831−3301265	52.53 ± 0.09	−764.17	54.56	12.570	14.276	11.314	8.744	—
12 04 12.57	+05 14 12.88	3894986960344055680	12041256+0514128	45.85 ± 0.12	−190.00	−149.60	13.605	15.676	12.252	9.317	—
12 04 15.53	−40 37 52.55	6149067058064798208	12041550−4037521	48.60 ± 0.05	321.44	−590.34	12.328	13.754	11.164	8.747	—
12 05 46.63	−18 49 32.12	3518918112077486720	12054662−1849315	43.65 ± 0.08	−17.10	−316.73	14.504	16.507	13.170	10.317	—
12 06 24.96	+00 16 02.45	3699014096618129792	12062495+0016025	40.92 ± 0.57	21.04	−130.38	13.468	15.272	12.183	9.475	—
12 06 39.11	−44 27 53.59	6144529373579791488	12063910−4427535	60.97 ± 0.07	199.85	−297.14	11.528	13.058	10.344	7.825	—
12 06 58.53	−35 00 52.05	3462607925435602560	12065853−3500518	40.45 ± 0.21	−314.44	−273.05	13.202	14.943	11.898	9.127	—
12 08 18.25	−21 01 05.35	3517619520125627904	12081824−2101049	54.88 ± 0.10	34.81	−271.90	14.567	16.790	13.188	10.231	—
12 08 43.76	−11 33 45.14	3574445407785255296	12084374−1133446	56.85 ± 0.12	247.59	−329.41	14.449	16.713	13.065	10.175	—
12 09 23.61	−38 15 42.57	3459586677937737088	12092361−3815424	56.17 ± 0.06	−137.56	−211.03	13.470	15.316	12.181	9.453	—
12 09 46.96	−32 13 21.73	3472352592050451968	12094695−3213217	46.92 ± 0.06	−191.75	1.98	13.694	15.471	12.418	9.731	—

Table 2: List of M dwarf systems within 25 pc drawn from *Gaia* DR2, as described in §2.3.

These systems have not been vetted to distinguish single stars from multiples, but in cases

where a system was resolved in *Gaia* but not 2MASS, a “J” flag is listed in column 12.

12 09 58.17	−46 11 32.23	6143175943486753152	12095813−4611323	50.58 ± 0.06	−384.49	−79.70	12.009	13.516	10.822	8.298	−
12 10 04.45	+12 44 09.93	3920481233377933824	12100445+1244101	61.66 ± 0.09	−34.27	−31.93	13.451	15.279	12.166	9.449	−
12 10 05.60	−15 04 16.96	3569610404187997696	12100559−1504156	81.55 ± 0.10	−56.24	−713.34	10.735	12.357	9.525	6.863	−
12 10 11.58	−31 58 23.54	3472374376124622336	12101156−3158235	46.89 ± 0.07	−596.81	−105.23	14.506	16.632	13.151	10.216	−
12 10 28.38	−13 10 24.03	3571124882669324800	12102834−1310234	45.45 ± 0.08	246.65	−343.83	12.315	14.034	11.062	8.412	−
12 10 42.18	−22 13 09.15	3490286416972291584	12104215−2213094	52.75 ± 0.08	157.83	245.67	12.009	13.424	10.848	8.370	−
12 11 11.76	−19 57 38.07	3517841209157902720	12111179−1957376	78.35 ± 0.06	−213.09	−184.36	10.580	11.965	9.447	7.044	−
12 11 16.95	−19 58 21.71	3517841140438425600	12111697−1958213	78.52 ± 0.11	−205.35	−188.22	11.398	12.919	10.232	7.743	−
12 13 03.34	−04 32 43.74	3597096309389074816	12130336−0432437	59.48 ± 1.02	−368.11	−34.60	19.884	20.936	18.132	13.014	−
12 13 32.91	−25 55 24.62	3488261563231724032	12133287−2555240	44.11 ± 0.04	267.87	−342.83	10.656	11.713	9.664	7.547	−
12 14 08.68	−23 45 16.91	3489874340631095936	12140866−2345172	92.80 ± 0.08	44.15	84.41	12.303	14.185	11.001	8.234	−
12 14 16.55	+00 37 26.37	3698534434669937024	12141654+0037263	123.77 ± 0.11	−951.93	−284.29	11.839	13.885	10.502	7.540	−
12 14 39.99	−46 03 14.29	6143501502007380608	12144002−4603141	63.89 ± 0.09	−735.27	−243.31	13.796	15.932	12.437	9.441	−
12 16 51.86	+02 58 04.88	3701290326205270784	12165190+0258046	42.75 ± 0.08	−651.20	258.20	12.088	13.534	10.901	8.422	−
12 18 34.87	−06 25 23.22	3584226658929871232	12183488−0625232	51.06 ± 0.10	−378.80	−42.28	12.415	13.930	11.223	8.710	−
12 18 41.88	−06 09 12.37	3584656640992625280	12184187−0609123	44.14 ± 0.09	102.60	−34.43	13.232	14.988	11.957	9.280	−
12 18 59.40	+11 07 33.77	3907283967108054528	12185939+1107338	154.51 ± 0.11	−1269.93	203.62	11.937	14.121	10.573	7.570	−
12 20 05.10	−18 12 59.49	3519902656020508288	12200512−1812596	42.50 ± 0.34	−223.42	42.95	13.853	15.808	12.522	9.623	−
12 20 33.68	−82 25 57.54	5783027130236367744	12203376−8225577	81.75 ± 0.61	14.88	244.93	10.633	12.241	9.425	6.842	−
12 21 27.71	+02 57 19.77	3701479918946381184	12212770+0257198	53.95 ± 0.25	−145.35	−43.50	17.860	20.923	16.227	11.953	−
12 21 29.06	−50 04 08.78	6126746594071444480	12212906−5004086	40.06 ± 0.07	−110.44	32.29	13.134	14.797	11.890	9.235	−
12 22 03.99	−06 29 12.66	3584388909910567680	12220398−0629123	42.51 ± 0.08	55.21	−333.61	14.226	16.146	12.912	10.118	−
12 22 06.71	−78 38 27.41	5788368866963535104	12220676−7838272	48.24 ± 0.04	−392.45	−175.44	10.990	12.340	9.874	7.481	−
12 23 01.43	−46 37 08.43	6131272458806020736	12230147−4637082	63.13 ± 0.07	−752.50	−346.60	12.169	13.849	10.926	8.362	−
12 23 38.59	−46 06 20.30	6131349562059299712	12233860−4606203	43.63 ± 0.05	−232.78	−12.79	12.437	14.005	11.224	8.702	−
12 23 52.08	−08 58 43.50	3582675080520660992	12235208−0858432	52.26 ± 0.12	−231.61	−275.78	15.702	18.527	14.225	10.955	−
12 23 56.19	−27 57 46.50	3474993275382942208	12235633−2757468	47.57 ± 0.13	−1257.98	308.27	15.803	18.698	14.331	11.069	−
12 24 39.80	−82 05 53.22	5783786274295781760	12243981−8205532	44.28 ± 0.05	−23.44	−264.83	13.747	15.504	12.472	9.812	−
12 24 52.19	−12 38 35.71	3576327737332306688	12245222−1238352	58.11 ± 0.19	−304.58	−188.97	17.113	19.685	15.519	11.353	−
12 24 52.50	−18 14 32.25	3519785523672576384	12245243−1814303	112.74 ± 0.07	1095.88	−2309.28	10.280	11.557	9.194	6.950	−
12 25 01.03	+23 23 17.13	3953845192168088576	12250105+2323175	45.47 ± 0.08	−130.49	−304.60	14.754	16.828	13.413	10.619	−

Table 2: List of M dwarf systems within 25 pc drawn from *Gaia* DR2, as described in §2.3.

These systems have not been vetted to distinguish single stars from multiples, but in cases

where a system was resolved in *Gaia* but not 2MASS, a “J” flag is listed in column 12.

12 25 32.03	-15 59 41.82	3521407509481957120	12253211-1559418	77.25 ± 0.12	-817.52	33.93	13.355	15.483	11.990	8.998	-
12 27 29.25	-67 16 16.93	5859826196420495616	12272924-6716168	46.27 ± 0.04	-45.47	-0.88	11.474	12.721	10.396	8.141	-
12 27 43.56	-43 32 49.61	6145487494885361408	12274356-4332495	43.25 ± 0.06	-22.16	-54.41	13.375	15.050	12.126	9.511	-
12 27 44.70	-03 15 00.81	3693536394118295808	12274471-0315006	40.50 ± 0.06	-293.82	-29.42	11.770	13.098	10.484	7.852	-
12 28 39.98	-71 27 51.49	5843144887000900736	12283989-7127503	46.66 ± 0.03	-446.17	1095.84	12.526	13.946	11.367	9.051	-
12 28 43.05	-71 27 56.46	5843144887000900992	12284295-7127553	46.81 ± 0.04	-447.41	1093.67	14.069	15.891	12.787	10.181	-
12 28 53.16	-10 39 48.64	3578493912677730048	12285316-1039488	51.47 ± 0.06	-279.44	3.53	10.643	11.869	9.565	6.857	-
12 28 57.60	+08 25 31.10	3902745286187581312	12285759+0825316	68.62 ± 0.89	-649.47	-240.22	10.757	12.339	9.550	6.956	-
12 29 27.12	+22 59 46.73	3953011178238339584	12292712+2259467	44.07 ± 0.07	-172.38	-22.45	12.809	14.442	11.581	9.003	-
12 29 34.54	-55 59 37.05	6072726969332631552	12293453-5559371	76.48 ± 0.06	-902.48	-811.07	11.872	13.545	10.638	8.065	-
12 29 45.31	+07 52 37.79	3901165013100805248	12294530+0752379	48.14 ± 0.16	-442.02	63.59	15.842	18.570	14.377	11.090	-
12 29 54.18	-05 27 24.36	3680612219043341824	12295422-0527241	47.12 ± 0.09	-570.08	-304.43	11.752	13.332	10.545	7.962	-
12 29 54.65	-05 27 20.51	3680612223338027392	12295469-0527203	47.15 ± 0.09	-560.82	-293.85	12.845	14.501	11.601	8.924	-
12 30 01.73	-34 11 24.11	6158476403698590464	12300177-3411238	49.99 ± 0.30	-420.98	-279.42	12.566	14.421	11.268	8.439	-
12 30 15.92	-31 24 04.74	3470386321662727040	12301592-3124048	46.84 ± 0.12	-117.11	-13.66	15.076	17.515	13.646	10.391	-
12 31 15.80	+08 48 38.19	3902785109124370432	12311578+0848380	73.76 ± 0.41	-632.47	-523.76	8.951	9.930	8.000	5.892	-
12 31 16.21	-15 29 49.75	3526709869947149440	12311620-1529495	46.59 ± 0.07	33.48	-113.79	14.250	16.223	12.930	10.096	-
12 32 17.75	-68 56 00.70	5856405272135505024	12321772-6856005	47.42 ± 0.12	-216.04	-100.04	16.964	20.445	15.364	11.318	-
12 32 26.32	+20 23 27.57	3949199167129128832	12322631+2023274	43.68 ± 0.07	42.59	25.33	11.815	13.231	10.663	8.213	-
12 32 32.17	-26 10 14.28	3499614570544095232	12323218-2610144	43.71 ± 0.06	721.54	-683.29	12.429	13.787	11.287	9.020	-
12 32 44.45	-15 30 54.73	3526665614604204160	12324445-1530545	43.91 ± 0.11	-174.43	-184.82	14.885	17.120	13.506	10.462	-
12 33 33.08	-48 26 11.38	6128439395302574720	12333310-4826111	48.09 ± 0.78	-245.21	97.25	10.842	12.312	9.673	7.142	-
12 34 39.90	-54 14 59.45	6074572293432378240	12343989-5414594	40.25 ± 0.07	-462.17	-134.22	12.454	13.985	11.252	8.728	-
12 35 00.71	+09 49 42.57	3903318372263850368	12350069+0949425	55.04 ± 0.05	-449.28	-319.34	10.445	11.666	9.375	7.153	-
12 35 37.50	-31 01 06.43	3470292824518708864	12353750-3101063	42.52 ± 0.07	94.17	57.29	11.728	13.032	10.616	8.273	-
12 35 58.40	-45 56 20.49	6131930516518662144	12355841-4556202	48.21 ± 0.60	-102.99	-717.74	10.155	11.351	9.103	6.844	-
12 36 39.58	-17 22 17.27	3523229125371172608	12363959-1722170	42.59 ± 0.16	9.87	-80.19	15.557	18.044	14.046	10.712	-
12 36 57.35	-42 15 47.48	6145852528447523456	12365733-4215475	41.04 ± 0.08	126.23	-18.69	12.659	14.069	11.502	9.093	-
12 37 21.57	-20 52 35.51	3515253160648329088	12372157-2052349	41.83 ± 0.07	-40.21	-427.80	11.966	13.555	10.748	8.085	-
12 37 21.65	-32 00 36.68	6160315989731008768	12372164-3200364	56.10 ± 0.19	227.64	-433.74	13.385	15.238	12.087	9.288	-
12 37 26.14	-35 27 17.17	6157380018807576192	12372612-3527172	49.77 ± 0.10	66.41	-16.25	14.664	16.821	13.298	10.381	-

Table 2: List of M dwarf systems within 25 pc drawn from *Gaia* DR2, as described in §2.3.

These systems have not been vetted to distinguish single stars from multiples, but in cases

where a system was resolved in *Gaia* but not 2MASS, a “J” flag is listed in column 12.

12 37 52.22	−52 00 05.32	6078114541943893888	12375231−5200055	105.51 ± 0.06	−1034.45	29.72	9.559	10.931	8.434	6.020	—
12 37 58.88	−09 29 55.67	3579017589450369280	12375884−0929551	42.37 ± 0.05	489.29	−563.84	13.361	14.932	12.143	9.659	—
12 38 19.16	−65 14 45.45	5861048509766415616	12381916−6514455	55.31 ± 0.05	3.50	62.73	11.511	12.802	10.411	8.134	—
12 38 37.14	−27 03 35.12	3496359397652313856	12383713−2703348	40.19 ± 0.15	−184.60	−175.74	11.351	12.683	10.243	7.844	—
12 38 47.27	−04 19 17.06	3680458326070745728	12384731−0419168	53.39 ± 0.08	−747.51	−198.57	12.230	13.798	11.016	8.455	—
12 38 47.89	+09 58 04.28	3903379292080122368	12384789+0958041	40.16 ± 0.06	−168.22	−134.56	13.290	14.968	12.039	9.394	—
12 38 49.10	−38 22 53.67	6153483658836320384	12384914−3822527	149.84 ± 0.08	−665.08	−1312.57	11.226	13.034	9.968	7.386	—
12 38 52.44	+11 41 46.15	3928391218812375808	12385241+1141461	70.22 ± 0.07	−1155.70	−251.04	10.325	11.770	9.174	6.691	—
12 39 33.92	−28 50 04.63	3471143919533988224	12393391−2850045	46.46 ± 0.09	127.97	−90.54	12.099	13.561	10.925	8.452	—
12 39 36.44	−26 58 10.96	3496355755520065408	12393641−2658111	91.11 ± 0.09	−585.41	−188.45	13.418	15.554	12.065	9.233	—
12 39 46.73	+04 10 47.57	3707083515533601280	12394672+0410471	46.96 ± 0.15	−486.38	−482.03	14.781	17.089	13.359	10.042	—
12 40 46.29	−43 33 59.00	6133474952391837824	12404633−4333595	124.25 ± 0.10	−782.18	689.87	10.979	12.489	9.813	7.413	—
12 41 03.26	−46 55 23.44	6128965305457482752	12410327−4655234	47.10 ± 0.08	−242.52	−51.86	11.193	12.433	10.113	7.809	—
12 41 08.05	−38 43 12.89	6153267707880611584	12410805−3843124	44.08 ± 0.39	−440.71	−219.25	15.388	17.953	13.921	10.450	—
12 41 29.01	+19 05 00.53	3948128006581121408	12412898+1905012	41.63 ± 0.08	73.42	−306.48	13.502	15.286	12.220	9.477	—
12 42 19.63	−71 38 20.11	5842905399625203328	12421964−7138202	69.20 ± 0.04	−755.51	−14.21	12.081	13.718	10.857	8.222	—
12 44 00.74	−11 10 30.39	3530383784971799680	12440075−1110302	70.48 ± 0.08	−479.40	−152.91	12.650	14.452	11.367	8.674	—
12 44 22.77	+04 21 23.50	3704193243061410944	12442278+0421233	46.21 ± 0.08	621.34	−385.46	14.076	16.053	12.746	9.958	—
12 44 30.97	−11 42 14.76	3530280499598321792	12443097−1142145	48.16 ± 0.12	−206.53	−165.54	12.888	14.517	11.655	9.073	—
12 45 29.19	−70 40 05.23	5843101456298985984	12452918−7040051	45.39 ± 0.05	73.50	129.87	14.305	16.251	12.992	10.166	—
12 45 52.52	−55 06 50.14	6073573215330461952	12455254−5506502	98.18 ± 0.07	350.76	−137.04	12.114	13.938	10.838	8.124	—
12 46 09.42	+07 06 24.91	3709637096929192960	12460939+0706248	48.18 ± 0.11	−308.78	−465.09	15.452	18.076	14.000	10.635	—
12 47 09.78	−03 34 17.73	3681919233426269056	12470977−0334177	47.93 ± 0.07	−508.02	−13.81	11.451	12.856	10.320	7.886	—
12 47 10.03	−22 22 37.08	3502412621478297088	12471005−2222369	42.91 ± 0.06	−266.64	−57.37	11.283	12.572	10.195	7.835	—
12 47 14.72	−05 25 13.31	3677094164086948736	12471472−0525130	50.44 ± 0.11	−485.28	562.71	13.252	15.056	11.968	9.291	—
12 47 56.62	+09 45 05.03	3735000631158990976	12475664+0945050	123.82 ± 0.06	−1008.60	−459.80	10.094	11.665	8.902	6.362	—
12 49 34.20	+09 28 31.06	3734930606012228096	12493419+0928309	45.70 ± 0.07	−425.13	33.60	11.880	13.362	10.702	8.248	—
12 49 59.17	+03 57 47.71	3705361680324471552	12495915+0357476	41.74 ± 0.08	−419.90	−115.87	13.797	15.525	12.535	9.872	—
12 50 47.16	−55 27 14.33	6061693095281495424	12504704−5527161	62.61 ± 1.07	−78.96	−113.20	18.553	19.467	17.461	14.458	—
12 50 52.65	−21 21 13.61	3502592975744957824	12505265−2121136	56.08 ± 0.25	448.24	−330.32	15.373	18.573	13.826	10.128	—
12 53 10.96	−57 09 24.85	6060561079334177664	12531092−5709248	60.02 ± 0.26	−1563.84	−431.86	18.256	20.049	16.612	12.051	—

Table 2: List of M dwarf systems within 25 pc drawn from *Gaia* DR2, as described in §2.3.

These systems have not been vetted to distinguish single stars from multiples, but in cases

where a system was resolved in *Gaia* but not 2MASS, a “J” flag is listed in column 12.

12 53 48.68	−08 42 16.15	3627381669982295168	12534870−0842160	47.16 ± 0.09	−267.83	−166.04	14.049	16.053	12.714	9.855	—
12 54 50.79	+11 59 14.52	3927886100593557888	12545079+1159143	56.09 ± 0.08	−273.95	−393.73	13.924	16.040	12.565	9.621	—
12 55 12.14	−59 28 17.11	6056881391901174528	12551214−5928172	57.92 ± 0.08	24.70	−386.61	14.864	17.371	13.434	10.209	—
12 56 13.34	−22 04 58.59	3499296429434610304	12561336−2204580	50.59 ± 0.07	−294.86	−285.76	11.481	12.798	10.367	8.053	—
12 59 04.77	−43 36 24.42	6135947032490329472	12590470−4336243	129.05 ± 0.14	1103.61	−265.36	14.857	18.330	13.288	9.520	—
12 59 24.04	+07 43 54.84	3730621070186855424	12592403+0743551	54.95 ± 0.07	−678.01	0.12	14.105	16.195	12.756	9.838	—
12 59 41.67	−26 50 15.63	6187224127342923776	12594169−2650156	43.22 ± 0.06	−203.01	3.62	12.442	13.928	11.261	8.784	—
13 00 03.95	−05 37 47.80	3677448412989388032	13000398−0537477	52.83 ± 0.15	−344.48	43.70	11.372	12.834	10.228	7.780	—
13 00 25.80	−34 36 24.28	6155259541913716608	13002579−3436243	47.68 ± 0.06	−59.00	79.12	9.849	10.871	8.875	6.715	—
13 00 33.52	+05 41 08.00	3705324881043314304	13003350+0541081	116.81 ± 0.20	−939.56	227.32	11.767	13.676	10.480	7.660	—
13 00 46.56	+12 22 32.72	3737308025028857600	13004666+1222325	86.86 ± 0.15	−632.15	−36.02	8.908	10.033	7.876	5.578	—
13 01 19.65	−63 11 42.19	5863130980814698112	13011965−6311422	59.32 ± 0.04	−391.40	−411.19	10.084	11.179	9.083	6.934	—
13 04 29.07	−37 47 36.17	6142630035959679616	13042904−3747361	40.75 ± 0.04	286.56	−55.80	12.369	13.584	11.294	9.081	—
13 05 40.17	−25 41 05.83	6187779556809793024	13054019−2541059	53.85 ± 0.71	−313.48	−20.03	18.658	21.436	16.788	11.747	—
13 05 41.06	+20 46 39.46	3943239882828182784	13054106+2046394	50.43 ± 0.84	−52.20	81.44	20.380	21.467	18.639	13.368	—
13 07 04.31	+20 48 38.68	3943234217765374336	13070434+2048390	41.06 ± 0.07	−94.96	−81.84	11.511	12.710	10.458	8.216	—
13 08 25.08	+07 25 51.14	3730679138144442496	13082507+0725512	44.56 ± 0.19	233.74	−417.64	17.766	20.806	16.153	12.004	—
13 08 51.21	−01 31 07.55	3685703546290587392	13085124−0131075	42.43 ± 0.09	−404.98	8.06	11.636	13.037	10.494	8.081	—
13 09 20.41	−40 09 27.07	6140884286374656000	13092037−4009264	59.91 ± 0.05	719.83	−997.31	11.640	13.135	10.458	7.989	—
13 09 21.86	−23 30 35.76	3504014060164255104	13092185−2330350	66.67 ± 0.19	16.53	−382.82	16.141	19.472	14.584	10.669	—
13 09 51.92	−54 38 48.26	6067637295632046464	13095193−5438480	48.36 ± 0.20	−170.33	−185.08	17.928	20.229	16.277	11.960	—
13 10 52.02	−71 07 10.69	5843636265629936000	13105199−7107108	41.53 ± 0.05	−543.04	−215.83	13.655	15.352	12.404	9.724	—
13 13 04.77	+20 11 26.69	3940052815229913344	13130478+2011265	45.52 ± 0.07	−610.51	146.79	11.697	13.191	10.523	8.019	—
13 13 09.32	−41 30 39.76	6137710099384586240	13130939−4130396	84.27 ± 0.24	−1024.98	24.54	11.412	13.148	10.163	7.412	—
13 14 05.84	+03 53 58.85	3716608138087936128	13140583+0353587	51.25 ± 0.05	−736.55	9.64	12.309	13.811	11.117	8.590	—
13 15 25.91	+16 15 07.69	3936753661871508096	13152591+1615077	40.02 ± 0.05	164.52	−681.70	12.939	14.321	11.788	9.443	—
13 15 30.86	−26 49 51.84	6186534394250282752	13153094−2649513	53.87 ± 1.13	−688.63	−288.12	20.365	21.833	18.570	13.462	—
13 16 45.41	−12 20 20.38	3621610157353795584	13164546−1220203	45.50 ± 1.20	−289.04	−51.63	12.396	13.948	11.188	8.639	—
13 18 01.73	+02 14 02.01	3688439268658769664	13180180+0214011	74.45 ± 0.64	−274.24	−96.57	12.069	13.249	10.508	7.924	—
13 20 03.86	−35 24 43.92	6166376978860425600	13200391−3524437	73.31 ± 0.07	−851.19	−465.43	11.633	13.130	10.462	7.981	—
13 20 12.56	−01 40 40.97	3686259727375524864	13201255−0140407	44.33 ± 0.07	131.05	−253.32	12.277	13.672	11.126	8.780	—

Table 2: List of M dwarf systems within 25 pc drawn from *Gaia* DR2, as described in §2.3.

These systems have not been vetted to distinguish single stars from multiples, but in cases

where a system was resolved in *Gaia* but not 2MASS, a “J” flag is listed in column 12.

13	20	24.94	−01	39	27.05	3686261307923490688	13202492−0139266	44.38 ± 0.05	129.32	−253.33	10.733	11.846	9.716	7.527	−
13	20	27.00	−03	56	14.61	3636256549884389248	13202705−0356147	44.22 ± 0.09	−857.26	284.18	14.342	16.197	13.049	10.481	−
13	21	35.25	+03	45	55.22	3715722687629983104	13213523+0345551	43.38 ± 0.05	−517.55	−42.58	10.998	12.181	9.947	7.676	−
13	21	54.09	−14	24	09.73	3608334005420675584	13215411−1424098	51.53 ± 0.08	−220.80	73.57	12.888	14.608	11.634	8.985	−
13	22	04.73	−55	00	59.14	6066971747504719232	13220473−5500591	68.52 ± 0.11	−267.43	−135.25	12.258	13.918	11.022	8.434	−
13	22	56.75	+24	28	03.60	1446540213584440704	13225673+2428034	72.74 ± 0.06	−615.95	−865.13	11.627	13.222	10.420	7.957	−
13	23	38.03	−25	54	45.14	6192641081831733760	13233804−2554449	70.81 ± 0.07	−613.99	−230.98	11.574	13.154	10.371	7.781	−
13	25	48.85	−28	22	26.35	6188331614726318720	13254887−2822263	64.99 ± 0.05	−451.90	−103.76	10.109	11.292	9.070	6.876	−
13	27	27.01	−33	45	50.62	6168093900626704512	13272695−3345502	40.96 ± 0.07	434.15	−249.26	12.366	13.739	11.222	8.833	−
13	27	30.95	+01	49	38.37	3711482627195848576	13273095+0149384	41.80 ± 0.23	−176.62	7.10	16.505	19.679	14.988	11.432	−
13	27	53.97	−26	57	01.48	6189329043571426944	13275397−2657013	50.60 ± 0.07	−197.33	−108.50	10.836	12.032	9.782	7.543	−
13	28	21.08	−02	21	37.11	3637980103080373888	13282106−0221365	76.21 ± 0.35	151.97	−493.64	10.179	11.577	9.041	6.613	−
13	29	01.01	−41	47	13.53	6136908241874304640	13290099−4147133	46.07 ± 0.36	228.01	−278.31	18.370	21.282	16.781	12.273	−
13	29	21.31	+11	26	26.65	3738495703745045120	13292131+1126264	52.30 ± 0.05	328.84	−1190.83	11.014	12.401	9.884	7.535	−
13	29	24.09	−14	22	12.32	3608139353206904192	13292408−1422122	41.26 ± 0.06	108.58	−41.64	11.871	13.338	10.703	8.197	−
13	29	59.79	+10	22	37.78	3738099879558957952	13295979+1022376	131.24 ± 0.05	1127.51	−1073.88	8.206	9.285	7.196	5.036	−
13	30	02.80	−08	42	25.47	3630015546177181952	13300285−0842251	62.14 ± 0.08	−1114.53	−473.36	12.724	14.523	11.443	8.749	−
13	30	25.80	−52	02	40.24	6069775296000876416	13302576−5202403	56.61 ± 0.10	−565.62	−366.74	11.915	13.385	10.744	8.314	−
13	30	31.06	+19	09	34.06	3746973763029907328	13303106+1909340	66.75 ± 0.08	−503.65	−1283.42	13.219	15.053	11.931	9.221	−
13	30	40.95	−20	39	03.75	6196627086360009600	13304092−2039030	58.87 ± 0.14	298.17	−513.18	11.173	12.740	9.981	7.393	−
13	31	01.43	−45	35	09.55	6087242378235260800	13310146−4535096	65.20 ± 0.06	−619.50	223.02	12.256	13.753	11.077	8.702	−
13	31	39.37	−65	13	05.59	5864005027836957952	13313937−6513056	62.41 ± 0.16	−17.23	12.33	17.383	20.194	15.747	11.572	−
13	31	50.58	+23	23	20.38	1443068608699851008	13315057+2323203	51.66 ± 0.07	−280.17	47.88	11.200	12.514	10.127	7.815	−
13	32	44.61	+16	48	39.11	3745619095984248448	13324460+1648397	60.30 ± 0.11	287.56	−206.79	10.845	12.176	9.729	6.828	−
13	33	06.07	−39	57	15.46	6161174910174799360	13330607−3957154	43.47 ± 0.05	18.07	−106.03	11.969	13.298	10.844	8.508	−
13	34	11.49	−71	21	51.25	5840719364353028096	13341148−7121513	59.64 ± 0.06	−452.66	−337.20	13.408	15.421	12.068	9.200	−
13	34	23.60	−26	22	11.79	6189035061649770752	13342364−2622114	41.83 ± 0.06	−705.58	−358.12	12.574	14.205	11.346	8.749	−
13	34	28.03	−62	57	35.55	5865271012355608704	13342803−6257356	47.15 ± 0.54	−216.80	−32.53	17.189	20.099	15.573	11.318	−
13	35	11.44	−48	21	25.69	6082806153754882304	13351149−4821258	50.92 ± 0.09	359.88	−64.26	10.436	11.503	9.441	7.302	−
13	35	42.20	−18	15	12.56	6293217116979986560	13354218−1815123	41.26 ± 0.04	118.82	−110.76	10.216	11.177	9.285	7.242	−
13	35	50.88	−23	22	33.11	6191885339386292736	13355086−2322329	49.03 ± 0.08	86.01	−12.30	12.950	14.362	11.800	9.452	−

Table 2: List of M dwarf systems within 25 pc drawn from *Gaia* DR2, as described in §2.3.

These systems have not been vetted to distinguish single stars from multiples, but in cases

where a system was resolved in *Gaia* but not 2MASS, a “J” flag is listed in column 12.

13 36 55.23	+22 58 00.92	1442207244418843264	13365521+2258011	42.50 ± 0.05	102.33	−169.85	11.620	12.929	10.512	8.141	—
13 36 55.90	−32 12 21.77	6168707015798163328	13365588−3212215	41.72 ± 0.08	186.68	−273.93	13.590	15.336	12.324	9.603	—
13 38 26.45	−37 52 50.46	6163457878567757696	13382653−3752504	41.21 ± 0.10	−1274.58	−15.90	14.973	17.021	13.639	10.965	—
13 38 40.88	−11 32 07.75	3610474857638415616	13384087−1132077	50.72 ± 0.10	149.24	−86.40	12.768	14.517	11.500	8.814	—
13 38 53.44	−02 15 47.27	3637468383496879104	13385345−0215471	55.43 ± 0.07	−301.87	−77.32	11.114	12.383	10.039	7.747	—
13 40 24.63	+12 13 23.62	3740258186524389888	13402467+1213236	41.91 ± 0.06	−562.86	−64.02	13.553	15.158	12.326	9.861	—
13 41 21.23	−09 07 17.05	3618109522784875008	13412122−0907171	40.15 ± 0.04	95.23	39.86	12.175	13.563	11.033	8.668	—
13 41 32.93	+08 05 04.87	3724596914697213056	13413291+0805048	40.36 ± 0.19	−267.68	−12.96	16.021	18.701	14.556	11.131	—
13 42 09.83	−16 00 23.33	3605249596515311360	13420990−1600233	47.48 ± 0.52	−496.64	−49.15	12.179	13.715	10.768	8.089	—
13 43 01.26	+09 04 23.62	3724962880270554752	13430127+0904235	49.43 ± 0.35	−324.47	−115.56	11.914	13.388	10.736	8.200	—
13 43 41.49	−40 02 29.23	6113324752547911040	13434146−4002292	59.06 ± 0.08	189.65	−97.78	13.395	15.318	12.083	9.248	—
13 44 20.91	−26 18 35.18	6190352001701947520	13442092−2618350	49.18 ± 0.08	−326.20	−184.02	11.998	13.507	10.808	8.285	—
13 44 25.48	−40 20 15.53	6113245033656232448	13442546−4020155	44.33 ± 0.07	151.52	69.02	12.257	13.716	11.088	8.632	—
13 44 27.57	−40 18 40.04	6113271494953274752	13442755−4018400	44.46 ± 0.09	151.78	72.72	13.289	14.968	12.041	9.426	—
13 44 37.09	−19 54 43.55	6292376372837063808	13443711−1954433	48.30 ± 0.06	−380.48	−176.96	12.412	13.931	11.222	8.716	—
13 44 48.81	−54 07 17.94	6065791696645045248	13444880−5407181	51.12 ± 0.04	−253.83	−376.48	11.424	12.712	10.334	8.068	—
13 45 05.08	+17 47 07.57	1244644727396803584	13450502+1747105	77.45 ± 0.04	450.84	−1833.19	9.106	10.021	8.187	6.220	—
13 45 41.45	−51 01 00.54	6069407131407996544	13454144−5101002	42.43 ± 0.07	88.42	−491.24	13.978	15.763	12.694	10.119	—
13 45 50.71	−17 58 05.61	6294928369390563968	13455074−1758047	89.23 ± 0.08	−307.30	−552.53	10.595	12.120	9.412	6.902	—
13 46 46.05	−31 49 25.53	6171593062022433920	13464607−3149258	73.23 ± 0.16	−343.36	158.62	14.854	17.697	13.373	10.038	—
13 48 07.28	−13 44 31.60	3606183188877989376	13480721−1344321	55.00 ± 0.08	−687.60	−512.98	13.537	15.372	12.250	9.664	—
13 48 13.41	+23 36 48.70	1251824607045654016	13481341+2336486	84.18 ± 0.07	−1482.68	122.48	13.467	15.648	12.103	9.179	—
13 48 24.56	−42 27 44.11	6112093093362734336	13482456−4227441	41.78 ± 1.16	−158.35	−83.22	20.136	21.605	18.455	13.337	—
13 48 40.77	−05 17 08.35	3632779859757659008	13484075−0517081	40.14 ± 0.08	246.43	−465.71	13.405	15.146	12.135	9.403	—
13 48 48.61	+04 06 02.33	3713826030072008192	13484861+0406022	61.16 ± 0.10	−1.20	−179.82	12.855	14.646	11.586	8.882	—
13 49 01.00	+02 47 28.97	3665076433275547904	13490104+0247281	55.78 ± 0.75	149.68	−333.14	10.825	11.448	9.216	6.935	—
13 49 01.27	−42 28 42.27	6112090855684709248	13490127−4228421	40.61 ± 0.07	−160.48	−83.93	12.169	13.560	11.023	8.622	—
13 50 23.77	−21 37 19.87	6288413183175704960	13502377−2137193	47.51 ± 0.07	−33.50	−376.21	12.319	13.868	11.119	8.626	—
13 50 44.00	−21 41 26.98	6288409919000551424	13504400−2141263	47.49 ± 0.06	−35.89	−377.30	11.606	13.021	10.463	8.061	—
13 51 21.76	−53 32 45.90	6065173805485251072	13512172−5332457	59.01 ± 0.05	353.21	−414.96	11.722	13.149	10.566	8.123	—
13 52 36.21	+14 25 20.17	3728979323235476352	13523620+1425209	40.63 ± 0.06	46.51	−280.81	10.783	11.915	9.570	7.144	—

Table 2: List of M dwarf systems within 25 pc drawn from *Gaia* DR2, as described in §2.3.

These systems have not been vetted to distinguish single stars from multiples, but in cases

where a system was resolved in *Gaia* but not 2MASS, a “J” flag is listed in column 12.

13 52 53.47	-18 20 16.87	6293916376311538944	13525350-1820165	44.32 ± 0.05	-275.41	-120.40	10.891	12.066	9.844	7.610	-
13 53 55.63	-20 14 43.43	6289177958320337408	13535557-2014439	60.48 ± 0.04	432.25	283.61	11.579	12.834	10.491	8.206	-
13 54 53.90	-71 21 47.73	5845972349875278720	13545390-7121476	43.76 ± 0.06	-145.66	-128.16	11.117	12.399	10.034	7.672	-
13 55 27.97	-73 29 40.87	5791509037818118656	13552796-7329409	48.87 ± 0.03	-374.63	179.15	10.519	11.633	9.502	7.352	-
13 55 35.12	-07 23 16.67	3619515385839767936	13553511-0723165	48.33 ± 0.05	254.72	-104.91	11.501	12.857	10.370	7.947	-
13 57 13.06	-29 22 25.93	6173812151364882688	13571306-2922252	75.41 ± 0.07	-23.81	-453.39	11.380	12.812	10.225	7.789	-
13 57 53.77	+23 08 46.33	1250871227385237888	13575378+2308464	40.07 ± 0.10	-92.68	-26.73	14.786	16.833	13.445	10.596	-
13 58 05.41	-39 37 55.14	6114232433761438208	13580529-3937545	86.53 ± 0.06	1736.05	-888.01	12.638	14.286	11.409	8.948	-
13 58 13.92	+12 34 43.91	3727747870210462464	13581392+1234438	106.92 ± 0.09	-329.51	719.98	11.057	12.558	9.886	7.439	-
13 58 16.17	-12 02 59.05	3612684120096472192	13581621-1202591	57.94 ± 0.09	-338.01	43.11	12.898	14.700	11.621	8.887	-
13 58 19.59	-13 16 25.01	6302599662016881664	13581955-1316248	63.92 ± 0.10	342.88	-59.42	12.546	14.252	11.299	8.653	-
13 58 20.70	+11 00 49.78	3727298827083333504	13582069+1100496	48.64 ± 0.10	198.89	-483.95	14.196	16.262	12.848	9.988	-
13 58 38.84	-00 20 12.69	3660416565557981440	13583885-0020124	43.21 ± 0.06	-249.19	-317.30	12.985	14.476	11.800	9.366	-
13 59 10.41	-19 50 03.66	6290519435137636224	13591045-1950034	92.43 ± 0.08	-559.84	-186.65	11.408	13.172	10.153	7.445	-
13 59 55.11	-40 34 58.52	6111126966247119232	13595510-4034582	47.51 ± 0.27	26.59	-507.64	18.430	20.569	16.742	12.566	-
14 01 03.19	-02 39 17.51	3657653114880309248	14010324-0239180	96.04 ± 0.09	-825.42	598.11	8.859	9.961	7.842	5.683	-
14 01 05.25	-12 20 38.33	3612604950963820160	14010525-1220381	43.66 ± 0.17	-21.00	-163.54	15.284	17.615	13.881	10.815	-
14 02 06.08	+21 02 45.26	1247332788512753536	14020606+2102454	54.20 ± 0.07	15.95	25.25	11.977	13.601	10.728	8.076	-
14 02 10.36	-03 55 01.14	3645393972547522560	14021035-0355010	43.24 ± 0.06	116.64	-31.22	11.633	13.026	10.486	8.111	-
14 02 19.63	+13 41 22.69	1229977414080680192	14021961+1341229	49.17 ± 0.05	98.76	-140.55	9.835	10.883	8.857	6.706	-
14 02 28.88	-21 00 36.71	6289594093023609984	14022888-2100369	49.80 ± 0.10	482.27	-387.27	11.984	13.480	10.801	8.252	-
14 02 46.67	-24 31 49.72	6274832977622107264	14024670-2431502	55.41 ± 0.06	-364.01	374.17	11.149	12.398	10.076	7.840	-
14 03 51.55	-42 41 53.01	6109610086872510592	14035157-4241528	100.61 ± 0.12	-379.48	-290.23	11.708	13.394	10.473	7.890	-
14 04 06.60	-43 55 16.23	6109281367252825216	14040658-4355170	40.59 ± 0.74	-30.03	-65.91	16.627	17.218	14.744	12.378	-
14 04 08.18	-66 14 38.08	5851167679807239808	14040823-6614378	72.26 ± 0.51	468.71	130.53	10.490	11.863	9.363	6.915	-
14 05 18.50	-12 36 01.50	6302708689761652096	14051848-1236017	41.99 ± 0.05	83.56	92.61	11.721	12.937	10.642	8.385	-
14 06 36.12	+24 55 43.45	1257462971392301440	14063612+2455434	42.56 ± 0.06	87.27	39.73	12.741	14.142	11.591	9.212	-
14 06 49.36	-30 18 28.00	6173042836822996224	14064928-3018281	44.42 ± 0.12	-832.55	-58.41	15.031	17.391	13.626	10.366	-
14 07 56.85	-34 03 46.99	6122285222557114752	14075685-3403470	43.30 ± 0.06	74.03	-32.15	12.580	14.212	11.357	8.772	-
14 09 03.11	-33 57 56.49	6123776156029125760	14090310-3357565	41.54 ± 0.60	88.50	44.93	19.105	20.684	17.446	12.865	-
14 09 58.97	-24 03 39.56	6274553461150416000	14095897-2403396	49.62 ± 0.07	-113.11	35.75	12.321	13.899	11.111	8.604	-

Table 2: List of M dwarf systems within 25 pc drawn from *Gaia* DR2, as described in §2.3.

These systems have not been vetted to distinguish single stars from multiples, but in cases

where a system was resolved in *Gaia* but not 2MASS, a “J” flag is listed in column 12.

14	10	24.79	-15	27	31.28	6301109896776440960	14102462-1527320	64.18 ± 0.59	-170.64	-50.11	15.862	16.957	14.659	12.289	-
14	10	57.46	-31	17	25.18	6124711741640147712	14105747-3117253	62.88 ± 0.05	-320.43	127.22	9.923	11.061	8.900	6.693	-
14	11	08.73	-61	55	47.06	5866128597052432128	14110874-6155469	50.96 ± 0.03	154.93	-45.29	10.033	11.097	9.046	6.921	-
14	11	59.91	-41	32	22.06	6109949904687424640	14115998-4132211	111.03 ± 0.35	-712.62	-58.54	13.431	15.943	11.988	8.620	-
14	13	12.87	-56	44	31.41	5895265380327966464	14131288-5644314	85.75 ± 0.04	353.92	179.35	9.341	10.471	8.315	6.136	-
14	13	21.95	-80	31	35.60	5784922310327353984	14132192-8031356	44.64 ± 0.05	-295.62	-8.46	13.671	15.438	12.397	9.715	-
14	13	29.55	-44	31	54.69	6097323972147451648	14132953-4431546	47.87 ± 0.17	126.81	-138.27	13.240	14.912	11.998	9.414	-
14	13	31.19	-06	57	32.34	3640244581637740416	14133119-0657323	54.68 ± 0.06	110.26	136.80	9.475	10.395	8.561	6.571	-
14	13	53.08	+24	47	51.36	1257273099478139008	14135308+2447512	42.55 ± 0.05	-8.08	291.33	11.906	13.252	10.772	8.450	-
14	15	20.48	+15	23	03.53	1231853730673656960	14152047+1523035	42.72 ± 0.07	137.73	-126.33	11.146	12.362	10.081	7.838	-
14	15	32.55	+04	39	31.41	3668176368871118208	14153253+0439312	71.11 ± 0.39	-744.93	-766.43	12.674	14.632	11.350	8.618	-
14	15	46.35	-13	29	33.42	6302909449418261120	14154638-1329334	64.04 ± 0.04	-416.76	-116.67	11.547	12.877	10.425	8.106	-
14	16	47.53	-44	53	20.96	6096529059601571200	14164754-4453210	64.94 ± 0.11	-400.94	100.72	11.072	12.512	9.936	7.446	-
14	17	04.86	+10	35	36.02	1225145747671533056	14170487+1035359	49.46 ± 0.04	-282.42	-105.89	10.580	11.773	9.526	7.279	-
14	17	25.88	-40	18	15.32	6116110468338455680	14172590-4018154	66.43 ± 0.05	-388.76	12.27	11.271	12.634	10.155	7.810	-
14	17	59.05	-00	31	29.44	3653827329811719680	14175905-0031295	46.83 ± 0.04	-279.37	-275.19	11.680	12.982	10.572	8.281	-
14	18	05.21	-28	03	36.68	6269287689510453504	14180520-2803366	45.12 ± 0.04	-47.63	6.61	11.941	13.253	10.824	8.480	-
14	18	25.48	-55	28	37.29	5895473600324039680	14182547-5528373	46.91 ± 0.04	-291.09	-109.05	11.596	12.905	10.496	8.181	-
14	19	11.01	-07	18	11.91	3639794778302745088	14191106-0718113	56.89 ± 0.08	-1118.13	-758.42	12.334	13.709	11.191	8.917	-
14	19	29.58	+02	54	36.47	3666992950762141312	14192958+0254365	48.00 ± 0.10	-195.33	-149.49	13.264	15.217	11.943	9.072	-
14	19	43.05	+07	58	25.43	3673771439947412864	14194304+0758254	44.15 ± 0.09	-543.34	-139.43	14.224	16.207	12.892	10.034	-
14	20	07.37	-09	37	13.39	6329012134635132544	14200739-0937127	72.44 ± 0.07	-608.97	-838.74	11.598	13.135	10.404	7.976	-
14	21	15.13	-01	07	19.81	3652796572020424448	14211512-0107199	74.56 ± 0.08	168.72	-626.18	11.837	13.403	10.634	8.093	-
14	21	31.42	+18	27	40.50	1239625559894563968	14213145+1827407	52.67 ± 0.26	-753.54	-164.42	17.863	20.013	16.238	11.943	-
14	21	34.06	-07	55	16.63	3639512375613095424	14213406-0755165	42.28 ± 0.06	-97.28	-87.09	12.343	13.881	11.143	8.630	-
14	22	19.47	-70	23	37.01	5846275093531511936	14221943-7023371	77.76 ± 0.07	-793.59	-418.29	13.587	15.689	12.242	9.374	-
14	22	20.08	+23	52	35.06	1255420869061901440	14222009+2352351	46.11 ± 0.08	-248.69	44.60	13.818	15.771	12.493	9.647	-
14	23	07.81	-22	17	09.12	6276491659631783424	14230784-2217083	40.96 ± 0.07	-277.01	-470.42	13.510	15.243	12.243	9.504	-
14	23	23.85	-14	55	34.77	6299557386358126976	14232385-1455354	48.69 ± 0.09	-161.75	313.57	14.300	16.254	12.985	10.191	-
14	23	43.75	+14	26	51.33	1228555023991501184	14234378+1426515	55.00 ± 0.29	354.04	-536.75	15.014	17.609	13.564	10.256	-
14	24	18.71	-35	14	32.74	6119528334597735296	14241870-3514325	52.39 ± 0.24	-8.05	-76.49	15.810	18.681	14.315	10.806	-

Table 2: List of M dwarf systems within 25 pc drawn from *Gaia* DR2, as described in §2.3.

These systems have not been vetted to distinguish single stars from multiples, but in cases

where a system was resolved in *Gaia* but not 2MASS, a “J” flag is listed in column 12.

14 24 55.98	+08 53 15.45	1175938925836488448	14245599+0853155	77.09 ± 0.08	547.96	160.79	11.095	12.500	9.962	7.590	—
14 25 13.32	−16 24 55.99	6298364691119997440	14251336−1624559	42.83 ± 0.14	−364.21	20.57	15.200	17.577	13.776	10.488	—
14 26 05.60	−29 46 49.70	6221167631840454400	14260559−2946494	50.78 ± 0.08	89.30	−143.92	12.887	14.619	11.633	8.948	—
14 27 56.07	−00 22 31.13	3652910371473481344	14275607−0022310	57.08 ± 0.06	−361.50	41.64	12.469	14.287	11.185	8.403	—
14 28 04.16	+13 56 13.32	1227705135863076864	14280419+1356137	75.45 ± 0.13	−365.65	−494.96	14.922	17.867	13.440	10.026	—
14 28 21.52	+05 19 01.30	3669916380381791104	14282151+0519014	52.70 ± 0.07	−373.17	−60.33	11.394	12.788	10.253	7.843	—
14 28 31.07	−06 44 33.76	6331354197480725120	14283106−0644337	42.32 ± 1.22	−100.79	−122.75	20.205	21.476	18.375	13.627	—
14 29 18.19	−58 45 59.11	5890960105080869632	14291819−5845591	47.10 ± 0.05	−150.77	115.20	12.144	13.514	11.010	8.636	—
14 29 29.70	+15 31 57.50	1229089524081628416	14292971+1531578	70.18 ± 0.05	−1054.73	1299.49	9.723	10.931	8.666	6.393	—
14 29 41.37	−48 08 31.50	6091907056321709312	14294137−4808312	49.35 ± 0.07	−132.15	748.14	14.523	16.621	13.182	10.448	—
14 29 42.95	−62 40 46.17	5853498713160606720	14294291−6240465	768.50 ± 0.20	−3781.31	769.77	8.954	11.383	7.586	4.384	—
14 30 56.70	−31 14 36.67	6219675839377104128	14305669−3114367	47.39 ± 0.16	−403.51	−122.93	16.507	19.750	14.968	11.310	—
14 31 01.16	−12 17 45.95	6324308389531786112	14310120−1217451	92.07 ± 0.10	−407.97	−398.94	10.662	12.190	9.483	6.961	—
14 31 04.50	−03 07 16.89	3649114960414008064	14310451−0307170	40.02 ± 0.08	−332.86	12.72	13.327	15.106	12.043	9.327	—
14 31 10.21	−21 28 58.00	6279645574376722432	14311020−2128581	41.61 ± 0.09	127.92	−25.26	14.834	16.979	13.474	10.532	—
14 31 15.61	−13 18 25.14	6300158578700499712	14311564−1318247	41.07 ± 0.18	−268.48	−186.16	14.692	16.884	13.298	10.097	—
14 32 08.51	+08 11 31.25	1172618435080418176	14320849+0811313	78.32 ± 0.11	−476.96	10.10	13.679	15.972	12.295	9.166	—
14 32 09.92	−73 57 39.04	5796351145286316160	14320992−7357389	42.50 ± 0.07	151.33	65.34	13.068	14.790	11.805	9.113	—
14 32 10.81	+16 00 49.32	1235125877277843840	14321078+1600494	63.27 ± 0.06	178.19	−70.67	12.258	13.902	11.026	8.471	—
14 32 36.72	−03 14 07.49	3649057407852320640	14323673−0314072	44.60 ± 0.13	−154.14	−225.45	16.297	—	—	11.327	—
14 33 09.00	+24 32 06.25	1255034459444168704	14330900+2432062	42.12 ± 0.19	−196.15	−30.95	17.306	20.320	15.712	11.773	—
14 34 16.81	−12 31 10.42	6324325225803432320	14341683−1231106	160.11 ± 0.11	−355.04	593.22	9.879	11.594	8.662	5.939	—
14 38 39.37	−02 57 23.87	3648394677218755584	14383936−0257237	40.08 ± 0.06	−210.53	−30.79	12.725	14.255	11.523	9.031	—
14 40 22.14	−27 52 42.38	6222568134778281984	14402215−2752419	49.83 ± 0.05	−145.53	−211.78	12.389	13.879	11.210	8.753	—
14 40 43.58	−00 58 57.72	3649861009118391296	14404355−0058576	41.01 ± 0.07	−192.29	15.23	13.078	14.624	11.868	9.283	—
14 41 09.95	−08 59 20.51	6326945362011635584	14410995−0859204	41.46 ± 0.07	−257.69	44.30	12.194	13.672	11.015	8.505	—
14 41 46.00	−14 27 17.35	6311012064136913920	14414598−1427173	56.49 ± 0.07	−145.38	−182.26	14.383	16.557	13.029	10.098	—
14 41 58.86	−16 49 00.73	6285682717847042560	14415883−1649008	46.64 ± 0.08	−171.65	−247.08	13.371	15.164	12.092	9.390	—
14 41 59.10	−16 53 13.18	6285679964774140928	14415908−1653133	46.68 ± 0.05	−170.94	−247.73	12.113	13.580	10.941	8.507	—
14 43 25.37	−44 29 03.01	6098895724014519936	14432538−4429028	44.96 ± 0.06	−251.47	−165.54	12.172	13.601	11.011	8.582	—
14 44 06.56	−34 26 47.07	6203502160773159424	14440656−3426465	64.94 ± 0.09	−83.07	−437.93	12.757	14.456	11.512	8.883	—

Table 2: List of M dwarf systems within 25 pc drawn from *Gaia* DR2, as described in §2.3.

These systems have not been vetted to distinguish single stars from multiples, but in cases

where a system was resolved in *Gaia* but not 2MASS, a “J” flag is listed in column 12.

14 47 55.18	−03 09 35.44	6338748894214299264	14475520−0309357	54.90 ± 0.07	−545.27	377.27	12.306	13.583	11.204	9.060	−
14 49 33.25	−26 06 20.81	6228695270697905280	14493338−2606205	48.27 ± 0.04	−1201.17	−185.82	10.791	11.907	9.769	7.640	−
14 50 02.85	−37 42 09.78	6201523658320811008	14500286−3742095	42.45 ± 0.13	−253.08	−360.33	12.751	14.278	11.559	9.074	−
14 52 28.53	+12 23 32.80	1181472011945052928	14522854+1223330	48.34 ± 0.04	−61.31	−227.80	10.565	11.835	9.479	7.115	−
14 53 17.79	+13 46 56.18	1185087343615401600	14531754+1346541	41.38 ± 0.30	−180.77	−131.65	14.956	16.573	13.711	11.113	−
14 53 37.19	+11 34 12.52	1181168684174651392	14533718+1134124	51.24 ± 0.07	83.95	−741.32	13.752	15.624	12.453	9.652	−
14 53 51.40	+23 33 21.02	1266092694561970432	14535144+2333208	87.94 ± 0.18	−693.84	90.35	10.683	11.978	9.218	6.572	−
14 54 29.24	+16 06 03.80	1187851653287128576	14542923+1606039	100.68 ± 0.05	279.34	−117.96	9.126	10.350	8.059	5.770	J
14 54 53.48	+09 56 36.53	1174189362317947776	14545347+0956364	40.23 ± 0.11	−311.60	−401.41	10.475	11.498	9.500	7.388	−
14 55 59.81	−21 58 05.63	6232094067297707392	14555981−2158054	42.19 ± 0.06	−8.00	−59.30	12.000	13.356	10.866	8.481	−
14 56 27.16	+17 54 59.76	1188693088919917952	14562713+1755001	53.41 ± 0.07	−848.04	488.40	14.078	16.124	12.741	9.852	−
14 56 38.26	−28 09 48.62	6224387727748521344	14563831−2809473	141.69 ± 0.11	−491.06	−843.27	14.083	17.352	12.550	8.928	−
15 00 10.92	−41 02 56.98	6197011365679426688	15001090−4102568	44.60 ± 0.14	202.84	−62.29	14.776	16.788	13.451	10.622	−
15 01 08.19	+22 50 02.12	1262763648230973440	15010818+2250020	93.45 ± 0.19	−43.77	−64.00	16.530	19.959	14.927	10.706	−
15 01 16.50	−43 39 31.11	5908372482296952064	15011648−4339311	70.70 ± 0.07	93.76	30.20	9.644	11.039	8.515	6.074	−
15 01 20.11	+05 32 55.54	1159745146784043264	15012011+0532553	66.69 ± 0.06	83.47	−442.48	11.065	12.510	9.921	7.432	−
15 02 07.66	−71 18 01.43	5798502241016325120	15020765−7118013	52.24 ± 0.04	−242.01	−235.73	11.753	13.339	10.542	7.962	−
15 02 21.25	+16 17 30.30	1187167168643550208	15022125+1617303	48.57 ± 0.51	29.24	−15.08	17.010	17.997	15.564	13.222	−
15 02 50.30	−62 39 17.11	5874433139633560576	15025025−6239175	45.82 ± 2.61	−5.14	−32.94	19.976	20.115	18.150	15.213	−
15 04 16.18	−23 55 56.58	6227871564690336512	15041621−2355564	50.80 ± 0.18	−331.34	−87.61	16.235	19.433	14.686	11.032	−
15 04 58.28	−21 07 00.72	6231840080111876992	15045835−2107003	40.68 ± 0.08	−656.94	−198.56	13.132	14.769	11.897	9.462	−
15 06 06.60	+15 12 31.58	1183850942790617856	15060658+1512316	40.94 ± 0.04	99.87	−54.24	10.779	11.838	9.785	7.627	−
15 06 41.54	−42 30 55.10	6004484268320338944	15064152−4230551	40.06 ± 0.08	−511.25	−53.10	15.096	17.267	13.733	10.853	−
15 07 27.81	−20 00 43.31	6256677841624904320	15072779−2000431	41.80 ± 0.22	96.69	−73.32	15.905	19.130	14.355	10.661	−
15 08 23.39	−23 51 37.20	6228198531960352768	15082343−2351371	44.04 ± 0.04	−230.88	−226.76	10.945	12.149	9.887	7.634	−
15 08 28.05	−12 29 59.02	6312500665441926912	15082796−1229586	48.83 ± 0.51	−85.23	−19.22	14.671	15.631	13.688	11.531	J
15 08 41.32	−62 49 56.23	5873758486184093952	15084135−6249561	52.91 ± 1.98	10.30	12.45	20.163	21.675	18.729	14.698	−
15 09 31.95	−15 46 47.76	6307627763050869632	15093196−1546476	41.08 ± 0.81	7.43	26.94	11.365	12.500	10.316	8.072	−
15 09 35.59	+03 10 00.55	1155276250492687616	15093558+0310007	68.49 ± 0.06	−602.11	481.32	10.368	11.731	9.245	6.858	−
15 09 55.92	−23 58 59.87	6228000276276576896	15095591−2359002	41.22 ± 0.05	−86.64	235.74	10.891	11.921	9.911	7.822	−
15 10 04.82	+19 21 27.48	1212774313804554752	15100481+1921286	57.86 ± 0.09	5.84	−452.15	12.033	13.662	10.808	8.250	−

Table 2: List of M dwarf systems within 25 pc drawn from *Gaia* DR2, as described in §2.3.

These systems have not been vetted to distinguish single stars from multiples, but in cases

where a system was resolved in *Gaia* but not 2MASS, a “J” flag is listed in column 12.

15	10	16.84	−02	41	08.05	6336552379219937920	15101685−0241078	55.43 ± 0.35	−399.09	32.14	17.238	20.280	15.638	11.347	−
15	10	34.96	−35	27	01.89	6200911539578946432	15103497−3527019	81.46 ± 1.48	11.04	0.50	19.177	20.386	17.642	15.007	−
15	10	40.48	−52	48	19.04	5888257093214433920	15104047−5248189	40.97 ± 0.23	−137.33	−170.97	10.496	11.675	9.244	6.847	J
15	10	56.56	−51	41	35.59	5900432500841313920	15105657−5141356	55.13 ± 0.04	−337.20	63.58	11.983	13.316	10.864	8.577	−
15	11	00.66	−79	26	48.34	5773317961528696832	15110067−7926484	44.13 ± 0.07	88.32	−252.45	11.736	13.222	10.555	8.099	−
15	11	50.60	−10	14	18.07	6319027263385067264	15115065−1014178	65.37 ± 0.10	−967.85	−250.24	12.762	14.536	11.494	8.867	−
15	11	55.96	+17	57	16.41	1211589731374380544	15115602+1757175	41.23 ± 0.07	−415.73	−562.96	12.330	13.769	11.161	8.768	−
15	12	08.17	−39	41	59.30	6005425828227820160	15120816−3941593	42.28 ± 0.06	77.62	108.11	10.635	11.734	9.627	7.402	−
15	12	50.78	−39	01	18.07	6006981087424136576	15125078−3901180	62.29 ± 0.20	−52.63	−133.99	13.714	15.767	12.376	9.422	−
15	14	16.89	−09	58	38.85	6319402059411076224	15141690−0958386	44.20 ± 0.08	−113.53	−114.07	12.706	14.434	11.446	8.780	−
15	14	29.68	−57	53	19.82	5877160615677467520	15142970−5753196	55.61 ± 0.06	−373.74	−388.47	12.539	14.252	11.289	8.266	−
15	16	24.93	−32	10	23.15	6207588323936193536	15162497−3210230	77.58 ± 2.05	−9.06	−3.17	19.699	20.968	17.959	14.793	−
15	16	53.06	−28	32	16.43	6213843239430821248	15165310−2832162	59.25 ± 0.09	−838.08	−314.52	13.668	15.572	12.364	9.613	−
15	18	31.46	+20	36	28.16	1214076070761755008	15183145+2036279	61.21 ± 0.43	4.59	95.99	13.553	15.761	12.187	9.268	−
15	18	34.85	−32	14	32.24	6207547504569849728	15183485−3214320	48.05 ± 1.39	−5.63	−9.13	19.589	20.675	17.956	14.987	−
15	19	01.79	−74	16	13.46	5792730526510790144	15190181−7416133	40.64 ± 0.18	254.59	104.21	17.953	21.567	16.332	12.441	−
15	19	11.73	−12	45	06.27	6314466489153193344	15191181−1245061	46.85 ± 0.77	−726.94	−188.93	11.490	13.096	10.266	7.582	−
15	19	26.83	−07	43	20.19	6322070093095493504	15192689−0743200	158.75 ± 0.05	−1221.47	−97.13	9.411	10.836	8.268	5.837	−
15	19	45.85	+04	39	34.43	1155910118945913728	15194584+0439344	59.69 ± 0.08	28.75	98.23	12.489	14.108	11.264	8.703	−
15	20	12.73	−35	59	24.62	6199925071490964992	15201272−3559244	48.31 ± 0.17	52.46	−205.17	15.003	17.336	13.610	10.639	−
15	20	39.90	−36	44	42.50	6007639003393866496	15203991−3644427	43.13 ± 0.97	−13.58	3.87	19.203	20.137	17.790	15.324	−
15	21	34.31	−02	16	58.16	4414858219987352320	15213429−0216580	48.88 ± 0.04	33.44	−286.90	10.495	11.616	9.472	7.255	−
15	21	52.93	+20	58	39.91	1214160733157163008	15215291+2058394	87.38 ± 0.05	81.45	128.07	9.107	10.276	8.060	5.756	−
15	22	12.98	−27	49	42.58	6213248060043565184	15221293−2749436	85.57 ± 0.06	436.51	606.76	11.952	13.509	10.750	8.274	−
15	23	51.14	+17	27	57.44	1208695640675619584	15235112+1727569	89.18 ± 0.08	−392.16	−1258.73	12.207	14.002	10.935	8.279	−
15	24	48.49	−49	29	47.51	5890493602926306048	15244849−4929473	46.21 ± 0.33	−122.72	−242.51	10.652	11.886	9.580	7.299	−
15	27	04.53	−09	18	16.60	6317869099684480768	15270453−0918163	43.67 ± 0.10	−118.45	−270.17	15.202	17.514	13.810	10.811	−
15	27	45.06	−09	01	32.23	6317928267153806976	15274506−0901319	47.57 ± 0.09	25.30	−308.02	13.780	15.648	12.472	9.632	−
15	27	45.18	+07	40	30.72	1162946718485093632	15274518+0740308	48.33 ± 0.06	97.60	12.66	10.505	11.633	9.479	7.278	−
15	28	45.83	−56	41	52.96	5883479539047399936	15284584−5641530	44.56 ± 0.05	47.95	−140.39	12.453	14.001	11.252	8.651	−
15	30	21.12	−53	42	34.85	5888509602928271488	15302112−5342348	45.24 ± 0.17	25.39	−50.16	16.965	20.128	15.381	11.603	−

Table 2: List of M dwarf systems within 25 pc drawn from *Gaia* DR2, as described in §2.3.

These systems have not been vetted to distinguish single stars from multiples, but in cases

where a system was resolved in *Gaia* but not 2MASS, a “J” flag is listed in column 12.

15 30 30.33	+09 26 01.43	1165479168642900992	15303032+0926014	115.76 ± 0.14	−178.99	184.49	13.092	15.421	11.703	8.661	—
15 30 52.05	−68 01 17.79	5823352234601659008	15305202−6801175	46.78 ± 0.46	184.03	2.67	12.224	13.815	10.866	8.225	—
15 32 16.14	−35 21 03.18	6013642341180098432	15321613−3521030	55.50 ± 0.10	71.55	−85.59	12.459	14.066	11.242	8.715	—
15 32 35.35	−23 33 59.40	6239491684610275328	15323534−2333592	42.35 ± 0.09	33.60	−280.98	14.975	17.084	13.619	10.740	—
15 32 43.82	−61 50 29.50	5827483512137991040	15324381−6150296	45.81 ± 0.05	−208.86	−207.60	11.668	12.954	10.569	8.335	—
15 32 50.28	−54 10 27.49	5885471411757745408	15325031−5410276	65.95 ± 0.05	169.14	−119.00	11.609	13.191	10.414	7.898	—
15 34 00.26	+04 36 51.93	4427595924756992256	15340026+0436519	41.20 ± 0.05	−134.55	−204.24	12.226	13.537	11.110	8.767	—
15 34 30.50	+14 16 17.84	1193998747920687872	15343054+1416181	44.15 ± 0.07	−669.51	−148.60	12.567	14.151	11.356	8.809	—
15 34 50.81	+18 00 12.41	1209432042883668480	15345086+1800131	58.55 ± 0.16	−207.05	−333.59	13.912	15.945	12.581	9.713	—
15 34 53.26	+12 19 49.41	1193465794018333824	15345325+1219495	49.89 ± 1.65	174.55	−38.16	20.626	21.372	18.916	13.827	—
15 34 56.93	−14 18 49.25	6265453524968112640	15345704−1418486	91.68 ± 0.17	−918.55	−330.20	15.770	19.327	14.153	10.305	—
15 35 20.52	+17 42 46.88	1209281375431039104	15352059+1742470	66.96 ± 0.04	−1211.18	−164.34	11.351	12.685	10.239	7.940	—
15 35 41.68	+22 25 25.73	1217510223537123712	15354167+2225254	90.79 ± 0.59	−2.38	−19.28	16.968	18.497	15.728	13.171	—
15 35 46.13	+22 09 03.75	1217467067705592576	15354610+2209037	54.57 ± 0.07	−707.38	−131.99	11.496	12.995	10.339	7.920	—
15 35 53.23	−32 13 54.41	6208256169875566208	15355326−3213547	61.53 ± 1.57	−1.90	−4.22	19.740	20.560	18.357	15.992	—
15 36 34.49	−37 54 22.95	6012446244330608768	15363450−3754223	99.20 ± 0.09	−338.77	−802.15	11.363	13.024	10.158	7.671	—
15 36 58.62	−14 08 01.76	6265472113586221696	15365868−1408006	71.65 ± 0.08	−449.87	−629.15	11.353	12.977	10.159	7.572	—
15 37 12.78	−39 54 09.90	6002992162332713856	15371278−3954097	45.82 ± 0.15	−290.00	−244.08	16.434	19.535	14.901	11.321	—
15 38 57.60	−87 45 50.25	5765079905013035264	15385751−8745503	40.66 ± 0.09	−187.69	−186.26	14.599	16.695	13.246	10.310	—
15 39 41.92	−05 20 42.76	4400638923299410048	15394189−0520428	58.82 ± 0.42	590.20	104.57	19.010	20.371	17.319	12.575	—
15 40 29.61	−26 13 42.95	6234648404610590208	15402966−2613422	67.24 ± 0.20	−1149.90	−1131.01	15.750	19.131	14.214	10.730	—
15 40 43.54	−51 01 35.97	5985290231327158144	15404341−5101357	188.05 ± 0.09	1949.17	−324.64	12.756	15.537	11.297	7.943	—
15 42 06.54	−19 28 18.27	6254033894120917760	15420677−1928167	105.89 ± 0.45	−2013.05	−1040.93	10.675	12.132	9.521	7.168	—
15 42 37.53	−61 28 28.93	5827358099092820608	15423752−6128290	40.40 ± 0.04	−201.63	−389.17	12.690	14.120	11.527	9.092	—
15 43 18.33	−20 15 32.91	6241924010489984896	15431836−2015310	42.80 ± 0.04	−303.99	−1128.54	12.206	13.360	11.152	9.018	—
15 43 59.10	+14 27 07.89	1194206418179409280	15435905+1427079	43.55 ± 0.09	400.05	15.26	14.205	16.038	12.915	10.328	—
15 44 23.68	+15 05 44.25	1195788477975819008	15442369+1505443	40.11 ± 0.06	−335.71	−120.65	13.207	14.693	12.023	9.586	—
15 45 41.61	−43 30 28.45	5989551315565681664	15454163−4330287	48.40 ± 0.11	−267.07	−394.85	11.824	13.340	10.638	8.077	—
15 46 41.69	−55 34 47.49	5884382654716110848	15464185−5534468	119.10 ± 0.70	−254.53	−251.34	14.576	17.887	13.008	9.112	—
15 47 15.11	+01 49 21.97	4423007800173036544	15471513+0149218	54.38 ± 0.41	−211.35	−64.93	14.414	16.933	12.968	9.667	—
15 47 24.55	−10 53 47.27	6268621389764361344	15472464−1053471	62.52 ± 0.28	−309.01	−370.77	10.208	11.538	9.096	6.743	—

Table 2: List of M dwarf systems within 25 pc drawn from *Gaia* DR2, as described in §2.3.

These systems have not been vetted to distinguish single stars from multiples, but in cases

where a system was resolved in *Gaia* but not 2MASS, a “J” flag is listed in column 12.

15 47 29.81	-27 55 12.11	6233452028580863744	15472982-2755121	40.28 ± 0.10	96.15	24.53	12.144	13.397	10.941	8.473	-
15 47 34.90	-27 53 42.91	6233827481743360128	15473488-2753426	40.84 ± 0.54	91.15	30.72	14.738	17.008	13.345	10.346	-
15 47 51.39	-16 18 54.02	6261833108052952576	15475143-1618534	48.78 ± 0.07	-255.49	-307.45	12.893	14.367	11.709	9.254	-
15 50 04.75	+06 16 46.68	4429874387730820608	15500475+0616467	40.03 ± 0.11	-399.92	-139.02	15.491	17.903	14.082	11.082	-
15 50 11.21	+00 57 32.74	4410702581435191296	15501121+0057325	59.21 ± 0.08	183.62	-47.68	11.343	12.742	10.218	7.831	-
15 52 06.55	-33 59 19.02	6012127622177717760	15520654-3359191	63.68 ± 0.20	-98.99	54.00	12.166	13.848	10.925	8.355	-
15 52 44.61	-26 23 13.71	6235533167875990272	15524460-2623134	94.16 ± 0.17	211.62	-452.80	14.100	16.750	12.650	9.315	-
15 55 14.47	-10 10 23.04	4346481103689544832	15551446-1010232	47.13 ± 0.09	14.91	129.07	11.069	12.403	9.971	7.616	-
15 55 36.89	-32 00 00.41	6039413759870675072	15553689-3200001	45.92 ± 0.06	-129.09	-89.76	12.493	14.168	11.254	8.654	-
15 55 46.90	-31 57 41.38	6039437399371019136	15554690-3157409	46.17 ± 0.07	-126.78	-87.98	11.585	12.960	10.469	8.074	-
15 55 52.17	-11 54 19.73	4345978351997277056	15555218-1154195	43.78 ± 0.07	-321.24	-98.94	11.686	13.091	10.540	8.122	-
15 56 34.43	-19 42 41.65	6247047562878494848	15563443-1942409	42.68 ± 0.08	-15.69	-355.10	13.572	15.192	12.343	9.800	-
15 57 12.38	-61 28 55.63	5832599952051348992	15571239-6128557	61.18 ± 0.05	-36.00	-815.30	12.166	13.815	10.934	8.345	-
15 57 48.26	+09 01 10.08	4454532237354157568	15574826+0901099	52.25 ± 0.05	146.00	-153.90	12.253	13.884	11.025	8.434	-
15 57 50.42	-51 31 48.99	5981695893418544128	15575044-5131486	59.72 ± 0.27	81.70	47.70	14.540	17.232	13.084	9.669	-
15 58 27.82	-06 51 45.21	4349759744283934336	15582783-0651450	46.54 ± 0.10	-145.77	-201.82	11.286	12.608	10.195	7.811	-
15 59 53.38	-08 15 11.54	4347870370990204928	15595337-0815114	75.23 ± 0.05	202.55	-25.53	9.594	10.747	8.561	6.343	-
16 00 27.84	-34 43 17.26	6011142532786032000	16002794-3443167	44.13 ± 0.05	-920.79	-287.90	12.464	13.872	11.308	8.975	-
16 01 39.75	-26 25 15.90	6043237998751210880	16013973-2625157	40.98 ± 0.06	138.08	-43.54	10.113	11.050	9.191	7.178	-
16 01 51.61	-41 40 38.09	5995278018798610816	16015161-4140381	45.23 ± 0.05	-47.41	-126.23	12.362	13.829	11.188	8.719	-
16 01 55.68	-34 21 56.84	6011177614079629952	16015561-3421563	46.31 ± 0.09	550.77	-309.24	14.435	16.467	13.060	9.978	-
16 02 41.64	+01 31 58.19	4412417304175836544	16024164+0131580	60.07 ± 0.10	-163.98	-558.83	14.466	16.829	13.062	10.033	-
16 02 50.94	+20 35 21.03	1205070452055788928	16025098+2035218	99.90 ± 0.06	-961.09	-1242.23	11.156	12.830	9.942	7.369	-
16 04 13.22	+23 31 38.55	1206795169186219264	16041322+2331386	47.83 ± 0.34	-161.00	18.13	13.317	15.323	11.980	9.065	-
16 04 19.99	-06 16 45.99	4350216075969473408	16041999-0616453	56.93 ± 0.11	-71.69	-866.61	13.814	15.853	12.477	9.548	-
16 05 09.38	-49 47 55.41	5983356259047553792	16050935-4947553	61.83 ± 0.08	121.11	-213.25	14.178	16.433	12.789	9.644	-
16 05 23.84	-61 15 13.07	5832781680707896192	16052383-6115132	41.10 ± 0.03	-169.98	-244.09	11.856	13.133	10.754	8.446	-
16 06 29.47	-24 07 24.68	6242063304871870592	16062950-2407249	58.34 ± 0.10	-324.22	206.09	13.462	15.248	12.189	9.511	-
16 07 31.24	-04 42 09.63	4404521333221783680	16073123-0442091	65.60 ± 0.22	-14.72	-422.67	16.368	19.642	14.795	10.717	-
16 07 41.05	-28 25 03.87	6042005308777992192	16074105-2825037	42.85 ± 0.08	-122.05	-109.49	12.970	14.589	11.742	9.124	-
16 08 14.96	-10 26 14.27	4343596947252195200	16081497-1026133	46.61 ± 0.07	-368.39	-1302.19	13.310	15.013	12.054	9.529	-

Table 2: List of M dwarf systems within 25 pc drawn from *Gaia* DR2, as described in §2.3.

These systems have not been vetted to distinguish single stars from multiples, but in cases

where a system was resolved in *Gaia* but not 2MASS, a “J” flag is listed in column 12.

16 08 43.94	−44 42 28.67	5991166914825299712	16084394−4442283	42.06 ± 0.07	−143.59	−608.76	13.960	15.707	12.695	10.102	−
16 09 16.27	+09 21 07.54	4453239765733463936	16091625+0921077	73.86 ± 0.06	−340.99	218.76	10.653	12.024	9.527	7.136	−
16 10 58.43	−06 31 32.57	4349305645979265920	16105843−0631325	59.84 ± 0.13	−55.78	−184.03	15.094	17.750	13.642	10.371	−
16 12 10.25	−25 12 10.22	6049547340064301952	16121023−2512098	41.94 ± 0.07	119.10	−253.56	14.164	15.984	12.858	10.129	−
16 12 41.78	−18 52 31.81	6245870673116518784	16124178−1852317	68.78 ± 0.12	35.71	−214.05	10.235	11.633	9.111	6.589	−
16 13 05.93	−70 09 08.09	5819260642586368896	16130591−7009081	57.64 ± 0.04	−226.27	−571.54	12.292	13.990	11.041	8.388	−
16 14 21.94	−28 30 36.65	6039144001564707072	16142197−2830362	52.86 ± 0.07	−410.26	−338.79	11.713	13.224	10.539	8.114	−
16 14 25.20	−02 51 00.76	4405150047715392128	16142520−0251009	68.70 ± 0.13	−7.22	367.83	15.249	18.251	13.748	10.280	−
16 14 32.62	+19 06 10.87	1201405126966213760	16143285+1906101	58.95 ± 0.11	−2003.13	363.49	11.732	13.187	10.586	8.262	−
16 15 42.46	+05 46 40.07	4438043930922131072	16154245+0546400	56.09 ± 0.20	141.60	−103.22	17.572	20.901	15.944	11.741	−
16 16 58.94	−31 36 37.60	6037396465276491776	16165895−3136375	54.54 ± 0.30	−120.42	−107.40	12.466	14.275	11.181	8.475	−
16 19 10.60	+19 57 25.83	1201927669866633088	16191059+1957259	40.66 ± 0.08	−382.05	243.96	14.170	16.034	12.872	10.156	−
16 19 11.13	+01 40 41.08	4408913744737288320	16191111+0140411	45.16 ± 0.09	−150.56	−12.82	12.936	14.633	11.685	9.041	−
16 20 03.51	−37 31 44.41	6021430250773348736	16200353−3731449	117.36 ± 0.06	−747.69	988.21	9.491	10.861	8.367	5.950	−
16 21 04.48	−37 11 37.52	6021535941318934912	16210447−3711373	41.76 ± 0.17	−68.26	−312.73	16.688	19.948	15.161	11.565	−
16 22 40.96	−48 39 20.02	5941478335062267392	16224099−4839198	42.29 ± 0.06	−586.92	−484.55	10.917	12.078	9.871	7.637	−
16 23 02.75	−69 05 36.93	5808918155180366336	16230269−6905373	54.82 ± 0.06	−1045.77	−1275.37	14.734	17.025	13.356	10.535	−
16 23 07.64	−24 42 35.23	6049221163063960320	16230768−2442340	60.47 ± 0.05	−344.56	−675.98	9.450	10.461	8.483	6.393	−
16 23 21.71	−21 46 43.79	6052153251338962688	16232170−2146436	47.08 ± 0.08	−149.17	−146.38	14.103	16.117	12.765	9.866	−
16 24 43.88	+22 54 20.86	1298694726154793856	16244387+2254209	42.92 ± 0.33	−145.09	−96.73	10.355	11.421	9.362	7.208	−
16 25 13.01	−21 56 14.50	6051948158061617024	16251302−2156141	53.81 ± 0.05	−570.98	−337.68	9.675	10.624	8.744	6.725	−
16 26 01.34	−06 39 26.07	4352067894065551744	16260134−0639257	43.93 ± 0.19	−80.69	−383.43	17.162	20.427	15.573	11.846	−
16 26 51.68	−38 12 32.59	6018209128388194688	16265168−3812326	71.42 ± 0.12	−296.05	−258.73	13.902	16.114	12.507	9.443	−
16 27 33.23	−10 00 28.45	4344429586787123072	16273324−1000282	47.79 ± 0.05	−206.17	−324.63	10.002	11.074	9.005	6.834	−
16 30 13.09	−14 39 49.55	4325701192912743424	16301314−1439494	45.90 ± 0.25	−520.69	−218.85	11.131	12.526	9.998	7.598	−
16 30 18.06	−12 39 45.32	4330690742322011520	16301808−1239434	232.21 ± 0.06	−94.03	−1183.78	8.794	10.343	7.604	5.075	−
16 30 27.30	−36 33 55.82	6018950572865687808	16302725−3633559	59.37 ± 0.12	−424.78	−166.25	13.705	15.692	12.343	9.028	−
16 31 35.06	+17 33 48.86	4467057362718750080	16313507+1733494	59.47 ± 0.09	−324.76	−810.54	11.654	13.069	10.507	8.178	−
16 32 45.19	+12 36 46.00	4459548724797475200	16324524+1236460	54.05 ± 0.15	−764.81	−136.21	11.055	12.394	9.963	7.675	−
16 32 52.84	+09 50 25.97	4446574040918651904	16325284+0950259	65.05 ± 0.07	228.73	155.62	11.806	13.302	10.633	8.160	−
16 32 58.82	−06 31 48.40	4352307381441947392	16325882−0631481	47.80 ± 0.22	17.80	−346.87	17.175	20.411	15.591	11.621	−

Table 2: List of M dwarf systems within 25 pc drawn from *Gaia* DR2, as described in §2.3.

These systems have not been vetted to distinguish single stars from multiples, but in cases

where a system was resolved in *Gaia* but not 2MASS, a “J” flag is listed in column 12.

16 33 13.08	-75 53 22.89	5781043783061254272	16331306-7553232	43.97 ± 0.14	-138.70	-811.84	17.616	20.944	16.030	12.126	-
16 33 19.67	-52 07 56.25	5934097210481810432	16331968-5207561	74.07 ± 0.08	-201.72	-350.76	11.110	12.606	9.959	7.434	-
16 33 49.07	-68 08 48.21	5809399363316632064	16334908-6808480	65.67 ± 0.18	-218.77	-314.77	15.303	18.360	13.798	10.072	-
16 34 55.18	-53 34 38.34	5930619695722133760	16345519-5334381	59.96 ± 0.08	-174.75	-652.55	11.075	12.386	9.993	7.706	-
16 35 24.64	-27 18 54.59	6044721476534419584	16352464-2718533	50.81 ± 0.07	-6.21	-894.62	12.769	14.440	11.525	8.998	-
16 35 37.20	-52 02 00.82	5931193640795532288	16353720-5202008	65.27 ± 0.09	-192.11	89.15	13.743	15.818	12.399	9.559	-
16 35 40.41	-30 51 20.21	6031475835680030720	16354037-3051205	51.51 ± 0.08	-802.95	-842.57	11.550	12.944	10.418	8.075	-
16 36 05.65	+08 48 49.26	4446207564241339520	16360563+0848491	66.08 ± 0.06	-518.19	-158.66	12.402	14.112	11.152	8.510	-
16 36 57.57	-40 41 08.91	5968887716837842048	16365758-4041086	44.72 ± 0.07	-72.86	-283.07	12.138	13.696	10.936	8.312	-
16 37 33.57	-53 41 55.62	5930579185585956992	16373358-5341555	53.16 ± 0.05	-313.08	-166.56	10.585	11.735	9.551	7.361	-
16 37 43.20	-20 13 33.93	4130971047908354304	16374318-2013338	50.85 ± 0.07	89.14	-81.89	12.341	13.981	11.105	8.492	-
16 39 25.81	-46 53 00.34	5942630107855861888	16392581-4653002	51.75 ± 0.07	-73.22	-292.13	12.058	13.516	10.890	8.434	-
16 39 37.00	-55 24 36.10	5930139823230549120	16393700-5524360	49.84 ± 0.08	-90.60	-131.13	13.692	15.570	12.396	9.604	-
16 40 05.98	+00 42 18.85	4383790518216171264	16400599+0042188	88.72 ± 0.07	175.60	-158.04	12.193	13.962	10.929	8.209	-
16 40 45.25	-45 59 59.30	5942777301034031104	16404524-4559590	59.11 ± 0.06	354.86	-399.80	11.565	12.946	10.432	8.050	-
16 41 28.26	-43 59 11.26	5943550124208359552	16412829-4359109	63.51 ± 0.06	-376.24	-485.04	10.641	11.851	9.582	7.334	-
16 42 06.03	-17 09 56.75	4132033901994675456	16420607-1709559	40.53 ± 0.08	-327.69	-419.16	14.353	16.271	13.044	10.244	-
16 46 13.74	+16 28 40.79	4558856584955186432	16461372+1628407	63.41 ± 0.04	-354.76	-471.97	10.587	11.921	9.475	7.094	-
16 46 24.24	-52 50 42.20	5930862138021206656	16462424-5250421	45.71 ± 0.07	55.87	45.93	11.482	12.804	10.382	8.037	-
16 47 55.15	-65 09 11.60	5815970800722940800	16475517-6509116	68.55 ± 0.05	349.74	-100.78	12.637	14.271	11.410	8.879	-
16 48 24.32	-29 13 10.02	6031367499416648192	16482431-2913100	50.00 ± 0.76	-62.37	-115.01	20.004	21.530	18.305	13.133	-
16 48 24.47	-72 58 33.91	5805810454276181120	16482446-7258342	63.44 ± 0.03	-478.98	-532.35	10.438	11.574	9.417	7.224	-
16 48 45.96	-15 44 20.16	4134107168607042816	16484597-1544198	52.74 ± 0.05	-6.74	-220.14	10.022	11.148	9.000	6.774	-
16 49 04.19	+04 44 57.02	4434578579508991360	16490419+0444571	40.18 ± 0.17	53.81	72.52	17.376	20.626	15.788	11.882	-
16 49 13.57	-00 31 27.91	4382616720834062848	16491360-0031278	75.53 ± 1.81	45.73	4.83	19.357	20.326	17.727	14.667	-
16 50 53.79	-04 50 35.06	4353476020565733632	16505382-0450349	55.16 ± 0.06	-750.01	-235.37	12.234	13.722	11.050	8.676	-
16 50 57.94	+22 27 05.66	4566158991430299520	16505794+2227058	95.56 ± 0.06	36.60	400.30	12.413	14.339	11.103	8.309	-
16 52 35.14	-29 00 19.09	6032685745182407040	16523515-2900186	51.05 ± 0.09	-110.18	-349.40	14.055	16.060	12.676	9.706	-
16 53 33.72	-56 32 52.52	5929051723344715008	16533371-5632524	41.15 ± 0.04	-162.19	-361.80	11.991	13.271	10.890	8.567	-
16 54 12.03	+11 54 52.86	4448223656247483904	16541202+1154529	49.79 ± 0.04	-543.80	316.26	10.040	10.991	9.107	7.106	-
16 55 25.22	-08 19 21.30	4339465360508118912	16552527-0819207	153.92 ± 0.13	-816.94	-898.33	10.435	12.026	9.243	6.724	-

Table 2: List of M dwarf systems within 25 pc drawn from *Gaia* DR2, as described in §2.3.

These systems have not been vetted to distinguish single stars from multiples, but in cases

where a system was resolved in *Gaia* but not 2MASS, a “J” flag is listed in column 12.

16 55 35.26	−08 23 40.75	4339417394313320192	16553529−0823401	153.81 ± 0.11	−813.42	−870.61	13.838	17.075	12.321	8.816	−
16 56 33.61	−20 46 37.58	4127182375667696128	16563362−2046373	61.09 ± 0.11	−194.34	−194.02	15.015	17.620	13.566	10.368	−
16 56 44.62	−34 59 17.99	5977903849656045824	16564462−3459181	51.30 ± 0.58	30.72	−1.70	18.791	19.409	17.342	14.650	−
16 56 45.13	−37 03 38.68	5971414119713770240	16564514−3703385	49.30 ± 0.04	−147.52	−454.71	10.564	11.699	9.542	7.344	−
16 56 48.57	−39 05 38.16	5970189504223192960	16564855−3905380	63.81 ± 0.06	56.32	−106.53	10.385	11.771	9.248	6.489	−
16 57 05.74	−04 20 56.32	4365609170043180416	16570570−0420559	115.03 ± 0.08	481.54	−376.24	10.906	12.541	9.698	7.120	−
16 57 34.55	+10 54 23.46	4447496977846072960	16573454+1054233	41.91 ± 0.34	−96.18	−91.18	19.111	21.832	17.415	12.801	−
16 58 56.13	−53 11 42.89	5935907693782592000	16585612−5311430	43.96 ± 0.09	−151.29	−199.76	13.677	15.557	12.373	9.560	−
16 59 03.91	−53 12 29.91	5935904773205046912	16590389−5312299	44.63 ± 0.13	−158.44	−193.54	14.529	16.448	13.141	10.014	−
16 59 09.61	+20 58 16.37	4561968271578549632	16590962+2058160	56.18 ± 0.57	−22.32	123.14	11.357	12.662	10.007	7.513	−
16 59 28.13	−69 58 18.33	5808063765921988864	16592811−6958185	48.09 ± 0.08	−380.49	−585.67	13.712	15.651	12.403	9.696	−
17 00 17.41	−16 54 44.97	4132842313621569792	17001742−1654448	40.83 ± 0.16	−112.73	−61.37	16.046	18.816	14.587	11.227	−
17 01 02.12	+08 12 26.42	4443110789740420480	17010211+0812264	51.02 ± 0.04	−246.57	−182.29	12.241	13.758	11.048	8.553	−
17 02 08.25	−27 40 24.62	6030284102539737728	17020825−2740242	41.86 ± 0.09	−129.85	−220.40	12.943	14.658	11.691	9.041	−
17 02 49.59	−06 04 06.25	4364314662596822528	17024958−0604063	50.53 ± 0.06	−126.27	−83.66	10.052	11.083	9.075	6.945	−
17 04 22.34	+16 55 55.57	4547881191164080768	17042234+1655552	60.83 ± 0.06	133.50	−1132.06	11.224	12.570	10.121	7.795	−
17 05 13.78	−05 05 39.25	4364480521350598144	17051383−0505385	95.64 ± 0.06	−917.28	−1131.95	9.168	10.311	8.133	5.975	−
17 05 48.35	−05 16 46.34	4364462551205872000	17054834−0516462	52.67 ± 0.35	116.74	−120.24	18.179	21.048	16.549	12.032	−
17 06 50.05	−82 11 41.92	5774108991423344000	17065001−8211420	41.87 ± 0.05	−166.13	−257.51	13.142	14.793	11.899	9.275	−
17 06 54.86	−13 14 39.97	4140696473069943424	17065487−1314396	51.48 ± 0.52	−12.61	−187.82	19.668	21.599	17.945	13.095	−
17 07 07.49	+21 33 14.47	4568060562432051584	17070752+2133144	71.16 ± 0.04	−463.40	−25.44	10.555	11.916	9.431	7.042	−
17 07 23.43	−05 58 25.22	4364185165038935040	17072343−0558249	85.01 ± 0.44	87.37	17.86	16.942	20.420	15.236	10.711	−
17 08 14.80	−34 36 22.64	5977390652584004480	17081482−3436213	49.75 ± 0.13	−266.00	−838.61	14.265	16.308	12.907	10.006	−
17 09 52.76	+11 55 34.03	4540984195244025088	17095274+1155341	51.93 ± 0.15	−365.29	−79.01	12.641	14.332	11.393	8.729	−
17 10 19.00	−14 44 57.33	4139489552908817920	17101899−1444575	52.66 ± 0.06	27.63	90.73	10.909	12.132	9.842	7.607	−
17 10 44.33	−53 00 25.58	5924057019994083712	17104431−5300250	45.05 ± 0.15	−45.45	−170.66	11.096	12.176	9.647	7.163	−
17 10 59.15	−52 30 55.84	5924187617032756736	17105916−5230559	78.36 ± 0.04	−247.58	156.56	9.207	10.294	8.203	6.026	−
17 11 19.63	−27 32 50.93	4108574893750868480	17111967−2732509	47.98 ± 2.68	−5.82	−5.51	20.134	21.388	18.494	15.141	−
17 12 01.21	−27 46 02.17	4108554857678482432	17120120−2746023	44.24 ± 0.06	−219.30	−126.65	12.249	13.677	11.089	8.656	−
17 12 04.32	−03 23 30.26	4366633811793952896	17120433−0323300	51.07 ± 0.12	−371.24	−181.54	15.530	18.246	14.048	10.637	−
17 12 51.28	−05 07 31.35	4364702279101280256	17125127−0507311	43.25 ± 0.42	189.05	−705.98	10.872	11.869	9.907	7.937	−

Table 2: List of M dwarf systems within 25 pc drawn from *Gaia* DR2, as described in §2.3.

These systems have not been vetted to distinguish single stars from multiples, but in cases

where a system was resolved in *Gaia* but not 2MASS, a “J” flag is listed in column 12.

17 12 51.50	-43 20 31.07	5965209575545481216	17125151-4320311	44.64 ± 0.09	24.23	-288.34	10.395	11.499	9.391	7.234	-
17 13 11.55	-18 34 24.82	4134597202897079936	17131153-1834250	47.99 ± 0.05	24.76	-105.75	10.018	11.031	9.047	6.479	-
17 13 40.47	-08 25 14.82	4359809585500446720	17134048-0825144	50.03 ± 0.31	-438.21	-408.18	10.862	12.285	9.715	7.253	-
17 13 40.48	-39 52 11.87	5972124644679705728	17134048-3952120	51.45 ± 0.27	108.68	-285.98	18.153	20.395	16.487	12.104	-
17 14 19.45	-15 01 17.40	4136502179820402304	17141946-1501172	41.87 ± 0.10	-99.63	-102.97	15.134	17.395	13.746	10.696	-
17 15 18.93	+04 57 50.06	4393265392167891712	17151894+0457496	68.27 ± 0.17	580.45	-749.59	13.009	14.932	11.696	8.782	-
17 15 50.12	+19 00 00.08	4548562265603840768	17155010+1900000	73.11 ± 0.03	-150.00	14.03	9.644	10.630	8.598	6.450	-
17 16 00.64	+11 03 27.61	4540061704988054400	17160063+1103274	55.08 ± 0.05	-137.31	-347.32	9.983	11.095	8.967	6.816	-
17 16 20.65	-05 23 51.37	4361639417663824768	17162064-0523512	51.15 ± 0.10	168.67	-124.32	11.379	12.768	10.258	7.829	-
17 16 40.98	+08 03 30.20	4395113392038461312	17164097+0803302	66.14 ± 0.04	-278.77	-67.20	10.470	11.732	9.389	7.106	-
17 16 47.80	+11 33 52.32	4540115306180362368	17164779+1133523	40.39 ± 0.05	-130.32	135.34	12.814	14.472	11.571	8.918	-
17 17 44.09	+11 40 12.43	4540481374832743040	17174408+1140117	80.80 ± 0.17	-352.90	-445.56	13.238	15.354	11.881	8.931	-
17 18 32.31	-07 39 15.26	4360144043194583296	17183232-0739151	41.92 ± 0.06	-278.60	-150.13	12.623	14.046	11.466	9.052	-
17 18 54.55	-41 31 40.09	5959737748540750592	17185456-4131395	88.79 ± 0.18	-220.05	-911.54	14.578	17.425	13.089	9.621	-
17 18 58.83	-34 59 48.61	5975663354131618304	17185868-3459483	138.02 ± 0.09	1131.61	-215.54	9.380	10.615	8.311	6.036	-
17 19 19.35	-47 36 18.46	5950974851364748160	17191934-4736182	43.55 ± 0.14	131.09	-276.16	16.500	19.181	14.942	11.552	-
17 19 20.33	-29 49 24.04	4059215823975992960	17192033-2949233	40.36 ± 0.11	-35.64	-515.99	12.841	14.400	11.641	9.110	-
17 19 47.97	-38 55 29.00	5972467791084770688	17194793-3855287	41.70 ± 0.68	-39.28	26.46	18.233	19.059	16.840	13.129	-
17 19 50.54	-22 24 11.41	4114726279009806976	17195055-2224115	47.43 ± 0.08	-96.48	-26.09	14.708	16.905	13.326	10.344	-
17 21 54.62	+21 25 47.35	4567274927016803328	17215464+2125468	63.00 ± 0.10	-159.79	246.64	12.459	14.175	11.206	8.492	-
17 22 33.91	+05 31 15.39	4390370373754096128	17223390+0531153	40.84 ± 0.06	-97.59	-18.86	11.570	12.886	10.465	8.120	-
17 23 49.23	-32 15 16.28	5979367986779538432	17234924-3215153	45.51 ± 0.05	-168.22	-617.49	10.766	11.896	9.739	7.519	-
17 23 51.12	-35 41 10.16	5975349615358601856	17235113-3541093	44.34 ± 0.06	-142.26	-559.84	12.772	14.158	11.633	9.223	-
17 23 56.80	+13 38 20.18	4542284161585626496	17235678+1338204	49.51 ± 0.05	97.41	-132.52	12.425	14.017	11.207	8.668	-
17 24 16.94	-04 21 52.09	4363125648147587328	17241695-0421520	48.47 ± 0.07	-234.39	-122.87	11.101	12.417	10.007	7.655	-
17 26 08.32	-24 41 12.34	4110096961504087168	17260832-2441124	42.91 ± 0.06	-6.87	84.71	14.156	16.077	12.843	9.971	-
17 26 15.26	-03 11 30.96	4363875373342033664	17261525-0311308	53.83 ± 0.07	-30.24	-103.34	13.575	15.483	12.263	9.501	-
17 26 22.93	-84 33 08.30	5767542123866994304	17262298-8433082	48.82 ± 0.06	355.46	-372.65	12.898	14.557	11.658	9.021	-
17 26 41.68	-47 12 07.17	5950304355429385984	17264170-4712069	50.95 ± 0.07	-542.68	-488.41	12.576	13.992	11.412	9.083	-
17 27 06.90	-60 16 07.57	5912492318012378752	17270690-6016076	44.81 ± 0.07	-91.17	-80.01	12.542	14.127	11.327	8.716	-
17 27 14.08	-25 09 36.43	4110023156763233408	17271403-2509357	50.76 ± 0.06	426.20	-451.29	12.114	13.652	10.920	8.494	-

Table 2: List of M dwarf systems within 25 pc drawn from *Gaia* DR2, as described in §2.3.

These systems have not been vetted to distinguish single stars from multiples, but in cases

where a system was resolved in *Gaia* but not 2MASS, a “J” flag is listed in column 12.

17 27 39.88	+14 29 01.89	4542821410453751680	17274007+1429027	54.04 ± 0.05	−1117.94	−343.34	12.513	14.011	11.322	8.958	—
17 27 59.23	−01 11 09.48	4373221192113292928	17275921−0111092	41.66 ± 1.16	308.74	−313.40	20.610	21.367	18.818	13.852	—
17 28 07.32	−62 27 14.27	5910710976034819584	17280732−6227145	60.77 ± 0.07	−287.20	−936.03	11.395	13.029	10.193	7.567	—
17 28 39.95	−46 53 42.69	5951824121022278144	17283991−4653424	219.80 ± 0.05	572.58	−880.25	8.331	9.681	7.216	4.855	—
17 29 27.32	−80 08 57.30	5776161813992756992	17292729−8008573	78.47 ± 0.04	−518.14	473.07	10.922	12.429	9.752	7.299	—
17 29 46.20	−25 03 53.62	4110388293316278528	17294620−2503529	55.39 ± 0.81	−39.48	−463.79	12.223	13.815	11.012	8.459	—
17 30 10.34	−20 04 51.42	4121448452584163840	17301035−2004509	42.57 ± 1.64	−2.63	3.72	20.333	20.486	18.299	15.162	—
17 30 22.26	+19 12 32.28	4554019214828782848	17302224+1912323	52.97 ± 0.04	381.99	−101.18	12.428	13.795	11.285	8.944	—
17 30 22.73	+05 32 54.66	4389844948935164544	17302272+0532547	98.85 ± 0.04	29.84	−249.21	8.530	9.548	7.556	5.422	—
17 30 49.90	−19 58 39.82	4121455981682434176	17304988−1958398	40.41 ± 2.11	−3.66	−10.86	20.217	20.477	18.385	15.074	—
17 31 27.17	−07 59 49.04	4169232338868860160	17312716−0759488	54.17 ± 0.17	40.76	−227.52	16.527	—	—	11.150	—
17 31 38.16	+01 47 49.67	4376455233769489536	17313816+0147496	40.55 ± 0.04	−179.57	−105.37	11.089	12.255	10.045	7.771	—
17 31 44.95	−78 51 25.69	5776716483248901760	17314492−7851257	42.91 ± 0.07	−96.77	−360.56	15.302	17.682	13.884	10.675	—
17 32 15.27	−21 13 51.12	4117946443687177472	17321530−2113507	45.23 ± 1.91	−23.20	11.90	19.860	20.920	18.240	16.080	—
17 32 21.94	−47 36 58.06	5951535219996858624	17322194−4736580	50.93 ± 0.07	−229.18	−184.40	12.600	14.261	11.358	8.682	—
17 32 33.76	−09 01 17.86	4166869660174061312	17323375−0901178	41.72 ± 0.05	214.61	−78.76	11.594	12.786	10.535	8.341	—
17 33 06.12	−30 35 08.13	4058369298708349824	17330612−3035079	54.71 ± 0.06	−113.45	−123.01	12.450	13.931	11.277	8.795	—
17 33 40.63	−42 55 43.33	5958896763938010624	17334063−4255429	42.78 ± 0.33	−11.79	68.42	13.234	14.241	11.332	8.676	—
17 33 42.28	−16 54 50.12	4124397553254685440	17334227−1654500	55.32 ± 0.36	71.18	−38.40	18.416	19.528	16.674	12.350	—
17 33 53.16	+16 55 12.84	4549983418742839808	17335314+1655129	62.37 ± 0.39	−122.08	−116.00	12.399	14.570	11.028	7.995	—
17 34 03.51	−71 15 29.01	5803999970941812224	17340353−7115289	40.10 ± 0.06	9.13	50.89	14.995	17.116	13.636	10.718	—
17 34 08.68	−08 49 51.75	4168368844280868992	17340869−0849514	61.92 ± 0.08	−183.01	−311.45	14.138	16.162	12.815	10.055	—
17 34 30.54	−11 51 39.04	4162703606326651392	17343053−1151388	48.66 ± 0.24	119.78	−372.65	17.687	20.940	16.067	11.883	—
17 34 50.34	+22 54 19.41	4557368602127213056	17345033+2254193	41.21 ± 0.04	−72.72	−82.71	13.632	15.312	12.385	9.773	—
17 35 13.62	−48 40 51.12	5946986063684477056	17351362−4840510	103.35 ± 0.05	74.41	470.34	9.283	10.496	8.219	5.829	—
17 35 15.17	−52 10 06.43	5922125556008846208	17351517−5210064	51.45 ± 0.10	93.09	−129.53	12.836	14.591	11.566	8.812	—
17 35 37.49	+00 12 21.08	4373813863241766784	17353749+0012209	40.81 ± 0.11	−2.28	−319.29	15.293	17.586	13.906	10.874	—
17 36 01.77	−07 08 18.78	4169409974417144192	17360176−0708187	42.91 ± 0.08	−36.72	−17.69	12.960	14.665	11.713	9.031	—
17 36 31.17	−25 15 00.94	4062191480304598656	17363114−2515007	60.24 ± 0.83	−24.24	6.89	14.721	16.575	13.146	7.887	—
17 36 41.81	−34 25 46.19	4053559111471124608	17364180−3425459	53.08 ± 0.12	−122.50	−146.84	15.328	18.042	13.843	10.498	—
17 36 45.79	−22 20 43.91	4116840541184279296	17364579−2220429	46.87 ± 0.20	−92.12	−590.65	13.016	14.842	11.715	8.988	—

Table 2: List of M dwarf systems within 25 pc drawn from *Gaia* DR2, as described in §2.3.

These systems have not been vetted to distinguish single stars from multiples, but in cases

where a system was resolved in *Gaia* but not 2MASS, a “J” flag is listed in column 12.

17 37 03.67	−44 19 09.17	5955305209191546112	17370367−4419088	199.70 ± 0.08	−706.12	−937.91	9.570	11.223	8.336	5.606	−
17 37 30.61	−66 33 13.93	5812456039998285312	17373061−6633141	40.21 ± 0.04	−61.91	−480.84	12.583	14.048	11.406	8.943	−
17 37 32.26	−66 34 24.01	5812455902555239424	17373235−6634238	40.28 ± 0.07	−68.35	−469.61	10.366	11.383	9.380	6.818	J
17 37 36.49	+22 05 50.17	4557080701880013824	17373648+2205510	48.75 ± 0.05	29.66	−308.71	12.756	14.397	11.520	8.888	−
17 37 53.35	+18 35 30.16	4550763526539955712	17375330+1835295	122.56 ± 0.03	926.74	984.70	8.739	9.840	7.723	5.572	−
17 38 32.50	−58 32 34.42	5912921509809469952	17383251−5832342	61.21 ± 0.05	19.73	−333.60	11.311	12.801	10.148	7.667	−
17 38 51.25	+08 01 35.28	4487343970727152128	17385125+0801352	49.44 ± 0.11	−81.90	−221.53	11.239	12.512	10.165	7.847	−
17 39 24.35	−23 27 07.19	4116504399886241792	17392440−2327071	53.52 ± 0.10	−453.38	−43.20	13.856	15.757	12.544	9.776	−
17 39 25.15	+24 54 42.38	4581695915363428736	17392515+2454421	41.70 ± 0.94	80.38	−600.04	20.697	21.560	18.985	13.946	−
17 39 59.98	−27 07 06.86	4060950333528619904	17395997−2707071	59.66 ± 0.05	80.20	147.74	11.324	12.542	10.255	8.046	−
17 41 54.41	+09 40 53.95	4489306942580947584	17415439+0940537	54.66 ± 0.14	−339.77	−259.10	15.955	18.940	14.432	10.968	−
17 42 10.76	−08 49 00.19	4165225959018604288	17421079−0848598	46.99 ± 0.06	−839.89	−473.99	12.494	13.863	11.357	9.065	−
17 42 27.34	−23 06 54.37	4116870812104603520	17422732−2306543	45.96 ± 0.08	88.85	−17.56	13.570	15.365	12.290	9.557	−
17 42 32.27	−16 38 24.83	4124051889957546624	17423229−1638236	49.28 ± 0.06	−107.56	−691.05	12.035	13.322	10.941	8.678	−
17 44 24.96	−58 34 15.17	5918136424731578240	17442494−5834151	45.23 ± 0.12	81.52	−28.90	15.747	18.380	14.300	11.132	−
17 45 34.67	−16 40 53.96	4123874907297370240	17453466−1640538	51.03 ± 0.30	106.92	−100.33	18.429	20.268	16.754	12.402	−
17 46 04.65	+24 39 04.92	4581486217883307008	17460465+2439049	66.76 ± 0.05	−371.16	508.40	11.546	12.985	10.398	8.059	−
17 46 12.75	−32 06 09.14	4055585060376248832	17461275−3206088	70.76 ± 0.05	−76.84	−271.89	9.588	10.771	8.543	6.251	−
17 46 23.52	−05 51 49.10	4175226257790341504	17462352−0551490	40.07 ± 0.10	−9.99	−226.78	15.583	17.955	14.175	11.081	−
17 46 29.33	−08 42 36.50	4165561928540617856	17462934−0842362	76.59 ± 0.08	−44.20	−428.04	11.273	13.001	10.028	7.353	−
17 46 34.23	−57 19 08.56	5918660719981686144	17463427−5719081	169.86 ± 0.12	−1117.14	−1353.82	9.581	11.018	8.432	6.016	−
17 46 40.66	−32 14 04.50	4055579464064558592	17464063−3214045	82.92 ± 0.11	205.39	102.98	13.973	16.394	12.567	9.381	−
17 48 27.73	−74 27 55.94	5802998414627070080	17482771−7427560	51.88 ± 0.04	−7.11	−145.45	11.392	12.715	10.284	7.918	−
17 49 16.42	−35 53 42.24	4040285772776989056	17491641−3553419	40.50 ± 0.07	13.28	−296.96	12.298	13.874	11.087	8.520	−
17 49 59.50	+22 41 06.82	4580216762992082048	17495948+2241069	44.05 ± 0.46	−776.64	−113.20	16.094	19.059	14.602	11.287	−
17 50 15.13	+23 45 50.93	4580620038939265920	17501513+2345511	46.81 ± 0.04	−340.24	449.53	12.224	13.774	11.020	8.450	−
17 50 59.01	−56 36 06.87	5918765792061510144	17505894−5636072	40.51 ± 0.04	−1058.45	−685.39	11.283	12.352	10.286	8.187	−
17 51 50.25	+07 14 47.20	4475839844988727808	17515024+0714473	46.12 ± 0.05	−97.32	57.60	12.313	13.825	11.122	8.621	−
17 53 00.59	+16 55 03.36	4502798839309818368	17530062+1655029	44.15 ± 1.02	−243.94	−240.05	12.025	13.086	10.437	7.874	−
17 53 22.64	−15 54 23.61	4147993588172928640	17532264−1554236	43.13 ± 0.05	−1.05	121.47	12.196	13.668	11.024	8.547	−
17 53 45.19	−65 59 55.67	5908794218026022144	17534518−6559559	63.82 ± 0.32	−52.88	−341.97	19.344	21.260	17.712	12.424	−

Table 2: List of M dwarf systems within 25 pc drawn from *Gaia* DR2, as described in §2.3.

These systems have not been vetted to distinguish single stars from multiples, but in cases

where a system was resolved in *Gaia* but not 2MASS, a “J” flag is listed in column 12.

17 54 02.47	−04 32 46.29	4175841812495567104	17540246−0432459	46.37 ± 2.50	−20.94	11.16	20.127	21.036	18.497	16.741	—
17 54 02.99	−34 40 18.15	4040839376832467584	17540302−3440177	52.31 ± 0.05	−309.14	−240.06	12.285	13.792	11.096	8.550	—
17 54 17.12	+07 22 44.80	4475881317196185728	17541710+0722446	62.22 ± 0.06	−598.98	−287.97	11.819	13.469	10.592	7.974	—
17 54 43.33	+12 51 20.67	4496250461589918080	17544332+1251206	48.33 ± 0.05	−79.44	−130.79	11.187	12.350	10.147	7.948	—
17 56 13.60	−41 05 56.69	5957041127551353088	17561359−4105566	43.74 ± 0.11	28.64	−9.25	13.678	15.450	12.407	9.704	—
17 56 36.02	−20 42 29.72	4071058526222980096	missing	145.81 ± 1.32	−36.91	9.45	19.311	19.777	17.364	—	—
17 56 56.21	−48 05 09.63	5947766235872922624	17565620−4805096	47.15 ± 0.23	77.11	29.86	18.190	—	—	12.190	—
17 57 03.54	+15 46 43.03	4501735993818529664	17570356+1546432	46.87 ± 0.21	−193.90	−233.34	11.854	12.750	10.146	7.514	—
17 57 14.22	−41 59 29.17	5956746565858482176	17571423−4159290	56.52 ± 0.04	−69.03	−370.25	10.405	11.556	9.366	7.143	—
17 57 22.63	−52 29 06.78	5945333635111767040	17572263−5229068	46.60 ± 0.05	95.70	−232.86	12.025	13.308	10.918	8.611	—
17 57 41.29	−11 12 18.33	4152047350078302592	17574130−1112188	75.35 ± 1.78	146.53	−155.71	19.612	19.936	18.071	15.395	—
17 57 46.38	−44 19 17.70	5956044179742203520	17574638−4419177	47.67 ± 0.12	−92.37	−157.92	15.375	17.979	13.923	10.652	—
17 57 48.50	+04 41 36.11	4472832130942575872	17574849+0441405	547.45 ± 0.29	−802.80	10362.54	8.195	9.810	6.970	4.524	—
17 58 22.13	+12 45 42.71	4496383055821714816	17582208+1245433	55.34 ± 0.05	334.59	−294.84	12.483	13.933	11.315	8.922	—
17 58 39.56	−58 39 21.80	5918299904067162240	missing	52.24 ± 0.12	−271.59	−974.01	14.912	17.218	13.481	—	—
17 59 41.87	−16 26 08.47	4145033393613641984	17594186−1626082	53.32 ± 0.10	19.97	−163.94	13.308	15.117	12.023	9.260	—
18 00 01.17	−15 59 23.97	4145132555890838784	18000116−1559235	80.90 ± 0.34	−7.45	−296.09	18.616	20.075	16.795	11.981	—
18 01 52.66	−27 06 54.38	4063191108246057472	18015266−2706540	41.71 ± 0.07	−248.46	−517.17	13.654	15.418	12.380	9.604	—
18 03 36.04	−18 58 49.93	4095396422225930624	18033605−1858503	76.20 ± 0.79	173.16	−341.84	12.456	14.417	11.138	8.275	—
18 04 06.30	−13 21 32.07	4150249919153716480	18040630−1321320	41.61 ± 0.13	68.70	−22.81	12.999	14.410	11.856	9.447	—
18 04 14.62	−31 29 28.90	4043852481204049536	18041462−3129284	46.15 ± 0.15	−15.27	−811.67	15.153	17.345	13.748	10.877	—
18 04 33.02	−15 34 37.44	4145205501565331712	18043303−1534373	49.26 ± 0.38	−23.55	−24.72	18.870	20.704	17.160	12.547	—
18 04 38.71	+13 54 14.20	4498055584805914752	18043871+1354143	52.15 ± 0.04	151.38	43.36	12.118	13.482	10.982	8.639	—
18 05 07.58	−03 01 52.75	4177731838628465408	18050755−0301523	129.39 ± 0.06	569.73	−332.46	8.517	9.622	7.494	5.306	—
18 05 29.13	+01 32 35.95	4468161302457071360	18052911+0132359	46.64 ± 0.05	−270.65	−32.22	11.896	13.367	10.720	8.261	—
18 05 38.06	−20 17 09.01	4094926445417081472	18053805−2017088	40.40 ± 1.16	−7.26	−3.19	18.996	19.959	17.131	10.834	—
18 05 44.65	−14 22 42.49	4147112604476417792	18054470−1422425	105.56 ± 0.14	−344.94	24.89	13.277	15.572	11.888	8.861	—
18 06 17.05	−21 25 45.75	4070042165108311680	18061706−2125454	64.29 ± 1.56	−7.12	3.66	19.524	20.797	17.748	13.810	—
18 06 48.56	+17 20 47.17	4502369583096912896	18064856+1720472	66.99 ± 0.05	20.11	165.78	12.477	14.126	11.248	8.652	—
18 07 06.22	−06 25 47.23	4171383636445972096	18070621−0625471	53.40 ± 0.47	124.01	−206.12	17.624	20.597	15.997	11.852	—
18 07 32.84	−15 57 47.07	4145870293808914688	18073292−1557464	125.59 ± 0.07	−618.43	−347.10	11.878	13.802	10.580	7.827	—

Table 2: List of M dwarf systems within 25 pc drawn from *Gaia* DR2, as described in §2.3.

These systems have not been vetted to distinguish single stars from multiples, but in cases

where a system was resolved in *Gaia* but not 2MASS, a “J” flag is listed in column 12.

18 08 12.14	+11 34 46.59	4495301445619547904	18081215+1134467	44.55 ± 0.07	−452.86	−404.19	13.977	15.933	12.646	9.715	—
18 08 47.54	−26 32 39.76	4064593187342783488	18084755−2632395	48.07 ± 0.12	−261.50	−438.39	13.246	14.760	12.032	9.494	—
18 08 53.51	−02 06 58.56	4177911333902753280	18085349−0206586	54.47 ± 0.08	191.12	63.62	13.864	15.893	12.522	9.704	—
18 08 59.14	−35 46 44.96	4038797789974368128	18085914−3546448	45.65 ± 0.07	−83.47	−96.17	13.005	14.491	11.814	9.316	—
18 09 43.70	−02 19 35.06	4177855052651068928	18094366−0219347	61.25 ± 0.45	6.33	−533.34	13.452	15.382	12.135	9.271	—
18 09 50.15	−02 47 43.16	41747997847111199616	18095018−0247421	42.78 ± 0.14	−576.85	−829.09	14.608	16.567	13.293	10.675	—
18 10 52.54	−07 08 49.97	4171084878520425216	18105253−0708497	42.31 ± 0.07	6.57	−351.73	13.488	15.193	12.235	9.586	—
18 11 15.25	−78 59 22.87	6364795328246346112	18111528−7859227	85.84 ± 0.39	60.50	304.05	11.220	12.953	9.845	6.964	—
18 13 20.37	−39 50 35.91	6725832095922016256	18132037−3950357	53.01 ± 0.09	−31.11	−144.85	11.739	13.127	10.600	8.187	—
18 14 59.85	+19 39 25.94	4527029949581078016	18145985+1939259	48.70 ± 0.04	95.43	−123.60	12.030	13.300	10.930	8.681	—
18 15 12.42	−19 24 06.66	4094679437572611712	18151241−1924063	68.50 ± 0.05	109.10	−397.24	9.987	11.163	8.949	6.453	—
18 15 29.75	+06 10 33.66	4471720799558032384	18152976+0610337	40.95 ± 0.63	−23.49	−105.06	15.653	17.515	13.733	10.477	—
18 15 41.09	−22 37 34.20	4090479921678998272	missing	122.03 ± 1.77	5.51	0.12	19.442	19.649	17.645	—	—
18 15 43.59	+18 56 19.55	4526778333217510656	18154360+1856199	43.54 ± 0.34	−39.39	−426.24	10.047	11.078	9.062	6.964	—
18 16 02.25	+13 54 48.20	4497494077967197568	18160224+1354480	54.76 ± 0.05	98.86	−500.95	9.474	10.412	8.548	6.557	—
18 16 08.83	+00 19 47.98	4274925505435880704	18160883+0019481	45.00 ± 0.06	16.44	44.13	10.441	11.527	9.435	7.243	—
18 16 18.18	+01 31 27.36	4277318077096011264	18161819+0131277	63.00 ± 0.06	−408.91	−638.26	11.450	12.814	10.319	7.891	—
18 16 31.54	+04 52 45.78	4470812298018311296	18163154+0452456	68.15 ± 0.11	−155.72	407.39	13.038	14.968	11.729	8.832	—
18 17 26.92	−09 37 29.17	4157616097307511168	18172692−0937291	42.27 ± 0.05	53.12	−46.90	11.604	12.928	10.485	8.111	—
18 19 17.07	−77 02 49.76	6413248744098317568	18191700−7702501	46.76 ± 0.04	−224.66	−575.73	12.751	14.349	11.529	9.058	—
18 19 19.64	−40 32 58.00	6726429375571878912	18191963−4032578	42.23 ± 0.10	28.23	−259.54	15.721	18.157	14.260	10.919	—
18 19 29.31	+05 17 26.56	4470666028607218176	18192930+0517262	46.09 ± 1.29	−16.86	−4.40	19.970	20.262	18.115	15.486	—
18 22 06.68	+06 20 37.58	4477025122831072768	18220671+0620376	67.59 ± 0.06	−1190.50	111.16	11.384	12.820	10.227	7.935	—
18 22 52.48	−00 23 31.79	4271633361463061376	18225249−0023315	40.68 ± 0.08	−144.94	−242.74	14.008	15.708	12.756	10.158	—
18 23 28.56	+12 21 34.28	4485035198170569856	18232856+1221344	42.34 ± 0.05	31.99	−15.76	11.782	13.194	10.627	8.196	—
18 23 49.11	−34 51 59.29	4044295274980460416	18234909−3451594	42.31 ± 0.08	107.34	63.97	12.070	13.512	10.909	8.489	—
18 23 53.79	−01 54 36.07	4271143185424456320	18235380−0154361	45.96 ± 2.86	2.89	−0.80	20.365	19.837	18.026	14.547	—
18 24 05.19	+01 41 16.15	4276632394156013440	18240518+0141161	57.66 ± 0.04	150.17	−238.23	10.862	12.122	9.779	7.487	—
18 24 23.59	−05 36 49.25	4161034758178900224	18242359−0536488	75.50 ± 0.10	50.82	−447.63	14.447	17.039	12.996	9.620	—
18 24 53.31	−12 12 12.20	4153194449969231104	18245327−1212118	48.20 ± 1.61	−40.89	16.16	20.066	20.840	17.790	10.107	—
18 25 04.79	+24 38 04.48	4536614495522394112	18250478+2438044	43.79 ± 0.03	−40.23	−448.53	10.026	11.024	9.071	6.980	—

Table 2: List of M dwarf systems within 25 pc drawn from *Gaia* DR2, as described in §2.3.

These systems have not been vetted to distinguish single stars from multiples, but in cases

where a system was resolved in *Gaia* but not 2MASS, a “J” flag is listed in column 12.

18 25 17.98	+18 39 09.11	4523577620507728768	18251798+1839091	47.21 ± 0.04	−115.06	−48.98	12.413	13.928	11.222	8.701	—
18 25 55.97	−57 45 01.57	6648040999716899200	18255597−5745017	41.84 ± 0.08	14.56	319.53	12.955	14.374	11.794	9.398	—
18 26 16.55	+01 46 20.98	4276822089967374336	18261655+0146210	55.33 ± 0.09	−135.94	304.43	13.296	15.164	11.996	9.165	—
18 26 19.76	−65 47 40.81	6437366909611503104	18261976−6547410	57.32 ± 0.06	−12.42	−619.02	13.653	15.623	12.331	9.445	—
18 26 31.59	−19 23 30.82	4092990622155744000	18263162−1923300	50.35 ± 0.06	−297.76	−463.87	12.700	14.271	11.495	8.916	—
18 26 53.52	−33 06 18.88	4045112624470837888	18265347−3306190	43.99 ± 0.05	345.31	84.02	12.180	13.529	11.059	8.706	—
18 29 16.91	−30 59 49.11	4047622985664694656	18291690−3059489	44.85 ± 0.05	456.89	−251.29	12.869	14.183	11.757	9.487	—
18 29 18.99	−14 39 01.93	4104121283206946688	18291894−1439014	55.89 ± 0.53	−46.90	19.91	16.715	17.982	15.421	11.334	—
18 29 24.24	−34 57 45.24	6734485286788609664	18292423−3457451	71.81 ± 0.05	−54.08	−237.71	10.756	12.145	9.621	7.327	—
18 29 34.65	+02 15 54.94	4276948538120524288	18293465+0215549	40.12 ± 0.28	21.48	−42.04	17.481	20.913	15.879	11.934	—
18 29 43.38	+21 58 18.47	4529151148024705792	18294337+2158185	43.20 ± 1.18	−7.82	18.36	19.152	20.084	17.761	15.414	—
18 30 12.01	−58 16 27.48	6635966781495628672	18301200−5816274	69.55 ± 0.07	−27.89	−446.76	9.074	10.089	8.106	5.963	—
18 30 39.45	−03 56 18.88	4257891802569298048	18303947−0356189	54.68 ± 0.19	−214.26	−105.09	12.849	14.676	11.568	8.859	—
18 31 16.05	+06 50 09.97	4477295014267164800	18311606+0650099	59.78 ± 0.04	144.92	−110.52	9.889	10.974	8.893	6.744	—
18 31 18.15	−07 32 25.18	4159791176135290752	18311816−0732250	54.00 ± 0.40	136.96	−154.84	17.225	20.351	15.511	11.200	—
18 31 26.08	+05 54 36.50	4284947760072791296	18312608+0554363	41.07 ± 1.02	−0.47	−5.79	19.584	20.242	18.279	15.005	—
18 32 02.57	+00 46 36.19	4273456111216132480	18320256+0046361	40.22 ± 0.08	20.44	−135.67	14.077	15.981	12.765	9.962	—
18 32 33.31	+04 04 20.58	4283420018727986560	18323330+0404205	43.45 ± 0.08	−179.88	−221.75	12.900	14.339	11.735	9.327	—
18 33 09.27	−06 51 17.67	4255925978875831424	18330925−0651177	42.35 ± 2.45	−33.51	23.51	20.221	20.474	18.278	13.511	—
18 34 16.13	−14 26 15.22	4103719347337431168	18341610−1426154	50.72 ± 0.08	236.70	91.38	13.574	15.218	12.292	9.614	—
18 35 21.54	−31 23 38.32	4046709772499428608	18352154−3123385	58.24 ± 0.08	23.40	−383.06	11.611	13.227	10.403	7.803	—
18 35 26.35	−19 43 49.26	4092388708225823616	18352637−1943485	45.12 ± 0.04	−286.45	−482.06	12.214	13.595	11.079	8.674	—
18 35 42.80	−79 12 04.41	6364037936533088384	18354285−7912046	45.22 ± 0.05	398.19	−783.33	14.394	—	—	10.252	—
18 35 48.48	−39 36 06.73	6723777800190040960	18354848−3936067	47.28 ± 0.11	−62.45	21.48	13.312	15.026	12.060	9.381	—
18 36 19.23	+13 36 26.37	4508377078422114944	18361922+1336261	83.03 ± 0.08	179.14	278.91	11.146	12.768	9.943	7.367	—
18 36 58.43	−35 07 17.44	6733860940302404864	18365842−3507176	52.46 ± 0.12	77.05	−253.73	16.169	19.348	14.634	11.195	—
18 37 31.81	+20 30 42.03	4525711600783788160	18373180+2030424	57.55 ± 0.07	86.33	−287.39	14.642	17.031	13.243	10.149	—
18 38 39.20	−06 47 09.65	4252972072151393408	18383923−0647095	45.52 ± 0.58	18.32	−12.12	18.750	20.112	17.032	14.157	—
18 38 44.75	−14 29 26.02	4103671239732631936	18384474−1429249	74.71 ± 0.16	112.38	−568.82	10.235	11.523	9.150	6.849	—
18 38 47.80	+04 46 03.16	4283815022597925376	18384782+0446031	40.23 ± 1.37	−163.33	−91.25	10.525	11.480	9.561	7.511	—
18 38 47.80	+04 46 03.16	4283815022597925376	18384782+0446031	40.23 ± 1.37	−163.33	−91.25	10.525	11.480	9.561	7.511	—

Table 2: List of M dwarf systems within 25 pc drawn from *Gaia* DR2, as described in §2.3.

These systems have not been vetted to distinguish single stars from multiples, but in cases

where a system was resolved in *Gaia* but not 2MASS, a “J” flag is listed in column 12.

18 39 48.43	+16 48 49.59	4511615999154663296	18394841+1648497	41.97 ± 0.08	132.72	−99.71	14.832	16.969	13.472	10.528	—
18 40 17.84	−10 27 55.17	4155146598548456064	18401783−1027550	56.33 ± 0.05	−143.16	−556.81	10.638	11.750	9.628	7.460	—
18 40 35.48	−00 19 18.63	4272344298801279488	18403548−0019185	42.72 ± 2.22	−14.42	27.59	20.319	20.398	18.199	14.234	—
18 40 50.24	−08 04 58.46	4251808514080675712	18405024−0804583	44.80 ± 0.06	−132.03	−253.09	12.520	14.116	11.300	8.736	—
18 40 57.31	−13 22 46.60	4105386718001211392	18405732−1322455	58.91 ± 0.05	−94.32	−671.25	9.769	10.881	8.748	6.546	—
18 40 59.36	−09 59 13.67	4155202364362108544	18405934−0959136	40.57 ± 0.55	23.90	−245.19	18.812	20.382	16.780	12.823	—
18 41 09.76	+24 47 14.43	4535928365908540416	18410977+2447143	100.72 ± 0.05	505.30	87.06	10.723	12.564	9.456	6.616	—
18 41 09.82	−43 47 32.74	6709964635600548992	18410977−4347327	79.83 ± 0.10	−796.91	−85.49	14.163	16.729	12.728	9.603	—
18 41 47.92	+24 21 59.69	4535850438020392704	18414791+2421595	47.41 ± 0.08	−116.90	−751.31	15.315	17.846	13.894	10.759	—
18 41 51.40	−03 23 05.07	4258546939721676288	18415139−0323052	44.92 ± 1.19	−5.22	−7.12	19.383	19.954	17.693	14.674	—
18 42 11.10	−23 28 58.63	4078319494857310336	18421107−2328582	94.15 ± 0.05	181.15	−242.54	10.967	12.376	9.832	7.436	—
18 42 44.98	+13 54 16.73	4505805591300126080	18424498+1354168	91.43 ± 0.07	−31.06	354.21	11.399	13.082	10.172	7.551	—
18 43 06.97	−54 36 48.37	6650117736660187136	18430697−5436481	97.66 ± 0.06	−137.31	−492.52	11.506	13.254	10.248	7.488	—
18 43 12.50	−33 22 46.13	6735656923825446144	18431250−3322462	62.38 ± 0.09	−128.39	−370.90	9.481	10.538	8.487	6.328	—
18 44 16.78	+22 09 23.61	4531940505956457984	18441672+2209231	49.10 ± 0.04	262.51	194.32	12.809	14.241	11.639	9.234	—
18 45 00.79	−14 09 03.96	4105057482987021184	18450079−1409036	54.97 ± 0.09	47.60	−85.72	12.217	14.151	10.898	7.650	—
18 45 05.25	−63 57 47.46	6439125097425259776	18450541−6357475	249.92 ± 0.16	2584.30	589.00	14.023	17.592	12.450	8.508	—
18 45 10.27	+06 20 15.93	4285624303318368512	18451027+0620158	53.05 ± 0.10	−37.51	−77.21	10.004	11.100	9.003	6.806	—
18 45 18.04	−25 03 40.47	4073475012238397440	18451804−2503403	43.15 ± 0.07	−338.93	−159.93	12.848	14.288	11.685	9.270	—
18 45 21.48	+07 11 58.55	4286113482922764288	18452147+0711584	43.68 ± 0.13	−224.75	−269.00	16.304	19.212	14.792	11.149	—
18 45 22.95	+18 51 58.54	4512525016089353472	18452294+1851585	70.97 ± 0.04	−138.71	−262.62	12.291	13.981	11.049	8.431	—
18 45 23.82	−32 53 38.62	6736067076020049024	18452383−3253385	45.72 ± 0.05	117.42	49.06	10.437	11.537	9.433	7.240	J
18 45 57.46	−28 55 53.66	4071372539860350464	18455748−2855533	53.29 ± 0.58	308.43	−254.00	11.369	12.960	10.160	7.603	—
18 46 07.64	−32 50 10.62	6736068072442493312	18460763−3250107	48.72 ± 0.12	12.72	−257.14	15.010	17.367	13.606	10.549	—
18 46 46.76	+00 43 26.02	4278483868667724032	18464675+0043260	46.07 ± 0.05	101.17	−33.73	12.552	14.186	11.320	8.733	—
18 47 16.70	−19 22 20.81	4086259033953267328	18471674−1922202	48.36 ± 0.10	−481.35	−401.33	12.948	14.638	11.700	9.089	—
18 47 36.50	−33 42 06.75	6735410976814156672	18473652−3342066	42.77 ± 0.07	−283.90	−117.69	13.522	15.194	12.283	9.742	—
18 48 01.27	−14 34 51.20	4101968375059565568	18480129−1434507	58.54 ± 0.06	−236.49	−237.03	11.013	12.342	9.913	7.558	—
18 48 17.54	+07 41 21.18	4286249341336984576	18481752+0741210	131.20 ± 0.08	376.33	249.30	12.313	14.476	10.955	7.913	—
18 48 20.97	−68 55 34.39	6431977687725247104	18482096−6855350	44.15 ± 0.16	−329.42	−1221.99	15.508	17.167	14.020	11.100	—
18 48 38.68	−61 35 25.80	6631993077750824960	18483868−6135259	40.90 ± 0.05	−154.99	−535.85	11.715	13.065	10.589	8.168	—

Table 2: List of M dwarf systems within 25 pc drawn from *Gaia* DR2, as described in §2.3.

These systems have not been vetted to distinguish single stars from multiples, but in cases

where a system was resolved in *Gaia* but not 2MASS, a “J” flag is listed in column 12.

18 48 41.30	−46 47 08.66	6704729998176610176	18484134−4647078	56.80 ± 0.10	215.85	135.90	11.155	12.517	9.997	6.985	—
18 48 51.15	−82 14 42.14	6359521108406068992	18485108−8214422	56.93 ± 0.10	−50.53	−272.51	15.607	18.652	14.100	10.503	—
18 49 06.40	−03 15 17.48	4258787045551023104	18490639−0315174	58.07 ± 0.10	269.52	−10.66	12.716	14.494	11.448	8.702	—
18 49 49.36	−23 50 10.45	4075141768785646848	18494929−2350101	336.12 ± 0.06	639.35	−193.55	9.126	10.751	7.913	5.370	—
18 49 51.21	−57 26 48.60	6636988399594203648	18495119−5726486	79.41 ± 0.06	−654.93	−184.15	11.318	12.942	10.099	7.455	—
18 49 54.47	+18 40 28.66	4518262684390915200	18495449+1840295	83.88 ± 0.07	−109.30	−278.65	12.544	14.399	11.250	8.509	—
18 50 00.83	+03 05 17.19	4279492361332301056	18500082+0305173	47.11 ± 0.06	−185.04	−408.23	9.956	10.986	8.979	6.857	—
18 50 26.64	−62 03 03.72	6631770869026896512	18502667−6203038	59.75 ± 0.05	89.20	60.23	9.881	10.969	8.873	6.704	—
18 51 40.86	+24 27 32.21	4534214948839463040	18514084+2427322	55.21 ± 0.04	−355.73	−34.98	11.645	13.034	10.504	8.116	—
18 51 51.18	+16 34 59.81	4510987662629223424	18515118+1634599	65.76 ± 0.05	−226.07	−481.64	9.380	10.380	8.422	6.319	—
18 52 00.19	−60 46 11.05	6632099970897367680	18520010−6046109	49.73 ± 0.07	−639.53	334.80	12.119	13.620	10.933	8.457	—
18 52 15.49	−03 05 55.00	4258755778197107200	18521549−0305552	42.85 ± 0.11	−85.64	251.44	15.891	18.489	14.432	11.123	—
18 52 25.31	−37 30 36.48	6730934796246420608	18522528−3730363	64.75 ± 0.09	425.74	−79.15	11.367	13.035	10.133	7.559	—
18 52 46.33	+19 18 50.10	4518409297395588736	18524633+1918501	41.61 ± 0.05	−22.87	−28.20	12.088	13.388	10.972	8.685	—
18 53 25.36	+02 50 48.61	4279261876207080576	18532537+0250490	51.42 ± 0.11	300.54	51.19	11.433	12.643	10.334	8.104	—
18 53 31.13	+20 22 35.72	4519089139177681664	18533112+2022357	47.16 ± 0.07	−31.54	−282.76	13.870	15.672	12.589	9.952	—
18 53 39.91	−38 36 44.46	6729187672268648832	18533991−3836442	80.25 ± 0.08	353.40	−924.60	11.334	12.943	10.119	7.589	—
18 54 17.12	+10 58 09.24	4311982650767794176	18541711+1058091	53.89 ± 0.06	20.02	112.86	12.374	14.060	11.129	8.483	—
18 54 50.93	−57 04 41.73	6637017330494491648	18545092−5704417	57.04 ± 0.21	−469.77	−322.90	15.953	19.023	14.424	10.790	—
18 55 27.41	+08 24 09.03	4310275491469537152	18552740+0824090	89.80 ± 0.05	91.80	−69.01	9.019	10.422	7.879	5.434	—
18 55 47.87	−69 14 14.93	6421389047155380352	18554792−6914153	86.12 ± 0.08	458.96	−693.19	14.253	16.869	12.812	9.512	—
18 56 04.37	−69 22 00.39	6421374031949679744	18560436−6922003	61.30 ± 0.05	−12.22	−118.62	11.275	12.711	10.140	7.698	—
18 56 09.02	−08 22 39.00	4203875751318123904	18560903−0822382	45.81 ± 0.25	−82.69	−1093.41	18.308	20.518	16.665	12.521	—
18 56 31.11	−46 30 50.69	6710598435331928192	18563112−4630505	44.93 ± 0.09	−130.27	−126.87	12.863	14.431	11.659	9.113	—
18 56 50.09	+14 53 48.51	4507557663079927680	18565009+1453484	51.29 ± 3.35	−13.48	1.55	20.515	21.184	18.591	15.502	—
18 57 01.11	−40 11 51.28	6716791228418408192	18570106−4011511	42.30 ± 0.07	30.40	−198.27	13.598	15.377	12.297	9.075	—
18 58 00.14	+05 54 29.24	4282578724832056576	18580014+0554296	90.05 ± 0.05	−196.30	−1220.47	8.456	9.473	7.488	5.357	—
18 58 45.42	+15 04 49.69	4507586907526491392	18584541+1504496	41.64 ± 0.06	124.55	130.98	13.826	15.620	12.549	9.838	—
18 59 07.46	−48 16 28.06	6662167868705713664	18590745−4816279	70.65 ± 0.08	150.85	−492.53	10.086	11.390	8.991	6.700	—
18 59 15.09	−17 01 52.08	4088457984145905280	18591512−1701514	43.96 ± 0.08	−212.75	−364.03	14.231	16.195	12.910	10.034	—
18 59 38.88	+08 29 00.37	4310146505003156992	18593888+0829005	52.75 ± 0.07	−377.76	−254.02	13.782	15.686	12.480	9.706	—

Table 2: List of M dwarf systems within 25 pc drawn from *Gaia* DR2, as described in §2.3.

These systems have not been vetted to distinguish single stars from multiples, but in cases

where a system was resolved in *Gaia* but not 2MASS, a “J” flag is listed in column 12.

18 59 40.71	−63 27 22.11	6439209141342705536	18594068−6327218	60.43 ± 1.51	95.68	189.89	11.782	13.288	10.573	8.077	—
19 03 13.60	+03 24 02.73	4269203303374311552	19031361+0324027	46.00 ± 0.05	−187.16	−84.51	11.305	12.640	10.194	7.828	—
19 03 14.69	−09 32 07.64	4202659377841518720	19031470−0932075	57.24 ± 0.07	−35.12	−84.30	11.751	13.197	10.592	8.136	—
19 03 16.65	−13 34 05.03	4101582957531738112	19031664−1334051	53.81 ± 0.05	−493.75	−490.80	13.447	15.216	12.178	9.537	—
19 03 20.63	−12 43 48.96	4198522985063559296	19032063−1243490	42.08 ± 0.07	−148.98	−256.44	13.329	14.892	12.121	9.648	—
19 03 30.61	+12 24 36.15	4313780700197743744	19033059+1224360	44.13 ± 0.76	−14.37	−5.52	19.271	19.706	17.825	14.858	—
19 04 09.61	−14 10 22.22	4101357699404676736	19040960−1410222	45.65 ± 0.12	−84.65	−68.31	13.229	15.001	11.960	9.284	—
19 06 06.93	−05 15 04.33	4206320171755704320	19060693−0515043	49.12 ± 0.61	223.82	−45.20	17.424	19.648	15.788	11.811	—
19 06 32.81	+03 54 10.37	4269294730306503936	19063280+0354103	42.76 ± 0.06	196.22	50.79	12.354	13.844	11.172	8.656	—
19 07 05.57	+20 53 16.92	4519789321933481856	19070556+2053168	113.34 ± 0.10	−478.82	−347.64	9.802	11.033	8.742	6.521	—
19 07 13.20	+20 52 37.26	4519789081415296128	19071320+2052372	113.21 ± 0.05	−480.69	−332.34	9.794	11.027	8.733	6.517	—
19 07 22.14	+04 43 55.32	4269411798275964800	19072214+0443554	50.65 ± 0.12	−249.87	−153.88	15.279	17.888	13.824	10.601	—
19 08 22.11	−37 05 28.00	6719043646702291968	19082211−3705278	42.50 ± 0.05	176.74	−170.32	12.604	14.108	11.422	8.932	—
19 09 08.20	−19 37 48.06	4083994314834200960	19090821−1937479	45.24 ± 0.52	−35.54	−155.64	19.488	21.356	17.828	12.915	—
19 09 19.89	−14 44 54.85	4185275209966301568	19091989−1444551	48.38 ± 0.05	172.76	−470.25	10.967	12.233	9.882	7.634	—
19 09 37.63	+04 42 15.89	4293417882279257216	19093760+0442156	51.03 ± 2.33	−17.99	−0.80	19.814	20.446	17.993	14.282	—
19 09 38.14	+10 16 42.97	4312248118403812352	19093813+1016425	44.78 ± 2.70	6.09	−19.65	20.347	20.523	18.548	14.767	—
19 09 41.66	+09 48 58.21	4309224392703603584	19094165+0948584	42.53 ± 0.06	126.70	−353.75	13.340	14.973	12.106	9.455	—
19 09 50.87	+17 40 06.41	4514347014274847744	19095098+1740074	97.45 ± 0.16	−641.45	−424.54	11.956	13.797	10.673	7.902	—
19 09 51.39	+07 42 07.99	4307174761290443776	19095139+0742077	40.83 ± 1.14	26.10	−79.32	11.336	12.227	9.832	7.475	—
19 12 14.62	+02 53 11.44	4268226078065241600	19121455+0253111	106.28 ± 1.06	1760.99	−554.09	9.891	11.379	8.723	6.294	—
19 12 25.26	−55 52 07.63	6643046944883125376	19122525−5552076	42.50 ± 0.03	−278.20	−170.96	10.540	11.608	9.547	7.378	—
19 12 39.25	−36 14 56.56	6743125734489663104	19123922−3614555	87.24 ± 0.21	772.89	−1956.08	12.494	14.206	11.251	8.769	—
19 12 39.27	−50 16 17.28	6658123517042686464	19123926−5016173	51.36 ± 0.16	66.81	−67.52	13.418	15.358	12.097	9.208	—
19 13 06.07	−23 12 04.99	4080825969002728320	19130608−2312052	44.11 ± 0.19	191.18	−358.46	14.991	17.263	13.589	10.516	—
19 13 07.97	−39 01 53.92	6717813842950778880	19130794−3901536	46.80 ± 0.05	444.80	−245.24	11.341	12.664	10.128	7.658	—
19 14 39.16	+19 19 03.72	4516199240734836608	19143925+1919025	55.24 ± 0.06	−613.83	435.54	10.370	11.790	9.219	6.813	—
19 15 22.39	−23 12 11.03	6770968152052164608	19152238−2312113	41.39 ± 0.07	141.74	231.14	12.089	13.528	10.926	8.442	—
19 16 13.10	+00 51 49.75	4264640944245035264	19161309+0051495	43.55 ± 0.26	86.74	14.69	18.007	20.081	16.331	12.207	—
19 16 55.26	+05 10 08.04	4293318823182081408	19165526+0510086	169.16 ± 0.05	−579.04	−1332.74	8.098	9.375	6.994	4.673	—
19 16 57.61	+05 09 01.59	4293315765165489536	19165762+0509021	168.96 ± 0.13	−598.18	−1365.27	14.321	17.726	12.754	8.765	—

Table 2: List of M dwarf systems within 25 pc drawn from *Gaia* DR2, as described in §2.3.

These systems have not been vetted to distinguish single stars from multiples, but in cases

where a system was resolved in *Gaia* but not 2MASS, a “J” flag is listed in column 12.

19 17 04.52	−30 19 20.10	6758930664392303232	19170448−3019198	42.91 ± 0.11	183.51	−189.63	15.423	17.788	13.984	10.876	−
19 18 29.47	−45 54 30.46	6664246083120889344	19182944−4554308	50.96 ± 0.10	−416.86	−500.59	14.660	16.906	13.283	10.296	−
19 19 12.96	−05 14 52.91	4211396238979741952	19191294−0514529	56.01 ± 0.74	30.30	−35.97	18.116	−	−	14.541	−
19 19 27.86	+14 38 01.99	4319899070070496128	19192785+1438019	43.73 ± 0.07	503.30	−67.55	14.349	16.359	13.019	10.159	−
19 19 30.28	+09 02 59.23	4308175076364495360	19193027+0902590	41.50 ± 0.05	19.40	−388.19	11.955	13.270	10.834	8.547	−
19 19 41.21	−59 55 19.52	6446274293824799488	19194119−5955194	58.68 ± 0.05	−244.67	−244.23	12.405	14.022	11.179	8.609	−
19 19 55.14	−04 46 29.39	4211801099777745920	19195513−0446293	46.48 ± 0.08	96.39	−101.78	11.084	12.514	9.942	7.477	−
19 20 47.98	−45 33 29.63	6663600360559308672	19204795−4533283	169.09 ± 0.22	659.33	−2897.03	10.740	12.544	9.491	6.845	−
19 20 54.38	−82 33 16.17	6347643496607835520	19205439−8233170	80.09 ± 0.04	342.18	−1230.22	11.417	12.960	10.228	7.686	−
19 21 29.78	−29 15 50.54	6759481141756109056	19212977−2915507	66.67 ± 0.22	512.18	250.76	15.560	18.683	14.033	10.441	−
19 21 38.70	+20 52 03.27	4516795626642787456	19213867+2052028	94.20 ± 0.24	−948.34	−1455.73	11.950	13.731	10.647	7.935	−
19 22 02.07	+07 02 30.31	4295619138933719808	19220206+0702310	94.19 ± 0.07	−740.03	−444.91	11.259	12.698	10.106	7.688	−
19 22 05.64	−35 03 44.95	6742962972412390912	19220562−3503445	53.30 ± 0.08	119.54	−219.68	13.423	15.199	12.151	9.465	−
19 22 43.69	−43 19 20.76	6665143937443906816	19224368−4319206	40.03 ± 0.05	38.89	−168.45	11.841	13.107	10.754	8.456	−
19 22 50.39	−24 11 13.90	6769967321590585344	19225038−2411138	41.85 ± 0.08	24.32	−212.31	14.014	15.843	12.724	10.027	−
19 25 30.91	+09 38 23.29	4308488780772030336	19253089+0938235	59.43 ± 0.29	83.79	−240.82	15.673	19.143	14.064	10.024	−
19 26 01.62	+24 26 17.12	2022893621784904064	19260160+2426170	53.87 ± 0.05	182.17	97.60	12.767	14.542	11.494	8.729	−
19 26 08.60	−43 10 56.86	6665111226973054208	19260859−4310563	42.06 ± 0.09	−157.84	−1098.04	15.324	17.665	13.935	11.119	−
19 26 49.38	+16 43 01.57	4322492440039701120	19264937+1643019	47.71 ± 0.05	34.95	−207.27	11.817	13.309	10.644	8.157	−
19 27 13.01	−04 09 49.00	4213398965047338880	19271300−0409491	45.74 ± 0.10	54.98	−273.69	13.740	15.618	12.441	9.676	−
19 27 52.72	−28 11 15.80	6764810715133775744	19275268−2811150	66.49 ± 0.36	76.08	−456.14	13.323	15.145	11.703	8.786	−
19 28 19.73	+23 54 59.49	2019813992789300608	19281972+2354594	57.69 ± 2.32	−7.48	6.23	19.930	21.322	18.587	16.337	−
19 29 03.38	+19 04 28.98	4323439463157504512	19290334+1904288	58.04 ± 3.48	−22.56	−32.12	20.205	21.031	18.235	13.937	−
19 29 10.67	−29 32 11.58	6764432753712671104	19291066−2932115	41.72 ± 0.06	−24.65	31.49	12.583	14.141	11.379	8.833	−
19 29 38.30	−74 44 42.16	6367463327570835328	19293833−7444422	61.62 ± 0.04	294.77	11.84	10.823	12.083	9.741	7.448	−
19 29 43.80	+11 01 57.08	4314878631298620160	19294379+1101571	49.42 ± 0.13	−196.00	40.98	16.191	19.208	14.662	10.987	−
19 31 01.40	−73 37 05.22	6415630939116638464	19310138−7337058	56.89 ± 0.46	241.35	−151.17	12.000	13.084	10.800	8.244	−
19 31 04.60	−03 06 18.12	4213581106021661184	19310458−0306186	54.16 ± 0.12	197.95	480.63	14.682	17.017	13.283	10.228	−
19 31 52.42	+19 06 58.48	1825387390297688832	19315239+1906592	42.20 ± 0.11	40.08	−241.84	13.571	15.466	12.089	9.036	J
19 32 08.11	−11 19 57.37	4187836934609063552	19320809−1119573	56.56 ± 0.07	235.57	22.90	12.548	14.184	11.317	8.706	−
19 32 27.98	+20 22 55.57	2017773269160819328	19322802+2022555	44.76 ± 1.94	0.96	−14.68	19.474	−	−	12.954	−

Table 2: List of M dwarf systems within 25 pc drawn from *Gaia* DR2, as described in §2.3.

These systems have not been vetted to distinguish single stars from multiples, but in cases

where a system was resolved in *Gaia* but not 2MASS, a “J” flag is listed in column 12.

19 32 29.83	+21 05 30.32	2017880467232804736	19322982+2105307	47.92 ± 2.30	12.07	−0.48	19.967	20.908	18.117	15.606	—
19 34 03.95	−52 25 14.14	6645504151509887744	19340394−5225144	54.54 ± 0.07	41.46	−257.06	11.607	13.098	10.431	7.920	—
19 34 14.23	+23 23 40.73	2019504312771688832	19341425+2323409	44.57 ± 2.84	4.14	−29.72	20.283	20.808	18.308	14.887	—
19 34 49.30	+24 11 38.24	2021114611956315008	19344929+2411385	46.08 ± 1.30	−7.99	7.31	18.684	—	—	14.732	—
19 36 33.29	−48 16 53.43	6659271205321359872	19363328−4816535	40.18 ± 0.09	290.80	97.22	14.250	16.120	12.955	10.177	—
19 37 31.75	+18 00 11.98	1824265132576021632	19373175+1800121	52.41 ± 1.08	−9.13	−11.91	18.533	18.951	16.929	14.944	—
19 37 59.65	−15 26 47.43	4181999352495280000	19375964−1526473	42.03 ± 0.09	64.67	−18.23	14.378	16.318	13.054	10.229	—
19 38 27.40	−32 31 25.46	6744957928883188736	19382738−3231248	50.47 ± 0.06	91.06	−337.43	12.575	14.055	11.401	8.972	—
19 38 36.88	−24 16 58.66	6768045340904025088	19383689−2416586	42.04 ± 0.18	45.07	82.88	12.014	13.368	10.879	8.511	—
19 38 42.66	+21 28 14.36	2018317110778667264	19384265+2128142	45.62 ± 2.02	−5.75	−11.00	19.735	21.385	18.110	14.386	—
19 38 44.69	+24 29 27.50	2021161379905981696	19384468+2429274	47.48 ± 0.95	−3.39	−10.75	19.129	20.097	17.739	13.576	—
19 39 18.86	+06 30 19.64	4291878634719894016	19391887+0630201	52.13 ± 1.14	−6.92	31.68	19.059	—	—	14.891	—
19 39 52.01	−57 50 33.84	6448329418495400960	19395199−5750339	46.96 ± 0.13	75.17	114.24	16.405	19.480	14.880	11.204	—
19 40 44.13	+24 41 26.71	2021182304939695104	19404414+2441268	61.50 ± 1.66	−8.34	−10.15	19.020	19.658	17.583	14.836	—
19 41 53.21	−46 02 31.00	6684504722300935680	19415319−4602310	48.68 ± 0.05	−20.85	−24.37	11.502	12.771	10.417	8.113	—
19 41 54.22	+03 09 16.07	4289793067314163072	19415421+0309163	43.82 ± 0.33	−271.16	−484.47	11.927	13.145	10.816	8.518	—
19 42 00.65	−21 04 05.38	6868107358662346112	19420065−2104051	53.55 ± 0.08	76.76	−250.12	11.772	13.498	10.519	7.816	—
19 42 02.25	+24 57 56.96	2021565759618910592	19420225+2457570	41.65 ± 0.70	−3.26	−5.30	17.217	18.473	16.047	12.825	—
19 42 12.82	−20 45 47.97	6868221463056407168	19421282−2045477	63.11 ± 0.09	−10.24	−154.34	12.725	14.515	11.448	8.756	—
19 42 21.20	−06 20 23.99	4208730438673343488	19422119−0620238	44.03 ± 0.10	55.93	−162.99	13.847	15.760	12.528	9.706	—
19 42 30.08	−41 15 12.46	6689574432978156160	19423007−4115124	40.22 ± 0.17	−9.30	56.60	16.065	18.824	14.593	11.298	—
19 42 43.22	−17 23 24.34	6870168805525824384	19424321−1723228	45.07 ± 0.13	40.67	−892.85	12.952	14.698	11.688	8.975	—
19 43 15.72	+08 34 09.15	4301201801807687680	19431571+0834090	42.79 ± 0.05	−117.27	−185.69	12.419	13.978	11.210	8.634	—
19 43 24.69	−37 22 11.00	6739809744861879040	19432464−3722108	41.26 ± 0.06	162.89	−183.23	12.266	13.893	11.017	8.247	—
19 43 51.62	+24 41 41.28	2020815617836409472	19435163+2441412	45.17 ± 0.71	−0.67	−7.61	17.718	18.693	16.563	14.133	—
19 43 51.80	−32 24 04.06	6747926786376161536	19435179−3224035	57.90 ± 0.04	−24.46	−415.32	10.679	11.947	9.591	7.291	—
19 44 32.28	+18 13 27.27	1824156791978550016	19443225+1813270	83.59 ± 1.44	−15.74	−13.23	17.724	18.768	16.403	13.953	—
19 44 53.81	−23 38 00.18	6768500534421789440	19445376−2337591	69.09 ± 0.59	318.23	−134.14	12.742	14.340	11.052	8.265	—
19 45 28.84	+19 00 22.95	1824624157487746048	19452883+1900229	44.69 ± 1.21	−25.84	3.35	19.260	19.750	17.709	15.220	—
19 45 35.57	−25 57 21.89	6766848728654380160	19453551−2557215	49.33 ± 0.15	592.99	−176.53	16.316	19.584	14.773	11.509	—
19 46 50.51	−01 57 39.64	4234960284989103744	19465050−0157397	43.51 ± 0.37	113.75	−27.06	11.078	12.382	9.995	7.749	—

Table 2: List of M dwarf systems within 25 pc drawn from *Gaia* DR2, as described in §2.3.

These systems have not been vetted to distinguish single stars from multiples, but in cases

where a system was resolved in *Gaia* but not 2MASS, a “J” flag is listed in column 12.

19 48 22.67	−08 22 52.20	4195469572528982144	19482268−0822520	51.11 ± 0.08	−428.51	−350.00	14.585	16.822	13.207	10.191	−
19 48 31.80	+23 44 02.19	2020463361775898496	19483178+2344026	49.60 ± 1.96	−4.78	−7.78	20.086	20.651	18.111	14.232	−
19 48 51.08	+24 49 48.02	2020691613528108544	19485106+2449479	46.15 ± 0.88	−1.13	−6.86	19.019	21.007	17.463	13.362	−
19 49 29.43	+17 13 02.71	1820834656271108864	19492942+1713027	48.16 ± 0.38	177.07	−88.94	19.262	21.071	17.591	12.819	−
19 49 51.64	−20 38 52.79	6865562672142017920	19495163−2038527	46.74 ± 0.08	15.73	19.38	13.024	14.760	11.758	9.082	−
19 50 19.99	−43 27 02.57	6685171129426977408	19501998−4327025	44.44 ± 0.06	93.77	−108.78	13.230	14.932	11.981	9.301	−
19 50 35.84	+24 36 47.50	2020624298493806336	19503583+2436474	44.98 ± 1.57	−17.17	−7.49	19.581	21.172	17.903	13.735	−
19 50 53.40	+23 52 11.07	1828398845273827584	19505338+2352111	42.87 ± 1.73	−18.12	−10.94	18.994	19.981	17.465	14.781	−
19 51 35.83	−35 10 37.48	6746465363619405696	19513587−3510375	88.20 ± 0.08	382.47	97.56	12.204	13.881	10.793	7.735	−
19 51 35.98	−35 10 38.02	6746465363619405824	19513587−3510375	88.27 ± 0.09	351.27	45.36	12.441	14.217	11.179	7.735	−
19 51 40.39	−31 00 22.19	6748527772559539328	19514041−3100217	76.44 ± 0.86	48.90	−127.52	11.070	12.576	9.907	7.409	−
19 53 02.09	−41 02 18.60	6690155009477092224	19530209−4102186	41.28 ± 0.09	−45.75	20.53	14.977	17.163	13.611	10.601	−
19 53 27.72	−46 11 32.17	6683916311780897664	19532771−4611322	43.23 ± 0.08	2.55	112.85	13.382	15.118	12.122	9.440	−
19 54 00.14	−47 48 37.28	6671213104187807872	19540013−4748370	51.05 ± 0.11	−137.15	−1051.38	11.571	12.791	10.493	8.286	−
19 54 01.61	+24 18 15.69	1834395890930656768	19540157+2418153	44.36 ± 4.39	−18.50	−14.65	20.809	21.056	19.016	15.318	−
19 54 18.33	+17 38 29.28	1821193578108774784	19541829+1738289	42.78 ± 0.05	205.16	145.78	13.505	15.140	12.272	9.719	−
19 54 20.64	−23 56 40.55	6863536001631204608	19542064−2356398	70.60 ± 0.08	−127.11	−407.32	13.246	15.299	11.894	8.839	−
19 54 24.88	−31 47 59.79	6748241006182314368	19542484−3148000	41.02 ± 0.26	−463.27	−110.97	11.886	13.311	10.728	8.316	−
19 54 43.59	+18 01 58.29	1821315795663331456	19544358+1801581	50.09 ± 0.15	−40.33	−454.16	16.513	19.656	14.965	11.113	−
19 56 17.71	+24 51 17.05	1834487463935484800	19561768+2451169	87.01 ± 1.94	−8.50	−14.56	20.667	20.861	18.772	15.112	−
19 56 26.44	−21 38 31.19	6864448905520369280	19562645−2138307	46.95 ± 0.21	−198.99	−746.05	13.617	15.755	12.261	9.237	−
19 57 23.80	−12 33 50.22	4188996885011268608	19572380−1233499	56.22 ± 0.10	−89.27	−518.03	13.553	15.661	12.207	9.318	−
19 57 51.98	−10 53 05.22	4189472728736232704	19575199−1053050	41.56 ± 0.08	−390.50	−287.53	12.853	14.625	11.576	8.843	−
19 58 02.41	+24 10 35.99	1834203476393599616	19580240+2410360	45.33 ± 1.10	−7.30	−18.90	18.577	19.718	17.126	14.633	−
19 58 15.74	+02 02 15.64	4240815184408080512	19581572+0202151	64.23 ± 0.05	−337.65	−820.45	10.949	12.246	9.857	7.561	−
20 01 06.15	+00 16 15.53	4237021938009045248	20010615+0016155	50.36 ± 0.04	55.46	−217.58	10.561	11.774	9.496	7.206	−
20 02 13.45	−54 25 55.91	6473160651658069120	20021341−5425558	55.30 ± 0.11	61.13	−365.00	15.512	18.342	14.041	10.644	−
20 02 50.71	−05 21 52.58	4220379661283166720	20025073−0521524	56.72 ± 1.48	−111.38	−114.70	20.634	21.067	18.832	13.417	−
20 03 51.00	+05 59 44.24	4248817876711932416	20035098+0559440	75.39 ± 0.06	−495.67	−799.60	11.118	12.366	10.056	7.868	−
20 03 58.91	−08 07 47.49	4192723988912416256	20035892−0807472	51.94 ± 0.07	−501.31	−247.37	12.164	13.801	10.931	8.286	−
20 04 04.74	−65 36 01.19	6427708902548969216	20040474−6536016	77.76 ± 0.05	132.94	−852.22	10.333	11.585	9.254	7.057	−

Table 2: List of M dwarf systems within 25 pc drawn from *Gaia* DR2, as described in §2.3.

These systems have not been vetted to distinguish single stars from multiples, but in cases

where a system was resolved in *Gaia* but not 2MASS, a “J” flag is listed in column 12.

20 04 06.76	−31 41 48.02	6748764545515650944	20040671−3141469	42.60 ± 0.11	320.74	−764.96	12.973	14.678	11.730	9.028	—
20 04 30.79	−23 42 02.27	6851779920225659136	20043077−2342018	55.00 ± 0.12	119.10	−338.92	11.581	13.293	10.340	7.701	—
20 04 57.10	+03 21 07.73	4247106761739962880	20045709+0321076	58.77 ± 0.09	−102.27	−336.73	13.421	15.422	12.087	9.181	—
20 05 35.18	−22 18 16.31	6853658057885526912	20053518−2218161	50.40 ± 0.05	55.52	−97.31	12.589	14.176	11.375	8.834	—
20 05 50.45	+19 11 19.46	1822574770834494208	20055044+1911189	50.70 ± 0.96	−32.65	−119.46	13.924	15.345	12.565	10.079	—
20 06 48.60	−67 36 51.06	6424217300298269568	20064858−6736510	51.41 ± 0.04	−161.54	18.67	12.655	14.138	11.476	9.037	—
20 07 03.71	+24 33 57.44	1833863834676183680	20070374+2433572	40.79 ± 0.50	−4.81	−18.80	16.534	16.918	14.774	12.098	—
20 07 42.66	+18 59 00.44	1822370978937299456	20074265+1859002	42.83 ± 0.05	172.85	−203.89	12.339	13.898	11.133	8.601	—
20 07 48.05	−31 45 29.07	6748796362632835968	20074802−3145284	68.01 ± 0.09	287.49	−750.65	11.070	12.483	9.943	7.591	—
20 07 55.24	−42 05 14.66	6686474256863996672	20075523−4205144	64.92 ± 0.08	51.95	−748.24	12.725	14.595	11.428	8.610	—
20 07 57.55	−01 32 27.97	4223777873773440384	20075751−0132278	47.45 ± 0.07	340.51	−220.18	12.400	13.878	11.217	8.745	—
20 08 23.77	−55 21 25.64	6472836050915560448	20082378−5521256	53.71 ± 0.06	203.44	−185.41	13.345	15.139	12.066	9.376	—
20 09 18.25	−01 13 38.32	4223813264304668288	20091824−0113377	92.52 ± 0.12	−43.63	−373.73	12.694	14.704	11.364	8.512	—
20 09 51.61	−47 31 34.29	6672112470338969856	20095160−4731341	52.00 ± 0.09	15.71	−342.87	13.101	14.907	11.818	9.009	—
20 10 34.44	+06 32 13.91	4250327300012527872	20103444+0632140	62.37 ± 0.08	43.13	−203.60	10.915	12.499	9.724	7.182	—
20 10 35.39	+06 34 36.83	4250327781042868224	20103539+0634367	62.01 ± 0.17	45.16	−208.87	17.140	20.654	15.516	11.425	—
20 10 55.52	−25 35 09.34	6847570886634835200	20105549−2535081	45.66 ± 0.07	198.64	−831.39	13.401	15.219	12.119	9.352	—
20 11 13.26	+16 11 07.99	1809359465717142656	20111329+1611074	49.38 ± 0.07	−417.56	399.72	12.628	14.271	11.388	8.883	—
20 12 52.58	+12 46 31.72	1803225427774999680	20125255+1246315	51.86 ± 0.10	272.86	150.91	16.140	19.254	14.616	11.035	—
20 12 59.94	+01 12 58.28	4242728884389090944	20125995+0112584	50.39 ± 0.30	243.35	−80.45	13.909	15.971	12.552	9.585	—
20 13 53.40	−45 09 50.47	6673000841376349696	20135335−4509506	162.32 ± 0.05	778.24	−159.74	7.235	8.209	6.293	4.281	—
20 13 58.98	+06 41 16.16	4249667627392687488	20135898+0641161	43.58 ± 0.06	−251.94	−582.52	11.961	13.482	10.767	8.167	—
20 15 11.91	+20 30 09.65	1828594150330084608	20151189+2030101	111.65 ± 2.14	−29.98	4.31	19.167	19.609	17.493	15.114	—
20 15 22.68	−56 45 54.45	6468714875175231232	20152266−5645543	41.25 ± 0.46	−44.97	−340.56	11.700	13.089	10.382	7.765	—
20 15 38.30	−39 53 21.94	6692782017633230848	20153830−3953221	41.41 ± 0.09	238.43	−278.20	14.902	17.129	13.522	10.564	—
20 16 11.25	−75 31 04.54	6366571314402539008	20161129−7531044	66.22 ± 0.08	251.60	37.60	13.895	16.084	12.527	9.509	—
20 16 50.56	−10 45 59.47	6881163470829624320	20165054−1045595	41.93 ± 0.16	175.18	139.11	15.985	18.739	14.524	11.404	—
20 18 44.56	+15 50 46.24	1808403096750183168	20184454+1550463	57.27 ± 0.05	174.38	−59.07	10.759	12.043	9.670	7.367	—
20 19 49.81	−58 16 42.99	6468337884421010048	20194981−5816431	61.18 ± 0.10	−24.64	−340.82	14.613	17.503	13.118	9.715	—
20 20 43.60	−28 06 06.52	6846064551407418112	20204362−2806066	43.80 ± 0.05	−205.83	51.90	12.600	14.202	11.375	8.716	—
20 22 41.95	−58 17 08.39	6467586746180725248	20224191−5817083	49.80 ± 0.15	759.80	−435.94	9.899	10.841	8.976	6.969	—

Table 2: List of M dwarf systems within 25 pc drawn from *Gaia* DR2, as described in §2.3.

These systems have not been vetted to distinguish single stars from multiples, but in cases

where a system was resolved in *Gaia* but not 2MASS, a “J” flag is listed in column 12.

20 23 22.12	+08 00 15.05	1752189568342546048	20232212+0800149	50.40 ± 0.06	15.20	−209.33	13.571	15.476	12.261	9.407	—
20 23 52.23	−13 03 17.49	6876824767881427328	20235220−1303169	44.98 ± 0.11	292.29	−353.03	14.871	16.962	13.517	10.665	—
20 25 29.98	−35 45 46.06	6695913186230672512	20252998−3545460	40.30 ± 0.11	−251.56	−1.03	12.969	14.603	11.736	9.044	—
20 27 37.35	−54 52 59.21	6469383588698276480	20273733−5452592	57.78 ± 0.07	−258.04	200.66	11.553	13.015	10.392	7.921	—
20 27 41.66	−27 44 51.74	6798111275908572032	20274166−2744506	69.88 ± 0.07	−201.20	−876.21	10.338	11.694	9.223	6.864	—
20 27 42.08	−56 27 25.16	6468968316900356736	20274210−5627262	49.06 ± 0.05	424.41	−1230.62	11.236	12.481	10.161	7.915	—
20 28 03.73	−76 40 15.86	6363251682639715968	20280382−7640164	77.70 ± 0.05	723.68	−1242.43	12.393	14.136	11.137	8.600	—
20 28 22.17	+05 24 32.75	4246382183568597120	20282216+0524327	40.06 ± 0.06	−221.15	−146.08	13.629	15.330	12.369	9.783	—
20 28 43.62	−11 28 30.87	6904064446906104832	20284361−1128307	54.64 ± 0.10	159.31	−96.74	11.209	12.717	10.046	7.496	—
20 28 56.45	−04 20 41.20	4218602403817112192	20285643−0420413	45.56 ± 0.08	171.21	66.42	14.281	16.269	12.948	10.090	—
20 29 12.98	−11 11 03.21	6904166426608411008	20291299−1111031	42.02 ± 0.05	−324.29	−78.39	11.479	12.558	10.472	8.401	—
20 29 48.32	+09 41 20.59	1752805741531173632	20294834+0941202	133.81 ± 1.39	669.34	101.33	11.467	13.369	10.188	7.307	—
20 30 01.90	+00 23 55.12	4229940258483255296	20300192+0023553	52.98 ± 0.81	144.37	17.29	13.107	14.833	11.708	9.093	—
20 33 01.89	−49 03 11.10	6476114936322488960	20330186−4903105	55.51 ± 0.54	102.62	−180.46	13.519	15.566	12.173	9.194	—
20 33 36.68	−21 20 10.11	6856077189625042688	20333668−2120096	57.33 ± 0.11	−120.24	−71.83	11.463	12.829	10.355	8.018	—
20 34 43.03	+03 20 51.29	4233129014004310656	20344303+0320509	47.60 ± 0.06	287.64	−479.03	10.983	12.264	9.898	7.629	—
20 35 06.79	+02 18 29.05	4232452638259239936	20350677+0218289	49.85 ± 0.05	−101.14	−33.54	12.278	13.790	11.087	8.592	—
20 36 03.16	+10 51 29.58	1754495583527340416	20360316+1051295	42.37 ± 0.42	−123.96	−179.35	19.009	21.794	17.356	12.447	—
20 36 08.31	−36 07 11.51	6683306151547010688	20360829−3607115	59.23 ± 0.07	6.17	40.10	10.582	11.883	9.483	7.172	—
20 37 07.16	−11 37 57.35	6901234269614405888	20370715−1137569	46.68 ± 0.14	−2.44	−378.98	16.409	19.621	14.856	11.257	—
20 37 21.71	−46 43 52.41	6674554829263069440	20372170−4643523	58.09 ± 0.07	−4.06	−12.18	13.080	14.683	11.859	9.308	—
20 38 46.17	−21 06 45.91	6856237271645944320	20384619−2106458	44.43 ± 0.09	−207.58	60.43	14.308	16.309	12.973	10.115	—
20 39 23.82	−29 26 34.67	6798222846275675520	20392378−2926335	55.68 ± 0.14	319.69	−737.30	15.203	17.869	13.751	10.367	—
20 40 12.39	−55 01 25.62	6470597999291000448	20401242−5501258	43.75 ± 0.06	408.57	−284.84	13.697	15.470	12.421	9.688	—
20 40 33.86	+15 29 58.73	1810616448010879488	20403364+1529572	104.89 ± 0.09	1321.00	662.24	11.845	13.709	10.558	7.749	—
20 40 56.17	−82 45 09.33	6348139685588865792	20405616−8245093	44.47 ± 0.05	83.60	−123.20	12.597	14.388	11.323	8.638	—
20 41 51.13	−32 26 06.68	6792436799475128960	20415111−3226073	101.20 ± 0.08	247.20	−415.56	9.555	11.244	8.182	4.944	J
20 42 45.17	−05 00 19.18	6914281796143286784	20424514−0500193	59.64 ± 0.10	241.33	117.30	15.200	17.869	13.744	10.539	—
20 42 57.15	−18 55 06.09	6858312737278836736	20425709−1855048	52.49 ± 0.04	601.49	−858.95	9.901	10.985	8.893	6.739	—
20 43 23.87	+04 45 55.26	1735245338242513536	20432387+0445552	64.82 ± 0.12	446.86	−149.66	13.543	15.653	12.188	9.136	—
20 43 34.52	+24 07 40.85	1843206728575513472	20433453+2407407	46.96 ± 0.05	145.07	−40.41	10.795	12.050	9.714	7.396	—

Table 2: List of M dwarf systems within 25 pc drawn from *Gaia* DR2, as described in §2.3.

These systems have not been vetted to distinguish single stars from multiples, but in cases

where a system was resolved in *Gaia* but not 2MASS, a “J” flag is listed in column 12.

20 44 22.08	+13 39 00.91	1762070089066876288	20442205+1339002	44.35 ± 0.06	273.56	441.74	14.446	16.413	13.116	10.251	—
20 44 30.72	+08 54 11.00	1750816656275568000	20443072+0854107	40.49 ± 0.04	201.45	97.72	10.457	11.530	9.454	7.304	—
20 44 37.48	+15 17 34.78	1762523981210977664	20443743+1517352	96.09 ± 0.10	303.72	−155.17	15.290	18.620	13.717	10.061	—
20 45 02.40	−63 32 06.58	6450595924277607040	20450238−6332066	43.69 ± 0.20	78.46	−214.70	17.615	20.885	15.863	11.207	—
20 45 45.40	−29 27 29.23	6795084084175092480	20454538−2927295	43.37 ± 0.05	−329.24	−403.86	12.154	13.634	10.972	8.512	—
20 46 37.07	−81 43 13.65	6349094336559890944	20463725−8143141	93.72 ± 0.03	539.70	−544.15	10.383	11.781	9.253	6.826	—
20 46 43.65	−11 48 13.36	6900333494712655616	20464360−1148132	51.63 ± 0.07	345.91	−65.83	12.367	14.040	11.116	8.435	—
20 47 24.74	+14 21 52.36	1762216079299019008	20472471+1421526	44.19 ± 0.13	210.19	−106.17	17.437	20.726	15.843	11.877	—
20 48 51.00	+11 27 20.03	1751865311194729344	20485102+1127201	56.74 ± 0.06	438.03	−61.13	12.424	13.838	11.262	8.874	—
20 48 57.18	−00 53 47.48	4227064966858434304	20485716−0053473	40.21 ± 0.10	77.69	−63.15	14.945	16.954	13.615	10.863	—
20 49 09.96	−40 12 06.03	6678510081826546048	20490993−4012062	105.16 ± 0.27	−67.71	−9.69	11.839	13.777	10.533	7.704	—
20 49 39.54	−00 21 03.39	4227165812690769408	20493951−0021031	40.41 ± 0.05	303.12	−205.77	11.883	13.337	10.714	8.208	—
20 49 52.73	−17 16 08.47	6858958940879829248	20495272−1716083	53.39 ± 0.10	301.91	−98.57	15.777	18.612	14.284	10.807	—
20 50 07.94	−23 42 49.57	6806697710102769920	20500793−2342495	48.41 ± 0.06	83.09	−73.41	10.886	12.073	9.835	7.622	—
20 50 16.16	−34 24 42.60	6779821003058453120	20501615−3424424	104.07 ± 0.09	335.61	−296.94	12.065	13.960	10.767	7.997	—
20 51 09.77	−24 58 17.52	6805803738429787904	20510974−2458174	44.14 ± 0.07	186.68	−90.02	13.165	14.776	11.932	9.368	—
20 51 41.58	−79 18 39.98	6349915534307041152	20514174−7918403	58.80 ± 0.03	708.78	−983.81	10.904	12.089	9.851	7.664	—
20 52 08.59	−23 18 10.14	6806826799639247744	20520861−2318096	40.83 ± 0.15	−184.50	−303.61	16.084	18.832	14.612	11.293	—
20 52 28.09	−47 58 44.29	6481588305207220864	20522808−4758442	42.63 ± 0.20	6.74	−448.72	17.311	20.580	15.723	11.881	—
20 52 31.50	−01 47 09.10	6916916844479162880	20523149−0147089	49.41 ± 0.05	−91.58	−55.97	14.022	—	—	10.070	—
20 52 33.02	−16 58 29.01	6882963066420161664	20523304−1658289	178.12 ± 0.08	−309.22	37.35	10.072	11.762	8.850	6.199	—
20 53 09.14	−01 33 04.36	6916929660661726208	20530910−0133039	58.46 ± 0.07	399.96	−215.73	13.973	—	—	9.793	—
20 53 28.01	−73 08 10.42	6370294123335198464	20532801−7308105	43.59 ± 0.04	87.48	−185.89	11.750	13.046	10.642	8.351	—
20 53 33.06	+10 37 02.20	1750765357185849856	20533304+1037020	77.84 ± 0.07	−492.56	−447.03	12.455	14.222	11.189	8.481	—
20 53 55.50	−62 23 57.84	6451144236982039680	20535550−6223578	46.34 ± 0.05	104.81	−53.00	12.489	14.066	11.275	8.703	—
20 53 57.33	−55 06 31.48	6470039653542791552	20535735−5506315	42.60 ± 0.05	277.72	−131.74	13.617	15.377	12.347	9.690	—
20 54 15.04	−53 29 55.71	6470468772315704448	20541502−5329557	40.18 ± 0.04	−39.03	−189.90	11.193	12.313	10.181	8.049	—
20 54 31.89	+00 51 28.42	4227727388253995648	20543189+0051282	40.11 ± 0.08	62.09	−21.05	13.865	15.622	12.590	9.922	—
20 55 37.12	−14 03 54.88	6887025727524300416	20553706−1403545	80.23 ± 0.09	1420.74	−472.12	12.920	14.844	11.606	8.915	—
20 55 37.74	−14 02 08.13	6887029163498137856	20553771−1402078	77.01 ± 0.40	1425.50	−464.31	11.045	12.708	9.839	7.365	—
20 56 27.14	−24 00 12.54	6805970245721550080	20562711−2400123	52.59 ± 0.08	333.86	−117.47	13.483	15.375	12.172	9.375	—

Table 2: List of M dwarf systems within 25 pc drawn from *Gaia* DR2, as described in §2.3.

These systems have not been vetted to distinguish single stars from multiples, but in cases

where a system was resolved in *Gaia* but not 2MASS, a “J” flag is listed in column 12.

20 56 46.60	−10 26 54.75	6890353330746858368	20564659−1026534	62.12 ± 0.07	−37.20	−1124.32	10.408	11.738	9.300	6.884	—
20 57 25.36	+22 21 45.81	1838855376946302720	20572537+2221457	69.31 ± 0.07	769.82	−213.27	11.003	12.285	9.921	7.640	—
20 57 54.09	−02 52 30.25	6915795853718552960	20575409−0252302	64.47 ± 0.24	−2.87	−102.22	18.066	20.726	16.430	11.724	—
20 59 40.42	−40 14 34.06	6773742009427000704	20594043−4014341	41.60 ± 0.05	−88.42	149.53	11.974	13.203	10.891	8.636	—
21 00 54.94	−41 31 43.98	6773423224070637952	21005492−4131438	53.25 ± 0.06	358.68	−253.97	12.420	14.030	11.193	8.600	—
21 01 03.82	−41 14 33.28	6773453838597541760	21010380−4114331	53.31 ± 0.10	358.55	−253.16	13.021	14.749	11.763	9.094	—
21 01 04.79	+03 07 04.97	1731137528439917568	21010483+0307047	54.34 ± 0.16	1023.18	−55.15	15.886	18.983	14.345	10.567	—
21 01 07.40	−49 07 25.07	6478328150150225664	21010742−4907248	65.65 ± 0.49	−282.95	−210.79	12.000	13.599	10.786	8.193	—
21 01 58.64	−06 19 07.48	6910371005081903488	21015865−0619070	69.14 ± 0.12	−230.06	−442.01	10.173	11.489	9.069	6.692	—
21 02 40.72	−18 31 16.95	6881661519529805952	21024074−1831169	49.01 ± 0.05	337.62	−113.79	10.520	11.608	9.517	7.408	—
21 03 13.95	−56 57 48.35	6456884409233519360	21031390−5657479	80.06 ± 0.06	−357.00	354.64	11.550	13.065	10.378	7.902	—
21 03 21.66	−50 22 52.41	6478007127114271104	21032165−5022522	41.30 ± 0.11	296.00	−386.28	11.873	13.364	10.692	8.192	—
21 04 48.00	−04 18 26.51	6912395304772726144	21044799−0418264	40.19 ± 0.10	47.79	−10.06	12.893	14.570	11.648	9.052	—
21 04 53.38	−16 57 31.95	6882393725554653056	21045341−1657311	54.70 ± 0.04	−916.24	−2039.76	10.620	11.716	9.608	7.545	—
21 05 13.80	−55 03 56.25	6463883281779253120	21051377−5503562	62.88 ± 0.06	44.46	−327.30	12.530	14.218	11.284	8.643	—
21 05 22.21	+20 51 34.09	1838036133406428288	21052221+2051341	46.79 ± 0.08	272.32	−87.75	12.112	13.478	10.977	8.657	—
21 05 32.06	+06 09 15.47	1736707482548494848	21053205+0609155	44.34 ± 0.06	27.88	45.13	11.452	12.877	10.306	7.802	—
21 06 26.81	−51 42 37.14	6476864837612387584	21062685−5142369	44.18 ± 0.04	−335.30	−207.84	11.644	12.836	10.467	8.078	—
21 07 36.79	−13 04 58.19	6885822307751773568	21073678−1304581	48.25 ± 0.15	61.32	−87.10	11.459	12.904	10.323	7.843	—
21 09 17.43	−13 18 09.02	6885776098199761024	21091740−1318080	84.70 ± 0.07	714.80	−1995.21	10.016	11.129	9.006	6.909	—
21 11 24.20	−09 40 33.24	6895572437565417856	21112419−0940334	52.67 ± 0.10	−28.78	−349.45	14.478	16.739	13.089	9.950	—
21 11 49.57	−43 36 49.15	6579894402894605824	21114955−4336489	63.34 ± 0.05	215.50	−691.26	11.009	12.252	9.935	7.667	—
21 11 57.28	−34 54 10.74	6777414279481335936	21115725−3454105	45.26 ± 0.08	252.74	−152.67	13.363	15.018	12.119	9.490	—
21 12 17.00	−63 18 10.88	6449957142381556480	21121700−6318109	43.77 ± 0.07	−88.43	−110.39	14.288	16.345	12.945	9.933	—
21 12 40.50	−18 47 57.61	6833711267686909952	21124050−1847576	40.30 ± 0.07	212.96	−53.64	13.425	15.078	12.184	9.559	—
21 14 12.20	−76 33 25.29	6368299918479525632	21141217−7633256	51.21 ± 0.69	92.02	−219.00	11.150	12.482	9.821	7.237	—
21 16 06.31	+22 38 46.43	1791810263689791488	21160629+2238462	47.84 ± 0.11	67.52	176.05	15.611	18.247	14.154	10.827	—
21 16 08.08	−33 46 26.16	6783572399293314560	21160807−3346261	63.17 ± 1.28	−17.47	−3.72	18.974	19.706	17.878	15.936	—
21 16 27.28	+02 34 51.39	2692455319291894400	21162729+0234514	56.69 ± 0.06	247.52	−39.68	10.860	12.224	9.740	7.324	—
21 17 34.08	−44 44 35.31	6576809826100275456	21173406−4444358	56.97 ± 0.65	6.06	108.36	13.201	14.312	11.241	8.526	—
21 20 09.80	−67 39 05.63	6399966162596931712	21200974−6739054	47.93 ± 0.28	−431.98	87.98	10.066	11.159	9.057	6.834	—

Table 2: List of M dwarf systems within 25 pc drawn from *Gaia* DR2, as described in §2.3.

These systems have not been vetted to distinguish single stars from multiples, but in cases

where a system was resolved in *Gaia* but not 2MASS, a “J” flag is listed in column 12.

21	21	14.20	-59	27	50.43	6453242173886773376	21211420-5927505	40.88 ± 0.06	-100.27	154.47	12.826	14.344	11.631	9.133	-
21	22	06.28	+22	55	53.14	1791995119082190848	21220626+2255531	64.59 ± 0.05	108.84	117.87	9.770	10.848	8.769	6.595	-
21	22	16.93	-43	14	04.83	6577290140883225984	21221691-4314049	46.36 ± 0.05	-42.60	-228.28	12.033	13.605	10.818	8.212	-
21	23	52.72	-39	08	17.60	6582502959872402944	21235271-3908176	41.09 ± 0.07	-82.83	-41.75	12.175	13.746	10.964	8.457	-
21	24	18.36	-46	41	35.11	6575581499814748800	21241840-4641352	44.96 ± 0.09	737.92	-54.48	11.473	12.700	10.400	8.135	-
21	26	34.04	-31	43	22.52	6784262587654030336	21263403-3143224	40.87 ± 0.58	203.68	-233.90	17.950	21.138	16.323	12.362	-
21	26	52.91	-44	48	46.52	6576207602966235392	21265289-4448466	42.38 ± 0.06	251.18	177.08	12.181	13.781	10.956	8.345	-
21	27	04.58	-38	44	50.83	6582903697500334464	21270455-3844505	48.78 ± 0.09	566.29	-705.05	13.129	14.855	11.868	9.278	-
21	27	16.86	-06	50	39.38	6898272524589700608	21271685-0650391	59.53 ± 0.10	29.26	-398.96	10.288	11.352	9.302	7.166	-
21	27	56.51	-72	17	17.70	6371660537113102976	21275652-7217177	54.49 ± 0.03	120.85	68.16	11.913	13.310	10.770	8.386	-
21	28	17.68	-32	54	06.58	6783123184369906816	21281779-3254062	46.18 ± 0.20	302.50	-156.85	16.494	19.545	14.918	10.511	-
21	28	17.84	-32	54	06.15	6783123184369906944	21281779-3254062	46.43 ± 0.16	309.03	-157.43	15.821	18.495	14.334	10.511	-
21	28	18.28	-22	18	32.36	6828140347214896000	21281830-2218319	47.49 ± 0.10	-209.62	-259.81	11.112	12.439	10.019	7.633	-
21	29	03.49	-14	06	28.33	6842531927921853440	21290348-1406282	46.69 ± 0.09	-12.65	79.60	10.589	11.771	9.540	7.280	-
21	29	17.28	-73	27	10.70	6370787700976287744	21291726-7327108	41.47 ± 0.07	-82.86	-136.83	15.283	17.640	13.881	10.753	-
21	29	23.39	-18	55	07.84	6831300038686921088	21292339-1855075	47.88 ± 0.10	-38.01	-186.25	14.880	17.204	13.480	10.301	-
21	29	36.81	+17	38	35.86	1784473016438653056	21293671+1738353	147.61 ± 0.10	1007.02	378.78	9.101	10.591	7.933	5.453	-
21	30	07.00	-77	10	37.32	6356570053556464128	21300712-7710377	47.36 ± 0.08	510.72	-272.91	14.883	17.203	13.483	10.365	-
21	30	47.67	-40	42	29.45	6579485487647973888	21304763-4042290	82.19 ± 0.08	1046.86	-1396.29	11.786	13.400	10.566	8.134	-
21	31	18.57	-09	47	26.48	6894054664842632448	21311859-0947263	134.08 ± 1.11	1246.51	-61.07	10.483	12.300	9.224	6.379	-
21	32	21.98	+24	33	41.82	1798246358080104448	21322198+2433419	48.84 ± 0.09	211.92	-44.18	12.278	12.903	10.443	7.589	J
21	32	29.77	-05	11	59.03	2671157366745568256	21322975-0511585	49.76 ± 0.09	116.21	-341.57	15.121	17.579	13.697	10.379	-
21	33	33.97	-49	00	32.40	6562924609150908416	21333397-4900323	201.41 ± 0.04	-45.83	-816.60	7.738	8.920	6.676	4.501	-
21	33	48.91	-06	51	10.36	2670661109044300160	21334890-0651099	59.63 ± 0.06	126.26	-502.67	12.625	14.360	11.369	8.655	-
21	33	49.13	+01	46	56.51	2688566793341935360	21334913+0146561	59.46 ± 0.07	-14.93	-726.90	12.570	14.171	11.348	8.775	-
21	34	22.30	-43	16	10.64	6577933973662574080	21342228-4316102	59.11 ± 0.09	146.53	-793.74	14.294	16.588	12.896	9.685	-
21	35	39.62	-53	25	31.56	6462049502543522688	21353962-5325315	50.25 ± 0.07	-91.10	167.60	14.077	16.042	12.756	9.915	-
21	36	25.30	-44	01	00.08	6577573677445347584	21362532-4401005	70.54 ± 0.07	485.03	-679.68	12.591	14.396	11.307	8.530	-
21	37	10.46	+14	50	47.70	1770881266011697920	21371044+1450475	42.38 ± 0.32	-156.84	-136.30	19.012	21.214	17.393	12.815	-
21	37	31.19	-10	14	25.75	6893412618771209088	21373116-1014250	51.86 ± 0.10	207.80	-591.03	13.321	15.106	12.040	9.428	-
21	37	49.19	-07	57	14.64	2667332230216493440	21374917-0757145	46.59 ± 0.25	19.43	-5.25	13.042	14.685	11.812	9.186	-

Table 2: List of M dwarf systems within 25 pc drawn from *Gaia* DR2, as described in §2.3.

These systems have not been vetted to distinguish single stars from multiples, but in cases

where a system was resolved in *Gaia* but not 2MASS, a “J” flag is listed in column 12.

21	38	43.66	-33	39	55.20	6592223158057230592	21384369-3339555	82.88 ± 0.11	1039.75	-518.82	11.276	12.817	10.099	7.574	-
21	39	03.72	-10	48	44.57	6892947044316282368	21390367-1048437	48.37 ± 0.07	441.49	-576.89	14.408	16.352	13.098	10.507	-
21	39	13.77	-71	23	53.41	6371430640400532480	21391379-7123536	43.53 ± 0.03	37.26	-222.25	11.393	12.698	10.291	7.911	-
21	41	40.51	-14	01	39.96	6841809067745428992	21414051-1401396	42.66 ± 0.08	-292.79	-273.61	13.032	14.610	11.814	9.248	-
21	41	46.81	-27	04	54.64	6810820947424835712	21414678-2704542	49.29 ± 0.08	146.74	-267.78	14.023	16.005	12.695	9.786	-
21	41	55.08	-51	18	50.62	6558741070485093632	21415505-5118506	63.48 ± 0.90	705.21	-262.58	20.347	21.442	18.473	13.658	-
21	42	25.31	-26	24	04.07	6811417157605199104	21422531-2624036	41.90 ± 0.09	-39.21	-307.82	14.646	16.674	13.312	10.465	-
21	44	07.98	+17	04	37.31	1773497412196823680	21440795+1704372	58.52 ± 0.07	245.11	1.47	13.312	15.221	12.010	9.193	-
21	44	09.03	+17	03	34.95	1773485214494929536	21440900+1703348	58.39 ± 0.15	251.72	3.22	12.303	13.954	11.072	8.435	-
21	44	12.99	+06	38	29.28	2700417192226894976	21441297+0638292	49.01 ± 0.08	-324.04	-166.11	10.978	12.348	9.855	7.443	-
21	44	40.38	-18	47	55.78	6836547453635933056	21444037-1847557	42.78 ± 1.12	-42.90	25.01	20.292	21.446	18.525	13.964	-
21	44	41.29	-74	21	57.23	6370491382592592128	21444127-7421575	41.91 ± 0.05	-91.51	-393.99	13.093	14.550	11.915	9.534	-
21	45	00.78	-05	47	13.34	2668249051115631232	21450079-0547128	59.84 ± 0.06	-169.46	-435.34	11.745	13.156	10.596	8.193	-
21	45	24.89	-05	54	05.97	2668056572156599040	21452490-0554055	40.11 ± 0.06	-139.38	-343.87	12.404	13.883	11.219	8.776	-
21	45	44.32	+20	46	47.65	1792668153341911680	21454431+2046476	46.59 ± 0.09	255.08	-30.85	12.974	14.598	11.751	9.192	-
21	46	40.42	-00	10	23.77	2681122098893985408	21464040-0010233	80.77 ± 0.11	769.50	-505.67	11.314	12.928	10.095	7.489	-
21	46	42.69	-85	43	04.48	6342940473056949120	21464282-8543046	64.33 ± 0.05	236.26	-195.33	11.958	13.696	10.690	7.991	-
21	46	45.52	-21	17	46.95	6817950657560102016	21464549-2117468	64.19 ± 0.08	292.28	-52.81	12.285	13.961	11.046	8.379	-
21	47	17.45	-04	44	40.70	2669873515120908544	21471744-0444406	86.79 ± 0.10	257.13	5.46	12.624	14.534	11.323	8.501	-
21	48	53.03	-19	47	27.07	6824372698820338176	21485301-1947269	41.25 ± 0.09	303.68	-28.80	13.310	15.117	12.021	9.210	-
21	49	11.31	-41	33	28.71	6572227714472220416	21491134-4133295	69.32 ± 0.60	279.17	-229.06	10.944	12.351	9.766	6.882	-
21	49	25.91	-63	06	51.91	6402860489518406144	21492590-6306519	59.96 ± 0.05	289.81	439.39	11.429	12.836	10.297	7.886	-
21	49	35.80	+05	39	06.89	2697080449314615168	21493582+0539068	44.26 ± 0.04	541.61	-26.87	13.524	15.134	12.297	9.770	-
21	49	44.83	-41	38	32.77	6572223552647639552	21494480-4138327	46.25 ± 0.61	151.37	-52.77	12.267	13.805	11.067	8.544	-
21	50	15.77	-75	20	36.73	6358287868675805824	21501592-7520367	41.36 ± 0.28	888.63	-298.23	18.911	21.446	17.303	12.673	-
21	50	27.12	-63	40	53.84	6402563827535838592	21502708-6340537	43.52 ± 0.05	-176.62	164.07	12.600	14.138	11.398	8.936	-
21	50	48.19	-10	39	06.13	2617720998556760576	21504816-1039061	42.46 ± 0.08	-36.91	-245.67	13.213	14.764	11.861	9.081	-
21	51	05.09	+23	28	09.61	1795813379365971072	21510510+2328088	61.54 ± 0.37	20.64	-40.73	14.403	15.147	12.941	10.651	-
21	51	17.51	+12	50	30.67	1766511046596516608	21511741+1250303	42.13 ± 0.06	666.93	160.65	12.223	13.736	11.032	8.539	-
21	51	27.03	-01	27	14.30	2673992663636347520	21512700-0127144	50.10 ± 0.10	212.85	18.28	14.871	17.198	13.473	10.385	-
21	51	31.38	-40	17	23.17	6572811211549713792	21513137-4017229	56.11 ± 0.15	402.56	-265.50	15.418	18.144	13.930	10.413	-

Table 2: List of M dwarf systems within 25 pc drawn from *Gaia* DR2, as described in §2.3.

These systems have not been vetted to distinguish single stars from multiples, but in cases

where a system was resolved in *Gaia* but not 2MASS, a “J” flag is listed in column 12.

21	51	48.32	+13	36	15.21	1768825106253209984	21514831+1336154	55.01 ± 0.53	192.01	−87.33	12.602	14.197	11.184	8.423	—
21	51	59.56	−15	14	01.37	6839883788525745536	21515955−1514018	44.63 ± 0.08	106.94	−851.47	14.232	16.021	12.948	10.360	—
21	53	07.53	−12	49	40.89	6840822904599511936	21530753−1249408	41.47 ± 0.08	−145.51	−135.73	10.288	11.238	9.358	7.359	—
21	53	12.00	−25	59	56.92	6812057416969617280	21531204−2559567	41.35 ± 0.08	−343.32	−113.46	14.893	17.027	13.534	10.593	—
21	54	02.54	−47	54	02.37	6561011974314713856	21540252−4754023	42.47 ± 0.07	164.28	76.94	13.862	15.669	12.580	9.837	—
21	54	45.31	−46	59	33.84	6561146458331160320	21544531−4659338	64.36 ± 0.04	−320.56	−365.18	10.952	12.233	9.863	7.576	—
21	55	02.23	−20	14	26.94	6823449766182657280	21550221−2014271	52.33 ± 0.10	209.15	122.51	12.841	14.418	11.633	9.102	—
21	55	48.36	−33	13	14.82	6588749457226272512	21554835−3313151	43.71 ± 0.44	62.49	−218.39	11.477	13.000	10.291	7.695	—
21	56	19.50	+22	49	01.20	1794793582332461952	21561950+2249008	47.07 ± 0.99	−8.70	−12.75	19.131	19.448	17.230	14.832	—
21	56	19.81	−10	20	16.69	2617043665033540480	21561982−1020166	50.54 ± 0.08	−307.18	−272.34	13.286	14.954	11.818	9.086	—
21	56	37.93	+19	46	14.43	1780624347783836032	21563794+1946144	45.38 ± 0.07	−88.55	−479.24	11.746	13.185	10.584	8.067	—
21	56	55.25	−01	54	09.34	2679694971455927296	21565513−0154100	74.14 ± 0.10	1281.20	612.25	13.038	14.956	11.728	9.026	—
21	57	12.68	−09	03	26.86	2618333804489940992	21571265−0903267	51.27 ± 0.15	177.62	−126.52	13.394	15.298	12.066	9.239	—
21	57	26.23	+08	08	13.92	2724890053318383232	21572624+0808139	47.78 ± 0.08	373.75	100.16	10.127	11.280	9.094	6.845	—
21	57	39.30	−09	28	13.39	2617534627040896768	21573933−0928131	40.57 ± 0.07	−515.66	−195.26	13.467	15.178	12.208	9.537	—
21	58	49.12	−32	26	25.64	6612817835477756160	21584914−3226253	51.34 ± 0.59	−380.78	−355.22	14.014	16.025	12.677	9.761	—
21	58	50.19	−32	28	17.86	6612817217002464128	21585020−3228176	51.51 ± 0.08	−395.02	−360.89	13.341	14.968	12.109	9.558	—
21	59	34.70	−59	45	10.14	6409685433069148288	21593479−5945104	86.52 ± 0.04	886.11	−125.36	8.913	9.977	7.918	5.757	—
22	02	10.28	+01	24	00.83	2683023811628007296	22021026+0124006	94.74 ± 0.14	−452.43	−278.58	8.402	9.409	7.438	5.322	—
22	03	27.13	−50	38	38.26	6558265325547297536	22032712−5038382	47.66 ± 0.09	347.14	−485.90	11.127	12.352	10.068	7.812	—
22	04	21.52	+15	05	52.47	1768695093298872832	22042147+1505517	48.17 ± 0.31	653.21	484.83	14.397	16.633	13.023	9.981	—
22	05	35.73	−11	04	28.96	2614071100988460544	22053575−1104287	50.95 ± 0.12	−270.59	−175.31	15.380	17.907	13.938	10.723	—
22	06	09.63	−07	23	35.60	2620145937091715072	22060961−0723353	64.95 ± 0.08	175.42	−219.36	14.211	16.512	12.825	9.759	—
22	06	22.62	+17	22	20.77	1776179945695834368	22062259+1722206	56.83 ± 0.11	362.10	84.20	11.837	13.382	10.634	8.076	—
22	06	25.84	+21	39	43.96	1781723721971913856	22062584+2139439	40.19 ± 0.07	128.69	9.82	13.879	15.643	12.609	9.943	—
22	06	29.76	+02	22	31.82	2683209044978079616	22062976+0222320	50.94 ± 0.07	268.05	68.37	13.287	14.981	12.038	9.443	—
22	06	40.69	−44	58	07.53	6567609525117256576	22064072−4458067	58.02 ± 0.20	−459.05	−583.22	12.919	14.707	11.638	8.893	—
22	06	46.36	+03	25	03.86	2683714304930755712	22064638+0325037	56.65 ± 0.09	471.05	−319.83	12.296	13.910	11.078	8.512	—
22	06	54.88	−76	53	58.84	6357192995613035008	22065493−7653587	45.92 ± 0.04	100.02	45.59	10.981	12.218	9.909	7.619	—
22	06	57.20	−49	49	41.90	6559631640545167232	22065718−4949419	40.23 ± 0.04	370.94	−24.51	11.969	13.327	10.831	8.449	—
22	07	48.46	+05	39	09.94	2720293407519457280	22074847+0539099	40.25 ± 0.10	456.00	126.81	14.452	16.457	13.114	10.242	—

Table 2: List of M dwarf systems within 25 pc drawn from *Gaia* DR2, as described in §2.3.

These systems have not been vetted to distinguish single stars from multiples, but in cases

where a system was resolved in *Gaia* but not 2MASS, a “J” flag is listed in column 12.

22 08 38.72	−83 03 28.44	6345136988052055552	22083876−8303284	47.32 ± 0.03	295.61	0.95	11.756	13.163	10.609	8.219	—
22 08 44.76	−25 05 06.58	6620217750595836288	22084476−2505065	40.19 ± 0.06	−116.64	−53.31	12.222	13.616	11.077	8.729	—
22 09 40.34	−04 38 26.65	2627117287488522240	22094029−0438267	113.60 ± 0.05	1132.53	−22.13	9.224	10.632	8.086	5.594	—
22 10 13.19	−71 46 06.19	6383229053001389312	22101326−7146064	51.64 ± 0.08	512.22	−205.79	13.052	14.767	11.796	9.109	—
22 11 13.49	−02 32 37.09	2676023495972445184	22111347−0232369	44.85 ± 0.06	426.74	−71.88	11.190	12.430	10.113	7.818	—
22 11 30.09	+18 25 34.30	1776317182780536064	22113008+1825341	85.29 ± 0.04	329.20	180.82	9.253	10.493	8.179	5.823	—
22 12 35.94	+08 33 11.60	2723557788822526720	22123595+0833110	62.78 ± 0.10	106.80	−670.42	10.905	12.252	9.790	7.472	—
22 13 42.86	−17 41 08.68	6825822095663585536	22134277−1741081	97.51 ± 0.07	856.89	−306.30	12.081	13.914	10.807	8.115	—
22 13 50.20	−54 51 24.32	6508226723167166336	22135019−5451242	40.71 ± 0.14	108.70	−395.29	16.606	19.706	15.076	11.629	—
22 13 50.47	−63 42 10.01	6405457982659103872	22135048−6342100	72.10 ± 0.08	115.67	170.40	14.657	17.299	13.213	9.938	—
22 15 54.92	+23 21 02.52	1878388180082512000	22155488+2321026	44.27 ± 0.08	−113.99	−180.86	15.067	17.176	13.335	10.115	—
22 17 18.97	−08 48 12.26	2616132101175106816	22171899−0848122	89.80 ± 0.09	−458.51	−291.85	12.105	13.850	10.843	8.167	—
22 17 19.23	−34 44 03.51	6599565765426015232	22171923−3444031	52.92 ± 0.78	109.10	−455.35	13.571	15.710	12.207	9.170	—
22 17 53.27	−36 11 19.99	6598319159758429696	22175325−3611192	44.15 ± 0.06	111.48	−529.13	12.871	14.448	11.653	9.087	—
22 19 23.69	−28 23 20.71	6615656396543741952	22192359−2823204	47.02 ± 0.07	845.27	−249.53	13.300	15.075	12.021	9.359	—
22 19 26.44	−31 03 35.61	6613969195950456448	22192645−3103352	52.23 ± 0.21	−233.22	−412.36	12.339	13.649	11.219	8.921	—
22 20 13.26	+06 43 31.98	2708839657453920256	22201326+0643321	55.42 ± 0.09	284.49	280.95	12.197	13.600	11.052	8.695	—
22 21 42.92	−65 31 32.98	6404403585367962752	22214293−6531330	52.11 ± 0.04	−70.93	147.68	11.006	12.273	9.929	7.644	—
22 21 53.35	−31 31 22.57	6613707340384992896	22215333−3131225	41.46 ± 0.06	252.33	−74.02	12.316	13.824	11.122	8.603	—
22 23 07.00	−17 36 26.33	2595284016771502080	22230696−1736250	138.18 ± 0.25	308.43	−718.31	11.554	13.550	10.239	7.319	—
22 23 33.30	−57 13 14.26	6504705571539380992	22233334−5713146	52.68 ± 0.04	589.98	−374.94	9.895	10.967	8.899	6.730	—
22 24 22.95	−65 58 36.12	6398188767690594048	22242295−6558361	63.11 ± 0.05	−155.42	−54.39	11.485	12.921	10.334	7.931	—
22 24 24.65	−58 26 13.66	6408509574103239552	22242466−5826141	62.38 ± 0.19	−75.71	−37.18	13.565	15.599	12.224	9.286	—
22 24 42.38	+22 30 42.66	1875075420267288064	22244238+2230425	47.90 ± 0.09	−186.46	−86.05	15.519	18.133	14.076	10.875	—
22 25 05.07	−47 52 46.87	6518076320126449280	22250500−4752461	66.70 ± 0.10	487.81	−642.20	11.202	12.767	10.017	7.427	—
22 26 01.16	−15 18 13.04	2599176120046382336	22260112−1518128	41.00 ± 0.10	272.52	−53.52	14.988	17.209	13.602	10.561	—
22 26 44.42	−75 03 42.53	6357834388848708224	22264440−7503425	42.59 ± 0.14	58.40	11.60	16.815	20.097	15.235	11.246	—
22 27 02.81	+06 49 32.63	2710189960812052736	22270280+0649324	72.72 ± 0.08	182.93	−34.94	11.931	13.532	10.719	8.164	—
22 28 01.20	−04 11 58.87	2627941715050682752	22280118−0411587	48.51 ± 0.06	96.01	4.41	12.625	14.105	11.445	9.000	—
22 28 45.94	+18 55 54.11	2738145555048846080	22284590+1855544	44.90 ± 0.05	167.38	−127.66	10.009	11.006	9.065	6.978	—
22 28 54.35	−13 25 19.46	2601148128510120576	22285440−1325178	91.89 ± 0.09	−328.10	−1044.81	14.563	17.469	13.086	9.843	—

Table 2: List of M dwarf systems within 25 pc drawn from *Gaia* DR2, as described in §2.3.

These systems have not been vetted to distinguish single stars from multiples, but in cases

where a system was resolved in *Gaia* but not 2MASS, a “J” flag is listed in column 12.

22 30 09.41	−53 44 55.53	6509993810151618304	22300946−5344551	62.52 ± 0.17	−49.93	−741.82	12.806	14.743	11.494	8.629	—
22 32 41.95	−56 11 28.52	6505203753385335296	22324194−5611285	47.38 ± 0.06	50.79	−117.83	13.679	15.369	12.431	9.899	—
22 33 02.23	+09 22 40.72	2717105133036645760	22330225+0922410	77.03 ± 0.06	538.30	141.21	9.537	10.644	8.528	6.356	—
22 34 31.99	+19 58 13.27	2834386568038204416	22343196+1958137	40.81 ± 0.07	119.96	−203.70	13.558	15.272	12.298	9.653	—
22 34 46.21	+04 02 37.67	2705611005983192320	22344620+0402377	59.45 ± 0.05	−96.07	129.05	11.610	12.968	10.485	8.129	—
22 34 53.68	−01 04 58.04	2629732510254843136	22345363−0104581	45.09 ± 0.07	1097.11	218.64	13.416	15.143	12.155	9.518	—
22 38 24.67	−29 21 14.08	6608187792013441792	22382467−2921139	84.37 ± 0.04	1.72	−256.47	9.930	11.195	8.851	6.569	—
22 38 45.57	−20 37 16.09	2400808142038361088	22384559−2037160	112.37 ± 0.08	449.24	−79.06	8.163	9.372	7.098	4.800	—
22 38 51.71	−32 16 32.49	6600863910701061632	22385170−3216324	57.25 ± 0.06	113.31	−36.25	12.113	13.632	10.922	8.429	—
22 40 18.69	−49 31 04.48	6517274496976569344	22401867−4931045	83.95 ± 0.08	468.50	172.15	13.185	15.235	11.845	9.005	—
22 41 13.88	−10 44 47.43	2608006916403629056	22411384−1044475	45.53 ± 0.07	238.59	22.36	11.558	12.978	10.403	7.901	—
22 41 15.21	−25 54 25.97	6622965567593297536	22411520−2554257	42.06 ± 0.09	27.11	−128.15	12.950	14.423	11.771	9.370	—
22 41 58.12	−69 10 08.32	6385548541499112448	22415815−6910089	67.15 ± 0.05	334.36	−726.97	13.393	15.451	12.052	9.145	—
22 41 59.37	−75 00 33.06	6381623044470172672	22415937−7500329	80.44 ± 0.07	−76.01	217.12	13.943	16.234	12.562	9.600	—
22 42 01.03	−37 17 34.28	6595750597516482048	22420102−3717342	40.92 ± 0.06	220.65	−17.47	13.438	15.100	12.191	9.566	—
22 43 23.20	+22 08 18.03	2836510961942677376	22432313+2208179	50.79 ± 0.07	390.35	2.16	13.376	15.273	12.067	9.258	—
22 44 57.96	−33 15 01.75	6603693881832177792	22445794−3315015	47.94 ± 0.05	179.90	−123.10	10.736	12.324	9.539	6.932	—
22 45 06.07	−12 23 43.28	2604498958915619840	22450605−1223434	47.26 ± 0.05	133.37	140.10	12.643	14.272	11.417	8.788	—
22 46 26.35	−06 39 26.36	2611463952760479232	22462632−0639259	50.22 ± 0.10	694.99	−539.72	14.185	16.263	12.835	9.850	—
22 47 38.92	+18 26 37.04	2833336809311479936	22473884+1826364	40.89 ± 0.22	382.84	208.07	11.872	13.287	10.712	8.273	—
22 48 04.49	−24 22 07.72	6623351805412369024	22480446−2422075	130.30 ± 0.07	331.90	−183.47	11.136	12.904	9.881	7.206	—
22 48 17.37	−36 47 23.32	6548081373973468416	22481735−3647233	46.38 ± 0.06	756.20	−274.18	10.959	12.180	9.905	7.626	—
22 48 22.52	+12 32 10.42	2719512513745949184	22482247+1232105	51.15 ± 0.15	503.18	−13.44	14.851	17.242	13.441	10.232	—
22 48 38.39	−31 08 40.71	6604348434848487808	22483835−3108412	56.95 ± 0.62	427.43	−123.89	11.173	12.611	10.017	7.487	—
22 48 54.59	+18 19 58.97	2830318679957189632	22485459+1819592	52.91 ± 0.10	−21.52	−128.50	13.034	14.763	11.777	9.119	—
22 49 02.79	+04 59 36.05	2705239237909520128	22490279+0459360	43.45 ± 0.22	−137.55	17.08	12.891	14.552	11.655	9.109	—
22 50 19.42	−07 05 24.38	2611163717366876544	22501943−0705245	68.96 ± 0.05	−106.49	103.89	9.130	10.118	8.185	6.104	—
22 51 23.73	−34 19 36.13	6602601031698725632	22512369−3419359	41.03 ± 0.05	246.25	−183.69	10.683	11.788	9.668	7.491	—
22 52 48.07	−28 47 42.66	6609167869190786688	22524813−2847422	48.20 ± 0.05	−412.11	−273.97	10.894	12.108	9.841	7.578	—
22 53 16.73	−14 15 49.30	2603090003484152064	22531672−1415489	213.87 ± 0.08	957.96	−673.64	8.875	10.477	7.662	5.010	—
22 53 50.93	−71 28 07.06	6383963114451742464	22535091−7128069	47.12 ± 0.07	257.65	−159.52	14.366	16.488	13.011	9.955	—

Table 2: List of M dwarf systems within 25 pc drawn from *Gaia* DR2, as described in §2.3.

These systems have not been vetted to distinguish single stars from multiples, but in cases

where a system was resolved in *Gaia* but not 2MASS, a “J” flag is listed in column 12.

22 55 27.21	−52 18 09.75	6512664180298450688	22552718−5218094	42.06 ± 0.07	139.41	−88.61	10.657	11.771	9.639	7.418	—
22 55 45.51	−75 27 31.21	6378584028690858496	22554532−7527320	116.41 ± 0.03	−1026.33	−1059.32	9.283	10.635	8.163	5.811	—
22 55 59.85	+17 48 39.80	2830099469122381056	22555984+1748399	59.02 ± 0.06	24.68	−110.18	9.645	10.732	8.650	6.449	—
22 56 24.67	−60 03 49.25	6491249026683800832	22562466−6003490	96.22 ± 0.06	−521.01	−939.14	12.319	14.281	11.001	8.108	—
22 56 26.21	−11 09 38.84	2604921308819786624	22562617−1109392	46.27 ± 0.07	393.08	278.98	13.575	15.323	12.307	9.626	—
22 57 49.30	−46 38 44.64	6516332666486584064	22574930−4638447	42.63 ± 0.55	−180.29	200.37	18.208	20.933	16.545	12.595	—
22 59 06.45	−54 20 35.82	6506200976072829184	22590642−5420357	48.29 ± 0.13	480.00	−107.41	16.433	19.672	14.894	11.220	—
23 00 33.40	−23 57 10.31	2384000217021721600	23003338−2357097	50.78 ± 0.06	191.23	−345.22	10.681	11.835	9.645	7.407	—
23 00 36.59	−23 58 10.67	2383999392388000640	23003657−2358101	50.76 ± 0.05	194.26	−347.12	10.690	11.843	9.654	7.417	—
23 01 46.16	−06 14 22.72	2634902826245745664	23014614−0614225	44.55 ± 0.07	177.93	−80.18	12.211	13.627	11.052	8.648	—
23 03 20.86	−49 43 34.02	6514632718428652928	23032085−4943339	51.12 ± 0.06	−29.62	−106.77	9.898	10.927	8.924	6.809	—
23 03 35.60	−46 50 46.99	6539544319023472000	23033561−4650470	67.36 ± 0.85	−172.04	−25.41	12.330	14.136	11.053	8.360	—
23 03 59.72	−16 12 06.76	2409534686654407936	23035972−1612062	45.03 ± 0.10	−96.61	−339.07	13.201	14.848	11.955	9.293	—
23 06 29.37	−05 02 29.03	2635476908753563008	23062928−0502285	80.45 ± 0.12	930.88	−479.40	15.645	18.998	14.097	10.296	—
23 06 58.77	−50 08 58.94	6502618938988110848	23065876−5008589	48.00 ± 0.28	462.34	22.16	18.064	20.848	16.445	12.240	—
23 07 15.25	−23 07 53.82	2384348242516852864	23071524−2307533	45.30 ± 0.05	158.06	−254.07	12.391	13.875	11.210	8.738	—
23 07 19.70	−84 52 03.72	6343789261675614464	23071998−8452039	64.82 ± 0.06	604.18	−75.64	13.534	15.425	12.230	9.474	—
23 07 19.83	−04 15 25.34	2635679803009267968	23071981−0415254	47.36 ± 0.04	59.62	15.79	11.688	13.075	10.544	8.084	—
23 08 06.96	+03 19 44.37	2661803855688028800	23080698+0319444	60.75 ± 0.04	494.27	257.30	10.118	11.154	9.146	7.067	—
23 08 19.55	−15 24 35.77	2410011256225662208	23081954−1524354	40.14 ± 0.04	106.95	−18.74	10.183	11.177	9.227	7.114	—
23 10 15.74	−25 55 52.70	2379962604166006016	23101566−2555530	67.09 ± 0.05	715.74	25.22	10.318	11.534	9.259	6.995	—
23 10 18.59	+14 47 20.21	2815747234607015936	23101857+1447203	40.88 ± 0.09	−29.85	−65.39	13.897	15.665	12.616	9.946	—
23 11 34.57	−75 06 39.20	6378475623716304000	23113466−7506394	43.10 ± 0.05	517.22	−354.57	13.594	15.286	12.346	9.759	—
23 12 11.31	−14 06 12.07	2410261949172008064	23121132−1406108	55.89 ± 0.07	−180.46	−697.45	11.785	13.215	10.622	8.218	—
23 12 16.77	+14 14 27.81	2815480671757024512	23121677+1414279	40.45 ± 0.09	−123.22	−90.16	14.091	15.932	12.800	10.060	—
23 15 02.01	−35 28 24.76	6554995893362365952	23150199−3528247	61.40 ± 0.08	263.73	165.72	12.137	13.736	10.923	8.400	—
23 15 51.61	−37 33 30.70	6550040463175784192	23155156−3733306	49.11 ± 0.08	1281.61	256.15	13.472	15.252	12.198	9.592	—
23 15 54.51	−06 27 46.43	2631857350835259392	23155449−0627462	59.41 ± 0.08	315.54	−44.63	14.819	17.357	13.389	10.228	—
23 16 08.47	+06 44 36.22	2664368290465455232	23160847+0644360	48.96 ± 0.05	173.56	−250.42	12.005	13.468	10.832	8.407	—
23 17 00.22	−23 23 46.67	2384877214983800448	23170018−2323461	43.11 ± 0.04	306.91	−243.14	10.176	11.113	9.249	7.253	—
23 17 28.15	+19 36 47.08	2825274743381064320	23172807+1936469	60.61 ± 0.32	349.12	−121.04	10.832	12.319	9.663	7.173	—

Table 2: List of M dwarf systems within 25 pc drawn from *Gaia* DR2, as described in §2.3.

These systems have not been vetted to distinguish single stars from multiples, but in cases

where a system was resolved in *Gaia* but not 2MASS, a “J” flag is listed in column 12.

23 17 34.55	+06 23 28.47	2664156432614468864	23173454+0623282	49.03 ± 0.07	170.37	−249.28	11.432	12.796	10.302	7.878	—
23 17 47.11	−48 38 50.26	6526909899623917056	23174712−4838501	50.02 ± 1.27	249.00	65.79	20.613	21.135	18.890	13.181	—
23 17 50.32	−48 18 47.34	6527055859795615616	23175034−4818476	48.05 ± 0.06	293.20	−704.66	12.367	13.890	11.172	8.705	—
23 21 05.65	−16 51 49.36	2405722027006062080	23210564−1651492	46.42 ± 0.06	133.34	−418.09	11.827	13.166	10.696	8.339	—
23 21 37.45	+17 17 25.39	2817999068780218368	23213752+1717284	94.65 ± 0.09	−536.69	−1382.46	10.346	11.965	9.142	6.507	—
23 21 56.01	+24 12 31.65	2840714875932461440	23215594+2412321	40.42 ± 0.05	411.04	−188.67	12.580	14.064	11.393	8.940	—
23 22 46.83	−31 33 23.49	2328674716056981888	23224684−3133231	50.32 ± 0.56	−203.21	−540.48	18.324	21.746	16.697	12.324	—
23 23 24.71	+15 34 16.67	2814501281775322240	23232471+1534178	46.82 ± 0.04	4.21	−467.34	10.703	11.880	9.657	7.438	—
23 24 11.31	−17 45 50.29	2393504773489279232	23241131−1745504	43.67 ± 0.10	−164.70	−88.37	11.017	12.196	9.970	7.763	—
23 24 16.88	−15 22 22.98	2407573643242037888	23241688−1522228	54.92 ± 0.08	194.53	−49.08	14.701	17.055	13.303	10.196	—
23 26 11.84	+17 00 07.61	2823757279894208000	23261182+1700082	49.47 ± 0.40	142.25	−41.48	12.432	14.107	11.173	8.533	—
23 26 32.50	+12 09 33.66	2812500651648343552	23263239+1209328	40.65 ± 0.05	696.82	263.31	11.627	12.981	10.497	8.084	—
23 26 37.86	−46 51 05.71	6528276867455634176	23263788−4651060	44.38 ± 0.09	405.76	−373.01	14.032	15.886	12.738	10.114	—
23 27 26.45	−17 41 32.78	2393563872239260928	23272645−1741329	54.33 ± 0.08	44.32	−563.46	15.547	18.431	14.077	10.835	—
23 27 26.62	+08 45 16.75	2761165175302182656	23272661+0845166	40.66 ± 0.08	−23.51	−18.64	13.050	14.513	11.875	9.464	—
23 28 22.50	+00 28 39.54	2645345918966845440	23282251+0028395	42.75 ± 0.04	178.79	−1.62	12.084	13.481	10.934	8.519	—
23 28 24.58	−15 55 30.43	2407340615496379008	23282458−1555304	58.34 ± 0.06	−12.25	34.25	12.766	14.460	11.523	8.909	—
23 30 13.44	−20 23 27.45	2391670474561181440	23301341−2023271	62.67 ± 0.09	313.50	−205.41	9.921	11.340	8.792	6.329	—
23 30 16.17	−47 36 45.08	6526541563232943872	23301612−4736459	73.79 ± 0.16	−563.13	−973.57	15.249	18.338	13.730	10.279	—
23 30 38.09	−33 18 26.99	2325083848520121856	23303809−3318269	60.51 ± 0.15	−110.30	−42.73	13.333	15.227	12.032	9.317	—
23 30 38.18	−84 55 18.92	6343965492773694464	23303802−8455189	78.58 ± 0.06	−272.16	−62.87	12.905	14.691	11.635	8.995	—
23 30 53.70	+15 47 40.56	2814379579582643328	23305374+1547409	43.99 ± 0.04	−164.69	−109.29	10.740	11.821	9.735	7.606	—
23 31 21.74	−27 49 49.61	2331849006126794880	23312174−2749500	73.21 ± 0.16	90.39	745.20	15.884	19.352	14.330	10.651	—
23 31 52.17	+19 56 14.13	2824770686019003904	23315208+1956142	159.71 ± 0.08	577.61	−59.64	9.038	10.535	7.867	5.326	—
23 32 00.18	−39 17 37.18	6538208137513096448	23320018−3917368	42.27 ± 0.08	188.16	−184.66	11.690	13.192	10.534	8.022	—
23 33 40.63	−21 33 53.09	2388493745334271104	23334057−2133526	42.50 ± 0.10	694.13	−331.37	15.537	18.048	14.105	10.929	—
23 34 03.33	+00 10 45.88	2644439955745152512	23340328+0010452	71.37 ± 0.05	−992.97	−937.64	10.165	11.417	9.088	6.828	—
23 35 10.46	−02 23 20.61	2640434056928150400	23351050−0223214	139.31 ± 0.11	781.67	−841.42	12.640	14.974	11.253	8.183	—
23 36 00.42	−48 30 33.24	6523443723579266816	23360041−4830332	40.53 ± 0.11	−132.21	−24.71	14.931	17.170	13.531	10.430	—
23 36 51.77	+01 09 52.57	2646192130603302400	23365182+0109525	40.33 ± 0.05	1189.95	−109.43	12.181	13.344	11.120	9.012	—
23 36 52.30	−36 28 51.69	6539166877292779264	23365227−3628518	83.56 ± 0.07	1175.50	59.38	12.253	14.017	10.992	8.422	—

Table 2: List of M dwarf systems within 25 pc drawn from *Gaia* DR2, as described in §2.3.

These systems have not been vetted to distinguish single stars from multiples, but in cases

where a system was resolved in *Gaia* but not 2MASS, a “J” flag is listed in column 12.

23 37 35.98	+16 22 03.29	2819781274051096192	23373601+1622031	72.93 ± 0.11	361.16	−63.20	14.022	16.323	12.632	9.616	—
23 37 53.96	−76 45 20.23	6377426792701085056	23375392−7645202	42.09 ± 0.06	272.40	45.97	14.477	—	—	10.207	—
23 38 08.16	−16 14 10.20	2395413147718069504	23380819−1614100	76.06 ± 0.07	−280.69	−77.89	10.333	11.579	9.260	7.003	—
23 38 12.56	−69 05 57.46	6387062603370442624	23381267−6905576	44.88 ± 0.02	897.02	−118.07	12.328	13.649	11.206	8.961	—
23 38 17.42	−41 31 03.78	6536984484151135360	23381743−4131037	48.25 ± 0.07	207.35	−202.84	10.943	12.247	9.851	7.494	—
23 40 23.84	−40 21 46.96	6537148826779472512	23402384−4021470	40.86 ± 0.08	265.22	−125.01	11.859	13.195	10.735	8.342	—
23 41 00.73	−44 57 18.16	6531677691280151680	23410070−4457181	49.19 ± 0.05	735.08	−128.18	12.393	13.841	11.225	8.791	—
23 41 39.30	−06 35 50.45	2439763461052925824	23413925−0635502	47.64 ± 0.09	290.52	−91.52	13.558	15.421	12.263	9.396	—
23 44 20.88	+21 36 05.11	2826640989657988992	23442084+2136050	49.40 ± 0.07	455.52	80.33	12.033	13.618	10.819	8.225	—
23 45 56.59	−40 12 13.93	6534547176109685504	23455658−4012138	46.08 ± 0.07	307.60	−321.06	12.747	14.324	11.531	9.024	—
23 46 19.22	−11 56 43.29	2432708307254343808	23461921−1156429	43.26 ± 0.10	221.87	−130.12	14.002	15.983	12.672	9.755	—
23 46 32.05	−50 43 27.45	6522188390538224640	23463204−5043273	51.35 ± 0.06	−211.14	−469.04	13.086	14.806	11.832	9.256	—
23 46 38.24	−34 10 01.57	2312376723918929920	23463825−3410015	64.98 ± 0.06	−310.92	−1.24	11.488	12.848	10.356	8.044	—
23 46 46.03	+11 29 09.47	2760661255379706240	23464599+1129094	50.83 ± 0.19	−386.18	−83.59	17.392	20.716	15.794	11.605	—
23 47 21.75	−12 20 36.04	2420649585275393920	23472176−1220358	59.59 ± 0.08	−303.85	−140.15	14.025	16.084	12.688	9.763	—
23 49 49.00	+12 24 38.42	2769753357547997440	23494899+1224386	44.57 ± 0.18	32.76	−195.07	16.887	—	—	11.557	—
23 50 31.64	−09 33 32.66	2435125446129139712	23503159−0933320	58.97 ± 0.12	634.65	−425.98	12.007	13.669	10.769	8.043	—
23 50 36.16	+09 56 53.52	2759428629829608064	23503619+0956537	49.09 ± 0.14	648.76	251.46	10.590	11.815	9.336	6.807	—
23 50 39.56	+08 06 23.66	2758618568934035456	23503956+0806237	47.29 ± 0.13	373.78	285.88	16.172	19.185	14.671	11.345	—
23 50 52.63	−39 05 17.30	2307270076523103616	23505262−3905173	47.42 ± 0.07	800.60	−221.05	13.086	14.688	11.865	9.310	—
23 51 50.47	−25 37 36.84	2337628932595588608	23515044−2537367	49.13 ± 0.45	372.12	197.65	17.038	—	—	11.269	—
23 52 10.55	−19 39 16.04	2390021451933103616	23521054−1939159	40.76 ± 0.05	−198.43	58.77	10.948	11.942	9.990	7.985	—
23 52 23.47	−14 41 24.30	2419293853078963584	23522340−1441240	42.30 ± 0.55	409.84	−240.99	13.740	15.621	12.404	9.554	—
23 52 44.40	−57 56 02.96	6494854187871294336	23524442−5756029	44.98 ± 0.04	301.20	58.69	12.123	13.713	10.908	8.296	—
23 53 25.22	−70 56 41.15	6386280060329151616	23532520−7056410	80.99 ± 0.05	315.41	33.21	11.632	13.282	10.411	7.779	—
23 53 40.96	−35 59 05.88	2311039752138513536	23534095−3559058	40.78 ± 0.08	253.98	168.11	12.243	13.758	11.049	8.552	—
23 53 50.11	−75 37 57.12	6377828354964753792	23535017−7537575	98.86 ± 0.03	243.93	−379.25	9.003	10.267	7.915	5.549	—
23 53 59.46	−08 33 31.68	2435317585786753920	23535946−0833311	45.87 ± 0.27	−50.20	−383.19	17.510	20.773	15.912	11.932	—
23 54 09.28	−33 16 26.76	2313836153805786624	23540928−3316266	43.08 ± 0.19	−307.43	−410.25	17.579	20.736	15.980	11.884	—
23 54 41.31	−61 35 10.30	6487693790194944128	23544129−6135103	53.38 ± 0.03	278.76	−180.53	11.949	13.385	10.787	8.350	—
23 54 46.30	−21 46 28.24	2341178362288721536	23544630−2146282	42.68 ± 0.05	−42.00	127.22	10.087	11.062	9.160	7.117	—

Table 2: List of M dwarf systems within 25 pc drawn from *Gaia* DR2, as described in §2.3.

These systems have not been vetted to distinguish single stars from multiples, but in cases

where a system was resolved in *Gaia* but not 2MASS, a “J” flag is listed in column 12.

23 54 50.21	−09 57 01.13	2434874482600313728	23545023−0957011	41.04 ± 0.30	−51.12	−190.59	11.143	12.454	10.055	7.690	—
23 55 39.78	−06 08 33.35	2442996678074668288	23553981−0608327	56.14 ± 0.10	−479.08	−379.00	10.137	11.402	9.061	6.715	—
23 55 55.15	−13 21 23.92	2421043416597513856	23555512−1321238	43.01 ± 0.09	313.92	20.01	12.088	13.600	10.895	8.431	—
23 56 09.27	−13 58 17.58	2419457405433453696	23560928−1358174	41.29 ± 0.10	324.02	62.33	14.370	16.207	13.082	10.403	—
23 56 10.82	−34 26 04.59	2312952902371420800	23561081−3426044	53.01 ± 0.18	83.17	−312.28	17.480	20.629	15.873	11.965	—
23 56 40.87	−14 52 30.37	2419154936657147008	23564084−1452303	41.02 ± 0.09	220.76	71.46	13.225	15.033	11.938	9.110	—
23 57 19.36	−12 58 40.73	2421080250237097216	23571934−1258406	50.86 ± 0.28	208.31	24.70	11.841	13.272	10.688	8.234	—
23 57 44.15	+23 18 16.61	2848303052351577344	23574410+2318169	74.06 ± 1.03	1010.89	−1029.80	10.550	11.999	9.394	7.060	—
23 57 45.18	+19 46 11.14	2822328189657389824	23574516+1946112	48.99 ± 0.09	128.51	−486.55	11.844	13.349	10.668	8.161	—
23 58 32.66	+07 39 30.12	2746709861572970624	23583264+0739304	60.85 ± 0.25	77.66	−319.82	10.631	12.030	9.491	7.063	—
23 58 42.88	−62 45 42.43	6487483783474213632	23584285−6245423	50.27 ± 0.06	590.65	83.56	14.903	17.195	13.519	10.515	—
23 59 08.37	+23 38 31.03	2848408772970345600	23590836+2338311	43.32 ± 0.26	173.36	−366.08	18.267	21.015	16.659	12.296	—
23 59 38.76	−73 09 18.86	6379958624382356608	23593875−7309187	42.20 ± 0.04	313.20	162.14	11.207	12.474	10.121	7.833	—
23 59 44.77	−44 05 00.33	6532612963356913408	23594483−4404599	58.27 ± 0.53	11.00	272.04	11.644	13.098	10.470	8.043	—
23 59 51.37	−34 06 42.42	2313022171603701888	23595135−3406422	63.65 ± 0.09	698.30	−643.67	11.501	13.087	10.296	7.748	—

Table 3: Systems targeted for the M dwarf speckle interferometry program at SOAR. The WDS code (column 3) is the name each system would have in the Washington Double Star Catalog (Mason et al. 2001) if it were included there. The subsets justifying each target’s inclusion are marked in columns 8–10, and are discussed in §4.1.1, §4.1.2, and §4.1.3.

R.A. J2000.0	Decl. J2000.0	WDS, Discov.	Name	π (mas), ref.	V (mag), ref.	$V - K$ (mag)	0.9m PB	Lit. mult.	DR2 sus.	SOAR res.	Orbit ref.
(1)	(2)	(3)	(4)	(5)	(6)	(7)	(8)	(9)	(10)	(11)	(12)
00 06 39.24	−07 05 35.9	00067−0706 JNN 11	2MA0006-0705AB	46.960 ± 0.403 EDR3	14.72 APdr9	5.76		✓	✓	N	
00 08 53.92	+20 50 25.6	00089+2050 BEU 1	G131-026AB	55.256 ± 0.761 DR2	13.52 Rie14	5.51	✓	✓	✓	Y	Vri22
00 09 45.04	−42 01 39.3	00098−4202	LEHPM1-0255AB	60.889 ± 0.350 EDR3	13.62 Win15	5.40			✓	Y	
00 13 46.60	−04 57 37.2	00138−0458	LHS1042	42.627 ± 0.219 EDR3	17.98 estim	7.50			✓	N	
00 15 27.99	−16 08 01.8	00155−1608 HEI 299	GJ1005AB	169.522 ± 0.969 Vri20	11.48 Win15	5.09	✓	✓	✓	Y	Ben16
00 15 58.07	−16 36 57.6	00160−1637 BWL 2	2MA0015-1636AB	56.096 ± 0.093 EDR3	13.20 Win19	5.29		✓	✓	Y	Vri22
00 16 01.97	−48 15 39.1	00160−4816 TOK 808	L290-072AB	40.672 ± 0.525 EDR3	11.55 Koe10	4.44		✓	✓	Y	
00 16 14.63	+19 51 37.5	00162+1952	GJ1006AC	65.108 ± 0.041 EDR3	12.26 Wei96	5.17		✓	✓	Y	
00 21 37.26	−46 05 33.4	00216−4606	L290-028	51.569 ± 0.045 EDR3	12.24 Koe10	4.79			✓	N	
00 24 44.10	−27 08 24.0	00247−2653 LEI 1BC	GJ2005BC	129.317 ± 0.126 EDR3	15.28 Win15	7.04	✓	✓	✓	Y	Man19
00 24 44.19	−27 08 24.2	00247−2653 LEI 1AB	GJ2005AB	129.317 ± 0.126 EDR3	15.28 Win15	7.04	✓	✓	✓	Y	Koe12
00 25 04.31	−36 46 17.9	00251−3646	LTT00220AB	49.871 ± 0.110	12.48	4.65		✓	✓	Y	

Table 3: Systems targeted for the M dwarf speckle interferometry program at SOAR. The WDS code (column 3) is the name each system would have in the Washington Double Star Catalog (Mason et al. 2001) if it were included there. The subsets justifying each target’s inclusion are marked in columns 8–10, and are discussed in §4.1.1, §4.1.2, and §4.1.3.

					BRG 2			EDR3	Win15					
00 27 55.99	+22 19 32.8	00279+2220	LP349-025AB	70.781 ± 0.427		18.04	8.47	✓	✓	✓	Y		Dup10b	
		FRV 1		EDR3		Win17								
00 32 53.14	−04 34 07.0	00329−0434	GIC0050AB	52.853 ± 0.100		13.97	5.62	✓	✓	✓	Y			
		JNN 12AB		EDR3		Win15								
00 32 53.14	−04 34 07.0	00329−0434	GIC0050AC	52.853 ± 0.100		13.97	5.62	✓	✓	✓	Y			
		JNN 12AC		EDR3		Win15								
00 43 26.00	−41 17 34.0	00434−4118	LHS1134	97.661 ± 0.032		13.00	5.29	✓			N			
				EDR3		Win15								
00 48 13.33	−05 08 07.7	00482−0508	LTT00453	40.227 ± 0.030		12.03	4.10				✓	N		
				EDR3		Win15								
00 58 27.94	−27 51 25.4	00585−2751	GJ0046	84.979 ± 0.462		11.77	4.88				✓	N		
				EDR3		Bes90								
01 00 56.37	−04 26 56.6	01009−0427	GJ1025	80.788 ± 0.039		13.35	5.13	✓			N			
				EDR3		Jao05								
01 10 22.88	−67 26 41.9	01104−6727	GJ0054AB	121.449 ± 1.193		9.82	4.69	✓	✓	✓	Y		Ben16	
		GKI 3		DR2		Hen06								
01 11 25.42	+15 26 21.5	01114+1526	LP467-016AB	45.79 ± 1.78		14.46	6.25		✓	✓	Y			
		BEU 2		Rie14		Rie14								
01 13 16.43	−54 29 13.8	01133−5429	DEN0113-5429	56.553 ± 0.021		14.16	5.48	✓			N			
				EDR3		Win15								
01 22 10.33	+22 09 02.7	01222+2209	G034-023AB	85.68 ± 1.71		13.03	5.49		✓	✓	Y			
		CRC 44		Vri20		*								
01 28 39.51	−14 58 04.7	01287−1458	SCR0128-1458AB	74.896 ± 0.233		13.60	5.40	✓	✓	✓	Y			
				EDR3		Win19								
01 39 01.38	−17 57 02.4	01388−1758	GJ0065AB	367.712 ± 0.742		12.06	6.72	✓	✓	✓	Y		Ker16	
		LDS 838		EDR3		Bes91								

Table 3: Systems targeted for the M dwarf speckle interferometry program at SOAR. The WDS code (column 3) is the name each system would have in the Washington Double Star Catalog (Mason et al. 2001) if it were included there. The subsets justifying each target’s inclusion are marked in columns 8–10, and are discussed in §4.1.1, §4.1.2, and §4.1.3.

01 39 21.72	−39 36 09.0	01394−3936	LP991-084	114.604 ± 0.040	14.48	6.21	✓			N	
				EDR3	Win15						
01 46 36.84	−08 38 57.6	01466−0839	L870-044AB	39.103 ± 1.046	12.99	5.00	✓	✓	✓	Y	
		JOD 3		DR2	Wei99						
01 47 42.50	−48 36 05.3	01477−4836	LEHPM1-1882AB	64.088 ± 0.194	12.42	4.97	✓	✓	✓	Y	
				EDR3	Win15						
01 51 04.10	−06 07 05.0	01511−0607	LHS1302	94.711 ± 0.049	14.49	5.94	✓			N	
				EDR3	Hen06						
01 53 37.02	−66 53 33.7	01536−6654	L088-043AB	81.82 ± 3.21	11.68	4.69			✓	Y	
				Vri20	Win15						
01 59 12.60	+03 31 11.4	01592+0330	GJ1041BC	41.867 ± 0.023	12.32	5.20		✓		N	
				EDR3	Win19						
02 05 04.88	−17 36 52.8	02051−1737	GJ0084AB	107.300 ± 0.231	10.19	4.53		✓		Y	Man19
		BEU 3		EDR3	Bes90						
02 19 10.08	−36 46 41.2	02192−3647	GJ1046AB	65.585 ± 0.091	11.58	4.55		✓	✓	N	
				EDR3	Win15						
02 27 30.53	−19 07 40.8	02275−1908	LP770-020AB	51.874 ± 0.321	13.22	4.85			✓	Y	
				EDR3	APdr9						
02 27 45.86	+04 25 55.7	02278+0426	GJ0098AB	58.33 ± 1.08	8.67	3.56		✓	✓	Y	And07
		A 2329		HIP07	Koe10						
02 34 21.19	−53 05 36.8	02344−5306	L225-057AB	50.086 ± 0.758	12.53	5.22		✓	✓	Y	
				DR2	Win15						
02 36 32.46	−59 28 05.5	02365−5928	APM0018	99.523 ± 0.032	14.47	6.13	✓			N	
				EDR3	Hen06						
02 45 14.32	−43 44 10.6	02452−4344	LP993-115BC	90.177 ± 0.025	12.69	5.49	✓	✓	✓	Y	Vri22
		BRG 15Aa,Ab		EDR3	Rie14						
02 53 00.89	+16 52 52.6	02530+1653	TEE0253+1652	260.988 ± 0.093	15.14	7.55			✓	N	

Table 3: Systems targeted for the M dwarf speckle interferometry program at SOAR. The WDS code (column 3) is the name each system would have in the Washington Double Star Catalog (Mason et al. 2001) if it were included there. The subsets justifying each target’s inclusion are marked in columns 8–10, and are discussed in §4.1.1, §4.1.2, and §4.1.3.

						EDR3	Die14						
03 01 51.08	−16 35 31.1	03019−1633	LP771-095BC			145.692 ± 0.024	11.37	5.08	✓	✓	✓	Y	Win19
		RS292BC				EDR3	Hen06						
03 01 51.39	−16 35 36.0	03019−1633	LP771-095A			145.692 ± 0.024	11.22	4.72	✓			N	
						EDR3	Hen06						
03 07 55.75	−28 13 11.0	03079−2813	GJ1054AC			51.009 ± 0.019	10.24	3.87		✓		N	
						EDR3	Wei93						
03 14 18.16	−23 09 29.8	03143−2309	LP831-045AB			62.901 ± 0.050	12.58	4.95	✓	✓		N	
						EDR3	Win15						
03 14 51.31	−62 41 41.8	03149−6242	UPM0314-6241AB			37.880 ± 0.050	12.39	4.75		✓	✓	Y	
		DAM1299				EDR3	APdr9						
03 19 29.16	−30 59 44.1	03195−3060	LTT01578AB			39.022 ± 0.476	14.00	5.22			✓	Y	
						EDR3	Rei02						
03 34 39.63	−04 50 33.4	03347−0451	LHS1561AB			37.820 ± 0.611	13.07	5.14		✓	✓	Y	
						EDR3	Rie10						
03 35 59.70	−44 30 45.7	03360−4431	GJ1061			272.162 ± 0.032	13.09	6.48	✓			N	
						EDR3	Lur14						
03 42 29.43	+12 31 33.6	03425+1232	LHS0178			36.712 ± 0.184	12.87	3.99			✓	N	
						EDR3	Jao17						
03 43 22.06	−09 33 50.7	03434−0934	LHS1582AB			49.647 ± 0.254	14.69	5.84	✓	✓	✓	N	Vri20
						DR2	Lur14						
03 52 41.75	+17 01 04.2	03527+1701	LHS1610AB			103.501 ± 0.088	13.85	5.80	✓	✓	✓	N	
						EDR3	Hen18						
03 54 20.09	−14 37 38.6	03543−1438	DEN0354-1437AB			56.205 ± 0.663	18.01	7.68			✓	Y	
						EDR3	*						
04 07 20.48	−24 29 13.6	04073−2429	LHS1630AB			54.179 ± 0.048	12.38	4.94	✓	✓	✓	Y	
		BEU 5				EDR3	Rie10						

Table 3: Systems targeted for the M dwarf speckle interferometry program at SOAR. The WDS code (column 3) is the name each system would have in the Washington Double Star Catalog (Mason et al. 2001) if it were included there. The subsets justifying each target’s inclusion are marked in columns 8–10, and are discussed in §4.1.1, §4.1.2, and §4.1.3.

04 08 55.60	−31 28 53.9	04089−3129 NSN 207	LP889-037AB	55.326 ± 0.023 EDR3	14.56 Win15	5.74	✓		Y	
04 09 15.67	−53 22 25.3	04093−5322	GJ0163	66.071 ± 0.012 EDR3	11.84 Bes90	4.70	✓		N	
04 10 28.12	−53 36 08.1	04105−5336	GJ1068	140.696 ± 0.021 EDR3	13.60 Win15	5.70	✓		N	
04 15 49.05	−46 02 23.6	04158−4602	UPM0415-4602AB	51.970 ± 0.092 EDR3	11.85 APdr9	4.56		✓	Y	
04 16 41.68	−12 33 23.1	04167−1233 HDS 544	GJ2033AB	45.931 ± 0.286 EDR3	11.28 Win19	4.55	✓	✓	Y	
04 17 34.58	−48 34 39.1	04176−4835	LEHPM1-3719	60.517 ± 0.182 EDR3	15.91 *	6.57		✓	N	
04 20 12.55	−70 05 58.6	04202−7006	SCR0420-7005	60.571 ± 0.042 EDR3	17.09 Win11	6.84	✓		N	
04 24 11.57	−23 56 36.3	04242−2357	2MA0424-2356	64.870 ± 0.025 EDR3	12.12 APdr9	4.65		✓	N	
04 29 18.47	−31 23 56.8	04293−3124 SIG 4	2MA0429-3123AB	58.794 ± 0.142 EDR3	17.39 Hos15	7.62	✓	✓	Y	
04 31 09.04	−13 30 52.5	04312−1331 HDS 586	LP715-051AB	53.479 ± 0.019 EDR3	11.54 Koe10	4.49	✓		N	
04 32 42.63	−39 47 12.1	04327−3947	LHS1678	50.340 ± 0.015 EDR3	12.48 Win15	4.22	✓		N	
04 35 16.15	−16 06 57.3	04353−1607	LP775-031AB	94.305 ± 0.210 EDR3	17.70 Die14	8.35	✓	✓	N	
04 40 29.27	−09 11 46.4	04406−0912 WOR 17	HIP021765AB	49.429 ± 0.043 EDR3	10.26 Koe10	3.99	✓		Y	Tok20b
04 46 51.78	−11 16 47.7	04469−1117	2MA0446-1116AB	52.772 ± 0.032	12.25	4.96	✓		Y	

Table 3: Systems targeted for the M dwarf speckle interferometry program at SOAR. The WDS code (column 3) is the name each system would have in the Washington Double Star Catalog (Mason et al. 2001) if it were included there. The subsets justifying each target’s inclusion are marked in columns 8–10, and are discussed in §4.1.1, §4.1.2, and §4.1.3.

		JNN 28		EDR3	Rie18							
04 48 47.39	+10 03 02.7	04488+1003	LEP0448+1003AB	57.896 ± 0.397	12.09	4.78	✓	✓	Y			
				EDR3	APdr9							
04 52 04.02	−10 58 22.0	04521−1058	LP716-010AB	59.113 ± 0.495	16.24	6.63			✓	Y		
				EDR3	Win15							
04 52 24.41	−16 49 21.9	04524−1649	LP776-025	63.132 ± 0.025	11.63	4.74	✓			N		
				EDR3	Win15							
05 01 58.80	+09 58 59.0	05020+0959	LP476-207AB	41.039 ± 0.030	11.53	5.16	✓	✓		Y		
		HDS 654		EDR3	Rie14							
05 02 28.47	−21 15 24.0	05025−2115	GJ0185AB	119.574 ± 0.042	8.28	3.68		✓	✓	Y	Tok15c	
		DON 91AB		EDR3	Win15							
05 06 49.47	−21 35 03.3	05069−2135	BD-21-01074BC	50.523 ± 0.065	11.08	4.97	✓	✓	✓	Y	Tok20b	
		DON 93BC		EDR3	Rie14							
05 08 35.04	−18 10 19.4	05086−1810	GJ0190AB	108.325 ± 0.098	10.31	5.00	✓	✓		Y	Tok17b	
		WSI 72		EDR3	Win15							
05 10 09.67	−72 36 27.9	05102−7236	HD271076AB	45.91 ± 2.79	11.36	4.31		✓	✓	Y	Tok20a	
		WSI 122		Rie18	Rie18							
05 17 22.91	−35 21 54.6	05174−3522	L449-001AB	85.452 ± 0.290	11.69	5.13	✓	✓	✓	Y		
		TSN 1		EDR3	Rie14							
05 25 41.67	−09 09 12.5	05257−0909	LP717-036AB	46.197 ± 0.137	12.59	4.97		✓	✓	Y		
		DAE 2		EDR3	Win15							
05 28 14.60	+02 58 14.2	05282+0258	GJ1080AB	47.507 ± 0.057	12.81	4.59		✓	✓	N		
				EDR3	Wei96							
05 32 14.66	+09 49 14.9	05322+0949	GJ0206AB	77.136 ± 0.027	11.55	4.99		✓		N		
				EDR3	Bes90							
05 33 28.04	−42 57 20.6	05335−4257	SCR0533-4257AB	95.932 ± 0.246	12.58	5.46	✓	✓	✓	Y	Vri22	
		SYU 7		EDR3	Hos15							

Table 3: Systems targeted for the M dwarf speckle interferometry program at SOAR. The WDS code (column 3) is the name each system would have in the Washington Double Star Catalog (Mason et al. 2001) if it were included there. The subsets justifying each target’s inclusion are marked in columns 8–10, and are discussed in §4.1.1, §4.1.2, and §4.1.3.

05 33 44.80	+01 56 43.5	05337+0157	LTT11675	63.360 ± 0.048	11.53	4.67		✓	N	
				EDR3	Bes90					
05 40 25.73	+24 48 07.9	05404+2448	GJ1083AB	97.60 ± 2.80	14.87	6.83	✓	✓	Y	
		WNO 45		Dit14	Wei84					
05 44 57.04	−21 36 55.8	05450−2137	LP837-019AB	43.416 ± 0.165	12.31	4.49		✓	Y	
				EDR3	Rei02					
05 53 14.08	+24 15 31.1	05532+2416	GJ0220AB	47.731 ± 0.512	10.84	4.21	✓	✓	N	
				EDR3	Wei96					
06 04 52.15	−34 33 35.8	06049−3434	APCOL	115.398 ± 0.030	12.96	6.09	✓		N	
				EDR3	Rie11					
06 10 52.90	−43 24 20.1	06109−4324	GJ1088	89.371 ± 0.021	12.28	4.97	✓		N	
				EDR3	Rie10					
06 11 14.65	−00 35 37.8	06112−0036	UPM0611-3433	46.022 ± 0.220	16.04	6.35		✓	N	
				EDR3	estim					
06 24 08.52	−26 55 23.6	06241−2655	UPM0624-2655AB	49.214 ± 0.856	11.51	4.61		✓	Y	
				DR2	APdr9					
06 24 10.12	−00 16 30.5	06242−0017	G106-045AB	45.614 ± 0.200	14.04	5.20		✓	Y	
				EDR3	APdr9					
06 29 23.39	−02 48 48.8	06293−0248	GJ0234AB	242.966 ± 0.883	11.12	5.63	✓	✓	✓	Y
		B 2601AB		DR2	Win15					Man19
06 30 46.47	−76 43 09.6	06308−7643	SCR0630-7643AB	112.658 ± 0.093	14.82	6.90	✓	✓	✓	Y
		HEN 4		EDR3	Win11					
06 31 31.04	−88 11 36.6	06315−8812	SCR0631-8811AB	63.31 ± 2.07	15.65	6.58			✓	Y
				Win17	Win11					
06 32 20.30	−09 43 29.0	06323−0943	UPM0632-0943AB	38.388 ± 0.413	14.48	5.50	✓		✓	Y
				EDR3	*					
06 35 29.85	−04 03 18.4	06354−0403	2MA0635-0403AB	79.164 ± 0.309	14.59	6.28		✓	✓	Y

Table 3: Systems targeted for the M dwarf speckle interferometry program at SOAR. The WDS code (column 3) is the name each system would have in the Washington Double Star Catalog (Mason et al. 2001) if it were included there. The subsets justifying each target’s inclusion are marked in columns 8–10, and are discussed in §4.1.1, §4.1.2, and §4.1.3.

				JNN 271		EDR3	APdr9				
06 36 18.28	−40 00 23.6	06363−4000	LP381-004AB		52.000 ± 0.188	10.59	3.80		✓	Y	
					EDR3	Koe10					
06 39 37.41	−21 01 33.2	06396−2102	LP780-032AB		65.308 ± 0.325	12.77	5.12		✓	Y	
					EDR3	Win15					
06 43 40.67	−26 24 41.0	06437−2625	LTT02631AB		58.141 ± 0.017	12.92	4.79	✓		N	
					EDR3	Win15					
06 52 18.04	−05 11 24.0	06523−0510	GJ0250BC		114.291 ± 0.022	10.09	4.37	✓		N	
		WSI 125Ba,Bb			EDR3	Wei96					
06 57 46.62	−44 17 28.2	06579−4417	GJ0257AB		124.357 ± 0.040	10.85	4.79	✓		Y	Zir03
		LPM 248			EDR3	Koe02					
06 59 40.78	−56 22 47.6	06597−5623	SCR0659-5622AB		41.0 ± 8.5	14.81	5.32		✓	Y	
					Win15	Win15					
07 02 50.33	−61 02 47.5	07028−6103	SCR0702-6102AB		57.024 ± 0.197	16.62	7.10	✓		Y	
					EDR3	Win17					
07 04 17.70	−10 30 31.6	07043−1031	GJ0263AB		63.551 ± 0.514	11.30	4.87	✓	✓	Y	Man19
		BEU 9			EDR3	Bes90					
07 09 37.66	−57 03 42.1	07096−5704	APM0089		58.556 ± 0.059	13.64	5.34	(✓)		Y	
					EDR3	Win15					
07 20 03.25	−08 46 49.9	07200−0847	WIS0720-0846AB		148.80 ± 1.08	18.54	9.07	✓	✓	✓	Bur15b
		BUG 17			Hen18	Hen18					
07 23 59.62	−80 15 18.0	07240−8015	SCR0723-8015AB		61.730 ± 0.126	17.45	7.01	✓	✓	N	
					EDR3	Win15					
07 27 24.50	+05 13 32.8	07274+0514	GJ0273AB		264.127 ± 0.041	9.88	5.02		✓	✓	N
		WDK 2			EDR3	Dav15					
07 28 13.10	−18 47 35.7	07282−1848	LHS1918AB		73.969 ± 0.526	13.69	5.52	✓	✓	✓	Y
					EDR3	Win21					

Table 3: Systems targeted for the M dwarf speckle interferometry program at SOAR. The WDS code (column 3) is the name each system would have in the Washington Double Star Catalog (Mason et al. 2001) if it were included there. The subsets justifying each target’s inclusion are marked in columns 8–10, and are discussed in §4.1.1, §4.1.2, and §4.1.3.

07 28 51.37	−30 14 48.5	07289−3015 HDS1054AB	GJ2060AB	64.140 ± 0.473 EDR3	9.92 Koe10	4.20	✓	✓	Y	Tok18c
07 33 26.82	−27 49 04.1	07334−2749	SCR0733-2749AB	44.2 ± 8.7 Win15	16.03 Win15	5.95		✓	Y	
07 36 25.12	+07 04 43.1	07364+0705 HEN 3	G089-032AB	117.59 ± 0.83 Hen18	13.25 Hen18	5.97	✓	✓	✓	Y Tok18c
07 40 11.80	−42 57 40.3	07402−4258	SCR0740-4257	125.303 ± 0.022 EDR3	13.81 Win11	6.04	✓		N	
07 54 54.73	−29 20 56.3	07549−2920 KUI 32	LHS1955AB	80.098 ± 0.144 EDR3	12.79 Rie10	5.44	✓	✓	✓	Y Mas18
07 57 32.53	−71 14 53.8	07575−7115	SCR0757-7114AB	44.342 ± 0.020 EDR3	12.45 Rie14	5.03	(✓)		N	
08 02 57.81	−83 30 07.5	08030−8330	GAI0802-8330AB	42.911 ± 0.277 EDR3	16.03 estim	6.32		✓	Y	
08 08 16.85	−73 01 40.2	08083−7302	LEP0808-7301AC	43.371 ± 0.498 EDR3	14.05 APdr9	5.06		✓	Y	
08 10 34.29	−13 48 51.1	08107−1348 JOD 4Ba,Bb	GJ0297.2BC	44.520 ± 0.049 EDR3	11.82 Wei99	4.40	✓	✓	Y	
08 11 57.56	+08 46 23.0	08120+0846	GJ0299	147.722 ± 0.095 EDR3	12.86 Dav15	5.20		✓	N	
08 13 08.46	−13 55 01.1	08132−1354 HU 115A	GJ0301AB	46.559 ± 0.444 EDR3	9.37 Koe10	3.55	✓	✓	Y	Izm19
08 15 11.20	−23 44 15.6	08152−2344	UPM0815-2344AB	101.041 ± 0.027 EDR3	12.36 Hen18	5.14	✓	✓	N	
08 20 13.37	+05 32 08.1	08202+0532	LEP0820+0532	44.508 ± 0.036 EDR3	11.91 APdr9	4.24		✓	N	
08 22 47.41	−57 26 52.9	08228−5727	LHS2005AB	77.632 ± 0.037	13.39	5.59	✓		Y	

Table 3: Systems targeted for the M dwarf speckle interferometry program at SOAR. The WDS code (column 3) is the name each system would have in the Washington Double Star Catalog (Mason et al. 2001) if it were included there. The subsets justifying each target’s inclusion are marked in columns 8–10, and are discussed in §4.1.1, §4.1.2, and §4.1.3.

			BRG 27Aa,Ab		EDR3		*						
08 27 11.83	−44 59 21.1		08272−4459	LHS2010AB	72.614 ± 0.048	11.86	4.99		✓				N
			JOD 5		EDR3	Rie10							
08 31 37.43	+19 23 49.7		08317+1924	GJ2069BD	60.249 ± 0.076	13.37	5.65	✓	✓	✓		Y	
			DEL 1Ba,Bb		EDR3	Hos15							
08 31 37.57	+19 23 39.4		08317+1924	GJ2069ACE	60.060 ± 0.036	11.93	5.33	✓	✓	✓		Y	Seg00
			BEU 12Aa,Ab		EDR3	Hos15							
08 37 20.42	−28 19 57.5		08373−2820	SCR0837-2819AB	43.663 ± 0.795	15.59	5.70				✓	Y	
					EDR3	Win15							
08 38 02.17	−58 55 58.4		08380−5856	SCR0838-5855AB	89.993 ± 0.236	17.19	7.92	✓	✓	✓		Y	
					EDR3	Win15							
08 38 33.74	−28 43 26.3		08386−2843	UPM0838-2843AB	73.316 ± 0.036	11.85	4.57				✓	Y	
					EDR3	APdr9							
08 42 44.53	+09 33 24.1		08427+0935	GJ0319AC	64.681 ± 0.112	9.63	3.80		✓	✓		Y	
			ST 8AB		EDR3	Koe10							
08 52 49.87	−66 08 47.4		08528−6609	SCR0852-6608AB	40.0 ± 7.6	16.41	6.02				✓	Y	
					Win15	Win15							
08 54 05.33	−13 07 30.7		08539−1308	GJ0326AB	64.936 ± 0.150	11.93	4.67		✓	✓		Y	
			ST 9AB		EDR3	Wei96							
08 54 31.99	−05 51 25.7		08545−0551	2MA0854-0551AB	45.572 ± 0.121	13.44	5.12				✓	Y	
					EDR3	*							
08 55 20.25	−23 52 14.6		08553−2352	LHS2071AB	64.077 ± 0.223	13.88	5.68	✓	✓	✓		Y	Rie10
					EDR3	Rie10							
08 57 04.68	+11 38 48.8		08571+1139	GJ0330AB	61.324 ± 0.105	10.57	4.08		✓	✓		Y	Tok19c
			HDS1296		EDR3	Bes90							
08 58 15.07	+19 45 48.2		08582+1945	GJ1116AB	194.144 ± 0.123	13.69	6.80		✓			Y	Tok20b
			LDS3836		EDR3	Win19							

Table 3: Systems targeted for the M dwarf speckle interferometry program at SOAR. The WDS code (column 3) is the name each system would have in the Washington Double Star Catalog (Mason et al. 2001) if it were included there. The subsets justifying each target’s inclusion are marked in columns 8–10, and are discussed in §4.1.1, §4.1.2, and §4.1.3.

08 58 56.32	+08 28 26.1	08589+0829 DEL 2	G041-014AB	146.97 ± 1.51 Hen18	10.92 Hen06	5.23	✓	✓	Y	
09 01 10.48	+01 56 35.2	09012+0157 CRC 57Aa,Ab	LTT12366AC	42.633 ± 0.349 EDR3	11.84 *	4.78	✓	✓	Y	
09 15 36.40	−10 35 47.2	09156−1036 MTG 2	LHS6167AB	103.54 ± 0.77 Hen18	13.82 Win15	6.09	✓	✓	✓	Y Mas18
09 29 03.78	−24 29 04.2	09291−2429	WT1637AB	56.66 ± 0.97 Win17	16.87 Win15	6.96			✓	Y
09 31 19.41	−13 29 18.9	09313−1329 KUI 41	GJ0352AB	99.88 ± 3.60 HIP07	10.08 Bes90	4.57	✓	✓	Y	Man19
09 31 22.32	−17 17 42.3	09314−1718	LP788-001AB	63.759 ± 0.692 EDR3	17.55 Win15	7.48	✓	✓	✓	N
09 36 57.83	−26 10 11.2	09370−2610 WSI 127AB	2MA0936-2610AB	55.352 ± 0.750 EDR3	13.12 Rie18	5.16	✓	✓	Y	Tok20b
09 42 46.34	−68 53 06.0	09428−6853	GJ1128	153.759 ± 0.025 EDR3	12.74 Lur14	5.70	✓			N
09 44 23.73	−73 58 38.3	09444−7359	WT0244AB	40.845 ± 0.245 EDR3	15.17 Rie10	5.79			✓	Y
09 44 54.19	−12 20 54.4	09449−1221	G161-071	76.051 ± 0.034 EDR3	13.76 Win15	6.16	✓			N
09 45 40.08	−39 02 26.7	09457−3902 HDS1409	LP462-119AB	50.593 ± 0.315 EDR3	12.11 Win19	4.59	✓	✓	Y	Tok18c
09 45 58.43	−32 53 30.0	09460−3254	WT2458	83.250 ± 0.037 EDR3	14.04 Win15	5.76	✓		✓	N,
09 50 40.54	−13 48 38.6	09507−1349	LP728-070AB	51.14 ± 1.86 Win17	12.71 Win15	4.99	✓	✓	Y	
09 53 11.78	−03 41 24.5	09532−0341	GJ0372AB	63.612 ± 0.074	10.55	4.42	✓			N

Table 3: Systems targeted for the M dwarf speckle interferometry program at SOAR. The WDS code (column 3) is the name each system would have in the Washington Double Star Catalog (Mason et al. 2001) if it were included there. The subsets justifying each target’s inclusion are marked in columns 8–10, and are discussed in §4.1.1, §4.1.2, and §4.1.3.

				EDR3	Bes90								
09 55 23.86	−27 15 40.7	09554−2716	LP847-048	91.737 ± 0.039	12.08	4.94			✓		N		
				EDR3	Win15								
09 58 34.32	−46 25 30.4	09586−4626	GJ0375AB	64.719 ± 0.020	11.27	5.01	✓	✓			N		
				EDR3	Win15								
10 06 52.10	−12 46 54.4	10069−1247	2MA1006-1246AB	46.8 ± 4.9	14.51	5.61			✓		Y		
				Fin18	*								
10 12 04.67	−02 41 05.2	10121−0241	GJ0381AB	86.659 ± 0.701	10.64	4.45		✓	✓	Y		Tok18a	
		DEL 3		DR2	Bes90								
10 14 51.77	−47 09 24.2	10149−4709	LHS0281	79.321 ± 0.018	13.49	5.17	✓				N		
				EDR3	Jao05								
10 17 26.90	−53 54 26.5	10174−5354	TWA022AB	50.521 ± 0.199	14.05	6.36		✓	✓	Y		Tok19c	
		CVN 16Aa,Ab		EDR3	Win19								
10 19 53.71	−41 48 59.8	10199−4149	L392-039BC	43.402 ± 0.017	13.17	4.88			✓	Y			
				EDR3	Win17								
10 36 44.84	+15 21 39.9	10367+1522	2MA1036+1521AB	49.979 ± 0.089	13.33	5.43		✓	✓	Y		Cal17	
		DAE 3AB		EDR3	Win19								
10 36 44.92	+15 21 38.0	10367+1522	2MA1036+1521BC	49.979 ± 0.089	13.33	5.43		✓	✓	Y		Cal17	
		DAE 3BC		EDR3	Win19								
10 39 44.35	−37 55 13.5	10397−3755	LP465-084AB	71.51 ± 2.48	11.08	4.70		✓	✓	Y		Tok20b	
		HDS1523		HIP07	Win15								
10 41 09.34	−36 53 43.5	10412−3654	GJ1135AB	62.624 ± 0.145	9.94	3.95		✓		Y			
		HDS1528		EDR3	Koe10								
10 42 41.36	−24 16 04.1	10427−2416	LP848-050AB	96.149 ± 0.469	16.53	7.19	✓	✓	✓	N			
				DR2	Win17								
10 43 02.86	−09 12 40.9	10430−0913	WT1827AB	82.001 ± 0.286	15.11	7.38	✓	✓	✓	Y			
		WSI 112		EDR3	Win15								

Table 3: Systems targeted for the M dwarf speckle interferometry program at SOAR. The WDS code (column 3) is the name each system would have in the Washington Double Star Catalog (Mason et al. 2001) if it were included there. The subsets justifying each target’s inclusion are marked in columns 8–10, and are discussed in §4.1.1, §4.1.2, and §4.1.3.

10 48 12.62	−11 20 09.6	10482−1120	LHS0292	219.330 ± 0.060	15.78	7.85	✓			N
				EDR3	Die14					
10 48 14.57	−39 56 06.8	10482−3956	DEN1048-3956	247.216 ± 0.051	17.37	8.92	✓		✓	N
				EDR3	Lur14					
10 54 41.96	−07 18 33.4	10547−0719	LTT04004AB	48.807 ± 0.201	13.29	5.32	✓	✓	✓	Y
		CRC 62		EDR3	Win15					
10 55 15.31	−73 56 09.0	10553−7356	WIS1055-7356	77.499 ± 0.477	17.54	7.87			✓	N
				EDR3	estim					
10 56 28.83	+07 00 53.3	10565+0701	GJ0406	415.179 ± 0.068	13.58	7.50	✓		✓	N
				EDR3	Die14					
10 58 05.31	−55 25 17.6	10581−5525	GAI1058-5525AB	50.421 ± 0.100	15.72	6.14			✓	Y
				EDR3	estim					
11 30 41.83	−08 05 43.0	11307−0806	LP672-042	74.205 ± 0.025	12.06	4.91	✓			NA
				EDR3	Win15					
11 31 08.39	−14 57 21.3	11311−1457	LHS0306	86.900 ± 0.048	14.19	5.69	✓		✓	N
				EDR3	Win15					
11 35 26.95	−32 32 23.9	11354−3232	GJ0433	110.171 ± 0.020	9.84	4.22	✓			N
				EDR3	Bes90					
12 06 58.53	−35 00 52.0	12070−3501	SCR1206-3500AB	40.757 ± 0.165	14.67	5.54			✓	Y
				EDR3	Win11					
12 10 42.16	−22 13 06.0	12107−2213	2MA1210-2213BC	52.834 ± 0.029	13.06	4.54			✓	Y
			EDR3	APdr9					
12 14 16.56	+00 37 26.4	12143+0037	GJ1154AB	123.643 ± 0.045	13.66	6.12		✓		N
				EDR3	Dav15					
12 20 05.10	−18 12 59.5	12201−1813	LP794-053AB	39.641 ± 0.256	15.60	5.98			✓	Y
				EDR3	*					
12 20 33.68	−82 25 57.5	12206−8226	NLTT30359AB	81.749 ± 0.608	11.96	5.12	✓	✓	✓	Y

Table 3: Systems targeted for the M dwarf speckle interferometry program at SOAR. The WDS code (column 3) is the name each system would have in the Washington Double Star Catalog (Mason et al. 2001) if it were included there. The subsets justifying each target’s inclusion are marked in columns 8–10, and are discussed in §4.1.1, §4.1.2, and §4.1.3.

								DR2	Win15						
12 28 57.60	+08 25 31.1	12290+0826	GJ0469AB	72.266 ± 0.696	12.05	5.09	✓	✓	✓	Y	Ben16				
				WSI 113	EDR3	Hos15									
12 29 34.54	−55 59 37.0	12296−5560	GJ1158	76.353 ± 0.022	13.26	5.19	✓		✓	N					
				EDR3	Jao11										
12 30 01.73	−34 11 24.1	12300−3411	SCR1230-3411AB	52.556 ± 0.263	14.16	5.73	✓	✓	✓	Y	Win17				
				EDR3	Win11										
12 33 17.36	+09 01 15.8	12335+0901	GJ0473AB	231.119 ± 0.512	12.47	6.43	✓	✓	✓	Y	Sca19				
				REU 1	EDR3	Ben16									
12 33 33.08	−48 26 11.4	12336−4826	L327-121AB	48.090 ± 0.781	12.07	4.93	✓	✓	✓	Y					
				DR2	Win15										
12 35 58.40	−45 56 20.5	12360−4556	GJ0477AB	48.210 ± 0.596	11.12	4.28		✓	✓	N					
				DR2	Bes90										
12 41 08.05	−38 43 12.9	12411−3843	SIP1241-3843AB	42.845 ± 0.275	17.65	7.20			✓	Y					
				EDR3	estim										
12 43 59.05	−16 14 35.5	12440−1615	LP796-001AB	51.3 ± 3.4	14.75	5.85			✓	Y					
				Fin18	*										
12 50 52.65	−21 21 13.6	12509−2121	LEHPM2-0174	56.788 ± 0.188	18.36	8.23	✓		✓	N					
				EDR3	Die14										
12 56 02.15	−12 57 21.7	12560−1257	LP736-015AB	47.273 ± 0.473	17.76	7.72		✓	✓	Y					
				SJM 1Aa,Ab	EDR3	*									
13 00 46.56	+12 22 32.7	13008+1223	GJ0494AB	86.901 ± 0.117	9.73	4.15		✓		N	Hei94				
				BEU 16AB	EDR3	Bes90									
13 13 09.32	−41 30 39.8	13132−4131	ER2	84.314 ± 0.447	12.90	5.49	✓		✓	Y					
				EDR3	Win15										
13 14 20.38	+13 20 01.0	13143+1320	NLTT33370AB	61.0 ± 2.8	15.88	7.09		✓	✓	Y	Dup16				
				LAW 2	Lep09	Win19									

Table 3: Systems targeted for the M dwarf speckle interferometry program at SOAR. The WDS code (column 3) is the name each system would have in the Washington Double Star Catalog (Mason et al. 2001) if it were included there. The subsets justifying each target’s inclusion are marked in columns 8–10, and are discussed in §4.1.1, §4.1.2, and §4.1.3.

13 16 45.41	−12 20 20.4	13168−1220	LP737-014AB	44.797 ± 0.554 EDR3	13.65 APdr9	5.01		✓	Y
13 23 38.03	−25 54 45.1	13236−2555	LHS2729	71.119 ± 0.039 EDR3	12.89 Rie14	5.11	✓		N
13 24 46.48	−05 04 19.9	13248−0504	G014-052AB	40.562 ± 0.323 EDR3	13.88 Win15	5.32		✓	Y
13 28 21.08	−02 21 37.1	13283−0222	GJ0512A	75.878 ± 0.057 EDR3	11.35 Win15	4.74		✓	N
13 28 21.50	−02 21 31.7	13283−0222	GJ0512B	75.595 ± 0.440 EDR3	13.69 Bes90	5.39		✓	N
13 42 09.83	−16 00 23.3	13422−1600 WSI 114	LHS2783AB	49.458 ± 0.073 EDR3	13.42 Win15	5.33	✓	✓	Y
13 58 05.41	−39 37 55.1	13581−3938	SSS1358-3938	86.541 ± 0.026 EDR3	14.04 Win15	5.09	✓		N
14 04 08.18	−66 14 38.1	14041−6615	NLTT36064AB	61.860 ± 0.461 EDR3	11.59 Win15	4.67		✓	Y
14 11 59.91	−41 32 22.1	14120−4132 MTG 3	WT0460AB	109.732 ± 0.232 EDR3	15.65 Win15	7.03	✓	✓	Y
14 12 10.97	−00 35 04.5	14121−0035 WSI 129Aa,Ab	LHS2875AB	37.030 ± 0.166 EDR3	13.04 Bes91	4.49		✓	Y
14 15 32.55	+04 39 31.4	14155+0440	GJ1182AB	72.004 ± 0.367 EDR3	14.30 Wei96	5.68	✓	✓	N
14 20 36.83	−75 16 05.7	14206−7516	SCR1420-7516	40.832 ± 0.186 EDR3	13.78 Win11	5.15		✓	Y
14 29 42.95	−62 40 46.1	14396−6050	PROXIMA	768.067 ± 0.050 EDR3	11.13 Lur14	6.75		✓	N
14 34 04.88	−18 24 10.7	14341−1824	LHS5273AB	36.770 ± 0.316	14.35	5.64		✓	Y

Table 3: Systems targeted for the M dwarf speckle interferometry program at SOAR. The WDS code (column 3) is the name each system would have in the Washington Double Star Catalog (Mason et al. 2001) if it were included there. The subsets justifying each target’s inclusion are marked in columns 8–10, and are discussed in §4.1.1, §4.1.2, and §4.1.3.

								EDR3	*					
14 34	16.81	−12 31	10.4	14343−1231	GJ0555		159.923 ± 0.055	11.34	5.40	✓			N	
								EDR3	Win15					
14 44	06.56	−34 26	47.1	14441−3427	SCR1444-3426		65.044 ± 0.032	14.17	5.29	✓			N	
								EDR3	Win11					
14 53	51.40	+23 33	21.0	14540+2335	GJ0568AB		86.276 ± 0.186	11.68	5.11		✓		Y	Mas18
								REU 2	EDR3	Wei96				
14 54	10.43	−20 41	28.4	14542−2042	LP801-025AB		43.190 ± 0.335	15.03	5.69			✓	Y	
								EDR3	*					
14 54	29.42	+16 06	08.6	14545+1606	GJ0569BC		100.524 ± 0.021	17.16	11.39		✓	✓	N	Kon10
								MEL 2Ba,Bb	EDR3	estim				
14 57	26.53	−21 24	41.6	14575−2125	GJ0570BC		169.884 ± 0.065	8.07	4.27		✓		Y	For99
								H N 28Ba,Bb	EDR3	Koe10				
15 09	31.95	−15 46	47.8	15095−1547	GAI1509-1546AB		31.132 ± 0.063	12.21	4.14			✓	Y	
								EDR3	APdr9					
15 15	43.71	−07 25	21.2	15157−0725	G151-037AB		57.144 ± 0.123	12.93	5.22			✓	Y	
								EDR3	Win17					
15 19	11.73	−12 45	06.3	15192−1245	LHS3056AB		46.440 ± 0.318	12.87	5.29		✓	✓	Y	
								CRC 72	EDR3	Win15				
15 19	26.83	−07 43	20.2	15194−0743	GJ0581		158.718 ± 0.030	10.56	4.72			✓	N	
								EDR3	Lur14					
15 24	48.49	−49 29	47.5	15248−4930	L264-018		45.767 ± 0.290	11.64	4.34		✓	✓	N	
								EDR3	APdr9					
15 30	52.05	−68 01	17.8	15309−6801	NLTT40317AB		50.482 ± 0.194	13.52	5.29			✓	Y	
								EDR3	Win15					
15 31	54.16	+28 51	09.6	15319+2851	LHS3080AB		37.638 ± 0.686	14.32	5.50	✓	✓	✓	Y	
								EDR3	Rie10					

Table 3: Systems targeted for the M dwarf speckle interferometry program at SOAR. The WDS code (column 3) is the name each system would have in the Washington Double Star Catalog (Mason et al. 2001) if it were included there. The subsets justifying each target’s inclusion are marked in columns 8–10, and are discussed in §4.1.1, §4.1.2, and §4.1.3.

15 42 06.54	−19 28 18.3	15421–1928	GJ0595AB	103.180 ± 0.316	11.84	4.67	✓	✓	✓	N	Hen18
				EDR3	Win15						
15 45 41.61	−43 30 28.4	15457–4330	LTT06288AB	47.932 ± 0.140	13.06	4.98	✓	✓	✓	Y	Vri20
				EDR3	Win15						
15 46 41.69	−55 34 47.5	15467–5535	SCR1546-5534AB	119.096 ± 0.703	17.58	8.47	✓	✓	✓	Y	
				DR2	Win15						
15 47 24.55	−10 53 47.3	15474–1054	LHS3117AB	62.516 ± 0.277	11.28	4.54		✓	✓	Y	
				DR2	Koe10						
15 47 29.81	−27 55 12.1	15475–2755	UPM1547-2755AB	40.192 ± 0.030	13.08	4.61		✓		Y	
		GAT 18AB		EDR3	APdr9						
15 47 34.90	−27 53 42.9	15476–2754	UPM1547-2755CD	40.673 ± 0.395	16.71	6.36			✓	Y	
				EDR3	estim						
15 57 50.42	−51 31 49.0	15578–5132	GAI1557-5131AB	59.719 ± 0.271	16.93	7.26			✓	Y	
				DR2	estim						
16 01 56.10	−33 57 11.9	16019–3357	LP553-044AB	66.086 ± 0.234	12.17	5.24			✓	Y	
				EDR3	Rei04						
16 16 58.94	−31 36 37.6	16170–3137	GAI1616-3136AB	54.544 ± 0.301	14.04	5.56			✓	Y	
				DR2	APdr9						
16 20 03.21	−37 31 48.6	16202–3734	GJ0618B	117.679 ± 0.107	14.15	6.38			✓	NA	
				EDR3	Bes90						
16 20 03.51	−37 31 44.4	16202–3734	GJ0618A	117.472 ± 0.029	10.59	4.64		✓		N	
				EDR3	Koe10						
16 26 48.14	−17 23 34.2	16268–1724	LHS3197AB	55.661 ± 0.260	14.30	5.62		✓	✓	Y	
		WSI 131		EDR3	Rie10						
16 26 51.68	−38 12 32.6	16269–3813	SCR1626-3812	71.737 ± 0.049	15.75	6.31	✓			N	
				EDR3	Win15						
16 30 13.09	−14 39 49.5	16302–1440	GJ2121AB	44.161 ± 0.159	12.35	4.75		✓	✓	Y	Tok20a

Table 3: Systems targeted for the M dwarf speckle interferometry program at SOAR. The WDS code (column 3) is the name each system would have in the Washington Double Star Catalog (Mason et al. 2001) if it were included there. The subsets justifying each target’s inclusion are marked in columns 8–10, and are discussed in §4.1.1, §4.1.2, and §4.1.3.

			WSI 132		EDR3	Wei96									
16 30 27.30	−36 33 56.8	16305−3634	SCR1630-3633AB		59.474 ± 0.036	14.93	5.90		✓					Y	
		WSI 133			EDR3	obsli									
16 45 16.93	−38 48 33.5	16453−3848	GJ2122AB		67.233 ± 0.241	9.68	3.96		✓	✓	✓			Y	
		RST1900Aa,Ab			EDR3	Hos15									
16 50 57.94	+22 27 05.7	16510+2227	G169-029		95.520 ± 0.026	14.08	5.77		✓					NA	
					EDR3	Win17									
16 55 28.76	−08 20 10.8	16555−0820	GJ0644AB		155.43 ± 0.49	9.03	4.63		✓	✓				Y	Sod99
		KUI 75AB			Vri20	Bes90									
16 58 25.21	+13 58 10.8	16584+1358	G139-003AB		70.90 ± 2.06	13.16	5.19		✓	✓				Y	
		YSC 61			Win17	Win17									
17 07 40.85	+07 22 06.7	17077+0722	GJ1210AB		82.00 ± 2.30	14.02	5.60		✓	✓				Y	Mas18
		YSC 62			Dit14	Wei96									
17 10 44.33	−53 00 25.6	17107−5300	UPM1710-5300AB		45.777 ± 0.052	12.12	4.96		✓					Y	
		NSN 374			EDR3	Win15									
17 11 52.25	−01 51 06.3	17119−0151	GJ0660AB		98.19 ± 12.09	11.37	4.71		✓	✓				Y	Doc19
		LPM 629			HIP07	Bes90									
17 12 51.28	−05 07 31.4	17129−0508	GJ0660.1A		43.259 ± 0.356	11.61	3.67				✓			N	
					EDR3	Bes90									
17 13 40.47	−08 25 14.8	17137−0825	GJ1212AB		48.484 ± 0.329	12.03	4.78		✓	✓				Y	
					EDR3	Koe10									
17 17 44.09	+11 40 12.4	17177+1140	GJ1215AB		80.841 ± 0.145	15.10	6.17		✓	✓	✓			N	Dah88
					EDR3	Wei96									
17 18 21.71	−01 46 53.4	17184−0147	HIP084652AB		45.030 ± 0.191	10.59	3.87		✓	✓				Y	
		BAG 51			EDR3	Wei93									
17 18 58.83	−34 59 48.6	17190−3459	GJ0667C		138.066 ± 0.028	10.34	4.30							N	
					EDR3	Lur14									

Table 3: Systems targeted for the M dwarf speckle interferometry program at SOAR. The WDS code (column 3) is the name each system would have in the Washington Double Star Catalog (Mason et al. 2001) if it were included there. The subsets justifying each target’s inclusion are marked in columns 8–10, and are discussed in §4.1.1, §4.1.2, and §4.1.3.

17 28 11.05	−01 43 57.3	17282−0144	SCR1728-0143AB	37.375 ± 0.391	14.42	5.41		✓	Y	
				EDR3	Win15					
17 29 46.20	−25 03 53.6	17298−2504	LP864-014AB	55.391 ± 0.806	13.55	5.09		✓	Y	
				DR2	APdr9					
17 33 40.66	−42 55 42.3	17337−4256	GAI1733-4255AB	44.786 ± 0.104	13.96	5.28	✓	✓	Y	
		GAT 23		EDR3	estim					
17 36 31.17	−25 15 00.9	17365−2515	GAI1736-2515AB	60.239 ± 0.831	16.39	8.50		✓	Y	
				DR2	estim					
17 37 03.67	−44 19 09.2	17371−4419	GJ0682AB	199.694 ± 0.031	10.99	5.38	✓	✓	N	
		WDK 3		EDR3	Win15					
17 43 00.80	+05 47 21.6	17430+0547	G140-009AB	47.828 ± 0.657	10.67	4.04		✓	✓	Y Tok19c
		HDS2506		EDR3	Wei86					
17 46 14.42	−32 06 08.4	17462−3206	GJ2130BC	70.734 ± 0.116	11.51	4.92		✓	✓	N
				EDR3	Ben16					
17 46 34.23	−57 19 08.7	17466−5719	GJ0693	169.804 ± 0.047	10.77	4.75	✓		N	
				EDR3	Win15					
17 57 48.50	+04 41 36.1	17578+0441	BARNARDS	546.976 ± 0.040	9.54	5.02			✓	NA
				EDR3	Dav15					
18 03 36.04	−18 58 49.9	18036−1859	G154-043AB	75.604 ± 0.681	14.13	5.85	✓	✓	✓	Y
				EDR3	Win15					
18 09 43.70	−02 19 35.1	18097−0220	LSR1809-0219	61.245 ± 0.453	15.10	5.83			✓	N
				DR2	Win15					
18 09 51.97	−10 27 13.3	18099−1027	UPM1809-1027AB	31.326 ± 0.383	13.12	5.00			✓	Y
				EDR3	*					
18 11 15.25	−78 59 22.9	18113−7859	L043-072AB	85.634 ± 0.462	12.57	5.61		✓	✓	Y
		KPP3056		EDR3	Win15					
18 20 57.16	−01 02 58.0	18210−0101	GJ1226AB	56.265 ± 0.045	13.07	5.12		✓	✓	Y

Table 3: Systems targeted for the M dwarf speckle interferometry program at SOAR. The WDS code (column 3) is the name each system would have in the Washington Double Star Catalog (Mason et al. 2001) if it were included there. The subsets justifying each target’s inclusion are marked in columns 8–10, and are discussed in §4.1.1, §4.1.2, and §4.1.3.

			VKI 46		EDR3	Jao05						
18 26 46.83	−65 42 40.0	18268−6543	SCR1826-6542AB	66.40 ± 0.73	17.35	7.80	✓	✓	N			
				Win17	Win11							
18 38 44.75	−14 29 26.0	18387−1429	GJ2138AB	74.792 ± 0.053	11.22	4.37	✓		N			
				HDS2641AB	EDR3	Koe10						
18 41 09.76	+24 47 14.4	18411+2447	GJ1230AC	100.685 ± 0.022	12.32	5.70	✓		N			
				EDR3	Win19							
18 45 05.25	−63 57 47.5	18451−6358	SCR1845-6357AB	249.665 ± 0.133	17.40	8.89	✓	✓	✓	NA		
				BIL 1	EDR3	Win11						
18 45 57.46	−28 55 53.7	18460−2856	LTT07434AB	53.207 ± 0.647	12.68	5.08	✓	✓	✓	Y		
				EDR3	Win15							
18 48 20.97	−68 55 34.4	18483−6856	SCR1848-6855AB	43.924 ± 0.098	16.86	5.76	✓	✓	✓	N	Jao14	
				JAO 8	EDR3	Jao14						
18 55 27.41	+08 24 09.0	18555+0824	GJ0735AB	89.907 ± 0.026	10.12	4.69	✓		N			
				EDR3	Bes90							
18 59 40.71	−63 27 22.1	18597−6327	L159-126AB	60.426 ± 1.512	13.05	4.97			✓	Y		
				DR2	*							
19 12 14.62	+02 53 11.4	19121+0254	GJ0748AB	106.279 ± 1.063	11.10	4.81	✓	✓	✓	Y	Ben16	
				AST 1	DR2	Lur14						
19 12 39.25	−36 14 56.6	19127−3615	WIS1912-3615	87.084 ± 0.072	13.91	5.14			✓	N		
				EDR3	Win15							
19 13 07.97	−39 01 53.9	19131−3902	LHS3443AB	46.936 ± 0.026	12.39	4.73		✓	✓	Y		
				WSI 135	EDR3	Rie10						
19 20 47.98	−45 33 29.6	19208−4534	GJ0754	169.235 ± 0.059	12.25	5.40	✓		✓	N		
				EDR3	Win15							
19 21 38.70	+20 52 03.3	19216+2052	GJ1235	94.399 ± 0.043	13.48	5.54			✓	N		
				EDR3	Hen18							

Table 3: Systems targeted for the M dwarf speckle interferometry program at SOAR. The WDS code (column 3) is the name each system would have in the Washington Double Star Catalog (Mason et al. 2001) if it were included there. The subsets justifying each target’s inclusion are marked in columns 8–10, and are discussed in §4.1.1, §4.1.2, and §4.1.3.

19 24 10.93	−09 31 33.5	19242−0932	SCR1924-0931AB	27.540 ± 0.454	13.89	4.96		✓	Y	
				EDR3	Win15					
19 27 52.71	−28 11 15.8	19279−2811	LHS5348AB	66.218 ± 0.070	14.85	6.06		✓	✓	Y
		WJG 6		EDR3	Win15					
19 31 01.40	−73 37 05.2	19310−7337	LEP1931-7337AB	51.687 ± 0.092	12.89	4.65			✓	Y
				EDR3	APdr9					
19 34 03.95	−52 25 14.1	19341−5225	L275-026	54.510 ± 0.029	12.83	4.91	✓			N
				EDR3	Win15					
19 42 00.65	−21 04 05.4	19420−2104	LP869-019AB	53.582 ± 0.047	13.22	5.40		✓		N
				EDR3	Win15					
19 43 24.58	−37 22 10.1	19434−3722	2MA1943-3722AB	41.387 ± 0.028	13.68	5.43		✓	✓	Y
		BRG 29		EDR3	*					
19 44 53.81	−23 38 00.2	19449−2338	LP869-026AB	67.388 ± 0.175	14.09	5.82		✓	✓	Y
		MTG 4		EDR3	Win15					Mas18
19 46 50.51	−01 57 39.6	19468−0158	LEP1946-0157	42.588 ± 0.409	12.14	4.39			✓	N
				EDR3	APdr9					
19 51 35.83	−35 10 37.5	19516−3511	2MA1951-3510AB	88.207 ± 0.075	13.06	5.32		✓		Y
		NSN 488		EDR3	Win15					
19 51 40.39	−31 00 22.2	19517−3100	UPM1951-3100AB	76.440 ± 0.860	12.28	4.87	✓	✓	✓	Y
				DR2	*					
19 54 24.88	−31 47 59.8	19544−3148	LP926-055AB	41.277 ± 0.438	13.07	4.75			✓	Y
				EDR3	*					
20 15 22.68	−56 45 54.5	20154−5646	L209-071AC	41.371 ± 0.290	12.85	5.08	✓		✓	Y
				EDR3	Win15					
20 25 18.95	−22 59 06.0	20253−2259	SCR2025-2259AB	14.123 ± 0.633	14.22	5.06			✓	Y
				EDR3	Win11					
20 29 48.32	+09 41 20.6	20298+0941	GJ0791.2AB	133.811 ± 1.387	13.13	5.82	✓	✓	✓	Y
										Tok19b

Table 3: Systems targeted for the M dwarf speckle interferometry program at SOAR. The WDS code (column 3) is the name each system would have in the Washington Double Star Catalog (Mason et al. 2001) if it were included there. The subsets justifying each target’s inclusion are marked in columns 8–10, and are discussed in §4.1.1, §4.1.2, and §4.1.3.

				AST 2AB		DR2	Win19							
20 33 01.89	−49 03 11.1	20330−4903	LEHPM2-1265AB	55.510 ± 0.536	15.33	6.14	✓	✓	✓	N				
				DR2	Win15									
20 49 09.96	−40 12 06.0	20492−4012	SCR2049-4012AB	105.156 ± 0.266	13.53	5.83	✓	✓	✓	Y	Hen18			
				DR2	Hos15									
20 55 37.74	−14 02 08.1	20556−1402	LHS0501AC	84.856 ± 0.471	12.48	5.11	✓	✓	✓	Y	Vri22			
				EDR3	Jao11									
21 01 07.40	−49 07 25.1	21011−4907	WT0766AC	74.455 ± 0.761	13.35	5.16		✓	✓	N				
				EDR3	Sub17									
21 14 12.20	−76 33 25.3	21142−7633	2MA2114-7633AB	51.210 ± 0.081	12.23	4.99			✓	Y				
				EDR3	APdr9									
21 17 34.09	−44 44 34.5	21176−4445	2MA2117-4444AB	55.889 ± 0.087	14.02	5.49			✓	Y				
				EDR3	APdr9									
21 20 09.80	−67 39 05.6	21202−6739	L117-123	47.022 ± 0.306	10.90	4.07			✓	N				
				EDR3	Koe10									
21 28 18.28	−22 18 32.4	21283−2219	L714-046	47.325 ± 0.028	12.17	4.54			✓	N				
				EDR3	Win15									
21 29 36.80	+17 38 35.9	21296+1739	GJ0829AB	147.496 ± 0.026	10.30	4.85		✓		Y				
				EDR3	Wei91									
21 30 47.67	−40 42 29.5	21308−4043	LHS0510	82.092 ± 0.028	13.12	4.99	✓			N				
				EDR3	Win15									
21 31 18.57	−09 47 26.5	21313−0947	GJ0831AB	134.083 ± 1.113	12.02	5.64	✓	✓	✓	Y	Ben16			
				BLA 9	DR2	Win15								
21 34 22.30	−43 16 10.6	21344−4316	WT0792	59.021 ± 0.033	16.38	6.69	✓			N				
				EDR3	Win15									
21 36 25.30	−44 01 00.1	21364−4401	WT0795	70.492 ± 0.033	14.15	5.62	✓			N				
				EDR3	Rie10									

Table 3: Systems targeted for the M dwarf speckle interferometry program at SOAR. The WDS code (column 3) is the name each system would have in the Washington Double Star Catalog (Mason et al. 2001) if it were included there. The subsets justifying each target’s inclusion are marked in columns 8–10, and are discussed in §4.1.1, §4.1.2, and §4.1.3.

21 38 43.65	−33 39 55.2	21387–3340	LHS0512	82.678 ± 0.045	12.55	4.98	✓			N	
				EDR3	Win15						
21 39 00.93	−24 09 29.3	21390–2409	GJ0836AB	51.399 ± 0.071	13.45	5.09	✓		✓	N	
				EDR3	Bes90						
21 49 05.76	−72 06 09.1	21491–7206	GJ1264AB	60.776 ± 0.069	9.62	3.97		✓	✓	Y	Tok20b
		HEI 598		EDR3	Koe10						
21 49 11.31	−41 33 28.7	21492–4133	L427-034A	65.399 ± 0.453	13.14	6.26			✓	N	
				EDR3	Win17						
21 49 44.83	−41 38 32.8	21497–4139	WT0818AB	38.623 ± 0.589	13.56	5.02	✓		✓	Y	
				EDR3	Win15						
21 55 48.36	−33 13 14.8	21558–3313	LP983-034AB	42.999 ± 0.485	12.73	5.03			✓	Y	
				EDR3	APdr9						
21 56 55.25	−01 54 09.3	21569–0154	LHS0516	74.220 ± 0.037	14.65	5.62	✓			N	
				EDR3	Wei96						
21 58 49.12	−32 26 25.6	21588–3226	LHS3739BC	55.686 ± 0.633	15.78	6.02	✓	✓	✓	N	Lur14
				EDR3	Lur14						
22 01 49.05	+16 28 02.8	22018+1628	GJ0844AB	61.79 ± 2.23	10.65	4.47		✓	✓	Y	Man19
		YSC 165		HIP07	Koe10						
22 02 29.38	−37 04 51.4	22025–3705	LHS3746	130.419 ± 0.053	11.76	5.04	✓		✓	N	
				EDR3	Hen06						
22 06 40.69	−44 58 07.5	22067–4458	WT0870AB	56.561 ± 0.138	14.43	5.54			✓	Y	
				EDR3	Rie10						
22 16 40.67	−48 00 36.4	22167–4801	SCR2216-4800AB	36.371 ± 0.205	13.66	5.06			✓	Y	
				EDR3	*						
22 17 18.70	−08 48 19.3	22173–0847	GJ0852BC	90.489 ± 0.222	14.43	5.90		✓		Y	
		BEU 22Ba,Bb		EDR3	Wei96						
22 17 19.23	−34 44 03.5	22173–3444	LP984-001AB	51.503 ± 0.088	15.48	6.31			✓	Y	

Table 3: Systems targeted for the M dwarf speckle interferometry program at SOAR. The WDS code (column 3) is the name each system would have in the Washington Double Star Catalog (Mason et al. 2001) if it were included there. The subsets justifying each target’s inclusion are marked in columns 8–10, and are discussed in §4.1.1, §4.1.2, and §4.1.3.

					EDR3	Win15							
22 23 07.00	−17 36 26.3	22231−1736	LHS3799		138.228 ± 0.048	13.30	5.98	✓				N	
					EDR3	Rie14							
22 28 23.24	−25 54 10.6	22284−2553	LP876-026AC		42.417 ± 0.024	13.36	5.85		✓	✓	Y		
		LDS2944AB			EDR3	*							
22 28 23.42	−25 54 07.7	22284−2553	LP876-026AB		42.417 ± 0.024	12.45	5.00		✓	✓	Y		
		WSI 137Aa,Ab			EDR3	*							
22 30 09.41	−53 44 55.5	22302−5345	LEHPM1-4771AB		64.358 ± 0.389	14.47	5.84	✓	✓	✓	Y	Vri20	
					EDR3	Win15							
22 35 04.89	−42 17 48.0	22351−4218	LTT09084AB		66.2 ± 10.5	13.34	5.13		✓	✓	Y		
					Win15	Win15							
22 36 09.69	−00 50 29.8	22360−0050	GJ0864AB		60.384 ± 0.041	9.99	3.83		✓		Y		
		JOD 25AB			EDR3	Bes90							
22 38 29.75	−65 22 42.6	22384−6523	GJ0865AB		76.33 ± 1.44	11.48	5.05		✓	✓	Y	Tok18c	
		HDS3215			Vri20	Bes90							
22 38 33.58	−15 17 59.8	22385−1519	GJ0866AB		293.600 ± 0.900	12.37	6.83		✓	✓	Y	Seg00	
		BLA 10AB			Tor10	Bes90							
22 38 45.28	−20 36 51.8	22388−2037	GJ0867BD		112.987 ± 0.039	11.45	4.96		✓		N		
					EDR3	Bes90							
22 38 45.57	−20 37 16.1	22388−2037	GJ0867AC		112.386 ± 0.056	9.09	4.29		✓		N		
					EDR3	Bes90							
22 48 38.39	−31 08 40.7	22486−3109	LP932-081		49.663 ± 0.737	12.33	4.84			✓	N		
					EDR3	Win15							
23 03 35.60	−46 50 47.0	23036−4651	SCR2303-4650AB		67.359 ± 0.855	13.89	5.53	✓	✓	✓	Y	Tok20b	
		WSI 139			EDR3	Win17							
23 05 52.04	−35 51 11.1	23059−3551	GJ0887AB		304.135 ± 0.020	7.34	3.87		✓		N		
					EDR3	Bes90							

Table 3: Systems targeted for the M dwarf speckle interferometry program at SOAR. The WDS code (column 3) is the name each system would have in the Washington Double Star Catalog (Mason et al. 2001) if it were included there. The subsets justifying each target’s inclusion are marked in columns 8–10, and are discussed in §4.1.1, §4.1.2, and §4.1.3.

23 07 19.88	−04 15 32.8	23073−0416	2MA2307-0415AC	48.356 ± 0.234 EDR3	10.73 APdr9	3.99		✓	Y	
23 08 19.55	−15 24 35.8	23083−1525	GJ0890	40.100 ± 0.024 EDR3	10.84 Bes90	3.73	(✓)		Y	
23 10 42.16	−19 13 34.4	23107−1914	GJ1281	46.822 ± 0.061 EDR3	12.45 Jao05	4.22	✓	✓	N	
23 11 57.79	−17 01 58.8	23120−1702	LP822-037AB	53.2 ± 14.4 Win15	13.95 *	5.25		✓	Y	
23 24 11.31	−17 45 50.3	23242−1746	G273-033AB	43.881 ± 0.381 EDR3	11.93 APdr9	4.17		✓	Y	
23 25 24.90	−67 40 07.2	23254−6740	SCR2325-6740AB	31.63 ± 1.53 Vri20	14.38 Win11	5.33		✓	Y	
23 30 13.44	−20 23 27.4	23302−2023	GJ1284AB	62.868 ± 0.076 EDR3	11.14 Rie14	4.81	✓		N	
23 36 52.30	−36 28 51.7	23369−3629	LHS0547	83.676 ± 0.023 EDR3	13.76 Jao05	5.34	✓		N	
23 45 31.28	−16 10 19.4	23455−1610	LHS4009AB	79.97 ± 1.37 Rie10	14.38 Rie10	6.07	✓	✓	Y	Man19
23 48 36.06	−27 39 38.9	23486−2740	LHS4016AB	38.233 ± 0.040 EDR3	12.34 Rie14	4.60	✓		N	
23 52 23.47	−14 41 24.3	23524−1441	LHS4032AB	39.108 ± 0.483 EDR3	15.30 Wei96	5.75		✓	Y	
23 54 50.21	−09 57 01.1	23548−0957	LP763-082AB	38.920 ± 0.146 EDR3	12.19 Rei03	4.50		✓	Y	
23 55 39.78	−06 08 33.4	23557−0609	GJ0912AB	55.920 ± 0.044 EDR3	11.16 Bes90	4.44	(✓)		Y	
23 57 19.36	−12 58 40.7	23573−1259	LP704-014AC	50.413 ± 0.067	12.98	4.75	✓		Y	

Table 3: Systems targeted for the M dwarf speckle interferometry program at SOAR. The WDS code (column 3) is the name each system would have in the Washington Double Star Catalog (Mason et al. 2001) if it were included there. The subsets justifying each target’s inclusion are marked in columns 8–10, and are discussed in §4.1.1, §4.1.2, and §4.1.3.

				BWL 67Aa,Ab		EDR3	Wei91						
23 58 32.66	+07 39 30.1	23585+0740	LTT17066AB		59.094 ± 0.278	11.71	4.65				✓	Y	
					EDR3	Wei86							
23 59 44.77	−44 05 00.3	23597−4405	LTT09828AB		58.267 ± 0.530	12.81	4.77	✓	✓	✓	Y	Vri20	
				WSI 140	DR2	Win15							

Table 4: Results of the SOAR speckle interferometry campaign for nearby M dwarfs. The meanings of columns 8–10 differ depending on whether or not the companion was resolved in that observation, hence the two lines in those columns’ headers. The “:” flag in the last column indicates highly uncertain results; the rest of the flags are described in §4.2.

WDS	Name	Date of obs. (yr)	N	Fil.	Res? (Y/N)	ρ (if Y) ρ_{\min} (if N) (mas)	θ (if Y) $\Delta m_{0.15}$ (if N) ($^{\circ}$ or mag)	Δm (if Y) $\Delta m_{1.0}$ (if N) (mag)	flag
(1)	(2)	(3)	(4)	(5)	(6)	(7)	(8)	(9)	(10)
00067-0706	2MA0006-0705AB	2019.8568	2	<i>I</i>	N	0.0768	2.3	2.9	
00067-0706	2MA0006-0705AB	2020.8342	2	<i>I</i>	N	0.0594	2.3	2.8	
00067-0706	2MA0006-0705AB	2022.4419	4	<i>I</i>	Y	0.1019	204.8	0.7	q
00067-0706	2MA0006-0705AB	2022.6823	2	<i>I</i>	Y	0.1135	201.9	0.9	:
00067-0706	2MA0006-0705AB	2023.0063	2	<i>I</i>	Y	0.1349	198.1	1.0	q
00089+2050	G131-026AB	2019.5397	2	<i>I</i>	Y	0.1110	154.4	0.0	
00089+2050	G131-026AB	2019.8564	2	<i>I</i>	Y	0.1233	130.0	0.3	
00089+2050	G131-026AB	2020.8340	2	<i>I</i>	Y	0.1522	77.5	0.0	
00089+2050	G131-026AB	2020.9241	2	<i>I</i>	Y	0.1514	74.2	0.2	
00089+2050	G131-026AB	2021.5684	2	<i>I</i>	Y	0.1436	42.8	0.3	
00089+2050	G131-026AB	2022.4420	2	<i>I</i>	Y	0.1243	349.3	0.2	
00098-4202	LEHPM1-0255AB	2019.6133	2	<i>I</i>	Y	0.0522	339.0	0.8	
00098-4202	LEHPM1-0255AB	2019.8567	2	<i>I</i>	N	0.0525	2.5	3.9	
00098-4202	LEHPM1-0255AB	2020.8341	2	<i>I</i>	Y	0.0959	115.7	1.0	
00098-4202	LEHPM1-0255AB	2020.9270	2	<i>I</i>	Y	0.1089	117.4	0.9	q
00098-4202	LEHPM1-0255AB	2021.5684	2	<i>I</i>	Y	0.1498	128.7	0.9	q
00098-4202	LEHPM1-0255AB	2022.4418	2	<i>I</i>	Y	0.1234	139.7	1.0	q
00098-4202	LEHPM1-0255AB	2022.8450	2	<i>I</i>	Y	0.0718	149.8	1.1	q
00138-0458	LHS1042	2019.8568	2	<i>I</i>	N	0.1145	1.6	2.5	:
00138-0458	LHS1042	2020.8342	2	<i>I</i>	N	0.1260	1.6	1.6	:
00155-1608	GJ1005AB	2019.5369	2	<i>I</i>	Y	0.3373	288.1	1.6	q

Table 4: Results of the SOAR speckle interferometry campaign for nearby M dwarfs. The meanings of columns 8–10 differ depending on whether or not the companion was resolved in that observation, hence the two lines in those columns’ headers. The “:” flag in the last column indicates highly uncertain results; the rest of the flags are described in §4.2.

00155-1608	GJ1005AB	2019.9495	2	<i>I</i>	Y	0.3950	269.8	1.6	q
00155-1608	GJ1005AB	2020.8342	2	<i>I</i>	Y	0.4238	239.8	1.6	q
00155-1608	GJ1005AB	2020.9270	2	<i>I</i>	Y	0.4168	236.6	1.6	q
00155-1608	GJ1005AB	2021.5657	2	<i>I</i>	Y	0.3346	210.3	1.5	q
00155-1608	GJ1005AB	2022.4445	2	<i>I</i>	Y	0.1884	118.1	1.6	q
00155-1608	GJ1005AB	2023.0062	2	<i>I</i>	Y	0.2073	32.3	1.6	q
00160-1637	2MA0015-1636AB	2019.5369	2	<i>I</i>	Y	0.0894	70.8	0.0	
00160-1637	2MA0015-1636AB	2019.8568	2	<i>I</i>	Y	0.1006	85.3	0.0	
00160-1637	2MA0015-1636AB	2019.9495	2	<i>I</i>	Y	0.1046	87.4	0.0	
00160-1637	2MA0015-1636AB	2020.8342	2	<i>I</i>	Y	0.0652	126.7	0.0	
00160-1637	2MA0015-1636AB	2020.9270	2	<i>I</i>	Y	0.0506	140.9	0.0	
00160-1637	2MA0015-1636AB	2021.5657	2	<i>I</i>	Y	0.0833	246.9	0.0	
00160-1637	2MA0015-1636AB	2021.5684	4	<i>I</i>	Y	0.0808	247.7	0.0	:
00160-1637	2MA0015-1636AB	2021.7321	2	<i>I</i>	Y	0.0947	254.9	0.0	
00160-1637	2MA0015-1636AB	2022.4445	2	<i>I</i>	Y	0.1002	282.2	0.0	
00160-1637	2MA0015-1636AB	2022.6823	2	<i>I</i>	Y	0.0927	289.6	0.1	
00160-1637	2MA0015-1636AB	2023.0062	2	<i>I</i>	Y	0.0535	315.8	0.1	
00160-4816	L290-072AB	2019.6133	2	<i>I</i>	Y	0.1935	43.1	0.4	q
00160-4816	L290-072AB	2020.8341	2	<i>I</i>	Y	0.1778	76.9	0.4	q
00160-4816	L290-072AB	2021.5356	2	<i>I</i>	Y	0.1543	101.7	0.3	
00160-4816	L290-072AB	2022.4418	2	<i>I</i>	Y	0.1197	150.4	0.4	q
00160-4816	L290-072AB	2022.7738	2	<i>I</i>	Y	0.1101	174.6	0.4	q
00162+1952	GJ1006AC	2019.5397	2	<i>I</i>	N	0.0636	2.3	3.9	
00162+1952	GJ1006AC	2019.8564	2	<i>I</i>	N	0.0543	2.7	4.1	
00162+1952	GJ1006AC	2020.9241	2	<i>I</i>	Y	0.0312	44.8	1.0	

Table 4: Results of the SOAR speckle interferometry campaign for nearby M dwarfs. The meanings of columns 8–10 differ depending on whether or not the companion was resolved in that observation, hence the two lines in those columns’ headers. The “:” flag in the last column indicates highly uncertain results; the rest of the flags are described in §4.2.

00162+1952	GJ1006AC	2021.5684	2	<i>I</i>	N	0.0415	2.2	4.7	
00216-4606	L290-028	2019.6133	2	<i>I</i>	N	0.0470	3.0	4.2	
00216-4606	L290-028	2019.9523	2	<i>I</i>	N	0.0415	3.3	4.3	
00216-4606	L290-028	2020.9270	2	<i>I</i>	N	0.0415	2.8	5.2	
00247-2653	GJ2005AB	2019.5369	4	<i>I</i>	Y	0.9181	53.6	2.2	
00247-2653	GJ2005AB	2019.8568	2	<i>I</i>	Y	0.9238	54.6	2.3	
00247-2653	GJ2005AB	2020.8342	4	<i>I</i>	Y	0.9148	58.2	2.1	
00247-2653	GJ2005AB	2021.5686	2	<i>I</i>	Y	0.8944	62.1	2.0	:
00247-2653	GJ2005AB	2022.4446	2	<i>I</i>	Y	0.8796	68.7	2.3	
00247-2653	GJ2005AB	2022.8452	2	<i>I</i>	Y	0.8717	71.6	2.3	
00247-2653	GJ2005BC	2019.5369	4	<i>I</i>	Y	0.2766	151.7	0.4	
00247-2653	GJ2005BC	2019.8568	2	<i>I</i>	Y	0.3124	159.8	0.4	
00247-2653	GJ2005BC	2020.8342	4	<i>I</i>	Y	0.4107	175.5	0.5	
00247-2653	GJ2005BC	2021.5686	2	<i>I</i>	Y	0.4584	182.9	0.7	:
00247-2653	GJ2005BC	2022.4446	2	<i>I</i>	Y	0.4904	192.4	0.4	
00247-2653	GJ2005BC	2022.8452	2	<i>I</i>	Y	0.4908	195.2	0.4	
00251-3646	LTT00220AB	2019.5369	2	<i>I</i>	Y	0.4608	297.0	3.1	q
00251-3646	LTT00220AB	2019.8567	2	<i>I</i>	Y	0.4677	298.9	3.1	q
00251-3646	LTT00220AB	2021.5684	2	<i>I</i>	Y	0.4780	309.5	3.1	q
00251-3646	LTT00220AB	2022.4418	2	<i>I</i>	Y	0.4865	314.5	3.1	q
00279+2220	LP349-025AB	2019.8564	2	<i>I</i>	Y	0.1170	197.3	0.2	:
00279+2220	LP349-025AB	2020.8340	2	<i>I</i>	N	0.2625	1.8	1.8	:
00279+2220	LP349-025AB	2020.9241	2	<i>I</i>	Y	0.0917	313.7	0.4	:
00279+2220	LP349-025AB	2021.5684	2	<i>I</i>	N	0.0764	0.0	0.0	:
00279+2220	LP349-025AB	2021.7323	2	<i>I</i>	Y	0.0930	78.5	0.4	:

Table 4: Results of the SOAR speckle interferometry campaign for nearby M dwarfs. The meanings of columns 8–10 differ depending on whether or not the companion was resolved in that observation, hence the two lines in those columns’ headers. The “:” flag in the last column indicates highly uncertain results; the rest of the flags are described in §4.2.

00329-0434	GIC0050AB	2019.5397	2	<i>I</i>	Y	0.9308	192.4	2.7	
00329-0434	GIC0050AB	2019.8568	3	<i>I</i>	Y	0.9300	193.0	3.0	
00329-0434	GIC0050AB	2020.8342	2	<i>I</i>	Y	0.9782	194.4	2.7	q
00329-0434	GIC0050AB	2021.5657	2	<i>I</i>	Y	1.0101	194.7	2.6	
00329-0434	GIC0050AB	2022.4447	2	<i>I</i>	Y	0.9811	195.1	2.9	
00329-0434	GIC0050AC	2019.5397	2	<i>I</i>	Y	0.2048	195.3	2.4	
00329-0434	GIC0050AC	2019.8568	3	<i>I</i>	Y	0.2328	195.6	2.7	
00329-0434	GIC0050AC	2020.8342	2	<i>I</i>	Y	0.2228	198.9	2.4	q
00329-0434	GIC0050AC	2021.5657	2	<i>I</i>	Y	0.1902	199.9	2.6	
00329-0434	GIC0050AC	2022.4447	2	<i>I</i>	Y	0.1478	201.7	3.2	
00434-4118	LHS1134	2019.6133	2	<i>I</i>	N	0.0492	2.5	4.0	
00434-4118	LHS1134	2019.8567	2	<i>I</i>	N	0.0470	2.8	4.3	
00434-4118	LHS1134	2020.8341	2	<i>I</i>	N	0.0508	2.7	4.1	
00482-0508	LTT00453	2019.9495	2	<i>I</i>	N	0.0415	2.4	4.8	
00482-0508	LTT00453	2020.8342	2	<i>I</i>	N	0.0477	2.9	4.2	
00482-0508	LTT00453	2021.5657	2	<i>I</i>	N	0.0415	2.5	5.0	
00585-2751	GJ0046	2019.5369	2	<i>I</i>	N	0.0463	2.7	4.2	
00585-2751	GJ0046	2019.8568	2	<i>I</i>	N	0.0444	2.6	4.1	
00585-2751	GJ0046	2020.9271	2	<i>I</i>	N	0.0415	2.9	5.2	
01009-0427	GJ1025	2019.5397	3	<i>I</i>	N	0.0562	2.5	4.2	
01009-0427	GJ1025	2019.8568	2	<i>I</i>	N	0.0543	2.8	3.7	
01009-0427	GJ1025	2020.8365	2	<i>I</i>	N	0.0463	2.6	4.0	
01104-6727	GJ0054AB	2019.6132	2	<i>I</i>	Y	0.1401	260.4	0.8	q
01104-6727	GJ0054AB	2019.7911	2	<i>I</i>	Y	0.1052	226.7	0.8	q
01104-6727	GJ0054AB	2020.8368	2	<i>I</i>	Y	0.1295	247.8	0.8	q

Table 4: Results of the SOAR speckle interferometry campaign for nearby M dwarfs. The meanings of columns 8–10 differ depending on whether or not the companion was resolved in that observation, hence the two lines in those columns’ headers. The “:” flag in the last column indicates highly uncertain results; the rest of the flags are described in §4.2.

01104-6727	GJ0054AB	2020.9242	2	<i>I</i>	Y	0.1093	229.6	0.9	q
01104-6727	GJ0054AB	2021.5356	2	<i>I</i>	Y	0.0632	9.4	0.8	
01104-6727	GJ0054AB	2022.6849	2	<i>I</i>	Y	0.0614	8.0	0.6	q
01114+1526	LP467-016AB	2020.8367	2	<i>I</i>	Y	0.4410	284.6	0.9	q
01133-5429	DEN0113-5429	2020.1110	2	<i>I</i>	N	0.0643	2.3	3.3	
01133-5429	DEN0113-5429	2020.8365	2	<i>I</i>	N	0.0562	2.5	3.2	
01133-5429	DEN0113-5429	2022.7738	2	<i>I</i>	N	0.0415	3.1	3.8	
01222+2209	G034-023AB	2019.9521	2	<i>I</i>	Y	0.1049	18.4	0.0	:
01222+2209	G034-023AB	2020.8367	2	<i>I</i>	Y	0.2394	0.9	0.0	
01222+2209	G034-023AB	2020.9241	2	<i>I</i>	Y	0.2482	359.9	0.0	
01222+2209	G034-023AB	2021.5684	2	<i>I</i>	Y	0.2963	355.5	0.0	
01222+2209	G034-023AB	2022.6824	2	<i>I</i>	Y	0.2875	348.8	0.0	
01287-1458	SCR0128-1458AB	2019.6134	2	<i>I</i>	Y	0.3686	326.5	2.6	q
01287-1458	SCR0128-1458AB	2020.8344	2	<i>I</i>	Y	0.3241	307.8	2.6	q
01287-1458	SCR0128-1458AB	2020.9271	2	<i>I</i>	Y	0.3205	306.2	2.7	q
01287-1458	SCR0128-1458AB	2021.5657	4	<i>I</i>	Y	0.3014	294.7	2.5	q
01287-1458	SCR0128-1458AB	2022.4447	2	<i>I</i>	Y	0.2848	276.1	2.7	q
01287-1458	SCR0128-1458AB	2022.8453	2	<i>I</i>	Y	0.2797	267.5	2.5	q
01388-1758	GJ0065AB	2020.8344	2	<i>I</i>	Y	1.9345	341.7	0.3	*
01388-1758	GJ0065AB	2023.0063	2	<i>I</i>	Y	1.2632	318.1	0.4	*
01394-3936	LP991-084	2019.5370	2	<i>I</i>	N	0.0508	2.5	3.9	
01394-3936	LP991-084	2020.8344	2	<i>I</i>	N	0.0500	2.5	3.9	
01394-3936	LP991-084	2022.7738	2	<i>I</i>	N	0.0434	3.1	4.2	
01466-0839	L870-044AB	2019.5398	2	<i>I</i>	Y	0.2145	6.3	0.9	q
01466-0839	L870-044AB	2019.8568	2	<i>I</i>	Y	0.2083	6.0	1.1	q

Table 4: Results of the SOAR speckle interferometry campaign for nearby M dwarfs. The meanings of columns 8–10 differ depending on whether or not the companion was resolved in that observation, hence the two lines in those columns’ headers. The “:” flag in the last column indicates highly uncertain results; the rest of the flags are described in §4.2.

01466-0839	L870-044AB	2020.8367	2	<i>I</i>	Y	0.1820	5.3	1.0	q
01466-0839	L870-044AB	2022.7739	2	<i>I</i>	Y	0.1165	4.1	1.0	q
01477-4836	LEHPM1-1882AB	2019.5370	2	<i>I</i>	Y	0.5562	30.6	0.6	*
01477-4836	LEHPM1-1882AB	2019.8567	2	<i>I</i>	Y	0.5482	28.5	0.6	q
01477-4836	LEHPM1-1882AB	2020.8365	2	<i>I</i>	Y	0.5095	22.6	0.6	q
01477-4836	LEHPM1-1882AB	2022.6112	2	<i>I</i>	Y	0.4047	7.9	0.6	q
01477-4836	LEHPM1-1882AB	2022.9329	2	<i>I</i>	Y	0.3806	4.4	0.6	q
01511-0607	LHS1302	2019.5399	2	<i>I</i>	N	0.0670	2.3	3.7	
01511-0607	LHS1302	2019.8568	2	<i>I</i>	N	0.0553	2.5	3.5	
01511-0607	LHS1302	2020.8367	2	<i>I</i>	N	0.0508	2.7	4.0	
01536-6654	L088-043AB	2019.6132	2	<i>I</i>	N	0.0485	2.8	4.2	
01536-6654	L088-043AB	2019.8567	2	<i>I</i>	N	0.0508	2.6	4.2	
01536-6654	L088-043AB	2020.8368	2	<i>I</i>	Y	0.0914	245.5	3.0	
01536-6654	L088-043AB	2021.5355	2	<i>I</i>	Y	0.1837	272.3	3.0	
01536-6654	L088-043AB	2021.7512	2	<i>I</i>	Y	0.2043	278.6	2.9	q
01536-6654	L088-043AB	2022.6115	2	<i>I</i>	Y	0.2557	291.7	2.9	
01536-6654	L088-043AB	2022.8423	2	<i>I</i>	Y	0.2616	294.4	2.8	
01592+0330	GJ1041AB	2019.5399	1	<i>I</i>	Y	4.2358	53.4	0.4	*
01592+0330	GJ1041AB	2019.5399	1	<i>I</i>	Y	4.2372	53.4	0.4	*
01592+0330	GJ1041BC	2019.5399	1	<i>I</i>	N	0.0636	2.3	4.0	
02051-1737	GJ0084AB	2019.6134	2	<i>I</i>	Y	0.4071	101.0	4.5	
02051-1737	GJ0084AB	2019.8593	2	<i>I</i>	Y	0.3762	99.2	5.0	
02051-1737	GJ0084AB	2020.8345	2	<i>I</i>	Y	0.2438	100.7	4.5	
02051-1737	GJ0084AB	2022.6113	2	<i>I</i>	N	0.0457	2.3	4.5	
02192-3647	GJ1046AB	2019.5370	2	<i>I</i>	N	0.0437	2.4	3.8	

Table 4: Results of the SOAR speckle interferometry campaign for nearby M dwarfs. The meanings of columns 8–10 differ depending on whether or not the companion was resolved in that observation, hence the two lines in those columns’ headers. The “:” flag in the last column indicates highly uncertain results; the rest of the flags are described in §4.2.

02192-3647	GJ1046AB	2019.9498	2	<i>I</i>	N	0.0415	3.1	5.4	
02192-3647	GJ1046AB	2020.9269	2	<i>I</i>	N	0.0415	3.8	5.4	
02192-3647	GJ1046AB	2022.6112	2	<i>I</i>	N	0.0492	2.2	4.0	
02275-1908	LP770-020AB	2019.5398	2	<i>I</i>	Y	0.2249	196.2	1.8	q
02275-1908	LP770-020AB	2019.8593	2	<i>I</i>	Y	0.2068	201.4	1.8	
02275-1908	LP770-020AB	2020.8345	2	<i>I</i>	Y	0.1179	232.4	1.8	q
02275-1908	LP770-020AB	2021.5658	3	<i>I</i>	Y	0.0648	319.9	1.3	
02275-1908	LP770-020AB	2021.7540	2	<i>I</i>	Y	0.0763	4.4	1.8	q
02275-1908	LP770-020AB	2022.6113	2	<i>I</i>	Y	0.1293	69.6	1.7	
02275-1908	LP770-020AB	2022.8453	2	<i>I</i>	Y	0.1418	79.5	1.7	q
02278+0426	GJ0098AB	2020.8367	2	<i>I</i>	Y	0.6303	109.3	0.3	q
02344-5306	L225-057AB	2019.5344	2	<i>I</i>	Y	0.1504	312.0	0.1	
02344-5306	L225-057AB	2019.8567	2	<i>I</i>	Y	0.1357	330.9	0.1	
02344-5306	L225-057AB	2019.9470	2	<i>I</i>	Y	0.1314	337.1	0.1	
02344-5306	L225-057AB	2020.8344	2	<i>I</i>	Y	0.1122	59.2	0.1	
02344-5306	L225-057AB	2020.9243	2	<i>I</i>	Y	0.1149	68.2	0.1	
02344-5306	L225-057AB	2021.5686	4	<i>I</i>	Y	0.1398	116.4	0.1	
02344-5306	L225-057AB	2021.6367	2	<i>I</i>	Y	0.1449	120.9	0.0	
02344-5306	L225-057AB	2021.7512	2	<i>I</i>	Y	0.1472	127.0	0.1	
02344-5306	L225-057AB	2022.6115	2	<i>I</i>	Y	0.1630	170.3	0.0	
02344-5306	L225-057AB	2022.8424	3	<i>I</i>	Y	0.1639	180.5	0.0	
02365-5928	APM0018	2019.5345	3	<i>I</i>	N	0.0562	2.6	3.7	
02365-5928	APM0018	2019.8568	3	<i>I</i>	N	0.0553	2.5	3.5	
02365-5928	APM0018	2020.8368	2	<i>I</i>	N	0.0534	2.6	3.6	
02365-5928	APM0018	2022.7740	2	<i>I</i>	N	0.0458	2.5	4.0	

Table 4: Results of the SOAR speckle interferometry campaign for nearby M dwarfs. The meanings of columns 8–10 differ depending on whether or not the companion was resolved in that observation, hence the two lines in those columns’ headers. The “:” flag in the last column indicates highly uncertain results; the rest of the flags are described in §4.2.

02452-4344	LP993-115BC	2019.5370	2	<i>I</i>	Y	0.3352	72.6	0.6	q
02452-4344	LP993-115BC	2019.8594	2	<i>I</i>	Y	0.3393	66.1	0.6	q
02452-4344	LP993-115BC	2019.9498	2	<i>I</i>	Y	0.3406	64.4	0.6	q
02452-4344	LP993-115BC	2020.8345	2	<i>I</i>	Y	0.3643	48.1	0.6	q
02452-4344	LP993-115BC	2021.5685	2	<i>I</i>	Y	0.3972	36.6	0.6	:
02452-4344	LP993-115BC	2022.6115	2	<i>I</i>	Y	0.4554	23.7	0.6	
02530+1653	TEE0253+1652	2019.9496	2	<i>I</i>	N	0.0420	0.0	3.3	
02530+1653	TEE0253+1652	2020.8369	2	<i>I</i>	N	0.0516	2.8	3.9	
02530+1653	TEE0253+1652	2023.0090	2	<i>I</i>	N	0.0415	0.0	3.8	
02531+1652	TEE0253+1652	2019.8569	2	<i>I</i>	N	0.0630	2.4	3.8	
03019-1633	LP771-095A	2020.8345	2	<i>I</i>	N	0.0420	2.8	4.7	
03019-1633	LP771-095BC	2019.6136	2	<i>I</i>	Y	1.0333	317.5	0.7	*
03019-1633	LP771-095BC	2019.9498	2	<i>I</i>	Y	1.0773	317.3	0.8	*
03019-1633	LP771-095BC	2020.8345	2	<i>I</i>	Y	1.1769	317.4	0.8	*
03019-1633	LP771-095BC	2022.7739	2	<i>I</i>	Y	1.3458	317.7	0.8	*
03019-1633	LP771-095BC	2019.6136	2	<i>I</i>	N	0.0636	2.5	4.2	
03079-2813	GJ1054AC	2019.8593	2	<i>I</i>	N	0.0432	2.7	4.0	
03079-2813	GJ1054AC	2020.8236	2	<i>I</i>	N	0.0432	2.7	4.4	
03143-2309	LP831-045AB	2019.8593	3	<i>I</i>	N	0.0485	2.6	4.1	
03143-2309	LP831-045AB	2020.8236	2	<i>I</i>	N	0.0463	2.8	4.1	
03149-6242	UPM0314-6241AB	2019.9470	2	<i>I</i>	Y	0.9524	247.8	0.4	*
03149-6242	UPM0314-6241AB	2020.8368	2	<i>I</i>	Y	0.9426	246.5	0.4	*
03149-6242	UPM0314-6241AB	2022.7740	2	<i>I</i>	Y	0.9134	243.4	0.5	q
03195-3060	LTT01578AB	2019.6136	2	<i>I</i>	Y	0.5501	133.0	1.3	q
03195-3060	LTT01578AB	2019.8593	2	<i>I</i>	Y	0.5573	132.1	1.2	*

Table 4: Results of the SOAR speckle interferometry campaign for nearby M dwarfs. The meanings of columns 8–10 differ depending on whether or not the companion was resolved in that observation, hence the two lines in those columns’ headers. The “:” flag in the last column indicates highly uncertain results; the rest of the flags are described in §4.2.

03195-3060	LTT01578AB	2020.9269	2	<i>I</i>	Y	0.5804	129.8	1.3	:
03195-3060	LTT01578AB	2023.0066	2	<i>I</i>	Y	0.6200	125.3	1.3	q
03347-0451	LHS1561AB	2019.6136	2	<i>I</i>	Y	0.1365	188.3	0.9	q
03347-0451	LHS1561AB	2019.8571	2	<i>I</i>	Y	0.1430	181.1	0.9	q
03347-0451	LHS1561AB	2020.0182	2	<i>I</i>	Y	0.1401	176.6	0.9	
03347-0451	LHS1561AB	2020.8236	2	<i>I</i>	Y	0.1140	151.5	0.9	q
03347-0451	LHS1561AB	2020.9243	2	<i>I</i>	Y	0.1077	146.0	0.9	q
03347-0451	LHS1561AB	2021.7297	2	<i>I</i>	Y	0.0417	46.5	0.7	
03347-0451	LHS1561AB	2022.7743	2	<i>I</i>	Y	0.0962	215.7	0.8	q
03347-0451	LHS1561AB	2023.0065	2	<i>I</i>	Y	0.1111	206.2	0.8	
03360-4431	GJ1061	2019.6135	2	<i>I</i>	N	0.0636	2.7	4.7	
03360-4431	GJ1061	2019.8594	2	<i>I</i>	N	0.0477	2.8	4.1	
03360-4431	GJ1061	2020.8368	2	<i>I</i>	N	0.0492	2.9	4.4	
03425+1232	LHS0178	2019.8569	2	<i>I</i>	N	0.0759	2.2	3.9	
03425+1232	LHS0178	2020.9244	3	<i>I</i>	Y	0.1049	67.7	1.9	q
03425+1232	LHS0178	2021.7516	2	<i>I</i>	Y	0.1276	66.6	1.6	:
03425+1232	LHS0178	2022.7743	2	<i>I</i>	Y	0.1473	64.9	1.7	q
03434-0934	LHS1582AB	2020.8236	2	<i>I</i>	N	0.0534	2.4	3.3	
03434-0934	LHS1582AB	2021.7542	2	<i>I</i>	Y	0.0729	125.9	2.6	:
03434-0934	LHS1582AB	2022.7742	2	<i>I</i>	N	0.0485	2.1	4.2	
03527+1701	LHS1610AB	2019.8569	2	<i>I</i>	N	0.0553	2.5	3.7	
03527+1701	LHS1610AB	2020.8369	2	<i>I</i>	N	0.0534	2.5	3.9	
03527+1701	LHS1610AB	2022.7743	2	<i>I</i>	N	0.0415	3.2	4.7	
03543-1438	DEN0354-1437AB	2019.8571	2	<i>I</i>	Y	0.1875	130.8	0.4	:
03543-1438	DEN0354-1437AB	2020.8369	3	<i>I</i>	Y	0.1963	117.1	1.0	:

Table 4: Results of the SOAR speckle interferometry campaign for nearby M dwarfs. The meanings of columns 8–10 differ depending on whether or not the companion was resolved in that observation, hence the two lines in those columns’ headers. The “:” flag in the last column indicates highly uncertain results; the rest of the flags are described in §4.2.

03543-1438	DEN0354-1437AB	2021.7297	2	<i>I</i>	Y	0.1737	101.0	0.4	
03543-1438	DEN0354-1437AB	2022.7742	2	<i>I</i>	Y	0.1667	81.8	0.5	:
04073-2429	LHS1630AB	2019.8594	2	<i>I</i>	Y	1.3340	98.7	0.4	*
04073-2429	LHS1630AB	2021.7297	2	<i>I</i>	Y	1.3830	100.3	0.4	*
04089-3129	LP889-037AB	2019.8594	2	<i>I</i>	Y	1.2842	275.0	2.9	*
04089-3129	LP889-037AB	2020.8236	2	<i>I</i>	Y	1.2946	276.7	3.2	*
04089-3129	LP889-037AB	2021.7296	2	<i>I</i>	Y	1.3062	277.9	2.9	*
04089-3129	LP889-037AB	2022.0470	2	<i>I</i>	Y	1.2978	278.7	2.9	*
04093-5322	GJ0163	2019.6136	2	<i>I</i>	N	0.0636	2.7	4.6	
04093-5322	GJ0163	2020.1111	2	<i>I</i>	N	0.0463	2.4	3.8	
04093-5322	GJ0163	2021.1624	2	<i>I</i>	N	0.0426	2.5	4.0	
04158-4602	UPM0415-4602AB	2019.6136	2	<i>I</i>	Y	0.7318	84.6	0.5	*
04158-4602	UPM0415-4602AB	2019.8594	2	<i>I</i>	Y	0.7270	83.5	0.4	*
04158-4602	UPM0415-4602AB	2020.1111	2	<i>I</i>	Y	0.7199	82.8	0.5	*
04158-4602	UPM0415-4602AB	2022.6115	2	<i>I</i>	Y	0.6340	73.6	0.6	q
04167-1233	GJ2033AB	2019.8571	2	<i>I</i>	Y	3.1128	101.6	0.8	*
04176-4835	LEHPM1-3719	2019.6138	2	<i>I</i>	N	0.0716	2.6	4.0	
04176-4835	LEHPM1-3719	2019.8594	2	<i>I</i>	N	0.0716	2.1	3.7	
04176-4835	LEHPM1-3719	2020.9271	2	<i>I</i>	N	0.0573	2.2	3.0	
04176-4835	LEHPM1-3719	2022.7740	2	<i>I</i>	N	0.0548	2.0	2.8	
04202-7006	SCR0420-7005	2019.9469	2	<i>I</i>	N	0.0415	2.2	4.3	
04202-7006	SCR0420-7005	2020.8286	2	<i>I</i>	N	0.1068	1.8	2.6	:
04242-2357	2MA0424-2356	2019.9500	2	<i>I</i>	N	0.0415	3.0	5.5	
04242-2357	2MA0424-2356	2020.8237	2	<i>I</i>	N	0.0450	2.7	4.2	
04242-2357	2MA0424-2356	2022.1945	2	<i>I</i>	N	0.0415	3.7	4.9	

Table 4: Results of the SOAR speckle interferometry campaign for nearby M dwarfs. The meanings of columns 8–10 differ depending on whether or not the companion was resolved in that observation, hence the two lines in those columns’ headers. The “:” flag in the last column indicates highly uncertain results; the rest of the flags are described in §4.2.

04293-3124	2MA0429-3123AB	2019.6136	2	<i>I</i>	Y	0.4984	196.3	1.8	:
04293-3124	2MA0429-3123AB	2020.8237	2	<i>I</i>	Y	0.4977	188.4	1.8	:
04293-3124	2MA0429-3123AB	2021.7297	2	<i>I</i>	Y	0.4991	181.9	1.7	q
04293-3124	2MA0429-3123AB	2022.7740	2	<i>I</i>	Y	0.5001	175.2	1.6	:
04327-3947	LHS1678	2019.8594	3	<i>I</i>	N	0.0470	2.8	4.1	
04327-3947	LHS1678	2019.9500	2	<i>I</i>	N	0.0415	2.4	4.9	
04327-3947	LHS1678	2020.0182	2	<i>I</i>	N	0.0415	2.8	4.3	
04327-3947	LHS1678	2020.8369	2	<i>I</i>	N	0.0500	2.8	4.0	
04353-1607	LP775-031AB	2019.8571	2	<i>I</i>	N	0.0670	2.3	3.6	
04353-1607	LP775-031AB	2020.8237	4	<i>I</i>	N	0.0606	2.1	2.9	
04353-1607	LP775-031AB	2022.7742	2	<i>I</i>	N	0.0586	1.6	3.0	
04406-0912	HIP021765AB	2019.6191	2	<i>I</i>	Y	1.9103	192.4	0.6	*
04406-0912	HIP021765AB	2019.8571	2	<i>I</i>	Y	1.9052	192.7	0.1	*
04406-0912	HIP021765AB	2021.7299	2	<i>I</i>	Y	1.9797	194.2	0.5	*
04469-1117	2MA0446-1116AB	2019.6191	3	<i>I</i>	Y	1.5458	287.3	1.1	*
04469-1117	2MA0446-1116AB	2021.7299	2	<i>I</i>	Y	1.5380	288.1	0.9	*
04469-1117	2MA0446-1116AB	2022.1945	2	<i>I</i>	Y	1.5363	285.2	0.8	:
04488+1003	LEP0448+1003AB	2019.9498	2	<i>I</i>	Y	0.1075	302.5	0.4	q
04488+1003	LEP0448+1003AB	2020.1111	2	<i>I</i>	Y	0.0885	316.7	0.5	
04488+1003	LEP0448+1003AB	2020.8346	2	<i>I</i>	Y	0.0784	91.3	0.3	q
04488+1003	LEP0448+1003AB	2020.9244	2	<i>I</i>	Y	0.0824	103.0	0.3	
04488+1003	LEP0448+1003AB	2021.1594	2	<i>I</i>	Y	0.0720	132.8	0.3	
04488+1003	LEP0448+1003AB	2022.1945	2	<i>I</i>	Y	0.1207	275.1	0.4	q
04488+1003	LEP0448+1003AB	2022.6826	2	<i>I</i>	Y	0.1030	304.1	0.3	
04488+1003	LEP0448+1003AB	2022.8455	2	<i>I</i>	Y	0.0866	322.4	0.4	q

Table 4: Results of the SOAR speckle interferometry campaign for nearby M dwarfs. The meanings of columns 8–10 differ depending on whether or not the companion was resolved in that observation, hence the two lines in those columns’ headers. The “:” flag in the last column indicates highly uncertain results; the rest of the flags are described in §4.2.

04521-1058	LP716-010AB	2019.8571	3	<i>I</i>	Y	0.2393	51.3	2.6	
04521-1058	LP716-010AB	2020.1111	2	<i>I</i>	Y	0.2390	42.3	2.9	
04521-1058	LP716-010AB	2020.8237	3	<i>I</i>	Y	0.2443	31.9	2.8	
04521-1058	LP716-010AB	2021.1595	3	<i>I</i>	Y	0.2510	24.9	2.7	
04521-1058	LP716-010AB	2021.7299	2	<i>I</i>	Y	0.2614	18.6	2.9	
04521-1058	LP716-010AB	2022.1945	2	<i>I</i>	Y	0.2525	6.6	2.9	
04521-1058	LP716-010AB	2022.8452	4	<i>I</i>	Y	0.2537	358.5	2.6	q
04524-1649	LP776-025	2020.1110	3	<i>I</i>	N	0.0437	2.5	3.7	
04524-1649	LP776-025	2020.9271	2	<i>I</i>	N	0.0415	2.7	5.7	
04524-1649	LP776-025	2022.8452	2	<i>I</i>	N	0.0463	2.5	4.5	
05020+0959	LP476-207AB	2019.8569	2	<i>I</i>	Y	1.4293	143.6	0.9	*
05020+0959	LP476-207AB	2020.8346	2	<i>I</i>	Y	1.4300	142.9	1.0	*
05025-2115	GJ0185AB	2019.9497	2	<i>I</i>	Y	0.9787	0.6	1.6	*
05025-2115	GJ0185AB	2020.8237	2	<i>I</i>	Y	0.9976	3.7	1.6	*
05025-2115	GJ0185AB	2022.0470	2	<i>I</i>	Y	1.0133	7.9	1.5	*
05025-2115	GJ0185AB	2022.1946	2	<i>I</i>	Y	1.0229	8.0	1.6	*
05025-2115	GJ0185AB	2022.6827	2	<i>I</i>	Y	1.0384	9.7	2.1	q
05025-2115	GJ0185AB	2022.8425	2	<i>I</i>	Y	1.0374	10.0	1.7	*
05025-2115	GJ0185AB	2023.0090	2	<i>I</i>	Y	1.0420	10.5	1.6	*
05069-2135	BD-21-01074BC	2019.8595	2	<i>I</i>	Y	1.0803	98.4	0.7	*
05069-2135	BD-21-01074BC	2020.8237	2	<i>I</i>	Y	1.1047	95.5	0.7	*
05069-2135	BD-21-01074BC	2021.7299	2	<i>I</i>	Y	1.1281	92.8	0.6	*
05069-2135	BD-21-01074BC	2022.0470	2	<i>I</i>	Y	1.1279	92.2	0.7	*
05086-1810	GJ0190AB	2019.8595	2	<i>I</i>	Y	0.0307	28.3	0.0	
05086-1810	GJ0190AB	2019.9524	2	<i>I</i>	Y	0.0342	226.8	0.0	

Table 4: Results of the SOAR speckle interferometry campaign for nearby M dwarfs. The meanings of columns 8–10 differ depending on whether or not the companion was resolved in that observation, hence the two lines in those columns’ headers. The “:” flag in the last column indicates highly uncertain results; the rest of the flags are described in §4.2.

05086-1810	GJ0190AB	2020.1112	2	<i>I</i>	Y	0.0675	218.2	0.2	
05086-1810	GJ0190AB	2020.9271	2	<i>I</i>	Y	0.0410	224.5	0.0	
05086-1810	GJ0190AB	2021.1625	3	<i>I</i>	Y	0.0231	206.4	0.0	
05102-7236	HD271076AB	2019.9469	2	<i>I</i>	Y	0.5859	229.6	0.3	*
05102-7236	HD271076AB	2020.9271	2	<i>I</i>	Y	0.6264	225.1	0.3	
05174-3522	L449-001AB	2019.6138	2	<i>I</i>	Y	0.0454	154.5	0.7	
05174-3522	L449-001AB	2019.8595	2	<i>I</i>	Y	0.0525	0.4	0.7	
05174-3522	L449-001AB	2019.9497	2	<i>I</i>	Y	0.0688	350.9	0.9	
05174-3522	L449-001AB	2020.1112	2	<i>I</i>	Y	0.0360	320.7	0.8	
05174-3522	L449-001AB	2020.8370	2	<i>I</i>	Y	0.0284	315.8	0.1	
05174-3522	L449-001AB	2021.1598	2	<i>I</i>	Y	0.0211	258.3	0.8	:
05174-3522	L449-001AB	2021.3154	2	<i>I</i>	Y	0.0609	175.6	1.0	q
05174-3522	L449-001AB	2021.7299	2	<i>I</i>	Y	0.0463	158.4	0.9	
05174-3522	L449-001AB	2022.1946	2	<i>I</i>	Y	0.0541	155.0	0.9	q
05174-3522	L449-001AB	2022.6829	2	<i>I</i>	Y	0.0464	186.4	0.3	:
05174-3522	L449-001AB	2022.8451	2	<i>I</i>	Y	0.0662	162.8	0.9	q
05174-3522	L449-001AB	2023.0090	2	<i>I</i>	N	0.0415	2.9	5.4	
05257-0909	LP717-036AB	2019.8571	2	<i>I</i>	Y	0.7234	33.9	0.5	*
05257-0909	LP717-036AB	2020.8237	2	<i>I</i>	Y	0.7121	31.9	0.5	*
05257-0909	LP717-036AB	2022.1946	2	<i>I</i>	Y	0.6884	28.7	0.5	q
05282+0258	GJ1080AB	2019.7914	2	<i>I</i>	N	0.0677	2.6	4.3	
05282+0258	GJ1080AB	2019.8571	2	<i>I</i>	N	0.0534	2.5	3.9	
05282+0258	GJ1080AB	2019.9471	2	<i>I</i>	N	0.0415	2.7	4.9	
05282+0258	GJ1080AB	2020.9272	2	<i>I</i>	N	0.0415	3.1	5.0	
05322+0949	GJ0206AB	2019.7914	2	<i>I</i>	N	0.0636	2.7	4.7	

Table 4: Results of the SOAR speckle interferometry campaign for nearby M dwarfs. The meanings of columns 8–10 differ depending on whether or not the companion was resolved in that observation, hence the two lines in those columns’ headers. The “:” flag in the last column indicates highly uncertain results; the rest of the flags are described in §4.2.

05322+0949	GJ0206AB	2019.8571	2	<i>I</i>	N	0.0463	2.5	3.7	
05322+0949	GJ0206AB	2020.9272	2	<i>I</i>	N	0.0415	2.7	5.5	
05335-4257	SCR0533-4257AB	2019.6138	2	<i>I</i>	Y	0.0661	224.6	0.7	q
05335-4257	SCR0533-4257AB	2019.8594	2	<i>I</i>	Y	0.0252	38.0	0.0	:
05335-4257	SCR0533-4257AB	2019.9470	2	<i>I</i>	Y	0.0513	309.4	0.7	q
05335-4257	SCR0533-4257AB	2020.0182	2	<i>I</i>	Y	0.0664	284.0	0.5	q
05335-4257	SCR0533-4257AB	2020.1112	2	<i>I</i>	Y	0.0769	262.8	0.6	q
05335-4257	SCR0533-4257AB	2020.8370	2	<i>I</i>	Y	0.0766	251.5	0.5	
05335-4257	SCR0533-4257AB	2021.1598	2	<i>I</i>	Y	0.0292	269.5	0.2	
05335-4257	SCR0533-4257AB	2021.3154	2	<i>I</i>	Y	0.0562	298.9	0.6	q
05335-4257	SCR0533-4257AB	2021.7300	2	<i>I</i>	Y	0.0446	1.1	0.5	
05335-4257	SCR0533-4257AB	2022.1946	2	<i>I</i>	Y	0.0763	249.5	0.7	q
05335-4257	SCR0533-4257AB	2022.6829	2	<i>I</i>	Y	0.0625	287.5	0.0	:
05335-4257	SCR0533-4257AB	2022.8425	2	<i>I</i>	Y	0.0778	252.7	0.5	
05335-4257	SCR0533-4257AB	2023.0066	2	<i>I</i>	Y	0.0580	216.0	0.6	
05337+0157	LTT11675	2019.9471	2	<i>I</i>	N	0.0415	2.3	5.5	
05337+0157	LTT11675	2020.8373	2	<i>I</i>	N	0.0470	2.7	4.3	
05337+0157	LTT11675	2022.6827	2	<i>I</i>	N	0.0508	2.6	3.8	
05404+2448	GJ1083AB	2019.9471	2	<i>I</i>	Y	0.6042	83.5	0.3	
05404+2448	GJ1083AB	2020.8373	2	<i>I</i>	Y	0.6579	92.2	0.4	:
05450-2137	LP837-019AB	2019.8595	2	<i>I</i>	Y	0.1665	24.2	0.2	
05450-2137	LP837-019AB	2019.9497	2	<i>I</i>	Y	0.1632	22.8	0.1	
05450-2137	LP837-019AB	2020.1112	2	<i>I</i>	Y	0.1568	20.5	0.0	
05450-2137	LP837-019AB	2020.8370	2	<i>I</i>	Y	0.1113	5.0	0.2	
05450-2137	LP837-019AB	2021.1597	2	<i>I</i>	Y	0.0699	350.3	0.1	

Table 4: Results of the SOAR speckle interferometry campaign for nearby M dwarfs. The meanings of columns 8–10 differ depending on whether or not the companion was resolved in that observation, hence the two lines in those columns’ headers. The “:” flag in the last column indicates highly uncertain results; the rest of the flags are described in §4.2.

05450-2137	LP837-019AB	2021.3156	3	<i>I</i>	Y	0.0400	331.6	0.0	
05450-2137	LP837-019AB	2021.7517	2	<i>I</i>	Y	0.0612	261.3	0.0	
05450-2137	LP837-019AB	2022.1946	2	<i>I</i>	Y	0.1120	237.0	0.2	
05450-2137	LP837-019AB	2022.8425	2	<i>I</i>	Y	0.1506	43.5	0.2	
05532+2416	GJ0220AB	2019.8600	3	<i>I</i>	N	0.0492	2.5	4.1	
05532+2416	GJ0220AB	2020.9274	2	<i>I</i>	N	0.0415	2.8	4.7	
06049-3434	APCOL	2019.8595	2	<i>I</i>	N	0.0477	2.5	4.4	
06049-3434	APCOL	2020.8370	2	<i>I</i>	N	0.0492	2.9	4.3	
06109-4324	GJ1088	2020.1112	2	<i>I</i>	N	0.0450	2.6	4.0	
06109-4324	GJ1088	2020.9271	2	<i>I</i>	N	0.0415	3.0	5.2	
06109-4324	GJ1088	2021.7327	2	<i>I</i>	N	0.0525	2.7	4.4	
06112-0036	UPM0611-3433AB	2019.8596	2	<i>I</i>	N	0.0955	2.1	3.1	
06112-0036	UPM0611-3433AB	2020.8373	2	<i>I</i>	N	0.0656	1.8	2.6	:
06112-0036	UPM0611-3433AB	2022.1946	2	<i>I</i>	Y	0.1056	279.4	0.7	
06112-0036	UPM0611-3433AB	2022.7744	2	<i>I</i>	Y	0.1357	274.4	0.5	q
06112-0036	UPM0611-3433AB	2022.9302	2	<i>I</i>	Y	0.1352	274.2	0.5	:
06241-2655	UPM0624-2655AB	2019.8595	2	<i>I</i>	Y	0.1618	29.7	0.5	q
06241-2655	UPM0624-2655AB	2019.9524	2	<i>I</i>	Y	0.1569	26.1	0.4	
06241-2655	UPM0624-2655AB	2020.8372	2	<i>I</i>	Y	0.0559	294.3	0.3	q
06241-2655	UPM0624-2655AB	2020.9244	2	<i>I</i>	Y	0.0538	267.3	0.5	
06241-2655	UPM0624-2655AB	2021.0780	2	<i>I</i>	Y	0.0574	215.1	0.6	q
06241-2655	UPM0624-2655AB	2021.3156	2	<i>I</i>	Y	0.0691	154.7	0.5	
06241-2655	UPM0624-2655AB	2021.7327	2	<i>I</i>	Y	0.1078	99.0	0.5	q
06241-2655	UPM0624-2655AB	2022.1290	2	<i>I</i>	Y	0.1433	75.1	0.5	q
06241-2655	UPM0624-2655AB	2022.2874	2	<i>I</i>	Y	0.1541	68.0	0.5	q

Table 4: Results of the SOAR speckle interferometry campaign for nearby M dwarfs. The meanings of columns 8–10 differ depending on whether or not the companion was resolved in that observation, hence the two lines in those columns’ headers. The “:” flag in the last column indicates highly uncertain results; the rest of the flags are described in §4.2.

06241-2655	UPM0624-2655AB	2022.8427	2	<i>I</i>	Y	0.1730	48.3	0.4	q
06242-0017	G106-045AB	2019.8599	4	<i>I</i>	Y	0.0248	36.4	0.2	
06242-0017	G106-045AB	2019.9473	2	<i>I</i>	N	0.0458	2.0	4.0	
06242-0017	G106-045AB	2020.1115	2	<i>I</i>	Y	0.0453	108.2	0.4	
06242-0017	G106-045AB	2020.8373	2	<i>I</i>	Y	0.0954	133.4	0.0	
06242-0017	G106-045AB	2020.9246	2	<i>I</i>	Y	0.1014	136.4	0.0	
06242-0017	G106-045AB	2021.1595	2	<i>I</i>	Y	0.1090	138.7	0.0	
06242-0017	G106-045AB	2021.7327	2	<i>I</i>	Y	0.1044	143.1	0.1	
06242-0017	G106-045AB	2022.1946	2	<i>I</i>	Y	0.0747	151.3	0.1	
06242-0017	G106-045AB	2022.2875	2	<i>I</i>	Y	0.0667	155.1	0.0	
06242-0017	G106-045AB	2022.7744	1	<i>I</i>	N	0.0427	1.9	4.2	
06242-0017	G106-045AB	2022.9302	2	<i>I</i>	N	0.0553	2.5	3.8	
06293-0248	GJ0234AB	2019.8599	2	<i>I</i>	Y	1.2022	23.3	2.4	*
06293-0248	GJ0234AB	2020.8373	2	<i>I</i>	Y	1.3361	32.0	2.4	*
06293-0248	GJ0234AB	2021.7327	2	<i>I</i>	Y	1.3881	39.0	2.1	*
06293-0248	GJ0234AB	2022.2875	2	<i>I</i>	Y	1.3894	43.2	2.3	*
06308-7643	SCR0630-7643AB	2019.9528	4	<i>I</i>	Y	1.3167	89.4	0.2	*
06308-7643	SCR0630-7643AB	2020.9272	2	<i>I</i>	Y	1.3067	92.8	0.3	*
06308-7643	SCR0630-7643AB	2022.1971	2	<i>I</i>	Y	1.2884	97.8	0.1	*
06315-8812	SCR0631-8811AB	2019.9469	2	<i>I</i>	Y	0.1195	330.8	0.6	q
06315-8812	SCR0631-8811AB	2020.0183	1	<i>I</i>	Y	0.1331	330.5	0.8	:
06315-8812	SCR0631-8811AB	2020.8346	3	<i>I</i>	Y	0.0757	348.2	0.0	:
06315-8812	SCR0631-8811AB	2021.0781	2	<i>I</i>	Y	0.0343	21.0	0.0	:
06315-8812	SCR0631-8811AB	2021.3157	2	<i>I</i>	Y	0.0386	156.9	0.0	
06315-8812	SCR0631-8811AB	2022.1949	2	<i>I</i>	Y	0.1633	0.2	0.4	

Table 4: Results of the SOAR speckle interferometry campaign for nearby M dwarfs. The meanings of columns 8–10 differ depending on whether or not the companion was resolved in that observation, hence the two lines in those columns’ headers. The “:” flag in the last column indicates highly uncertain results; the rest of the flags are described in §4.2.

06315-8812	SCR0631-8811AB	2022.7742	2	<i>I</i>	Y	0.2056	5.7	0.3	:
06323-0943	UPM0632-0943AB	2019.8596	2	<i>I</i>	Y	0.2180	62.0	0.4	q
06323-0943	UPM0632-0943AB	2020.1115	2	<i>I</i>	Y	0.2254	62.0	0.4	q
06323-0943	UPM0632-0943AB	2020.8372	2	<i>I</i>	Y	0.2372	62.2	0.4	
06323-0943	UPM0632-0943AB	2022.7744	2	<i>I</i>	Y	0.2590	62.7	0.4	
06354-0403	2MA0635-0403AB	2019.8599	3	<i>I</i>	Y	0.0952	175.5	0.4	
06354-0403	2MA0635-0403AB	2019.9473	2	<i>I</i>	Y	0.0813	175.5	0.3	
06354-0403	2MA0635-0403AB	2020.1115	2	<i>I</i>	Y	0.0584	175.9	0.0	
06354-0403	2MA0635-0403AB	2020.8373	2	<i>I</i>	Y	0.0428	165.0	0.0	
06354-0403	2MA0635-0403AB	2021.1595	2	<i>I</i>	Y	0.0582	170.4	0.0	
06354-0403	2MA0635-0403AB	2022.1946	2	<i>I</i>	Y	0.1485	170.7	0.3	
06354-0403	2MA0635-0403AB	2022.7744	2	<i>I</i>	Y	0.1413	172.7	0.2	q
06363-4000	LP381-004AB	2019.8597	2	<i>I</i>	Y	0.1782	73.2	2.3	q
06363-4000	LP381-004AB	2019.9524	2	<i>I</i>	Y	0.1720	73.7	2.3	q
06363-4000	LP381-004AB	2020.8372	2	<i>I</i>	Y	0.0858	79.7	2.1	
06363-4000	LP381-004AB	2021.0780	2	<i>I</i>	N	0.0415	2.6	5.4	
06363-4000	LP381-004AB	2021.7300	2	<i>I</i>	N	0.0432	2.3	4.1	
06363-4000	LP381-004AB	2022.1947	2	<i>I</i>	Y	0.0842	241.9	2.6	
06363-4000	LP381-004AB	2022.2874	2	<i>I</i>	Y	0.0942	243.9	2.4	q
06363-4000	LP381-004AB	2022.8425	2	<i>I</i>	Y	0.1522	247.8	2.3	q
06396-2102	LP780-032AB	2019.8596	2	<i>I</i>	Y	0.5306	249.7	0.3	
06396-2102	LP780-032AB	2020.1115	2	<i>I</i>	Y	0.5301	252.1	0.1	q
06396-2102	LP780-032AB	2020.8372	2	<i>I</i>	Y	0.5303	259.1	0.2	q
06396-2102	LP780-032AB	2021.7327	2	<i>I</i>	Y	0.5318	267.6	0.3	q
06396-2102	LP780-032AB	2023.0070	2	<i>I</i>	Y	0.5376	279.5	0.2	q

Table 4: Results of the SOAR speckle interferometry campaign for nearby M dwarfs. The meanings of columns 8–10 differ depending on whether or not the companion was resolved in that observation, hence the two lines in those columns’ headers. The “:” flag in the last column indicates highly uncertain results; the rest of the flags are described in §4.2.

06437-2625	LTT02631AB	2019.8596	2	<i>I</i>	N	0.0477	2.4	3.8	
06437-2625	LTT02631AB	2020.8372	2	<i>I</i>	N	0.0508	2.5	3.9	
06437-2625	LTT02631AB	2021.7327	2	<i>I</i>	N	0.0516	2.6	4.1	
06523-0510	GJ0250BC	2019.9473	2	<i>I</i>	N	0.0415	2.0	5.0	
06579-4417	GJ0257AB	2019.7915	2	<i>I</i>	Y	2.6808	243.2	1.3	
06579-4417	GJ0257AB	2019.9471	3	<i>I</i>	Y	2.6891	243.0	0.0	*
06579-4417	GJ0257AB	2020.1115	2	<i>I</i>	Y	2.6961	242.9	0.0	*
06579-4417	GJ0257AB	2020.8372	2	<i>I</i>	Y	2.7438	242.3	0.0	*
06579-4417	GJ0257AB	2020.9957	3	<i>I</i>	Y	2.7504	242.2	0.0	*
06579-4417	GJ0257AB	2021.3156	2	<i>I</i>	Y	2.7712	241.9	0.1	*
06579-4417	GJ0257AB	2021.7300	2	<i>I</i>	Y	2.7839	241.5	0.0	*
06579-4417	GJ0257A	2021.7518	2	<i>I</i>	N	0.0485	2.5	4.2	
06579-4417	GJ0257B	2021.7518	2	<i>I</i>	N	0.0463	2.6	4.0	
06597-5623	SCR0659-5622AB	2019.8571	2	<i>I</i>	Y	0.2314	142.4	0.0	
06597-5623	SCR0659-5622AB	2020.1111	2	<i>I</i>	Y	0.2326	141.4	0.1	
06597-5623	SCR0659-5622AB	2020.8374	2	<i>I</i>	Y	0.2321	137.5	0.0	
06597-5623	SCR0659-5622AB	2022.1948	2	<i>I</i>	Y	0.2172	130.3	0.1	
07028-6103	SCR0702-6102AB	2019.8571	3	<i>I</i>	Y	0.0753	26.5	0.0	:
07028-6103	SCR0702-6102AB	2019.9475	4	<i>I</i>	Y	0.0776	16.2	0.4	
07028-6103	SCR0702-6102AB	2020.0182	2	<i>I</i>	Y	0.0928	358.1	0.2	:
07028-6103	SCR0702-6102AB	2020.1111	2	<i>I</i>	Y	0.0635	7.4	0.3	:
07028-6103	SCR0702-6102AB	2020.8374	2	<i>I</i>	Y	0.0644	12.7	0.5	:
07028-6103	SCR0702-6102AB	2020.9246	4	<i>I</i>	Y	0.0509	348.5	0.0	
07028-6103	SCR0702-6102AB	2020.9957	2	<i>I</i>	Y	0.0601	344.7	0.0	:
07028-6103	SCR0702-6102AB	2021.3156	3	<i>I</i>	Y	0.0740	297.8	0.4	

Table 4: Results of the SOAR speckle interferometry campaign for nearby M dwarfs. The meanings of columns 8–10 differ depending on whether or not the companion was resolved in that observation, hence the two lines in those columns’ headers. The “:” flag in the last column indicates highly uncertain results; the rest of the flags are described in §4.2.

07028-6103	SCR0702-6102AB	2021.7545	2	<i>I</i>	Y	0.0844	258.8	0.0	
07028-6103	SCR0702-6102AB	2022.1292	2	<i>I</i>	Y	0.0883	45.0	0.0	:
07028-6103	SCR0702-6102AB	2022.2902	4	<i>I</i>	Y	0.0874	28.4	0.2	
07028-6103	SCR0702-6102AB	2022.8428	3	<i>I</i>	Y	0.0504	318.0	0.0	:
07043-1031	GJ0263AB	2019.8599	2	<i>I</i>	Y	0.0492	0.5	0.5	q
07043-1031	GJ0263AB	2019.9525	2	<i>I</i>	Y	0.0504	348.4	0.0	
07043-1031	GJ0263AB	2020.1115	2	<i>I</i>	Y	0.0567	329.3	0.6	
07043-1031	GJ0263AB	2020.8372	2	<i>I</i>	Y	0.1082	289.7	0.5	q
07043-1031	GJ0263AB	2021.0780	2	<i>I</i>	Y	0.1226	283.6	0.6	q
07043-1031	GJ0263AB	2021.3156	2	<i>I</i>	Y	0.1345	278.8	0.6	q
07043-1031	GJ0263AB	2021.7327	2	<i>I</i>	Y	0.1382	271.5	0.6	q
07043-1031	GJ0263AB	2022.1946	2	<i>I</i>	Y	0.0939	261.1	0.6	q
07043-1031	GJ0263AB	2022.8428	2	<i>I</i>	Y	0.0733	60.9	0.5	q
07096-5704	APM0089AB	2019.8571	2	<i>I</i>	N	0.0618	2.3	3.2	
07096-5704	APM0089AB	2020.1111	2	<i>I</i>	N	0.0562	2.3	3.4	
07096-5704	APM0089AB	2020.9957	2	<i>I</i>	Y	0.0351	70.9	0.1	
07096-5704	APM0089AB	2021.7545	2	<i>I</i>	Y	0.0361	102.6	0.0	
07096-5704	APM0089AB	2022.1292	2	<i>I</i>	Y	0.0312	122.4	0.0	
07096-5704	APM0089AB	2022.2902	2	<i>I</i>	Y	0.0293	199.5	0.0	
07096-5704	APM0089AB	2022.8427	2	<i>I</i>	Y	0.0295	132.9	0.0	
07096-5704	APM0089AB	2022.9329	2	<i>I</i>	Y	0.0301	175.7	0.0	
07200-0847	WIS0720-0846AB	2019.9473	2	<i>I</i>	N	0.0474	1.8	3.4	
07200-0847	WIS0720-0846AB	2020.8373	2	<i>I</i>	N	0.1086	1.4	1.4	:
07240-8015	SCR0723-8015AB	2019.9469	3	<i>I</i>	N	0.0448	1.6	3.0	
07240-8015	SCR0723-8015AB	2020.1113	2	<i>I</i>	N	0.0875	1.7	2.8	:

Table 4: Results of the SOAR speckle interferometry campaign for nearby M dwarfs. The meanings of columns 8–10 differ depending on whether or not the companion was resolved in that observation, hence the two lines in those columns’ headers. The “:” flag in the last column indicates highly uncertain results; the rest of the flags are described in §4.2.

07240-8015	SCR0723-8015AB	2020.8347	2	<i>I</i>	N	0.1312	1.6	1.9	:
07274+0514	GJ0273AB	2020.8373	2	<i>I</i>	N	0.0432	2.6	4.6	
07274+0514	GJ0273AB	2020.9247	2	<i>I</i>	N	0.0415	2.7	5.4	
07282-1848	LHS1918AB	2019.8599	2	<i>I</i>	Y	0.5315	210.6	1.5	q
07282-1848	LHS1918AB	2020.1115	2	<i>I</i>	Y	0.5315	213.2	1.4	q
07282-1848	LHS1918AB	2020.8373	2	<i>I</i>	Y	0.5300	221.0	1.5	q
07282-1848	LHS1918AB	2022.1947	2	<i>I</i>	Y	0.5280	235.3	1.5	q
07289-3015	GJ2060AB	2019.7916	2	<i>I</i>	Y	0.2946	191.1	1.2	q
07289-3015	GJ2060AB	2020.1115	3	<i>I</i>	Y	0.2365	196.4	1.2	q
07289-3015	GJ2060AB	2020.8374	2	<i>I</i>	N	0.0463	2.7	4.2	
07289-3015	GJ2060AB	2021.3157	2	<i>I</i>	Y	0.1608	137.0	1.4	q
07289-3015	GJ2060AB	2022.8427	2	<i>I</i>	Y	0.3908	161.3	1.2	q
07334-2749	SCR0733-2749AB	2019.8599	2	<i>I</i>	Y	0.4295	232.9	0.2	:
07334-2749	SCR0733-2749AB	2020.1115	2	<i>I</i>	Y	0.4270	233.8	0.4	:
07334-2749	SCR0733-2749AB	2022.8427	2	<i>I</i>	Y	0.4051	245.3	0.3	:
07364+0705	G089-032AB	2019.9473	2	<i>I</i>	Y	0.6400	269.3	0.3	q
07364+0705	G089-032AB	2020.8373	2	<i>I</i>	Y	0.7217	279.0	0.6	q
07364+0705	G089-032AB	2022.8456	2	<i>I</i>	Y	0.8572	294.9	0.5	q
07402-4258	SCR0740-4257	2019.8597	2	<i>I</i>	N	0.0492	2.7	3.9	
07402-4258	SCR0740-4257	2020.1116	2	<i>I</i>	N	0.0500	2.6	3.9	
07402-4258	SCR0740-4257	2020.9246	2	<i>I</i>	N	0.0415	2.7	5.0	
07549-2920	LHS1955AB	2019.8599	2	<i>I</i>	Y	0.8554	17.9	0.3	*
07549-2920	LHS1955AB	2020.8374	2	<i>I</i>	Y	0.8348	12.2	0.3	*
07549-2920	LHS1955AB	2022.1294	2	<i>I</i>	Y	0.8055	4.4	0.3	
07575-7115	SCR0757-7114AB	2019.8572	2	<i>I</i>	N	0.0562	2.6	4.0	

Table 4: Results of the SOAR speckle interferometry campaign for nearby M dwarfs. The meanings of columns 8–10 differ depending on whether or not the companion was resolved in that observation, hence the two lines in those columns’ headers. The “:” flag in the last column indicates highly uncertain results; the rest of the flags are described in §4.2.

07575-7115	SCR0757-7114AB	2020.8346	2	<i>I</i>	N	0.0516	2.7	3.9	
07575-7115	SCR0757-7114AB	2022.1293	2	<i>I</i>	N	0.0525	2.8	4.2	
08030-8330	GAI0802-8330AB	2019.8573	4	<i>I</i>	Y	0.1168	152.0	0.0	:
08030-8330	GAI0802-8330AB	2019.9469	4	<i>I</i>	Y	0.1232	151.8	0.5	
08030-8330	GAI0802-8330AB	2020.1113	2	<i>I</i>	Y	0.1328	134.5	0.0	:
08030-8330	GAI0802-8330AB	2020.8346	3	<i>I</i>	Y	0.1373	139.2	0.0	:
08030-8330	GAI0802-8330AB	2021.0781	2	<i>I</i>	Y	0.1512	134.5	0.4	
08030-8330	GAI0802-8330AB	2022.1949	2	<i>I</i>	Y	0.1389	119.8	0.4	:
08030-8330	GAI0802-8330AB	2022.9330	2	<i>I</i>	Y	0.1220	104.4	0.4	:
08083-7302	LEP0808-7301AC	2019.9528	3	<i>I</i>	Y	0.2798	343.5	0.5	:
08083-7302	LEP0808-7301AC	2020.1113	2	<i>I</i>	Y	0.2778	343.9	0.5	:
08083-7302	LEP0808-7301AC	2021.1599	2	<i>I</i>	Y	0.3024	348.5	0.5	
08083-7302	LEP0808-7301AC	2022.0474	2	<i>I</i>	Y	0.3092	353.0	0.5	:
08083-7302	LEP0808-7301AC	2022.8429	2	<i>I</i>	Y	0.3138	355.3	0.5	:
08107-1348	GJ0297.2BC	2019.9501	2	<i>I</i>	Y	0.8242	284.7	1.7	*
08107-1348	GJ0297.2BC	2022.2876	2	<i>I</i>	Y	0.7458	285.4	1.7	q
08120+0846	GJ0299	2019.9474	2	<i>I</i>	N	0.0415	2.4	4.8	
08120+0846	GJ0299	2021.0780	2	<i>I</i>	N	0.0415	2.1	5.1	
08132-1354	GJ0301AB	2022.2876	2	<i>I</i>	Y	1.3279	125.7	0.6	*
08152-2344	UPM0815-2344AB	2019.9528	2	<i>I</i>	N	0.0415	2.8	4.9	
08152-2344	UPM0815-2344AB	2020.9274	2	<i>I</i>	N	0.0415	2.8	5.4	
08152-2344	UPM0815-2344AB	2022.1294	2	<i>I</i>	N	0.0470	2.8	4.2	
08202+0532	LEP0820+0532	2019.9474	2	<i>I</i>	N	0.0415	3.0	5.2	
08202+0532	LEP0820+0532	2021.0781	2	<i>I</i>	N	0.0415	2.4	5.1	
08228-5727	LHS2005AB	2020.1113	2	<i>I</i>	Y	1.2393	177.5	2.8	*

Table 4: Results of the SOAR speckle interferometry campaign for nearby M dwarfs. The meanings of columns 8–10 differ depending on whether or not the companion was resolved in that observation, hence the two lines in those columns’ headers. The “:” flag in the last column indicates highly uncertain results; the rest of the flags are described in §4.2.

08228-5727	LHS2005AB	2020.8374	2	<i>I</i>	Y	1.2704	179.2	2.6	*
08228-5727	LHS2005AB	2022.1948	2	<i>I</i>	Y	1.3220	182.0	2.7	*
08272-4459	LHS2010AB	2019.8597	3	<i>I</i>	N	0.0470	2.6	4.1	
08272-4459	LHS2010AB	2020.9274	2	<i>I</i>	N	0.0415	3.0	5.3	
08272-4459	LHS2010AB	2022.1293	2	<i>I</i>	N	0.0492	2.5	4.4	
08317+1924	GJ2069ACE	2019.9474	2	<i>I</i>	Y	0.3560	216.5	3.6	
08317+1924	GJ2069ACE	2020.9960	2	<i>I</i>	Y	0.3452	222.9	3.8	
08317+1924	GJ2069BD	2019.9474	2	<i>I</i>	Y	0.9271	177.9	0.8	*
08317+1924	GJ2069BD	2020.9960	1	<i>I</i>	Y	0.9036	176.1	1.0	
08373-2820	SCR0837-2819AB	2019.9501	2	<i>I</i>	Y	0.1219	246.5	0.5	q
08373-2820	SCR0837-2819AB	2020.1116	2	<i>I</i>	Y	0.1216	243.5	0.8	q
08373-2820	SCR0837-2819AB	2020.8374	3	<i>I</i>	Y	0.1055	237.4	0.7	:
08373-2820	SCR0837-2819AB	2021.1600	2	<i>I</i>	Y	0.0931	233.8	0.9	q
08373-2820	SCR0837-2819AB	2022.1949	2	<i>I</i>	Y	0.0686	220.1	0.7	
08373-2820	SCR0837-2819AB	2022.2823	2	<i>I</i>	Y	0.0696	216.0	0.8	:
08373-2820	SCR0837-2819AB	2022.8456	3	<i>I</i>	Y	0.0576	212.6	0.2	:
08380-5856	SCR0838-5855AB	2019.8572	2	<i>I</i>	Y	0.4781	348.7	1.7	q
08380-5856	SCR0838-5855AB	2020.1113	2	<i>I</i>	Y	0.4768	347.0	1.9	q
08380-5856	SCR0838-5855AB	2022.1948	2	<i>I</i>	Y	0.4324	327.6	1.9	q
08380-5856	SCR0838-5855AB	2022.9330	2	<i>I</i>	Y	0.4090	319.4	1.9	q
08386-2843	UPM0838-2843AB	2019.9501	2	<i>I</i>	Y	0.0478	98.4	0.0	
08386-2843	UPM0838-2843AB	2020.1116	2	<i>I</i>	Y	0.0303	167.5	0.1	:
08386-2843	UPM0838-2843AB	2020.8374	2	<i>I</i>	Y	0.0329	148.5	0.0	
08386-2843	UPM0838-2843AB	2020.9274	2	<i>I</i>	Y	0.0387	90.7	0.0	
08386-2843	UPM0838-2843AB	2021.1600	2	<i>I</i>	Y	0.0488	336.9	0.0	

Table 4: Results of the SOAR speckle interferometry campaign for nearby M dwarfs. The meanings of columns 8–10 differ depending on whether or not the companion was resolved in that observation, hence the two lines in those columns’ headers. The “:” flag in the last column indicates highly uncertain results; the rest of the flags are described in §4.2.

08386-2843	UPM0838-2843AB	2021.3157	2	<i>I</i>	Y	0.0502	286.9	0.0	
08386-2843	UPM0838-2843AB	2022.1949	2	<i>I</i>	Y	0.0271	192.3	0.0	
08386-2843	UPM0838-2843AB	2022.2823	2	<i>I</i>	Y	0.0359	118.0	0.0	
08386-2843	UPM0838-2843AB	2022.8456	2	<i>I</i>	Y	0.0350	232.6	0.0	
08386-2843	UPM0838-2843AB	2023.0066	2	<i>I</i>	Y	0.0374	105.4	0.0	
08427+0935	GJ0319AC	2019.9474	2	<i>I</i>	Y	1.6403	33.0	2.8	*
08528-6609	SCR0852-6608AB	2019.9475	2	<i>I</i>	Y	0.2944	46.1	0.3	
08528-6609	SCR0852-6608AB	2020.1113	2	<i>I</i>	Y	0.2924	45.9	0.1	:
08528-6609	SCR0852-6608AB	2022.0474	2	<i>I</i>	Y	0.2796	40.5	0.3	:
08539-1308	GJ0326AB	2019.9501	2	<i>I</i>	Y	0.8639	291.2	0.2	*
08539-1308	GJ0326AB	2020.0184	2	<i>I</i>	Y	0.8634	291.5	0.2	*
08539-1308	GJ0326AB	2020.1116	2	<i>I</i>	Y	0.8618	291.8	0.2	*
08539-1308	GJ0326AB	2020.8374	2	<i>I</i>	Y	0.8540	295.1	0.2	*
08539-1308	GJ0326AB	2020.9247	2	<i>I</i>	Y	0.8511	295.4	0.1	*
08539-1308	GJ0326AB	2021.0781	2	<i>I</i>	Y	0.8517	295.9	0.1	*
08539-1308	GJ0326AB	2021.1598	2	<i>I</i>	Y	0.8503	296.3	0.3	*
08545-0551	2MA0854-0551AB	2019.9474	2	<i>I</i>	Y	0.1612	266.9	3.1	q
08545-0551	2MA0854-0551AB	2020.0186	1	<i>I</i>	Y	0.1529	268.3	3.0	
08545-0551	2MA0854-0551AB	2020.1116	2	<i>I</i>	Y	0.1588	267.5	3.4	
08545-0551	2MA0854-0551AB	2022.1947	2	<i>I</i>	N	0.0415	2.1	4.9	
08545-0551	2MA0854-0551AB	2022.8456	2	<i>I</i>	Y	0.1088	295.1	3.2	
08545-0551	2MA0854-0551AB	2023.0094	3	<i>I</i>	N	0.0415	2.3	4.4	
08553-2352	LHS2071AB	2019.9501	2	<i>I</i>	Y	0.3299	219.1	2.5	q
08553-2352	LHS2071AB	2020.1116	2	<i>I</i>	Y	0.3168	222.7	2.5	q
08553-2352	LHS2071AB	2020.8374	2	<i>I</i>	Y	0.2912	231.0	2.4	q

Table 4: Results of the SOAR speckle interferometry campaign for nearby M dwarfs. The meanings of columns 8–10 differ depending on whether or not the companion was resolved in that observation, hence the two lines in those columns’ headers. The “:” flag in the last column indicates highly uncertain results; the rest of the flags are described in §4.2.

08553-2352	LHS2071AB	2022.1949	2	<i>I</i>	Y	0.2449	257.2	2.5	q
08553-2352	LHS2071AB	2022.8456	2	<i>I</i>	Y	0.2352	270.5	2.5	q
08571+1139	GJ0330AB	2021.1597	2	<i>I</i>	Y	0.7449	235.3	1.4	*
08582+1945	GJ1116AB	2019.9474	2	<i>I</i>	Y	2.5478	244.8	0.6	*
08582+1945	GJ1116AB	2020.1116	2	<i>I</i>	Y	2.5624	245.3	0.5	*
08582+1945	GJ1116AB	2020.9960	2	<i>I</i>	Y	2.6436	248.1	0.5	*
08582+1945	GJ1116AB	2021.0780	2	<i>I</i>	Y	2.6501	248.1	0.6	*
08582+1945	GJ1116AB	2021.1597	3	<i>I</i>	Y	2.6483	248.4	0.5	*
08589+0829	G041-014AB	2019.9474	2	<i>I</i>	Y	0.6730	91.1	0.6	*
08589+0829	G041-014AB	2021.0781	2	<i>I</i>	Y	0.5917	81.4	0.6	*
08589+0829	G041-014AB	2022.8456	2	<i>I</i>	Y	0.1001	343.6	0.6	q
09012+0157	LTT12366AC	2019.9474	2	<i>I</i>	Y	0.1870	147.9	1.3	q
09012+0157	LTT12366AC	2020.1116	2	<i>I</i>	Y	0.1819	148.8	1.2	q
09012+0157	LTT12366AC	2021.0781	2	<i>I</i>	Y	0.1126	152.6	1.2	q
09012+0157	LTT12366AC	2022.1947	2	<i>I</i>	N	0.0415	2.0	5.3	
09012+0157	LTT12366AC	2022.4407	2	<i>I</i>	Y	0.0373	309.8	1.1	:
09012+0157	LTT12366AC	2022.8456	2	<i>I</i>	Y	0.0788	320.1	1.3	q
09156-1036	LHS6167AB	2019.9502	2	<i>I</i>	Y	0.1715	283.3	0.3	q
09156-1036	LHS6167AB	2020.9958	2	<i>I</i>	Y	0.1456	62.1	0.0	
09156-1036	LHS6167AB	2021.3184	2	<i>I</i>	Y	0.1342	44.5	0.0	
09156-1036	LHS6167AB	2022.0471	2	<i>I</i>	Y	0.1368	358.6	0.2	
09291-2429	WT1637AB	2019.9502	2	<i>I</i>	Y	0.4203	199.1	0.1	
09291-2429	WT1637AB	2020.1117	2	<i>I</i>	Y	0.4184	199.0	0.0	
09291-2429	WT1637AB	2020.9958	2	<i>I</i>	Y	0.4190	197.2	0.1	:
09291-2429	WT1637AB	2022.4408	2	<i>I</i>	Y	0.4072	194.0	0.0	

Table 4: Results of the SOAR speckle interferometry campaign for nearby M dwarfs. The meanings of columns 8–10 differ depending on whether or not the companion was resolved in that observation, hence the two lines in those columns’ headers. The “:” flag in the last column indicates highly uncertain results; the rest of the flags are described in §4.2.

09313-1329	GJ0352AB	2020.9958	2	<i>I</i>	Y	0.3793	102.5	0.2	q
09313-1329	GJ0352AB	2022.1294	2	<i>I</i>	Y	0.4861	65.6	0.2	q
09313-1329	GJ0352AB	2023.0094	2	<i>I</i>	Y	0.5519	46.1	0.3	q
09314-1718	LP788-001AB	2019.9502	2	<i>I</i>	N	0.0415	1.3	3.9	
09314-1718	LP788-001AB	2021.3158	2	<i>I</i>	N	0.0700	2.2	2.6	
09370-2610	2MA0936-2610AB	2019.9502	2	<i>I</i>	Y	0.3906	31.2	0.4	q
09370-2610	2MA0936-2610AB	2020.9958	2	<i>I</i>	Y	0.3905	43.4	0.4	q
09370-2610	2MA0936-2610AB	2023.0094	2	<i>I</i>	Y	0.3817	67.3	0.4	q
09428-6853	GJ1128	2019.9528	2	<i>I</i>	N	0.0415	2.7	4.2	
09428-6853	GJ1128	2021.1573	2	<i>I</i>	N	0.0463	2.6	4.1	
09428-6853	GJ1128	2022.2825	2	<i>I</i>	N	0.0470	3.1	4.4	
09444-7359	WT0244AB	2019.8573	4	<i>I</i>	Y	0.3322	279.4	1.7	q
09444-7359	WT0244AB	2019.9530	4	<i>I</i>	Y	0.3284	278.1	1.5	:
09444-7359	WT0244AB	2021.0781	2	<i>I</i>	Y	0.3043	279.8	1.8	*
09444-7359	WT0244AB	2022.0474	2	<i>I</i>	Y	0.2834	280.2	1.7	q
09444-7359	WT0244AB	2023.0099	2	<i>I</i>	Y	0.2607	281.4	1.8	q
09449-1221	G161-071	2019.9502	2	<i>I</i>	N	0.0415	2.0	5.1	
09449-1221	G161-071	2021.1598	2	<i>I</i>	N	0.0508	3.0	4.1	
09449-1221	G161-071	2022.0471	2	<i>I</i>	N	0.0415	2.6	5.3	
09457-3902	LP462-119AB	2021.1575	2	<i>I</i>	Y	0.5951	40.4	0.5	q
09460-3254	WT2458	2019.9502	2	<i>I</i>	N	0.0415	2.1	5.3	
09460-3254	WT2458	2021.1575	2	<i>I</i>	N	0.0508	2.6	3.7	
09460-3254	WT2458	2022.4408	3	<i>I</i>	N	0.0508	2.3	3.8	
09507-1349	LP728-070AB	2019.9502	2	<i>I</i>	Y	0.3552	302.6	0.0	q
09507-1349	LP728-070AB	2020.1116	2	<i>I</i>	Y	0.3541	302.4	0.1	

Table 4: Results of the SOAR speckle interferometry campaign for nearby M dwarfs. The meanings of columns 8–10 differ depending on whether or not the companion was resolved in that observation, hence the two lines in those columns’ headers. The “:” flag in the last column indicates highly uncertain results; the rest of the flags are described in §4.2.

09507-1349	LP728-070AB	2021.1598	2	<i>I</i>	Y	0.3433	301.2	0.0	
09507-1349	LP728-070AB	2022.0471	2	<i>I</i>	Y	0.3283	300.5	0.0	
09532-0341	GJ0372AB	2019.9502	2	<i>I</i>	N	0.0415	1.8	4.8	
09532-0341	GJ0372AB	2021.0781	2	<i>I</i>	N	0.0415	0.0	5.5	
09554-2716	LP847-048	2019.9502	2	<i>I</i>	N	0.0415	2.5	5.4	
09554-2716	LP847-048	2020.9957	3	<i>I</i>	N	0.0415	2.4	5.4	
09586-4626	GJ0375AB	2019.9474	2	<i>I</i>	N	0.0415	2.9	5.6	
09586-4626	GJ0375AB	2020.9961	2	<i>I</i>	N	0.0415	2.8	5.1	
10069-1247	2MA1006-1246AB	2019.9503	2	<i>I</i>	Y	0.1801	202.5	0.0	
10069-1247	2MA1006-1246AB	2020.0184	2	<i>I</i>	Y	0.1883	205.7	0.0	:
10069-1247	2MA1006-1246AB	2021.1598	2	<i>I</i>	Y	0.2094	233.4	0.0	:
10069-1247	2MA1006-1246AB	2022.1951	2	<i>I</i>	Y	0.2298	254.1	0.0	
10069-1247	2MA1006-1246AB	2023.0094	2	<i>I</i>	Y	0.2396	268.5	0.0	
10121-0241	GJ0381AB	2019.9502	2	<i>I</i>	Y	0.0400	25.2	1.1	
10121-0241	GJ0381AB	2020.9960	2	<i>I</i>	Y	0.0714	270.1	1.0	q
10149-4709	LHS0281	2019.9528	3	<i>I</i>	N	0.0415	2.5	3.9	
10149-4709	LHS0281	2020.2004	2	<i>I</i>	N	0.0415	2.6	4.9	
10149-4709	LHS0281	2021.1600	2	<i>I</i>	N	0.0463	2.9	4.2	
10174-5354	TWA022AB	2019.9529	2	<i>I</i>	Y	0.1089	86.9	0.4	
10174-5354	TWA022AB	2020.9961	2	<i>I</i>	Y	0.0997	146.1	0.4	
10174-5354	TWA022AB	2021.3158	2	<i>I</i>	Y	0.0926	167.1	0.6	q
10174-5354	TWA022AB	2022.0472	2	<i>I</i>	Y	0.0799	230.7	0.5	
10174-5354	TWA022AB	2022.2825	2	<i>I</i>	Y	0.0854	251.8	0.4	
10174-5354	TWA022AB	2022.4409	2	<i>I</i>	Y	0.0855	265.0	0.6	q
10174-5354	TWA022AB	2023.0096	2	<i>I</i>	Y	0.0977	309.9	0.6	q

Table 4: Results of the SOAR speckle interferometry campaign for nearby M dwarfs. The meanings of columns 8–10 differ depending on whether or not the companion was resolved in that observation, hence the two lines in those columns’ headers. The “:” flag in the last column indicates highly uncertain results; the rest of the flags are described in §4.2.

10199-4149	L392-039BC	2019.9475	2	<i>I</i>	Y	0.1683	127.9	0.2	
10199-4149	L392-039BC	2020.0184	2	<i>I</i>	Y	0.1738	129.7	0.1	
10199-4149	L392-039BC	2020.9961	2	<i>I</i>	Y	0.2304	146.4	0.2	:
10199-4149	L392-039BC	2022.0472	2	<i>I</i>	Y	0.2752	157.8	0.1	q
10199-4149	L392-039BC	2022.4409	2	<i>I</i>	Y	0.2897	161.0	0.1	q
10199-4149	L392-039BC	2022.9331	2	<i>I</i>	Y	0.3046	164.5	0.2	q
10367+1522	2MA1036+1521AB	2022.1975	2	<i>I</i>	Y	0.7095	244.4	1.4	
10367+1522	2MA1036+1521AB	2019.9530	2	<i>I</i>	Y	0.7974	239.7	1.5	
10367+1522	2MA1036+1521AB	2020.9960	2	<i>I</i>	Y	0.7326	242.5	1.2	
10367+1522	2MA1036+1521BC	2019.9530	2	<i>I</i>	Y	0.0864	166.0	0.1	
10367+1522	2MA1036+1521BC	2020.9960	2	<i>I</i>	Y	0.1323	237.9	0.1	
10367+1522	2MA1036+1521BC	2022.1975	2	<i>I</i>	Y	0.1773	278.6	0.0	
10397-3755	LP465-084AB	2019.9475	2	<i>I</i>	Y	0.2952	240.6	1.2	q
10397-3755	LP465-084AB	2020.0184	2	<i>I</i>	Y	0.3049	238.3	1.2	q
10397-3755	LP465-084AB	2020.9961	2	<i>I</i>	Y	0.4412	216.3	1.2	q
10397-3755	LP465-084AB	2022.0472	2	<i>I</i>	Y	0.5730	204.2	1.3	q
10397-3755	LP465-084AB	2022.9331	2	<i>I</i>	Y	0.6808	197.1	1.3	q
10412-3654	GJ1135AB	2019.9475	2	<i>I</i>	Y	0.7867	35.2	2.1	*
10412-3654	GJ1135AB	2021.1626	2	<i>I</i>	Y	0.7758	26.3	2.2	*
10412-3654	GJ1135AB	2022.9331	2	<i>I</i>	Y	0.7711	12.7	2.2	q
10427-2416	LP848-050AB	2020.9958	2	<i>I</i>	N	0.0600	0.5	1.3	:
10427-2416	LP848-050AB	2022.4463	2	<i>I</i>	N	0.0643	2.0	2.6	
10430-0913	WT1827AB	2019.9503	2	<i>I</i>	Y	0.5752	136.2	2.0	*
10430-0913	WT1827AB	2021.1575	2	<i>I</i>	Y	0.5991	128.7	2.1	q
10430-0913	WT1827AB	2022.4462	2	<i>I</i>	Y	0.6060	122.1	2.1	q

Table 4: Results of the SOAR speckle interferometry campaign for nearby M dwarfs. The meanings of columns 8–10 differ depending on whether or not the companion was resolved in that observation, hence the two lines in those columns’ headers. The “:” flag in the last column indicates highly uncertain results; the rest of the flags are described in §4.2.

10482-1120	LHS0292	2019.9503	3	<i>I</i>	N	0.0415	2.5	4.8	
10482-1120	LHS0292	2022.1951	2	<i>I</i>	N	0.0450	2.2	3.7	
10482-3956	DEN1048-3956	2019.9475	2	<i>I</i>	N	0.0415	2.3	4.6	
10482-3956	DEN1048-3956	2022.0472	3	<i>I</i>	N	0.0415	1.8	4.0	
10547-0719	LTT04004AB	2019.9503	2	<i>I</i>	Y	0.8709	74.8	0.9	*
10547-0719	LTT04004AB	2021.1575	2	<i>I</i>	Y	0.8741	77.5	0.8	*
10547-0719	LTT04004AB	2022.4408	2	<i>I</i>	Y	0.8664	80.7	0.9	*
10553-7356	WIS1055-7356AB	2020.2006	3	<i>I</i>	N	0.0663	0.0	2.0	:
10553-7356	WIS1055-7356AB	2021.1573	2	<i>I</i>	Y	0.0589	5.2	0.0	
10553-7356	WIS1055-7356AB	2022.0474	2	<i>I</i>	Y	0.0687	5.8	0.0	:
10553-7356	WIS1055-7356AB	2022.2825	2	<i>I</i>	Y	0.0631	9.2	0.5	:
10553-7356	WIS1055-7356AB	2022.4434	2	<i>I</i>	Y	0.0378	5.9	0.0	:
10553-7356	WIS1055-7356AB	2023.0099	2	<i>I</i>	N	0.0615	0.0	0.0	:
10565+0701	GJ0406	2019.9530	2	<i>I</i>	N	0.0415	2.7	4.9	
10565+0701	GJ0406	2021.1627	2	<i>I</i>	N	0.0450	2.7	4.5	:
10565+0701	GJ0406	2022.4407	2	<i>I</i>	N	0.0437	2.4	4.2	
10581-5525	GAI1058-5525AB	2020.1117	2	<i>I</i>	Y	0.0949	9.9	0.0	
10581-5525	GAI1058-5525AB	2020.9961	2	<i>I</i>	Y	0.0740	52.1	0.3	:
10581-5525	GAI1058-5525AB	2021.3159	4	<i>I</i>	N	0.0543	2.3	3.5	
10581-5525	GAI1058-5525AB	2022.0472	2	<i>I</i>	Y	0.0793	174.2	0.0	:
10581-5525	GAI1058-5525AB	2022.2825	2	<i>I</i>	Y	0.0939	185.1	0.0	
10581-5525	GAI1058-5525AB	2023.0096	2	<i>I</i>	Y	0.0881	212.5	0.2	
11307-0806	LP672-042	2021.1576	2	<i>I</i>	N	0.0463	2.7	4.4	
11307-0806	LP672-042	2022.1294	2	<i>I</i>	N	0.0508	2.9	4.4	
11307-0806	LP672-042	2022.4462	2	<i>I</i>	N	0.0463	2.8	4.3	

Table 4: Results of the SOAR speckle interferometry campaign for nearby M dwarfs. The meanings of columns 8–10 differ depending on whether or not the companion was resolved in that observation, hence the two lines in those columns’ headers. The “:” flag in the last column indicates highly uncertain results; the rest of the flags are described in §4.2.

11311-1457	LHS0306	2019.9503	2	<i>I</i>	N	0.0415	2.0	4.9	
11311-1457	LHS0306	2021.1577	2	<i>I</i>	N	0.0525	2.6	3.7	
11311-1457	LHS0306	2022.0472	2	<i>I</i>	N	0.0415	2.4	4.3	
11354-3232	GJ0433	2019.5359	2	<i>I</i>	N	0.0414	2.7	4.1	
11354-3232	GJ0433	2019.9529	2	<i>I</i>	N	0.0415	2.8	5.7	
11354-3232	GJ0433	2021.1577	2	<i>I</i>	N	0.0432	2.8	4.6	
12070-3501	SCR1206-3500AB	2019.5359	2	<i>I</i>	Y	0.6156	45.9	2.0	*
12070-3501	SCR1206-3500AB	2020.0186	2	<i>I</i>	Y	0.6310	45.7	1.9	*
12070-3501	SCR1206-3500AB	2022.2166	2	<i>I</i>	Y	0.6984	46.7	2.0	q
12107-2213	2MA1210-2213BC	2019.5359	2	<i>I</i>	Y	0.0221	123.0	1.3	:
12107-2213	2MA1210-2213BC	2020.1171	3	<i>I</i>	N	0.0508	2.5	4.0	
12107-2213	2MA1210-2213BC	2021.1627	3	<i>I</i>	N	0.0534	2.3	3.3	
12107-2213	2MA1210-2213BC	2022.1976	2	<i>I</i>	N	0.0458	1.9	3.6	
12143+0037	GJ1154AB	2020.0187	2	<i>I</i>	N	0.0415	2.7	4.6	
12143+0037	GJ1154AB	2021.1576	2	<i>I</i>	N	0.0543	2.8	3.7	
12143+0037	GJ1154AB	2022.1295	2	<i>I</i>	N	0.0534	2.4	4.0	
12201-1813	LP794-053AB	2019.5359	2	<i>I</i>	Y	0.1147	309.7	1.4	
12201-1813	LP794-053AB	2020.0187	2	<i>I</i>	Y	0.0969	311.1	0.7	:
12201-1813	LP794-053AB	2021.1602	2	<i>I</i>	N	0.0534	2.4	3.2	
12201-1813	LP794-053AB	2021.5674	2	<i>I</i>	N	0.0638	0.0	0.0	:
12201-1813	LP794-053AB	2022.1976	2	<i>I</i>	Y	0.0734	113.5	2.2	
12201-1813	LP794-053AB	2022.4410	2	<i>I</i>	Y	0.0666	117.4	0.8	:
12206-8226	NLTT30359AB	2019.5386	2	<i>I</i>	Y	0.1175	69.5	2.3	
12206-8226	NLTT30359AB	2020.1117	2	<i>I</i>	Y	0.1939	54.6	2.3	q
12206-8226	NLTT30359AB	2020.2006	2	<i>I</i>	Y	0.1981	53.0	2.2	q

Table 4: Results of the SOAR speckle interferometry campaign for nearby M dwarfs. The meanings of columns 8–10 differ depending on whether or not the companion was resolved in that observation, hence the two lines in those columns’ headers. The “:” flag in the last column indicates highly uncertain results; the rest of the flags are described in §4.2.

12206-8226	NLTT30359AB	2021.0782	2	<i>I</i>	Y	0.1375	34.5	2.3	q
12206-8226	NLTT30359AB	2021.3160	2	<i>I</i>	Y	0.0487	19.3	1.9	
12206-8226	NLTT30359AB	2021.5674	2	<i>I</i>	N	0.0415	2.9	3.2	
12206-8226	NLTT30359AB	2022.0474	2	<i>I</i>	Y	0.1517	63.6	2.1	q
12206-8226	NLTT30359AB	2022.2086	2	<i>I</i>	Y	0.1721	59.8	2.2	
12206-8226	NLTT30359AB	2022.4412	2	<i>I</i>	Y	0.1919	54.7	2.3	q
12206-8226	NLTT30359AB	2023.0099	2	<i>I</i>	Y	0.1903	44.6	2.2	q
12290+0826	GJ0469AB	2020.0188	2	<i>I</i>	Y	0.0719	69.8	1.2	
12290+0826	GJ0469AB	2021.1576	2	<i>I</i>	Y	0.2464	15.6	1.3	q
12290+0826	GJ0469AB	2022.1295	2	<i>I</i>	Y	0.3001	4.7	1.4	q
12296-5560	GJ1158	2020.0188	2	<i>I</i>	N	0.0420	2.9	3.4	
12296-5560	GJ1158	2021.0782	2	<i>I</i>	N	0.0415	1.3	4.7	
12296-5560	GJ1158	2022.4412	2	<i>I</i>	N	0.0477	2.4	4.1	
12300-3411	SCR1230-3411AB	2019.5359	2	<i>I</i>	Y	0.1260	56.3	2.0	q
12300-3411	SCR1230-3411AB	2020.0187	2	<i>I</i>	Y	0.1100	61.6	1.8	q
12300-3411	SCR1230-3411AB	2020.1171	3	<i>I</i>	Y	0.1003	64.0	1.7	q
12300-3411	SCR1230-3411AB	2021.1577	2	<i>I</i>	N	0.0583	2.5	3.3	
12300-3411	SCR1230-3411AB	2021.2451	2	<i>I</i>	Y	0.0508	227.5	1.8	
12300-3411	SCR1230-3411AB	2021.5674	2	<i>I</i>	Y	0.0662	244.3	1.0	:
12300-3411	SCR1230-3411AB	2022.2085	2	<i>I</i>	Y	0.0520	244.9	1.2	:
12300-3411	SCR1230-3411AB	2022.4410	2	<i>I</i>	N	0.0516	2.4	3.8	
12300-3411	SCR1230-3411AB	2023.0096	2	<i>I</i>	Y	0.0609	49.1	1.5	q
12335+0901	GJ0473AB	2020.0188	2	<i>I</i>	Y	0.7161	128.9	0.3	*
12335+0901	GJ0473AB	2021.1576	2	<i>I</i>	Y	0.3563	290.2	0.0	
12335+0901	GJ0473AB	2022.1295	2	<i>I</i>	Y	0.1955	204.8	0.1	

Table 4: Results of the SOAR speckle interferometry campaign for nearby M dwarfs. The meanings of columns 8–10 differ depending on whether or not the companion was resolved in that observation, hence the two lines in those columns’ headers. The “:” flag in the last column indicates highly uncertain results; the rest of the flags are described in §4.2.

12335+0901	GJ0473AB	2022.4410	2	<i>I</i>	Y	0.2670	178.9	0.2	
12336-4826	L327-121AB	2019.5333	2	<i>I</i>	Y	0.1151	355.8	0.4	q
12336-4826	L327-121AB	2020.0187	2	<i>I</i>	Y	0.1544	13.3	0.4	
12336-4826	L327-121AB	2020.1169	2	<i>I</i>	Y	0.1602	15.9	0.4	q
12336-4826	L327-121AB	2021.0782	2	<i>I</i>	Y	0.1958	34.3	0.4	q
12336-4826	L327-121AB	2021.3185	2	<i>I</i>	Y	0.1960	38.6	0.4	q
12336-4826	L327-121AB	2021.5674	2	<i>I</i>	Y	0.1897	42.6	0.3	
12336-4826	L327-121AB	2022.0475	2	<i>I</i>	Y	0.1677	52.3	0.4	q
12336-4826	L327-121AB	2022.4412	2	<i>I</i>	Y	0.1431	62.3	0.4	q
12336-4826	L327-121AB	2023.0098	2	<i>I</i>	Y	0.1035	87.4	0.4	q
12360-4556	GJ0477AB	2019.5333	2	<i>I</i>	N	0.0477	2.7	4.2	
12360-4556	GJ0477AB	2021.1600	2	<i>I</i>	N	0.0437	2.7	4.4	
12411-3843	SIP1241-3843AB	2019.5333	2	<i>I</i>	Y	0.2962	171.4	1.8	:
12411-3843	SIP1241-3843AB	2020.1171	3	<i>I</i>	Y	0.2992	174.0	2.2	:
12411-3843	SIP1241-3843AB	2021.2451	2	<i>I</i>	Y	0.3019	164.6	2.0	:
12411-3843	SIP1241-3843AB	2022.2173	2	<i>I</i>	Y	0.2985	158.6	1.8	:
12440-1615	LP796-001AB	2019.5359	2	<i>I</i>	Y	0.3377	88.9	0.0	
12440-1615	LP796-001AB	2020.0187	2	<i>I</i>	Y	0.3301	85.2	0.0	
12440-1615	LP796-001AB	2021.1602	2	<i>I</i>	Y	0.3072	75.7	0.0	
12440-1615	LP796-001AB	2021.5674	2	<i>I</i>	Y	0.2935	71.9	0.0	:
12440-1615	LP796-001AB	2022.0475	2	<i>I</i>	Y	0.2756	67.2	0.1	:
12440-1615	LP796-001AB	2022.4410	2	<i>I</i>	Y	0.2607	62.5	0.0	
12509-2121	LEHPM2-0174	2019.5359	2	<i>I</i>	N	0.0969	2.0	3.4	:
12509-2121	LEHPM2-0174	2020.1171	3	<i>I</i>	N	0.0875	2.0	2.7	
12509-2121	LEHPM2-0174	2021.1602	2	<i>I</i>	N	0.0829	1.9	1.9	:

Table 4: Results of the SOAR speckle interferometry campaign for nearby M dwarfs. The meanings of columns 8–10 differ depending on whether or not the companion was resolved in that observation, hence the two lines in those columns’ headers. The “:” flag in the last column indicates highly uncertain results; the rest of the flags are described in §4.2.

12560-1257	LP736-015AB	2019.5359	2	<i>I</i>	Y	0.0983	149.4	0.0	:
12560-1257	LP736-015AB	2020.1171	3	<i>I</i>	Y	0.0785	141.3	0.0	:
12560-1257	LP736-015AB	2021.1602	2	<i>I</i>	N	0.0750	2.1	2.3	
12560-1257	LP736-015AB	2022.0475	2	<i>I</i>	Y	0.0392	166.6	0.5	:
12560-1257	LP736-015AB	2022.4410	2	<i>I</i>	Y	0.0994	171.8	0.4	:
12560-1257	LP736-015AB	2023.0098	4	<i>I</i>	Y	0.1239	169.1	0.1	:
13008+1223	GJ0494AB	2022.4410	2	<i>I</i>	N	0.0437	2.5	4.5	
13132-4131	ER2	2019.5333	2	<i>I</i>	Y	0.0602	89.3	2.5	:
13132-4131	ER2	2020.0188	2	<i>I</i>	N	0.0415	3.3	4.3	
13132-4131	ER2	2020.1168	3	<i>I</i>	N	0.0485	2.5	4.0	
13132-4131	ER2	2021.1600	2	<i>I</i>	N	0.0477	2.9	4.1	
13143+1320	NLTT33370AB	2020.1173	4	<i>I</i>	Y	0.1717	96.4	0.1	
13143+1320	NLTT33370AB	2021.1576	2	<i>I</i>	Y	0.1363	121.4	0.4	:
13143+1320	NLTT33370AB	2022.1295	2	<i>I</i>	Y	0.0716	165.3	0.0	:
13143+1320	NLTT33370AB	2022.4410	2	<i>I</i>	Y	0.0624	189.6	0.0	
13168-1220	LP737-014AB	2019.5359	4	<i>I</i>	Y	0.1690	232.1	1.6	q
13168-1220	LP737-014AB	2020.0188	2	<i>I</i>	Y	0.1771	241.7	1.4	
13168-1220	LP737-014AB	2021.1602	2	<i>I</i>	Y	0.2036	261.6	1.5	q
13168-1220	LP737-014AB	2021.5674	2	<i>I</i>	Y	0.2120	267.5	1.4	q
13168-1220	LP737-014AB	2022.1976	2	<i>I</i>	Y	0.2294	275.6	1.5	q
13168-1220	LP737-014AB	2023.0098	2	<i>I</i>	Y	0.2478	284.7	1.4	q
13236-2555	LHS2729	2020.0188	2	<i>I</i>	N	0.0415	2.9	4.3	
13236-2555	LHS2729	2021.1602	2	<i>I</i>	N	0.0470	2.5	4.0	
13236-2555	LHS2729	2022.2167	2	<i>I</i>	N	0.0470	2.4	4.1	
13248-0504	G014-052AB	2019.5360	2	<i>I</i>	Y	0.6043	280.6	0.6	*

Table 4: Results of the SOAR speckle interferometry campaign for nearby M dwarfs. The meanings of columns 8–10 differ depending on whether or not the companion was resolved in that observation, hence the two lines in those columns’ headers. The “:” flag in the last column indicates highly uncertain results; the rest of the flags are described in §4.2.

13248-0504	G014-052AB	2020.1173	3	<i>I</i>	Y	0.5978	279.4	0.4	:
13248-0504	G014-052AB	2022.1296	2	<i>I</i>	Y	0.5648	275.8	0.5	q
13284-0222	GJ0512A	2019.5360	2	<i>I</i>	N	0.0477	2.2	3.4	
13284-0222	GJ0512B	2019.5360	2	<i>I</i>	N	0.0553	2.1	3.2	
13422-1600	LHS2783AB	2020.0188	2	<i>I</i>	Y	0.7370	17.7	1.0	q
13422-1600	LHS2783AB	2021.1602	2	<i>I</i>	Y	0.7787	14.2	1.0	*
13422-1600	LHS2783AB	2022.4467	2	<i>I</i>	Y	0.8200	10.6	1.0	*
13581-3938	SSS1358-3938	2019.5334	2	<i>I</i>	N	0.0636	2.3	4.1	
13581-3938	SSS1358-3938	2020.1172	2	<i>I</i>	N	0.0508	2.4	4.1	
13581-3938	SSS1358-3938	2021.1603	2	<i>I</i>	N	0.0485	2.5	3.9	
14041-6615	NLTT36064AB	2019.5386	2	<i>I</i>	Y	0.1709	32.1	3.9	:
14041-6615	NLTT36064AB	2020.1118	2	<i>I</i>	N	0.0492	2.4	4.2	
14041-6615	NLTT36064AB	2020.2006	3	<i>I</i>	N	0.0415	2.4	5.5	
14041-6615	NLTT36064AB	2021.1578	2	<i>I</i>	N	0.0457	2.7	4.3	
14041-6615	NLTT36064AB	2022.3073	2	<i>I</i>	Y	0.1628	30.8	3.8	
14041-6615	NLTT36064AB	2022.4412	2	<i>I</i>	Y	0.1589	30.8	4.0	
14120-4132	WT0460AB	2019.5334	4	<i>I</i>	Y	0.5334	182.1	3.2	*
14120-4132	WT0460AB	2020.1171	4	<i>I</i>	Y	0.5343	189.7	4.1	*
14120-4132	WT0460AB	2021.3185	4	<i>I</i>	Y	0.5231	204.6	4.0	
14120-4132	WT0460AB	2022.2168	2	<i>I</i>	Y	0.5060	216.7	4.1	q
14121-0035	LHS2875AB	2019.5360	2	<i>I</i>	Y	0.5392	170.8	1.1	*
14121-0035	LHS2875AB	2020.1176	3	<i>I</i>	Y	0.5286	170.5	1.0	q
14121-0035	LHS2875AB	2021.1631	2	<i>I</i>	Y	0.5046	170.9	1.0	*
14121-0035	LHS2875AB	2021.3186	2	<i>I</i>	Y	0.4995	170.6	1.1	q
14121-0035	LHS2875AB	2022.1296	2	<i>I</i>	Y	0.4766	170.7	1.0	q

Table 4: Results of the SOAR speckle interferometry campaign for nearby M dwarfs. The meanings of columns 8–10 differ depending on whether or not the companion was resolved in that observation, hence the two lines in those columns’ headers. The “:” flag in the last column indicates highly uncertain results; the rest of the flags are described in §4.2.

14155+0440	GJ1182AB	2019.5360	2	<i>I</i>	N	0.0606	2.3	3.1	:
14155+0440	GJ1182AB	2019.6127	3	<i>I</i>	N	0.0318	2.8	5.2	
14155+0440	GJ1182AB	2021.1631	2	<i>I</i>	N	0.0508	2.7	3.8	
14206-7516	SCR1420-7516AB	2019.5386	2	<i>I</i>	N	0.1920	1.7	2.5	:
14206-7516	SCR1420-7516AB	2020.2006	2	<i>I</i>	Y	0.0877	154.0	0.0	:
14206-7516	SCR1420-7516AB	2021.1578	2	<i>I</i>	Y	0.1024	181.4	0.0	
14206-7516	SCR1420-7516AB	2021.3160	2	<i>I</i>	Y	0.1025	185.0	0.0	
14206-7516	SCR1420-7516AB	2022.1981	2	<i>I</i>	Y	0.1034	206.4	0.0	
14206-7516	SCR1420-7516AB	2022.4412	2	<i>I</i>	Y	0.1047	213.0	0.0	
14341-1824	LHS5273AB	2020.1172	3	<i>I</i>	Y	0.1438	64.6	1.3	
14341-1824	LHS5273AB	2021.0784	2	<i>I</i>	Y	0.1379	68.1	1.4	q
14341-1824	LHS5273AB	2022.1296	2	<i>I</i>	Y	0.1041	80.1	1.4	q
14341-1824	LHS5273AB	2022.4437	3	<i>I</i>	Y	0.0902	84.5	1.6	q
14341-1824	LHS5273AB	2022.6816	3	<i>I</i>	Y	0.0695	86.9	0.0	:
14343-1231	GJ0555	2019.5387	2	<i>I</i>	N	0.0477	2.6	4.4	
14343-1231	GJ0555	2020.1174	2	<i>I</i>	N	0.0450	2.4	4.1	
14343-1231	GJ0555	2021.1604	2	<i>I</i>	N	0.0420	3.1	4.5	
14396-6050	PROXIMA	2020.1118	2	<i>I</i>	N	0.0437	2.8	4.4	
14396-6050	PROXIMA	2021.1578	2	<i>I</i>	N	0.0426	2.8	4.3	
14396-6050	PROXIMA	2021.2452	2	<i>I</i>	N	0.0437	2.7	4.5	
14396-6050	PROXIMA	2021.3160	2	<i>I</i>	N	0.0414	2.8	4.3	
14441-3427	SCR1444-3426	2020.1172	3	<i>I</i>	N	0.0508	2.6	3.5	
14441-3427	SCR1444-3426	2021.0784	2	<i>I</i>	N	0.0415	1.5	4.7	
14441-3427	SCR1444-3426	2022.2168	2	<i>I</i>	N	0.0492	2.4	3.8	
14540+2335	GJ0568AB	2021.1632	2	<i>I</i>	Y	0.4887	69.3	1.1	q

Table 4: Results of the SOAR speckle interferometry campaign for nearby M dwarfs. The meanings of columns 8–10 differ depending on whether or not the companion was resolved in that observation, hence the two lines in those columns’ headers. The “:” flag in the last column indicates highly uncertain results; the rest of the flags are described in §4.2.

14540+2335	GJ0568AB	2022.2881	2	<i>I</i>	Y	0.3740	58.1	1.0	q
14540+2335	GJ0568AB	2022.4437	2	<i>I</i>	Y	0.3590	56.1	1.0	q
14542-2042	LP801-025AB	2020.1172	2	<i>I</i>	Y	0.3018	351.4	1.1	q
14542-2042	LP801-025AB	2021.0784	2	<i>I</i>	Y	0.3060	341.9	1.2	q
14542-2042	LP801-025AB	2022.1296	2	<i>I</i>	Y	0.3097	332.3	1.1	:
14542-2042	LP801-025AB	2022.6816	2	<i>I</i>	Y	0.3095	327.9	1.1	:
14545+1606	GJ0569A	2021.1631	1	<i>I</i>	N	0.0444	2.7	4.4	
14545+1606	GJ0569AB	2021.1631	1	<i>I</i>	Y	4.9163	45.0	8.2	*
14545+1606	GJ0569BC	2019.5360	2	<i>I</i>	N	0.1312	2.0	2.0	:
14545+1606	GJ0569BC	2021.5675	4	<i>I</i>	N	0.0415	2.8	5.4	
14575-2125	GJ0570BC	2020.1172	2	<i>I</i>	Y	0.1120	194.7	1.4	q
14575-2125	GJ0570BC	2021.1604	2	<i>y</i>	Y	0.0470	280.2	1.7	q
14575-2125	GJ0570BC	2021.5647	2	<i>I</i>	Y	0.1927	210.1	1.3	q
14575-2125	GJ0570BC	2022.1979	3	<i>I</i>	Y	0.1357	223.8	1.4	q
15095-1547	GAI1509-1546AB	2020.1174	2	<i>I</i>	Y	0.5795	199.0	2.1	*
15095-1547	GAI1509-1546AB	2021.0784	2	<i>I</i>	Y	0.6068	199.2	2.2	*
15095-1547	GAI1509-1546AB	2022.1296	2	<i>I</i>	Y	0.6299	200.1	2.2	q
15157-0725	G151-037AB	2019.5387	2	<i>I</i>	Y	0.5390	26.2	0.1	
15157-0725	G151-037AB	2020.1119	2	<i>I</i>	Y	0.5311	28.2	0.0	
15157-0725	G151-037AB	2021.3187	2	<i>I</i>	Y	0.5112	33.2	0.0	
15157-0725	G151-037AB	2022.1296	2	<i>I</i>	Y	0.4969	36.8	0.2	
15192-1245	LHS3056AB	2020.1174	2	<i>I</i>	Y	0.1354	8.2	2.4	q
15192-1245	LHS3056AB	2021.0785	2	<i>I</i>	Y	0.1348	49.8	2.1	q
15192-1245	LHS3056AB	2022.1295	3	<i>I</i>	Y	0.1118	100.5	2.3	q
15192-1245	LHS3056AB	2022.3895	2	<i>I</i>	Y	0.1025	116.8	2.4	q

Table 4: Results of the SOAR speckle interferometry campaign for nearby M dwarfs. The meanings of columns 8–10 differ depending on whether or not the companion was resolved in that observation, hence the two lines in those columns’ headers. The “:” flag in the last column indicates highly uncertain results; the rest of the flags are described in §4.2.

15192-1245	LHS3056AB	2022.6844	3	<i>I</i>	Y	0.0830	141.7	2.5	
15194-0743	GJ0581	2019.5387	2	<i>I</i>	N	0.0450	2.5	4.4	
15194-0743	GJ0581	2021.1604	2	<i>I</i>	N	0.0420	2.8	4.5	
15194-0743	GJ0581	2022.2828	2	<i>I</i>	N	0.0444	2.5	4.1	
15248-4930	L264-018	2019.5363	4	<i>I</i>	N	0.0485	2.2	3.7	
15248-4930	L264-018	2020.1118	2	<i>I</i>	N	0.0534	2.6	4.4	
15248-4930	L264-018	2021.1632	2	<i>I</i>	N	0.0426	2.6	4.3	
15309-6801	NLTT40317AB	2019.5386	2	<i>I</i>	Y	0.3354	304.4	1.2	:
15309-6801	NLTT40317AB	2020.1119	2	<i>I</i>	Y	0.2936	305.1	1.2	q
15309-6801	NLTT40317AB	2021.1633	2	<i>I</i>	Y	0.2106	307.8	1.2	q
15309-6801	NLTT40317AB	2022.1982	3	<i>I</i>	Y	0.1146	313.1	1.5	
15309-6801	NLTT40317AB	2022.4412	2	<i>I</i>	Y	0.0921	313.1	1.4	q
15309-6801	NLTT40317AB	2022.6843	2	<i>I</i>	Y	0.0606	323.3	0.3	:
15319+2851	LHS3080AB	2019.6125	2	<i>I</i>	Y	0.0952	13.3	0.0	:
15319+2851	LHS3080AB	2021.3188	2	<i>I</i>	Y	0.1632	356.3	0.0	
15319+2851	LHS3080AB	2022.2828	3	<i>I</i>	Y	0.1618	348.8	0.1	
15421-1928	GJ0595AB	2020.1119	2	<i>I</i>	N	0.0470	2.4	4.1	
15457-4330	LTT06288AB	2019.5364	2	<i>I</i>	Y	0.2538	335.6	2.5	q
15457-4330	LTT06288AB	2020.1119	2	<i>I</i>	Y	0.2345	335.1	2.5	q
15457-4330	LTT06288AB	2021.1578	4	<i>I</i>	Y	0.1665	335.1	2.6	q
15457-4330	LTT06288AB	2022.1298	2	<i>I</i>	Y	0.0432	309.2	1.4	
15457-4330	LTT06288AB	2022.3073	2	<i>I</i>	Y	0.0425	332.9	2.2	:
15457-4330	LTT06288AB	2022.4437	3	<i>I</i>	N	0.0463	2.5	3.8	
15457-4330	LTT06288AB	2022.6818	2	<i>I</i>	N	0.0562	2.4	3.0	
15467-5535	SCR1546-5534AB	2019.5363	3	<i>I</i>	Y	0.2715	12.3	1.6	q

Table 4: Results of the SOAR speckle interferometry campaign for nearby M dwarfs. The meanings of columns 8–10 differ depending on whether or not the companion was resolved in that observation, hence the two lines in those columns’ headers. The “:” flag in the last column indicates highly uncertain results; the rest of the flags are described in §4.2.

15467-5535	SCR1546-5534AB	2020.1118	2	<i>I</i>	Y	0.2625	29.8	1.6	:
15467-5535	SCR1546-5534AB	2021.1632	2	<i>I</i>	Y	0.2240	68.6	1.6	q
15467-5535	SCR1546-5534AB	2021.3162	2	<i>I</i>	Y	0.2126	75.8	1.5	q
15467-5535	SCR1546-5534AB	2022.1298	2	<i>I</i>	Y	0.1496	134.4	1.4	q
15467-5535	SCR1546-5534AB	2022.3893	2	<i>I</i>	Y	0.1524	158.8	1.7	q
15467-5535	SCR1546-5534AB	2022.6818	2	<i>I</i>	Y	0.1252	190.1	1.4	:
15474-1054	LHS3117AB	2019.5387	2	<i>I</i>	Y	0.2282	241.1	0.9	q
15474-1054	LHS3117AB	2020.1119	2	<i>I</i>	Y	0.1837	226.6	0.8	q
15474-1054	LHS3117AB	2020.2008	2	<i>I</i>	Y	0.1774	224.3	1.0	q
15474-1054	LHS3117AB	2021.0784	2	<i>I</i>	Y	0.1326	182.5	1.0	q
15474-1054	LHS3117AB	2021.3187	2	<i>I</i>	Y	0.1280	168.5	0.9	q
15474-1054	LHS3117AB	2022.1298	2	<i>I</i>	Y	0.1537	124.8	0.8	q
15474-1054	LHS3117AB	2022.2827	2	<i>I</i>	Y	0.1594	117.9	0.9	q
15474-1054	LHS3117AB	2022.4436	2	<i>I</i>	Y	0.1622	112.2	1.0	q
15475-2755	UPM1547-2755AB	2020.1119	2	<i>I</i>	Y	1.3298	122.3	1.5	*
15475-2755	UPM1547-2755AB	2021.1603	2	<i>I</i>	Y	1.3442	123.3	1.6	*
15475-2755	UPM1547-2755AB	2022.1296	2	<i>I</i>	Y	1.3516	124.4	1.7	*
15476-2754	UPM1547-2755CD	2019.5364	2	<i>I</i>	Y	0.1051	150.5	0.2	
15476-2754	UPM1547-2755CD	2020.1119	2	<i>I</i>	Y	0.0740	163.5	0.0	:
15476-2754	UPM1547-2755CD	2021.1603	3	<i>I</i>	Y	0.0640	262.8	0.6	
15476-2754	UPM1547-2755CD	2021.3187	2	<i>I</i>	Y	0.0660	280.2	0.5	:
15476-2754	UPM1547-2755CD	2021.5675	2	<i>I</i>	Y	0.0877	286.8	0.4	:
15476-2754	UPM1547-2755CD	2022.1296	2	<i>I</i>	Y	0.1057	297.0	0.3	:
15578-5132	GAI1557-5131AB	2019.5363	2	<i>I</i>	Y	0.3261	331.9	0.8	q
15578-5132	GAI1557-5131AB	2020.1119	2	<i>I</i>	Y	0.3541	333.6	0.9	q

Table 4: Results of the SOAR speckle interferometry campaign for nearby M dwarfs. The meanings of columns 8–10 differ depending on whether or not the companion was resolved in that observation, hence the two lines in those columns’ headers. The “:” flag in the last column indicates highly uncertain results; the rest of the flags are described in §4.2.

15578-5132	GAI1557-5131AB	2021.1632	2	<i>I</i>	Y	0.3848	337.5	0.9	:
15578-5132	GAI1557-5131AB	2022.1298	2	<i>I</i>	Y	0.4025	340.1	0.8	q
16019-3357	LP553-044AB	2019.5364	2	<i>I</i>	Y	0.6939	61.6	0.2	*
16019-3357	LP553-044AB	2020.1119	2	<i>I</i>	Y	0.6714	61.3	0.0	*
16019-3357	LP553-044AB	2022.1952	2	<i>I</i>	Y	0.5437	60.7	0.2	
16170-3137	GAI1616-3136AB	2019.5365	2	<i>I</i>	Y	0.2691	46.2	0.2	
16170-3137	GAI1616-3136AB	2020.2007	2	<i>I</i>	Y	0.2790	37.1	0.0	
16170-3137	GAI1616-3136AB	2021.3162	1	<i>I</i>	Y	0.2856	23.0	0.3	
16170-3137	GAI1616-3136AB	2022.1953	2	<i>I</i>	Y	0.2801	11.6	0.2	:
16170-3137	GAI1616-3136AB	2022.6844	2	<i>I</i>	Y	0.2704	5.2	0.1	:
16202-3734	GJ0618AB	2021.1605	1	<i>I</i>	Y	3.7394	226.7	3.4	*
16202-3734	GJ0618A	2019.5364	2	<i>I</i>	N	0.0534	2.1	3.2	
16202-3734	GJ0618A	2021.1605	2	<i>I</i>	N	0.0404	2.6	4.1	
16202-3734	GJ0618A	2021.3162	2	<i>I</i>	N	0.0420	2.7	4.1	
16202-3734	GJ0618A	2021.5676	2	<i>I</i>	N	0.0415	3.0	5.4	
16268-1724	LHS3197AB	2021.3188	2	<i>I</i>	Y	0.7062	170.0	0.0	
16269-3813	SCR1626-3812	2019.5364	2	<i>I</i>	N	0.0643	2.1	3.0	
16269-3813	SCR1626-3812	2021.1605	2	<i>I</i>	N	0.0508	2.5	3.4	
16269-3813	SCR1626-3812	2022.2909	2	<i>I</i>	N	0.0583	2.3	3.2	
16302-1440	GJ2121AB	2020.2007	3	<i>I</i>	Y	0.1046	100.5	2.2	
16302-1440	GJ2121AB	2021.1605	3	<i>I</i>	Y	0.0786	3.7	1.7	q
16302-1440	GJ2121AB	2021.5675	2	<i>I</i>	Y	0.0843	307.2	2.0	q
16302-1440	GJ2121AB	2022.3895	2	<i>I</i>	Y	0.1615	261.9	2.0	q
16302-1440	GJ2121AB	2022.4437	2	<i>I</i>	Y	0.1669	259.1	2.1	q
16453-3848	GJ2122AB	2019.5364	2	<i>I</i>	Y	0.7735	245.3	1.3	*

Table 4: Results of the SOAR speckle interferometry campaign for nearby M dwarfs. The meanings of columns 8–10 differ depending on whether or not the companion was resolved in that observation, hence the two lines in those columns’ headers. The “:” flag in the last column indicates highly uncertain results; the rest of the flags are described in §4.2.

16453-3848	GJ2122AB	2021.1578	2	<i>I</i>	Y	0.8010	242.9	1.3	*
16453-3848	GJ2122AB	2022.1953	2	<i>I</i>	Y	0.7939	241.6	1.3	q
16510+2227	G169-029	2021.2454	2	<i>I</i>	N	0.0573	2.3	2.8	
16510+2227	G169-029	2022.2828	2	<i>I</i>	N	0.0543	2.3	3.8	
16555-0820	GJ0644AB	2019.5361	2	<i>I</i>	Y	0.2250	122.9	0.4	q
16555-0820	GJ0644AB	2019.6128	2	<i>I</i>	Y	0.2248	106.9	0.4	q
16555-0820	GJ0644AB	2022.4438	2	<i>I</i>	Y	0.2108	237.3	0.3	q
16584+1358	G139-003AB	2019.5360	2	<i>I</i>	Y	0.5494	236.4	0.5	*
16584+1358	G139-003AB	2021.2454	2	<i>I</i>	Y	0.5411	223.0	0.3	
16584+1358	G139-003AB	2022.3895	2	<i>I</i>	Y	0.5406	214.1	0.3	q
17077+0722	GJ1210AB	2021.2454	2	<i>I</i>	Y	0.1107	33.2	0.0	
17077+0722	GJ1210AB	2021.5676	2	<i>I</i>	Y	0.0780	3.4	0.0	
17077+0722	GJ1210AB	2022.2174	2	<i>I</i>	Y	0.1102	287.2	0.2	
17107-5300	UPM1710-5300AB	2019.5365	3	<i>I</i>	Y	1.2178	341.4	0.5	*
17107-5300	UPM1710-5300AB	2021.1632	3	<i>I</i>	Y	1.1933	343.0	0.5	*
17107-5300	UPM1710-5300AB	2022.1954	2	<i>I</i>	Y	1.1682	343.7	0.5	*
17119-0151	GJ0660AB	2021.3190	2	<i>I</i>	Y	0.6221	341.0	0.2	*
17119-0151	GJ0660AB	2021.5676	2	<i>I</i>	Y	0.6165	344.8	0.2	
17119-0151	GJ0660AB	2022.4438	2	<i>I</i>	Y	0.6052	358.4	0.2	q
17129-0508	GJ0660.1A	2019.5361	2	<i>I</i>	N	0.0492	2.2	3.3	
17129-0508	GJ0660.1A	2021.1605	2	<i>I</i>	N	0.0457	2.9	4.4	
17129-0508	GJ0660.1A	2022.1954	2	<i>I</i>	N	0.0415	2.6	5.1	
17137-0825	GJ1212AB	2019.5361	2	<i>I</i>	Y	0.0345	30.7	0.2	
17137-0825	GJ1212AB	2019.6128	2	<i>I</i>	Y	0.0401	54.8	0.2	
17137-0825	GJ1212AB	2020.2008	1	<i>I</i>	Y	0.0420	148.0	0.0	

Table 4: Results of the SOAR speckle interferometry campaign for nearby M dwarfs. The meanings of columns 8–10 differ depending on whether or not the companion was resolved in that observation, hence the two lines in those columns’ headers. The “:” flag in the last column indicates highly uncertain results; the rest of the flags are described in §4.2.

17137-0825	GJ1212AB	2021.1605	2	<i>I</i>	Y	0.0367	221.2	0.2	
17137-0825	GJ1212AB	2021.3190	2	<i>I</i>	Y	0.0373	260.1	0.5	
17137-0825	GJ1212AB	2021.3190	2	<i>y</i>	Y	0.0415	252.1	0.4	:
17137-0825	GJ1212AB	2021.5676	2	<i>I</i>	Y	0.0472	301.6	0.4	
17137-0825	GJ1212AB	2021.7289	2	<i>I</i>	Y	0.0484	317.1	0.3	
17137-0825	GJ1212AB	2022.1954	2	<i>I</i>	Y	0.0559	152.6	0.4	
17137-0825	GJ1212AB	2022.3073	2	<i>I</i>	Y	0.0574	162.6	0.4	q
17137-0825	GJ1212AB	2022.4438	2	<i>I</i>	Y	0.0552	176.3	0.5	q
17177+1140	GJ1215AB	2019.5361	2	<i>I</i>	N	0.0573	2.2	2.9	
17177+1140	GJ1215AB	2021.2454	2	<i>I</i>	N	0.0562	2.4	2.9	
17177+1140	GJ1215AB	2022.4440	2	<i>I</i>	N	0.0534	2.4	3.4	
17184-0147	HIP084652AB	2019.5361	2	<i>I</i>	Y	0.5211	291.3	2.4	*
17184-0147	HIP084652AB	2021.2454	2	<i>I</i>	Y	0.5149	299.5	2.3	q
17184-0147	HIP084652AB	2022.3895	2	<i>I</i>	Y	0.4920	305.4	2.3	q
17190-3459	GJ0667C	2019.6129	2	<i>I</i>	N	0.0437	2.6	4.3	*
17190-3459	GJ0667AB?	2019.5338	2	<i>I</i>	Y	0.6560	0.2	0.8	*
17190-3459	GJ0667AB?	2019.6129	2	<i>I</i>	Y	0.6784	357.8	0.8	*
17190-3459	GJ0667AB?	2021.2452	2	<i>y</i>	Y	1.1551	327.8	1.2	*
17190-3459	GJ0667AB?	2021.3162	2	<i>I</i>	Y	1.1705	327.1	0.7	*
17190-3459	GJ0667AB?	2021.5651	2	<i>I</i>	Y	1.2289	324.5	0.7	*
17190-3459	GJ0667AB?	2021.5651	2	<i>y</i>	Y	1.2318	324.5	1.1	*
17190-3459	GJ0667AB?	2021.6362	2	<i>y</i>	Y	1.2507	324.1	1.3	*
17190-3459	GJ0667AB?	2021.7509	2	<i>I</i>	Y	1.2752	322.8	0.7	*
17190-3459	GJ0667AB?	2022.1953	2	<i>I</i>	Y	1.3753	319.3	0.8	*
17190-3459	GJ0667AB?	2022.2909	2	<i>I</i>	Y	1.3943	318.7	0.8	*

Table 4: Results of the SOAR speckle interferometry campaign for nearby M dwarfs. The meanings of columns 8–10 differ depending on whether or not the companion was resolved in that observation, hence the two lines in those columns’ headers. The “:” flag in the last column indicates highly uncertain results; the rest of the flags are described in §4.2.

17190-3459	GJ0667AB?	2022.4438	2	<i>I</i>	Y	1.4284	317.6	0.7	*
17282-0144	SCR1728-0143AB	2019.5361	2	<i>I</i>	Y	0.0736	22.7	0.7	
17282-0144	SCR1728-0143AB	2021.2454	2	<i>I</i>	Y	0.1310	90.6	0.9	q
17282-0144	SCR1728-0143AB	2021.3190	2	<i>I</i>	Y	0.1369	91.6	1.0	q
17282-0144	SCR1728-0143AB	2021.7289	2	<i>I</i>	Y	0.1376	100.9	1.0	:
17282-0144	SCR1728-0143AB	2022.2174	2	<i>I</i>	Y	0.1349	112.9	1.0	q
17282-0144	SCR1728-0143AB	2022.4438	2	<i>I</i>	Y	0.1320	119.5	0.9	q
17298-2504	LP864-014AB	2019.5338	2	<i>I</i>	Y	0.1435	203.3	0.5	
17298-2504	LP864-014AB	2020.2008	2	<i>I</i>	Y	0.1659	201.5	0.6	
17298-2504	LP864-014AB	2021.1605	2	<i>I</i>	Y	0.1299	200.4	0.5	q
17298-2504	LP864-014AB	2021.7317	2	<i>I</i>	Y	0.0928	195.9	0.6	
17298-2504	LP864-014AB	2022.1954	2	<i>I</i>	Y	0.0556	195.1	0.2	
17298-2504	LP864-014AB	2022.4438	2	<i>I</i>	Y	0.0340	193.1	0.0	:
17337-4256	GAI1733-4255AB	2019.5365	2	<i>I</i>	Y	0.7786	26.8	0.1	
17337-4256	GAI1733-4255AB	2020.2008	2	<i>I</i>	Y	0.7640	27.6	0.0	
17337-4256	GAI1733-4255AB	2022.3074	2	<i>I</i>	Y	0.6982	31.2	0.2	
17365-2515	GAI1736-2515AB	2019.5338	2	<i>I</i>	Y	0.4553	258.1	1.4	:
17365-2515	GAI1736-2515AB	2020.2008	1	<i>I</i>	Y	0.4543	257.3	1.8	:
17365-2515	GAI1736-2515AB	2021.1605	2	<i>I</i>	Y	0.4543	259.1	2.2	q
17365-2515	GAI1736-2515AB	2022.2909	2	<i>I</i>	Y	0.4509	259.7	0.4	:
17371-4419	GJ0682AB	2019.5365	2	<i>I</i>	N	0.0437	2.3	4.2	
17371-4419	GJ0682AB	2020.2008	2	<i>I</i>	N	0.0415	3.6	5.3	
17371-4419	GJ0682AB	2021.1633	2	<i>I</i>	N	0.0534	2.1	3.1	
17371-4419	GJ0682AB	2022.4438	2	<i>I</i>	N	0.0444	2.6	4.3	
17430+0547	G140-009AB	2019.5363	2	<i>I</i>	Y	0.2547	99.2	1.2	q

Table 4: Results of the SOAR speckle interferometry campaign for nearby M dwarfs. The meanings of columns 8–10 differ depending on whether or not the companion was resolved in that observation, hence the two lines in those columns’ headers. The “:” flag in the last column indicates highly uncertain results; the rest of the flags are described in §4.2.

17430+0547	G140-009AB	2021.2455	2	<i>I</i>	Y	0.1638	78.7	1.2	q
17430+0547	G140-009AB	2021.2455	4	<i>y</i>	Y	0.1640	80.4	1.4	
17430+0547	G140-009AB	2022.2883	2	<i>I</i>	Y	0.1212	50.7	1.2	q
17462-3206	GJ2130BC	2019.6129	2	<i>I</i>	N	0.0636	2.5	4.3	
17462-3206	GJ2130BC	2020.2008	2	<i>I</i>	N	0.0415	2.6	4.9	
17462-3206	GJ2130BC	2022.1954	2	<i>I</i>	N	0.0415	0.0	4.8	
17466-5719	GJ0693	2020.2009	2	<i>I</i>	N	0.0415	2.2	5.6	
17466-5719	GJ0693	2021.6364	2	<i>I</i>	N	0.0444	2.7	4.7	
18036-1859	G154-043AB	2019.5338	2	<i>I</i>	Y	0.2190	351.9	1.3	q
18036-1859	G154-043AB	2020.8228	2	<i>I</i>	Y	0.1648	325.3	1.4	q
18036-1859	G154-043AB	2021.2454	2	<i>I</i>	Y	0.1354	312.2	1.4	q
18036-1859	G154-043AB	2021.5677	2	<i>I</i>	Y	0.1226	295.5	1.4	:
18036-1859	G154-043AB	2021.7289	2	<i>I</i>	Y	0.1136	288.0	1.3	q
18036-1859	G154-043AB	2022.2174	4	<i>I</i>	Y	0.1184	258.9	1.3	q
18036-1859	G154-043AB	2022.3896	3	<i>I</i>	Y	0.1283	249.4	1.5	q
18097-0220	LSR1809-0219AB	2019.5361	2	<i>I</i>	N	0.0583	2.1	2.6	
18097-0220	LSR1809-0219AB	2021.3192	2	<i>I</i>	N	0.0534	2.5	3.6	
18097-0220	LSR1809-0219AB	2022.2883	2	<i>I</i>	Y	0.1322	198.8	2.5	
18097-0220	LSR1809-0219AB	2022.4440	2	<i>I</i>	Y	0.1343	191.5	2.9	
18099-1027	UPM1809-1027AB	2019.5361	2	<i>I</i>	Y	0.7285	36.2	0.2	*
18099-1027	UPM1809-1027AB	2020.8228	2	<i>I</i>	Y	0.7596	37.8	0.3	*
18099-1027	UPM1809-1027AB	2021.3191	2	<i>I</i>	Y	0.7713	38.2	0.3	*
18099-1027	UPM1809-1027AB	2022.2883	2	<i>I</i>	Y	0.7872	39.2	0.3	*
18113-7859	L043-072AB	2019.5366	2	<i>I</i>	Y	1.5457	132.8	1.2	*
18113-7859	L043-072AC	2021.3165	2	<i>I</i>	Y	0.0654	148.8	0.4	

Table 4: Results of the SOAR speckle interferometry campaign for nearby M dwarfs. The meanings of columns 8–10 differ depending on whether or not the companion was resolved in that observation, hence the two lines in those columns’ headers. The “:” flag in the last column indicates highly uncertain results; the rest of the flags are described in §4.2.

18113-7859	L043-072AC	2022.3076	2	<i>I</i>	Y	0.0729	327.5	0.9	
18113-7859	L043-072AC	2022.3894	2	<i>I</i>	Y	0.0798	322.2	0.8	
18113-7859	L043-072AC	2022.4413	2	<i>I</i>	Y	0.0794	315.0	0.9	
18113-7859	L043-072AC	2022.6819	2	<i>I</i>	Y	0.0522	320.3	0.8	:
18113-7859	L043-072AB	2021.3165	2	<i>I</i>	Y	1.6171	132.2	1.0	
18113-7859	L043-072AB	2022.3076	2	<i>I</i>	Y	1.5554	131.6	1.2	
18113-7859	L043-072AB	2022.3894	2	<i>I</i>	Y	1.5452	131.6	1.3	
18113-7859	L043-072AB	2022.4413	2	<i>I</i>	Y	1.5584	131.5	1.4	
18113-7859	L043-072AB	2022.6819	2	<i>I</i>	Y	1.5750	131.4	1.7	:
18210-0101	GJ1226AB	2019.5361	2	<i>I</i>	Y	1.4118	3.6	0.2	*
18210-0101	GJ1226AB	2021.3192	2	<i>I</i>	Y	1.4049	2.3	0.2	*
18210-0101	GJ1226AB	2021.5677	2	<i>I</i>	Y	1.4009	2.2	0.1	*
18210-0101	GJ1226AB	2022.4440	2	<i>I</i>	Y	1.3840	1.7	0.2	*
18268-6543	SCR1826-6542AB	2019.5365	2	<i>I</i>	N	0.0926	1.9	2.4	
18268-6543	SCR1826-6542AB	2020.8337	2	<i>I</i>	N	0.2250	1.6	1.6	:
18268-6543	SCR1826-6542AB	2021.3163	2	<i>I</i>	Y	0.1050	335.9	0.0	
18268-6543	SCR1826-6542AB	2021.6364	2	<i>I</i>	Y	0.1329	334.2	0.0	:
18268-6543	SCR1826-6542AB	2021.7510	2	<i>I</i>	Y	0.1272	334.0	0.0	:
18268-6543	SCR1826-6542AB	2022.3075	2	<i>I</i>	Y	0.1698	332.2	0.3	:
18268-6543	SCR1826-6542AB	2022.4413	2	<i>I</i>	Y	0.1732	332.0	0.0	
18387-1429	GJ2138AB	2021.7510	2	<i>I</i>	N	0.0426	2.2	2.9	
18411+2447	GJ1230AC	2019.6130	2	<i>I</i>	N	0.0543	2.4	3.6	
18411+2447	GJ1230AC	2021.3192	2	<i>I</i>	N	0.0477	2.6	4.4	
18411+2447	GJ1230AC	2022.4415	2	<i>I</i>	N	0.0477	2.4	3.9	
18460-2856	LTT07434AB	2019.6130	2	<i>I</i>	Y	0.3485	182.3	1.4	q

Table 4: Results of the SOAR speckle interferometry campaign for nearby M dwarfs. The meanings of columns 8–10 differ depending on whether or not the companion was resolved in that observation, hence the two lines in those columns’ headers. The “:” flag in the last column indicates highly uncertain results; the rest of the flags are described in §4.2.

18460-2856	LTT07434AB	2020.7694	2	<i>I</i>	Y	0.3949	172.4	1.4	q
18460-2856	LTT07434AB	2021.2454	2	<i>I</i>	Y	0.4146	168.7	1.4	q
18460-2856	LTT07434AB	2022.2909	2	<i>I</i>	Y	0.4475	162.1	1.4	q
18483-6856	SCR1848-6855AB	2019.5365	2	<i>I</i>	Y	0.7475	265.2	2.5	*
18483-6856	SCR1848-6855AB	2020.8337	2	<i>I</i>	N	0.2864	1.8	1.8	:
18483-6856	SCR1848-6855AB	2021.3164	3	<i>I</i>	Y	0.7656	265.7	2.8	*
18483-6856	SCR1848-6855AB	2022.3077	2	<i>I</i>	Y	0.7780	264.7	2.8	:
18555+0824	GJ0735AB	2019.5363	2	<i>I</i>	N	0.0457	2.2	3.3	
18555+0824	GJ0735AB	2021.2455	1	<i>I</i>	N	0.0437	2.8	4.3	
18555+0824	GJ0735AB	2022.2885	2	<i>I</i>	N	0.0420	2.6	3.9	
18597-6327	L159-126AB	2019.5366	2	<i>I</i>	Y	0.0563	44.8	0.3	
18597-6327	L159-126AB	2020.7693	2	<i>I</i>	Y	0.0297	20.8	0.0	:
18597-6327	L159-126AB	2020.8364	2	<i>I</i>	Y	0.0343	191.4	0.0	
18597-6327	L159-126AB	2021.3163	2	<i>I</i>	Y	0.0693	199.8	0.8	q
18597-6327	L159-126AB	2021.7510	2	<i>I</i>	Y	0.0994	203.3	0.8	q
18597-6327	L159-126AB	2022.2913	2	<i>I</i>	Y	0.1335	205.6	0.8	q
18597-6327	L159-126AB	2022.4413	2	<i>I</i>	Y	0.1430	206.2	0.8	q
18597-6327	L159-126AB	2022.6818	2	<i>I</i>	Y	0.1574	206.0	0.7	q
19121+0254	GJ0748AB	2019.5339	2	<i>I</i>	Y	0.1915	333.0	1.4	q
19121+0254	GJ0748AB	2021.3193	2	<i>I</i>	Y	0.1822	5.2	1.4	q
19121+0254	GJ0748AB	2022.2885	3	<i>I</i>	Y	0.1584	315.8	1.4	q
19127-3615	WIS1912-3615	2019.6130	2	<i>I</i>	N	0.0636	2.4	4.2	
19127-3615	WIS1912-3615	2020.8364	2	<i>I</i>	N	0.0508	2.7	3.7	
19127-3615	WIS1912-3615	2021.3164	2	<i>I</i>	N	0.0470	2.7	3.9	
19131-3902	LHS3443AB	2021.3164	2	<i>I</i>	Y	1.3149	329.5	2.4	*

Table 4: Results of the SOAR speckle interferometry campaign for nearby M dwarfs. The meanings of columns 8–10 differ depending on whether or not the companion was resolved in that observation, hence the two lines in those columns’ headers. The “:” flag in the last column indicates highly uncertain results; the rest of the flags are described in §4.2.

19208-4534	GJ0754	2019.6129	3	<i>I</i>	N	0.0492	2.5	4.5	
19208-4534	GJ0754	2021.3164	2	<i>I</i>	N	0.0450	2.5	4.0	
19216+2052	GJ1235	2019.6130	2	<i>I</i>	N	0.0573	2.6	3.4	
19216+2052	GJ1235	2021.3193	2	<i>I</i>	N	0.0492	2.6	4.1	
19216+2052	GJ1235	2022.3896	2	<i>I</i>	N	0.0415	2.6	4.9	
19242-0932	SCR1924-0931AB	2019.5339	2	<i>I</i>	Y	0.4212	244.2	0.3	:
19242-0932	SCR1924-0931AB	2020.8228	2	<i>I</i>	Y	0.4321	239.3	0.3	q
19242-0932	SCR1924-0931AB	2021.5682	6	<i>I</i>	Y	0.4362	236.4	0.3	:
19242-0932	SCR1924-0931AB	2022.2885	2	<i>I</i>	Y	0.4401	233.9	0.2	q
19279-2811	LHS5348AB	2019.6132	2	<i>I</i>	Y	0.7239	250.7	0.5	*
19279-2811	LHS5348AB	2020.8339	2	<i>I</i>	Y	0.7165	243.1	0.4	q
19279-2811	LHS5348AB	2021.5653	2	<i>I</i>	Y	0.7090	238.7	0.5	:
19279-2811	LHS5348AB	2022.3075	2	<i>I</i>	Y	0.7066	234.3	0.6	q
19310-7337	LEP1931-7337AB	2019.5366	2	<i>I</i>	Y	0.6704	175.4	3.5	q
19310-7337	LEP1931-7337AB	2020.7693	2	<i>I</i>	Y	0.6299	169.1	3.5	
19310-7337	LEP1931-7337AB	2021.5679	2	<i>I</i>	Y	0.6106	164.3	3.2	:
19310-7337	LEP1931-7337AB	2022.3077	2	<i>I</i>	Y	0.5813	159.5	3.5	q
19341-5225	L275-026	2019.5366	2	<i>I</i>	N	0.0534	2.4	3.7	
19341-5225	L275-026	2020.2009	2	<i>I</i>	N	0.0415	2.4	5.1	
19341-5225	L275-026	2021.7510	2	<i>I</i>	N	0.0485	2.8	4.1	
19420-2104	LP869-019AB	2019.5391	2	<i>I</i>	N	0.0716	2.4	4.2	
19420-2104	LP869-019AB	2020.8364	2	<i>I</i>	N	0.0516	2.7	3.9	
19420-2104	LP869-019AB	2021.7511	2	<i>I</i>	N	0.0463	2.4	3.8	
19434-3722	2MA1943-3722AB	2019.5391	2	<i>I</i>	Y	1.6783	302.3	3.0	*
19449-2338	LP869-026AB	2019.5286	2	<i>I</i>	Y	0.3869	328.9	0.0	:

Table 4: Results of the SOAR speckle interferometry campaign for nearby M dwarfs. The meanings of columns 8–10 differ depending on whether or not the companion was resolved in that observation, hence the two lines in those columns’ headers. The “:” flag in the last column indicates highly uncertain results; the rest of the flags are described in §4.2.

19449-2338	LP869-026AB	2020.8364	2	<i>I</i>	Y	0.2983	320.4	0.0	
19449-2338	LP869-026AB	2021.3164	2	<i>I</i>	Y	0.2650	315.9	0.0	
19449-2338	LP869-026AB	2021.5653	2	<i>I</i>	Y	0.2471	312.7	0.0	
19449-2338	LP869-026AB	2022.2886	2	<i>I</i>	Y	0.2026	301.9	0.1	
19449-2338	LP869-026AB	2022.6821	2	<i>I</i>	Y	0.1743	292.8	0.0	:
19468-0158	LEP1946-0157	2019.5339	2	<i>I</i>	N	0.0543	2.4	3.9	
19468-0158	LEP1946-0157	2020.8228	2	<i>I</i>	N	0.0500	2.6	4.1	
19468-0158	LEP1946-0157	2022.2886	2	<i>I</i>	N	0.0463	2.6	4.0	
19516-3511	2MA1951-3510AB	2019.5391	2	<i>I</i>	Y	2.0015	140.8	0.2	*
19516-3511	2MA1951-3510AB	2020.8339	2	<i>I</i>	Y	2.0153	143.0	0.2	*
19517-3100	UPM1951-3100AB	2019.5391	2	<i>I</i>	Y	0.1215	13.8	1.9	q
19517-3100	UPM1951-3100AB	2019.8564	1	<i>I</i>	Y	0.1567	22.3	1.9	q
19517-3100	UPM1951-3100AB	2020.8339	2	<i>I</i>	Y	0.1274	37.4	1.9	
19517-3100	UPM1951-3100AB	2021.3164	2	<i>I</i>	N	0.0485	2.5	3.6	
19517-3100	UPM1951-3100AB	2021.5653	2	<i>I</i>	Y	0.0489	231.7	1.4	:
19517-3100	UPM1951-3100AB	2021.6365	2	<i>I</i>	Y	0.0392	236.5	1.7	
19517-3100	UPM1951-3100AB	2021.7511	2	<i>I</i>	N	0.0444	2.5	3.9	
19517-3100	UPM1951-3100AB	2022.4414	2	<i>I</i>	Y	0.1309	18.5	1.9	q
19517-3100	UPM1951-3100AB	2022.6821	2	<i>I</i>	Y	0.1566	22.1	1.8	q
19544-3148	LP926-055AB	2019.5391	2	<i>I</i>	Y	0.1367	139.5	0.8	q
19544-3148	LP926-055AB	2019.8564	2	<i>I</i>	Y	0.1409	147.4	0.9	q
19544-3148	LP926-055AB	2020.8339	2	<i>I</i>	Y	0.1555	167.4	0.8	q
19544-3148	LP926-055AB	2021.3164	2	<i>I</i>	Y	0.1630	175.7	0.8	q
19544-3148	LP926-055AB	2021.6365	2	<i>I</i>	Y	0.1667	180.8	0.8	q
19544-3148	LP926-055AB	2022.4413	2	<i>I</i>	Y	0.1728	193.2	0.8	q

Table 4: Results of the SOAR speckle interferometry campaign for nearby M dwarfs. The meanings of columns 8–10 differ depending on whether or not the companion was resolved in that observation, hence the two lines in those columns’ headers. The “:” flag in the last column indicates highly uncertain results; the rest of the flags are described in §4.2.

19544-3148	LP926-055AB	2022.6821	3	<i>I</i>	Y	0.1738	196.0	0.8	q
20154-5646	L209-071AC	2019.5366	2	<i>I</i>	Y	0.7991	31.2	1.8	*
20154-5646	L209-071AC	2020.8337	2	<i>I</i>	Y	0.8113	34.8	1.3	*
20154-5646	L209-071AC	2022.3077	2	<i>I</i>	Y	0.8169	39.6	1.8	*
20253-2259	SCR2025-2259AB	2019.5391	2	<i>I</i>	Y	0.9363	270.6	0.2	:
20253-2259	SCR2025-2259AB	2020.8229	2	<i>I</i>	Y	0.9338	268.8	0.4	*
20253-2259	SCR2025-2259AC	2022.4414	3	<i>I</i>	Y	0.0778	190.5	0.8	
20253-2259	SCR2025-2259AC	2022.7737	2	<i>I</i>	Y	0.0786	182.1	0.6	:
20253-2259	SCR2025-2259AB	2022.4414	3	<i>I</i>	Y	0.9503	266.3	0.0	
20253-2259	SCR2025-2259AB	2022.7737	2	<i>I</i>	Y	0.9489	265.7	0.2	:
20298+0941	GJ0791.2AB	2019.5394	2	<i>I</i>	Y	0.1283	118.6	2.2	
20298+0941	GJ0791.2AB	2019.8563	2	<i>I</i>	Y	0.1604	93.8	2.3	q
20298+0941	GJ0791.2AB	2021.3303	2	<i>I</i>	Y	0.1552	94.2	2.0	
20298+0941	GJ0791.2AB	2022.3896	2	<i>I</i>	Y	0.1137	131.2	2.4	
20298+0941	GJ0791.2AB	2022.4417	2	<i>I</i>	Y	0.1201	124.0	2.3	q
20330-4903	LEHPM2-1265AB	2019.5392	2	<i>I</i>	N	0.0797	1.8	3.1	:
20330-4903	LEHPM2-1265AB	2021.3165	2	<i>I</i>	N	0.0500	2.5	3.6	
20330-4903	LEHPM2-1265AB	2022.3077	2	<i>I</i>	N	0.0562	2.4	3.3	
20492-4012	SCR2049-4012AB	2019.5392	4	<i>I</i>	Y	0.0938	20.2	1.1	
20492-4012	SCR2049-4012AB	2019.6135	2	<i>I</i>	Y	0.0976	20.9	1.2	q
20492-4012	SCR2049-4012AB	2020.8284	2	<i>I</i>	N	0.0500	2.4	3.7	
20492-4012	SCR2049-4012AB	2020.9241	2	<i>I</i>	Y	0.0490	186.6	1.4	
20492-4012	SCR2049-4012AB	2021.3165	2	<i>I</i>	Y	0.0930	21.8	1.3	q
20492-4012	SCR2049-4012AB	2021.5681	2	<i>I</i>	Y	0.0942	24.0	1.1	q
20492-4012	SCR2049-4012AB	2021.7513	2	<i>I</i>	Y	0.0786	25.7	1.3	q

Table 4: Results of the SOAR speckle interferometry campaign for nearby M dwarfs. The meanings of columns 8–10 differ depending on whether or not the companion was resolved in that observation, hence the two lines in those columns’ headers. The “:” flag in the last column indicates highly uncertain results; the rest of the flags are described in §4.2.

20492-4012	SCR2049-4012AB	2022.3077	2	<i>I</i>	N	0.0553	2.4	3.8	
20492-4012	SCR2049-4012AB	2022.4414	2	<i>I</i>	N	0.0477	2.3	4.0	
20492-4012	SCR2049-4012AB	2022.6846	2	<i>I</i>	Y	0.0402	199.1	1.0	
20492-4012	SCR2049-4012AB	2022.8420	2	<i>I</i>	Y	0.0611	200.0	1.0	
20556-1402	LHS0501AC	2019.5287	3	<i>I</i>	Y	0.1024	235.6	0.3	
20556-1402	LHS0501AC	2019.8563	2	<i>I</i>	Y	0.1027	197.7	0.4	q
20556-1402	LHS0501AC	2020.8339	2	<i>I</i>	Y	0.0589	189.6	0.0	
20556-1402	LHS0501AC	2021.3193	2	<i>I</i>	Y	0.0994	240.9	0.4	q
20556-1402	LHS0501AC	2021.5654	2	<i>I</i>	Y	0.1059	214.0	0.3	
20556-1402	LHS0501AC	2022.2887	2	<i>I</i>	Y	0.0803	100.1	0.4	q
20556-1402	LHS0501AC	2022.3898	2	<i>I</i>	Y	0.0783	80.2	0.3	
20556-1402	LHS0501AC	2022.4415	2	<i>I</i>	Y	0.0770	70.1	0.4	q
20556-1402	LHS0501AC	2022.6820	2	<i>I</i>	Y	0.0598	7.4	0.3	q
20556-1402	LHS0501AC	2022.8419	2	<i>I</i>	Y	0.0613	305.5	0.0	:
21011-4907	WT0766AC	2019.5392	2	<i>I</i>	N	0.0636	2.6	4.1	
21011-4907	WT0766AC	2020.8337	2	<i>I</i>	N	0.0534	2.5	3.5	
21142-7633	2MA2114-7633AB	2019.6132	2	<i>I</i>	Y	0.7786	68.9	0.8	*
21142-7633	2MA2114-7633AB	2020.8336	2	<i>I</i>	Y	0.8351	69.7	0.8	:
21142-7633	2MA2114-7633AB	2021.3165	2	<i>I</i>	Y	0.8618	70.0	0.8	*
21142-7633	2MA2114-7633AB	2022.3076	2	<i>I</i>	Y	0.9020	70.9	0.8	*
21176-4445	2MA2117-4444AB	2019.5392	2	<i>I</i>	Y	0.7954	357.8	0.0	
21176-4445	2MA2117-4444AB	2020.7694	2	<i>I</i>	Y	0.7725	357.5	0.1	:
21176-4445	2MA2117-4444AB	2022.3079	2	<i>I</i>	Y	0.7395	356.9	0.1	
21202-6739	L117-123	2019.6132	2	<i>I</i>	N	0.0492	2.6	4.0	
21202-6739	L117-123	2020.8337	2	<i>I</i>	N	0.0508	3.0	4.3	

Table 4: Results of the SOAR speckle interferometry campaign for nearby M dwarfs. The meanings of columns 8–10 differ depending on whether or not the companion was resolved in that observation, hence the two lines in those columns’ headers. The “:” flag in the last column indicates highly uncertain results; the rest of the flags are described in §4.2.

21202-6739	L117-123	2021.7512	2	<i>I</i>	N	0.0444	2.7	4.2	
21283-2219	L714-046	2019.9495	2	<i>I</i>	N	0.0415	2.2	4.7	
21283-2219	L714-046	2020.8339	2	<i>I</i>	N	0.0508	2.7	4.2	
21296+1739	GJ0829AB	2019.5394	2	<i>I</i>	N	0.0525	2.8	4.3	
21296+1739	GJ0829AB	2019.8563	2	<i>I</i>	Y	0.0367	96.4	0.0	
21296+1739	GJ0829AB	2020.8228	2	<i>I</i>	Y	0.0307	209.0	0.2	
21296+1739	GJ0829AB	2020.8228	2	<i>y</i>	Y	0.0250	193.9	0.0	:
21296+1739	GJ0829AB	2021.3195	2	<i>I</i>	Y	0.0373	82.8	0.0	:
21296+1739	GJ0829AB	2021.3195	2	<i>y</i>	Y	0.0369	84.4	0.3	
21296+1739	GJ0829AB	2021.7318	2	<i>I</i>	Y	0.0302	122.7	0.0	:
21296+1739	GJ0829AB	2021.7318	1	<i>y</i>	Y	0.0322	120.3	0.0	
21296+1739	GJ0829AB	2022.4417	2	<i>I</i>	Y	0.0284	164.6	0.0	:
21296+1739	GJ0829AB	2022.6820	2	<i>I</i>	Y	0.0233	193.9	0.0	
21296+1739	GJ0829AB	2022.8419	2	<i>I</i>	N	0.0500	2.9	4.3	
21308-4043	LHS0510	2019.5392	2	<i>I</i>	N	0.0636	2.7	4.2	
21308-4043	LHS0510	2019.8564	2	<i>I</i>	N	0.0477	2.4	4.0	
21308-4043	LHS0510	2020.8339	2	<i>I</i>	N	0.0508	2.6	3.9	
21308-4043	LHS0510	2022.3898	2	<i>I</i>	N	0.0415	2.9	4.9	
21313-0947	GJ0831AB	2021.5656	2	<i>I</i>	Y	0.1469	180.7	1.6	
21313-0947	GJ0831AB	2022.4442	2	<i>I</i>	Y	0.0979	87.0	1.7	q
21344-4316	WT0792	2019.8564	2	<i>I</i>	N	0.0643	2.2	3.3	
21344-4316	WT0792	2021.3167	2	<i>I</i>	N	0.0553	2.1	3.1	
21344-4316	WT0792	2022.4414	2	<i>I</i>	N	0.0562	2.2	2.9	
21364-4401	WT0795	2020.8339	2	<i>I</i>	N	0.0534	2.5	3.3	
21364-4401	WT0795	2022.4414	2	<i>I</i>	N	0.0508	2.4	3.8	

Table 4: Results of the SOAR speckle interferometry campaign for nearby M dwarfs. The meanings of columns 8–10 differ depending on whether or not the companion was resolved in that observation, hence the two lines in those columns’ headers. The “:” flag in the last column indicates highly uncertain results; the rest of the flags are described in §4.2.

21387-3340	LHS0512	2019.5392	2	<i>I</i>	N	0.0636	2.6	4.4	
21387-3340	LHS0512	2019.8564	2	<i>I</i>	N	0.0470	2.8	4.2	
21387-3340	LHS0512	2020.8339	2	<i>I</i>	N	0.0508	2.7	4.1	
21390-2409	GJ0836AB	2019.5392	1	<i>I</i>	N	0.0741	2.1	3.5	
21390-2409	GJ0836AB	2020.8339	2	<i>I</i>	N	0.0516	2.8	3.7	
21491-7206	GJ1264AB	2019.5287	2	<i>I</i>	Y	0.6402	129.4	0.7	:
21491-7206	GJ1264AB	2020.8336	2	<i>I</i>	Y	0.6591	142.3	0.8	q
21491-7206	GJ1264AB	2022.4441	2	<i>I</i>	Y	0.7096	157.6	0.8	q
21491-7206	GJ1264AB	2022.6110	2	<i>I</i>	Y	0.7154	158.8	1.0	q
21491-7206	GJ1264AB	2022.6819	2	<i>I</i>	Y	0.7160	159.2	1.0	q
21491-7206	GJ1264AB	2022.8419	2	<i>I</i>	Y	0.7295	160.4	0.8	q
21491-7206	GJ1264AB	2022.8447	2	<i>I</i>	Y	0.7297	160.6	0.8	q
21492-4133	L427-034AB	2019.6135	2	<i>I</i>	Y	2.6906	128.5	0.4	*
21492-4133	L427-034AB	2021.7513	2	<i>I</i>	Y	2.6917	125.9	0.4	*
21497-4139	WT0818AB	2019.5392	2	<i>I</i>	Y	0.2030	320.5	1.6	q
21497-4139	WT0818AB	2019.8564	2	<i>I</i>	Y	0.1934	317.1	1.6	q
21497-4139	WT0818AB	2020.7694	3	<i>I</i>	Y	0.1540	303.6	1.5	:
21497-4139	WT0818AB	2020.9242	2	<i>I</i>	Y	0.1495	302.6	1.7	q
21497-4139	WT0818AB	2021.5682	2	<i>I</i>	Y	0.0933	284.5	1.4	q
21497-4139	WT0818AB	2022.3898	2	<i>I</i>	N	0.0427	0.0	4.4	
21497-4139	WT0818AB	2022.6846	2	<i>I</i>	Y	0.0423	102.7	0.5	:
21497-4139	WT0818AB	2022.8448	2	<i>I</i>	Y	0.0426	69.9	1.5	
21558-3313	LP983-034AB	2019.5392	2	<i>I</i>	N	0.0708	2.4	4.0	
21558-3313	LP983-034AB	2019.8564	2	<i>I</i>	Y	0.0490	207.8	1.1	
21558-3313	LP983-034AB	2020.8339	2	<i>I</i>	Y	0.0420	229.1	0.8	

Table 4: Results of the SOAR speckle interferometry campaign for nearby M dwarfs. The meanings of columns 8–10 differ depending on whether or not the companion was resolved in that observation, hence the two lines in those columns’ headers. The “:” flag in the last column indicates highly uncertain results; the rest of the flags are described in §4.2.

21558-3313	LP983-034AB	2021.3167	2	<i>I</i>	Y	0.0805	3.4	1.1	q
21558-3313	LP983-034AB	2021.5682	2	<i>I</i>	Y	0.0749	347.0	1.1	q
21558-3313	LP983-034AB	2021.7513	2	<i>I</i>	Y	0.0649	333.1	1.1	q
21558-3313	LP983-034AB	2022.3898	2	<i>I</i>	Y	0.0450	212.0	0.9	
21558-3313	LP983-034AB	2022.4442	2	<i>I</i>	Y	0.0507	204.3	0.9	q
21558-3313	LP983-034AB	2022.6846	2	<i>I</i>	Y	0.0574	179.2	0.8	:
21569-0154	LHS0516	2020.8339	2	<i>I</i>	N	0.0716	2.0	2.7	
21569-0154	LHS0516	2021.5656	2	<i>I</i>	N	0.0638	1.7	2.7	:
21588-3226	LHS3739BC	2019.5392	2	<i>I</i>	N	0.1260	1.2	1.8	:
21588-3226	LHS3739BC	2019.8566	2	<i>I</i>	N	0.0643	2.3	3.1	
21588-3226	LHS3739BC	2021.7513	2	<i>I</i>	Y	0.0888	126.0	1.8	:
22018+1628	GJ0844AB	2019.5396	2	<i>I</i>	Y	0.3545	216.3	0.4	
22018+1628	GJ0844AB	2021.7318	2	<i>I</i>	Y	0.3554	250.2	0.2	q
22018+1628	GJ0844AB	2022.6820	2	<i>I</i>	Y	0.3458	265.3	0.2	
22025-3705	LHS3746	2019.5392	2	<i>I</i>	N	0.0636	2.8	4.6	
22025-3705	LHS3746	2019.8566	2	<i>I</i>	N	0.0444	2.6	4.2	
22025-3705	LHS3746	2021.7513	2	<i>I</i>	N	0.0457	2.4	4.2	
22067-4458	WT0870AB	2019.5392	3	<i>I</i>	Y	0.2757	147.3	2.7	:
22067-4458	WT0870AB	2020.8339	2	<i>I</i>	Y	0.2990	144.5	2.7	:
22067-4458	WT0870AB	2021.3167	2	<i>I</i>	Y	0.3099	142.7	2.8	q
22067-4458	WT0870AB	2022.4442	2	<i>I</i>	Y	0.3159	139.4	2.7	
22167-4801	SCR2216-4800AB	2019.5367	2	<i>I</i>	Y	0.2036	240.3	2.7	q
22167-4801	SCR2216-4800AB	2019.8566	2	<i>I</i>	Y	0.1962	236.7	2.6	q
22167-4801	SCR2216-4800AB	2020.7694	1	<i>I</i>	Y	0.1576	224.8	2.6	:
22167-4801	SCR2216-4800AB	2021.3167	2	<i>I</i>	Y	0.1773	211.7	2.6	q

Table 4: Results of the SOAR speckle interferometry campaign for nearby M dwarfs. The meanings of columns 8–10 differ depending on whether or not the companion was resolved in that observation, hence the two lines in those columns’ headers. The “:” flag in the last column indicates highly uncertain results; the rest of the flags are described in §4.2.

22167-4801	SCR2216-4800AB	2021.5682	3	<i>I</i>	Y	0.1746	206.1	2.7	
22167-4801	SCR2216-4800AB	2022.4418	2	<i>I</i>	Y	0.1792	190.5	2.5	
22173-0847	GJ0852BC	2019.5394	2	<i>I</i>	Y	0.3564	354.7	1.8	:
22173-0847	GJ0852BC	2019.8590	3	<i>I</i>	Y	0.3207	357.5	2.0	q
22173-0847	GJ0852BC	2020.8340	1	<i>I</i>	Y	0.2294	18.3	1.9	q
22173-0847	GJ0852BC	2021.5682	2	<i>I</i>	Y	0.1875	45.3	2.0	q
22173-0847	GJ0852BC	2022.3899	2	<i>I</i>	Y	0.1963	80.6	2.0	q
22173-0847	GJ0852BC	2022.6820	3	<i>I</i>	Y	0.2022	89.6	1.5	:
22173-3444	LP984-001AB	2019.5392	2	<i>I</i>	Y	0.0734	76.4	0.0	:
22173-3444	LP984-001AB	2019.6134	2	<i>I</i>	Y	0.0726	73.1	0.0	
22173-3444	LP984-001AB	2019.8566	2	<i>I</i>	Y	0.0856	55.5	0.2	
22173-3444	LP984-001AB	2019.9495	2	<i>I</i>	Y	0.0900	49.0	0.1	
22173-3444	LP984-001AB	2020.8341	2	<i>I</i>	Y	0.1636	28.4	0.0	
22173-3444	LP984-001AB	2021.3167	2	<i>I</i>	Y	0.1811	21.9	0.0	
22173-3444	LP984-001AB	2021.7513	2	<i>I</i>	Y	0.1990	17.9	0.1	
22173-3444	LP984-001AB	2022.3898	2	<i>I</i>	Y	0.2149	12.5	0.0	
22173-3444	LP984-001AB	2022.6846	2	<i>I</i>	Y	0.2285	12.5	0.0	:
22231-1736	LHS3799	2019.5393	2	<i>I</i>	N	0.0685	2.3	3.9	
22231-1736	LHS3799	2021.7513	2	<i>I</i>	N	0.0463	2.2	3.8	
22231-1736	LHS3799	2022.4417	2	<i>I</i>	N	0.0525	2.1	3.7	
22284-2553	LP876-026AC	2019.5393	2	<i>I</i>	Y	3.1620	217.9	1.8	
22284-2553	LP876-026AC	2020.8341	2	<i>I</i>	Y	3.1154	218.2	0.9	
22284-2553	LP876-026AB	2019.5393	2	<i>I</i>	Y	0.3401	4.3	0.1	
22284-2553	LP876-026AB	2019.5393	2	<i>I</i>	Y	0.3490	4.5	0.7	
22284-2553	LP876-026AB	2019.8566	2	<i>I</i>	Y	0.3537	6.0	0.1	

Table 4: Results of the SOAR speckle interferometry campaign for nearby M dwarfs. The meanings of columns 8–10 differ depending on whether or not the companion was resolved in that observation, hence the two lines in those columns’ headers. The “:” flag in the last column indicates highly uncertain results; the rest of the flags are described in §4.2.

22284-2553	LP876-026AB	2020.8341	2	<i>I</i>	Y	0.3932	10.0	0.2	
22302-5345	LEHPM1-4771AB	2019.5367	2	<i>I</i>	Y	0.1620	80.1	1.1	q
22302-5345	LEHPM1-4771AB	2019.6135	2	<i>I</i>	Y	0.1530	79.5	1.1	q
22302-5345	LEHPM1-4771AB	2019.8566	2	<i>I</i>	Y	0.1457	76.2	1.1	q
22302-5345	LEHPM1-4771AB	2019.9495	2	<i>I</i>	Y	0.1424	74.3	1.2	q
22302-5345	LEHPM1-4771AB	2020.8337	4	<i>I</i>	Y	0.0668	41.9	0.9	:
22302-5345	LEHPM1-4771AB	2021.3167	2	<i>I</i>	Y	0.0473	167.6	1.0	
22302-5345	LEHPM1-4771AB	2021.5682	2	<i>I</i>	Y	0.0577	135.6	1.1	
22302-5345	LEHPM1-4771AB	2021.6366	2	<i>I</i>	Y	0.0644	127.5	1.0	
22302-5345	LEHPM1-4771AB	2021.7513	2	<i>I</i>	Y	0.0683	119.7	1.1	
22302-5345	LEHPM1-4771AB	2022.3899	2	<i>I</i>	Y	0.0970	270.3	1.3	q
22302-5345	LEHPM1-4771AB	2022.4418	2	<i>I</i>	Y	0.0943	270.9	1.1	q
22302-5345	LEHPM1-4771AB	2022.6110	3	<i>I</i>	Y	0.0892	264.1	0.3	:
22351-4218	LTT09084AB	2019.5393	2	<i>I</i>	Y	0.4275	350.7	0.0	
22351-4218	LTT09084AB	2019.8566	2	<i>I</i>	Y	0.4234	351.7	0.0	
22351-4218	LTT09084AB	2020.8341	2	<i>I</i>	Y	0.4009	354.8	0.0	
22351-4218	LTT09084AB	2021.3167	2	<i>I</i>	Y	0.3871	356.4	0.1	
22351-4218	LTT09084AB	2022.4442	2	<i>I</i>	Y	0.3438	0.8	0.0	
22360-0050	GJ0864AB	2019.5394	2	<i>I</i>	Y	0.6815	285.2	4.2	q
22360-0050	GJ0864AB	2019.8563	2	<i>I</i>	Y	0.6702	286.8	3.7	*
22360-0050	GJ0864AB	2020.8340	2	<i>I</i>	Y	0.6312	291.7	4.0	q
22360-0050	GJ0864AB	2022.4445	2	<i>I</i>	Y	0.5566	302.7	4.0	q
22384-6523	GJ0865AB	2019.5370	4	<i>I</i>	Y	0.8790	81.5	0.2	*
22384-6523	GJ0865AB	2020.7694	2	<i>I</i>	Y	0.8793	73.3	0.4	*
22384-6523	GJ0865AB	2021.6366	2	<i>I</i>	Y	0.8791	67.3	0.2	*

Table 4: Results of the SOAR speckle interferometry campaign for nearby M dwarfs. The meanings of columns 8–10 differ depending on whether or not the companion was resolved in that observation, hence the two lines in those columns’ headers. The “:” flag in the last column indicates highly uncertain results; the rest of the flags are described in §4.2.

22384-6523	GJ0865AB	2022.3899	2	<i>I</i>	Y	0.8737	62.2	0.2	*
22385-1519	GJ0866AB	2019.8566	2	<i>I</i>	Y	0.4759	349.7	0.5	q
22385-1519	GJ0866AB	2020.8341	2	<i>I</i>	Y	0.0947	245.8	0.4	q
22385-1519	GJ0866AB	2021.3303	2	<i>I</i>	Y	0.1181	89.5	0.0	:
22385-1519	GJ0866AB	2022.4417	2	<i>I</i>	Y	0.4730	340.8	0.5	q
22385-1519	GJ0866AB	2022.6821	2	<i>I</i>	Y	0.3828	331.9	0.5	q
22388-2037	GJ0867AC	2019.5393	2	<i>I</i>	N	0.0450	2.6	4.9	
22388-2037	GJ0867AC	2019.8566	2	<i>I</i>	N	0.0404	2.7	4.0	
22388-2037	GJ0867BD	2019.5393	2	<i>I</i>	N	0.0525	2.6	4.2	
22486-3109	LP932-081	2019.5393	2	<i>I</i>	N	0.0636	2.6	4.2	
22486-3109	LP932-081	2019.8566	2	<i>I</i>	N	0.0470	3.0	4.2	
22486-3109	LP932-081	2021.3167	2	<i>I</i>	N	0.0457	2.4	3.9	
23036-4651	SCR2303-4650AB	2019.5367	2	<i>I</i>	Y	0.0846	165.5	0.8	q
23036-4651	SCR2303-4650AB	2019.8566	2	<i>I</i>	Y	0.1143	162.1	0.8	q
23036-4651	SCR2303-4650AB	2019.9495	2	<i>I</i>	Y	0.1234	161.5	0.8	q
23036-4651	SCR2303-4650AB	2020.8341	2	<i>I</i>	Y	0.1960	158.0	0.7	
23036-4651	SCR2303-4650AB	2021.7537	2	<i>I</i>	Y	0.2523	155.7	0.8	q
23036-4651	SCR2303-4650AB	2022.4443	2	<i>I</i>	Y	0.2788	154.8	0.8	q
23059-3551	GJ0887AB	2019.5393	2	<i>I</i>	N	0.0409	2.7	4.9	
23059-3551	GJ0887AB	2020.8341	2	<i>I</i>	N	0.0399	2.8	4.3	
23073-0416	2MA2307-0415AC	2019.5396	2	<i>I</i>	Y	0.4514	111.6	2.1	q
23073-0416	2MA2307-0415AC	2019.8563	2	<i>I</i>	Y	0.4533	109.5	2.1	q
23073-0416	2MA2307-0415AC	2020.8340	2	<i>I</i>	Y	0.4470	103.8	2.0	q
23073-0416	2MA2307-0415AC	2022.4445	2	<i>I</i>	Y	0.4092	93.5	2.0	q
23083-1525	GJ0890AB	2019.5396	2	<i>I</i>	N	0.0500	2.8	4.3	

Table 4: Results of the SOAR speckle interferometry campaign for nearby M dwarfs. The meanings of columns 8–10 differ depending on whether or not the companion was resolved in that observation, hence the two lines in those columns’ headers. The “:” flag in the last column indicates highly uncertain results; the rest of the flags are described in §4.2.

23083-1525	GJ0890AB	2019.8566	2	<i>I</i>	N	0.0437	2.9	4.2	
23083-1525	GJ0890AB	2020.9241	2	<i>I</i>	Y	0.0307	102.9	1.0	:
23083-1525	GJ0890AB	2022.4443	2	<i>I</i>	N	0.0450	2.3	4.2	
23083-1525	GJ0890AB	2022.6821	2	<i>I</i>	N	0.0543	2.5	3.4	
23107-1914	GJ1281	2020.8342	2	<i>I</i>	N	0.0508	2.7	4.0	
23107-1914	GJ1281	2020.9242	2	<i>I</i>	N	0.0415	3.2	5.0	
23107-1914	GJ1281	2022.4443	2	<i>I</i>	N	0.0470	2.3	3.8	
23120-1702	LP822-037AB	2019.5396	2	<i>I</i>	Y	0.4874	34.0	0.0	:
23120-1702	LP822-037AB	2019.8566	2	<i>I</i>	Y	0.4960	35.1	0.0	
23120-1702	LP822-037AB	2020.8342	2	<i>I</i>	Y	0.5199	38.1	0.0	
23120-1702	LP822-037AB	2022.4443	2	<i>I</i>	Y	0.5513	42.8	0.0	q
23242-1746	G273-033AB	2019.9495	2	<i>I</i>	Y	0.0689	359.3	0.0	
23242-1746	G273-033AB	2020.8342	2	<i>I</i>	Y	0.1177	19.3	0.0	
23242-1746	G273-033AB	2020.9242	2	<i>I</i>	Y	0.1195	20.4	0.1	q
23242-1746	G273-033AB	2021.5358	2	<i>I</i>	Y	0.0798	33.4	0.0	
23242-1746	G273-033AB	2021.7538	2	<i>I</i>	Y	0.0604	42.7	0.0	
23242-1746	G273-033AB	2022.4445	2	<i>I</i>	Y	0.0515	183.1	0.0	
23242-1746	G273-033AB	2022.6821	2	<i>I</i>	Y	0.0688	198.5	0.0	:
23254-6740	SCR2325-6740AB	2019.6132	2	<i>I</i>	Y	0.1376	78.3	0.0	
23254-6740	SCR2325-6740AB	2019.8567	4	<i>I</i>	Y	0.1274	84.6	0.0	
23254-6740	SCR2325-6740AB	2019.9495	2	<i>I</i>	Y	0.1269	86.6	0.0	
23254-6740	SCR2325-6740AB	2020.7694	2	<i>I</i>	Y	0.1118	103.0	0.0	:
23254-6740	SCR2325-6740AB	2021.5684	2	<i>I</i>	Y	0.1113	125.1	0.0	:
23254-6740	SCR2325-6740AB	2022.4443	2	<i>I</i>	Y	0.1083	149.4	0.1	
23254-6740	SCR2325-6740AB	2022.7737	2	<i>I</i>	Y	0.0987	161.7	0.0	

Table 4: Results of the SOAR speckle interferometry campaign for nearby M dwarfs. The meanings of columns 8–10 differ depending on whether or not the companion was resolved in that observation, hence the two lines in those columns’ headers. The “:” flag in the last column indicates highly uncertain results; the rest of the flags are described in §4.2.

23302-2023	GJ1284AB	2020.9242	2	<i>I</i>	N	0.0415	2.8	5.4	
23302-2023	GJ1284AB	2022.4471	2	<i>I</i>	N	0.0492	2.3	4.4	
23369-3629	LHS0547	2019.5367	2	<i>I</i>	N	0.0508	2.5	3.4	
23369-3629	LHS0547	2020.8341	2	<i>I</i>	N	0.0525	2.6	3.7	
23369-3629	LHS0547	2021.7537	2	<i>I</i>	N	0.0516	2.7	3.9	
23455-1610	LHS4009AB	2019.5367	2	<i>I</i>	Y	0.3684	181.7	0.1	
23455-1610	LHS4009AB	2020.8342	2	<i>I</i>	Y	0.2275	175.9	0.0	
23455-1610	LHS4009AB	2021.5358	2	<i>I</i>	Y	0.1403	167.3	0.0	
23455-1610	LHS4009AB	2021.5656	2	<i>I</i>	Y	0.1394	167.7	0.2	
23455-1610	LHS4009AB	2022.4418	2	<i>I</i>	Y	0.0476	95.7	0.0	
23455-1610	LHS4009AB	2022.6821	3	<i>I</i>	Y	0.0872	61.0	0.8	:
23455-1610	LHS4009AB	2022.8450	2	<i>I</i>	Y	0.0794	42.9	0.4	q
23486-2740	LHS4016AB	2019.5367	2	<i>I</i>	N	0.0477	2.4	3.6	
23486-2740	LHS4016AB	2020.8342	2	<i>I</i>	N	0.0534	2.7	3.7	
23486-2740	LHS4016AB	2021.7538	2	<i>I</i>	N	0.0470	2.4	4.2	
23524-1441	LHS4032AB	2019.5367	2	<i>I</i>	Y	0.3780	252.9	1.9	q
23524-1441	LHS4032AB	2019.9495	2	<i>I</i>	Y	0.3781	250.3	1.9	q
23524-1441	LHS4032AB	2020.8342	2	<i>I</i>	Y	0.3801	245.4	1.8	:
23524-1441	LHS4032AB	2021.5656	1	<i>I</i>	Y	0.3857	241.2	1.8	:
23524-1441	LHS4032AB	2022.4419	2	<i>I</i>	Y	0.3925	237.1	1.9	q
23548-0957	LP763-082AB	2019.5396	2	<i>I</i>	Y	0.2525	249.5	2.6	q
23548-0957	LP763-082AB	2019.8590	2	<i>I</i>	Y	0.2636	251.1	2.5	q
23548-0957	LP763-082AB	2020.8342	2	<i>I</i>	Y	0.2842	262.4	2.6	q
23548-0957	LP763-082AB	2021.5358	2	<i>I</i>	Y	0.2921	268.6	2.5	q
23548-0957	LP763-082AB	2022.4419	2	<i>I</i>	Y	0.3054	276.9	2.5	q

Table 4: Results of the SOAR speckle interferometry campaign for nearby M dwarfs. The meanings of columns 8–10 differ depending on whether or not the companion was resolved in that observation, hence the two lines in those columns’ headers. The “:” flag in the last column indicates highly uncertain results; the rest of the flags are described in §4.2.

23557-0609	GJ0912AB	2019.5396	2	<i>I</i>	Y	0.3082	59.3	4.3	
23557-0609	GJ0912AB	2019.8590	3	<i>I</i>	Y	0.2890	53.0	4.6	
23557-0609	GJ0912AB	2020.8342	2	<i>I</i>	Y	0.2434	40.1	4.2	
23557-0609	GJ0912AB	2021.7321	2	<i>I</i>	Y	0.1982	18.5	4.2	
23557-0609	GJ0912AB	2022.4419	2	<i>I</i>	N	0.0437	2.4	4.5	
23557-0609	GJ0912AB	2022.6821	2	<i>I</i>	N	0.0500	3.0	4.5	
23585+0740	LTT17066AB	2019.5397	2	<i>I</i>	Y	0.2501	176.5	2.3	q
23585+0740	LTT17066AB	2020.8340	2	<i>I</i>	Y	0.2211	181.8	2.6	q
23585+0740	LTT17066AB	2021.5682	2	<i>I</i>	Y	0.1429	188.4	2.3	
23585+0740	LTT17066AB	2022.4447	2	<i>I</i>	Y	0.0408	215.1	2.1	
23585+0740	LTT17066AB	2022.6823	2	<i>I</i>	N	0.0492	2.7	4.2	
23597-4405	LTT09828AB	2019.6133	2	<i>I</i>	Y	0.3020	274.1	1.1	q
23597-4405	LTT09828AB	2020.8341	2	<i>I</i>	Y	0.2886	292.7	1.0	q
23597-4405	LTT09828AB	2021.5356	1	<i>V</i>	Y	0.2639	302.4	1.3	:
23597-4405	LTT09828AB	2021.5358	2	<i>I</i>	Y	0.2653	304.7	1.0	
23597-4405	LTT09828AB	2021.5358	1	<i>y</i>	Y	0.2897	305.5	0.6	
23597-4405	LTT09828AB	2022.4418	2	<i>I</i>	Y	0.2213	325.4	1.0	q
23597-4405	LTT09828AB	2022.8450	2	<i>I</i>	Y	0.1955	337.6	1.1	q

Table 5: Parameters for every orbit in this work, with the source of the orbit listed in column (1): RECONS refers to RECONS astrometry (Chapter 3), SOAR is speckle interferometry from SOAR (Chapter 4), and the 5-letter reference codes are defined in Table 1. Note that for all the RECONS orbits and many of the literature orbits, the semi-major axis given is photocentric rather than relative.

Orbit source (1)	System name (2)	Pair (3)	Num. comp. (4)	a (5)	a unit (6)	P_{orb} (7)	P_{orb} unit (8)	e (9)	i (deg) (10)	Ω (deg) (11)	ω (deg) (12)	T_0 (13)	T_0 unit (14)
SOAR	G131-026	AB	2	0.1475 ± 0.0017	as	5.91174 ± 0.01612	yr	0.0767 ± 0.0104	142.32 ± 1.37	83.05 ± 2.79	247.73 ± 7.39	2019.0110 ± 0.0940	yr
SOAR	LEHPM1-0255	AB	2	0.0956 ± 0.0018	as	3.35393 ± 0.01862	yr	0.5936 ± 0.0144	70.38 ± 1.17	130.91 ± 1.46	177.86 ± 5.22	2020.0631 ± 0.0394	yr
Ben16	GJ1005	AB	2	0.3037 ± 0.0005	as	1666.1 ± 2.5	d	0.364 ± 0.001	146.1 ± 0.2	62.8 ± 0.4	-13.4 ± 0.5	49850.4 ± 0.8	JD
SOAR	2MA0015-1636	AB	2	0.1109 ± 0.0038	as	4.24139 ± 0.04438	yr	0.0196 ± 0.0246	67.83 ± 3.21	90.98 ± 1.42	66.90 ± 44.10	2020.8500 ± 0.5172	yr
Bar18	GJ1006	AC	3	— —	— —	3.956523 ± 0.000092	d	0.00220 ± 0.00096	— —	— —	28 ± 23	709.24 ± 0.25	JD
Xia19	GJ2005	BC	3	3.80 ± 0.05	au	18.2 ± 0.5	yr	0.079 ± 0.04	63.8 ± 0.05	13.6 ± 0.05	184.0 ± 0.5	2005.5 ± 0.5	yr
Dup17	LP349-025	AB	2	145.99 ± 0.18	mas	7.698 ± 0.014	yr	0.0468 ± 0.0019	117.36 ± 0.11	36.64 ± 0.10	262.2 ± 1.8	2457758 ± 15	JD
Ben16	GJ0022	AC	3	0.5106 ± 0.0007	as	5694.2 ± 14.9	d	0.163 ± 0.002	43.7 ± 0.2	178.3 ± 0.2	104.5 ± 0.5	49850.4 ± 0.8	JD
RECONS	GIC0050	AC	3	48.30186 ± 2.56281	mas	5191.2065 ± 223.8426	d	0.15383 ± 0.07489	87.63176 ± 1.32732	17.66244 ± 1.23285	47.94209 ± 19.73337	2449184.4 ± 489.9	JD
Gaia3	GJ0046	AB	2	7.2375127 ± 0.085515	mas	147.02829 ± 0.072783	d	0.5046115 ± 0.011776	112.80806 ± 0.275703	92.402064 ± 0.430510	94.531558 ± 0.724865	48.461023 ± 0.645569	d
Win20	GJ1029	AB	2	— —	— —	95.76 ± 0.18	d	0.3786 ± 0.0067	— —	— —	210.0 ± 1.3	2457741.08 ± 0.56	BJD
Ben16	GJ0054	AB	2	0.1264 ± 0.0007	as	418.5 ± 0.2	d	0.174 ± 0.004	126.6 ± 0.4	92.2 ± 0.5	226.8 ± 1.4	53944.6 ± 1.6	JD
Gaia3	LP707-017	AB	2	2.3655559 ± 0.002073	mas	224.22364 ± 0.286031	d	0.2037968 ± 0.021277	62.265718 ± 1.080355	150.45981 ± 1.579310	175.22880 ± 4.957186	-72.65711 ± 2.960648	d
Ben16	GJ0065	AB	2	2.0458 ± 0.0066	as	9612 ± 12	d	0.617 ± 0.004	128.3 ± 0.3	147.6 ± 0.5	104.6 ± 0.5	41358.4 ± 12	JD

Table 5: Parameters for every orbit in this work, with the source of the orbit listed in column (1): RECONS refers to RECONS astrometry (Chapter 3), SOAR is speckle interferometry from SOAR (Chapter 4), and the 5-letter reference codes are defined in Table 1. Note that for all the RECONS orbits and many of the literature orbits, the semi-major axis given is photocentric rather than relative.

RECONS	LEHPM1-1882	AB	2	38.74030 ± 4.99821	mas	6473.5023 ± 114.7970	d	0.86941 ± 0.04126	132.12582 ± 8.77347	118.25965 ± 7.82891	71.81616 ± 7.97030	2447167.4 ± 122.1	JD
SOAR	GJ0084	AB	2	0.4917 ± 0.0204	as	13.30534 ± 0.17933	yr	0.3681 ± 0.0112	90.40 ± 0.36	100.88 ± 0.57	245.38 ± 7.11	2000.6267 ± 0.1930	yr
Man19	2MA0213+3648	AB	3	161.5 ± 1.3	mas	6.419 ± 0.071	yr	0.4232 ± 0.039	115.30 ± 0.24	83.73 ± 0.033	207.66 ± 0.73	57604.5 ± 2.9	d
Kur08	GJ1046	AB	2	— —	— —	168.848 ± 0.030	d	0.2792 ± 0.0015	— —	— —	92.70 ± 0.50	2453225.78 ± 0.32	BJD
SOAR	LP770-020	AB	2	0.2079 ± 0.0070	as	12.13572 ± 0.94703	yr	0.6459 ± 0.0196	35.29 ± 1.73	204.64 ± 2.79	125.64 ± 2.65	2021.6116 ± 0.0071	yr
Man19	GJ0098	AB	2	559.84 ± 0.66	mas	25.255 ± 0.021	yr	0.2354 ± 0.0013	73.389 ± 0.048	109.116 ± 0.022	231.49 ± 0.21	56417.3 ± 4.7	d
Man19	GJ0099	AB	2	360.53 ± 0.72	mas	24.015 ± 0.86	yr	0.2087 ± 0.0028	84.605 ± 0.049	98.836 ± 0.090	152.6 ± 1.9	56340. ± 43	d
SOAR	L225-057	AB	2	0.1586 ± 0.0024	as	6.35236 ± 0.18693	yr	0.2181 ± 0.0166	28.68 ± 1.21	121.79 ± 4.95	282.01 ± 7.18	2020.6965 ± 0.0315	yr
SOAR	LP993-116	BC	3	0.6303 ± 0.0375	as	28.46579 ± 2.05605	yr	0.2403 ± 0.0291	117.13 ± 1.98	158.70 ± 1.01	305.03 ± 8.74	2009.7143 ± 0.4337	yr
Man19	GJ0125	AB	2	534.5 ± 2.3	mas	25.67 ± 0.20	yr	0.2271 ± 0.044	97.186 ± 0.026	13.732 ± 0.082	181.38 ± 0.35	64226. ± 74	d
Spe19	BD+60-0637	AC	3	— —	— —	59.428 ± 0.005	d	0.642 ± 0.006	— —	— —	130.3 ± 0.8	2456470.94 ± 0.07	BJD
Bla10	SIP0320-0446	AB	2	— —	— —	246.9 ± 0.52	d	0.067 ± 0.015	— —	— —	167.2 ± 18.7	53529.9 ± 11.8	MJD
Gaia3	LT01628	AB	2	2.3092991 ± 0.027905	mas	90.192299 ± 0.036109	d	0.3281290 ± 0.015983	61.188629 ± 0.842641	85.812837 ± 1.113431	300.01806 ± 4.309562	-7.222555 ± 1.045613	d
SOAR	LHS1561	AB	2	0.0923 ± 0.0010	as	3.91379 ± 0.01684	yr	0.5256 ± 0.0093	143.85 ± 1.94	173.20 ± 3.08	173.05 ± 3.98	2021.8910 ± 0.0142	yr
RECONS	LHS1582	AB	2	23.69945 ± 0.67963	mas	1910.4690 ± 6.34995	d	0.27317 ± 0.04581	143.94120 ± 4.30654	112.02287 ± 6.49066	15.00402 ± 12.18412	2450018.8 ± 45.9	JD
Gaia3	LHS1610	AB	2	1.3910855	mas	10.588495	d	0.5239050	92.819743	162.59576	271.39623	0.6073069	d

Table 5: Parameters for every orbit in this work, with the source of the orbit listed in column (1): RECONS refers to RECONS astrometry (Chapter 3), SOAR is speckle interferometry from SOAR (Chapter 4), and the 5-letter reference codes are defined in Table 1. Note that for all the RECONS orbits and many of the literature orbits, the semi-major axis given is photocentric rather than relative.

				± 0.036712		± 0.001312		± 0.027422	± 1.903125	± 1.509986	± 2.873758	± 0.153265	
Mar09	GJ0164	AB	2	80.5	mas	736.9	d	0.161	121.9	271.8	311.7	1856	JD
				± 1.2		± 1.7		± 0.012	± 0.8	± 1.2	± 3.7	± 8	
Lub17	KELT0416-6200	AB	2	—	—	1.1112860702	d	0.03	83.4	—	271.2	2455255.96335	BJD
				—	—	± 0.000000370		± 0.01	± 0.1	—	± 0.2	± 0.00071	
Gaia3	LEHPM1-3719	AB	2	3.4655461	mas	142.51819	d	0.1748426	27.190651	176.33468	223.99335	-48.31705	d
				± 0.053385		± 0.081647		± 0.022331	± 1.490191	± 3.374812	± 7.654132	± 2.547950	
Dup17	LP415-020	AB	2	96.5	mas	14.82	yr	0.706	62.4	82.1	168	2458880.	JD
				± 1.4		± 0.24		± 0.012	± 1.6	± 1.1	± 4	$\pm 140.$	
Dup17	SDS0423-0414	AB	2	162.9	mas	12.3	yr	0.272	65.4	34.35	97.4	2458975.	JD
				± 0.5		± 0.06		± 0.008	± 0.3	± 0.23	± 0.3	$\pm 20.$	
Win20	LP655-043	AB	3	—	—	18.3715	d	0.1994	—	—	311.7	2458036.080	BJD
				—	—	± 0.0084		± 0.00078	—	—	± 2.7	± 0.069	
Mat97	DQTAU	AB	2	—	—	15.810	d	0.58	—	—	228	2449582.78	BJD
				—	—	± 0.006		± 0.07	—	—	± 5	± 0.23	
SOAR	LEP0448+1003	AB	2	0.1023	as	2.69806	yr	0.1982	52.31	282.61	171.39	2018.1868	yr
				± 0.0010		± 0.01114		± 0.0061	± 1.25	± 1.29	± 2.85	± 0.0176	
Gaia3	LSPM0448+3648	AB	2	1.1104699	mas	301.51811	d	0.5043747	116.90280	173.07100	126.05018	114.24924	d
				± 0.074667		± 2.699463		± 0.076621	± 6.036696	± 4.617607	± 10.26688	± 6.436705	
Del99	LP476-207	AC	3	—	—	11.9623	d	0.323	—	—	212.0	49799.47	JD
				—	—	± 0.0005		± 0.006	—	—	± 0.6	± 0.04	
Win20	LTT11586	AC	3	—	—	15.04547	d	0.5029	—	—	283.8	2458357.731	BJD
				\pm —	—	± 0.00041		± 0.0055	—	—	± 1.2	± 0.032	
Man19	GJ0190	AB	2	99.12	mas	0.96380	yr	0.2441	92.96	40.42	186.4	58182.4	d
				± 0.85		± 0.00024		± 0.0093	± 0.26	± 0.17	± 5.9	± 6.7	
Cas18	NGT0522-2507	AB	2	4.2945	R_{\odot}	1.74774445	d	0.00097	87.404	—	—	2457288.412922	BJD
				± 0.0158		± 0.00000054		± 0.00214	± 0.019	\pm —	—	± 0.000075	
Ben16	GJ1081	AB	2	0.2712	as	4066.1	d	0.848	97.1	231.5	231	48919.1	JD
				± 0.0027		± 27.5		± 0.004	± 0.2	± 0.2	± 0.7	± 28.9	
SOAR	SCR0533-4257	AB	2	0.0543	as	0.67037	yr	0.4505	147.85	91.66	23.66	2017.1513	yr
				± 0.0022		± 0.00214		± 0.0279	± 7.60	± 11.79	± 13.93	± 0.0131	

Table 5: Parameters for every orbit in this work, with the source of the orbit listed in column (1): RECONS refers to RECONS astrometry (Chapter 3), SOAR is speckle interferometry from SOAR (Chapter 4), and the 5-letter reference codes are defined in Table 1. Note that for all the RECONS orbits and many of the literature orbits, the semi-major axis given is photocentric rather than relative.

Gom12	PARANAGO-1802	AB	3	—	—	4.67390	d	0.017	—	—	1.48	2454849.9008	BJD
				\pm —	—	\pm 0.00006		\pm 0.003	—	—	\pm 0.01	\pm 0.0005	
Gaia3	APM0206	AB	2	3.2570241	mas	147.46727	d	0.5418394	166.13832	99.489185	131.46524	−48.61166	d
				\pm 0.097495		\pm 0.104131		\pm 0.025575	\pm 5.257562	\pm 14.56543	\pm 14.63436	\pm 0.968979	
SOAR	LP837-019	AB	2	0.0996	as	4.38358	yr	0.8468	150.70	347.22	131.50	2021.4523	yr
				\pm 0.0024		\pm 0.10861		\pm 0.0085	\pm 3.95	\pm 6.75	\pm 7.21	\pm 0.0114	
Zho15	LP827-020	AB	2	—	—	4.077017	d	0.002	—	—	274	2456374.0171	BJD
				—	—	\pm 0.000001		\pm 0.002	—	—	\pm 42	\pm 0.0001	
Bar18	GJ0220	AB	2	—	—	721.4	d	0.5089	—	—	109.2	1006.5	JD
				—	—	\pm 2.2		\pm 0.0089	—	—	\pm 1.7	\pm 1.6	
Ski18	G098-052	AB	2	—	—	2.63	d	0.010	—	—	128.94	2456261.747	BJD
				—	—	\pm 1.5		\pm 0.003	—	—	\pm 39.84	\pm 0.006	
Win20	LHS1817	AB	2	—	—	0.30992678	d	0.0063	—	—	93	2458357.731	BJD
				—	—	\pm 0.00000048		\pm 0.0031	—	—	\pm 37	\pm 0.032	
RECONS	SCR0613-2742	AB	2	8.93603	mas	2427.2605	d	0.84274	58.93405	21.48441	233.08614	2452758.9	JD
				\pm 1.72821		\pm 57.3312		\pm 0.07113	\pm 9.51929	\pm 10.13752	\pm 15.18826	\pm 169.7	
SOAR	UPM0624-2655	AB	2	0.1163	as	3.53956	yr	0.5199	145.87	32.17	159.28	2021.0312	yr
				\pm 0.0009		\pm 0.03184		\pm 0.0057	\pm 1.26	\pm 2.22	\pm 2.53	\pm 0.0045	
Ben16	GJ0234	AB	2	1.0932	as	6070.1	d	0.382	53.2	210.6	40.4	51277.1	JD
				\pm 0.0007		\pm 10.2		\pm 0.001	\pm 0.1	\pm 0.1	\pm 0.1	\pm 1.3	
Ben16	LHS0221	AB	2	0.4417	as	4946.3	d	0.482	109.7	107.8	58.9	54696.1	JD
				\pm 0.0009		\pm 2.2		\pm 0.002	\pm 0.1	\pm 0.1	\pm 0.2	\pm 1.7	
SOAR	SCR0702-6102	AB	2	0.0638	as	2.38183	yr	0.4022	164.78	−9.49	105.46	2020.6811	yr
				\pm 0.0031		\pm 0.03291		\pm 0.0302	\pm 17.17	\pm 65.41	\pm 62.95	\pm 0.0413	
Dup17	2MA0700+3157	AB	2	377	mas	23.9	yr	0.017	88.143	102.666	70.	2462500.	JD
				\pm 6		\pm 0.5		\pm 0.007	\pm 0.025	\pm 0.022	\pm 60.	\pm 1700.	
Ben16	LHS0224	AB	2	0.1564	as	1195.5	d	0.236	130.8	173.6	252.9	51340.5	JD
				\pm 0.0008		\pm 1.4		\pm 0.004	\pm 0.5	\pm 0.6	\pm 0.9	\pm 3.3	
Man19	GJ0263	AB	2	143.8	mas	3.6205	yr	0.7158	103.28	81.04	287.52	58416.0	d
				\pm 2.1		\pm 0.0021		\pm 0.0065	\pm 0.36	\pm 0.24	\pm 0.51	\pm 3.6	
SOAR	APM0089	AB	2	0.0346	as	0.69401	yr	0.1213	36.46	313.67	130.62	2021.3835	yr

Table 5: Parameters for every orbit in this work, with the source of the orbit listed in column (1): RECONS refers to RECONS astrometry (Chapter 3), SOAR is speckle interferometry from SOAR (Chapter 4), and the 5-letter reference codes are defined in Table 1. Note that for all the RECONS orbits and many of the literature orbits, the semi-major axis given is photocentric rather than relative.

				± 0.0023		± 0.00467		± 0.0602	± 9.45	± 11.45	± 10.80	± 0.0336	
Bar12	GJ0268	AB	2	11.10	mas	10.42672	d	0.3203	100.39	89.98	211.98	2450493.9853	JD
				± 0.05		± 0.00006		± 0.0009	± 0.03	± 0.07	± 0.19	± 0.0039	
Dup17	LHS1901	AB	2	287.7	mas	16.21	yr	0.8304	71.97	2.27	44.49	2460684.	JD
				± 0.8		± 0.08		± 0.05	± 0.05	± 0.05	± 0.15	$\pm 30.$	
Del99	GJ0268.3	AB	2	—	—	304.35	d	0.399	—	—	273.8	48826.0	JD
				—	—	± 0.25		± 0.008	—	—	± 0.9	± 1.5	
RECONS	WIS0720-0846	AB	2	126.15312	mas	3071.6587	d	0.25579	106.08327	60.57065	10.64022	2454256.4	JD
				± 3.94395		± 65.8720		± 0.00900	± 0.48875	± 0.43858	± 5.03874	± 44.0	
SOAR	GJ2060	AB	3	0.2543	as	7.78789	yr	0.8983	30.86	185.54	164.33	2013.0705	yr
				± 0.0018		± 0.00670		± 0.0031	± 2.29	± 3.65	± 4.33	± 0.0166	
SOAR	G089-032	AB	2	0.6377	as	23.68022	yr	0.5838	14.00	83.33	60.33	2016.2121	yr
				± 0.0029		± 0.22220		± 0.0031	± 1.27	± 4.65	± 4.84	± 0.0075	
Dup17	2MA0746+2000	AB	2	237.18	mas	12.736	yr	0.4854	138.56	29.77	355.6	2461877.	JD
				± 0.11		± 0.0310		± 0.003	± 0.21	± 0.30	± 0.6	$\pm 24.$	
Gaia3	LHS1955	AC	3	1.8734295	mas	14.325696	d	0.6166959	104.64619	170.41498	129.85968	2.3727361	d
				± 0.067767		± 0.001731		± 0.029570	± 0.730736	± 0.798222	± 2.461821	± 0.163313	
Sah15	DEN0823-4912	AB	2	4.62	mas	247.75	d	0.36	52.2	-13.8	41.8	55926.823928	MJD
				± 0.12		± 0.64		± 0.04	± 1.5	± 2.0	± 4.9	± 0.0	
Gaia3	LHS2010	AB	2	1.1433267	mas	51.796149	d	0.2228321	87.335893	158.45459	20.281939	7.1485523	d
				± 0.022576		± 0.026911		± 0.035247	± 1.111350	± 0.932677	± 8.856812	± 2.393316	
Man19	GJ0310	AB	2	552.6	mas	23.48	yr	0.6976	122.06	49.62	246.72	58432.5	d
				± 5.6		± 0.14		± 0.0074	± 0.57	± 0.39	± 0.37	± 5.3	
RECONS	SCR0838-5855	AB	2	92.76506	mas	8208.6213	d	0.23445	143.48352	166.15932	103.47027	2452271.7	JD
				± 10.73305		± 418.7722		± 0.04399	± 4.28150	± 7.45318	± 9.01940	± 263.3	
SOAR	UPM0838-2843	AB	2	0.0450	as	0.70178	yr	0.2147	144.78	109.70	317.31	2020.8398	yr
				± 0.0011		± 0.00237		± 0.0151	± 3.93	± 6.42	± 7.24	± 0.0062	
Gaia3	SCR0840-4044	AB	2	2.4395361	mas	83.383699	d	0.2945271	103.94548	149.29983	35.082058	-38.27105	d
				± 0.048046		± 0.045799		± 0.036476	± 0.766023	± 0.744065	± 5.424474	± 1.304741	
Gaia3	GJ0319	AB	2	1.4686946	mas	20.964576	d	0.1969016	119.78175	4.9747736	23.374571	2.1729976	d
				± 0.010601		± 0.002156		± 0.017267	± 0.989821	± 1.421525	± 5.196640	± 0.611830	

Table 5: Parameters for every orbit in this work, with the source of the orbit listed in column (1): RECONS refers to RECONS astrometry (Chapter 3), SOAR is speckle interferometry from SOAR (Chapter 4), and the 5-letter reference codes are defined in Table 1. Note that for all the RECONS orbits and many of the literature orbits, the semi-major axis given is photocentric rather than relative.

Har18	HAT-TR-318-007	AB	2	—	—	3.3439539	d	0.014	—	—	269.80	2457214.94178	JD
				—	—	± 0.0000002		± 0.03	—	—	± 0.03	± 0.00003	
Kra17	PTF0850+1948	AB	2	—	—	6.015742	d	0.0017	—	—	38	2457148.9041	JD
				—	—	± 0.000002		± 0.0006	—	—	± 17	± 0.0001	
RECONS	LHS2071	AB	2	184.49851	mas	12464.503	d	0.08887	64.90038	8.58040	24.10254	2445635.1	JD
				± 3.87648		± 100.529		± 0.01509	± 0.67647	± 0.69591	± 5.72160	± 243.5	
Del99	G041-014	AC	3	—	—	7.5555	d	0.014	—	—	7.0	50471.2	JD
				—	—	± 0.0002		± 0.002	—	—	± 9.3	± 0.2	
Tok15	G041-014	AB	3	0.398	as	5.566	yr	0.778	122.2	281.8	23.7	2006.445	yr
				± 0.008		± 0.024		± 0.019	± 3.1	± 1.7	± 3.2	± 0.039	
SOAR	LHS6167	AB	2	0.2003	as	5.04126	yr	0.4871	115.72	112.64	92.71	2019.2331	yr
				± 0.0012		± 0.00385		± 0.0050	± 0.32	± 0.34	± 0.24	± 0.0034	
Dup17	2MA0920+3517	AB	2	68.15	mas	7.258	yr	0.180	87.15	66.73	317.5	2457940.	JD
				± 0.23		± 0.009		± 0.007	± 0.17	± 0.12	± 1.5	± 11	
Win20	2MA0930+0227	AB	2	—	—	916.8	d	0.1928	—	—	240.5	2458262.3	BJD
				—	—	± 2.5		± 0.0046	—	—	± 1.2	± 2.6	
Man19	GJ0352	AB	2	638.0	mas	18.449	yr	0.3270	141.78	52.27	287.75	59074	d
				± 2.4		± 0.025		± 0.0035	± 0.60	± 0.51	± 0.75	± 13	
Spe19	HIP47133	AB	3	—	—	4.38804	d	0.474	—	—	140.2	2458055.344	BJD
				—	—	± 0.00001		± 0.005	—	—	± 1.9	± 0.015	
Har96	GJ0372	AB	2	—	—	47.709	d	0.53	—	—	81	2449345.44	yr
				—	—	± 0.053		± 0.02	—	—	± 2	± 0.52	
Dia07	GJ0375	AB	2	—	—	1.87844246	d	0.0072	—	—	—	2452779.422	HJD
				—	—	± 0.0000049		± 0.0070	—	—	—	± 0.005	
SOAR	GJ0381	AB	2	0.2920	as	7.60106	yr	0.7512	93.21	68.50	274.17	2016.8740	yr
				± 0.0060		± 0.01640		± 0.0117	± 0.14	± 0.26	± 0.20	± 0.0100	
Dup17	2MA1017+1308	AB	2	120.	mas	18.6	yr	0.158	35.4	72.7	5.0	2458650.	JD
				± 1.2		± 0.23		± 0.01	± 1.0	± 2.0	± 5.0	$\pm 150.$	
SOAR	TWA022	AB	2	0.0975	as	5.34326	yr	0.1357	17.02	120.78	111.06	2006.0272	yr
				± 0.0018		± 0.00769		± 0.0088	± 4.73	± 16.52	± 16.68	± 0.0526	
Bar18	LP790-002	AC	3	—	—	5.922845	d	0.01350	—	—	289.1	1007.42	JD

Table 5: Parameters for every orbit in this work, with the source of the orbit listed in column (1): RECONS refers to RECONS astrometry (Chapter 3), SOAR is speckle interferometry from SOAR (Chapter 4), and the 5-letter reference codes are defined in Table 1. Note that for all the RECONS orbits and many of the literature orbits, the semi-major axis given is photocentric rather than relative.

				—	—	± 0.000061		± 0.0012	—	—	± 6.4	± 0.107	
Bar18	LHS0283	AB	2	—	—	119.411	d	0.0655	—	—	326.0	718.42	JD
				—	—	± 0.035		± 0.0024	—	—	± 1.7	± 0.57	
SOAR	2MA1036+1521	BC	3	0.1481	as	8.51165	yr	0.3506	27.11	75.58	66.97	2011.1924	yr
				± 0.0012		± 0.02295		± 0.0068	± 1.54	± 3.37	± 3.47	± 0.0312	
RECONS	LP848-050	AB	2	71.95867	mas	2765.4649	d	0.05817	110.43925	22.88294	132.56650	2454399.7	JD
				± 1.83055		± 46.7516		± 0.02650	± 1.13357	± 1.15175	± 41.21267	± 320.9	
Gaia3	LP168-021	AB	2	7.1608430	mas	389.08611	d	0.1863472	160.71212	118.26233	40.083430	-75.96836	d
				± 0.083131		± 0.775708		± 0.011906	± 1.408958	± 6.204636	± 6.272141	± 2.574204	
Dup17	2MA1047+4026	BC	3	75.98	mas	6.562	yr	0.7485	30.0	85.5	63.5	2455822.5	JD
				± 0.22		± 0.029		± 0.0013	± 0.5	± 1.1	± 1.0	± 0.5	
Laz18	WIS1049-5319	AB	2	1784	mas	27.54	yr	0.343	100.26	139.67	128.1	2017.78	yr
				± 14		± 0.43		± 0.005	± 0.05	± 0.05	± 1.5	± 0.05	
Dup17	2MA1052+4422	AB	2	70.67	mas	8.608	yr	0.1399	62.1	126.8	187.3	2458987	JD
				± 0.24		± 0.0265		± 0.023	± 0.3	± 0.3	± 1.6	± 14	
Gaia3	WIS1055-7356	AB	2	14.192589	mas	775.71645	d	0.2207175	87.427405	6.7147627	60.663714	-384.3829	d
				± 0.157090		± 5.615055		± 0.014416	± 0.279520	± 0.386722	± 3.295789	± 8.308812	
SOAR	GAI1058-5525	AB	2	0.1014	as	4.32411	yr	0.07	63.64	199.29	280.62	2021.6189	yr
				± 0.0014		± 0.12958		± 0.0339	± 1.42	± 1.03	± 7.38	± 0.0919	
Dup17	GJ0417	BC	3	130.	mas	15.65	yr	0.105	102.9	101.01	348	2462370.	JD
				± 0.4		± 0.08		± 0.003	± 0.5	± 0.22	± 5	$\pm 50.$	
Irwin	LSPM1112+7626	AB	2	43.825	R_{\odot}	41.032363	d	0.23763	89.7339	—	50.10	2455290.04618	HJD
				± 0.069		± 0.000024		± 0.00086	± 0.0064	—	± 0.18	± 0.00018	
Dup17	LHS2397A	AB	3	214.8	mas	14.37	yr	0.351	42.55	74.7	221.2	2459093	JD
				± 0.8		± 0.05		± 0.003	± 0.29	± 0.8	± 1.3	± 23	
Spe19	HIP56229	AB	2	—	—	186.3	d	0.549	—	—	345.7	2458096.59	BJD
				—	—	± 0.73		± 0.050	—	—	± 1.7	± 1.04	
Win20	LP734-034	AB	2	—	—	33.6551	d	0.423	—	—	47.89	2457866.693	BJD
				—	—	± 0.0046		± 0.010	—	—	± 0.93	± 0.061	
SOAR	NLTT30359	AB	2	0.1230	as	2.31743	yr	0.8375	121.40	33.50	145.90	2021.3990	yr
				± 0.0028		± 0.01063		± 0.0134	± 1.16	± 2.66	± 4.09	± 0.0098	

Table 5: Parameters for every orbit in this work, with the source of the orbit listed in column (1): RECONS refers to RECONS astrometry (Chapter 3), SOAR is speckle interferometry from SOAR (Chapter 4), and the 5-letter reference codes are defined in Table 1. Note that for all the RECONS orbits and many of the literature orbits, the semi-major axis given is photocentric rather than relative.

Ben16	GJ0469	AB	2	0.3139 ± 0.0008	as	4223 ± 2.9	d	0.302 ± 0.003	107.6 ± 0.1	190.4 ± 0.2	89.2 ± 0.2	54548.2 ± 3.2	JD
SOAR	SCR1230-3411	AB	2	0.1048 ± 0.0020	as	4.46787 ± 0.12719	yr	0.2021 ± 0.0231	82.27 ± 1.24	57.82 ± 0.66	171.26 ± 10.00	2021.6381 ± 0.1181	yr
Ben16	GJ0473	AB	2	0.9167 ± 0.0017	as	5772.3 ± 9.4	d	0.301 ± 0.002	103.3 ± 0.7	143.5 ± 0.1	350.7 ± 0.5	54554 ± 8.7	JD
Win20	G123-045	AB	2	— —	— —	34.7557 ± 0.0041	d	0.3758 ± 0.0024	— ± —	— —	107.86 ± 0.35	2457755.218 ± 0.069	BJD
Gaia3	LHS5221	AB	2	2.4689465 ± 0.058949	mas	36.912219 ± 0.019372	d	0.3528583 ± 0.038868	50.943199 ± 2.160739	159.14340 ± 1.653231	265.90942 ± 6.099890	13.775994 ± 0.900969	d
Del99	GJ0487	AB	3	— —	— —	54.075 ± 0.006	d	0.081 ± 0.005	— —	— —	137.0 ± 3.0	50506.2 ± 0.05	JD
Man19	GJ0494	AB	3	427.73 ± 0.44	mas	13.709 ± 0.037	yr	0.2436 ± 0.0012	130.79 ± 0.20	56.13 ± 0.17	158.81 ± 0.62	59365. ± 18	d
Dup17	KELU-1	AB	2	227.9 ± 1.1	mas	24.98 ± 0.19	yr	0.709 ± 0.005	82.35 ± 0.08	44.78 ± 0.2	3.7 ± 2.1	2460410. ± 110.	JD
SOAR	NLTT33370	AB	2	0.1506 ± 0.0027	as	9.54198 ± 0.07456	yr	0.5926 ± 0.0063	50.37 ± 1.73	59.17 ± 2.17	208.68 ± 3.04	2013.5998 ± 0.0236	yr
Tok97	GJ0507	AB	3	— —	— —	200.26 ± 0.09	d	0.531 ± 0.011	— —	— —	348.8 ± 1.6	48780.30 ± 0.42	HJD
Spe19	GJ0508	AC	3	— —	— —	446.87 ± 0.43	d	0.082 ± 0.014	— —	— —	12.2 ± 8.4	2457009.7 ± 10.1	BJD
Dup17	2MA1404-3159	AB	2	133.7 ± 2.3	mas	16.52 ± 0.22	yr	0.825 ± 0.005	164 ± 8	207 ± 176	52 ± 172	2460690. ± 90.	JD
RECONS	WT0460	AB	2	134.30442 ± 0.83017	mas	6075.4019 ± 13.3419	d	0.31753 ± 0.00833	9.98989 ± 2.66668	114.74902 ± 14.97741	73.94811 ± 14.80984	2449716.1 ± 26.7	JD
Win20	GJ1182	AB	2	— —	— —	154.23 ± 0.51	d	0.5362 ± 0.0022	— —	— —	276.35 ± 0.58	2457713.3 ± 1.5	BJD
RECONS	DEN1454-6604	AB	2	111.23928 ± 11.42640	mas	6576.9713 ± 602.5020	d	0.32589 ± 0.04432	105.56886 ± 0.90129	129.89327 ± 1.38314	86.09474 ± 11.85654	2449286.6 ± 548.7	JD
Dup17	GJ0569	BC	3	93.64	mas	2.3707	yr	0.3186	32.7	142.5	81.19	2456159.2	JD

Table 5: Parameters for every orbit in this work, with the source of the orbit listed in column

(1): RECONS refers to RECONS astrometry (Chapter 3), SOAR is speckle interferometry from SOAR (Chapter 4), and the 5-letter reference codes are defined in Table 1. Note that for all the RECONS orbits and many of the literature orbits, the semi-major axis given is photocentric rather than relative.

				± 0.14		± 0.0005		± 0.001	± 0.23	± 0.3	± 0.29	± 0.4	
Gaia3	LHS3056	AC	3	6.3084675 ± 0.104760	mas	158.41203 ± 0.187614	d	0.7002550 ± 0.011502	55.804183 ± 0.926255	87.019966 ± 0.917694	231.67197 ± 1.674534	-6.784897 ± 1.828033	d
SOAR	LHS3056	AB	3	0.2329 ± 0.0043	as	13.54714 ± 0.36894	yr	0.4542 ± 0.0080	53.04 ± 0.82	74.68 ± 1.32	28.40 ± 1.35	2022.0279 ± 0.0354	yr
Lop05	GUBOO	AB	2	— —	— —	0.488728 ± 0.000002	d	0.0001 ± 0.0038	87.6 ± 0.2	— —	— —	2452723.9811 ± 0.0	BJD
Dup17	2MA1534-2952	AB	2	214.07 ± 0.27	mas	20.35 ± 0.06	yr	0.0027 ± 0.0028	85.56 ± 0.08	13.61 ± 0.05	80. $\pm 40.$	2462500. $\pm 900.$	JD
Nid02	GJ0595	AB	2	— —	— —	62.6277 ± 0.0001	d	0.26 ± 0.001	— —	— —	253 ± 0.1	2451999.50 ± 0.02	JD
RECONS	LTT06288	AB	2	36.61283 ± 1.06527	mas	3637.2862 ± 19.7605	d	0.51264 ± 0.05188	88.96396 ± 0.768091	152.24315 ± 0.84075	189.19239 ± 4.74322	2449306.8 ± 70.8	JD
SOAR	SCR1546-5534	AB	2	0.2037 ± 0.0032	as	5.42294 ± 0.42605	yr	0.3620 ± 0.0291	29.97 ± 8.02	181.51 ± 7.04	32.05 ± 11.04	2022.8118 ± 0.0547	yr
Kor16	LSR1610-0040	AB	2	9.89 ± 0.25	— —	633.0 ± 1.17	d	0.417 ± 0.032	83.5 ± 1.7	99.5 ± 1.8	146.6 ± 6.0	24535166 ± 10	JD
Dav16	EPIC203710387	AB	2	5.100 ± 0.043	R_{\odot}	2.808849 ± 0.000024	d	0.0156 ± 0.0087	82.84 ± 0.10	— —	259 ± 9.3	2456894.71388 ± 0.00051	BJD
Ben16	GJ0623	AB	2	0.2397 ± 0.0014	as	1367.4 ± 0.6	d	0.629 ± 0.004	152.5 ± 0.2	98.3 ± 0.5	245.4 ± 0.5	45838.7 ± 2.8	JD
SOAR	GJ2121	AB	2	0.2625 ± 0.0018	as	17.07924 ± 0.16891	yr	0.6873 ± 0.0031	137.73 ± 0.57	38.97 ± 0.93	16.84 ± 1.02	2020.9763 ± 0.0095	yr
Mor09	GJ0630.1	AB	2	3.7634 ± 0.0046	R_{\odot}	1.268389985 ± 0.000000005	d	0.0051 ± 0.0013	89.769 ± 0.073	— —	129 ± 16	2446058.56471 ± 0.00026	HJD
RECONS	GJ2122	AB	2	94.66970 ± 5.58066	mas	5985.2597 ± 82.7352	d	0.81768 ± 0.05032	107.29142 ± 2.28750	63.10332 ± 2.50848	191.80300 ± 6.77210	2450422.8 ± 122.7	JD
Maz01	GJ0644	AB	5	0.2256 ± 0.0011	as	625.8 ± 1.3	d	0.053 ± 0.028	163.1 ± 1.6	163.2 ± 3.1	115.6 ± 5.1	2447208 ± 45	HJD
Maz01	GJ0644	BD	5	— —	— —	2.965522 ± 0.000014	d	0.026 ± 0.007	— —	— —	166 ± 16	2447337.3 ± 0.14	HJD

Table 5: Parameters for every orbit in this work, with the source of the orbit listed in column (1): RECONS refers to RECONS astrometry (Chapter 3), SOAR is speckle interferometry from SOAR (Chapter 4), and the 5-letter reference codes are defined in Table 1. Note that for all the RECONS orbits and many of the literature orbits, the semi-major axis given is photocentric rather than relative.

SOAR	GJ1210	AB	2	0.3084 ± 0.0023	as	14.33994 ± 0.02900	yr	0.4865 ± 0.0040	112.31 ± 0.35	61.39 ± 0.50	203.35 ± 1.20	2006.5188 ± 0.0477	yr
Man19	GJ0661	AB	2	776.12 ± 1.01	mas	12.9551 ± 0.0043	yr	0.75167 ± 0.00062	146.96 ± 0.26	159.18 ± 0.67	98.31 ± 0.58	57730.0 ± 1.9	d
Gaia3	GJ0660.1	AB	2	9.0244201 ± 0.051291	mas	619.45972 ± 0.453215	d	0.6893240 ± 0.008188	55.783454 ± 0.419346	159.33112 ± 0.262961	187.81037 ± 0.423117	246.00364 ± 0.915719	d
SOAR	GJ1212	AB	2	0.0594 ± 0.0032	as	1.59170 ± 0.02243	yr	0.4593 ± 0.0555	65.63 ± 2.98	146.34 ± 4.16	261.76 ± 2.68	2020.3380 ± 0.0308	yr
RECONS	GJ1215	AB	3	46.50728 ± 1.10360	mas	3565.4532 ± 15.8338	d	0.11221 ± 0.03625	120.17789 ± 1.04462	169.49023 ± 1.06633	331.67412 ± 18.50755	2451109.1 ± 187.8	JD
RECONS	LHS0440	AB	2	38.49455 ± 4.77075	mas	10778.311 ± 793.282	d	0.42376 ± 0.11165	147.41673 ± 12.89470	126.87476 ± 19.35479	54.65653 ± 18.08734	2450662.4 ± 4679.7	JD
Ski18	G203-060	AB	2	— —	— —	3.29 ± 0.99	d	0.002 ± 0.002	— —	— —	54.47 ± 39.25	245649.3840 ± 0.3583	JD
Dup17	LP388-055	AB	2	283.2 ± 2.2	mas	21.65 ± 0.24	yr	0.497 ± 0.004	53.89 ± 0.110	179.08 ± 0.15	118.3 ± 0.4	2462870. ± 90.	JD
Win20	G258-017	AB	2	— —	— —	4.741475 ± 0.000018	d	0.00495 ± 0.00096	— —	— —	256.0 ± 9.5	2457828.76 ± 0.13	BJD
SOAR	G140-009	AB	2	0.3685 ± 0.0027	as	20.54797 ± 0.11549	yr	0.5424 ± 0.0066	104.20 ± 0.25	128.91 ± 0.28	234.64 ± 0.75	2007.3914 ± 0.0340	yr
Gaia3	G249-020	AB	2	6.9866742 ± 0.022336	mas	670.28830 ± 0.985803	d	0.1583456 ± 0.006200	57.915120 ± 0.259380	97.707602 ± 0.279589	183.81933 ± 1.861969	233.72044 ± 3.486808	d
Win20	LTT07077	AB	2	— —	— —	83.926 ± 0.032	d	0.0640 ± 0.0021	— —	— —	106.9 ± 1.6	2458294.34 ± 0.38	BJD
Gaia3	LP044-162	AB	2	7.0483434 ± 0.388444	mas	479.98901 ± 1.292692	d	0.5954590 ± 0.0523	65.787374 ± 1.132896	138.17582 ± 1.144182	301.05913 ± 2.575497	196.16699 ± 2.504982	d
SOAR	L043-072	AC	3	0.0752 ± 0.0035	as	1.99634 ± 0.04304	yr	0.0517 ± 0.0112	108.57 ± 4.37	139.85 ± 1.23	18.65 ± 50.99	2021.5448 ± 0.2842	yr
Del99	GJ1230	AC	3	— —	— —	5.06880 ± 0.00005	d	0.009 ± 0.001	— —	— ± —	230.0 ± 10.0	50643.7 ± 0.2	JD
RECONS	SCR1845-6357	AB	2	39.26953	mas	7020.3938	d	0.58714	41.31969	98.12510	151.72793	2445886.9	JD

Table 5: Parameters for every orbit in this work, with the source of the orbit listed in column

(1): RECONS refers to RECONS astrometry (Chapter 3), SOAR is speckle interferometry

from SOAR (Chapter 4), and the 5-letter reference codes are defined in Table 1. Note that

for all the RECONS orbits and many of the literature orbits, the semi-major axis given is

photocentric rather than relative.

				± 1.92811		± 134.4824		± 0.02886	± 2.53865	± 5.12689	± 5.31105	± 150.9	
RECONS	LTT07434	AB	2	62.82121	mas	8527.8578	d	0.72783	154.15708	153.51319	14.53715	2448510.3	JD
				± 2.12536		± 376.7276		± 0.03402	± 7.00990	± 15.28347	± 17.32617	± 402.5	
Duq88	GJ0735	AB	2	—	—	10.3191	d	0.200	—	—	177.2	2446188.981	JD
				—	—	± 0.0008		± 0.012	—	—	± 3.2	± 0.085	
Spe19	G229-018	AD	4	—	—	7.9461	d	0.044	—	—	291.9	2457609.65	BJD
				—	—	± 0.0002		± 0.007	—	—	± 12.8	± 0.28	
Seg00	GJ0747	AB	2	0.2881	as	2110.0	d	0.274	77.3	85.1	-29.1	50432.7	mJD
				± 0.0005		± 2.5		± 0.002	± 0.2	± 0.1	± 0.3	± 1.3	
Ben16	GJ0748	AB	2	0.148	as	901.7	d	0.45	131.6	-0.4	207.3	50033.2	JD
				± 0.0004		± 0.3		± 0.002	± 0.3	± 0.2	± 0.4	± 0.8	
Gaia3	2MA1912-5016	AB	2	5.0343065	mas	165.66557	d	0.5642821	119.98090	45.189540	68.112958	-21.16615	d
				± 0.203814		± 0.607364		± 0.038682	± 1.083311	± 3.094887	± 2.362920	± 3.458019	
Gaia3	L274-089	AB	3	4.3320445	mas	523.30323	d	0.1737850	110.67130	35.796589	252.23167	-237.5749	d
				± 0.054935		± 1.210355		± 0.027808	± 0.531972	± 0.708463	± 5.177429	± 7.175294	
Gaia3	G260-022	AB	2	3.6764836	mas	125.45001	d	0.5785184	102.31979	167.20287	121717224	-11.72326	d
				± 0.148544		± 0.046899		± 0.032081	± 0.624435	± 0.625053	± 2.439353	± 0.693267	
Gaia3	G125-018	AB	2	1.1385217	mas	209.31568	d	0.4698172	140.99209	145.74353	109.74534	5.4234106	d
				± 0.052939		± 0.739235		± 0.044447	± 3.998071	± 6.074409	± 6.441503	± 4.644838	
SOAR	UPM1951-3100	AB	2	0.1143	as	2.81908	yr	0.5711	72.41	32.13	157.14	2021.4374	yr
				± 0.0011		± 0.01606		± 0.0070	± 0.77	± 0.63	± 1.45	± 0.0068	
Ben16	GJ1245	AC	3	0.8267	as	6147	d	0.334	135.7	261.2	36.1	51506.8	JD
				± 0.0008		± 17		± 0.002	± 0.1	± 0.2	± 0.2	± 2.1	
Bar18	LP395-008	AC	3	—	—	1.1293392	d	0.00071	—	—	352	620.075	JD
				—	—	± 0.0000072		± 0.0026	—	—	± 12	± 0.039	
SOAR	GJ0791.2	AB	2	0.0985	as	1.47053	yr	0.6006	156.56	285.16	15.03	2019.1671	yr
				± 0.0011		± 0.00033		± 0.0087	± 3.38	± 2.16	± 2.84	± 0.0054	
RECONS	LEHPM2-1265	AB	2	29.59986	mas	1872.7103	d	0.58784	84.85068	173.22702	58.91194	2453288.9	JD
				± 1.34727		± 13.2281		± 0.04153	± 1.88134	± 1.49828	± 5.84728	± 39.0	
Ire08	GJ0802	AC	3	17.2	mas	1104	d	0.35	82.7	22.0	89.6	2453031	HJD
				± 1.0		± 9		± 0.05	± 3.0	± 1.3	± 4.8	± 13	

Table 5: Parameters for every orbit in this work, with the source of the orbit listed in column

(1): RECONS refers to RECONS astrometry (Chapter 3), SOAR is speckle interferometry

from SOAR (Chapter 4), and the 5-letter reference codes are defined in Table 1. Note that

for all the RECONS orbits and many of the literature orbits, the semi-major axis given is

photocentric rather than relative.

Ire08	GJ0802	AB	3	—	—	0.7395340	d	0.0	—	—	—	2454140.530	HJD
				—		± 0.000003		± 0.01	—	—	—	± 0.001	
SOAR	LHS0501	AC	3	0.0917	as	1.84367	yr	0.2422	141.71	237.51	231.98	2017.1359	yr
				± 0.0008	as	± 0.00209		± 0.0046	± 1.18	± 1.05	± 1.32	± 0.0062	
Duq88	GJ0815	AC	3	—	—	3.276188	d	0.007	—	—	0	2445912.5117	JD
				—	—	± 0.00005		± 0.007	—	—	± 0.0	± 0.0047	
RECONS	USN2101+0307	AB	2	32.43682	mas	2740.5760	d	0.50400	30.34936	162.40174	61.49448	2453056.2	JD
				± 0.99398		± 13.8945		± 0.04184	± 4.39000	± 9.23285	± 9.60322	± 36.4	
Gaia3	L117-123	AB	2	8.5058281	mas	381.17030	d	0.4014876	94.192807	11.474933	154.98840	-171.3100	d
				± 0.047571		± 0.139594		± 0.005953	± 0.247629	± 0.102816	± 0.523450	± 1.015409	
Ski18	G212-034	AB	2	—	—	8.17	d	0.062	—	—	127.78	2456488.0751	JD
				—	—	± 1.31		± 0.012	—	—	± 9.00	± 0.2036	
Del99	GJ0829	AB	2	—	—	53.221	d	0.374	—	—	300.0	48980.2	JD
				—	—	± 0.004		± 0.004	—	—	± 1.0	± 0.2	
Ben16	GJ0831	AB	2	0.1448	as	704.9	d	0.39	49.8	326.1	10.6	51164	JD
				± 0.0005		± 0.5		± 0.002	± 0.4	± 0.4	± 0.9	± 1.1	
Dup17	2MA2132+1341	AB	2	86.1	mas	10.74	yr	0.315	144.8	82.0	15	2458160.	JD
				± 0.4		± 0.17		± 0.005	± 0.6	± 2.2	± 5	$\pm 70.$	
Bal10	LTT16329	AB	2	0.2169	as	12.75	yr	0.294	—	—	—	—	—
				± 0.0026		± 0.13		± 0.0130	—	—	—	—	—
Dup17	2MA2140+1625	AB	2	143.0	mas	24.45	yr	0.196	37.3	100.5	186.6	2464380.	JD
				± 1.4		± 0.25		± 0.007	± 0.6	± 0.6	± 1.2	$\pm 90.$	
Gaia3	G093-033	AB	2	0.9076336	mas	14.646202	d	0.2232439	104.28876	19.445738	242.68999	3.8844248	d
				± 0.022553		± 0.003492		± 0.047969	± 1.367956	± 2.529461	± 14.66070	± 1.177080	
SOAR	WT0818	AB	2	0.1238	as	6.90482	yr	0.6440	129.70	142.63	356.23	2022.4841	yr
				± 0.0013		± 0.31003		± 0.0121	± 1.85	± 1.86	± 3.19	± 0.0165	
SOAR	LP983-034	AB	2	0.0693	as	2.56028	yr	0.1254	121.15	177.20	3.37	2022.7170	yr
				± 0.0011		± 0.01668		± 0.0084	± 1.76	± 1.36	± 6.87	± 0.0449	
RECONS	LHS3739	BC	3	30.71657	mas	2214.6135	d	0.29972	123.90136	137.14225	169.21578	2449388.8	JD
				± 0.48311		± 3.6716		± 0.02534	± 1.26176	± 1.14691	± 6.39904	± 37.5	
Dup17	2MA2140+1625	AB	2	143.0	mas	24.45	yr	0.196	37.3	100.5	186.6	2464380.	JD

Table 5: Parameters for every orbit in this work, with the source of the orbit listed in column (1): RECONS refers to RECONS astrometry (Chapter 3), SOAR is speckle interferometry from SOAR (Chapter 4), and the 5-letter reference codes are defined in Table 1. Note that for all the RECONS orbits and many of the literature orbits, the semi-major axis given is photocentric rather than relative.

				± 1.4		± 0.25		± 0.007	± 0.6	± 0.6	± 1.2	$\pm 90.$	
Act20	NGT2143-3801	AB	2	15.61805	R_{\odot}	7.61793	d	0.32034	87.58709	—	—	2457501.97719	BJD
				± 0.06457		± 0.00000544		± 0.00120	± 0.05265	—	—	± 0.00040	
Man19	GJ0844	AB	2	306.7	mas	11.798	yr	0.4838	38.21	151.8	267.2	57032.7	d
				± 2.6		± 0.067		± 0.0075	± 0.89	± 1.1	± 1.1	± 9.4	
Die18	GJ0845	BC	3	1.355	au	4165.09	d	0.47	75.90	148.58	316.99	2450967.7	JD
				± 0.0195		± 43.7		± 0.02	± 0.38	± 0.28	± 1.46	± 40.1	
Dup17	2MA2206-2047	AB	2	167.7	mas	23.96	yr	0.015	43.8	77.6	96	2463500.	JD
				± 0.5		± 0.23		± 0.008	± 0.5	± 0.4	± 13	$\pm 400.$	
SOAR	LEHPM1-4771	AB	2	0.1360	as	5.80759	yr	0.3345	108.06	90.09	218.66	2022.7401	yr
				± 0.0019		± 0.70943		± 0.0406	± 2.71	± 1.21	± 16.80	± 0.1148	
Seg00	GJ0866	AB	3	0.3473	as	822.6	d	0.439	112.6	-18.8	158.7	51810.3	mJD
				± 0.0005		± 0.2		± 0.001	± 0.1	± 0.1	± 0.3	± 0.4	
Her65	GJ0867	AC	4	—	—	4.08322	d	0.010	—	—	356	2437144.123	JD
				—	—	± 0.00004		± 0.010	—	—	± 32	± 0.006	
Gaia3	LEP2249+0459	AB	2	2.3483261	mas	134.66723	d	0.1980760	110.87619	142.73964	265.40140	55.493481	d
				± 0.053698		± 0.203825		± 0.041365	± 1.103878	± 1.286007	± 10.72544	± 4.538182	
Dup17	DEN2252-1730	AB	2	123.3	mas	8.822	yr	0.334	108.6	178.0	314.6	2460720.	JD
				± 0.8		± 0.027		± 0.009	± 0.5	± 0.3	± 1.2	$\pm 23.$	
SOAR	SCR2303-4650	AB	2	0.2434	as	13.55992	yr	0.1972	93.89	153.66	155.50	2015.2708	yr
				± 0.0047		± 0.81492		± 0.0275	± 0.62	± 0.67	± 18.44	± 0.5207	
SOAR	G273-033	AB	2	0.0941	as	4.01980	yr	0.2578	74.31	20.19	167.91	2022.6789	yr
				± 0.0032		± 0.20572		± 0.0370	± 1.00	± 1.03	± 9.42	± 0.0519	
SOAR	LHS4009	AB	2	0.4129	as	21.21853	yr	0.4905	98.93	9.47	353.90	2024.3277	yr
				± 0.0045		± 0.25750		± 0.0141	± 0.56	± 0.35	± 1.96	± 0.0719	
SOAR	LTT09828	AB	2	0.2170	as	10.71737	yr	0.4369	22.45	131.29	312.63	2003.0158	yr
				± 0.0011		± 0.05449		± 0.0066	± 1.32	± 4.21	± 4.30	± 0.0759	

REFERENCES

- Abt, H. A., Gomez, A. E., & Levy, S. G. 1990, *ApJS*, 74, 551
- Acton, J. S. et al. 2020, *MNRAS*, 494, 3950
- Alonso-Floriano, F. J., Caballero, J. A., Cortés-Contreras, M., Solano, E., & Montes, D. 2015, *A&A*, 583, A85
- Balega, I. I., Balega, Y. Y., & Malogolovets, E. V. 2010, *Astrophysical Bulletin*, 65, 250
- Baroch, D. et al. 2018, *A&A*, 619, A32
- Barry, R. K. et al. 2012, *ApJ*, 760, 55
- Basri, G., & Martín, E. L. 1999, *AJ*, 118, 2460
- Bate, M. R. 2012, *MNRAS*, 419, 3115
- Bate, M. R. 2015, in *Astronomical Society of the Pacific Conference Series*, Vol. 496, *Living Together: Planets, Host Stars and Binaries*, ed. S. M. Rucinski, G. Torres, & M. Zejda, 37
- . 2018, *MNRAS*, 475, 5618
- Bate, M. R., & Bonnell, I. A. 1997, *MNRAS*, 285, 33
- Bell, C. P. M., Mamajek, E. E., & Naylor, T. 2015, *MNRAS*, 454, 593
- Benedict, G. F. et al. 2016, *AJ*, 152, 141
- Bertin, E., & Arnouts, S. 1996, *A&AS*, 117, 393
- Blake, C. H., Charbonneau, D., & White, R. J. 2010, *ApJ*, 723, 684
- Brandner, W., Calissendorff, P., & Kopytova, T. 2023, *MNRAS*, 518, 662

- Burn, R., Schlecker, M., Mordasini, C., Emsenhuber, A., Alibert, Y., Henning, T., Klahr, H., & Benz, W. 2021, *A&A*, 656, A72
- Cañas, C. I. et al. 2022, *AJ*, 164, 50
- . 2023, arXiv e-prints, arXiv:2302.07714
- Casewell, S. L. et al. 2018, *MNRAS*, 481, 1897
- Chabrier, G., & Baraffe, I. 1997, *A&A*, 327, 1039
- Clarke, C. J., Gendrin, A., & Sotomayor, M. 2001, *MNRAS*, 328, 485
- Clarke, C. J., & Pringle, J. E. 1991a, *MNRAS*, 249, 584
- . 1991b, *MNRAS*, 249, 588
- Cuello, N., Ménard, F., & Price, D. J. 2023, *European Physical Journal Plus*, 138, 11
- Cutri, R. M. et al. 2003, *VizieR Online Data Catalog*, II/246
- Dal, H. A., & Evren, S. 2011, *PASP*, 123, 659
- David, T. J., Hillenbrand, L. A., Cody, A. M., Carpenter, J. M., & Howard, A. W. 2016, *ApJ*, 816, 21
- Delfosse, X., Forveille, T., Beuzit, J. L., Udry, S., Mayor, M., & Perrier, C. 1999, *A&A*, 344, 897
- Delfosse, X., Forveille, T., Ségransan, D., Beuzit, J. L., Udry, S., Perrier, C., & Mayor, M. 2000, *A&A*, 364, 217
- Díaz, R. F., González, J. F., Cincunegui, C., & Mauas, P. J. D. 2007, *A&A*, 474, 345
- Dieterich, S. 2018, *Sergedieterich/Mcmc_Sd: Mcmc_Sd V1.0*, Zenodo
- Dieterich, S. B., Henry, T. J., Jao, W.-C., Winters, J. G., Hosey, A. D., Riedel, A. R., &

- Subasavage, J. P. 2014, *AJ*, 147, 94
- Dieterich, S. B., Simler, A., Henry, T. J., & Jao, W.-C. 2021, *AJ*, 161, 172
- Dieterich, S. B. et al. 2018, *ApJ*, 865, 28
- Douglas, S. T., Agüeros, M. A., Covey, K. R., & Kraus, A. 2017, *ApJ*, 842, 83
- Dupuy, T. J., & Liu, M. C. 2017, *ApJS*, 231, 15
- Duquennoy, A., & Mayor, M. 1988, *A&A*, 200, 135
- . 1991, *A&A*, 248, 485
- El-Badry, K., Rix, H.-W., Tian, H., Duchêne, G., & Moe, M. 2019, *MNRAS*, 489, 5822
- Fabian, A. C., Pringle, J. E., & Rees, M. J. 1975, *MNRAS*, 172, 15
- Fabrycky, D., & Tremaine, S. 2007, *ApJ*, 669, 1298
- Fisher, R. T. 2004, *ApJ*, 600, 769
- Gaia Collaboration et al. 2022, arXiv e-prints, arXiv:2206.05595
- . 2016, *A&A*, 595, A1
- Gammie, C. F. 2001, *ApJ*, 553, 174
- Gómez Maqueo Chew, Y., Stassun, K. G., Prša, A., Stempels, E., Hebb, L., Barnes, R., Heller, R., & Mathieu, R. D. 2012, *ApJ*, 745, 58
- Gray, R. O., Corbally, C. J., Garrison, R. F., McFadden, M. T., Bubar, E. J., McGahee, C. E., O'Donoghue, A. A., & Knox, E. R. 2006, *AJ*, 132, 161
- Gray, R. O., Corbally, C. J., Garrison, R. F., McFadden, M. T., & Robinson, P. E. 2003, *AJ*, 126, 2048
- Guszejnov, D., Grudić, M. Y., Hopkins, P. F., Offner, S. S. R., & Faucher-Giguère, C.-A.

- 2021, MNRAS, 502, 3646
- Guszejnov, D., Hopkins, P. F., & Krumholz, M. R. 2017, MNRAS, 468, 4093
- Harlow, J. J. B. 1996, AJ, 112, 2222
- Harrington, R. S., & Miranian, M. 1977, PASP, 89, 400
- Hartkopf, W. I., Mason, B. D., & Worley, C. E. 2001, AJ, 122, 3472
- Hartman, J. D. et al. 2018, AJ, 155, 114
- Hawley, S. L., Gizis, J. E., & Reid, I. N. 1996, AJ, 112, 2799
- Henry, T. J., Franz, O. G., Wasserman, L. H., Benedict, G. F., Shelus, P. J., Ianna, P. A., Kirkpatrick, J. D., & McCarthy, Donald W., J. 1999, ApJ, 512, 864
- Henry, T. J., Jao, W.-C., Subasavage, J. P., Beaulieu, T. D., Ianna, P. A., Costa, E., & Méndez, R. A. 2006, AJ, 132, 2360
- Henry, T. J. et al. 2018, AJ, 155, 265
- Henry, T. J., & McCarthy, D. W., J. 1990, ApJ, 350, 334
- Henry, T. J., & McCarthy, Donald W., J. 1993, AJ, 106, 773
- Herbig, G. H., & Moorhead, J. M. 1965, ApJ, 141, 649
- Hilditch, R. W. 2001, *An Introduction to Close Binary Stars* (Cambridge, UK: Cambridge University Press)
- Holden, N., Henry, T., Vrijmoet, E., Couperus, A., Jao, W.-C., Dieterich, S., & Recons Team. 2023, in *American Astronomical Society Meeting Abstracts*, Vol. 55, American Astronomical Society Meeting Abstracts, 302.17
- Hoogerwerf, R., de Bruijne, J. H. J., & de Zeeuw, P. T. 2001, A&A, 365, 49

- Ireland, M. J., Kraus, A., Martinache, F., Lloyd, J. P., & Tuthill, P. G. 2008, *ApJ*, 678, 463
- Irwin, J., Charbonneau, D., Nutzman, P., & Falco, E. 2009, in *Transiting Planets*, ed. F. Pont, D. Sasselov, & M. J. Holman, Vol. 253, 37–43
- Irwin, J. M. et al. 2011, *ApJ*, 742, 123
- Jao, W.-C., Henry, T. J., Gies, D. R., & Hambly, N. C. 2018, *ApJ*, 861, L11
- Jao, W.-C., Henry, T. J., Subasavage, J. P., Brown, M. A., Ianna, P. A., Bartlett, J. L., Costa, E., & Méndez, R. A. 2005, *AJ*, 129, 1954
- Jefferys, W. H., Fitzpatrick, M. J., & McArthur, B. E. 1988, *Celestial Mechanics*, 41, 39
- Kanodia, S. et al. 2023, *AJ*, 165, 120
- Kirk, H. et al. 2017, *ApJ*, 838, 114
- Koren, S. C., Blake, C. H., Dahn, C. C., & Harris, H. C. 2016, *AJ*, 151, 57
- Kozai, Y. 1962, *AJ*, 67, 591
- Kratter, K. M. 2011, in *Astronomical Society of the Pacific Conference Series*, Vol. 447, *Evolution of Compact Binaries*, ed. L. Schmidtbreick, M. R. Schreiber, & C. Tappert, 47
- Kratter, K. M., & Murray-Clay, R. A. 2011, *ApJ*, 740, 1
- Kraus, A. L. et al. 2017, *ApJ*, 845, 72
- Kuffmeier, M., Calcutt, H., & Kristensen, L. E. 2019, *A&A*, 628, A112
- Kürster, M., Endl, M., & Reffert, S. 2008, *A&A*, 483, 869
- Lasker, B. M., Doggett, J., McLean, B., Sturch, C., Djorgovski, S., de Carvalho, R. R., & Reid, I. N. 1996, in *Astronomical Society of the Pacific Conference Series*, Vol. 101, *Astronomical Data Analysis Software and Systems V*, ed. G. H. Jacoby & J. Barnes, 88

- Law, N. M., Kraus, A. L., Street, R. R., Lister, T., Shporer, A., Hillenbrand, L. A., & Palomar Transient Factory Collaboration. 2011, in *Astronomical Society of the Pacific Conference Series*, Vol. 448, 16th Cambridge Workshop on Cool Stars, Stellar Systems, and the Sun, ed. C. Johns-Krull, M. K. Browning, & A. A. West, 1367
- Lazorenko, P. F., & Sahlmann, J. 2018, *A&A*, 618, A111
- Lee, A. T., Offner, S. S. R., Kratter, K. M., Smullen, R. A., & Li, P. S. 2019, *ApJ*, 887, 232
- Lee, Y.-N., & Hennebelle, P. 2018, *A&A*, 611, A89
- Lidov, M. L. 1962, *Planet. Space Sci.*, 9, 719
- Lindgren, L. et al. 2018, *A&A*, 616, A2
- López-Morales, M., & Ribas, I. 2005, *ApJ*, 631, 1120
- Lubin, J. B. et al. 2017, *ApJ*, 844, 134
- Lubow, S. H., & Artymowicz, P. 1996, in *NATO Advanced Study Institute (ASI) Series C*, Vol. 477, *Evolutionary Processes in Binary Stars*, ed. R. A. M. J. Wijers, M. B. Davies, & C. A. Tout, 53
- Lubow, S. H., & Artymowicz, P. 2000, in *Protostars and Planets IV*, ed. V. Mannings, A. P. Boss, & S. S. Russell, 731
- Ma, B., & Ge, J. 2014, *MNRAS*, 439, 2781
- Mamajek, E. E. 2009, in *American Institute of Physics Conference Series*, Vol. 1158, *Exoplanets and Disks: Their Formation and Diversity*, ed. T. Usuda, M. Tamura, & M. Ishii, 3–10
- Mann, A. W. et al. 2019, *ApJ*, 871, 63

- Mann, A. W., Feiden, G. A., Gaidos, E., Boyajian, T., & von Braun, K. 2015, *ApJ*, 804, 64
- Martinache, F., Rojas-Ayala, B., Ireland, M. J., Lloyd, J. P., & Tuthill, P. G. 2009, *ApJ*, 695, 1183
- Mason, B. D., Gies, D. R., Hartkopf, W. I., Bagnuolo, William G., J., ten Brummelaar, T., & McAlister, H. A. 1998, *AJ*, 115, 821
- Mason, B. D., Hartkopf, W. I., Gies, D. R., Henry, T. J., & Helsel, J. W. 2009, *AJ*, 137, 3358
- Mason, B. D., Wycoff, G. L., Hartkopf, W. I., Douglass, G. G., & Worley, C. E. 2001, *AJ*, 122, 3466
- Mathieu, R. D., & Mazeh, T. 1988, *ApJ*, 326, 256
- Mathieu, R. D., Stassun, K., Basri, G., Jensen, E. L. N., Johns-Krull, C. M., Valenti, J. A., & Hartmann, L. W. 1997, *AJ*, 113, 1841
- Mazeh, T. 2008, in *EAS Publications Series*, Vol. 29, *EAS Publications Series*, ed. M. J. Goupil & J. P. Zahn, 1–65
- Mazeh, T. et al. 2001, *MNRAS*, 325, 343
- McDonald, J. M., & Clarke, C. J. 1995, *MNRAS*, 275, 671
- Meibom, S., & Mathieu, R. D. 2005, *ApJ*, 620, 970
- Moe, M., & Di Stefano, R. 2017, *ApJS*, 230, 15
- Moe, M., & Kratter, K. M. 2018, *ApJ*, 854, 44
- Morales, J. C. et al. 2009, *ApJ*, 691, 1400
- Muñoz, D. J., Kratter, K., Vogelsberger, M., Hernquist, L., & Springel, V. 2015, *MNRAS*,

446, 2010

Muirhead, P. S., Dressing, C. D., Mann, A. W., Rojas-Ayala, B., Lépine, S., Paegert, M.,

De Lee, N., & Oelkers, R. 2018, *AJ*, 155, 180

Newton, E. R., Irwin, J., Charbonneau, D., Berta-Thompson, Z. K., Dittmann, J. A., &

West, A. A. 2016, *ApJ*, 821, 93

Nidever, D. L., Marcy, G. W., Butler, R. P., Fischer, D. A., & Vogt, S. S. 2002, *ApJS*, 141,

503

Offner, S. S. R., Dunham, M. M., Lee, K. I., Arce, H. G., & Fielding, D. B. 2016, *ApJ*, 827,

L11

Offner, S. S. R., Klein, R. I., McKee, C. F., & Krumholz, M. R. 2009, *ApJ*, 703, 131

Offner, S. S. R., Moe, M., Kratter, K. M., Sadavoy, S. I., Jensen, E. L. N., & Tobin, J. J.

2022, arXiv e-prints, arXiv:2203.10066

Olczak, C., Pfalzner, S., & Spurzem, R. 2006, *ApJ*, 642, 1140

Öpik, E. 1924, *Publications of the Tartu Astrofizica Observatory*, 25, 1

Pascucci, I. et al. 2016, *ApJ*, 831, 125

Pass, E. K., Charbonneau, D., Irwin, J. M., & Winters, J. G. 2022, *ApJ*, 936, 109

Perryman, M. 2012, *European Physical Journal H*, 37, 745

Pineda, J. E. et al. 2015, *Nature*, 518, 213

Popper, D. M. 1980, *ARA&A*, 18, 115

Raghavan, D. et al. 2010, *ApJS*, 190, 1

Reid, I. N. et al. 2003, *AJ*, 126, 3007

- Reid, I. N., Hawley, S. L., & Gizis, J. E. 1995, *AJ*, 110, 1838
- Reynolds, N. K. et al. 2021, *ApJ*, 907, L10
- Ribas, Á., Bouy, H., & Merín, B. 2015, *A&A*, 576, A52
- Ribas, I. et al. 2023, *A&A*, 670, A139
- Riedel, A. R. et al. 2014, *AJ*, 147, 85
- Rizzuto, A. C. et al. 2013, *MNRAS*, 436, 1694
- Rodriguez, J. E. et al. 2018, *ApJ*, 859, 150
- Sahlmann, J. et al. 2015, *A&A*, 579, A61
- Ségransan, D., Delfosse, X., Forveille, T., Beuzit, J. L., Udry, S., Perrier, C., & Mayor, M. 2000, *A&A*, 364, 665
- Shatsky, N., & Tokovinin, A. 2002, *A&A*, 382, 92
- Skinner, J. et al. 2018, *AJ*, 156, 45
- Skrutskie, M. F. et al. 2006, *AJ*, 131, 1163
- Sperauskas, J., Deveikis, V., & Tokovinin, A. 2019, *A&A*, 626, A31
- Tokovinin, A. 2014, *AJ*, 147, 86
- . 2016, *Orbit: Idl Software For Visual, Spectroscopic, And Combined Orbits*, Zenodo
- . 2018, *PASP*, 130, 035002
- Tokovinin, A., Cantarutti, R., Tighe, R., Schurter, P., Martinez, M., Thomas, S., & van der Blik, N. 2016, *PASP*, 128, 125003
- Tokovinin, A., & Kiyaeva, O. 2016, *MNRAS*, 456, 2070
- Tokovinin, A., Mason, B. D., & Hartkopf, W. I. 2010, *AJ*, 139, 743

- Tokovinin, A., Mason, B. D., Hartkopf, W. I., Mendez, R. A., & Horch, E. P. 2015, *AJ*, 150, 50
- Tokovinin, A., Mason, B. D., Mendez, R. A., & Costa, E. 2022, *AJ*, 164, 58
- Tokovinin, A., Mason, B. D., Mendez, R. A., Costa, E., & Horch, E. P. 2020, *AJ*, 160, 7
- Tokovinin, A., Mason, B. D., Mendez, R. A., Costa, E., Mann, A. W., & Henry, T. J. 2021, *AJ*, 162, 41
- Tokovinin, A., & Moe, M. 2020, *MNRAS*, 491, 5158
- Tokovinin, A. A. 1997, *A&AS*, 121, 71
- Udry, S., Mayor, M., Delfosse, X., Forveille, T., & Perrier-Bellet, C. 2000, *IAU Symposium*, 200, 158
- Valtonen, M., & Mikkola, S. 1991, *ARA&A*, 29, 9
- Van De Kamp, P. 1967, *Principles of astrometry* (San Francisco, CA: Freeman)
- Vrijmoet, E. H., Henry, T. J., Jao, W.-C., & Dieterich, S. B. 2020, *AJ*, 160, 215
- Vrijmoet, E. H., Tokovinin, A., Henry, T. J., Winters, J. G., Horch, E., & Jao, W.-C. 2022, *AJ*, 163, 178
- Weis, E. W. 1991, *AJ*, 101, 1882
- . 1996, *AJ*, 112, 2300
- Whitworth, A., Bate, M. R., Nordlund, Å., Reipurth, B., & Zinnecker, H. 2007, in *Protostars and Planets V*, ed. B. Reipurth, D. Jewitt, & K. Keil, 459
- Winters, J. G. et al. 2019, *AJ*, 157, 216
- . 2020, *AJ*, 159, 290

Xia, F., Fu, Y., & Wang, X. 2019, ApJ, 882, 147

Zahn, J. P. 1977, A&A, 57, 383

Zahn, J. P., & Bouchet, L. 1989, A&A, 223, 112

Zhao, B., & Li, Z.-Y. 2013, ApJ, 763, 7

Zhou, G. et al. 2015, MNRAS, 451, 2263